Final Report
Materials Research Center
University of Pittsburgh

Sponsored By
Air Force Office of Scientific Research
AFOSR-91-0441

Principal Investigators

F.S. Pettit
Materials Science & Engineering Department

D.M. Hercules
Department of Chemistry

University of Pittsburgh
Pittsburgh, PA 15261

Period Covered

November 1, 1991 - February 28, 1994

April 29, 1994

REPORT DOCUMENTATION PAGE

Form Approved
OMB No. 0704-0188

1. AGENCY USE ONLY (Leave blank)	2. REPORT DATE	3. REPORT TYPE AND DATES COVERED
	4/29/94	Final 11/1/91 to 2/28/94

4. TITLE AND SUBTITLE
Final Report
Materials Research Center, University of Pittsburgh

5. FUNDING NUMBERS
61103D 3484 B3

6. AUTHOR(S)
D.M. Hercules, F.S. Pettit, G. Mayer
University of Pittsburgh

7. PERFORMING ORGANIZATION NAME(S) AND ADDRESS(ES)
University of Pittsburgh
350 Thackeray Hall
Pittsburgh, PA 15260

8. PERFORMING ORGANIZATION REPORT NUMBER
AFOSR-TR- 94 0354

9. SPONSORING/MONITORING AGENCY NAME(S) AND ADDRESS(ES)
AFOSR/NE
Building 410, Bolling AFB DC
20332-6448

10. SPONSORING/MONITORING AGENCY REPORT NUMBER
AFOSR-91-0441

11. SUPPLEMENTARY NOTES

12a. DISTRIBUTION/AVAILABILITY STATEMENT
Approved for public release;
distribution unlimited.

12b. DISTRIBUTION CODE

13. ABSTRACT (Maximum 200 words)

The research and related activities at the Materials Research Center (MRC) of the University of Pittsburgh under AFOSR Grant 91-0441 are summarized. The research program has progressed in four technical areas. Nine projects under the heading of High-Performance Materials are discussed and include degradation of intermetallics and composites at elevated temperatures, deformation behavior of alloys during processing and service, and development of polymers with improved mechanical properties through microstructure control. Thirteen projects have involved Electro-optics. The development of new organic optoelectronic materials employing the design and synthesis of molecules, polymers, and molecular clusters is described and the tailoring of materials in specific device structures, such as IR detectors, light emitters, or filters is discussed. Five projects involve investigations related to Biotechnology where bioactive proteins as smart materials, viral proteins as templates for bioactive materials, and molecular recognition elements have been studied. In the Catalysis technical area, the results from studies on decomposition of nerve gases, and catalysts related to alternate fuels are presented. Educational aspects of the Center are also summarized. New equipment capabilities are reviewed, as well as internal and external collaborations of the MRC. Finally, the future plans for the MRC are addressed.

14. SUBJECT TERMS
High Performance Materials, Optoelectronics, Biotechnology, Catalysis, Diamond, Quantum Well Structures, Thin Film Ferroelectrics, Nonlinear Optical Materials, Biosensors, Molecular Recognition, Neurochemical Compounds, Smart Materials.

15. NUMBER OF PAGES

16. PRICE CODE

17. SECURITY CLASSIFICATION OF REPORT	18. SECURITY CLASSIFICATION OF THIS PAGE	19. SECURITY CLASSIFICATION OF ABSTRACT	20. LIMITATION OF ABSTRACT
UNCLASSIFIED	UNCLASSIFIED	UNCLASSIFIED	

TABLE OF CONTENTS

I. EXECUTIVE SUMMARY

ORGANIZATION AND TECHNICAL ACCOMPLISHMENTS

This report reviews the status and accomplishments of the two years of sponsored support of the new Materials Research Center at the University of Pittsburgh. This Materials Research Center (MRC) came into being as a result of an award from the Air Force Office of Scientific Research (AFOSR) to foster interdisciplinary research that would lead to breakthroughs in a variety of materials sectors of importance to the scientific, technological, and military competitiveness of the United States.

The plan presented in the original proposal for the MRC has been followed in implementing research during the two years of effort. Over thirty faculty from the Departments of Chemistry, Physics, Behavioral Neuroscience of the Faculty of Arts and Sciences, and from the Departments of Materials Science and Engineering, Chemical Engineering, Electrical Engineering, and Biotechnology from the School of Engineering, have directed this research. Two additional programs have been funded through matching funding by the University. One is in the Department of Chemistry and involves theoretical studies to elucidate the fundamental parameters determining the magnitude of the nonlinear response of a material. The other is in the Materials Science and Engineering Department and is directed at processing of polymers to control microstructures and thereby properties.

The research program has actually extended over a period of twenty-nine months (including a five-month no-cost extension). Over the period of the Grant, much has been accomplished in the four scientific thrust areas of the Center. Brief highlights of these include:

In High Performance Materials, an important advance in understanding and control of the high-temperature oxidation of nickel-based superalloys has been achieved. It was demonstrated that the lowering of sulfur content to less than 1 ppm improved oxidation resistance of such alloys by a factor of at least five.

Of note in the area of Catalysis has been a major breakthrough in the development of a new catalyst for the oxidative catalytic decomposition of toxic nerve gas agents. This catalyst, based upon $Pt\text{-}Al_2O_3$, exhibited lifetimes of six to eight times that of the current catalyst of choice employed by the Army for nerve gas agents.

In the Biotechnology scientific area, significant understanding has been developed of the thermodynamic requirements for the successful application of synthetic receptor-based materials.

In Optoelectronic Materials, methods were developed for preparation of monodispersed teflon spheres, which can be readily refractive-index matched for

optical switching. In a related program, methods were developed to polymerize arrays of highly charged colloidal particles into hydrogel arrays.

COLLABORATIONS

In the course of the research program, numerous collaborations, both within the Center and with outside partners, have been established. For example, in the area of superhard materials, faculty in the Departments of Materials Science and Engineering and Chemistry have launched a collaborative research program with the Westinghouse Science and Technology Center on diamond films, and with Kennametal's Corporate Technology Center on cubic boron nitride coatings. Also, the Catalysis Group has initiated joint efforts between the Departments of Chemistry and Materials Science and Engineering on several topics, including novel catalysts for destruction of nerve gas agents and new catalytic materials based on nanosized particle technology. Those efforts have proceeded in consultation with scientists at the Westinghouse Science and Technology Center and the ALCOA Technical Center, respectively. On the topic of smart materials, interactions between the Departments of Chemistry, Chemical Engineering, and Materials Science and Engineering resulted in a successfully prepared major research proposal. New collaborations have also been developed between MRC scientists and the Department of Civil And Environmental Engineering on the subject of durability of transportation materials.

NEW CAPABILITIES

With the assistance of grant funds, an important array of new scientific equipment and instrumentation has been acquired. These include such important apparati as a scanning tunneling microscope, an atomic force microscope, a new X-ray diffractometer with high-temperature capability, and a continuous wave UV laser. The new equipment has already been put to broad use in MRC inter-disciplinary research and will see extended use in many new problem areas of importance to the DoD and to industry. Industrial partners of the MRC have already made use of some of the new equipment.

EDUCATION

The research programs of the MRC have included training of 73 graduate students, 34 post-doctoral fellows, and 22 undergraduates, (including summer support). Of this group, two of the students were members of underrepresented racial minorities and three of the undergraduates were women. One of the female minority students is finishing her first year in graduate school in Electrical Engineering at the University of Pittsburgh. A faculty member from Hampton College, a historically black college, was involved during the first summer's program in theoretical aspects of electro-optical phenomena. That successful collaboration, with an MRC faculty member in the Chemistry Department, continues.

Five degrees at the Master's level and nine degrees at the Doctoral level were granted.

PUBLICATIONS and PATENTS

The productivity of the research program has been evidenced by 82 publications in the open literature or in press. An additional 20 papers have been submitted for publication or are in preparation. In addition, two patents from MRC-sponsored research have thus far been granted.

FUTURE DIRECTIONS

Many individual research and educational accomplishments have been achieved with the two years of funding provided to the MRC. For the future, program focal areas are being built which utilize both new and existing talents from within and outside the MRC. They will address need and opportunity areas of importance to defense, industry, and society. In brief, the future MRC focal areas will include: 1.) High Performance Durable Materials, addressing life extension in a wide array of systems from transportation to manufacturing to power generation and transmission, as well as the human body; 2.) Catalysis and Other Materials Approaches to Environmental Issues, treating both prevention and remediation of harmful environmental problems; and 3.) Novel Concepts, such as nanostructural materials for optoelectronics applications, and smart materials.

The future plans of the Center include heavy emphasis on collaborations with outside organizations, including industry, other universities, and federal laboratories.

II. INTRODUCTION

The Materials Research Center (MRC) at the University of Pittsburgh was established with the aid of a two-year grant sponsored by the Air Force Office of Scientific Research in October 1991. At its initiation, the multidisciplinary program consisted of four thrust areas, *High Performance Materials*, Catalysis, Optoelectronic Materials, and Biotechnology. During the second year, the area of Biotechnology was de-emphasized, as part of an effort to provide program focus. Interest in Biomaterials however persists through focus on Durable Materials and Smart Materials.

This report describes the second year of the operation of the Center and summarizes some of the highlights of the first year as well in this final report. The key scientific and technical accomplishments and milestones of the MRC are discussed. The details of the on-going research projects are described, followed by sections on internal and external interactions that have taken place. Data on publications and students supported are also provided. The report concludes with a discussion of future plans for the Center.

III. HIGHLIGHTS AND KEY ACCOMPLISHMENTS

The highlights and key accomplishments of the Materials Research Center are described in this section. These accomplishments are indicated in concise form since more details are provided in Section IV, Technical Reports.

The technical accomplishments of the two-year period of the grant include:

- In the area of environmental effects on titanium alloy composites, interstitial elements, especially oxygen, have been shown to degrade the mechanical properties of the matrix phase.

- It has been determined that lamellar microstructures which form in certain titanium aluminides, and hitherto described as fully transformed, and stable microstructures, are in fact, unstable at high temperatures. This is important because these alloys are intended for use at high temperatures (700 - 1000°C), and if the microstructure used in a finished part is not stable, the properties of the material may change unfavorably during service.

- Computer modeling and simulation studies have provided design criteria for tailoring copolymers that will bind to a surface and form a thick protective layer for property enhancement.

- In the area of crystalline colloidal arrays, a method has been developed to polymerize these arrays into a solid material. The use of such tailored systems as smart materials is being studied.

- A reproducible and inexpensive process, using moisture-tolerant precursors, was developed for the chemical deposition of thin films of ferroelectric and electro-optic materials. The achievement of high resistivity in PZT thin films should provide resistance against electrical breakdown during DRAM or non-volatile applications. Also, for electro-optic applications, the minimum porosity achieved in the films will assure highest optical properties.

- Computer-assisted design has been applied to Field Induced Dielectric Waveguides in a collaboration between the Chemistry and Electrical Engineering Departments. Technologically important effects, such as transition from confined to unconfined eigenmodes of the electromagnetic field in these structures at high applied voltages, were predicted.

- In research on molecular recognition, a model has been developed and tested for the reversible crosslinking of polymers in solution. This is a first important step in the development of smart materials.

- The removal of sulfur to level less than 1 ppm from superalloys such as PWA 1480 and PWA 1484 has been shown to improve the oxidation resistance of these alloys by a factor of at least five. Such alloys exhibit better oxidation than the same alloys with aluminide coatings.

- Hardness indentations to create cracks in $MoSi_2$ coupons have been shown to result in catastrophic oxidation (pesting) of $MoSi_2$ at 500°C in air.

- Diamond films have been shown to oxidize (at negligible rates) in oxygen at 400°C. At higher temperatures the rates are not negligible and the oxidation attack is dependent upon crystallographic orientation.

- In the projects concerned with the deformation of alloys during processing and service, it was observed that some dislocations may be bypassing some of the particles and shearing others. This observation has importance for understanding the mechanism of twinning in particle hardened systems.

- In the area of toughening of polymers, theoretical approaches using craze growth and experimental investigations involving the thread breaking technique have been used to develop microstructures suitable for increasing toughness. In addition, the evolution of the microstructure has been predicted from first principles as a function of the rheological and processing parameters.

- Methods were developed for preparing monodispersed teflon spheres which can then be easily refractive index matched for optical switching.

- A theoretical understanding of the dependence of the phase behavior of crystalline colloidal arrays on the interparticle interaction potential was developed.

- A model was developed that predicts crystalline colloidal nucleation at surfaces.

- Synthesis of highly charged, highly monodisperse SiO_2 spheres was achieved.

- A new low vapor pressure erbium complex for CVD deposition was developed for ultrahigh resolution laser diode fabrication.

- GaAs was grown epitaxially with various concentrations of an erbium complex in the gas stream.

- Multiquantum wells were fabricated with improved interface sharpness.

- Reduced adsorption in a waveguide with a MQW cladding layer was demonstrated.

- The theory that predicts nonlinear response of metal-dielectric composites was extended to treat metal-semiconductor composites.

- The first χ^3 measurement of an unsaturated transition-metal NLO chromophore was performed. The second order hyperpolarizability is 10-fold greater than that of its closest organic analogue.

- Preparation of the first metallabutadiynes (RC ≡ M-CR) and the examination of their molecular and electronic structures was achieved.

- Synthesis of the first conjugated metal-containing polymers was performed.

- Development of processes for reliably synthesizing pure and doped calcium hydroxyapatites.

- Developed methods to deposit Pt as an active and stable catalyst on the surface of calcium hydroxyapatite.

- Major breakthrough in developing a catalyst that far exceeds the lifetime (factor of 6 - 8) of the current catalyst of choice by the Army for the oxidative catalytic decomposition of toxic nerve gas agents.

- New synthetic methodology that will permit introduction of donor and acceptor substituents to create highly nonlinear materials has been achieved.

- Successful immobilization of a acetylcholine receptor peptide on polymer resin beads. This peptide retains the specific binding characteristics of the acetylcholine receptor.

- Development of molecular receptors which can be incorporated into membranes which selectively bind dicarboxylates.

- Development of a general motif for designing recognition elements which permit formation of self assembling helical structures in the solid state.

In addition to the technical accomplishments, new equipment has been installed and is operational (Section V). Numerous meetings with industry have been held to establish lines of communication for technology transfer and to develop out-year funding (Section VI).

IV. TECHNICAL PROGRESS REPORT

IV.A HIGH PERFORMANCE STRUCTURAL MATERIALS

IV.A.1 Oxidation Behavior of Selected Aluminides and Silicides

Principal Investigator:	Professor G. H. Meier Materials Science and Engineering Department University of Pittsburgh
Other Faculty Participants:	Dr. N. Birks Dr. F. S. Pettit Materials Science and Engineering Department University of Pittsburgh
	Dr. D. Hercules Department of Chemistry University of Pittsburgh
Students:	Dr. D. Monceau Dr. A. Proctor Mr. J. Rakowski Ms. D. Berztiss Mr. R. Cerchiara

IV.A.1.1 INTRODUCTION

The intermetallic compounds which have the greatest potential for near-term application as structural materials are the titanium aluminides (Ti_3Al, TiAl, and Orthorhombic Alloys), the refractory metal silicides (particularly $MoSi_2$), and NiAl. There is a critical need to develop a detailed understanding of the factors which affect the environmental resistance of these three compounds [1]. Each has particular areas of concern: Ti_3Al is extremely susceptible to embrittlement by oxygen (and possibly nitrogen) [2], TiAl shows oxidation rates which can vary by orders-of-magnitude as the result of small changes in temperature or slight changes in the composition of the oxidizing gas [3-6], $MoSi_2$ exhibits the characteristic of accelerated degradation at low temperatures (near 500°C) even though it is extremely resistant at high temperatures [7-14], and NiAl forms oxide layers which are poorly adherent to the substrate [15].

The objectives of this project for the second year included:

1. Characterization of the effect of temperature and nitrogen on the oxidation behavior and embrittlement of α_2-Ti_3Al and orthorhombic alloys.

2. Characterization of the effect of Al content, microstructure, and surface preparation on the oxidation behavior of γ-TiAl.

3. Further characterization of the oxidation behavior of $MoSi_2$ in the temperature range 400 - 600°C.

4. Initiate a study of how various factors, including impurities such as sulfur, affect the oxidation behavior and oxide adherence of NiAl.

5. Modification of existing apparatus to allow characterization of the effect of particle erosion on the oxidation behavior of intermetallics at temperatures above 800°C.

IV.A.1.2 ACCOMPLISHMENTS AND SIGNIFICANCE

A. Oxidation of Titanium Aluminides

Thermodynamics

An important aspect of the oxidation of Ti-Aluminides, compared to the aluminides of Ni and Fe, is the small difference in standard free energy of formation between alumina and the oxides of titanium, which is accentuated by a negative deviation from ideal solution behavior in the Ti-Al system. The aluminum activity is much smaller than unity in Ti_3Al and TiAl. In fact, combining the activities with standard free energy data for the oxides indicates that TiO is more stable in contact with the alloy than is Al_2O_3 for atom fractions of Al much less than about 0.5 [16, 17]. Thus, Al_2O_3 is unstable in contact with binary α_2 and is only marginally more stable than TiO in contact with γ-TiAl. This is extremely important since alumina layers are far more protective than the oxides of titanium.

Oxidation of Ti_3Al (α_2)

The oxidation of Ti_3Al alloys would not be expected, in light of the above thermodynamic considerations, to form continuous alumina scales. Instead they form mixed rutile-alumina scales. The oxidation kinetics of Ti_3Al between 600 and 950°C are reported to be those expected for rutile growth [3, 4].

Alloying of Ti_3Al with β-stabilizing elements, particularly Nb, reduces the oxidation rate [18]. The scales developed on α_2 alloys containing multiple additions of β-stabilizers have been described by Wallace etal [19] and Schaeffer [20].

An additional aspect of the oxidation of Ti_3Al alloys is dissolution of oxygen into the alloy at the scale/alloy interface. The embrittlement associated with this phenomenon can be more damaging to the mechanical properties than the surface recession caused by scale formation in the temperature range where Ti_3Al will likely be used (<700°C) [2].

The oxidation behavior of binary and Nb-modified α_2 alloys has been studied in this program as a function of temperature (600-900°C) and atmosphere [21]. The oxidation kinetics have been characterized by thermogravimetry and the oxidation morphologies have been characterized by a wide variety of metallographic techniques. Additionally, the penetration of interstitials into the alloys has been followed using hardness measurements and the effect of interstitial penetration on mechanical properties has been evaluated. The results of the characterization of the oxidation morphologies are presented schematically in Figure IV.A.1.1. The scale consists of an outer layer of single-phase TiO_2 (rutile), which has grown outward, and an inner layer containing rutile and discontinuous alumina particles, which has grown inward. These two layers are separated by a layer of large alumina crystals. The growth of the scale in both directions is consistent with the reported presence of both Ti-interstitials and O-vacancies as significant defects in rutile [22]. The presence of the large alumina crystals indicates that Al is rapidly transported through the inner rutile layer since their size precludes transport through alumina i.e continuous alumina layers for these times and temperatures are typically in the 0.1 μm thickness range. This morphology is typical of that observed for α_2 alloys over the entire temperature range studied. The addition of Nb, at levels of about 10 at %, slows the rate of oxidation as the result of doping of the TiO_2 in the mixed titania-alumina layer, Figure IV.A.1.2. The oxidation rates are generally lower in air than oxygen because of nitrides formed at the oxide/alloy interface during oxidation in air. The formation of nitride layers, which is more profuse for alloys containing Nb, also limits, but does not eliminate, interstitial penetration of the underlying alloy, Figure IV.A.1.1.

The nature of the layer of interstitial penetration is critical to the mechanical properties of the alloys. Interstitial penetration severely embrittles Nb-modified α_2, particularly in atmospheres containing water vapor. The results of a collaborative study with Mr. R. Perkins of Lockheed Palo Alto Research Laboratory [21] showed that room temperature ductility of Ti-21Al-11Nb was severely degraded by exposures to oxidizing atmospheres at temperatures from 600 to 900°C and that the embrittlement was sensitive to the composition of the exposure environment, Table IV.A.1.1. Oxygen caused severe embrittlement whereas high-purity nitrogen or argon did not. However, the presence of water vapor in the nitrogen or argon caused embrittlement and analysis of the fracture behavior suggested a synergistic effect between hydrogen and oxygen. The detailed mechanisms of these phenomena are a subject of continuing studies in the MRC.

Oxidation of Orthorhombic Alloys

There are relatively few oxidation data available on alloys in the Ti-Al-Nb system with significant volume fractions of the orthorhombic phase. However, data generated in this study indicate that the amount of Nb necessary to stabilize the orthorhombic phase results in more rapid oxidation than the α_2 alloys because of the formation of discrete Nb-oxides in the reaction products, (See Figure

IV.A.1.2). The presence of 27 at % Nb, which stabilizes a microstructure consisting of O + β, clearly accelerates the oxidation kinetics. Thus, additions of Nb which are small enough that the Nb remains in solution in the TiO_2 produce a beneficial doping effect whereas larger additions which produce discrete Nb-oxide are detrimental.

The orthorhombic alloys have been reported to be less susceptible to environmental embrittlement than the α_2 alloys [23]. However, the alloy microstructure is modified by the oxidation. A nitride layer and an interstial penetration zone form beneath the surface oxide layer. The effect of interstitial penetration on the mechanical properties of orthrorhombic alloys will be discussed in a subsequent section of this report on composites.

Oxidation of TiAl (γ)

The oxidation behavior of γ-TiAl (52 at % Al) was studied in the first year of the MRC over the temperature range 750 to 1100°C [6]. Exposures were carried out in pure oxygen and various oxygen-nitrogen mixtures. The oxidation behavior was found to depend on temperature and the composition of the oxidizing gas. Protective alumina scales formed in pure oxygen up to a critical temperature above which scales consisting primarily of intermixed TiO_2 and Al_2O_3 were formed and oxidation rates accelerated dramatically. Continuous alumina scales were not observed at any temperature when nitrogen was present in the oxidizing gas. The mechanism whereby nitrogen produces this effect was not completely defined but was shown to be associated with the initial development of the reaction product. The results of extensive experiments to characterize the nature of the non-protective mixed-oxide layers are summarized schematically in Figure IV.A.1.3. It is clear that, when protective alumina layers do not form, the oxidation morphologies on γ are very similar to those on α_2 (Figure IV.A.1.1).

Research during the second year has focussed on the effects of Al content, surface preparation, and microstructure of the alloy on the mechanisms of the above phenomena.

Effect of Aluminum Content

It is expected that increasing the amount of aluminum in a Ti-Al alloy would increase the temperature threshold for the formation of protective, continuous alumina. This has been previously noted to be about 1025°C for Ti-52Al. For lower aluminum alloys, at 900 C, mixed oxide nodules begin to disturb the alumina scales, leading to increased weight gain (Figure IV.A.1.4a-IV.A.1.4b). These nodules grow laterally and merge as the exposure time is increased, resulting in a complete layer of mixed oxide layer. This process occurs more rapidly at higher temperature (Figure IV.A.1.5). The oxidation kinetics generally decrease with increasing aluminum content (Figure IV.A.1.6). However, below 49 atomic percent aluminum, the alloys lie in a two phase field of γ + α_2. The distribution of the α_2 phase is critical, as will be explained in the next section.

Effect of Microstructure on Alpha-2 + Gamma Alloys

It has been noted in earlier work [24] that a lamellar distribution of α_2 is beneficial when compared to an equiaxed microstructure. One hypothesis is that the lamellar morphology allows alumina (forming on the γ lamellae) to overgrow rutile TiO_2 (forming on the α_2 lamellae). When the α_2 grains are equiaxed, the rutile nodules form on too large of a scale to be overgrown. The two alloys studied were Ti-46Al and Ti-48Al. Both lie in the two-phase field. The Ti-46Al alloy was heat-treated to form a duplex microstructure, consisting mostly of lamellar α_2 + γ, with a small amount of equiaxed γ. The Ti-48Al alloy was in the as-cast + HIP condition, so that the microstructure consisted of equiaxed γ, with a few small (5 to 10%, by volume) lamellar grains. The Ti-46Al alloy oxidized less rapidly in oxygen (Figure 6) and produced a different scale morphology consisting of a thin scale containing both titanium and aluminum oxides. The oxide mirrored the underlying alloy morphology with thicker, titanium rich oxide covering the lamellar regions and thin alumina covering the gamma grains. The Ti-48Al had very thin alumina over much of the surface, but in certain areas, the alumina was broken with very large mixed oxide nodules such as those in Figure IV.A.1.4b. These results suggest the possibility of influencing the oxidation behavior of γ alloys by microstructural, as well as compositional, control. The use of thermomechanical processing to control microstructure in titanium aluminides will be discussed in a subsequent section of this report.

The Effect of Surface Finish

Surface finish has been reported to alter the oxidation behavior of TiAl in oxygen [3]. Finer polishes are noted to produced more rapid oxidation kinetics. This behavior has been verified for Ti-50Al in the present experiments, Figure 7, where surface finish had a profound effect for exposures in oxygen but had no effect in air. Sequential exposures in air with both 600 grit and I micron surface polishes resulted in scales which begin with transient oxidation, forming mostly TiO_2, and some TiN. For the one micron finish, the α_2 phase (present in lamellar form) was initially covered with thicker oxides which was not apparent for the 600 grit finish. After two hours, however, the oxide morphologies had become virtually identical. Sequential exposures in oxygen with both 600 grit and I micron surface polishes reveal that after ten minutes, the 600 grit surface was covered with a thin, uniform oxide (Fig. IV.A.1.8a), while the one micron surface had patches of thick oxide and some regions of spalling/flaking (Fig. IV.A.1.8b-IV.A.1.8c). It is proposed that the rough polish smears over the finely distributed α_2 phase, lessening its effect on the formation of mixed oxide. A one micron polish does not obscure the finer features, leading to an increased rate of oxidation resulting from the formation of TiO_2. The oxidation kinetics for the fine polish in oxygen are comparable to the rapid kinetics for specimens exposed in air (Figure IV.A.1.7). Surface preparation has no effect in air because the nitrogen prevents the formation of continuous alumina, even on the single phase γ.

Application of XPS and Cross-section TEM to Oxide Characterization

The above results make it clear that complete understanding of the oxidation mechanisms of the titanium aluminides will require detailed knowledge of how the oxides nucleate and grow into mature layers. This requires the application of techniques which have high chemical sensitivity and high spatial resolution. To this end experiments have been begun to apply X-ray Photoelectron Spectroscopy (XPS) and cross-section Transmission Electron Microscopy (TEM) to the characterization of the oxidation products formed on α_2 and γ alloys.

The use of pure standards of Al_2O_3 and TiO_2 has allowed the determination of the relative amounts of these two oxides on the surface of titanium aluminides as they undergo oxidation. Typical results for binary alloys are presented in Figure IV.A.1.9. The relative concentrations of Al and Ti have been calculated from the ratio of the peak areas for Al2p and Ti2p. However, these ratios have been verified by deconvolution of the O1s peak which results form oxygen bound to both Al and Ti. Figure IV.A.1.9 indicates a substantial amount of Ti in the native oxide film on both α_2 and γ but shows the Al concentration increases at the surface during the initial growth of the oxide film. This result is currently being analyzed in terms of "Al segregation in an oxygen potential gradient" which can occur if Al is highly mobile in TiO_2. It is interesting that after about 1 hour oxidation the Al concentration at the surface falls to low values typical of the rutile outer layer depicted in Figures IV.A.1.1 and IV.A.1.3. The mechanism for this decrease has not yet been determined but these results indicate that XPS provides a powerful auxiliary tool for characterizing the development of oxide films on titanium aluminides.

A collaborative effort has been begun with Professor Manfred Ruhle (Max Planck Institut fur Metallforschung, Stuttgart, Germany) to apply cross-section TEM to the characterization of the oxide layers which form on titanium aluminides and the alloy layers which form immediately beneath the oxide. Figure IV.A.1.10 presents a micrograph of a specimen of γ-TiAl oxidized in pure oxygen. The thin oxide layer has been identified as α-Al_2O_3, however, the diffraction patterns from the Al-depleted alloy layer are not consistent with Ti_3Al, which would be expected from the binary phase diagram. In fact, the patterns are not consistent with any known phase in the Ti-Al-O system. These preliminary results must be verified and the structure identified, however, they indicate the usefuness of TEM in characterizing not only the oxide layers but also the underlying alloy which is so critical to the mechanical properties, as described above. This collaborative effort with Stuttgart will be expanded.

B. Oxidation of $MoSi_2$

The experiments performed in the first year of the MRC involved the oxidation of cast, HIPed, and single crystal $MoSi_2$ in air and in oxygen in the temperature range 400 - 1400°C Figure IV.A.1.11 summarizes weight change

data as a function of time. All materials fall into the ± 1 mg/cm^2 range for 600 - 1400°C in both air and oxygen. At 500°C all the materials oxidize rapidly and the cast material, showing the greatest weight gain, turns completely to powder, which is nonuniform in size and faceted in appearance. XRD indicated the reaction products were MoO_3 and amorphous SiO_2. HIPed and single crystal material showed the same reaction products, but the scale (20 - 40 μm thick) remained intact. The cast material did not exhibit pesting (disintegration to powder) at T > 500°C, but internal oxides of SiO_2 did form between 600 and 1000°C. The internal oxides appeared to form within grain boundaries, but it is also possible that these boundaries contained pre-existing cracks. There was no evidence of internal oxidation at 1200 or 1400°C where a silica layer covered the external surface.

The accelerated oxidation of HIPed material at 500°C is illustrated schematically in Figure IV.A.1.12. The oxidation involves oxidation of both Mo and Si and incorporation of small metallic particles into the scale, however, this material contains no pre-existing cracks and does not "pest". Scannining Auger analysis of specimens fractured after oxidation indicated penetration of oxygen into the material along grain boundaries but no oxide formation along the boundaries. The oxidation of the single crystal at 500°C was qualitatively the same as that for the HIPed material indicating that grain boundaries are not necessary for accelerated oxidation to occur. The volatility of MoO_3 plays an important role in the oxidation behavior of $MoSi_2$. MoO_3 is highly volatile with a melting point of 795°C and a high vapor pressure even at lower temperatures. At elevated temperatures (>1000°C), MoO_3 vaporizes and the diffusion of Si is rapid enough to form a continuous protective oxide scale to effectively seal the surface. At T < 600°C, mixed oxidation and volatilization of MoO_3 prevents continuous SiO_2 scale formation.

The oxidation behavior of cast material at 500°C is shown schematically in Figure IV.A.1.13. The oxide development was identical to that for the HIPed and single crystal material but the presence of cracks which existed in the starting material produced strikingly different results. In the cracks, oxygen has a short-circuit path for diffusion, thus SiO_2 can easily form within the cracks. At 500°C, MoO_3 can also form within the cracks, and at this temperature, little volatilization occurs. These processes enhance the widening of the pre-existing cracks leading to "pesting" (i.e. turning to powder). Thus cracking of $MoSi_2$ as a result of oxide formation within pre-existing cracks is an integral part of the oxidation process. This mechanism was further confirmed by showing that introducing cracks into HIPed $MoSi_2$ also lead to pesting.

Experiments in the second year have focussed on developing a better understanding of the low temperature behavior of $MoSi_2$, especially with regard to accelerated oxidation and "pesting" at or near 500°C. A number of experiments were performed.

1. $MoSi_2$ made by the HIPing process was exposed to air for one hour at both

500 and 800°C, more Si than Mo oxide forms, however both are evident. More importantly, more oxide forms at 500°C, than at 800°C as determined by intensities of the O1s peaks. This is in agreement with isothermal thermogravimetric studies of the oxidation behavior, where much larger weight gains were observed at 500°C than at 800°C and higher.

2. It is believed that the formation of MoO_3 impedes the growth of the protective SiO_2 at low tempertures, while at high temperatures the volatility of MoO3 is great allowing for continuous SiO_2 coverage. To find out what happens if the partial pressure of oxygen is below that to form MoO_3, a piece of $MoSi_2$ made by drop-casting was encapsulated in a quartz tube containing a Cu/Cu_2O and alumina powder mixture. This was done to ensure a fixed partial pressure of oxygen within the ampoule. The metal and powder were physically separated by a small amount of alumina wool. The tube was evacuated and backfilled with Ar to a pressure of 450 mm Hg. Subsequently a heat treatment of 500°C for 100 hours was performed. At high oxygen pressures, such as in air and pure oxygen, the cast material disintegrates to powder as a result of Mo and Si oxides growing within preexisting cracks in the material. The volume expansion of the oxides results in a wedging mechanism that breaks the material apart. At low partial pressures of oxygen, the oxide layer is very thin and cannot be resolved with glancing angle x-ray diffraction. The grains can be distringuished clearly by observation under a light optical microscope noting different interference colors on different grains, indicating that the grains have different thicknesses of oxide. There may be an orientation effect in oxide growth at low partial pressure of oxygen. XPS results of the oxide indicate some Mo oxide forming, but mostly oxides of Si are found. The Mo oxide should be MoO_2, as MoO_3 cannot form under these conditions.

These results further confirm that the formation of MoO_3 prevents the formation of continuous silica at low temperatures and, therefore, is the underlying cause of "accelerated oxidation". Furthermore, the absence of accelerated oxidation prevents pesting, even in material which contains cracks.

C. Oxidation of NiAl

The compound NiAl is, perhaps, the most oxidation resistant of all the intermetallic compounds. However, it can be severely degraded under certain conditions. In particular, the protective alumina layer which forms on NiAl can spall profusely during thermal cycling [15] and can undergo severe degradation in an intermediate temperature range around 800°C [25]. Experiments have been initiated to ascertain the mechanisms of the above phenomena. Preliminary results have been obtained but will be reported at a later date.

D. Erosion/Oxidation of Intermetallic Compounds

Study of the erosion-oxidation behavior of TiAl was begun, during the first year of the MRC using a dedicated apparatus already available for such studies. Experiments carried out involved samples exposed to erosive streams containing 20μm alumina particles and flowing at 100 m/s, at normal impingement and at 700 and 800 °C for times up to 420 minutes and to erosion-only conditions at room temperature at 75 m/s (maximum velocity at room temperature), and to oxidation-only at both 700 and 800°C. The erosion-oxidation exposures at 700°C showed small weight losses. At 800°C under erosion-oxidation, substantial weight losses were seen and are consistent with the rapid formation and removal of oxide. In the absence of erosion at both 700 and 800°C, very small weight gains were observed over 420 minutes, which points to the formation of a protective oxide layer in the absence of erosion. In the absence of oxidation at room temperature, a 420 minute exposure showed a surprising loss of weight. This was tentatively attributed to a change from ductile behavior of the TiAl at high temperature to brittle behavior at room temperature.

The activity during the second year has involved modification of the erosion apparatus to allow the use of lower particle loadings and higher temperatures. This modified apparatus will now be used to further characterize the erosion oxidation behavior of TiAl and $MoSi_2$.

IV.A.1.3 REFERENCES

1. G. H. Meier, N. Birks, F. S. Pettit, R. A. Perkins, and H. J. Grabke, "Environmental Behavior of Intermetallic Materials", in Structural Intermetallics, TMS, 1993, p. 861.
2. S. J. Balsone, "The Effect of Elevated Temperature Exposure on the Tensile and Creep Properties of Ti-24Al-11Nb", in: Oxidation of High Temperature Intermetallics, Edited by T. Grobstein and J. Doychak, (TMS Publications, Warrendale, PA (1989), 219-234.
3. Choudhury N. S., Graham H. C., and Hinze J. W., in Foroulis Z. A. and Pettit F. S. (eds.), Properties of High Temperature Alloys, (The Electrochem. Soc., 1976) p. 668.
4. Mendiratta, M.G., and Choudhury, N.S., "Properties and Microstructure of High-Temperature Materials", AFML-TR-78-112, Contract No. F33615-75--C-1005, (Systems Research Laboratories, Inc., Ohio, August 1978).
5. Meier G. H., Appalonia D., Perkins R. A., and Chiang K. T., in Grobstein T. and Doychak J. (eds.), Oxidation of High-Temperature Intermetallics, (TMS, 1989) p. 185.
6. G. H. Meier, F. S. Pettit, and S. Hu, "Oxidation Behavior of Titanium Aluminides" J. de Physique, in press.
7. E. Fitzer, "Molybdandisilizid als Hochtemperaturwerkstoffe", Warmfest und Korrosionbestandige Sinterwerkstoffe, 2nd Plansee Seminar, 19-23 June

1955, Reutte/Tirol, F. Benesovsky, ed., Vienna, Springer Verlag, 1956, p. 56.
8. J.B. Berkowitz-Mattuck, P.E. Blackburn and E.J. Felton, Trans AIME, 233, June 1965, p. 1093.
9. J.B. Berkowitz-Mattuck, M. Rosetti and D.W. Lee, Met. Trans., 1, Feb. 1970, p. 479.
10. J.H. Westbrook and D.L. Wood, J. Nucl. Mater., 12 1964, p. 208.
11. J. Schlichting, High Temperatures-High Pressures, 10 1978, p. 241.
12. O. Rubisch, Berichte deutsche keramische Gesellschaft, 41 1964, p. 120.
13. P. J. Meschter, Met. Trans., 23A, 1992, p. 1763.
14. D. A. Berztiss, R. R. Cerchiara, E. A. Gulbransen, F. S. Pettit, and G. H. Meier, Materials", Mater. Sci. + Eng., A155, 1992, p. 165.
15. M. W. Brumm and H. J. Grabke, Corros. Sci., 34, 547, 1993.
16. Rahmel A. and Spencer P. J., Oxidation of Metals, 35, 1991, p. 53.
17. Luthra K. L., Oxidation of Metals, 36, 1991, p. 475.
18. M. Khobaib and F. W. Vahldiek, "High Temperature Oxidation Behavior of Ti_3Al Alloys", Second International SAMPE Metals Conference, F. H. Froes and R. A. Cull eds., Covina, Ca, 1988, pp.262-270.
19. T. A. Wallace, R. K. Clark, K. E. Wiedemann, and S. K. Sankaran, Oxid. Metals, 37, 1992, 111-124.
20. J. C. Schaeffer, Scripta Met., 28, 1993, 791-796. .
21. J. Rakowski, D. Monceau, F. S. Pettit, G. H. Meier, and R. A. Perkins, "The Oxidation and Embrittlement of Titanium Aluminides", Proc. of Inst. of Materials Conf. on Microscopy of Oxidation, The Institute of Materials, Cambridge, England, 1993, in press.
22. P. Kofstad, High Temperature Corrosion, 1988, 295, Elsevier, London.
23. P.R. Smith, J. A. Graves, and C. G. Rhodes, "Preliminary Mechanical Property Assessment of a SiC/Orthorhombic Titanium Aluminide Composite" in Structural Intermetallics, TMS, 1993, p. 765.
24. A. Gil, H. Haven, E. Walbura, and W.J. Quadakkers, Corr. Sci., 34, 615 (1993).
25. M. W. Brumm, H. J. Grabke, and B. Wagemann, Corr. Sci., 36, 1994, 37-53.

Table IV.A.1.1

Contamination Embrittlement of Ti_3Al in Vacuum

Exposure Conditions	Elongation — %
Vacuum — 2 h at 900 °C	
As-annealed	1.9
0.127 mm removed	> 18.0, > 26.5, > 22.2
0.254 mm removed	> 20.6, > 27.9, > 24.3
Vacuum — 24 h at 900 °C	
As-annealed	3.4
0.076 mm removed	12.2
0.127 mm removed	12.3

Contamination Embrittlement of Ti_3Al in Various Gases

Exposure Conditions	Elongation — %	
	24 h – 900 °C Purged System	20 h – 900 °C Evacuate & Backfill
Argon		
<1 ppm H_2O		> 20.3
< 10 ppm H_2O	3.60	
Nitrogen		
< 1 ppm H_2O		17.0
< 32 ppm H_2O	1.55	
Oxygen		
< 3 ppm		2.70
< 50 ppm	3.06	
Air		
< 3 ppm		3.60
<50 ppm	6.87	
CO_2		
Liquified	1.42	
82% CO — 18% CO_2	4.37	
Air — 46% H_2O	1.30	
Oxygen — 37% H_2O	1.91	
(82% CO — 18% CO_2) — 31% H_2O	1.35	
H_2 — 39% H_2O	1.11	

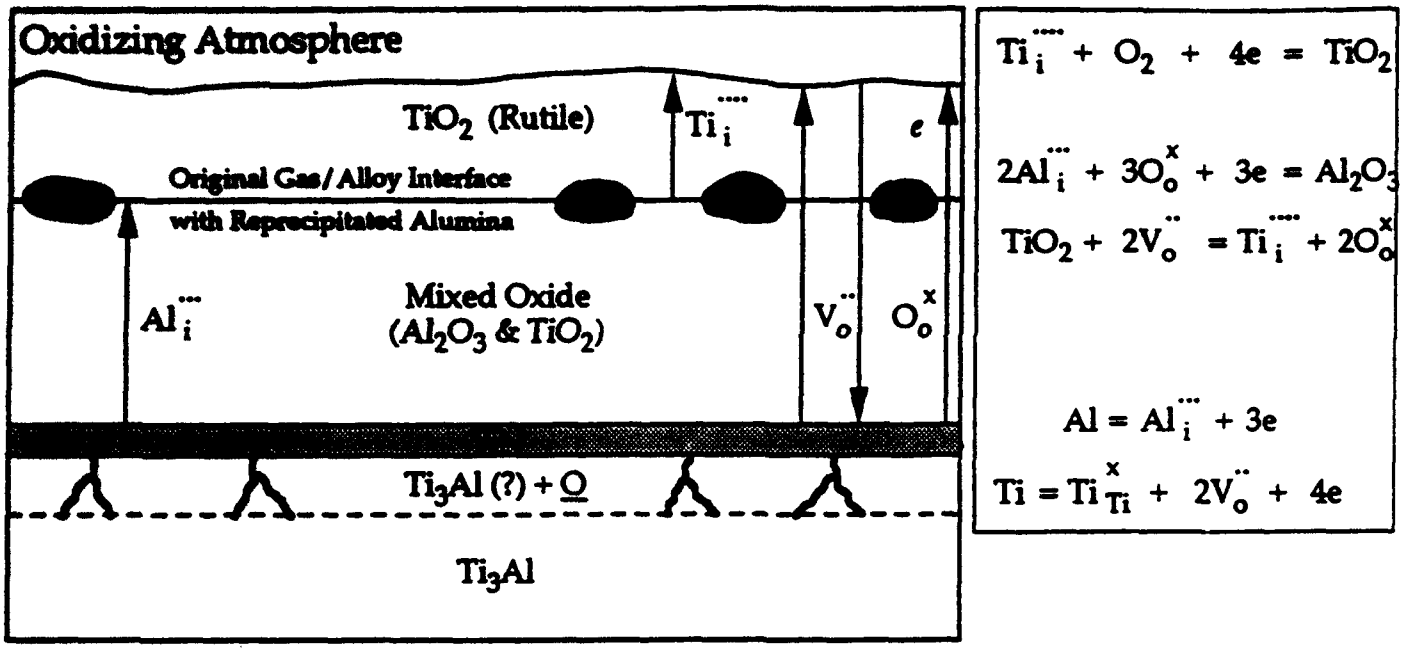

Figure IV.A.1.1 Schematic of oxide formed on Alpha-2Ti3Al in air with pertinent defect reactions.

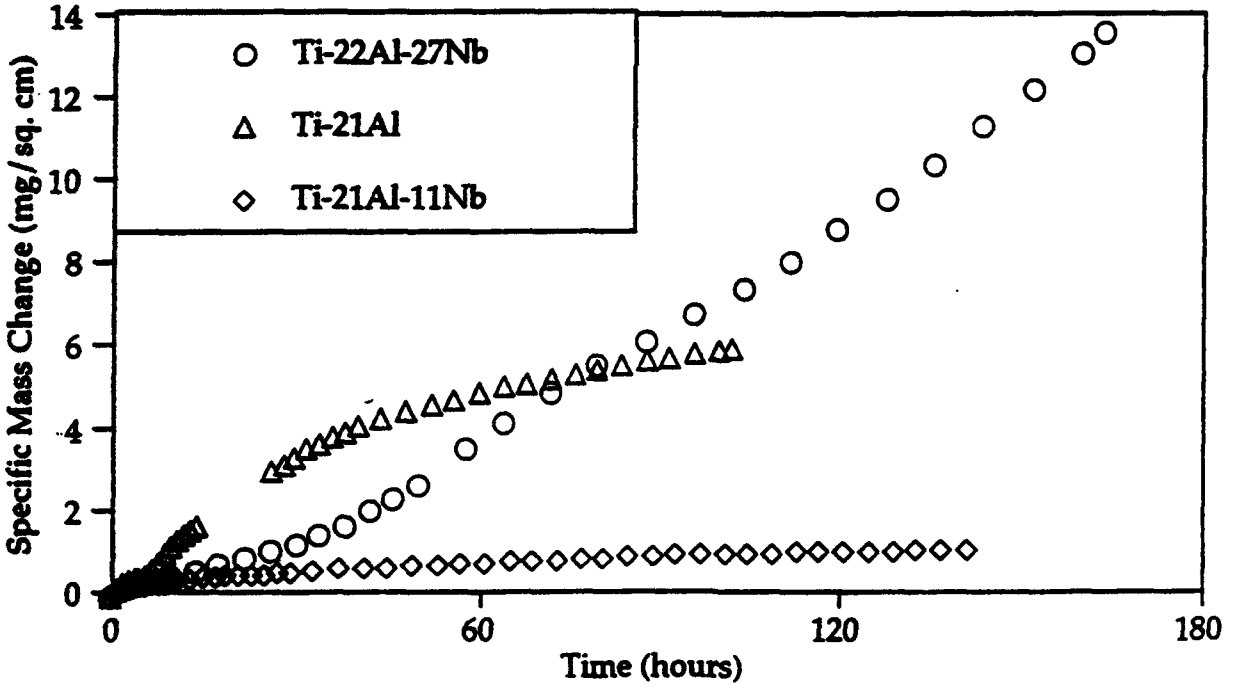

Figure IV.A.1.2 Isothermal oxidation results for titanium-base intermetallics, air exposure at 800°C.

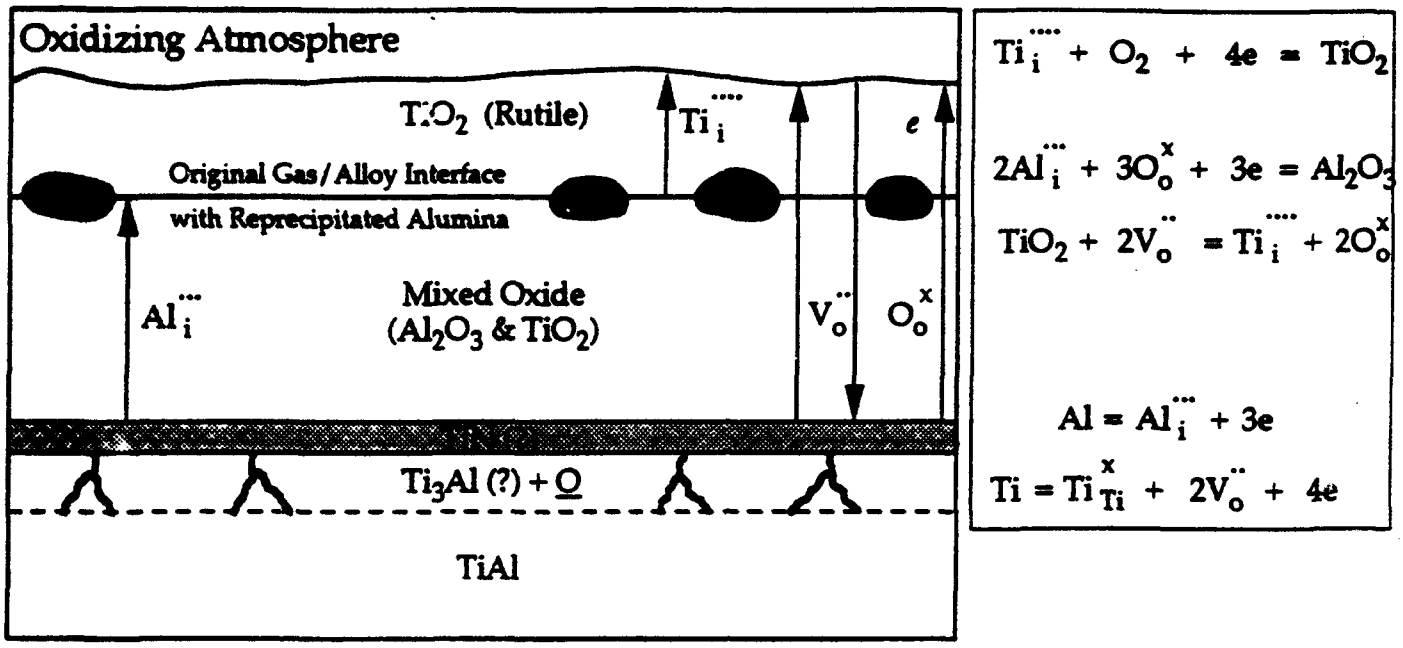

Figure IV.A.1.3 Schematic of oxide formed on gamma TiAl in air with pertinent defect reactions.

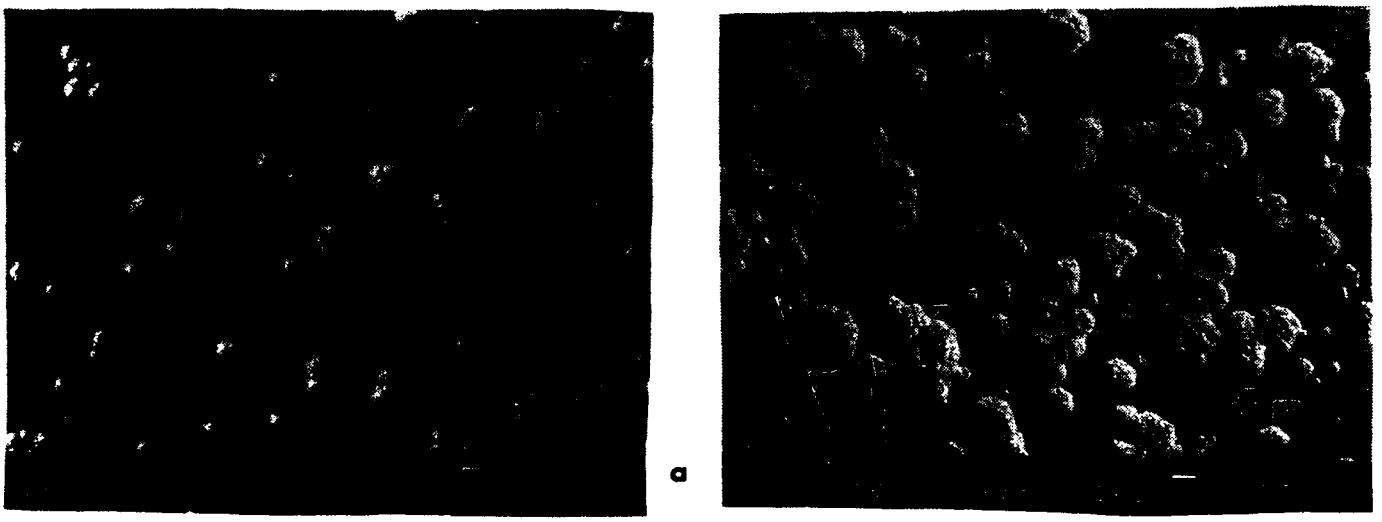

Figure IV.A.1.4 Ti-Al isothermal oxidation-samples exhibiting nodular oxide morphology.

a) Ti-50Al, 900°C, oxygen, approximately 1 week.
b) Ti-48Al, 900°C, oxygen, approximately 1 week.

Figure IV.A.1.5 Isothermal oxidation-Ti-48Al, 1000°C, oxygen, approximately 1 week.

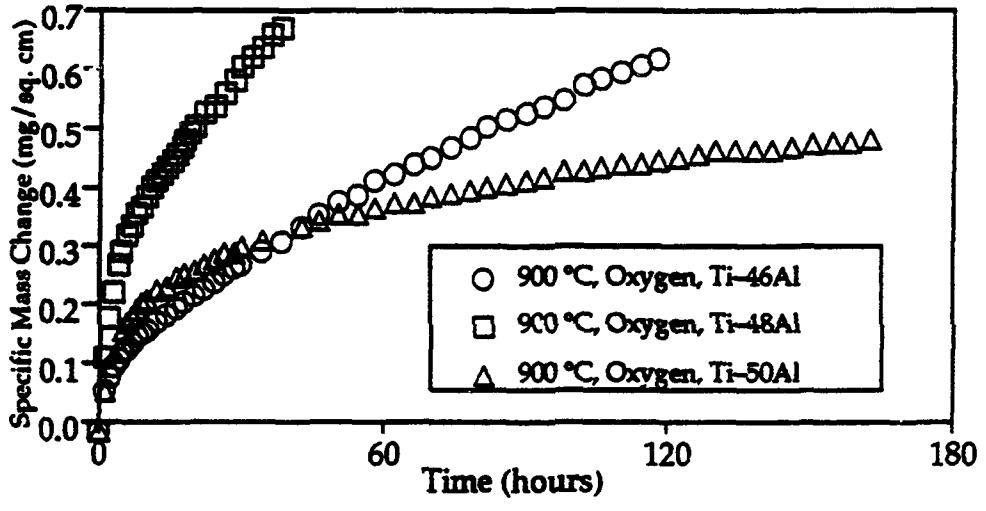

Figure IV.A.1.6 Isothermal oxidation results for gamma alloys, oxygen exposure at 900°C.

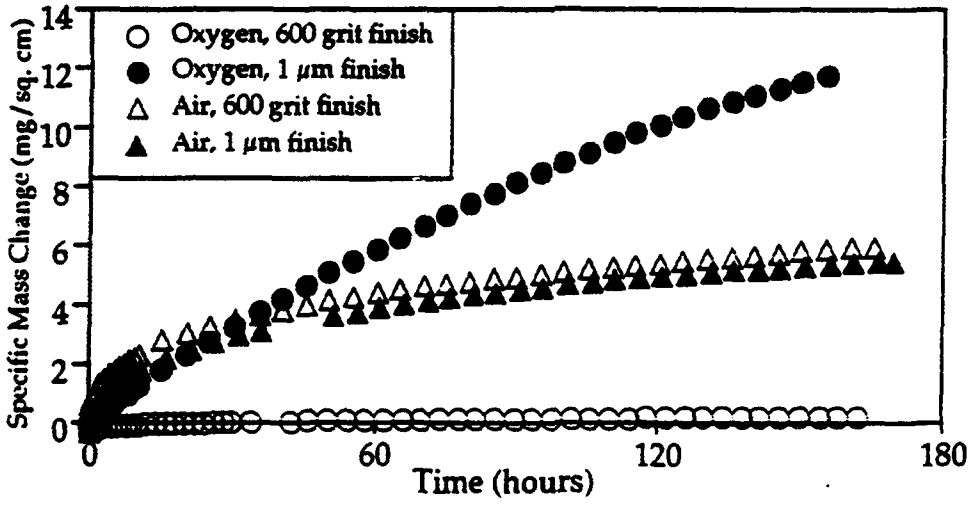

Figure IV.A.1.7 Isothermal oxidation results for Ti-50Al-effect of surface finish.

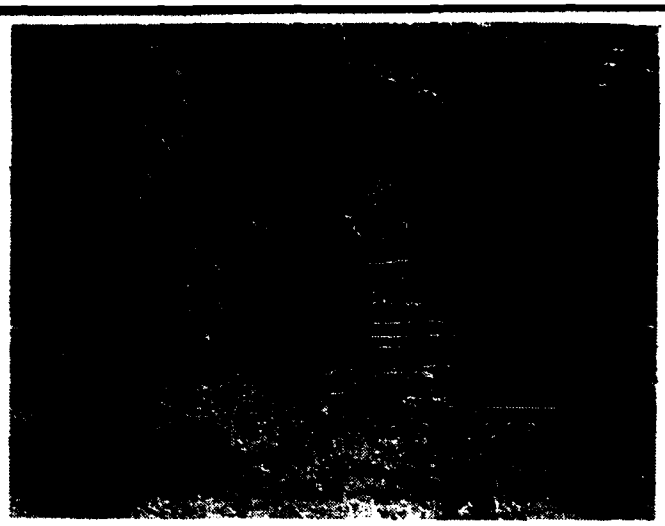

a

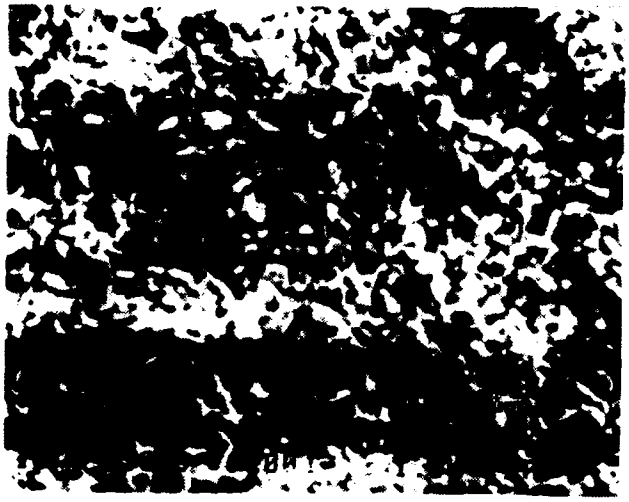

b

Figure IV.A.1.8

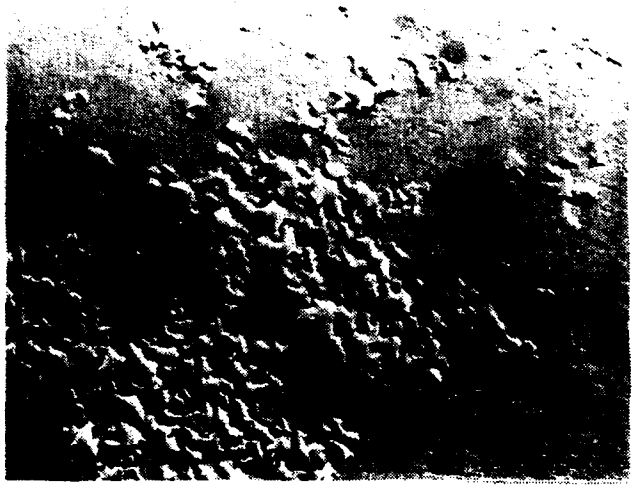

c

Short-term exposure micrographs of Ti-48Al at 900°C.

a) 15 minutes, 1 μm surface finish, air.
b) 2 hours, 1 μm surface finish, air.
c) 10 minutes, 1 μm surface finish, oxygen.

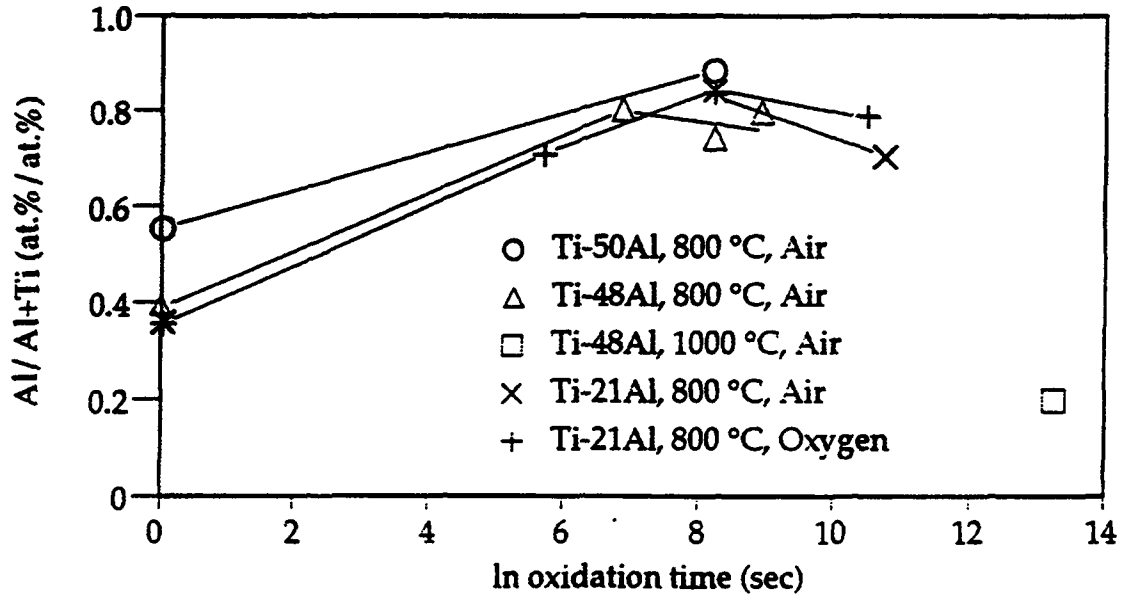

Figure IV.A.1.9 Aluminum Content vs. Time at Surface (XPS).

Figure IV.A.1.10 Cross-Section TEM Micrograph of Alumina on Gamma TiAl.

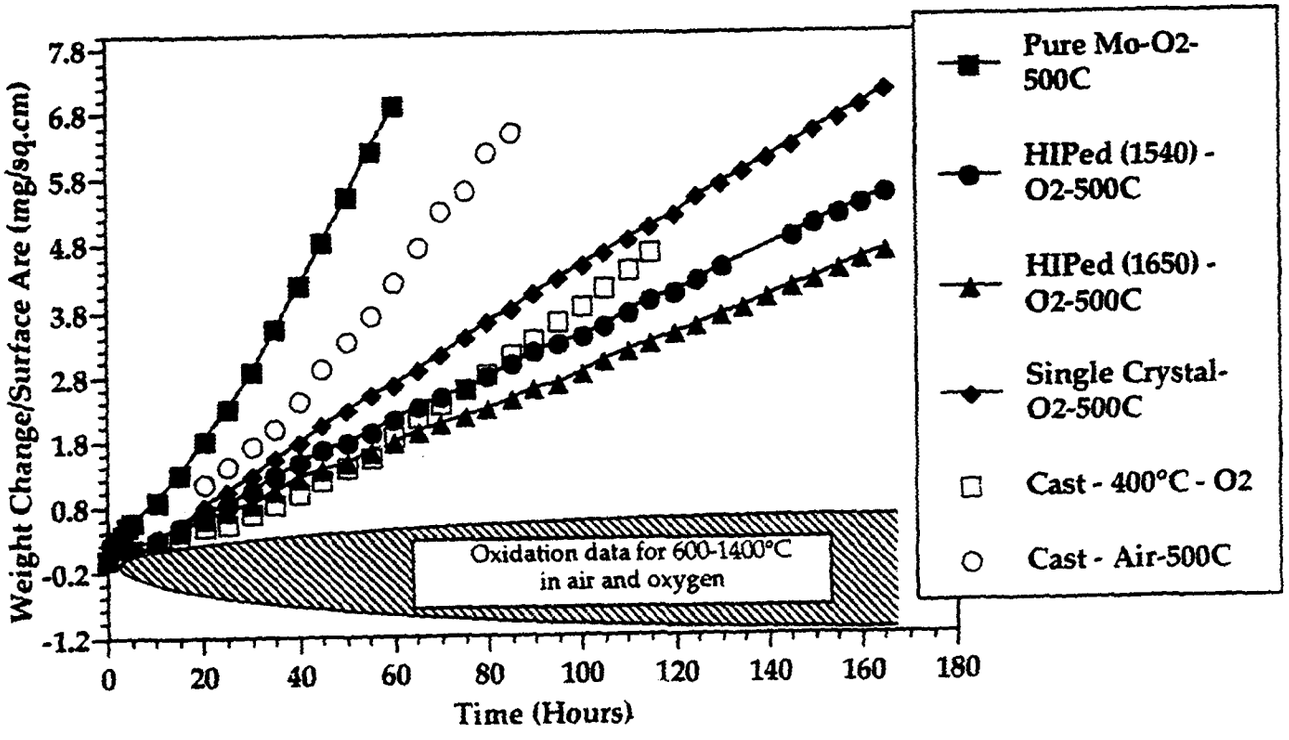

Figure IV.A.1.11 Weight change as a function of time for $MoSi_2$ oxidized in air and oxygen over a temperature range of 400 to 1400°C.

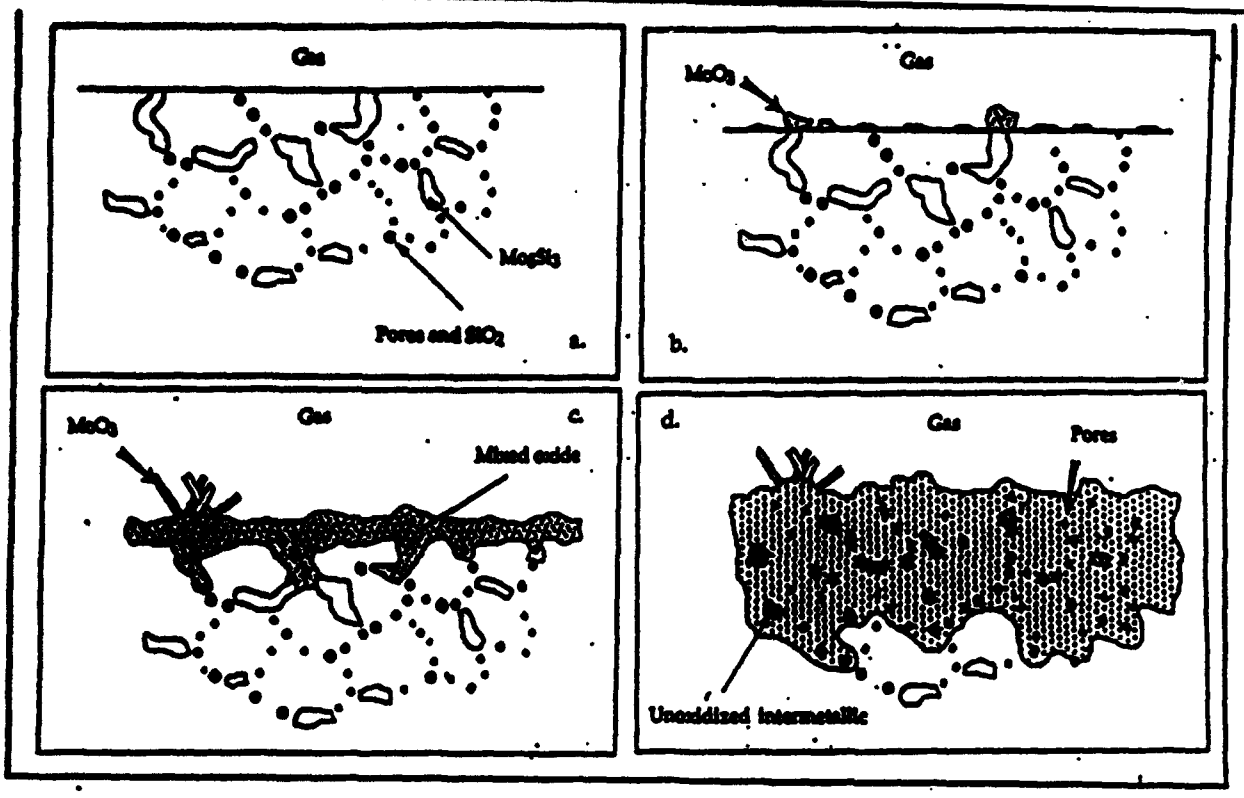

Figure IV.A.1.12 Schematic diagram of accelerated oxidation sequence of HIPed $MoSi_2$ at 500°C in air: a. As received, b. 30 mins., c. 47 hrs., d. 168 hrs.

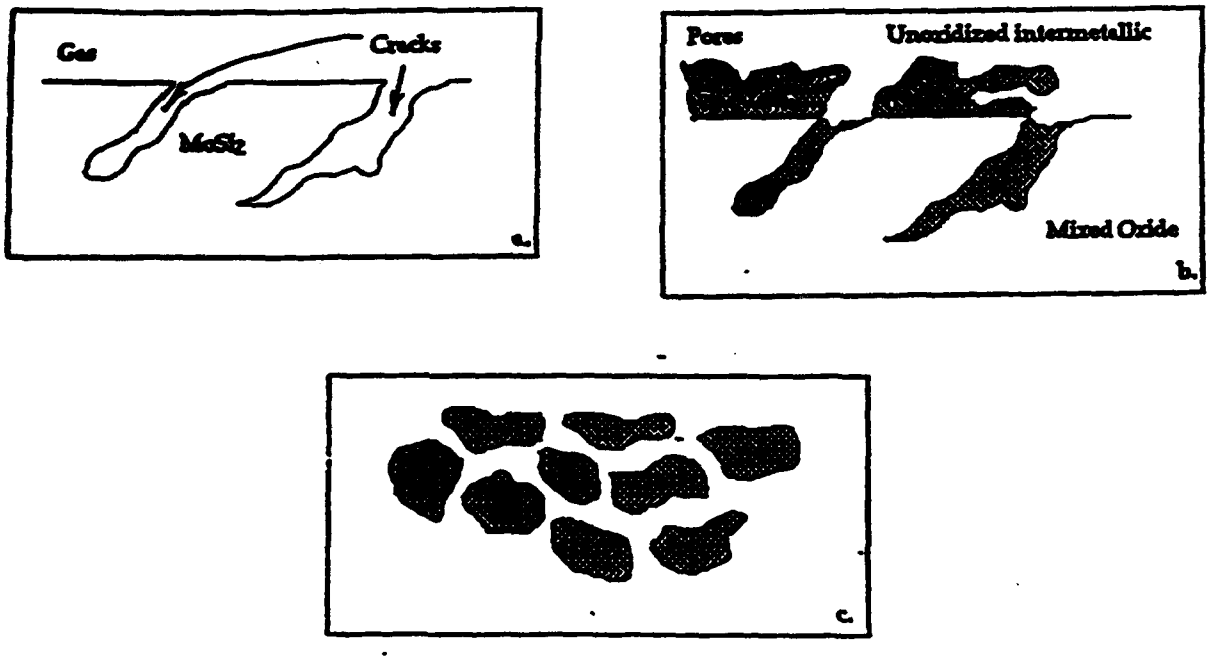

Figure IV.A.1.13 Schematic diagram sequence of oxidation at 500°C in air resulting in "pesting" of cast $MoSi_2$: a. As received, b. 43 hrs., c. 82 hrs.

IV.A.2 Coatings for Protection against High Temperature Corrosion

Principal Investigator:	**Professor G. H. Meier** **Materials Science and Engineering Department** **University of Pittsburgh**
Other Faculty Participants:	**Dr. N. Birks** **Dr. F. S. Pettit** **Materials Science and Engineering Department** **University of Pittsburgh**
Students:	**Dr. D. Rishel** **Mr. C. Stinner** **Mr. M. Stasik**

IV.A.2.1 INTRODUCTION

In the application of conventional materials, such as Ni-base superalloys and ferrous alloys it is often the case that the alloy compositions required for mechanical properties conflict with those required for oxidation and corrosion resistance. This situation is likely to be more severe in the case of the advanced materials, such as composites. The only current solution to this problem is the use of protective coatings. The following materials are among those which generally require coatings.

A. Superalloys in Gas Turbine Engines

Materials used in gas turbines may be subjected to a range of environmental conditions depending upon their location in the engine and the operating characteristics of the unit. Materials used for the high pressure turbine are exposed to high temperatures (600-1100°C) which can produce severe oxidation problems. Depending on the purity of the fuel and ingested air and temperature, deposits such as Na_2SO_4 and $NaVO_3$ can accumulate on hardware surfaces at metal temperatures in the range from 600 to about 1000°C. This can result in a rapid form of corrosion called "hot corrosion". The severe environments encountered in turbines generally require that the superalloy components be protected from corrosion by either diffusion or overlay coatings.

B. Ferrous Alloys

Ferrous alloys are used as structural materials for applications in a wide range of corrosive environments. These include applications where aqueous corrosion is of concern and where high-temperature oxidation is of concern. Often coatings are

required to provide corrosion resistance. Particularly important among these are galvanized and galvannealed coatings for aqueous corrosion resistance and diffusion chromized coatings for resistance to high-temperature oxidation. Despite the long use of these coatings there is still much unknown about the fundamentals of their formation mechanisms, adherence, and corrosion behavior.

C. Titanium Aluminides

The titanium aluminides, Ti_3Al and TiAl, have limited resistance to oxidation and react rapidly with dry hydrogen. They must be protected by surface coatings for extended service at elevated temperatures in hot structures and propulsion systems. However, the effort to develop these materials to date has concentrated on alloy design and manufacturing technology with little attention to the problem of coating for environmental protection under service conditions.

D. Carbon-Carbon Composites

Carbon-carbon composites are being considered for aerospace applications because of their light weight and excellent mechanical properties. Depending upon the application, carbon-carbon composites are expected to be used for periods ranging from about 10 hours to a few thousand hours at temperatures above 1000°C and approaching 2200°C. A major problem in using such materials in oxidizing environments is that carbon reacts with oxygen forming gaseous carbon oxides. A number of protective coatings are being considered to prevent oxygen from reacting with carbon. These coatings rely on the development of oxide films which provide protection by inhibiting oxygen diffusion. Typical coatings under consideration are chemical vapor deposited (CVD) silicon carbide and silicon nitride which form a silica film during oxidation that acts as a diffusion barrier. A problem arises in attempting to use coatings to protect carbon-carbon, since thermal expansion coefficient mismatch between the composite and the coatings causes the coating to crack.

The coating of Ti-aluminides and carbon-carbon composites is being addressed by existing projects in the MSE Department so the MRC effort is focussed on coatings for superalloys and ferrous alloys.

IV.A.2.2 OBJECTIVES

The objectives of this project during the second year include the following:

1. Characterization of the relationship between reactive element additions and sulfur content on the cyclic oxidation behavior of single crystal nickel-base superalloys and ferritic Fe-Cr-Al alloys.

2. Investigation of the formation mechanisms of Cr/Al diffusion coatings on Ni-

base superalloys.

3. Characterization of the effects of precious metals (Pt, Pd) on the formation of diffusion aluminide coatings on Ni-base superalloys and the oxidation behavior of these coatings.

IV.A.2.3 ACCOMPLISHMENTS AND SIGNIFICANCE:

A. Oxidation of Single Crystal Nickel-Base Superalloys and Ferritic Fe-Cr-Al Alloys

State-of-the-art superalloys and Fe-Cr-Al alloys rely on the formation of alumina scales for their oxidation protection thus alumina adherence is a critical factor. It is now well established that "reactive elements", such as Hf and Y substantially improve oxide scale adherence [1]. Over the last fifty years a number of mechanisms have been proposed for this effect [2-4]. These mechanisms extended from mechanical pegs to key the oxide to the alloy substrate to stress relief mechanisms for the oxide scale. More recently some investigators have proposed that alumina scales are intrinsically adherent and the reactive elements tie up detrimental elements, such as sulfur, and prevent them from diffusing to the alloy/oxide interface and degrading adherence [5, 6]. Hydrogen annealing has been shown to reduce the sulfur content of a single crystal superalloy PWA 1480 (to < 0.1 ppm) resulting in a dramatic increase in scale adherence [7]. Study in the first year of the MRC focussed on the relative effects of reactive element additions and sulfur removal on the adherence of alumina to single crystal substrates [8]. The results of this study showed sulfur removal improved the cyclic oxidation resistance of both 1480 and 1484. The improvement for 1484, which contains Hf, indicates that the sulfur removal somehow makes the Hf more effective. The magnitude of the effectiveness of the sulfur removal treatment was such that desulfurized 1480 and 1484 had oxidation resistances which were equal to or better than coated 1480.

The effects of sulfur on the adherence of alumina to FeCrAl alloys has not been extensively investigated. Sigler [9] vacuum annealed very thin (0.05 mm) foils at 1000°C for times up to 16 hours which lowered the sulfur content from about 200 ppm to the 10 ppm range. The annealing improved the cyclic oxidation resistance in relatively short time experiments (100 hrs.) at 900 and 1100°C and greatly decreased the amount of void formation at the alloy/oxide interface. Later experiments by Sigler [10] indicated the effectiveness of various reactive elements in promoting alumina adherence to FeCrAl could be correlated with the thermodynamic stability of the sulfides of the reactive elements. The more stable the sulfide the more effective was the element, particularly if the element did not form highly stable carbides and nitrides.

Work during the second year of the MRC has focussed on the effects of desulfurization and specimen thickness on the oxide adherence to FeCrAl alloys. It should be noted that, in principle, much thicker specimens of FeCrAl can be

desulfurized, relative to Ni-base alloys, because the diffusivity of sulfur in bcc iron [11] is approximately an order-of-magnitude greater than that in fcc nickel [12].

The alloys investigated were Fe-18Cr-6Al(wt %), Fe-18Cr-6Al-1Ti, Fe-18Cr-6Al-1Hf, and Fe-25Cr-5Al-0.1Y. The alloys were tungsten-arc melted and drop cast into a water-cooled copper chill. Most specimens had approximate dimensions 1cm X 1cm X 1mm, however, additional specimens of the undoped FeCrAl with thicknesses ranging from 0.3 to 1.5mm were annealed in Zr-gettered hydrogen for 100 hours at 1200°C to remove sulfur. This treatment lowered the sulfur contents of the alloys from initial values ranging between 12 and 25 ppm to 0.1 ppm for a 1.5 mm thick specimen and 0.05 ppm for a 0,3 mm thick specimen (Analyses by Shiva Technologies Inc.). Several "needle" specimens with dimensions 20 mm X 2 mm X 2mm were prepared to determine if length changes occurred during oxidation. One needle specimen of undoped FeCrAl was also hydrogen annealed. All specimens were polished through 600 grit SiC paper, washed in soapy water, and rinsed in ethanol prior to oxidation or hydrogen annealing. Hydrogen annealed specimens were oxidized with no further surface treatment. Cyclic oxidation was performed in air at 1100°C with one cycle consisting of 45 minutes in the hot zone and 15 minutes cooling above the furnace. The needle specimens were oxidized in an alumina crucible in air at 1200°C for successive 24 hour periods with the specimen length being measured after each period. The oxidized specimens were examined normal to the surface and in cross-section using optical and scanning electron metallography.

Figure IV.A.2.1 shows the effect of reactive element additions on the cyclic oxidation of FeCrAl in air at 1100°C. The undoped alloy shows an initial mass gain followed by a mass loss, resulting from spallation of a protective alumina film, followed by a large mass gain, resulting from the rapid growth of iron-containing oxides. All of the doped alloys exhibit small positive mass gains for the duration of the experiment. Indeed, previous work [13] has shown that the alumina on the doped alloys remains protective for several thousand hours under these exposure conditions. Figure 2 shows the effect of desulfurization of FeCrAl specimens of varying thicknesses. All of these specimens show small positive mass gains comparable to those for the doped alloys. The independence of oxidation behavior on specimen thickness is the result of the high sulfur diffusivity in FeCrAl. The thickness beyond which desulfurization would become less effective is still to be determined.

Figure IV.A.2.3 shows the effect of reactive element doping and desulfurization on the change in length of needle-shaped FeCrAl specimens during oxidation at 1200°C in air. The undoped specimen decreased in length as the result of oxidation and spalling from the specimen ends. The Ti-doped specimen increased in length indicating substantial stress generation. The Y-doped specimens exhibited negligible length changes. The result for the Y-doped alloy is consistent with the original proposal by Golightly et. al. [3] that Y alters the growth mechanism of the alumina such that lower growth stresses are generated. The

result for the desulfurized alloy comes from one specimen (whereas the results for the doped alloys have been confirmed for several specimens) but indicates length changes comparable to those for FeCrAlTi for the first 300 hours with negligible length changes during subsequent exposure. Spalling of the alumina was visually observed to begin at about the time when the length change ceased. If confirmed, this result would indicate that sulfur removal improves the adherence of the alumina but does not influence stress generation and that 2 mm has exceeded the thickness for which the 100 hr., 1200°C is completely effective. That is the sulfur content of this specimen, presumably greater than 0.1 ppm, is sufficient to degrade the adherence at longer times.

Examination of the oxide morphologies showed that the alumina film which develops on undoped FeCrAl was highly convoluted and spalled from the alloy over most of the surface. The alloy substrate exhibited large smooth areas where the oxide had lost contact at the oxidation temperature. The alumina spallation and the accompanying Al depletion from the alloy resulted in formation of thick Fe-rich oxides during cyclic oxidation. The alumina formed on the Ti-doped alloy during cyclic oxidation was adherent to the substrate but the oxide and alloy surface had undergone substantial deformation, which is consistent with the length changes in Figure 3. The alumina formed on the Y-doped alloy was smooth and planar, consistent with the absence of length changes in Figure IV.A.2.3. The oxide developed on the Hf-doped alloy after cyclic oxidation consisted primarily of alumina which had grown inward around internal oxide precipitates of HfO_2. This growth is responsible for the larger mass gains observed for the Hf-doped alloy in Figure 1, relative to that for Ti- or Y-doping. The alumina formed on the desulfurized alloys after cyclic oxidation was smooth and planar except at locations where a grain boundary had run through the specimen cross-section. Here the alloy appeared to have undergone grain boundary sliding to produce protrusions on opposite sides of the specimen.

The results of this study have shown that desulfurization of FeCrAl alloys by hydrogen annealing can result in improvements in cyclic oxidation comparable to that achieved by doping with reactive elements. Moreover, specimens of substantial thicknesses can be effectively desulfurized because of the high diffusivity of sulfur in bcc iron alloys. The results have also shown that there is less stress generation during the cyclic oxidation of Y-doped (and apparently desulfurized) FeCrAl compared to Ti-doped FeCrAl even though the alumina remained adherent to all the doped and desulfurized alloys. This indicates that the growth mechanism, as well as the strength of the oxide/alloy interface, must be considered in evaluating mechanisms for improved adherence.

B. Chrom-aluminizing of Nickel Base Alloys

1. Background

In halide-activated pack cementation, the pack consists of four components:

The object(s) to be coated, the master alloy (i.e., the element(s) to be deposited on the object), a halide salt activator (e.g., NaCl, NaF, NH_4Cl, etc.), and an inert filler (e.g., Al_2O_3). The object to be coated are immersed in a blend of master alloy, halide activator and inert filler powders. The retort containing the pack mixture, is heated to a high temperature in an inert or reducing gas. At the elevated temperature the master alloy reacts with the halide activator to form volatile metal halides. These metal halide vapors diffuse through the porous pack and react at the surface, of the object to be coated, to deposit the desire coating element.

The aluminizing and chromizing of materials via the pack-cementation process has been a commerically viable process for a number of years. The simulatenous codeposition of Al and Cr via the pack cementation process, using pure elemental powders, is however more difficult. The large difference in the thermodynamic stabilities of the Al and Cr chlorides makes it difficult to obtain comparable negative pressure gradients for the two elements to be deposited [14]. However, by employing binary chromium-aluminum (Cr-Al) master alloys, the high relative Al halide vapor pressures can be moderated. This is due to the fact that chromium-rich master alloys, exhibit highly negative deviations fromn ideality. The reduced thermodynamic activity of Al, results in generating lower vapor pressures for the otherwise favored halide species (e.g., AlCl, $AlCl_2$ etc.). Therefore comparable Al and Cr vapor pressures result. Thus provided a suitable activator and binary master alloy is chosen, the codeposition of Cr and Al into Ni base materials is possible.

Work during the first year of the MRC included:

a. The design and construction of a coating apparatus. This device permits the application of coatings on substrates at temperatures up to 1200°C in static or flowing inert (eg. Ar) gases.

b. Implementation and use of a computer program, (i.e., STANJAN), to facilitate determination of the relative vapor pressures of the various halide species within the pack atmosphere.

c. Experiments to ascertain the coating characteristics of several pack mixtures on pure Ni and two Ni-base superalloys, PWA 1480 and 1484. The results indicated that, consistent with the thermodynamic calculations, Al could be readily incorporated into the coatings but only very low Cr concentrations could be achieved.

Work during the second year of the MRC has focussed on the effects of the amount and composition of the source Cr-Al masteralloy on the composition of coatings formed on pure Ni and PWA 1480. It was found that decreasing the amount of masteralloy increased the amount of Cr, relative to Al in the coating. Typical results are presented in Figures IV.A.2.4 and IV.A.2.5 which are concentration profiles across coatings formed on pure nickel. Both coatings were formed at 1000°C in packs consisting of a 95%Cr-5%Al masteralloy, 2 wt% $CrCl_2$

activator, and an alumina filler. The only difference in the packs was the amount of masteralloy included. The coating formed with 25wt% of masteralloy, Fig. IV.A.2.4, contained more than 30% Al and less than 2% Cr. This result is consistent with previous results. However, when the amount of masteralloy was reduced to 10 wt%, Figure IV.A.2.5, the coating contained a large amount of Cr and almost no Al. These results are consistent with depletion of the Al from the source material resulting in a a change in the coating atmosphere being rich in Al-chlorides initially to rich in Cr-chlorides at longer times, as proposed by Geib and Rapp for coating of low-alloy steels [15]. Experiments are currently being performed with different exposure times to characterize this phenomenon. Similar results have been obtained on PWA 1480 but the interpretation is complicated by the presence of alloying elements, including Cr and Al, in the substrate.

C. Cyclic Oxidation Resistance of Precious Metal-Modified Aluminide Coatings on Nickel-Base Superalloys

Modern aluminide coatings on nickel-base superalloys are often modified with platinum to improve their oxidation resistance [16]. The presence of the Pt, which is electrodeposited prior to the aluminizing treatment, can increase the life of the coating by a factor of 3X. However, the mechanisms whereby the Pt exerts its effects are not clearly understood. Also, French investigators [17] have recently proposed that Pd additions can be as effective as Pt in improving the oxidation resistance of aluminide coatings. The present study focusses on determining the mechanisms for the effects of the precious metals and comparing the behavior of Pt and Pd additions.

The coatings studied were all applied to PWA 1480 substrates by Howmet Corporation. These consisted of:

i. A commercial Pt Aluminide.
ii. An Aluminide with one half the amount of Pt contained in the commercial coating.
iii. A Pd modified Aluminide.

The aluminizing treatment was the same for all three coatings so the only variation involved the precious metal addition. Also, a commercial aluminide coating which does not contain a precious metal, PWA 73, was studied for comparison.

The composition profiles of the as-received coatings are presented in Figure IV.A.2.6. The "typical Pt aluminide" coating is thicker and has a higher Al content than the other two coatings. The microstructure of this coating consisted of three distinct regions: an outer region containing two intermixed phases ($PtAl_2$ and Pt-rich β-NiAl), an intermediate region of single phase β-NiAl, and an interdiffusion zone adjacent to the substrate. The "reduced Pt aluminide" coating consisted of two regions: an outer region of single phase β-NiAl which contained Pt

and an interdiffusion zone. The Pd aluminide coating consisted of an outer region of β-NiAl which contained Pd and an interdiffusion zone.

The results of two separate cyclic oxidation experiments at 1100°C in air are presented in Figure IV.A.2.7. These results, which are quite reproducible, indicate that reducing the amount of Pt below that currently used in commercial coatings is detrimental and that the Pd-modified aluminide produces negligible improvement over an unmodified coating. Examination of the coatings after cyclic oxidation showed that the "typical Pt aluminide" coating still contained a substantial amount of β-NiAl whereas this phase had either dissappeared or become discontinuous in the other coatings. This is particular significant since the Pd aluminide and PWA 73 had been exposed for shorter times. Therefore, a major beneficial effect of the Pt is to cause more Al to be incorporated into the coating during aluminizing and to reduce the Al depletion during exposure which can occur both by oxidation and interdiffusion with the substrate. The Pd addition apparently does not produce this effect. The effect of interdiffusion was further evaluated by annealing the modified coatings at 1100°C in argon for times comparable to the oxidation exposures (450 hrs.). The argon essentially eliminated the oxidation component of the coating degradation. The "typical Pt aluminide" coating retained a zone of β which was approximately 120 μm thick whereas the β zones for the "reduced Pt" and Pd-modified aluminides were reduced to approximately 20 μm. These results indicate that Pt retards interdiffusion but also indicate that it must have some other effect since the "reduced Pt" coating showed similar interdiffusion behavior to the Pd-modified coating but clearly better cyclic oxidation resistance. This effect is still to be investigated.

IV.A.2.4 REFERENCES

1. J. L. Smialek and G. H. Meier, "High Temperature Oxidation", in Superalloys II, eds. C. T. Sims, N. S. Stoloff, and W. C. Hagel, John Wiley & Sons, 1987, Chap. 13.

2. J. K. Tien and F. S. Pettit, Met. Trans., 3, 1973, p. 1587.

3. F. A. Golightly, F. H. Stott, and G. C. Wood, Oxid. Met., 10, 1976, p. 163.

4. T. A. Ramanarayanan, R. Ayer, R. Petkovic, and D.P. Leta, Oxid. Met., 29, 1988, p. 445.

5. A. W. Funkenbusch, J. G. Smeggil, and N. S. Bornstein, Met. Trans., 16A, 1985, p. 1164.

6. J. G. Smeggil, A. W. Funkenbusch, and N. S. Bornstein, Met. Trans., 17A, 1986, p. 923.

7. B. K. Tubbs and J. K. Smialek, "Effect of Sulfur Removal on Scale Adhesion

to PWA 1480" Symposium on Corrosion and Particle Erosion at High Temperatures, eds. V. Srinivasan and K. Vedula, TMS, 1989, p.459.

8. R. V. McVay, P. Williams, G. H. Meier, F. S. Pettit, and J. L. Smialek, "Oxidation of Low Sulfur Single Crystal Nickel-Base Superalloys", Superalloys 1992, S. D. Antolovich, R. W. Stusrud, R. A. MacKay, D. L. Anton, T. Khan, R. D. Kissinger, and D. L. Klarstrom eds., p. 807, TMS (1992).

9. D. R. Sigler, Oxid. Met., 29, 23 (1988).

10. D. R. Sigler, Oxid. Met., 32, 337 (1989).

11. S. J. Wang and H. J. Grabke, Z. Metallk., 61, 597 (1970).

12. A. B. Vladimirov, V. N. Kaygordorov, S. M. Klotsman, and I. Sh. Trakhtenberg, Fiz. Metal. Metalloved., 39, 319 (1975).

13. G. H. Meier, Mater. Sci. and Eng., A120, 1 (1989).

14. S. C. Kung and R. A. Rapp, Oxid. Met., 32, 89 (1989).

15. F. D. Geib and R. A. Rapp, Oxid. Met., 40, 213 (1993).

16. R. Streiff and D. H. Boone, J. Mater. Eng., 10, 15 (1988).

17. S. Alperine, P. Steinmetz, P. Josso, and A. Constantani, Mater. Sci. and Eng., A121, 367 (1989).

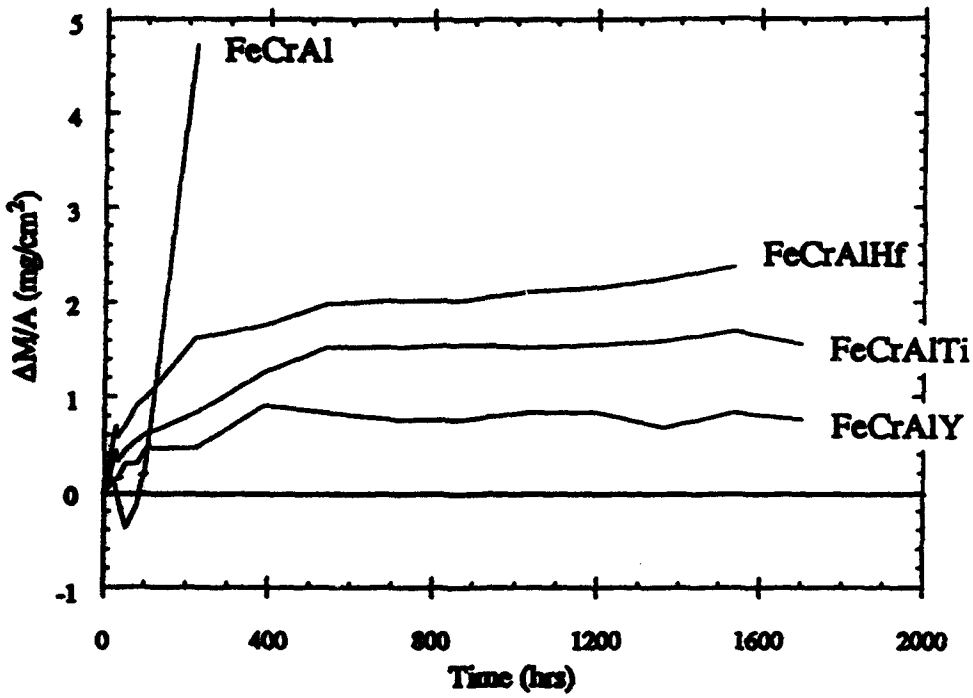

Figure IV.A.2.1 The effect of reactive elements on the cyclic oxidation of FeCrAl alloys at 1100°C in air.

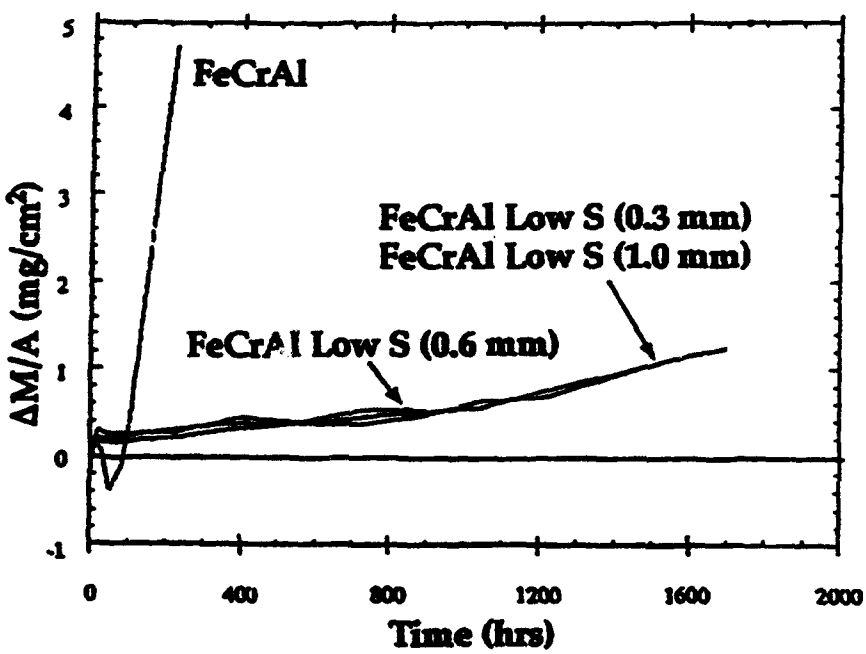

Figure IV.A.2.2 The effect of specimen thickness on the cyclic oxidation of desulfurized FeCrAl alloys in air at 1100°C.

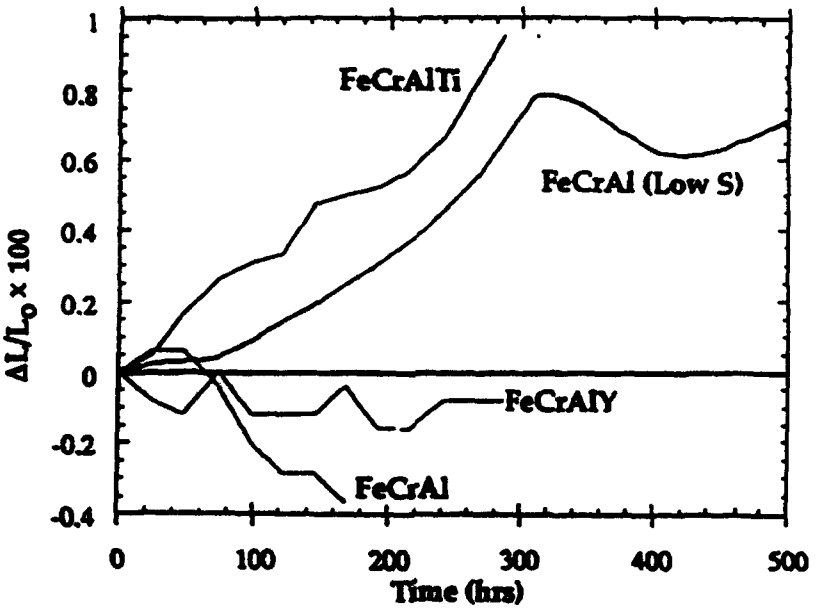

Figure IV.A.2.3 The effect of reactive elements and desulfurization on the change in length of needle-shaped specimens of FeCrAl during oxidation in air at 1200°C.

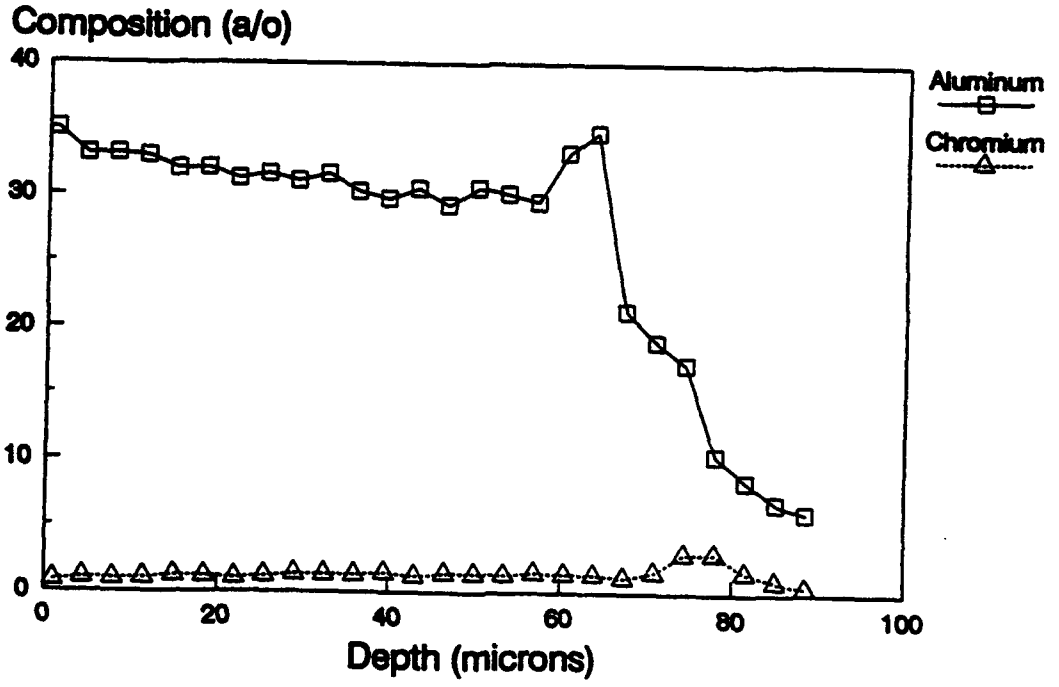

Figure IV.A.2.4 Concentration profiles for a chrom-aluminide coating formed after 20 hours on Ni at 1000°C in a pack consisting of 25 wt % of a 95Cr-5Al masteralloy and activated with $CrCl_2$.

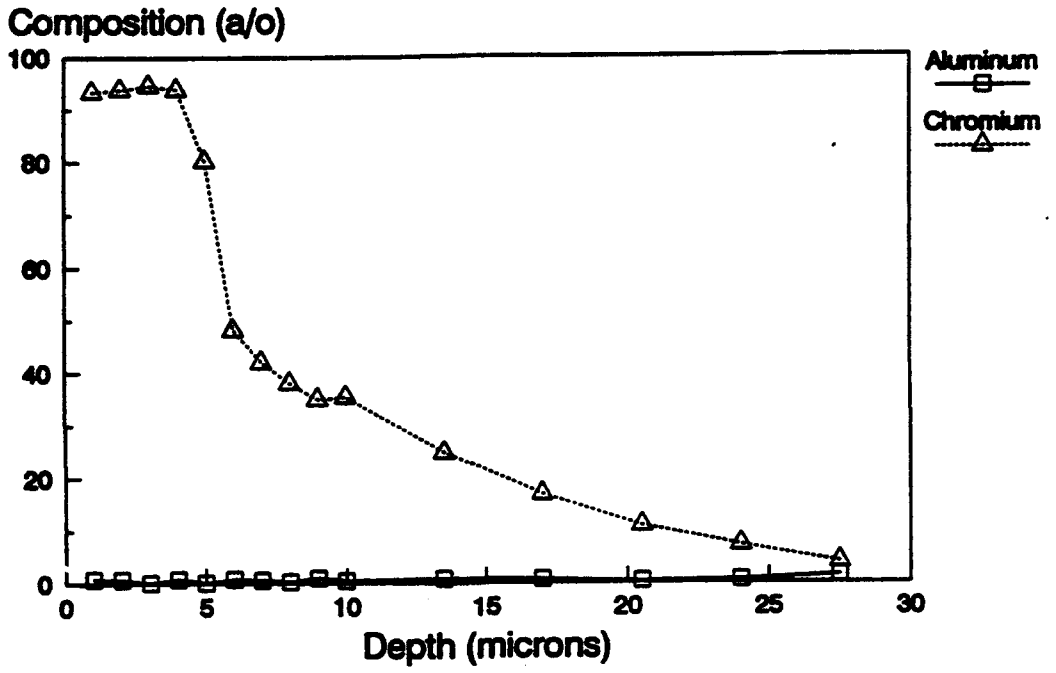

Figure IV.A.2.5 Concentration profiles for a chrom-aluminide coating formed after 20 hrs. on Ni at 1000°C in a pack consisting of 10 wt % of a 95 CR-5Al masteralloy and activated with $CrCl_2$.

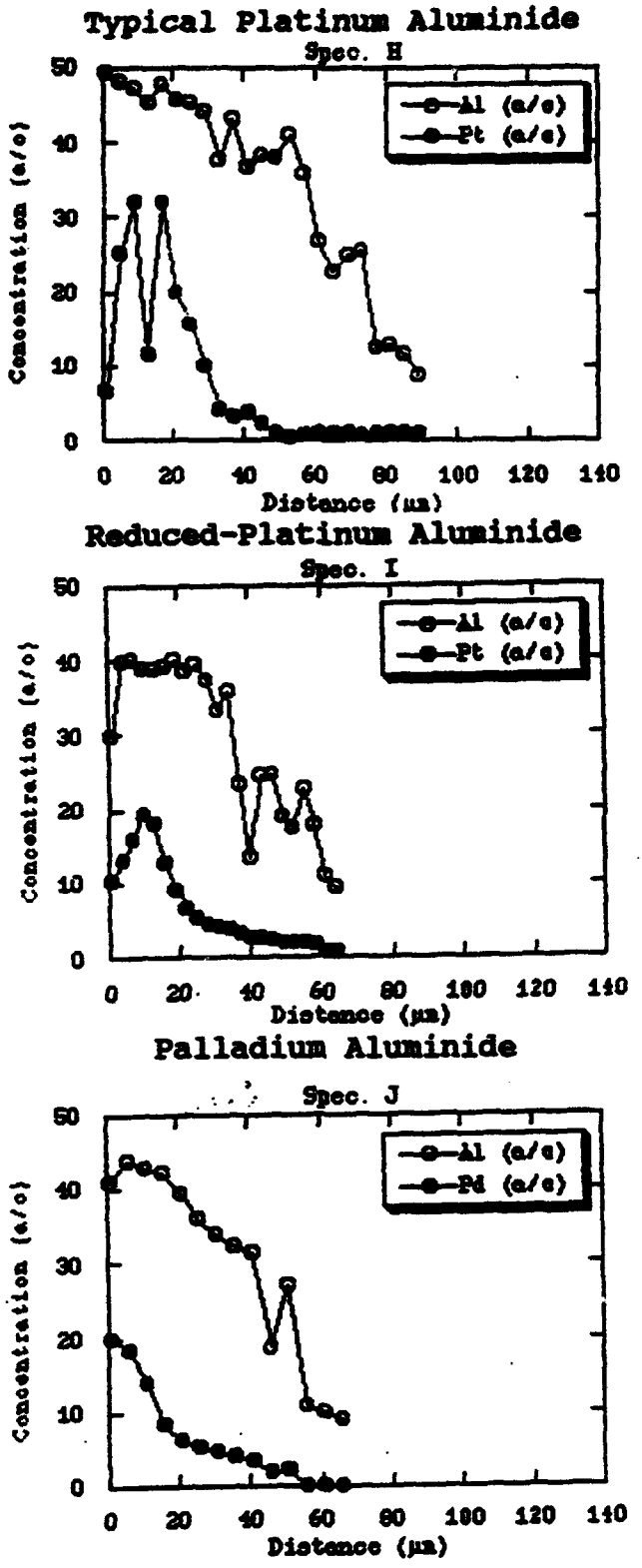

Figure IV.A.2.6 Concentration profiles across as-received Pt- and Pd-aluminide coatings on PWA 1480.

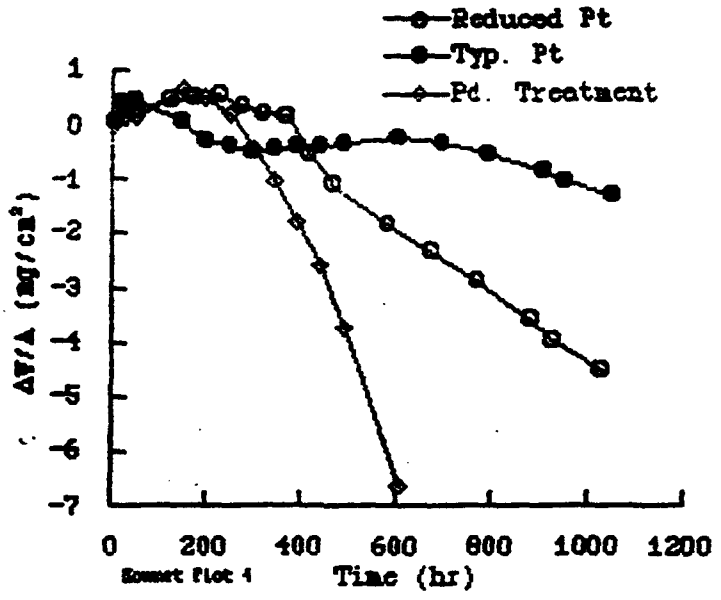

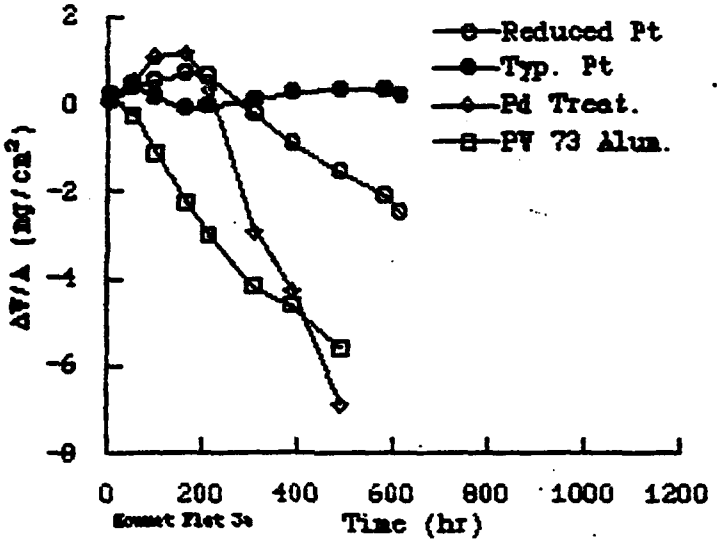

Figure IV.A.2.7 Result of two separate cyclic oxidation experiments at 1100°C in air to compare the relative effectiveness of Pt- and Pd-modification of aluminide coatings on PWA 1480.

IV.A.3 Metal and Ceramic-Matrix Composites

Principal Investigator:	**Professor F.S. Pettit** **Materials Science and Engineering Department** **University of Pittsburgh**
Other Faculty Participants:	**Dr. G.H. Meier** **Dr. N. Birks** **Materials Science and Engineering Department** **University of Pittsburgh**
Students:	**Mr. R. Cerchiara** **Mr. C. Sarioglu** **Mr. J.E. Spowart**

IV.A.3.1 INTRODUCTION

The possible development of composite materials using metal or ceramic matrixes containing fibers or whiskers of materials such as carbon, SiC, TiB_2 or Al_2O_3 may provide a variety of high performance materials. The mechanical properties of composite materials are very strongly influenced by the interaction between the matrix and the fiber. Consequently, it is of great concern to develop an understanding of the behavior of this interface. In addition to the fiber-matrix interactions, external environments can react with the matrixes as well as with fibers exposed to the external surface. Some reactants can dissolve into the matrix phase and affect mechanical properties or subsequently react with the fibers or whiskers.

The objectives of this research are to examine environmental effects at elevated temperatures on some relevant composite materials. Three composite systems have been studied, namely a titanium alloy matrix reinforced with continuous fibers of SiC, an aluminum alloy matrix reinforced with SiC whiskers, and a $MoSi_2$ matrix containing a variety of discontinuous phases (i.e. Al_2O_3, TiB_2, HfB_2, SiC).

IV.A.3.2 ACCOMPLISHMENTS AND SIGNIFICANCE

IV.A.3.2.1 Titanium Matrix Composite

As discussed in the first annual report for this program [1] the titanium matrix alloy that was investigated in this program had a composition of Ti-22Al-23Nb and the reinforcing phase was continuous SCS-6 SiC fibers. The matrix alloy consisted of three phases, namely, about 40% of an equiaxed α_2 (Ti_3Al) phase, and 60% of a two phase mixture consisting of continuous β_o phase, with lenticular orthorhombic

phase precipitates, (Ti_2AlNb). Both the β_o and orthorhombic phases were ordered. The objectives of the investigation were to compare the oxidation of neat panels (i.e. bonded panels of alloy with no fibers) to that of the composite, and to determine the effects of interstitials (i.e. oxygen, nitrogen, hydrogen) on the mechanical properties of the composite. Emphasis was placed upon different gaseous environments such as air, oxygen and these gases with water vapor. The temperature range was 500°C to 900°C. An objective was to determine at what temperatures this composite could be used in the uncoated condition.

Coupons of neat and composite panels have been exposed to air and oxygen (1atm.) at 500°C -900°C in a thermogravemetric apparatus. Kinetic data were obtained in the form of continuous weight change measurements. Surfaces and cross-sections of oxidized specimens were examined using optical microscopy, X-ray diffraction and scanning electron microscopy. Hardness measurements in the "interstitial affected zone" were performed at the Rockwell Science Center using a nanoindentation technique. The kinetic data to compare the oxidation of neat and composite specimens in air are presented in Figures IV.A.3.1. and IV.A.3.2. The oxidation kinetics for the neat panels obeyed a parabolic rate law for temperatures less than 700°C. There was a transition to a more rapid linear rate after an initial period of parabolic behavior at temperatures above 700°C, Figure IV.A.3.1. The kinetic data for oxidation of the composites in air obeyed a linear rate for temperatures between 700° and 900°C. Initial weight losses were evident because the oxidation of carbon predominated, Figure IV.A.3.2. Oxidation in pure oxygen did not differ substantially from that for air. The rates were slightly larger than air, perhaps due to the higher oxygen pressure. A significant difference between air and oxygen was not evident at 500°C.

The compositions of the scales that were formed did not vary with the gas composition. Above 700°C a thick scale composed of TiO_2, Al_2O_3 and Nb_2O_5 was evident, Figure IV.A.3.3. Below 700°C discrete Nb_2O_5 was not evident but Nb doped TiO_2 and Al_2O_3 were present along with an inner Ti/Nb nitride. The rates of oxidation were such that this composite could not be used uncoated at temperatures above 600°C.

Beneath the oxide scale an interstitial harden zone was evident as detected by hardness measurements, Figure IV.A.3.4. This interstitial affected zone consisted of an outer zone characterized by depletion of alloying elements and morphological changes in the β and orthorhombic phases, Figure IV.A.3.5. In the inner and outer zones a submicron size precipitate had been found at the interphase boundaries. This precipitate has not been identified as yet. Also it has not been conclusively determined if the hardened zone is caused by oxygen or nitrogen. Since nitrides have been observed above this zone separating it from the oxide scale, the observed hardening must be caused by oxygen.

The effects of water vapor have not been studied as yet, nor have the effects of the interstitial zone on ductility. The results that have been obtained indicate

embrittling effects at temperatures as low as 500°C may be significant.

IV.A.3.2.2 Aluminum Matrix Composites

The aluminum matrix composite consisted of an aluminum solid solution containing intermetallic phases (Al_6Fe, metastable; $Al_{13}Fe_4$ and $Al_{13}F_3Ce$, stable) as well as SiC particles. The oxidation of this composite in air was examined at temperatures of 350°C and 500°C. No significant oxidation in air was detected. The aqueous corrosion of this composite was examined in deaerated 0.1 M NaCl solution at 25°C. The pitting potential of this composite was observed to be more negative than that of the matrix with no SiC, Figures IV.A.3.6 and IV.A.3.7. Pitting corrosion was evident in the matrix near SiC particles, Figure IV.A.3.8. The corrosion also spread over the alloy between SiC particles, Figure IV.A.3.9. Pitting was also evident in the matrix alloy at sulfur rich impurities which may have been introduced into the alloy during processing of the composite.

The pitting corrosion susceptibility of the aluminum matrix composite appears to be poorer than this alloy without SiC. This may occur by the SiC acting as cathodic sites or providing crevices between the SiC and the alloy where corrosion occurs due to compositional changes in the aqueous solution.

The aqueous corrosion of the aluminum matrix composite requires more studies to develop a model to account for the attack. Studies are also planned to investigate the effects of water vapor and NaCl on the oxidation of this alloy.

IV.A.3.2.3 $MoSi_2$ Matrix Composites

The oxidation of $MoSi_2$ matrix composites containing SiC, TiB_2, HfB_2 and Al_2O_3 as the reinforcing phase have been investigated in air at temperatures between 500° and 1200°C. Typical oxidation kinetics for these materials at 500°C are presented in Figure IV.A.3.10. The $MoSi_2$ exhibited accelerated oxidation at 500°C since a continuous SiO_2 layer was not developed as discussed in Section IV.A.1.2.B. At 500°C the reinforcing phases did not exert a substantial effect on the oxidation behavior of the composites.

At temperatures above 600°C protective SiO_2 scales were formed on the $MoSi_2$ in all of these composites. As the oxidation temperatures were increased to about 1200°C the effect of the reinforcing phase began to become evident. The boride phases (e.g. TiB_2, HfB_2) caused the most deleterious effects, Figure IV.A.3.11 probably because of rapid transport through TiO_2 and HfO_2. B_2O_3 may also affect the protectiveness of SiO_2. The composites with Al_2O_3 and SiC did oxidize at rates greater than the matrix phase with no reinforcing phase. More research is required to account for these observations.

IV.A.3.3 SUMMARY

Environmental effects on some relevant composites have been investigated. A variety of significant effects have been documented. In the case of titanium alloy matrixes interstitial elements, especially oxygen, have been shown to influence mechanical properties of the matrix phase. An aluminum alloy matrix composite has been shown to be susceptible to aqueous corrosion attack in the matrix phase adjacent to the SiC reinforcing phase. Finally, reinforcing phases in $MoSi_2$ matrix composites have been shown to affect the oxidation of such composites when the oxides of the reinforcing phase elements are formed in relatively large quantities.

Numerous advanced composites are being considered for use in advanced machines and equipment. The results that have been obtained in this project show that environmental effects must be considered in the application of such composites.

IV.A.3.4 REFERENCE

1. S.A. Asher, F.S. Pettit, and G. Mayer "First Annual Progress Report", Materials Research Center, University of Pittsburgh, AFOSR Grant-91-0441, November 23, 1992, p. 51.

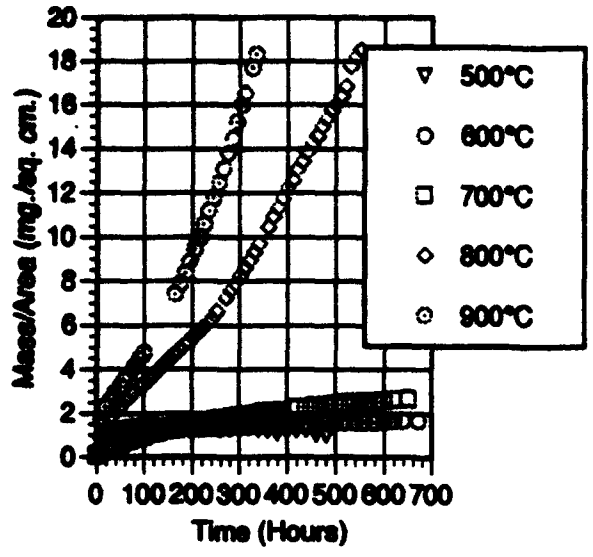

Figure IV.A.3.1. Oxidation kinetics in air for Ti-22Al-23Nb neat panels, 500 - 900°C.

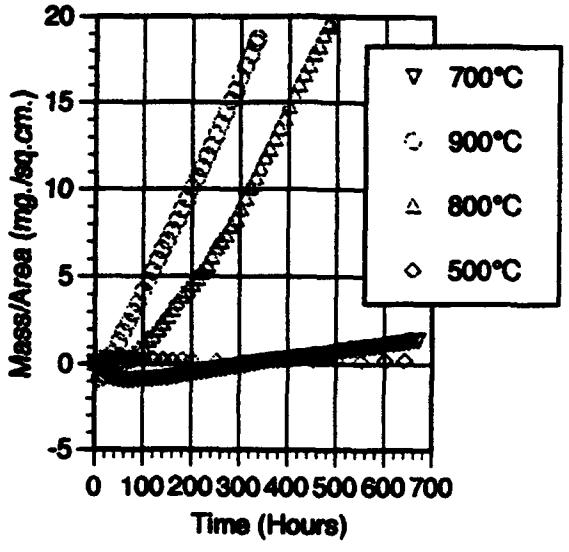

Figure IV.A.3.2. Oxidation kinetics in air for SCS-6/Ti-22Al-23Nb, 500 - 900°C.

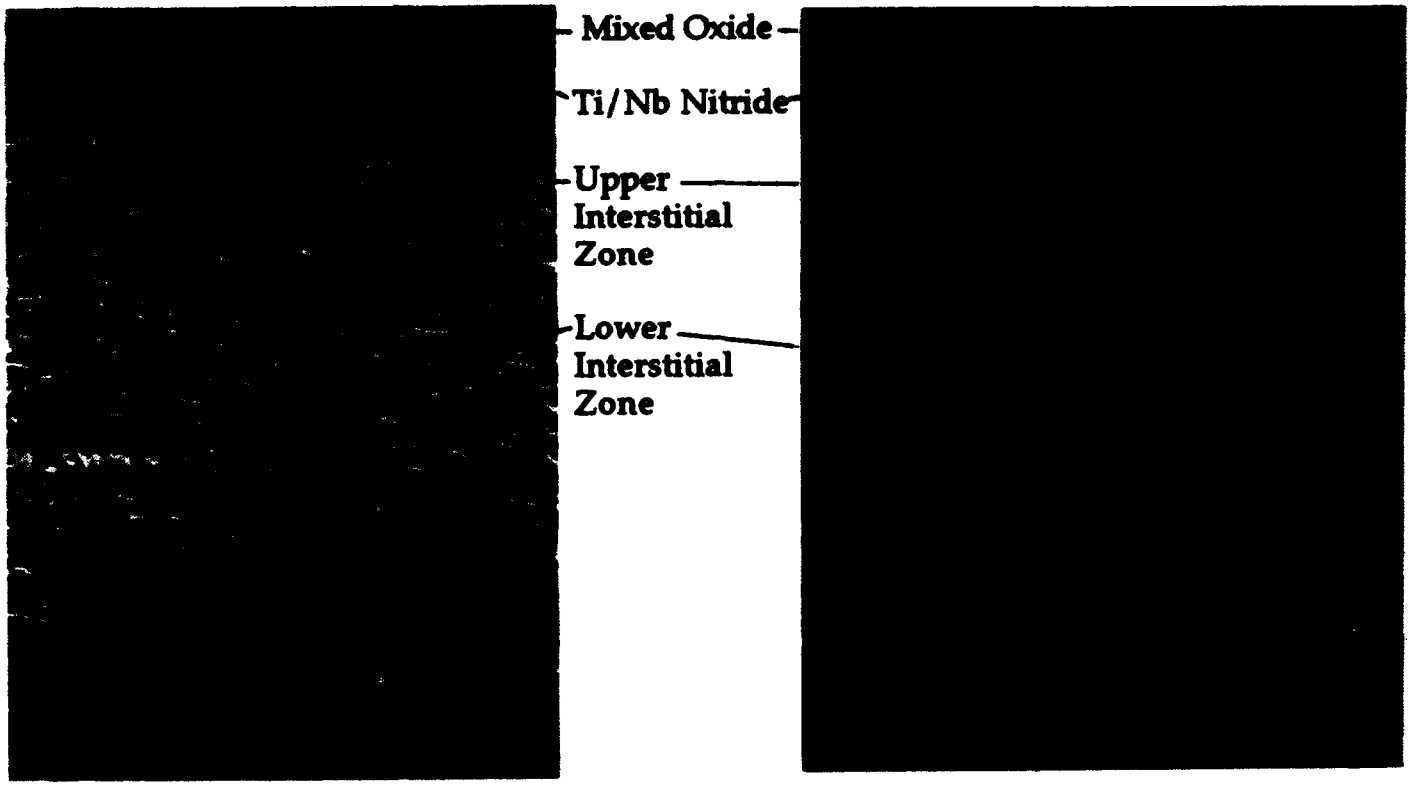

Figure IV.A.3.3. SEM(left) and optical micrograph (right) of Ti-22Al-23Nb neat panel oxidized in air at 800°C for 482 hrs. Ti/Nb nitride and two interstitial affected zones (~75μm total extent) are evident below a mixed oxide scale (~100μm in extent).

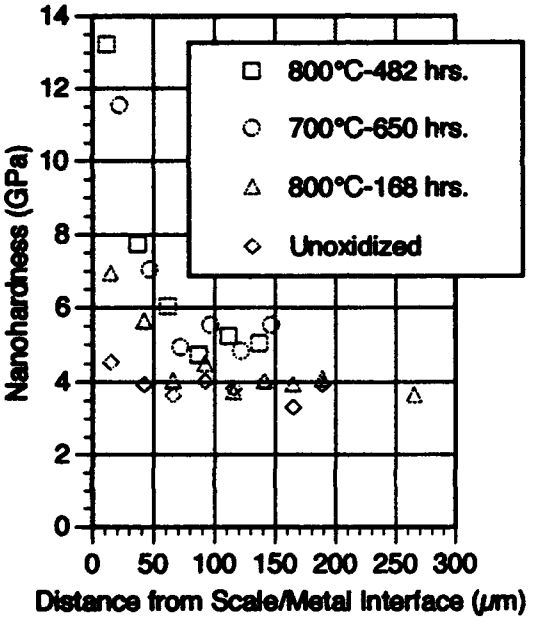

Figure IV.A.3.4. Hardness vs distance from metal/scale interface for Ti-22Al-23Nb neat panels oxidized in air at 700 and 800°C.

Figure IV.A.3.5. SCS-6/Ti-22Al-23Nb oxidizedin air at 700°C for 670 hrs. Morphological changes in the interstitial zone adjacent to theTi/Nb nitride. Submicron sized precipitate is indicated by arrow.

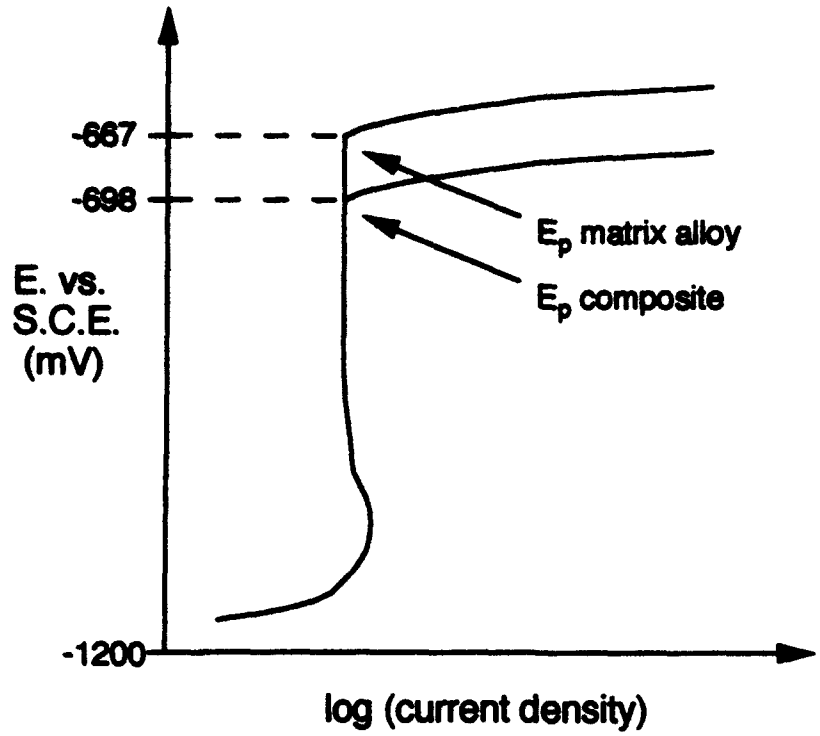

Figure IV.A.3.6 Schematic pitting curves for composite and matrix alloy in deaerated 0.1M NaCl solution under potentiostatic control.

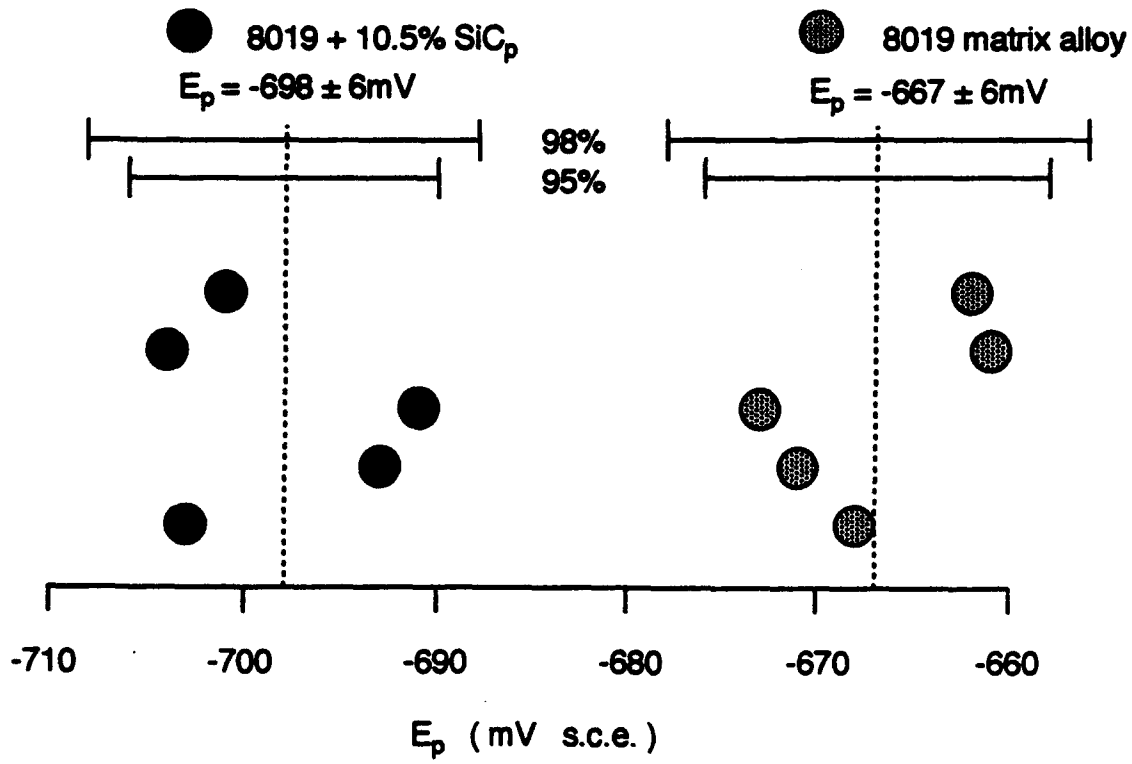

Figure IV.A.3.7 Comparison of pitting potentials for composite and matrix alloy.

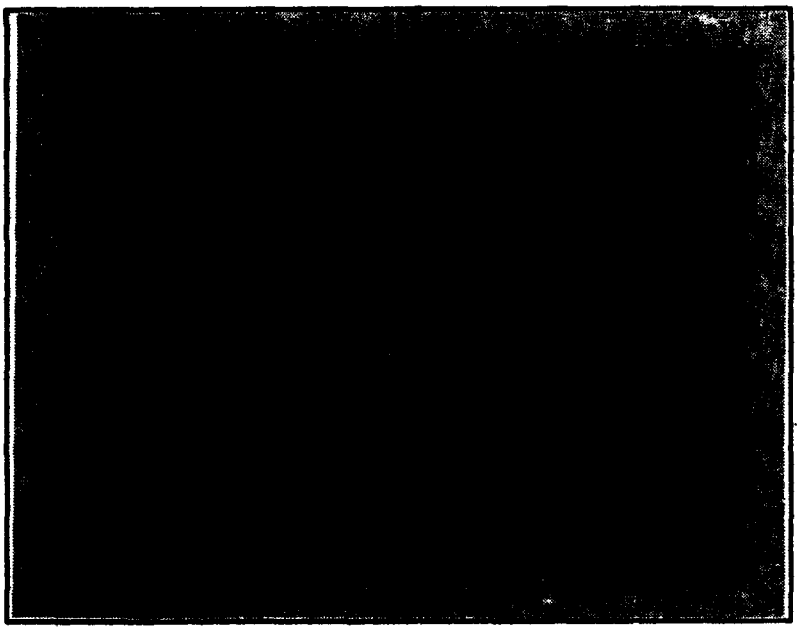

FigureIV.A.3.8. SEM micrograph of preferential attack around SiC particle reinforcement. Composite surface exposed to aerated 0.1M NaCl.

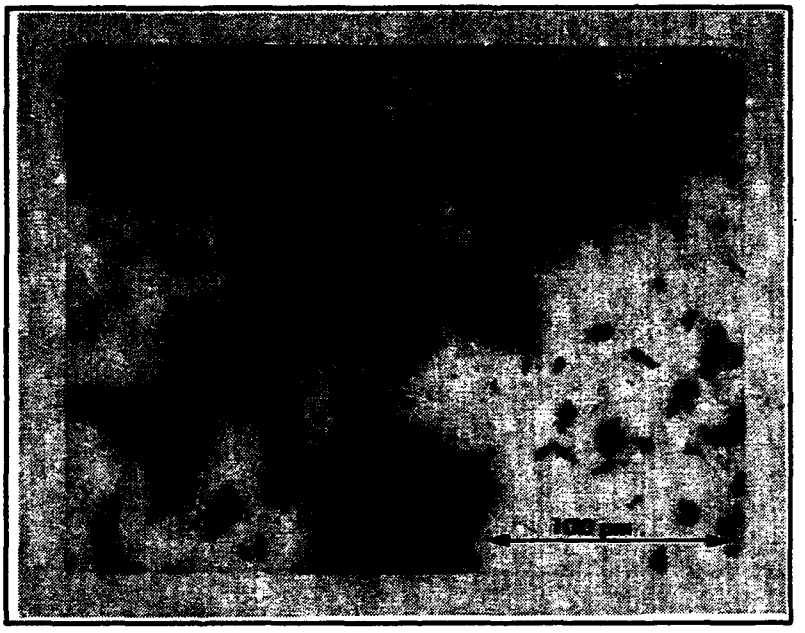

Figure IV.A.3.9. Optical micrograph of composite surface exposed to 0.1M NaCl for 18 hours total.

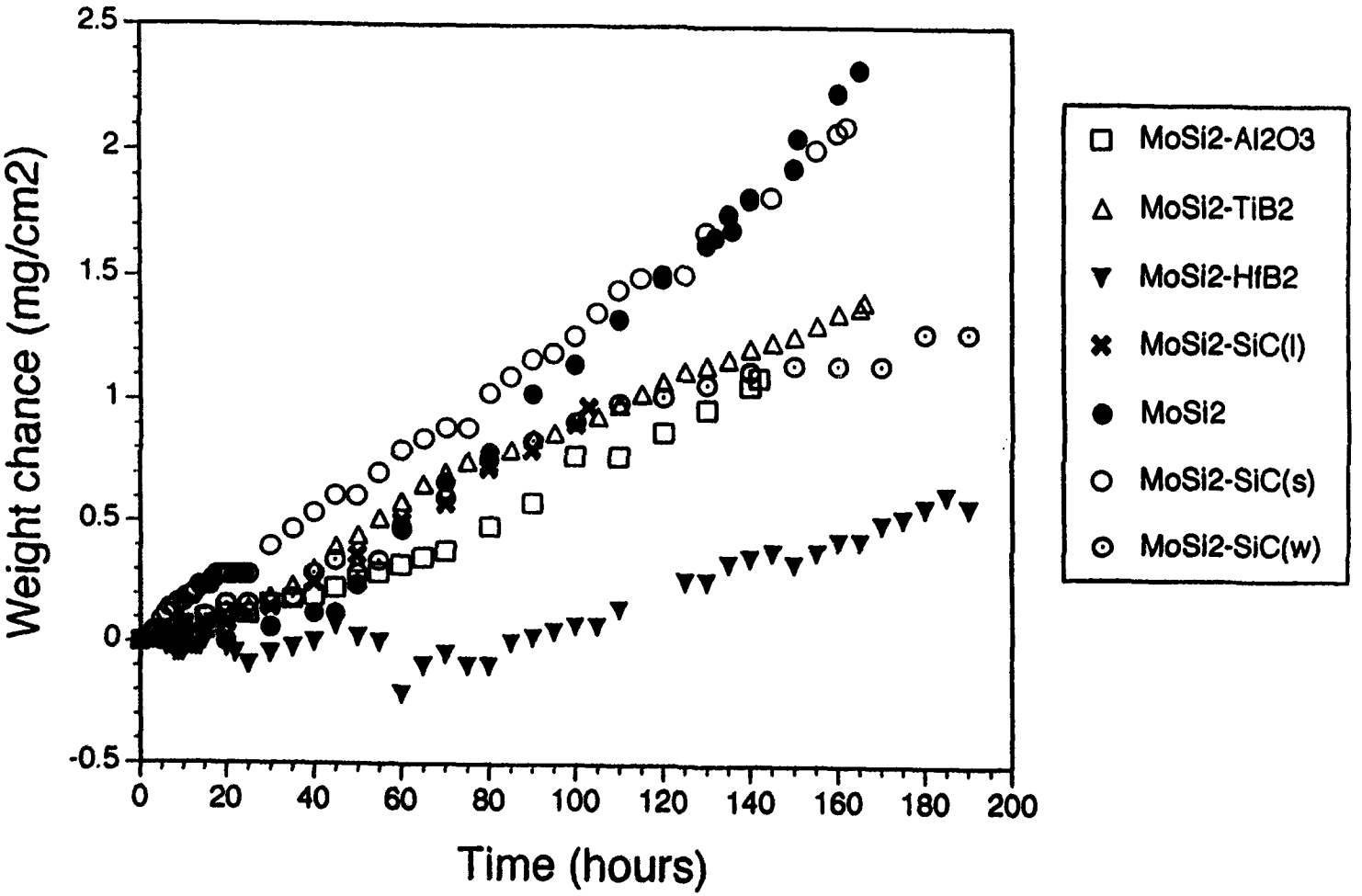

Figure IV.A.3.10. Weight change as a function of time for $MoSi_2$ and $MoSi_2$ - based composites at 500°C in air.

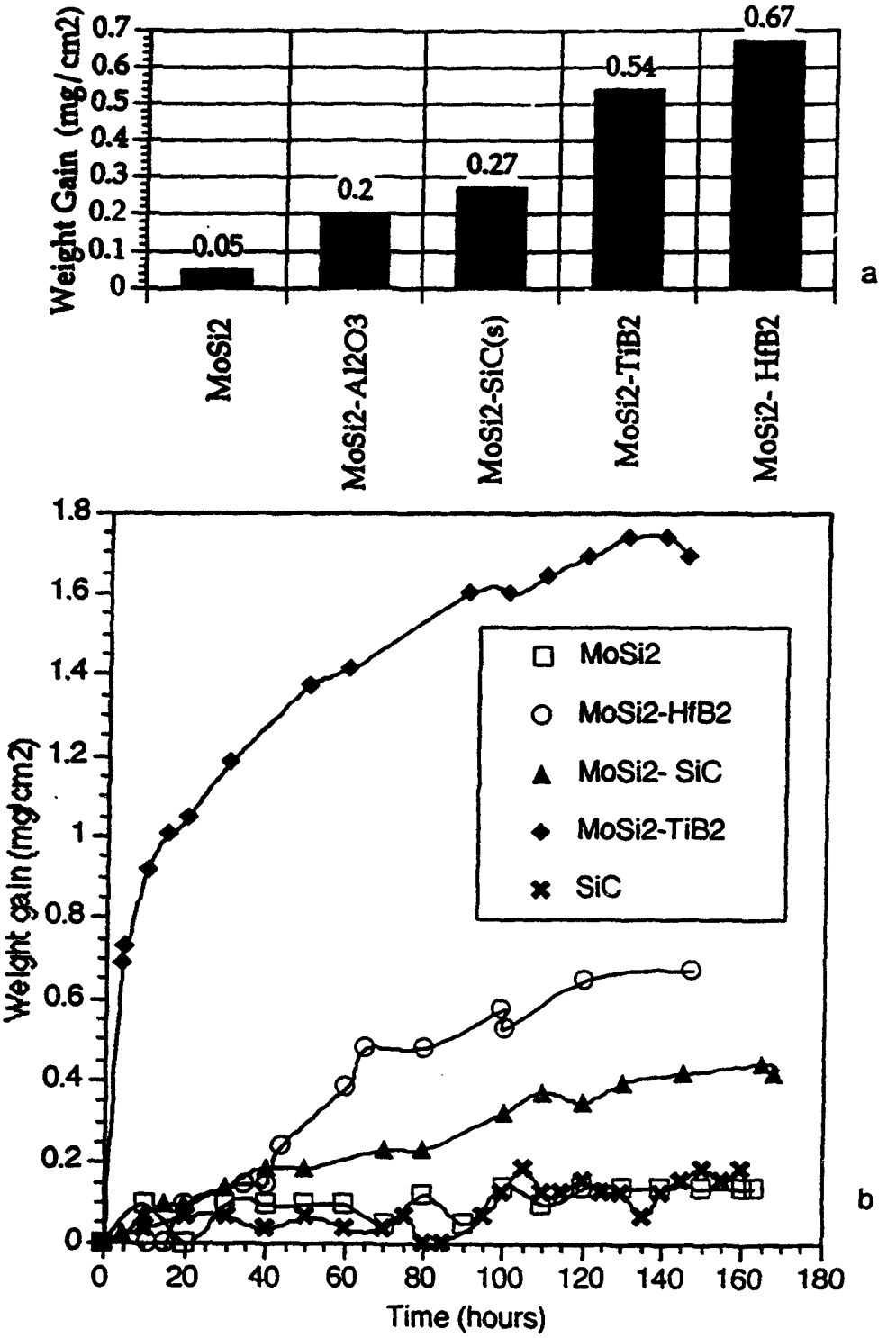

Figure IV.A.3.11. Weight gain as a function of time: a. weight gain after 1 week at 950°C in air, b. weight gain at 1200°C in air.

IV.A.4 Diamond Films for Use at Elevated Temperatures

Principal Investigator:	Professor F.S. Pettit Materials Science and Engineering Department University of Pittsburgh
Other Faculty	Dr. G.H. Meier Dr. N. Birks Materials Science and Engineering Department University of Pittsburgh
	Dr. S.A. Asher Dr. J.T. Yates, Jr. Department of Chemistry University of Pittsburgh
Students:	Mr. R. Lizewski Mr. R. Bormett

IV.A.4.1 INTRODUCTION

Diamond coatings possess numerous very useful properties such as high thermal conductivity, high hardness, wear resistance and chemical inertness. In some applications diamond films may be used at elevated temperatures in oxidizing environments and it is necessary to determine the effects of various environments and elevated temperature exposures on the properties of diamond films. In order to understand the surface chemistry of diamond at the fundamental structural level, it is necessary to study not only diamond films but also single crystal surfaces where periodic surface structure exists and where some understanding of both the surface reconstruction and the surface electronic behavior has been obtained. The goal of the investigation on diamond films and diamond crystals is to combine engineering studies of the behavior of polycrystalline diamond films with atomic level investigations of surface chemistry on single crystal diamond surfaces in reactive environments to determine how diamond performs at elevated temperatures in practical environments. The specific objectives of this research are as follows:

A. <u>Diamond Film Studies</u>

- Investigate the behavior of diamond films at temperatures between 200°C and 700°C in oxygen or water vapor + oxygen environments.
- Describe how and why any reactions occur.

B. Diamond Single Crystal Studies

- Study oxygen, atomic hydrogen, and atomic fluorine surface chemistry on diamond (100) and diamond (111) using STM for structural and electronic measurements.

- Compare STM measurements with vibrational spectra of modified diamond surfaces, to correlate local chemical structure with long range structure of single crystals surface.

- Study etching of diamond surfaces by H and F.

The approach to be used in the investigations on diamond films consists of:

- Fabrication of diamond films on molybdenum substrates.

- Characterization of free standing diamond films using SEM and Raman spectroscopy.

- Examination of the oxidation behavior of these diamond films by making weight change versus time measurements and by performing detailed characterization of these exposed films.

In the case of the studies with the diamond single crystals the approach involves:

- Use of a high pressure reactor to modify diamond surfaces with the adsorbates of interest.

- Transfer of the crystals to the UHV STM for studies of the surfaces.

- Determine the thermal behavior of the modified diamond in the STM.

- Study the modified and clean diamond surface with low energy electron diffraction.

- Correlate the STM studies with the spectroscopic studies of surface species.

IV.A.4.2 ACCOMPLISHMENTS AND SIGNIFICANCE OF DIAMOND FILM STUDIES

The work performed on diamond single crystals will be presented in Section IV.A.5. The present section will discuss results obtained with diamond films. In the first annual report for this program the diamond films which were

results from oxidation testing were presented. As documented in this report the as processed diamond films consisted of columnar grains that extended through the thickness of the film as is evident in Figure IV.A.4.1. The diameters of these grains were smaller on the substrate side, Figure IV.A.4.2a, compared to the growth side, Figure IV.A.4.3a. As mentioned in the first annual report the oxidation of these films in oxygen resulted in linear weight loss kinetics. Oxidation has now been performed over a range of temperatures and results are presented in Figure IV.A.4.4. Oxidation at temperatures of 400°C and lower was negligible. The oxidation kinetics obeyed an Arrhenius relationship, Figure IV.A.4.5, with an activation energy of 270 KJ/mole. These results indicate that the oxidation process is controlled by adsorption-dissociation reactions.

The use of Raman spectroscopy with ultra violet excitation has been shown to be very effective to differentiate between diamond and non-diamond species in the films. No polymorphs of carbon, other than diamond, were evident using Raman spectroscopy and visible radiation except in the vicinity of regions cut by the YAG laser used in preparing specimens; Figure IV.A.4.6a. When using ultra violet radiation, however, the as processed films were found to contain a small amount of non-diamond carbon, Figure IV.A.4.6b. The amount of non-diamond carbon in as processed diamond was found to depend on the fabrication method. For example more non-diamond carbon was detected in films prepared by microwave compared to DC arc.

Oxidation foils were studied as a function of exposure time to observe the initial stages of oxidation. The growth side of a diamond film is presented in Figure IV.A.4.3a and b after 5 minutes at 700°C and 60 hrs. of exposure at 600°C, respectively. The oxidation occurred preferentially at selective sites on crystal facets that appeared to be {111} crystal faces. Other investigators [1,2] have observed preferential oxidation of {111} surfaces of diamond compared to {100} surfaces. Moreover, the attack on the {111} surfaces consisted of localized pits which were attributed to defect sites created by dislocations [1]. After long periods of oxidation the attack was more general, Figure IV.A.4.3b, in that crystal facets were no longer evident but the oxidized surfaces were still uneven which suggested some preferential attack.

Since the individual grains of the diamond films were better defined on the substrate side, Figure IV.A.4.2.a, this surface was examined as a function time at 700°C. Scanning micrographs of substrate side surfaces after five and seven minutes of exposure are presented in Figures IV.A.4.2.b and c, respectively. The initial attack occurred at discrete boundaries in the grains. There is also attack at the edges of grains. This attack becomes more pronounced after seven minutes, where on some grains, boundaries are evident which extend completely across the grain. Close inspection of such surfaces has shown that oxidation occurred preferentially at two types of sites. The first type occurred at boundaries in the

crystal where oxidation divided the crystal into triangular shaped sections. The second type involved oxidation at points on the crystal surface which occurred first at edges of crystals but then extended to other planar portions of the grain surface.

Diamond films were also examined after short periods of oxidation by using UV Raman spectroscopy. Figure IV.A.4.6.b presents spectra after oxidation for 0, 2, 4 and 8 minutes in oxygen at 700°C. The data presented in this Figure show that the initial films contained a small amount of non-diamond carbon. The spectra were all normalized to have the same integrated area for the first order diamond phonon band. Figure IV.A.4.6.b shows the preferential oxidation of non-diamond carbon which exists in at least two phases. One phase has a Raman band only near 1570 cm^{-1} while a second non-diamond carbon phase has bands near 1570cm^{-1} and 3000 cm^{-1}. These two phases can be distinguished since the relative intensity of the 3000 cm^{-1} and 1570cm^{-1} bands decrease dramatically after only 2 minutes of oxidation. Figure IV.A.4.6.c also clearly demonstrates that the oxidized first order phonon band is narrower than that prior to oxidation. This presumably indicates preferential oxidation of defective diamond sites or stress relief of the sample. This apparently preferential oxidation of the non-diamond carbon may be correlated with the observed preferential oxidation at localized points and boundaries. The Raman spectroscopy results are also not indicative of diamond transforming to some other polymorph (e.g. graphite) which is then oxidized. These results are consistent with an oxidation reaction involving the gas reactive with diamond.

IV.A.4.3 SUMMARY

The results obtained for the oxidation of diamond films in one atmosphere of oxygen show that such films oxidize at substantial rates at temperatures above 500°C. The rate controlling process is proposed to be adsorption and dissociation of molecular oxygen. This process has been found to be influenced by the structure of the films and preferential reaction has been observed at what is believed to be twin boundaries [3]. Preferential attack has also been observed at points on {111} planes of these films. The cause for such attack may occur due to the preferential oxidation of non-diamond carbon at structural defects in the diamond film.

The oxidation rates of the diamond films are close to the rates for graphite, and observed differences may be due to the fact that the oxidation of both of these materials is affected by crystal orientation and defects in crystals. The rates of oxidation of these diamond films, therefore, may be significantly different in other gases such as water vapor or atomic oxygen.

IV.A.4.4 REFERENCES

1. W. Zhu, X.H. Wand, D. Pickrill, A.R. Badzian and R. Messier, in "New Diamond Science and Technology", MRS, p. 821, (1991).

2. Q. Sun and M. Alam, J. Electrochem. Soc., 139, 933 (1992).

3. Ch. Weld, N. Herres and P. Koidl, J. Appl. Phys. 68, 973 (1990).

Oxidation of Cross Section

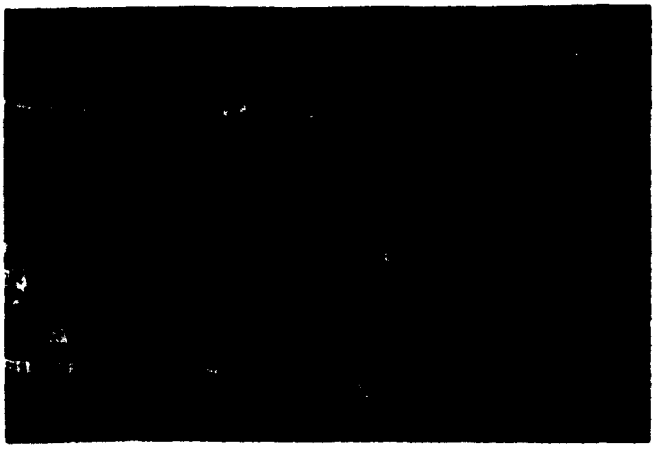

Figure IV.A.4.1 Cross-section of diamond film after 16 min. of oxidation at 700°C in oxygen. The oxidation has been preferential at boundaries revealing the columnar nature of the grains.

Oxidation of Substrate Side

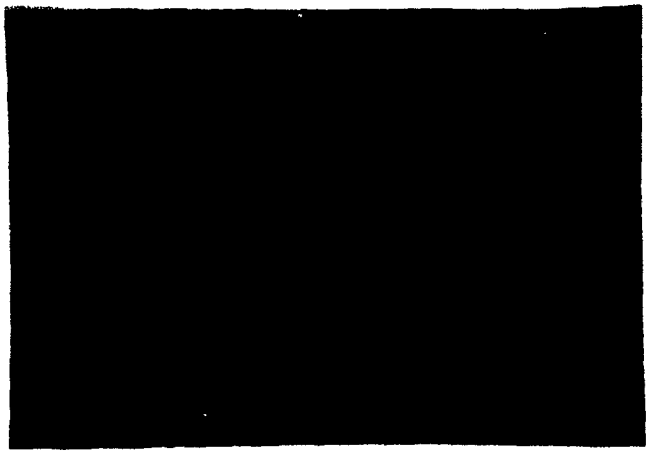

a. before oxidation

b. after 5 min. exposure at 700 C

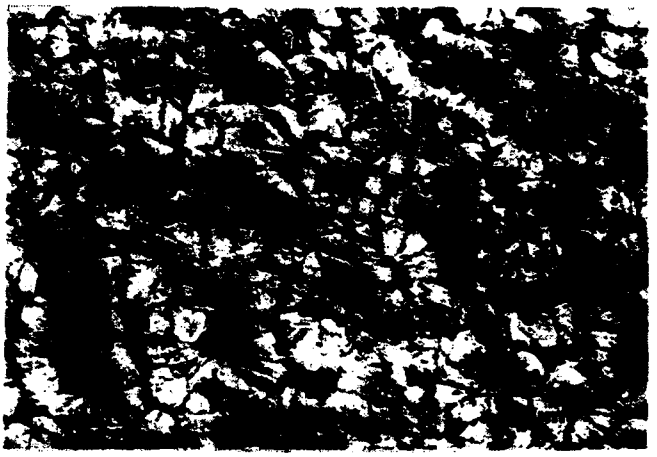

c. after 7 min. exposure at 700 C

Figure IV.A.4.2 Scanning micrographs showing the surface of diamond films at the substrate interface before oxidation and after 5 and 7 minutes of oxidation at 700°C in oxygen. The oxidation can be seen to take place preferentially at boundaries in these films.

a. in O_2 at 700 C for 5min.

b. in O_2 at 600 C for 60 hrs.

Figure IV.A.4.3 Scanning micrographs of diamond films at the growth interface after 5 minutes of oxidation at 700°C and after 60 hours of oxidation at 600°C in oxygen. After short oxidation exposures it is evident that the attack occurs at localized sites. Even after 60 hours of oxidation the oxidation does not produce a uniform surface.

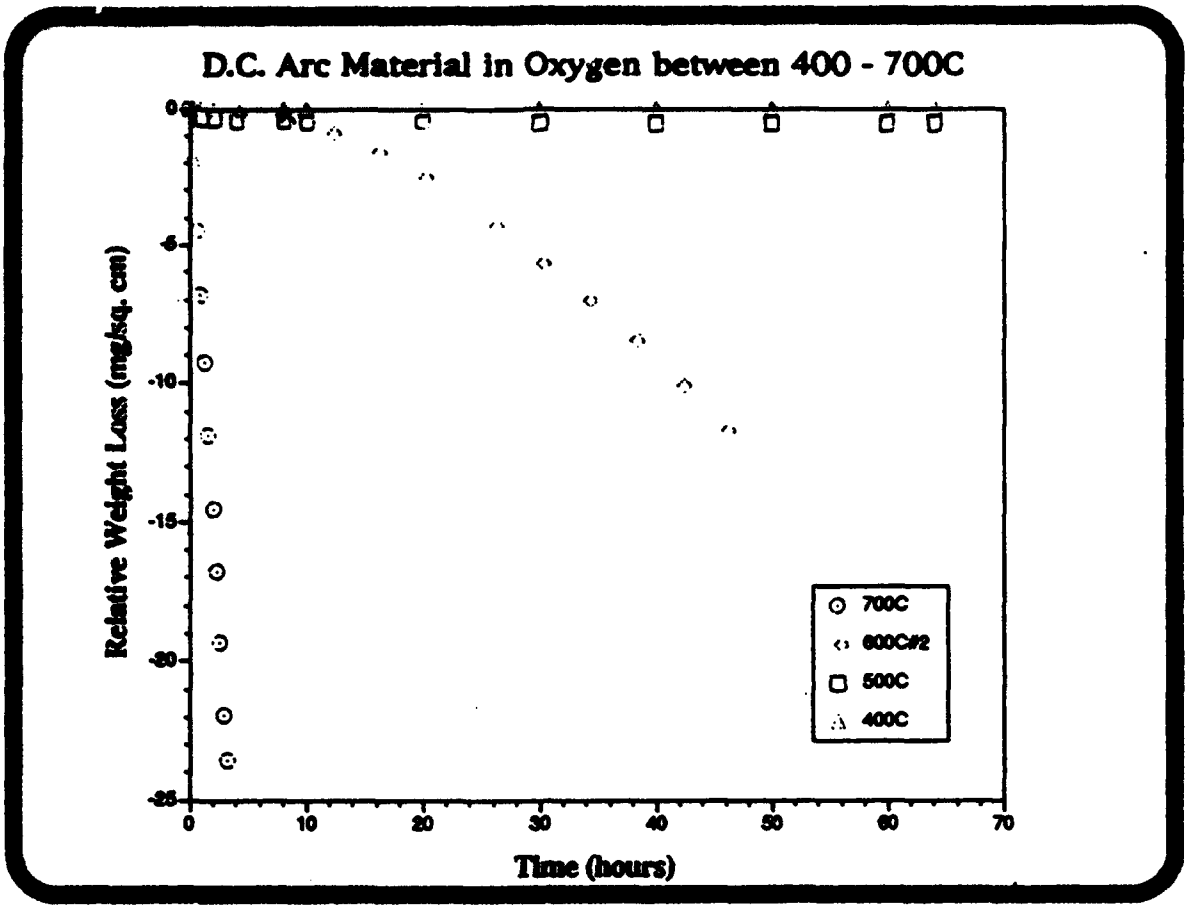

Figure IV.A.4.4 Weight loss versus time measurements for the oxidation of diamond films in oxygen at temperatures from 400°C to 700°C.

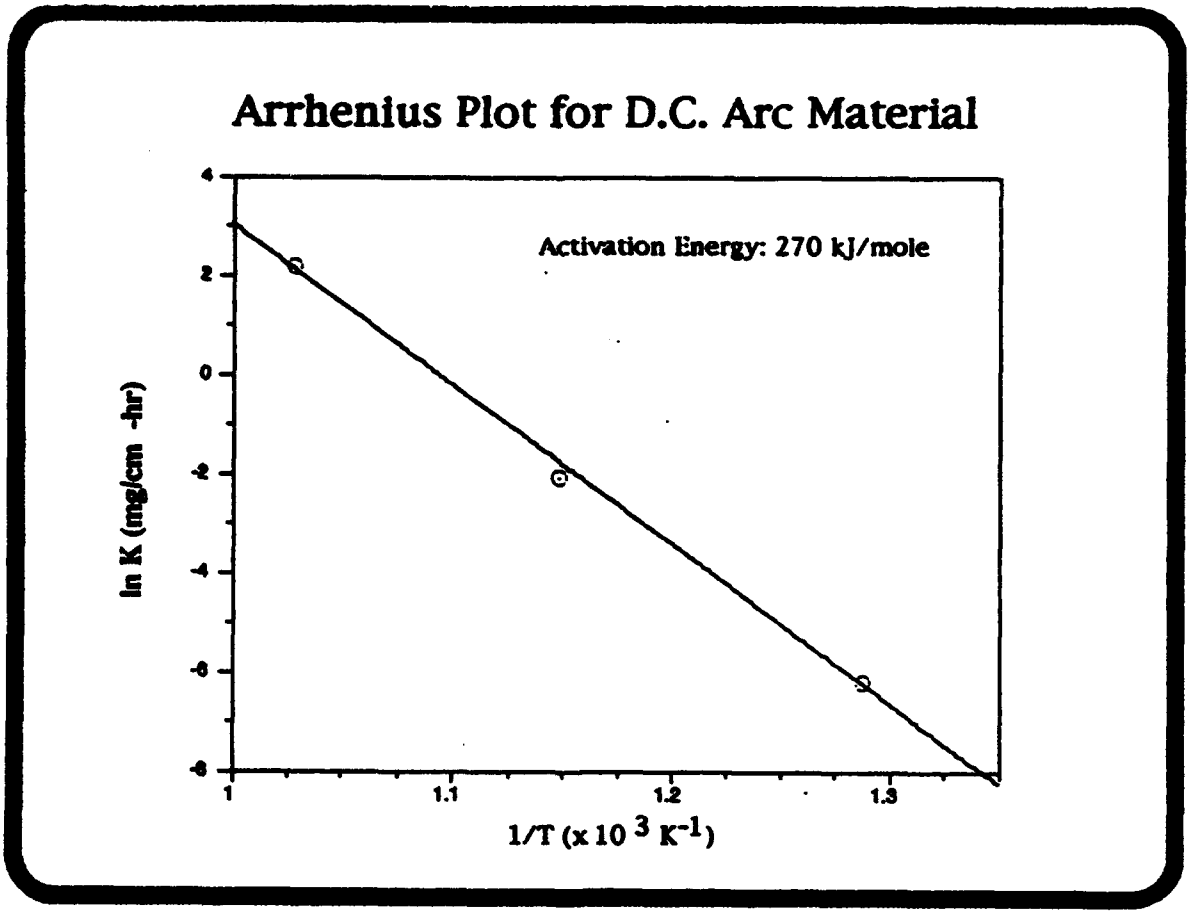

Figure IV.A.4.5 Linear rate constants for the oxidation of diamond films in oxygen.

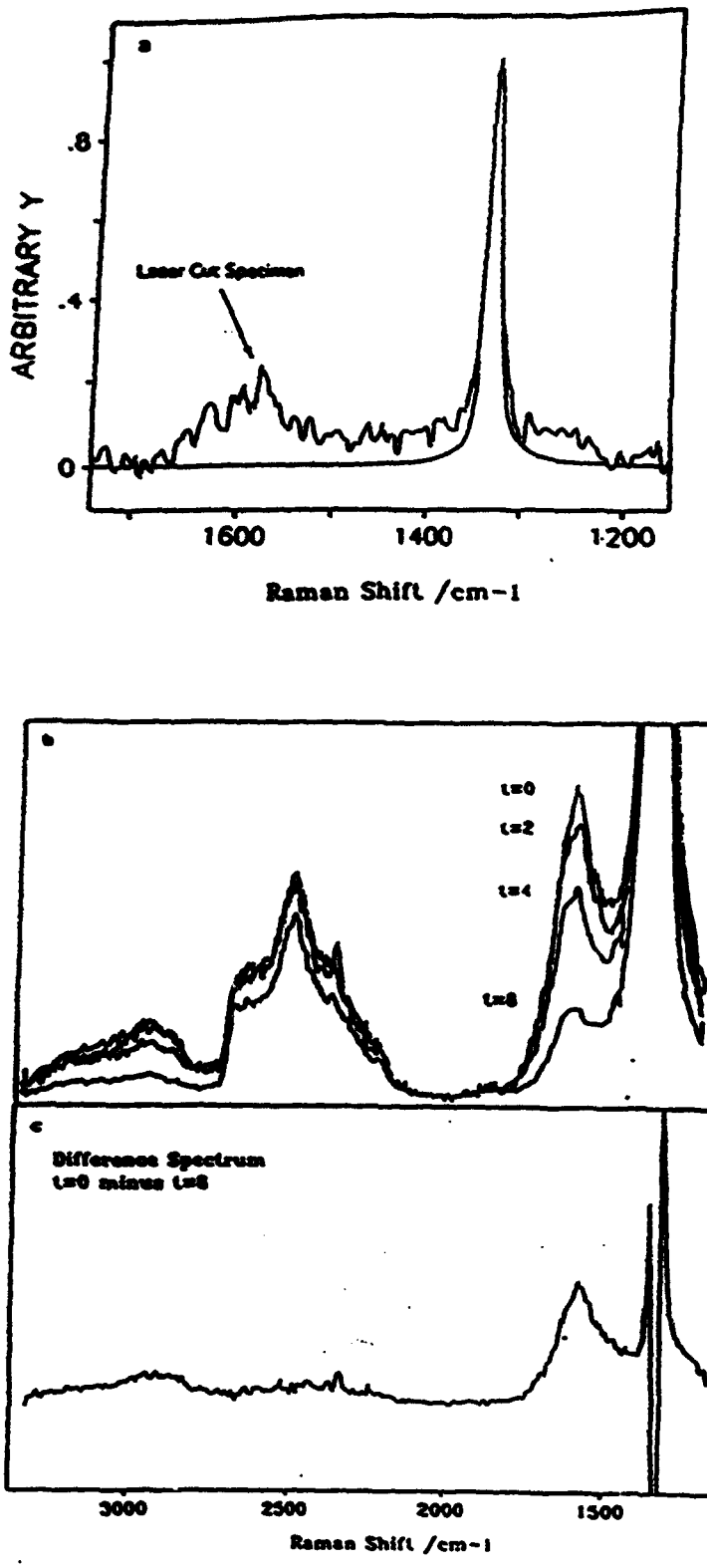

Figure IV.A.4.6. a. Raman spectra in arbitrary units with visible radiation (488 nm excitation) showing the first order Raman spectrum for diamond (1332 cm^{-1}) and for a non-diamond species (1570 cm^{-1}). The two spectra were scaled such that the 1332 cm^{-1} diamond peak intensities were identical. b. UV Raman spectra (228.9 nm excitation) of initial diamond film and after oxidation times of 2, 4, and 8 minutes. Second order Raman spectrum for diamond (2500 cm^{-1}) and for non-diamond carbon (3000 cm^{-1}) are evident. The spectra were scaled such that the 1332 cm^{-1} integrated diamond peak intensities were identical. c. Difference spectrum of 0 minus 8 minutes.

IV.A.5 Scanning Tunneling Microscope and Atomic Force Microscope Facility

Principal Investigator:	**Professor John T. Yates, Jr.** **Department of Chemistry** **Surface Science Center** **University of Pittsburgh**
Other Faculty Participants:	**Dr. Fred S. Pettit** **Materials Science and Engineering Department** **University of Pittsburgh**
Students:	**Dr. K. Wan** **Dr. V. Ukraintsev** **Mr. R. Amata** **Mr. K. Xu**

IV.A.5.1 INTRODUCTION

An Omicron scanning tunneling microscope (STM) was purchased as an add-on appendage instrument to an existing ultrahigh vacuum system which was donated to the project by Professor David M. Hercules. The ultrahigh vacuum system was extensively modified in order to make it suitable for the STM and other associated measurements. In addition, an Omicron atomic force microscope (AFM) was purchased. It will operate in the air or in a purge gas and it employs the same electronics and readout equipment as the STM, except that changes in the electronics must be manually installed for the AFM.

The STM will be employed in a number of studies of semiconductor and metal single crystals, both in the imaging mode and as a local probe of the density of electronic states from the surface atoms of the semiconductor single crystals to be studied.

The STM is operating but the AFM has just been received from the company and has been shown to operate at the micron level of horizontal resolution.

IV.A.5.2 UHV STM SYSTEM-ANALYTICAL COMPONENTS

Overview

A top view of the UHV STM is shown in Figure IV.A.5.1. It consists of a central vacuum chamber of 12 inch diameter, containing various surface analysis

components to be discussed later, a load lock system for insertion of the samples without breaking vacuum, and the STM. The double headed arrow shows the location where sample transfer is achieved from the load lock to a central carrousel

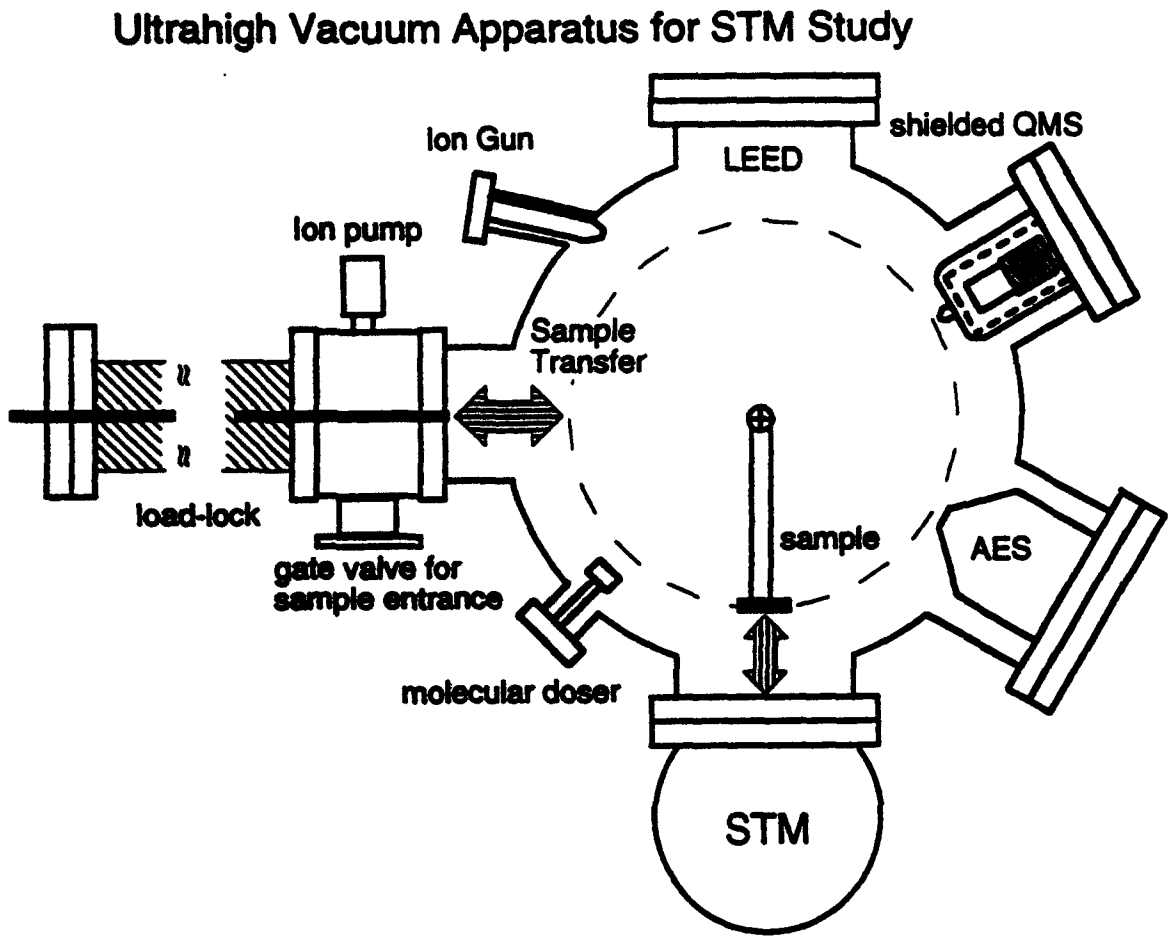

Figure IV.A.5.1 Ultrahigh Vacuum System + STM

manipulator; after study at the various ports in the central chamber, the sample may be transferred a second time to the STM as shown by the second double headed arrow.

Analysis of the single crystal sample may be done using LEED (homebuilt), a shielded quadrupole mass spectrometer (QMS), and an Auger spectrometer (AES). In addition, a controlled dosage of gas may be applied to the sample using the molecular beam doser. An ion gun is also supplied for sputtering the sample for surface cleaning. All of these components have been built from the ground up, or heavily modified for use in the STM facility.

Analytical Components Performance

One of the most critical factors in working with the STM samples in this apparatus is the ability to electrically heat the crystals reproducibly in the moveable sample holder in the main chamber, and to accurately measure the temperature achieved. We have designed a feedback temperature controller for this purpose which senses the thermocouple reading and adjusts the heating current accordingly. This controller will ramp the temperature linearly from 300 K to more than 1500 K. But it is very difficult to move a crystal from place to place while maintaining thermocouple contact. This difficulty was overcome by a new design which has been produced here and is shown in exploded view in Figure IV.A.5.2.

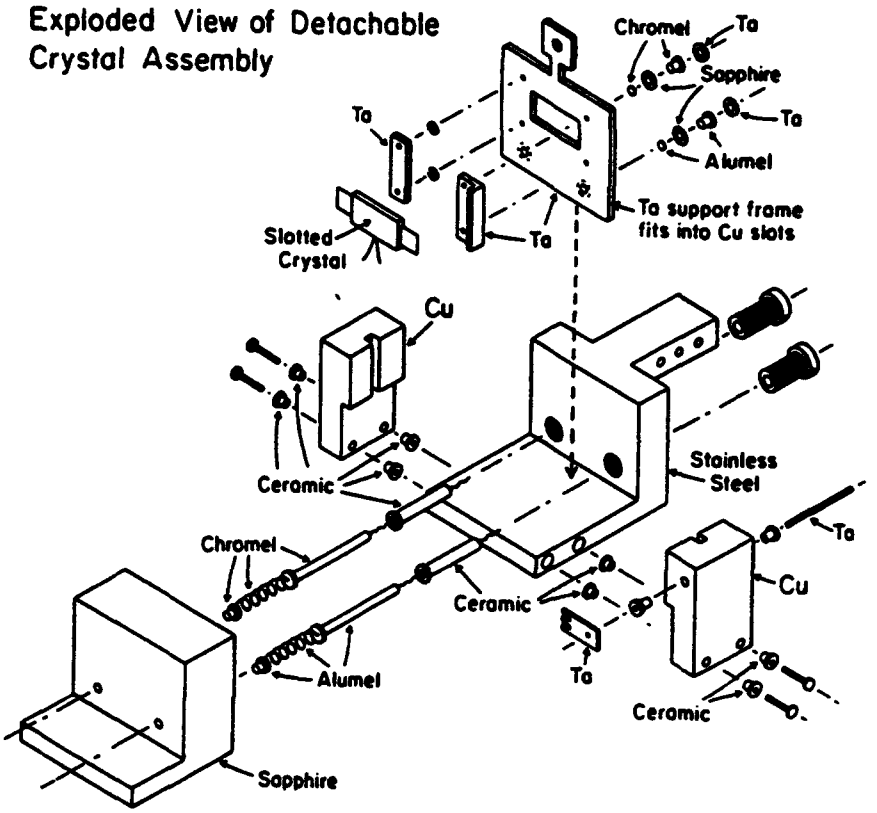

Figure IV.A.5.2 STM Sample Holder with Built-in Thermocouple

The slotted single crystal is held in a framework structure made of Ta metal, as shown in the picture. A small thermocouple is buried in a slot on the bottom of the crystal. Contact of the thermocouple to the outside world occurs via spring contacts made of the same thermocouple alloy materials (to avoid junction contact potentials). The Ta frame fits into a Cu holder which is mounted on a sapphire block. A springy Ta contact is made for ohmic contact to the crystal for applying electrical heating power. The crystal can be moved into the assembly by manipulation using an ultrahigh vacuum finger grip device which grabs the appendage handle at the top of the frame.

The performance of the device is excellent as monitored using two thermocouples, one going directly to a readout device and the second going through the spring contact arrangement in the holder. Figure IV.A.5.3 shows that errors less than 20 K are measured at a crystal temperature of 1350 K. The device and its performance have been described in a short paper which has now been accepted by The Journal of Vacuum Science and Technology [1].

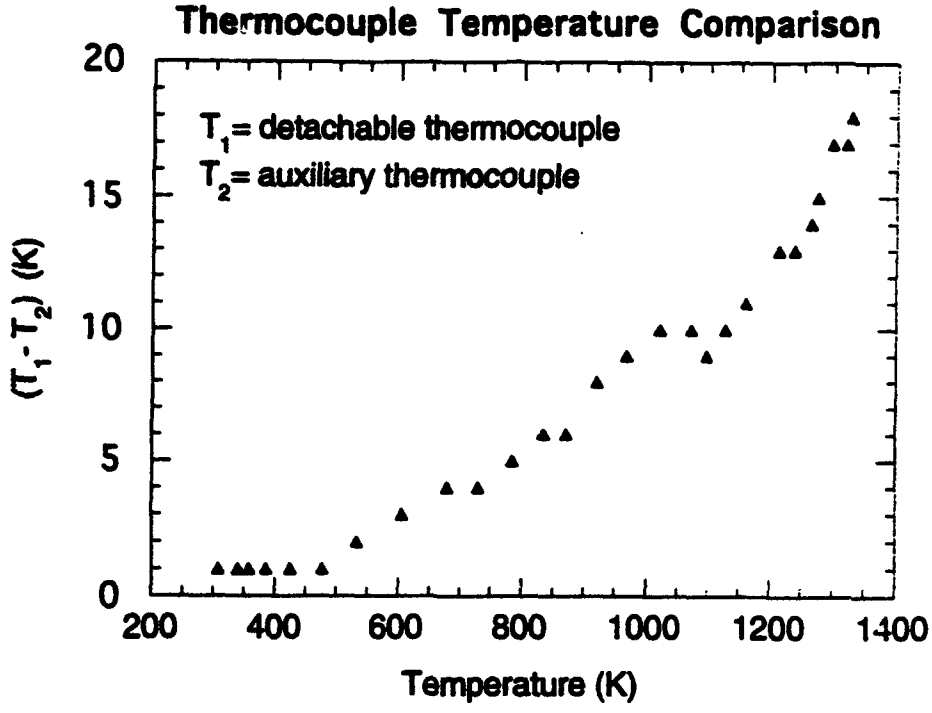

Figure IV.A.5.3. Comparison of Temperature Measurement with Detachable Thermocouple and Fixed Thermocouple.

The collimated molecular beam doser supplies gas to the crystal for controlled adsorption studies through a microchannel plate collimator. It must be calibrated absolutely, and this has been done as shown in Figure IV.A.5.4, using nitrogen. The calibration indicates that the laser drilled pinhole conductance which controls flow has a conductance of $1.81 \times 10^{13} N_2$/torrs. This conductance may be used to calculate the flow rate for any gas being used in the doser and will permit about 1 monolayer of gas to be applied to the crystal surface in 100 s, a convenient rate of adsorption. The gas doser is backed by an ultrahigh vacuum gas handling system which was designed here and built in our shops. The gas handling system is separately pumped using both ion pump and turbopump. It

contains calibrated volumes for doser calibration.

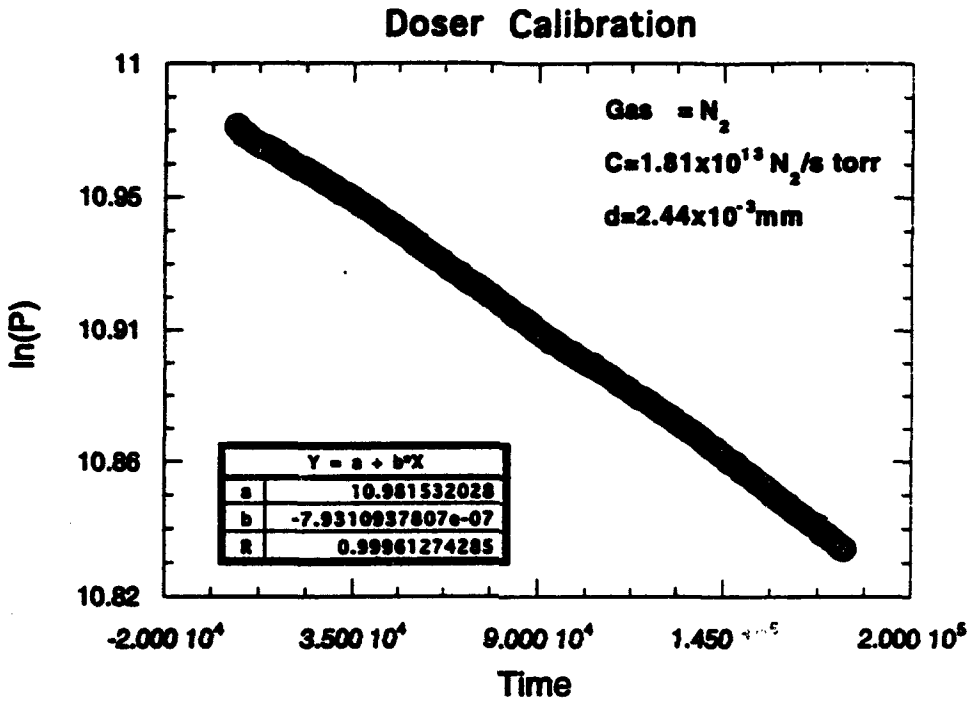

Figure IV.A.5.4 Calibration of Molecular Beam Doser with N_2

The Auger spectrometer was a surplus instrument with 20 year old electronics and electron optics. This was rebuilt by the electronic shop and works excellently now.

The LEED apparatus was designed and built in the Surface Science laboratory. Modeling of the electron optics was employed in the design, and a typical electron optic performance curve for the homebuilt electron gun is shown in Figure IV.A.5.5. The focus voltage calculated actually agrees with the actual focus voltage used to within 1 volt!

Modelling of the Electron Optics

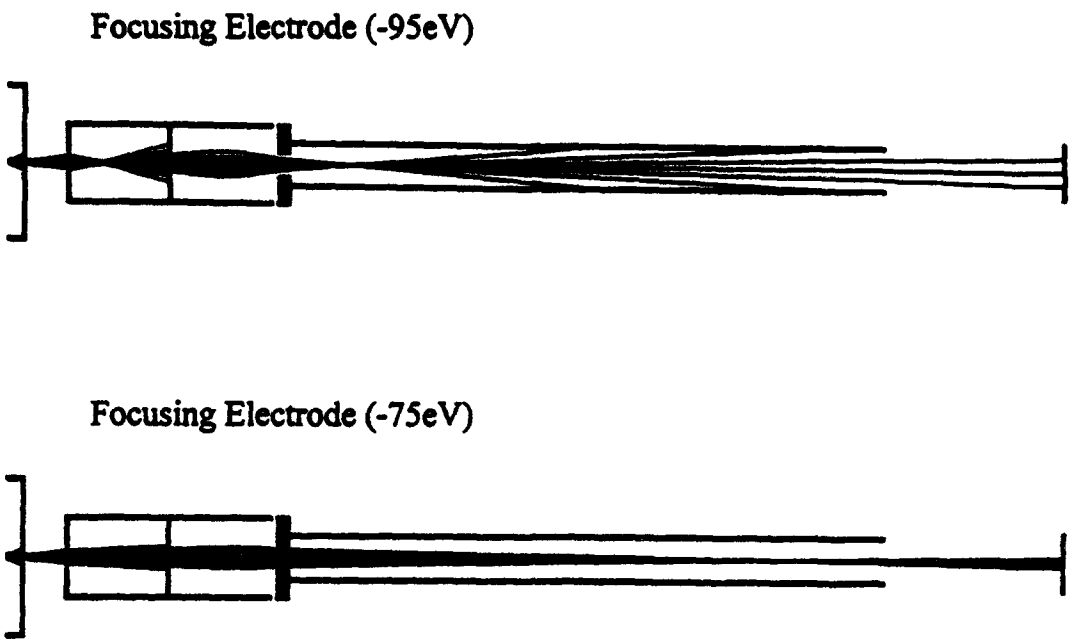

Figure IV.A.5.5 Modeled Performance of Electron Gun in Reverse View LEED Apparatus

A photograph of the reverse view LEED apparatus is shown in Figure IV.A.5.6. Figure IV.A.5.7 contains a photograph of the LEED pattern obtained from a reconstructed Si(100)-(2 x 1) surface, and it may be seen that the performance is superior. Home built power electronics were employed for this apparatus, as shown in Figure IV.A.5.8.

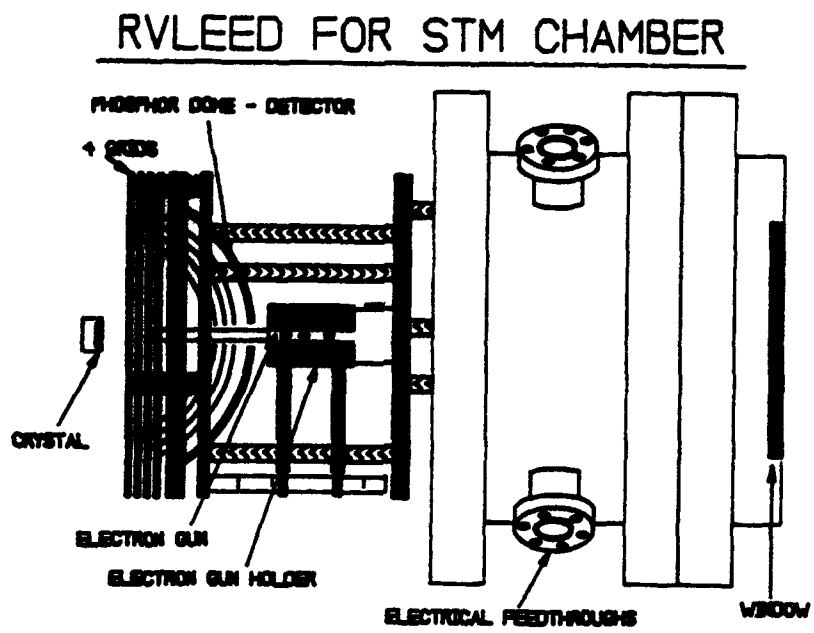

Figure IV.A.5.6 Schematic of RV LEED

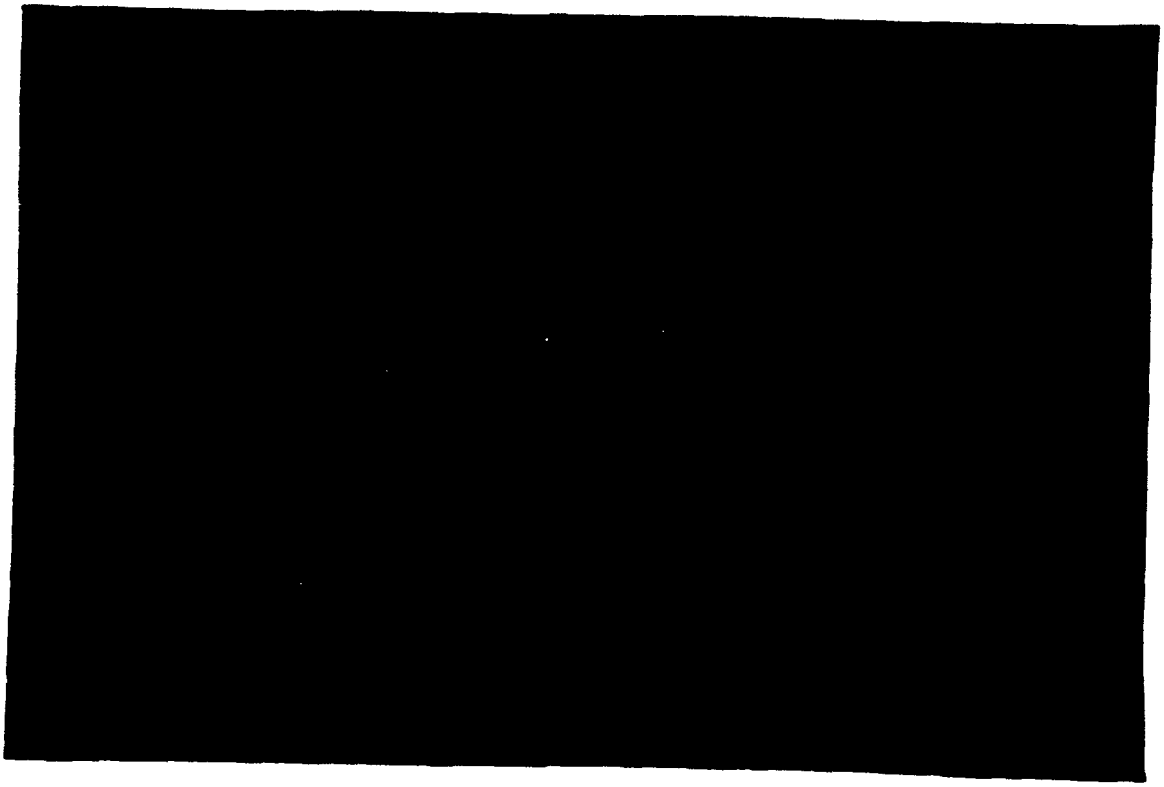

Figure IV.A.5.7. LEED Pattern - Si(100)-(2x1)

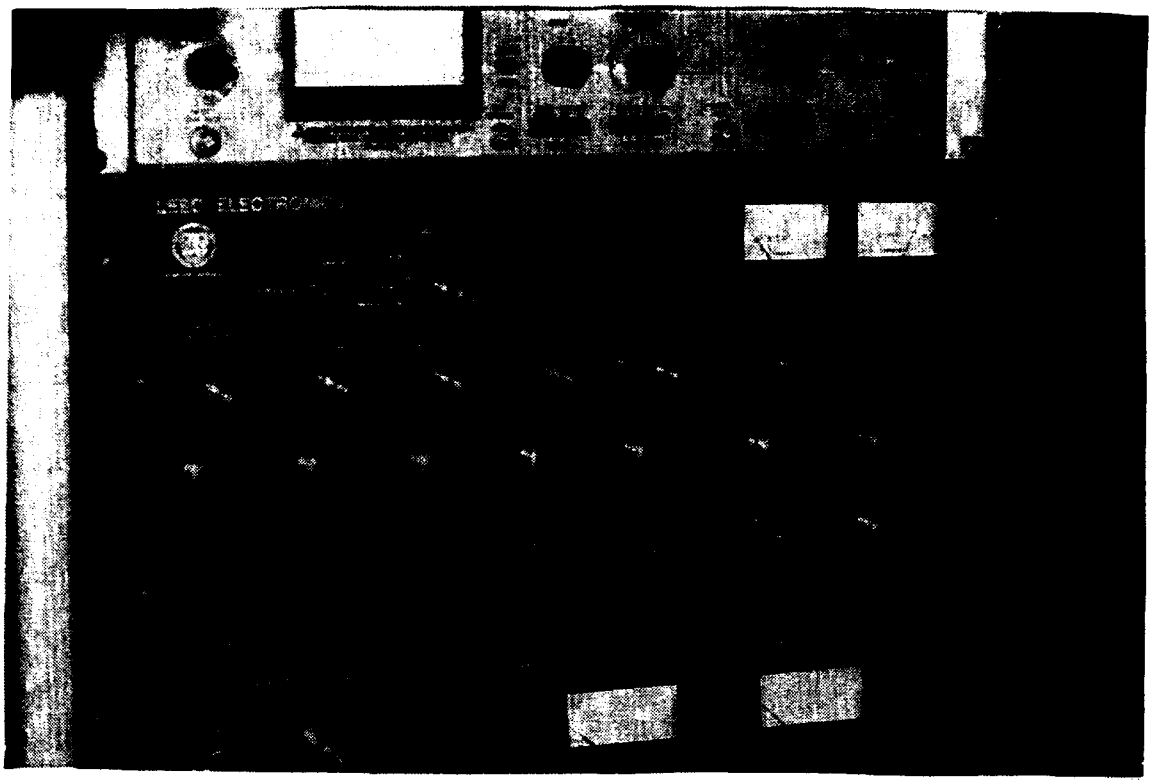

Figure IV.A.5.8 Homebuilt RV LEED Power Supply

STM Performance

The key mechanical requirement of an instrument with better than 1 Å resolution is adequate vibration isolation. Thus, the laboratory which houses the STM was custom designed to avoid both building vibration and acoustical vibration. All air conditioning was mounted on the outside walls of the laboratory which is itself made of heavy stone and concrete construction elements. Figure IV.A.5.9 shows a schematic drawing of the vibration isolation employed for the ultrahigh vacuum system. The vacuum chamber is mounted on about 1000 pounds of cold rolled steel flat stock which sits on a 4" thick sheet of styrofoam which makes contact with the concrete floor. The concrete floor is in turn poured on a cinder base which forms the foundation of the building. The styrofoam has been used to damp shear modes which are common in laboratory setups of this type.

STM vibration isolation:

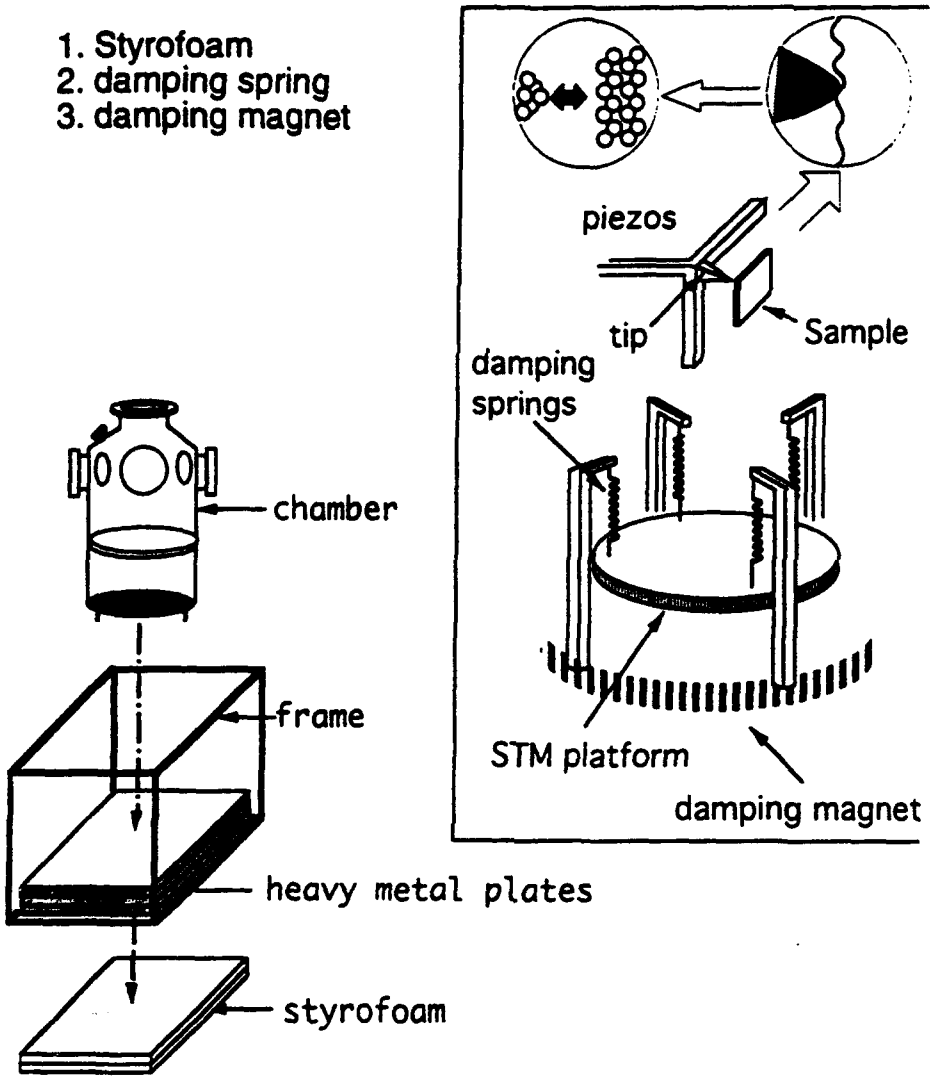

Figure IV.A.5.9 Schematic View of UHV-STM

Inside the STM chamber, two additional vibration damping arrangements are contained. The STM is supported on 4 springs, and the support assembly is suspended in a damping magnet assembly in which any motion produces an eddy current response in copper fins which are inside a sectored magnetic field. The piezo drive mechanism and a schematic of the STM tip in imaging position are also shown in Figure IV.A.5.9.

The Si(111)-(7 x 7) surface is a well known reconstruction of the primitive Si(111) surface, and a schematic diagram of the surface in top view and in side view is shown in Figure IV.A.5.10. Si atoms present filled and unfilled orbitals to vacuum from this surface. The two basic types of Si atoms are called adatoms and rest atoms. The adatoms contain partially empty orbitals which can be imaged with the STM tip biased negative. Figure IV.A.5.11 shows our STM image

Top and Side View of the DAS model for the Si(111) 7x7 reconstruction

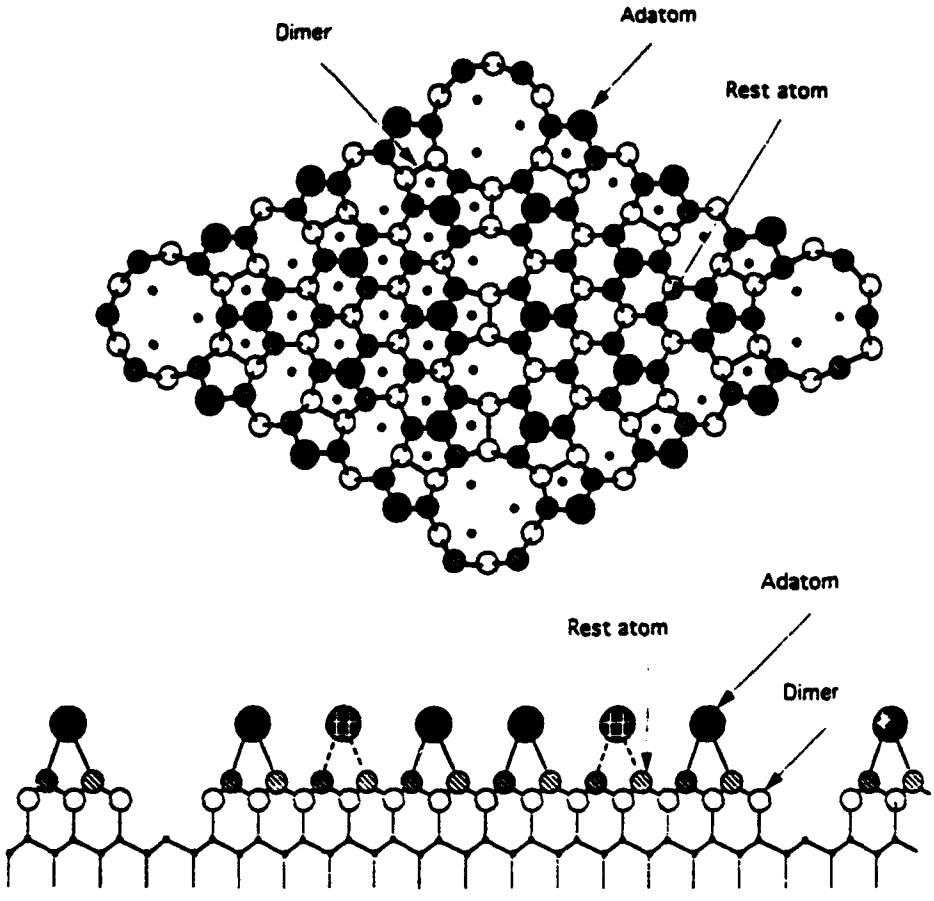

Figure IV.A.5.10 Si(111)-(7x7)-Schematic Structure

of the Si(111)-(7 x 7) surface, and an exact correspondence between the atomically resolved image and the model in Figure IV.A.5.10 is obtained. It is these projecting orbitals, as seen by the STM, which are the reactive acceptor orbitals responsible for certain types of surface chemistry on this surface.

The Si(100)-(2 x 1) surface is a reconstructed surface produced from the primitive surface. Figure IV.A.5.12 shows the reconstructed surface as a model, and Figure IV.A.5.13 shows the STM image of the surface obtained here. Atomic steps are observed, and these steps are associated with a 90° rotation of the rows of dimer atoms as one proceeds from terrace to adjacent terrace. Inspection of the Si(100) pattern shows that the terraces contain vacancy defect sites, and the

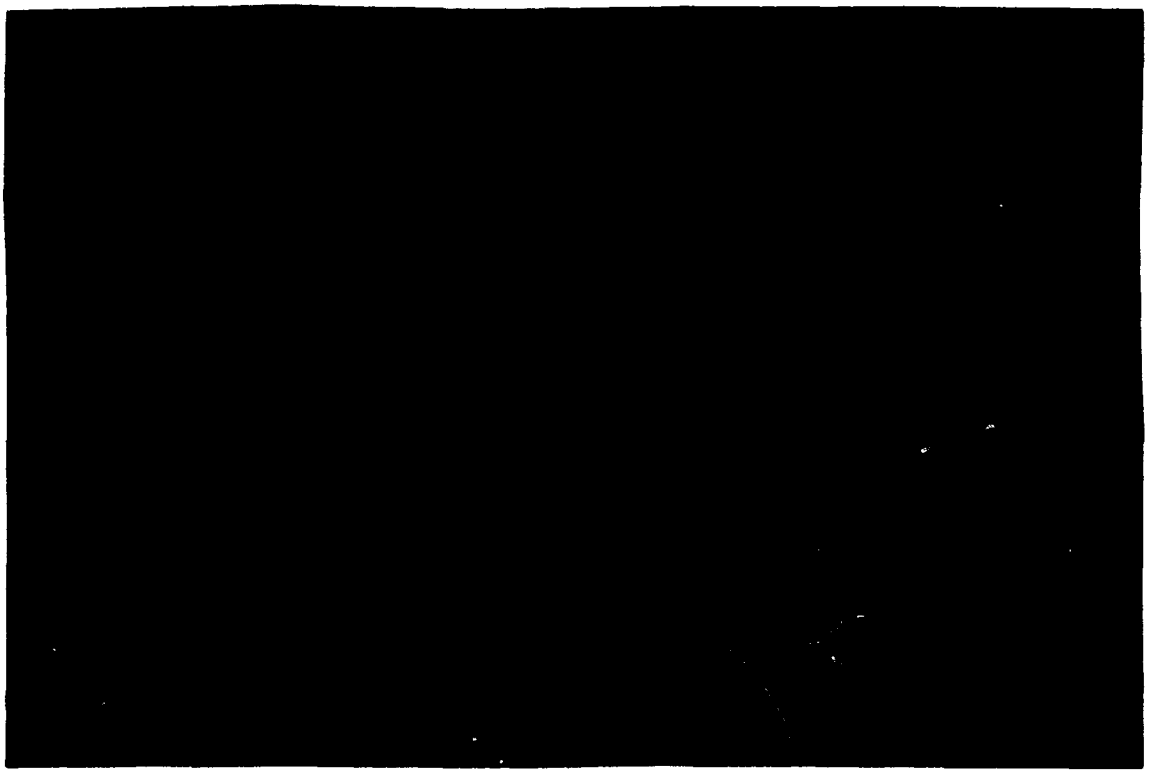

Figure IV.A.5.11 Si(111)-(7x7)-STM Image

origin of these defects is being investigated. A small level of defect site density is observed by others in all studies of Si(100).

Top and Tilted Views of Si(001) 2x1 Reconstruction

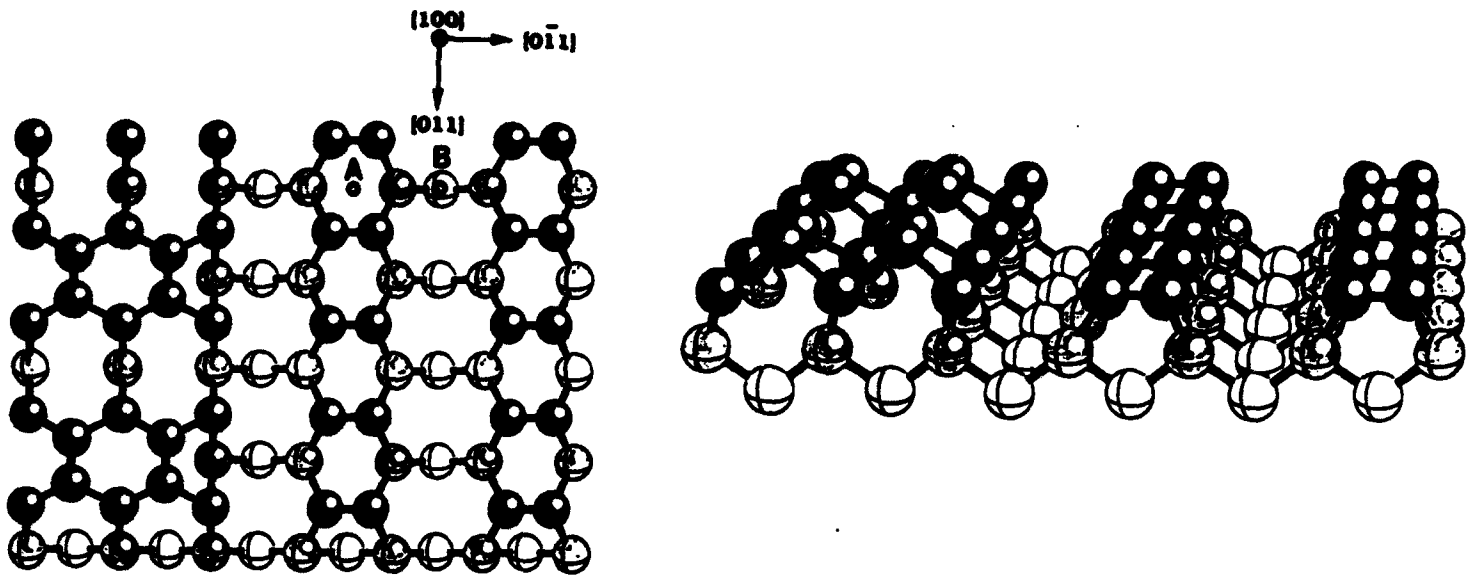

Figure IV.A.5.12 Si(100)-(2x1)-Schematic Structure

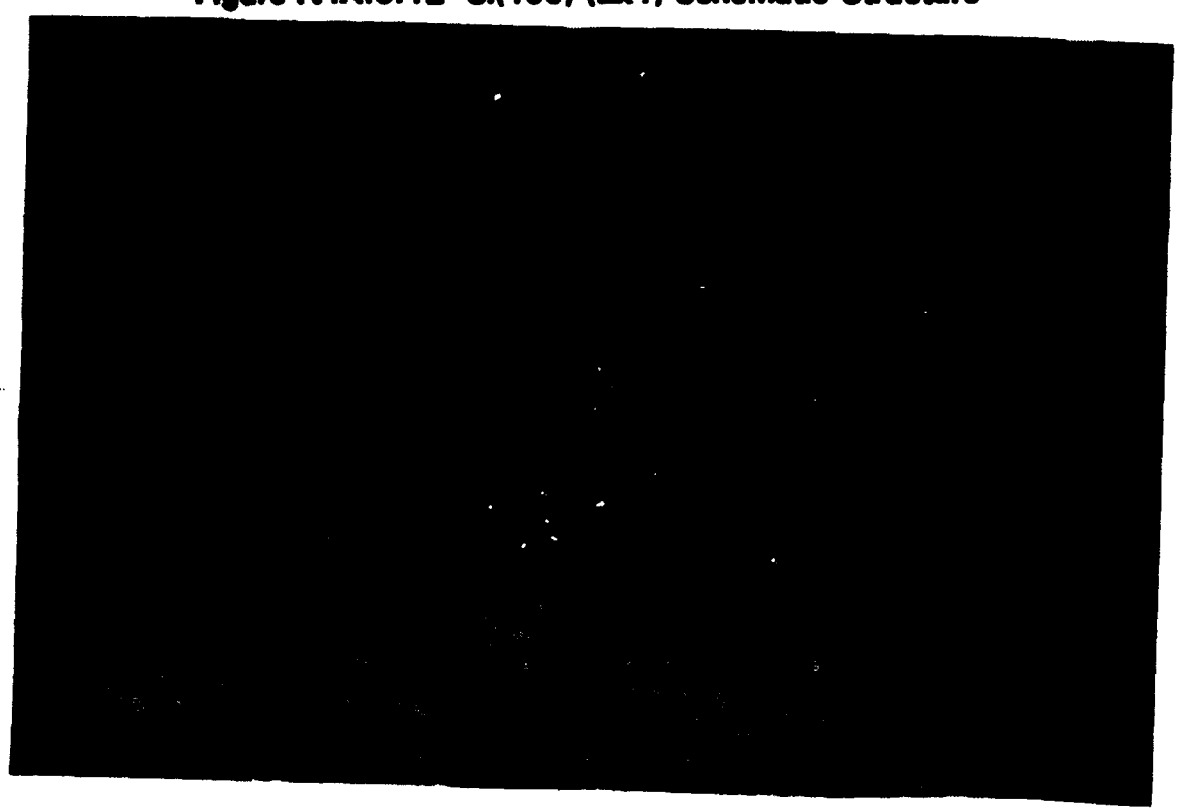

Figure IV.A.5.13 Si(100)-(2x1)-STM Image

AFM Performance

The AFM was received from Omicron. It was placed on a granite support block and then on a vibration isolation platform which is attached to the block. Although we have not yet been able to make images with this apparatus, an atomic resolution image of a stepped Si(100) single crystal was supplied by the company, and is shown in Figure IV.A.5.14.

Note: Subsequent to the preparation of this report, the Omicron AFM was exchanged for another AFM, manufactured by TOPOMETRIX, which is compatible with the Omicron STM electronics package, and is expected to provide greater ease of operation and maintenance.

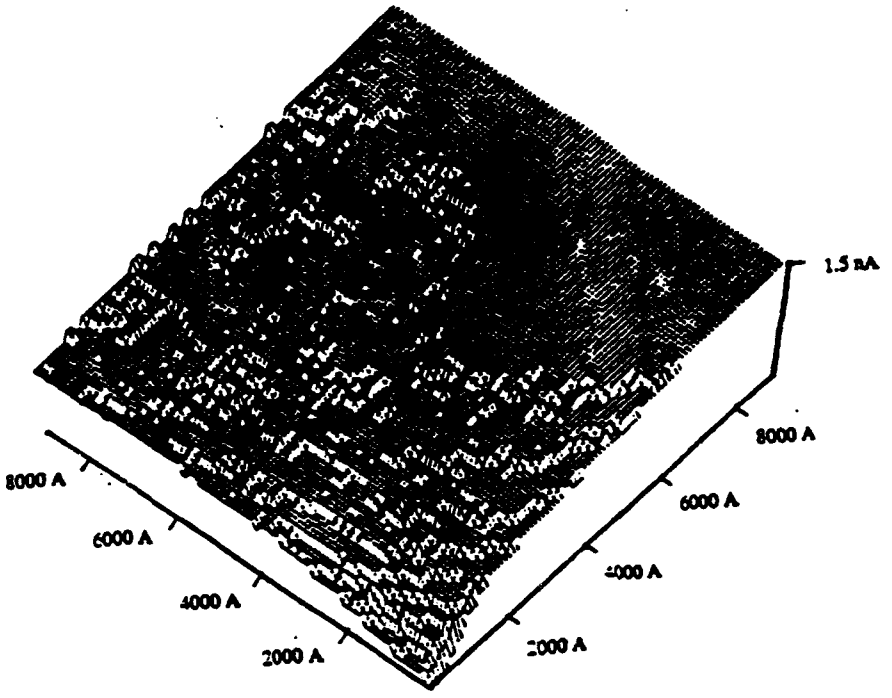

Figure IV.A.5.14 AFM Image - Made in Germany at Omicron

IV.A.5.3 PLANS FOR THE FUTURE

A number of STM projects involving the study of surface chemistry and surface photochemistry on semiconductor surfaces is planned. The STM will be used for imaging and for perturbing surface species, atom-by-atom. This work will be done using a no-cost extension using University funds, as on other contracts available to us.

The AFM is viewed mainly as a service instrument for microscopy. Professor Hercules plans to study ion-induced damage of polymer molecules supported on Ag surfaces in connection with the need to understand processes occurring in analytical SIMS.

REFERENCE

1. K. John, K. Wan and J.T.Yates, Jr. J. Vacuum Sci. and Technol., accepted.

IV.A.6 Twinning in Advanced Materials: The Interplay of Slip and Twinning in High-Strength Particle Hardened and $L1_2$ Ordered Alloys

Principal Investigator: Professor W.A. Soffa
Materials Science and Engineering Department
University of Pittsburgh

Students: Ms. Tamara Radetic
Mr. Hideyuki Okumura

IV.A.6.1 BACKGROUND

Deformation twinning generally has been considered of secondary importance at most in the plasticity of face-centered cubic (f.c.c.) and f.c.c.-based metals and alloys. Slip is almost always considered the primary mode of plastic flow in single phase and multiphase f.c.c. materials at low and moderate temperatures except under extraordinary conditions; however, it is becoming more and more evident that the interaction of slip and twinning can have a major influence on the flow and fracture of numerous f.c.c. related materials [1]. Under certain circumstances twinning appears to be a primary mechanism of plastic flow of equal importance to slip even replacing slip as the initial plastic response at yielding [2]. A perusal of the literature clearly shows that more fundamental work remains to be done to clarify the interplay of slip and twinning and that many of the conventional views of mechanical twinning in f.c.c. crystals and polycrystals are overly simplistic.

IV.A.6.2 HIGH-STRENGTH COPPER-TITANIUM ALLOYS

An interesting case for studying the interplay of slip and twinning is in the deformation of ultra-high strength, precipitation hardened copper-titanium alloys containing a few percent titanium. The attractive properties of these age hardened alloys have been known for almost four decades, but only recently have they started to displace the well-known copper-beryllium series in various technological applications. The high strengths of the Cu-Ti alloy (Y.S. ~ 90,000 psi) derive from the formation of a fine dispersion of coherent, metastable Cu_4Ti ($D1_a$) particles during aging between 350 - 450°C. At the higher titanium concentrations (~ 3 - 4 wt.% Ti) it has been suggested that the precipitation reaction stems from spinodal decomposition involving clustering and ordering [3]. The slip and twinning systems of the $D1_a$ particles and f.c.c. matrix are parallel and five a/2 <110> unit dislocations are required to produce an identify translation in the ordered particles; however, it is interesting to note that the motion of matrix twinning dislocations of the type a/6 <112> create antiphase boundaries (APB's) in only 1/3 of the particle variants. The age hardened Cu-Ti alloys have been reported to exhibit an anomalous age hardening response showing a pronounced double peak [4]. Furthermore, Saito [5] in his early studies showed that age hardened polycrystalline

Cu-4 wt.% Ti alloys strengthened by the so-called modulated structures exhibited profuse deformation twinning after initial yielding by slip. Extensive twinning in particle hardened single crystals of Cu-Ti and Cu-Ti-Al alloys also was found, and in suitably aged and oriented specimens plastic flow was observed to commence with mechanical twinning [2].

In this part of the research program the mechanical properties of particle hardened copper-titanium alloys were investigated with a primary focus on elucidating the fundamental basis for the anomalous, double-peak age hardening response and on the interplay between slip and twinning during plastic flow in these particle hardened alloys.

IV.A.6.3 RESULTS

The deformation studies of the age hardened copper-titanium alloys were carried out using a Cu-4.2wt.% Ti alloy. Tensile specimens were prepared from sheet material having a 1.0 in. gage length. The gage section was 0.25 in. wide and 0.008 in. thick. The specimens were solutionized at 875°C for 2 hours followed by an ice brine quench. The quenched specimens were aged at 375°C for times up to 1500 minutes. The grain size of the alloy was approximately 60 μm. Tensile testing was performed on a hydraulic machine at a strain rate $\dot{\epsilon} \sim 6.5 \times 10^{-4}$ sec^{-1}. For each aging time one sample was pulled until failure and another was deformed 5 percent. The as-deformed alloys were examined in the transmission electron microscope at 200 kV using specimens prepared from the gage length of the tensile samples.

The as-quenched specimens showed a yield strength $\sigma_{0.2} \sim$ 33,000 psi (229 MPa). After aging for 1500 minutes the alloy developed a yield strength of about 99,000 psi (680 MPa). No distinct double peak age hardening curve was observed. The high strength alloys aged near peak hardness exhibited profuse deformation twinning in conjunction with slip from the early stages of plastic flow ($\sim$ 5 percent). Twinning was observed to occur both on primary and secondary systems of the f.c.c. matrix. Thin twins $\sim$ 10 - 20 nm thick were observed to coalesce forming thicker ones. The twins apparently propagated through the array of particles in a manner which lead to the incorporation of small untwinned regions around some of the $D1_a$ particles. The deformation twins were often observed to stretch across the grains from one grain boundary to another. In alloys aged to strengths well-below 680 MPa, twinning did not occur until large amounts of plastic flow and significant workhardening had occurred.

These preliminary observations have lead the investigators to look carefully into models of deformation twinning which would allow for fine-scale twinning to occur around or through the $D1_a$ particles consistent with the crystallography and experimental results. Furthermore, a new series of systematic experiments involving an investigation of twinning in the high strength allows as a function of temperature and strain rate have commenced.

IV.A.6.4 DEFORMATION OF POLYTWINNED STRUCTURES

Another f.c.c.-based system where mechanical twinning appears to play a special role is in $L1_0$ ordered alloys. In the $L1_0$ ordering alloys the ordering transformation often produces a microstructure comprised of microtwins conjugated along the {110} planes of the parent phase. These polytwinned microstructures are well-known in the Cu-Au, Fe-Pd, Fe-Pt, Co-Pt and Ni-Pt systems. The microstructure is essentially a lamellar aggregate in which the c-axis of the tetragonal cell of the CuAuI-type structure changes by 90° in going from one structural domain or twin to another. The problem of plastic flow in these ordered phases which are partitioned into twinned domains on a scale ~ 10^2 - 10^3 Å is very interesting from a fundamental point of view. Recently, the technological relevance of flow in these laminated structures has been accentuated by the occurrence of twin-related lamellar microstructures in γ-TiAl intermetallic alloys. Pashley et. al [6] investigated the deformation of CuAuI in 1968 and called attention to the complexity of flow in these lamellar aggregates and the dislocation mechanisms involved in the transmission of shear across the twin boundaries. They also suggested that the predominant deformation mechanism in these microstructures is twinning and not slip as concluded by the earlier study by Syutkina and Yakoleva [7]. Since this earlier work very few studies had been directed at this unique problem of polycrystalline plasticity until the explosion of interest in the deformation mechanism of γ-TiAl. In the current research program the micromechanisms of plastic flow and fracture in polytwinned microstructures are being studied to develop a fundamental understanding of the role of slip and twinning in these lamellar aggregates in terms of the behavior of dislocations in the $L1_0$ structure. The work is focussing on the reversibly ordering CuAu and Fe-Pd alloys as model systems; however, these studies will be applied to clarify the influence of the lamellar structures on the behavior of the γ-TiAl alloys.

IV.A.6.5 RESULTS

The preliminary studies of the polytwinned alloys have focussed on the Fe-Pd equiatomic alloy. The materials were thermomechanically processed and heat treated to produce sheet material with a grain size of about 250 μm and a polytwinned structure on the scale ~ 0.1 - 1.0 μm. The sheet material was subjected to various modes of deformation including rolling, hammering, and indentation by a microhardness indentor. The initial experiments have yielded some important preliminary results.

Although a plethora of dislocation reactions has been suggested in the literature, the dislocation structures observed by transmission electron microscopy in this study are rather simple and limited. The deformation substructure appears to be dominated by single dislocations of the type a/2 <110>. The single dislocations often make an angle of 30° with respect to the Burgers vector. The dislocation configurations bounding planar faults appear to be of the type a/6 <112> and a/6 <145>. Also, there is a high density of {111} twins cutting

across the lamellar aggregates. These results have been used to design a series of experiments employing simple tension at various temperatures and strain rates.

IV.A.6.6 REFERENCES

1. L. Remy: Met. Trans., 12A, 387 (1981).

2. A.M. Li, Yu.I. Chumlyakov and A.D. Korotayev: Phys. Met. Metall., 59, 158 (1985).

3. A. Datta and W.A. Soffa: Acta Met., 24, 987 (1976).

4. J. Greggi and W.A. Soffa: Scripta Met., 14, 649 (1980).

5. K. Saito: Trans. Nat. Res. Inst. Japan, 12, 8 (1970).

6. D.W. Pashley, J.L. Robertson and M.J. Stowell: Phil. Mag., 19, 83 (1969).

7. V.I. Syutkina and E.S. Yakovleva: Phys. Stat. Sol., 21, 465 (1967).

IV.A.7 Thermomechanical Processing of Titanium Aluminides

Principal Investigator:	**Professor A.J. DeArdo** **Materials Science and Engineering Department** **University of Pittsburgh**
Other Faculty Participants:	**Dr. C.I.Garcia** **Dr. W.A. Soffa** **Materials Science and Engineering Department** **University of Pittsburgh**
Students:	**Dr. P. Pouli** **Mr. R. Mutschler** **Mr. M.J. Hua** **Mr. C.C. Cunningham**

IV.A.7.1 INTRODUCTION

Recent initiatives addressed by the aerospace industry include an increase in the propulsion capacity of gas turbine engines. This new demand has resulted in an increase in R&D efforts to develop new structural materials for high temperature applications. Owing to their high temperature strength retention, oxidation resistance, and low density, titanium aluminides have emerged as viable candidates for applications currently dominated by Ni and Fe based superalloys. Major drawbacks, however, including poor room temperature ductility (i.e. ~1% for single phase γ-TiAl)[1], low fracture toughness (7.7Mpa(m)$^{1/2}$ for single phase γ-TiAl)[2], and poor formability have prevented the extensive application of titanium aluminides in critical aerospace components. Recent work has shown that improvements in ductility and fracture toughness can be achieved with two phase titanium-aluminide alloys through proper alloy design and thermomechanical processing.[3]

The major objectives of this program are to develop a basic understanding of the nature of the phase transformations and recrystallization behavior, and to study the effect of thermomechanical processing (i.e. strain, strain rate, deformation temperature, and cooling rate) on the final microstructure.

IV.A.7.2 BACKGROUND

Previous studies by various investigators have shown that the dual phase TiAl alloys show the best potential for achieving a suitable combination of low and high temperature properties.[4-12] These studies have established four basic types of microstructures: fully lamellar, massive, equiaxed, and duplex (lamellar +

equiaxed). The fully lamellar and massive types are developed by slow or rapid cooling, respectively, from the single phase α region. Equiaxed and duplex microstructures are formed by heating to and cooling from the (α + γ) two phase region, with the specifics of the microstructure depending on possible prior deformation, reheating temperature and holding time.

The duplex microstructure has shown the best combination of room temperature strength and ductility, but suffers from low fracture toughness (<16 MPa(m)$^{1/2}$).[7] The fully lamellar structure exhibits superior fracture toughness, creep properties and retained strength at high temperatures.[5,8] However, it is limited by poor ductility and low temperature strength. It has been suggested that the inferior tensile properties of the lamellar microstructure are due to its large grain size (~500 to 1000μm) inherited from the parent α phase.[13] Additions of alloying elements such as Cr, Mn, or V to binary Ti-48Al have been shown to increase the room temperature ductility of the alloy from 2-4% in duplex specimens.[7]

Blackburn was the first to study the formation of the fully lamellar structure [12], which is often referred to in the literature as the fully transformed structure, on cooling from the α region. An orientation relationship was determined between the γ and α_2 plates as $\{111\}_\gamma // \{0001\}_{\alpha 2}$ and $<011>_\gamma // <1120>_{\alpha 2}$. Blackburn also suggested that the γ phase forms by a stacking fault mechanism, nucleating on stacking faults in the α phase during the formation of the lamellar structure. Kim has proposed three mechanisms/ paths to explain the formation of the fully lamellar structure.[8] His work suggests that stacking faults play a major role in the transformation. Kim's mechanism can be summarized as follows:

$$\alpha \rightarrow \alpha + \gamma_p \rightarrow L(\alpha,\gamma) \rightarrow L(\alpha_2,\gamma)$$

where γ_p refers to γ plates.

Despite the large amount of information on the physical metallurgy of titanium aluminides, there is a dearth of information on the transformation behavior of these alloys under isothermal conditions. This observation is surprising since these alloys were initially developed for high temperature applications. Due to the fact that most studies performed up to this time titanium aluminides have been continuous cooling studies, and that there has not yet been a comprehensive isothermal study, the investigations being reported here involve the isothermal transformation behavior of near-gamma TiAl alloys. The results of these studies will enable the more effective execution of a thermomechanical processing study leading to an optimal microstructure.

IV.A.7.3 EXPERIMENTAL PROCEDURE

The alloys examined in this study are Ti-48Al-2Mn-2Nb, Ti-45Al-2Cr-2Nb, and a binary Ti-49Al, with the alloying contents in atomic %. These alloys are

being studied so that the effects of the various alloying elements on microstructural development can be compared. Samples were homogenized in the single phase α region at 1380°C for 4 hours prior to subsequent heat treatment, in order to produce a uniform starting structure and eliminate the effects of previous processing.

The main set of experiments in this study to date involve isothermal heat treatments over a range of holding temperatures. A schematic diagram of the heat treatments used in the isothermal study is presented in Figure IV.A.7.1. Samples 1/8 inch thick were encapsulated in a quartz tube evacuated and back-filled with argon, and heated to 1380°C for one hour (ten minutes for the Ti-45Al-2Cr-2Nb alloy). The samples were then air cooled (14°C/s) to temperatures in the range of 1250°C to 1000°C in 50° intervals, and water quenched. Quantitative metallography was performed in order to determine the volume fraction of various constituents in the microstructure. Scanning electron microscopy (SEM) and transmission electron microscopy (TEM) were utilized in order to more closely examine the features of the microstructure. X-ray analysis was used to confirm that the phases present in the alloys after heat treatment matched the phase diagram.

IV.A.7.4 RESULTS AND DISCUSSION

When the alloys were heated into the single phase α region and air cooled, a lamellar microstructure with some Widmanstatten-like plates was formed (see Figure IV.A.7.2). This result occurred in all three alloys investigated. However, when the three alloys were water quenched from the α region, there was a difference in behavior. For example, the Ti-45Al-2Cr-2Nb alloy develops a lamellar microstructure similar to that obtained by air cooling, while the Ti-48Al-2Mn-2Nb and Ti-49Al alloys, however, have a massive microstructure, Figure IV.A.7.3, which is γ massively transformed from α. It is suggested here that the massive transformation is also possible in the chromium containing alloy, but the kinetics of the massive to lamellar morphology transformation are speeded up to the extent that the massive microstructure is not observed even after water quenching.

The isothermal experiments produced a transformation in the microstructure from lamellar to equiaxed which is represented in Figure IV.A.7.4. The results shown in Figure 4 are for the binary alloy held at 1150°C (but the trend holds true for the other alloys at a given temperature). Upon cooling to the respective holding temperature, the microstructure was initially fully lamellar, although the Mn containing alloy tended to retain some massive microstructure. This microstructure gradually transformed over time at temperature to a fully equiaxed structure. The kinetic results from the full range of temperatures for each alloy led to the construction of TTT diagrams. The TTT diagram for the Ti-45Al-2Cr-2Nb alloy is shown in Figure IV.A.7.5, with similar diagrams being produced for the other two alloys investigated. In examining this diagram, it is clear that the initial lamellar microstructure (of α and γ) will gradually transform to a fully equiaxed morphology

(also of α and γ) if held for a sufficient time at high temperature. It is important to emphasize that the transformation followed in the TTT curve does not involve a change in the phases present. It, instead, follows a change in the morphology of the phases in the microstructure. Also included in Figure IV.A.7.5 are representative microstructures from different stages in the transformation: fully lamellar at the 0% transformation curve, a mixed microstructure at the 50% transformation curve, and fully equiaxed after the 95% transformation curve.

In order to examine the effects of the alloying elements on the transformation, the 50% transformation curves for the three alloys were plotted on the same diagram, Figure IV.A.7.6. The results in this figure show that the quaternary alloys proceed at a faster transformation rate than the binary alloy, with the chromium addition having a greater effect than the manganese addition. An interesting effect of the manganese addition is that although it slows down the transformation from massive to lamellar (stabilizes the massive structure) with respect to the binary alloy, it speeds up the kinetics of the lamellar to equiaxed transformation. Not only do the alloying elements move the nose of the TTT curve to shorter times, they also appear to shift the nose to higher temperatures.

There appears to be two basic mechanisms by which the microstructure of these alloys transforms from a lamellar to an equiaxed morphology. The first, which is prevalent at relatively short times, is the nucleation and growth of γ grains. An example of this is shown in Figure IV.A.7.7. It is important to note that for both mechanisms, the α_2 phase is more or less globular, and often can be found anchored on planar defects such as grain or twin boundaries or γ stacking faults, see Figure IV.A.7.8a. However, these α_2 particles can also be found inside a γ grain, unconnected to any defect, Figure IV.A.7.8b.

The second mechanism which produces the equiaxed microstructure involves spheroidization of the α (or α_2) phase. This mechanism appears dominant at longer times and higher temperatures, and is demonstrated in Figure IV.A.7.9. Figure 9a not only gives evidence of spheroidization, but also shows how in some lamellar grains, the α plates thicken (selected plates thicken at the expense of others), forming a "zebra stripe" type structure, prior to spheroidizing. Figure IV.A.7.9b is simply a later stage of the transformation shown in Figure IV.A.7.9a. An explanation of the spheroidization process can be proposed via TEM examinations. Figure IV.A.7.10a shows a γ subgrain boundary across adjacent lamellae in a binary sample held at 1250°C for 24 hours, and the necking of an α_2 lamella is demonstrated in Figure IV.A.7.10b. The proposed spheroidization mechanism is illustrated in Figure IV.A.7.11, wherein subgrain boundaries sweeping through prior lamellar grains connect to each other through the γ-γ and α-γ interfaces, resulting in two distinct plates (Figure IV.A.7.11d), which subsequently become spherical. This transformation is probably driven by the reduction in interfacial free energy attained by the α (or α_2) phase changing from plates to a more spherical shape.

It is important to note a few other interesting microstructural observations. In many of the samples held at high temperature for long times, there were lamellar areas that had lamellar grains of size much smaller than the original lamellar grains, see Figure IV.A.7.12. In other words, there were many areas in the original lamellar grain which changed orientation when held for a long time at high temperature. The reason for this is unclear, but it may be related to the motion of subgrain boundaries similar to those mentioned in the spheroidization mechanism. Another observation is that the massive microstructure appears much more stable in the Ti-48Al-2Mn-2Nb alloy than in the other alloys. While the binary and Cr containing alloys are fully lamellar after air cooling to the holding temperature, the Mn containing alloy still retains a significant amount of the massive morphology at this point in the transformation sequence, Figure IV.A.7.13a. In fact, even after holding for 48 hours at 1000°C, some evidence of the massive structure was still found, Figure IV.A.7.13b.

In order to confirm the instability of the lamellar microstructure at high temperatures, Ti-48Al-2Mn-2Nb samples were first heat treated to form a fully lamellar microstructure, and then were reheated to a temperature of 1150°C, and held for a time ranging from 10 minutes to 72 hours, see Figure IV.A.7.14. The results are plotted in Figure IV.A.7.15, and are shown along with the results for the same alloy cooled from 1380°C and held at the same temperature, for the purposes of comparison. It is evident that the same basic events occur in the reheated samples that occur in the cooled samples: the lamellar microstructure transforms to an equiaxed microstructure, although the kinetics are much slower for the reheated samples. The equiaxed grains in this case appeared to nucleate and grow primarily at the lamellar (prior α) grain boundaries, see Figure IV.A.7.16.

Therefore, from the above results, it is evident that the lamellar microstructure, which is often referred to in the literature as the fully transformed microstructure, is in fact unstable at high temperature. This is important because these alloys are intended for use at high temperatures (700-1000°C)[14], and if the microstructure used in a finished part is not stable, the properties of the material may change unfavorably during service.

A summary of the microstructural evolution in Ti-48Al type alloys is illustrated in Figure IV.A.7.17. On water quenching from single phase α, a massive microstructure is formed. If this structure is held isothermally, or if the material is slowly cooled from α, a lamellar structure forms. If this lamellar microstructure is held for longer times at high temperature, it will gradually transform to the stable microstructure, which is the equiaxed structure. These observations lead to the proposal of a new mechanism for the microstructural transformation of Ti-48Al alloys from single phase α, in which stacking faults play a major role:

$$\alpha \rightarrow \alpha_{faulted} \rightarrow \text{Lamellar}(\alpha + \gamma) \rightarrow \text{Equiaxed}(\gamma + \alpha)$$
$$\searrow \qquad\qquad \searrow$$
$$\text{Lam}(\alpha_2 + \gamma) \qquad\qquad \text{Eq}(\gamma + \alpha_2).$$

The α phase, upon cooling, would form a heavily faulted structure, and on these stacking faults, initially disordered γ phase would nucleate. Upon ordering, the γ phase would grow to form plates, thus forming the lamellar phase, which would experience ordering of the α phase upon cooling. If the lamellar structure is not cooled from high temperature but instead held there, the equiaxed structure is formed.

IV.A.7.5 PROPOSED FUTURE WORK

1. Examine properties at high temperature of materials composed of 100% lamellar, 50% equiaxed, and 100% equiaxed microstructures.

2. Study in more detail the transformation mechanism involving speroidization.

3. Determine the volume percent α phase in various alloys held isothermally, in order to compare experimental values to the phase diagram, via an atom probe study. This study involves measuring oxygen contents in the α and γ phases, and calculating the volume fraction of α from these values and the known overall oxygen content, as described by Denquin et al.[15] This study will also investigate the segregation of alloying elements in the two phases during transformation.

4. Study high temperature deformation, flow curves, recrystallization, and grain coarsening behavior in α and $\alpha + \gamma$ fields. Also, study the kinetics of transformation as influenced by driving and pinning forces.

5. Measure properties of selected thermomechanically refined microstructures.

IV.A.7.6 REFERENCES

1. H.A. Lipsitt, D. Shechtman, and R.E. Schafrik, **Met. Trans., 6A, (1975), pp. 1991-1996.**

2. M.J. Blackburn et al., **AWFL Technical Report No. AFML-TR-79-4056, (1979).**

3. Y.W. Kim, **Journal of Metals, 41, (July 1989), pp. 24-30.**

4. Y.W. Kim and D.M. Dimiduk, **Journal of Metals, 43, (August 1991), pp. 40-47.**

5. J.C. Beddoes, W. Wallace, and M.C. de Malherbe, **Materials & Manufacturing Processes, 7 (4), (1992), pp. 527-559.**

6. J.C. Chesnutt and J.C. Williams, **Metals and Materials, 6, (August 1990), pp. 509-511.**

7. S.C. Huang and E.L. Hall, **Met. Trans., 22A, (1991), pp. 427-439.**

8. Y.W. Kim, **Acta Met., 40, (1992), pp. 1121-1130.**

9. S.A. Jones and M.J. Kaufman, **Acta Met., 41, (1993), pp. 426-435.**

10. Y.W. Kim, **High Temperature Ordered Intermetallic Alloys IV**, L.A. Johnson, D.P. Pope, and J.O. Stiegler, eds., (MRS, Pittsburgh, PA, 1991), pp. 777-794.

11. P. Wang, G.B. Viswanathan, and V.K. Vasudevan, **Met. Trans., 23A, (1992), pp. 690-697.**

12. M.J. Blackburn, **The Science, Technology, and Application of Titanium**, R.I. Jaffee and N.E. Promisel, eds., (Plenum Press, New York, 1970), Vol.3, pp. 633-643.

13. Y.W. Kim, **Microstructure/Mechanical Property Relationships in Titanium Aluminides and Alloys**, Y.W. Kim and R.R. Boyer, eds., (TMS, Warrendale, PA, 1991), pp. 91-103.

14. J.M. Larsen et al., **High Temperature Aluminides and Intermetallics**, S.H. Whang et al., eds., (TMS, Warrendale, PA, 1990), pp. 521-555.

15. A. Denquin et al, **Scripta Met., 28 (9), (1993), pp. 1131-1136.**

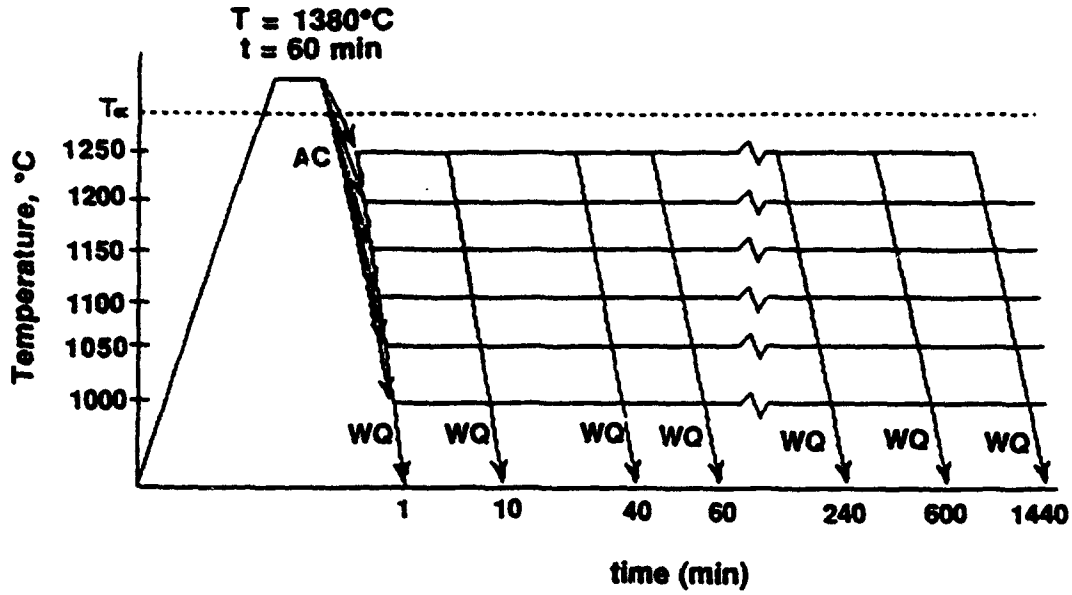

Figure IV.A.7.1 Schematic diagram of isothermal heat treatments.

Figure IV.A.7.2 Optical micrograph of lamellar structure obtained via air cooling from α, and also when Ti-45Al-2Mn-2Mn-2Nb is water quenched from α.

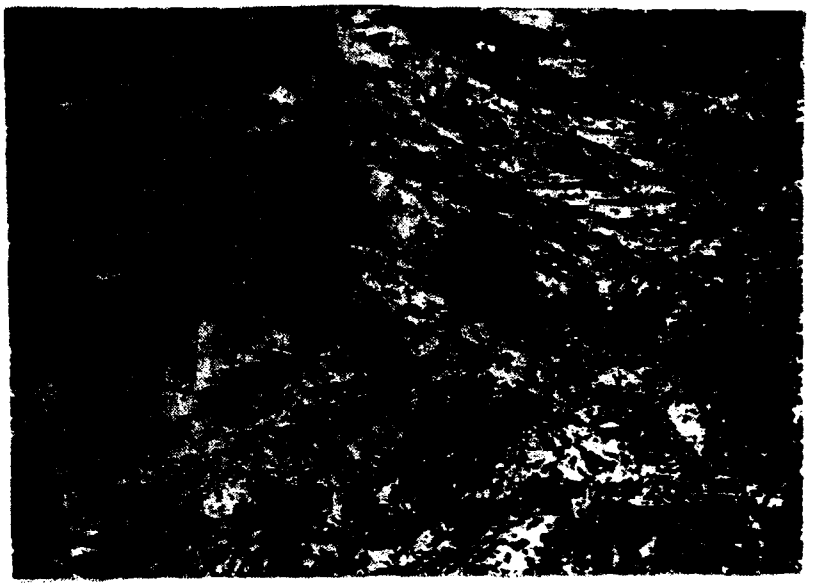

Figure IV.A.7.3 Massively transformed α, formed in Ti-49Al and Ti-48Al-2Mn-2Nb water quenched from α.

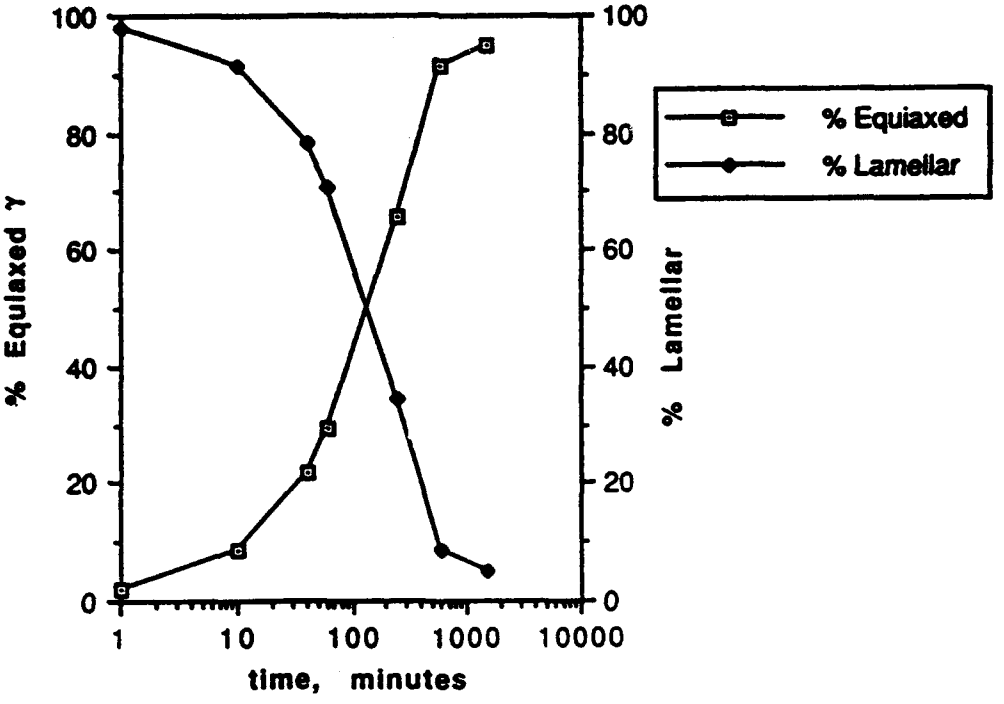

Figure IV.A.7.4 Microstructural transformation kinetics of Ti-49Al heated 1380°C, 1 hr, AC 1150°C, and held up to 24 hrs.

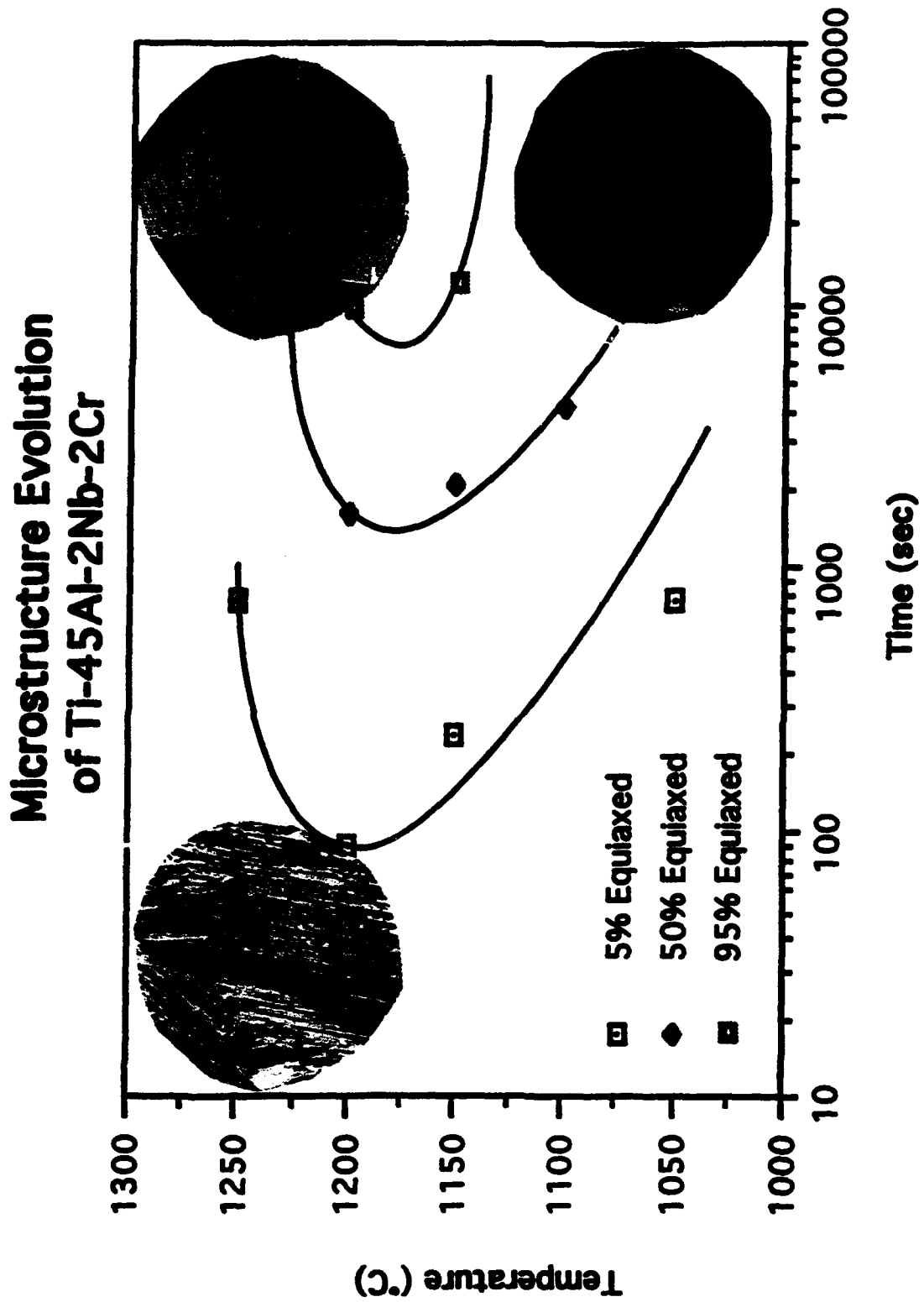

Figure IV.A.7.5 TTT diagram for Ti-45Al-2Cr-2Nb alloy, with representative micrographs at stages in the transformation.

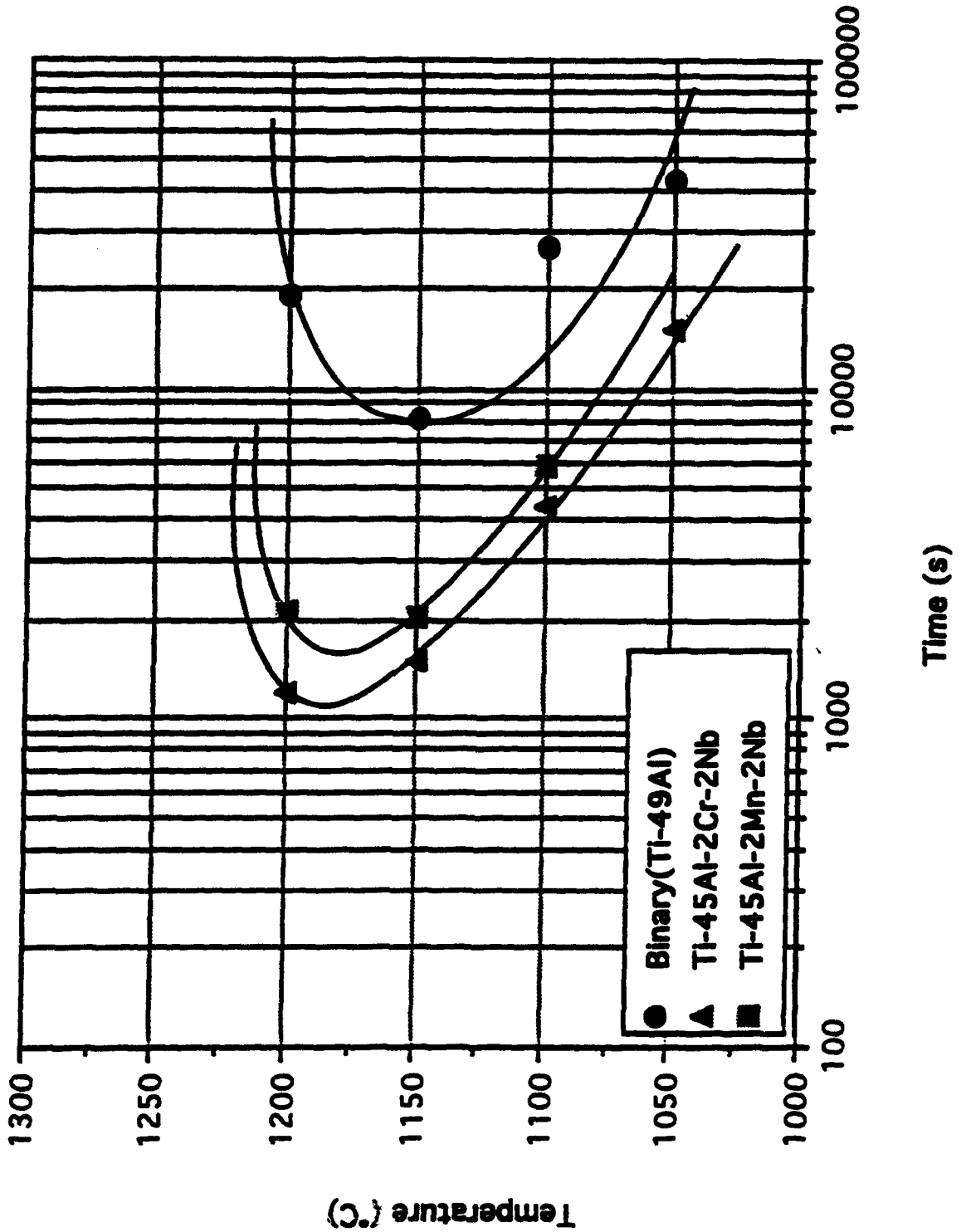

Figure IV.A.7.6 Partial TTT diagram showing 50% transformation curve Ti-49Al, Ti-45Al-2Cr-2Nb, and Ti-48Al-2Mn-2Nb.

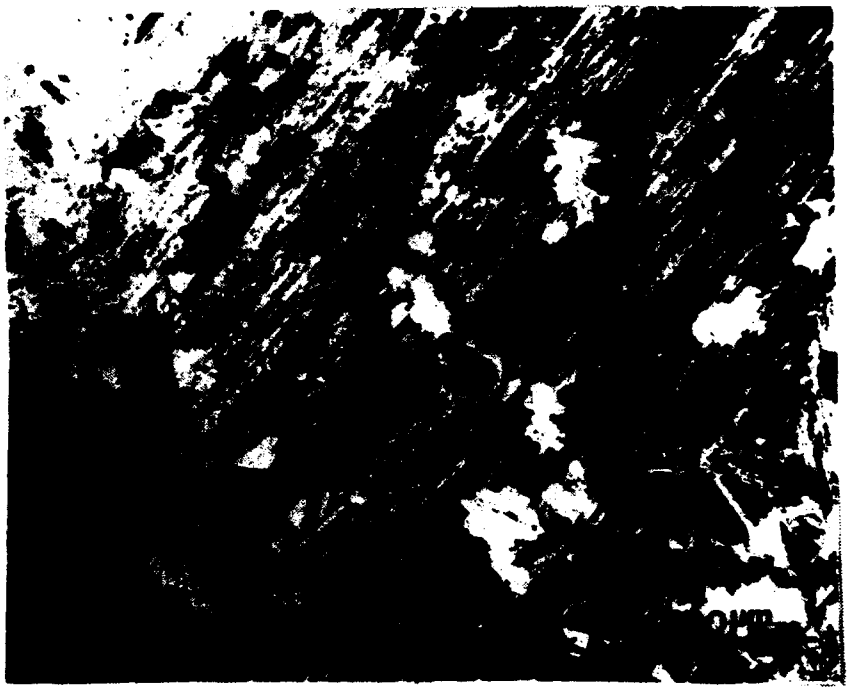

Figure IV.A.7.7 Ti-49Al heated at 1380°C for 1 hr, AC to 1100°C, held for 240 min., and WQ, showing growth of γ grains into the lamellar structure.

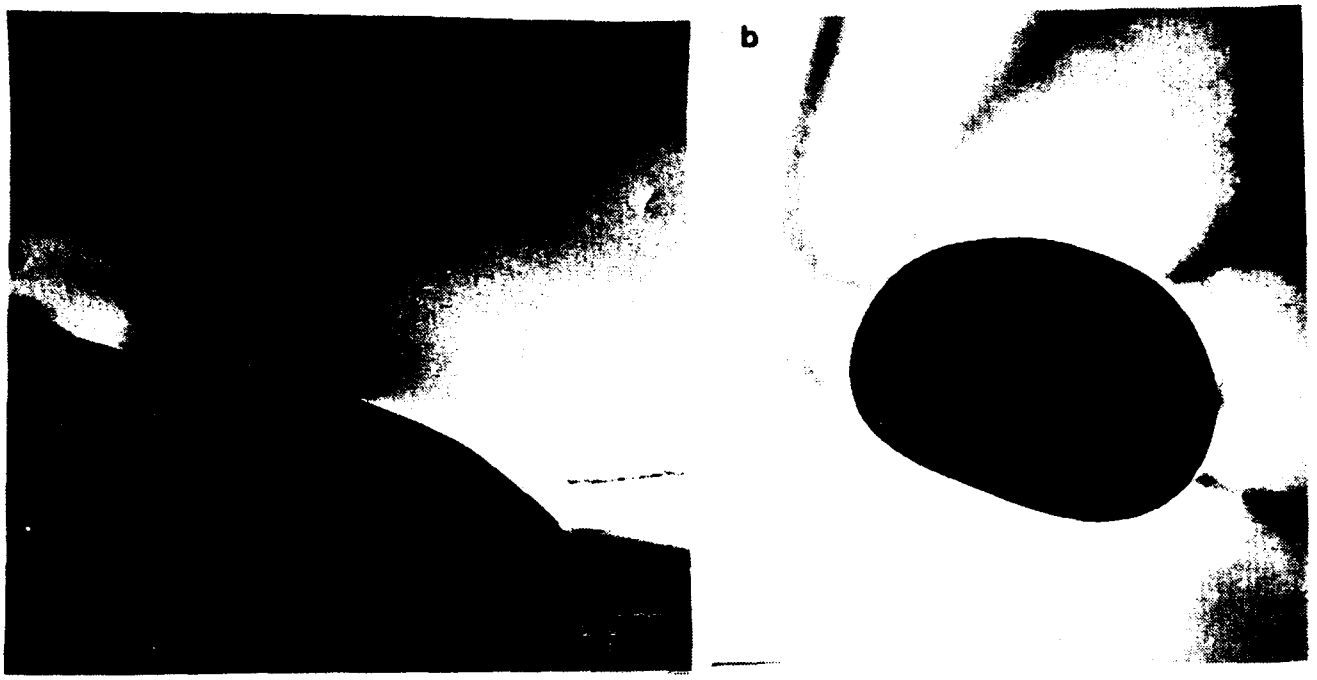

Figure IV.A.7.8(a,b) TEM micrograph of Ti-45Al-2Cr-2Nb heated at 1380°C for 1 hr., held at 1250°C for 24hr, and WQ, showing typical α particles.

Figure IV.A.7.9(a,b) Ti-49Al heated at 1380°C for 1 hr., AC to 1200°C, and held for a) 48 hr. and b) 72 hr.

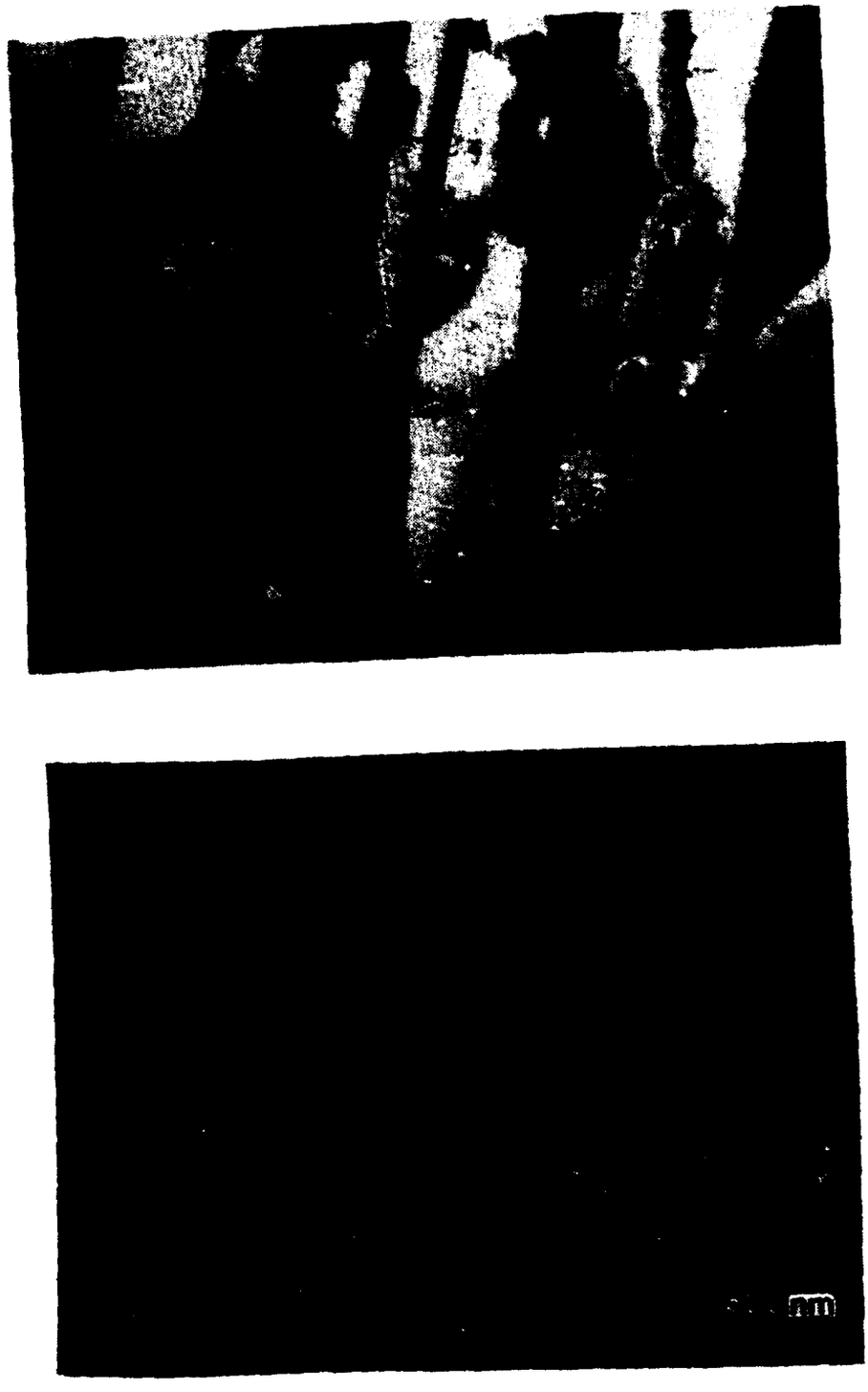

Figure IV.A.7.10 (a,b) TEM micrographs of Ti-49Al heated at 1380°C for 1 hr., held at 1250°C for 24 hrs. and WQ, showing: a) a γ subgrain boundary across adjacent lamellae, b) the necking of an α_2 lamella.

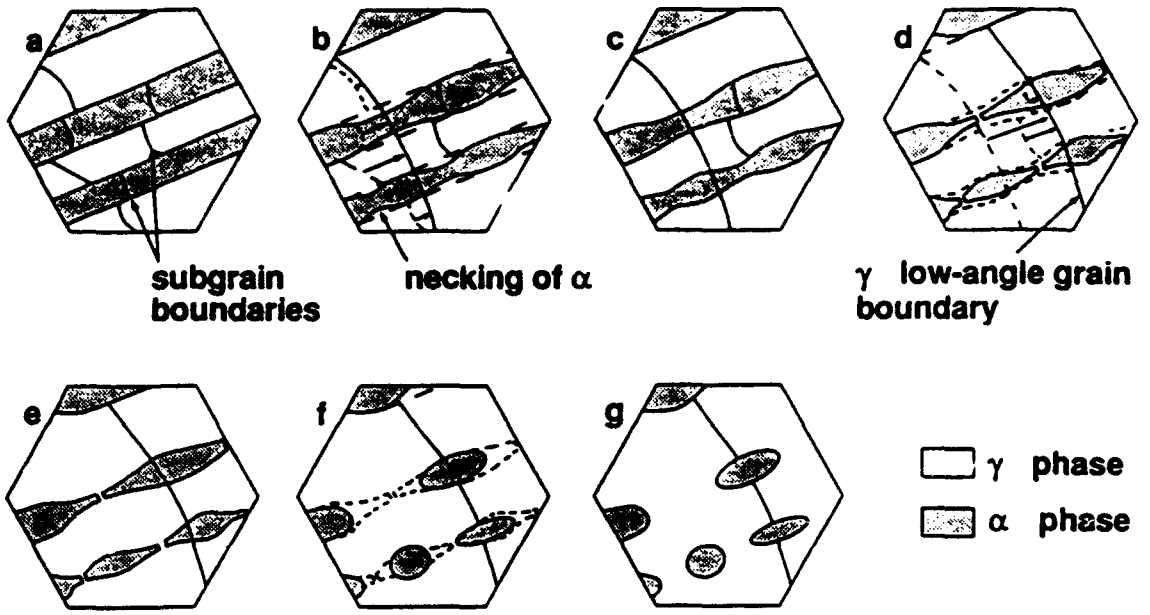

Figure IV.A.7.11 Proposed mechanism for the spheroidization process in the transformation from the fully lamellar to the equiaxed structure.

Figure IV.A.7.12 Ti-48Al-2Mn-2Nb heated at 1380°C for 1 hr., AC to 1250°C, held 48 hr., WQ.

Figure IV.A.7.13 (a,b) Ti-48Al-2Mn-2Nb optical micrographs showing retained massive microstructure. a) heated at 1380°C for 1 hr., AC to 1000°C, held 48 hr., WQ.

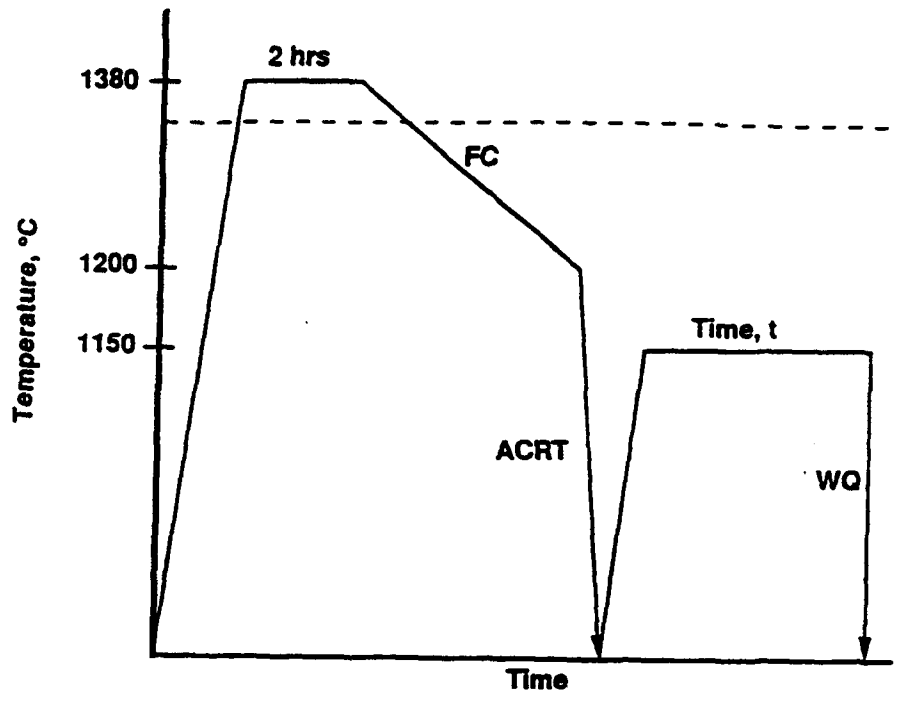

Figure IV.A.7.14 Schematic diagram of heat treatments to test stability of lamellar microstructure upon reheating.

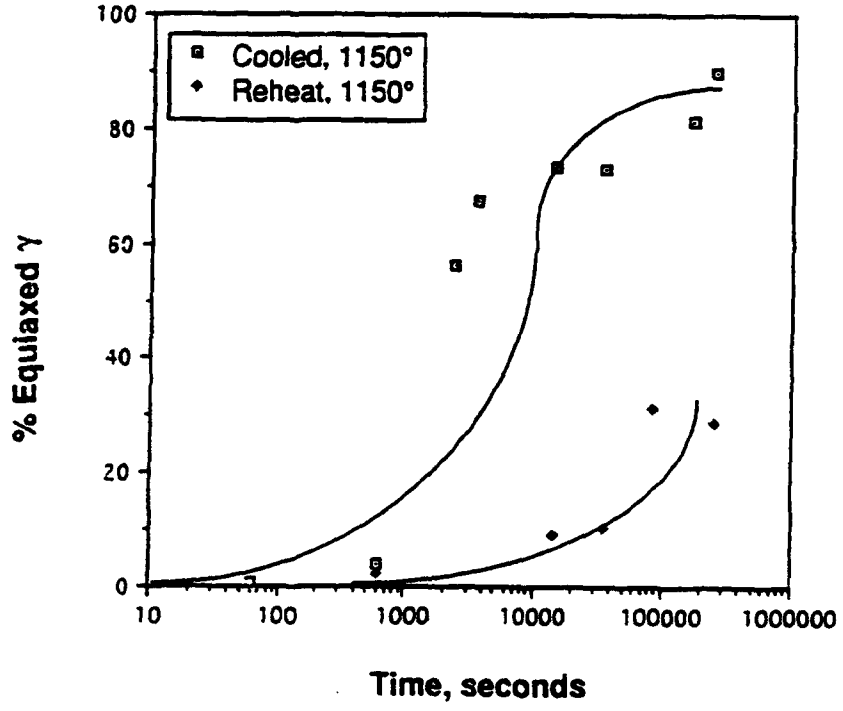

Figure IV.A.7.15 Comparison of lamellar to equiaxed transformations for reheated from RT and cooled from α Ti-48Al-2Mn-2Nb samples held at 1150°C.

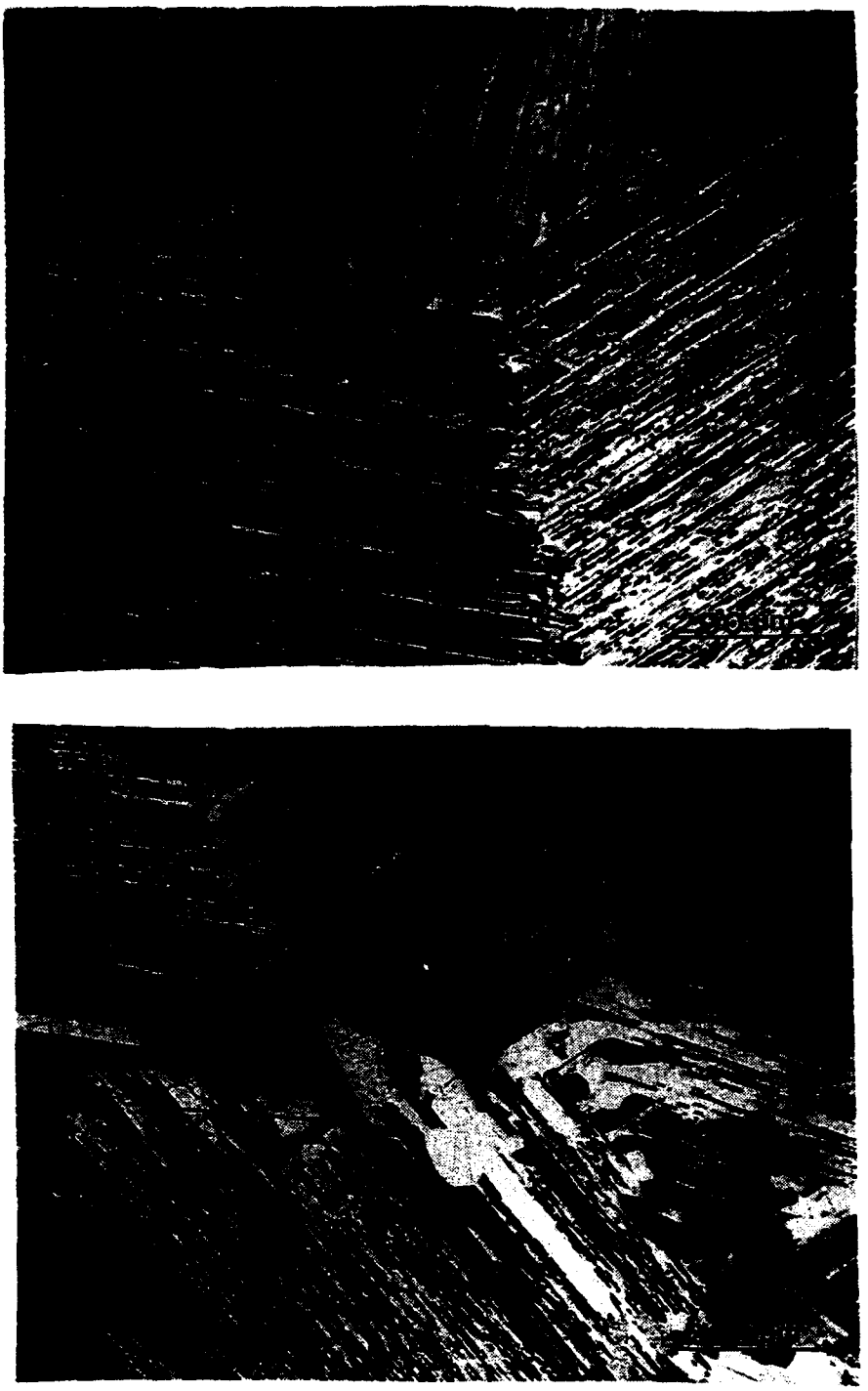

Figure IV.A.7.16 (a,b) Ti-48Al-2Mn-2Nb optical micrographs showing a) heated at 1380°C for 2 hr., FC to 1200°C, ACRT to obtain fully lamellar microstructure b) fully lamellar microstructure which was reheated to 1150°C and held for 4 hrs.

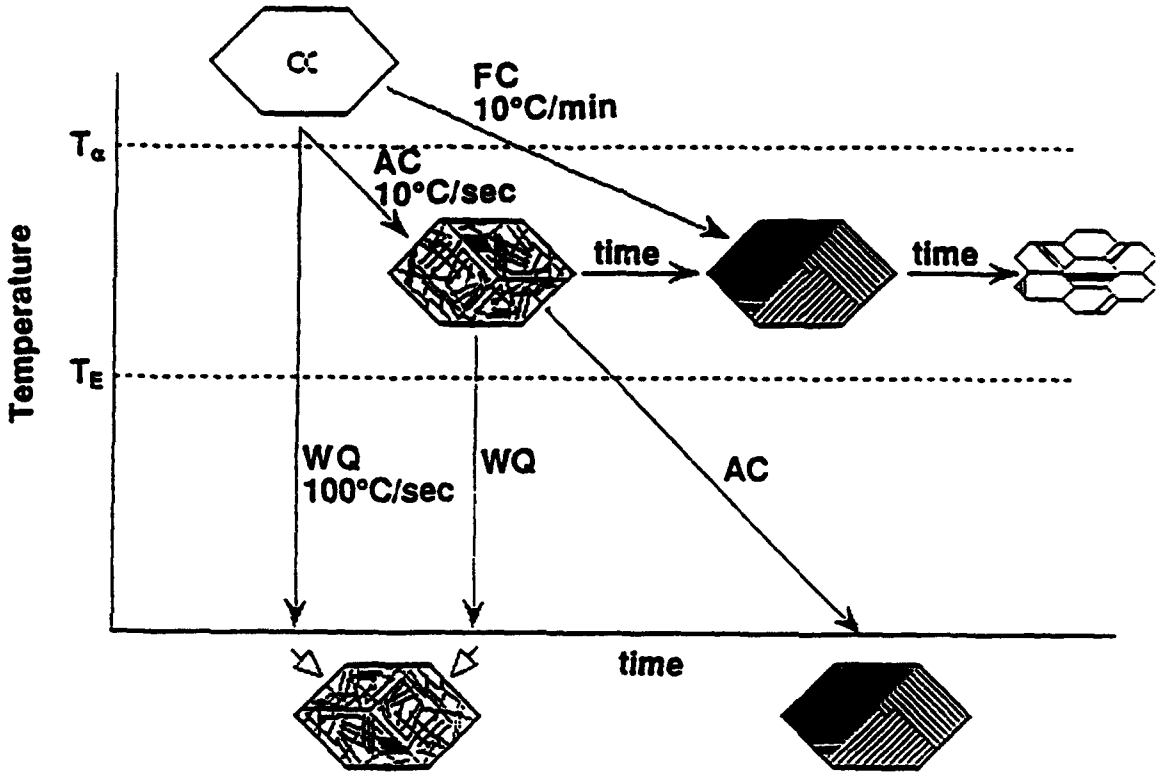

Figure IV.A.7.17 Schematic diagram of microstrctural evolution for Ti-48Al type alloys.

IV.A.8 Modelling and Simulation of Rubber Toughened Polymers and Polymer Coatings

Principal Investigator:	Professor Anna C. Balazs Materials Science and Engineering Department University of Pittsburgh
Other Faculty Participants:	Professor David Jasnow Department of Physics University of Pittsburgh
Students:	Dr. T.A. Issaevitch Dr. W. Li Dr. D. Gersappe Dr. C. Yeung Mr. P.K. Harm Mr. D.J. Irvine Mr. M. Fasolka

IV.A.8.1 INTRODUCTION

The focus of the first year of our research was to combine microscopic and macroscopic modeling and simulation to determine the material parameters necessary to achieve desired mechanical properties in toughened polymers. In particular, we were interested in rubber toughened thermoplastics and thermosets, though the techniques developed may be applied to other systems as well.

Our objective has been to develop a unified microscopic and macroscopic description of rubber toughened polymers that allows accurate quantitative predictions and the exploration of parameter values not yet accessible to experimental study. To this end, we have been developing two simulation programs, one microscopic, the other macroscopic. The two approaches are related since the results of the microscopic program are used as input to the macroscopic program.

The prior year's work and accomplishments have been detailed in the progress report of that effort. In brief, the following areas were addressed:

Our program to predict the mechanical properties of rubber toughened materials entails the combined study of complementary macroscopic and microscopic models with the latter to be used as input into the former:

The microscopic theory:

- Models the polymer matrix on the individual chain level.
- Allows one to control the statistical properties of the randomly distributed polymers.
- Will be used to study the adhesion and mechanical response of the polymer-rubber interface.

The macroscopic theory

- Models the polymer as an inhomogeneous continuum.
- Calculates local stress field dynamics and simulates craze evolution.
- Exactly reduces the three dimensional problem to an effective two-dimensional problem with commensurate savings in computer time.

The goal of the second year of our research was to use theoretical models and computer simulations to design polymer coatings that can protect and enhance the strength of the underlying substrate.

IV.A.8.2 ACCOMPLISHMENTS OF THE SECOND YEAR

In order to design such protective and strength-enhancing coatings, we must first understand the fundamental aspects of polymer-surface adsorption. With this aim in mind, we investigated the adsorption of copolymers onto a regular, patterned surface [1]. The copolymers contain sites that are capable of sticking to the surface ("stickers") and other sites that do not bind to the substrate. In a typical adsorbed conformation, the chains will attach to the surface at $L+1$ points, forming L loops and two tails. We studied the transition from infinite to finite-sized loops as a function of sticking energy, E, sticker concentration, C, and surface lattice constant, m. Three cases were studied in the limit of infinite chain length: finite substrates, infinite one-dimensional substrates, and infinite two-dimension substrates. In the first, case we found that there is a first order transition from infinite to finite loop sizes, and there exists a range of average loop sizes that is inaccessible. In the second and third cases, no such gap exists, and the transition is continuous.

The above results provide design criteria for tailoring copolymers that will bind to the surface and form large loops or a thick protective layer on the underlying surface. (The surface itself can be another polymeric material or some other substrate.) The work was also important in enhancing the collaboration

between members of the Materials Science Department and the Physics Department (Prof. David Jasnow.)

Another method of coating a substrate is to graft polymer chains onto the surface. Such grafted chains are referred to as polymer "brushes". We examined a model of polymer brushes in which polymers are grafted onto a flat surface at one end, and strongly interacting end-groups are attached on the free ends [2,3]. We showed that in the region where the attraction between the end-groups is strong and the chains are sufficiently long, the system undergoes a microphase separation, and the end-groups form microdomains of aggregates. Thus, by tailoring the interactions among the end-groups and the chain length, we can obtain polymer brushes with a variety of lateral structures. Furthermore, the attraction between the end-groups causes these sites to be "pulled up" and all lie within a narrow range of heights above the surface. Thus, the ends are now well exposed (not buried within the brush) and lie near or at the top of the layer. Consequently, they can readily react with a subsequent coating, which in turn can provide additional protection of the surface.

Our extended goal is to develop theoretical model and computer simulations to design copolymers that enhance the strength of polymer composites and thereby, facilitate the fabrication of tough polymeric materials. Very few polymer mixtures form a homogeneous, miscible phase. Instead, the polymers phase separate, forming distinct domains. In order to enhance the structural integrity and mechanical properties of these materials, a third polymer component or "compatibilizer" is added to the mixture. The compatibilizers sit at the interface between the immiscible polymers and act to "stitch" the phases together. Comb copolymers (polymers that contain a backbone and sidechains that emanate from the backbone) are commonly used as compatibilizers in large-scale industrial processes. Despite their commercial importance, very few fundamental studies have been undertaken to determine the comb architectures that would provide the optimal compatibilizing activity.

Our specific goal is to determine the properties of comb copolymers at penetrable or polymer/polymer interfaces using Monte Carlo simulations and self-consistent field lattice calculations.

The results of these above studies will indicate how to tailor the molecular architecture of the comb in order to:

> Modify the mechanical properties of polymer composites
> Fabricate toughening additives
> Produce high-strength materials

IV.A.8.3 PUBLICATIONS

1. Issaevitch, T.A., Jasnow, D., and Balazs, A.C., "Copolymer Adsorption onto Regular Surfaces", *J. Chem. Phys.* **99** (1993) 8244.

2. Li, W., and Balazs, A.C., "Cluster Formation in Grafted Polymers with Interactive End-Groups", *Molecular Simulations*, in press (an invited paper in a special issue devoted to simulations of polymer systems).

3. Li, W., and Balazs, A.C., "Cluster Formation in Grafted Polymers with Interactive End-Groups", Proceedings of the American Chemical Society, Division of Polymer Materials Science and Engineering Division, August 1993 Meeting, Chicago, IL.

IV.A.9 Interfacial Instability in Extrusion Processing of Polymer Blends

Principal Investigator: Professor J.T. Lindt
Department of Materials Science
and Engineering
University of Pittsburgh

Students: Mr. Ben Lander

IV.A.9.1 INTRODUCTION

Polymer alloys and blends constitute more than 30% of the commercial polymers market, and with the constant annual growth of some 9% (four-fold of the growth rate of plastics as a whole) their role is but to increase. Polymer blending is used mainly to improve mechanical properties of the matrix materials. It is expected that in the future, electrically, magnetically, and optically active polymeric blends will also become important.

In the past decade a number of high performance polymeric materials have been developed, such as polyphenyleneether (PPE), polyetheretherketone (PEEK), polyethersulfone (PES), and polyetherimide (PEI), known for their chemical and thermal stability. Blends of liquid crystal polymers (LCP) have received particular attention. Numerous attempts have been made to optimize the mechanical properties of these materials by blending them with other compatible or incompatible polymers. In high performance polymer based composites, optimized blends are used as the matrix materials. Such polymer based composites have found usage in a variety of DOD applications.

The existing blending technologies include mechanical mixing, dissolution in co-solvent followed by film casting, freeze/spray drying, latex blending, fine powder mixing and diverse inter-penetrating networks (IPN) based technologies. For economic reasons, the preparation of polymer blends by mechanical blending predominates.

The blend morphology depends on the thermodynamics and processing history. The choice of blend ingredients, their composition and spatial arrangement of the phases (morphology) determine the target blend properties. This work includes the final stages of mechanical blending in which the lamellar structures resulting from the initial melting and deformation of the initially macroscopically segregated polymer mixtures become unstable. These instabilities and the subsequent surface tension driven break-up control the transition to a dispersed droplet morphology that, in turn, control the mechanical properties of a given blend.

IV.A.9.2 OBJECTIVES

This work centers around the following aspects of the blending process:

i. The mixing environment that imposes the necessary deformation on the polymer articles including the simultaneous transition from the solid to the molten state and the deformation of the polymer particles. This necessitates the simultaneous analysis of melting and viscous flow.

ii. The onset of stratified two component flow. The kinematics resulting from (i) of the flow field is used to establish its effect on the topology of the planar lamellar structure formed.

iii. The onset of unstable flow. Mathematical stability analysis is performed to obtain solutions leading to predictions of domain size and the break-up time distributions.

IV.A.9.3 ACCOMPLISHMENTS AND SIGNIFICANCE

The overall strategy underlying this effort is illustrated in Figure IV.A.9.1. Within this scheme the following has been accomplished:

1. development of the interfacial tension measurement method using the breaking thread method; interfacial tension has been obtained for the polystyrene/nylon, polystyrene/ linear low density polyethylene, polycarbonate/ nylon, and polyetherimide/ polyether sulfone blend systems.

2. the extension of the breaking thread method to study the effects of interaction of neighboring threads on the kinetics of thread break-up and resulting morphology in the nylon/ polystyrene and the polyetherimide/ polyether sulfone blend systems.

3. selected theories have been examined dealing with the onset of instability in lamellar creeping two phase flows.

A. Instability Analysis

In the final stages of the blending process the lamellar structures resulting from the initial melting and deformation become continuously thinner and ultimately the interfaces between phases become unstable. These instabilities and the subsequent surface tension driven break-up controls the transition to a dispersed droplet morphology.

The stability of liquid threads in a liquid matrix stems from the work of Lord Rayleigh [1] who in 1879 developed a theory for the growth of instabilities in Newtonian liquid jets passing through air. Tomotika extended Rayleigh's theory to the instabilities present in a quiescent system consisting of a Newtonian liquid cylinder in a Newtonian liquid matrix. Expressions were found to describe the growth rate of disturbances and the dominant disturbance wavelength. Tomotika's work has become the basis for the study and modeling of thread break-up in polymer blend systems. Tomotika theory has been successfully used in measurement of polymer-polymer surface tension by the breaking thread technique. An extension of this technique is applied here to determine the influence of neighboring threads on the kinetics of thread break-up in polymer blend systems.

The use of Tomotika theory to measure polymer-polymer interfacial tensions seems particularly attractive in light of the facts that Tomotika theory describes a dynamic process and is independent of density differences between the phases. Use of Tomotika theory to measure interfacial surface tension between polymers would eliminate the waiting of hours or even days for equilibrium and the necessity of acquiring the very accurate density data required of more conventional methods such as sessile or pendant drop techniques. The method was first proposed and studied by Chappelear [4] and used to measure the interfacial surface tension between Polystyrene (PS) and Poly-ethylene-terepthalate (PET), PS and Nylon 6 (PA-6), PET and low density poly-ethylene (LDPE), and LDPE and PA-6 systems. Elemans [6] used the method to measure interfacial surface tension between high density poly-ethylene (HDPE) and PS, PS and LDPE, Nylon and PS, and Nylon and HDPE systems. This group, within this project, has also used the breaking thread method to evaluate interfacial surface tension between Nylon 6 and PS, linear-low density poly-ethylene (LLDPE) and PS, Nylon 6 and bisphenol-a-poly-carbonate (PC), and poly-ether-imide (PEI) and poly-ether-sulfone (PSF). The interfacial tension results for the PA-6/PS, LLDPE/PS and PA-6/PC blend systems agree well with previous data found in the literature and have been reported in last year's final report [10]. This report will focus on the interfacial tension measurements made on the PEI/PSF system and the extension of the breaking thread technique to determine the influence of neighboring threads on the kinetics and morphology of break-up in the PA-6/PS and PEI/PSF blend systems.

In execution of the breaking thread experiment, films of the matrix material are first prepared by compression molding above the melt temperature of the material. The film thicknesses are generally between 150 and 300 microns thick. Threads of the dispersed constituent, 20 to 70 microns in diameter, are then pulled from a molten pellet placed on a hot plate. The films and threads are then dried under vacuum for 24 hours at 80 degrees C. The thread is then placed between two films on a glass slide with a cover glass and placed inside a Metler FP-2 hot stage held isothermally at the test temperature. The hot stage is placed on a

microscope equipped with a long working distance objective and a camera for photographing the thread. Photomicrographs are taken at time intervals as the break-up proceeds. From the photomicrographs the disturbance wavelength λ and the diameter of the thickest a and thinnest part of the thread b is measured as a function of time. The disturbance amplitude σ is then found. The relative amplitude $\ln(2\sigma/D_o)$ is then plotted against time and the growth rate q is found from the slope. The surface tension can then be calculated from Tomotika theory.

In using the breaking thread method to determine the influence of neighboring threads the above procedure is followed with two parallel threads placed in the matrix. The growth rates are measured and an apparent surface tension is calculated. By comparing the measured surface tension from single thread experiments to the apparent surface tension measured in the two thread experiments the effect of the neighboring threads on the kinetics of thread break-up can be measured.

B. Results on PA-6/PS

A measure of interfacial tension for the PA-6/PS system was determined through 12 single thread experiments. The mean interfacial surface tension of $\sigma =$ 0.018 N/m with a standard deviation $v = 0.00387$ was reported from these experiments [10]. A series of experiments, using two threads, was then performed at varying thread separation to determine the observed interfacial tension for each thread. A series of micro graphs taken during one such experiment is shown in Figure IV.A.9.2. The experimental temperature was 220°C. The time to complete thread break-up ranged from 60 seconds to 9 minutes depending on thread diameter. The apparent interfacial tensions measured in these experiments were plotted as dots against the dimension-less separation distance (distance / average thread diameter) in Figure IV.A.9.3. The measured interfacial tension from single thread experiments is plotted as a line between lines depicting one standard deviation (i.e., upper and lower limits). The apparent interfacial tensions observed in the two thread experiments are almost all within two standard deviations of the mean surface tension measured in the single thread experiments. Although the apparent surface tension seems to decrease with decreasing distance between threads, the correlation is too weak and the experimental scatter too large for any conclusions to be drawn. Figure IV.A.9.4 shows the final micrographs taken in three of these experiments arranged in order from the smallest separation to the largest. Here it can be clearly seen, that as the separation distance decreases the droplets arrange themselves so that the centers of the droplets of one thread are shifted one half wavelength in relation to the droplets of the other thread. This arrangement, presumably due to the interaction of stress fields associated with the disturbance growth, suggests that some interaction definitely occurs between the threads.

C. Results on Polyetherimide / Polysulfone

A series of experiments using a higher viscosity system (Polyetherimide/ Polysulfone) was then performed. A higher viscosity system was chosen to increase the distances over which stress fields would be dissipated and to lengthen the time of break-up to minimize experimental error. The experimental evaluation of the interfacial tension was performed with 5 experiments using single threads. An interfacial tension of 3.3×10^{-3} N/m is reported from these experiments with a standard deviation of 9.5×10^{-4} (N/m). A total of 6 two thread experiments were performed with the distance between the threads ranging between 100 and 500 microns. The temperature of the experiments was 320°C. The time to complete break-up in these experiments ranged from 2 minutes to 35 minutes. Thermal degradation is not believed to be significant in these measurements as these two polymers have been shown to be very thermally stable. The polysulfone macromolecule has been shown to be thermally stable below 400°C.[11] The poly(ether-imide) resin spent over two weeks in our viscometer at temperatures between (250°C and 310°C) without any significant degradation of viscosity. These experiments are summarized in Figure IV.A.9.5 where the apparent surface tension, as determined by the growth rate of the disturbances, is plotted against the dimension-less separation distance. It is readily apparent in Figure IV.A.9.5 that the apparent surface tensions are quite scattered about the measured surface tension and that no correlation exists between the kinetics of break-up and separation distance. The system however does exhibit the same effect of separation distance on final morphology as shown in the PS/PA-6 system. The droplets order as the separation distance decreases. This is shown in figure IV.A.9.6 where the droplets appear to be shifting 1/4 of a wavelength as the separation distance decreases. This seems to be indicating again an interaction between the stress fields of the two threads.

D. Instability Calculations

Polymer blend compounding occurs in the flow environment of a screw extruder where the contribution of the flow field to the stability of the interface must be considered. The onset of interfacial instabilities in flowing systems has been studied through the perturbation techniques of hydrodynamic stability analysis as developed by Yih [7,8]. In this work Yih's perturbation solutions of the Orr-Somerfeld equations of hydrodynamic stability, in the limit of low Reynolds number, have been generalized to include combined Poiseuille and Couette flows as present in screw extruders. Some preliminary calculations of the instability damping parameter are presented.

The simplified two-layer flow system considered here is shown in Figure IV.A.9.7. The fluids are assumed to be Newtonian and isothermal. The use of Newtonian fluids allows us to use Squires theorem [12] and reduce the problem of considering three dimensional disturbances to that of considering only two dimensional disturbances.

In the small Reynolds number analysis the eigen functions and eigen values are expanded around Re=0, corresponding to creeping flow as found in polymer blend extrusion. Solutions are then found for the zeroth order terms by ignoring all terms containing Re or higher orders of Re. This results in a system of linear equations which may be solved for a zeroth order approximation of the eigen functions and the stability parameter c_i . Negative values of the stability parameter imply that intefacial disturbances are damped in time and the interface is stable. Positive values of the stability parameter imply that the interfacial disturbances will be amplified in time resulting in an unstable interface. The first order approximation is then found in like fashion by ignoring all terms in the system containing Re^2 or higher orders of Re .

The equation system was derived using a Fortran code for computation on a desktop computer. The system is non-singular thus standard linear algebra techniques such as Gaussian elimination or L-U decomposition can be used to solve the system and arrive at a solution vector. Upon back substitution of the solution vector into the boundary conditions it was found that the solution accuracy was very poor especially at higher wave numbers. The matrix is ill conditioned especially at higher wave numbers. This is demonstrated in Figure IV.A.9.8 where the condition of the matrix is shown to deteriorate rapidly with increasing wave number.

IV.A.9.4 SUMMARY

The ultimate goal of this program is to develop predictive techniques relevant to the design of polymer blends with optimized mechanical properties. In keeping with commercial practice, the blend morphology development in initially macrosegregated incompatible polymeric mixtures subject to continuous shear/ elongation mixing in the molten state is the physical domain of this work. In this situation the blend components are first molten and brought into intimate contact while the state of segregation is rapidly decreased to the micron level by intense shearing. Simultaneously with the reduction in thickness of the domains of the minor component, interfacial instabilities develop leading ultimately to the break-up of the minor phase into a spectrum of distributed globules that constitute the final blend morphology. In summation the mechanical properties of the blend are strongly affected by the interactions between the kinetics of the deformation process and the interfacial tension introduced instabilities.

In the second year of the program we have used the breaking thread method, verified during the first year of the program to measure interfacial tension in a high performance polymer blend system, polyetherimide/ polyether sulfone. This method has also been extended to the situation of two neighboring threads to determine the effect of interactions between neighboring layers of the minor component on the morphology and kinetics of thread break-up. We have demonstrated that an interaction occurs between the stress fields of neighboring threads undergoing surface tension driven break-up. This interaction results in an

alignment of the Rayleigh wave crests so as to minimize their interaction. The effect of this interaction upon the kinetics of thread break-up is undetectable within the scatter of the experimental data.

Further, we have examined the theories of hydrodynamic stability theory using non-singular perturbation techniques applied to the equation governing interfacial stability. As polymer blend extrusion typically involves low Reynolds number flow ($Re \sim 10^{-6}$) the analysis has been applied to study solution in the limit Re approaches zero. A solution of the Orr-Somerfeld equation governing interfacial stability has been formulated using perturbation analysis techniques in the limit of small Reynolds numbers. Numerical solution of the resulting equation system for the instability parameter governing the amplification of interfacial instability has been inaccurate due to the ill conditioned nature of the system. Future work will focus on improving the accuracy of the solution through more sophisticated numerical techniques.

IV.A.9.5 REFERENCES

1. Lord Rayleigh, Proc. London Math. Soc., 10, 4, (1879).

2.. S. Tomotika, Proc. Royal Soc. London, A150, 322, (1935).

3. S. Tomotika, Proc. Phys. Math. Soc.Japan, 18, 550, (1936).

4. D.C. Chappelear, Polym. Prepr., 5, 363, (1964).

5. J. J. Elmendorp, Polym. Eng. Sci., 26, 418, (1986).

6. P.H.M. Elemans, J.M.H. Jassen, H.E.H. Meijer, J. Rheol., 34, 1311, (1990).

7. C.S. Yih, J. Fluid Mech., 2, 554, (1957).

8. C.S. Yih, J. FLuid Mech., 27, 337, (1967).

9. W. Kuhn, Kolloid Z., 132, 84, (1953).

10. B. Lander, J.T. Lindt, Morphology Development in Polymer Blends: Year end report to MRC, (1992).

11. Amoco Performance Products, "Udel Polysulfone Design Engineering Data" pg 13.

12. H.B. Squire, Proc. Royal Soc. London, A142, 621, (1933).

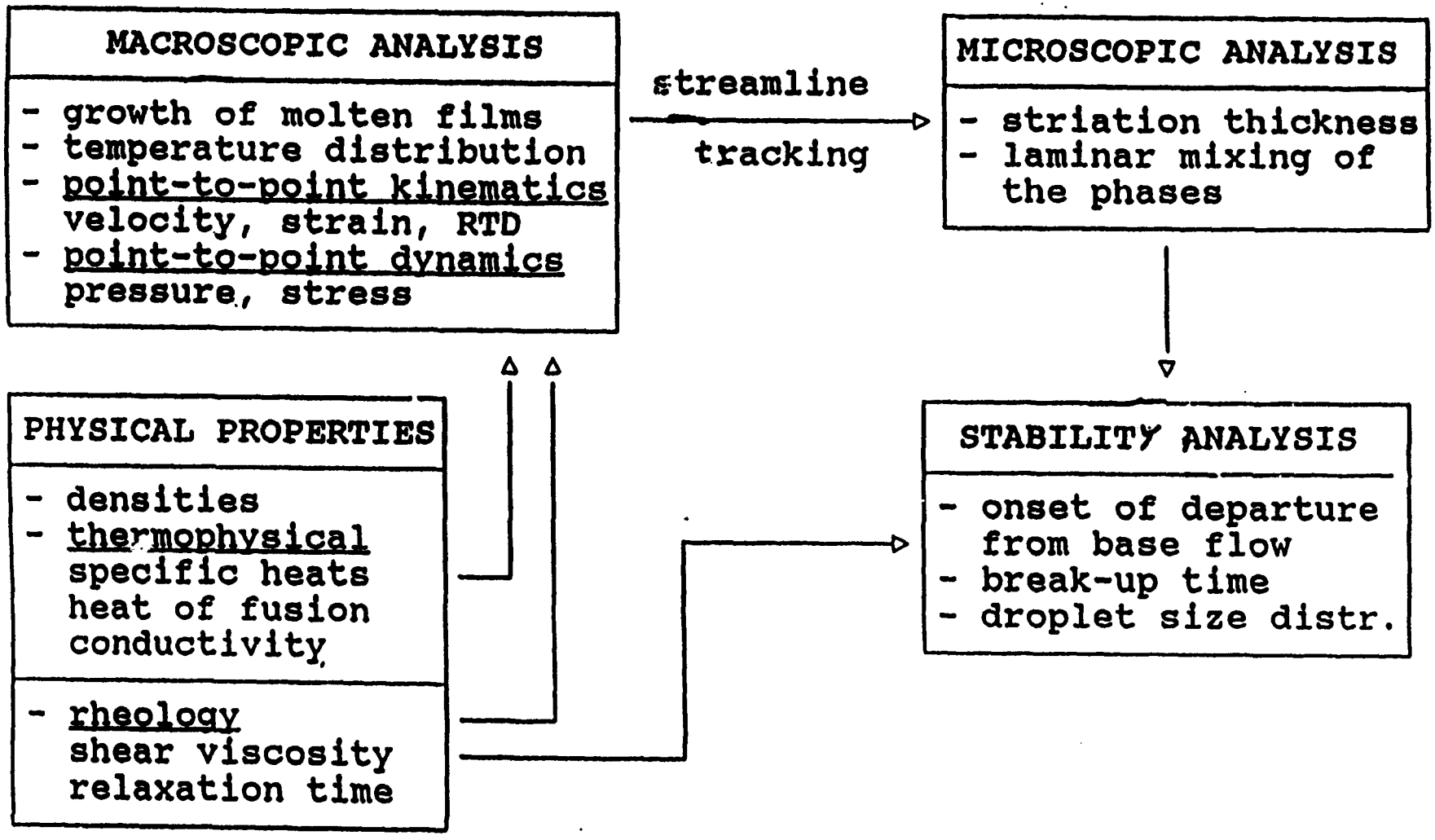

Figure IV.A.9.1 **BLEND MORPHOLOGY DEVELOPMENT IN SCREW EXTRUDERS DURING MELTING**

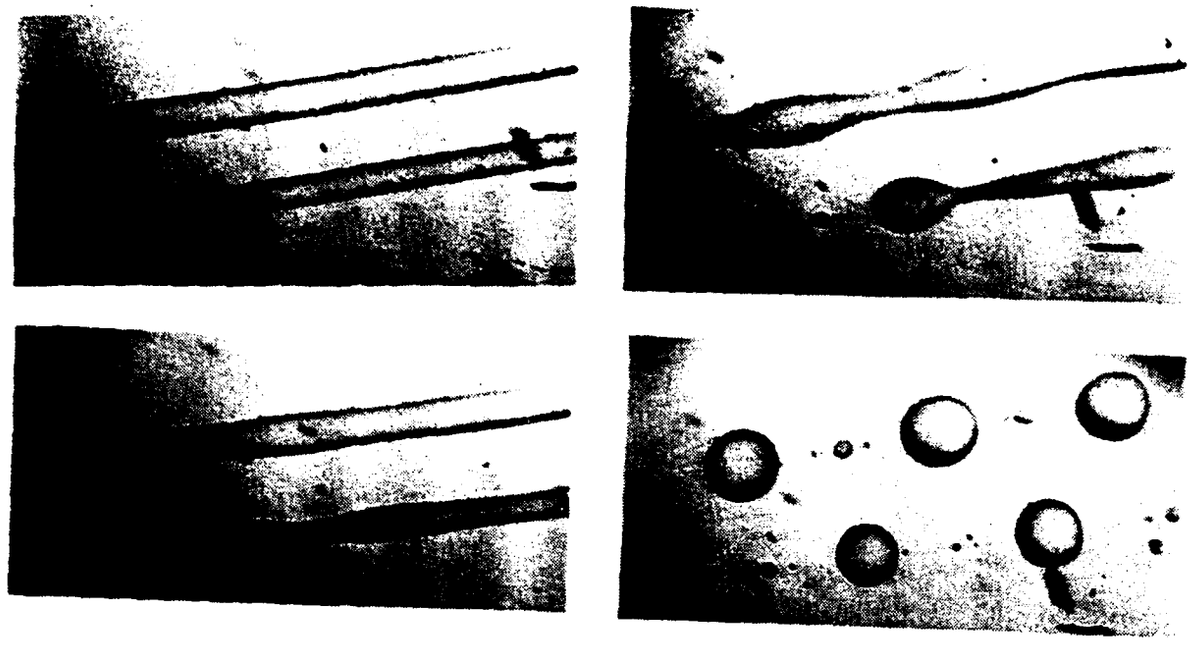

Figure IV.A.9.2 Two threads of PA-6 breaking up in a PS matrix at T = 227 C

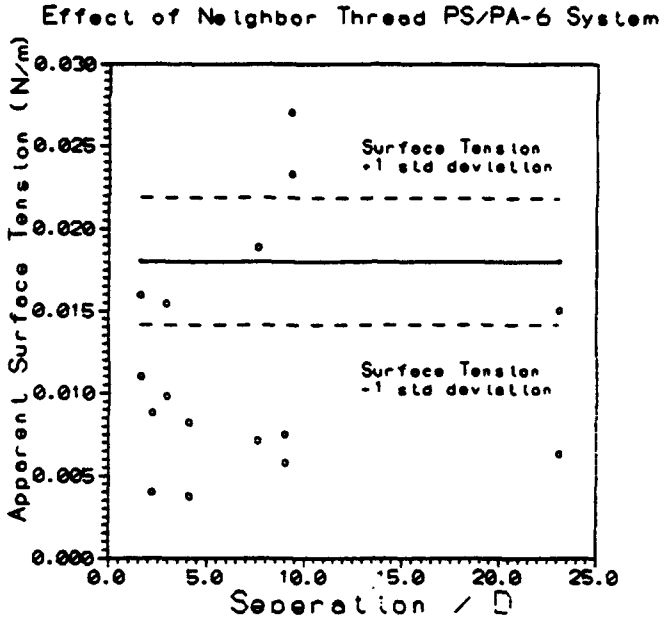

Figure IV.A.9.3 Apparent surface tension vs. relative separation distance PS/PA-6 two thread experiments.

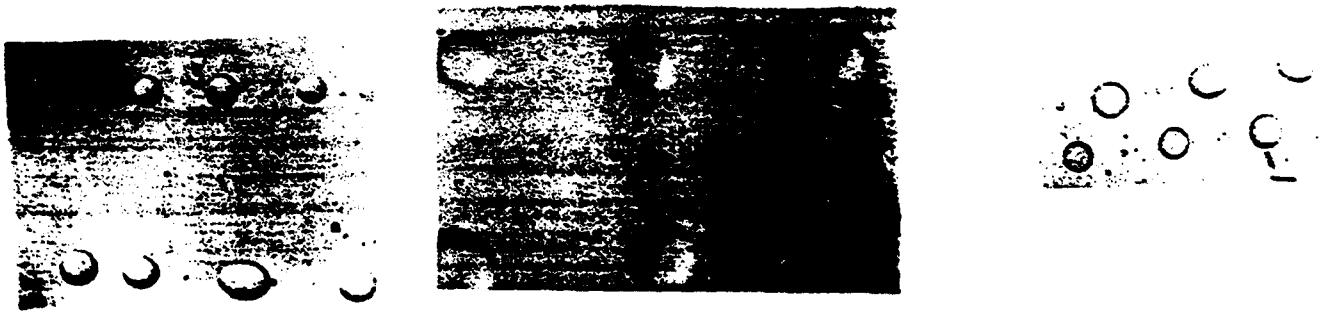

Figure IV.A.9.4 Effect of separation distance on final morphology in PS/PA-6 system.

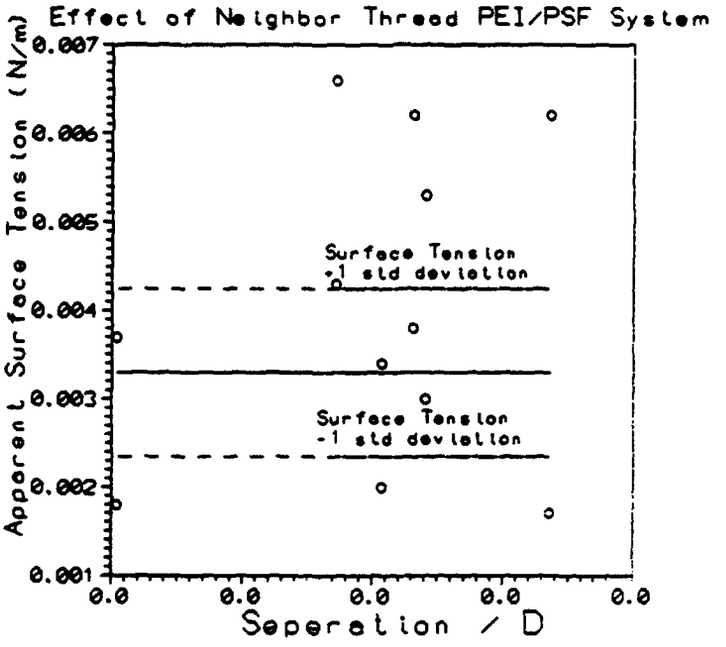

Figure IV.A.9.5 Apparent surface tension vs. relative separation distance. PSF/PEI two thread experiments.

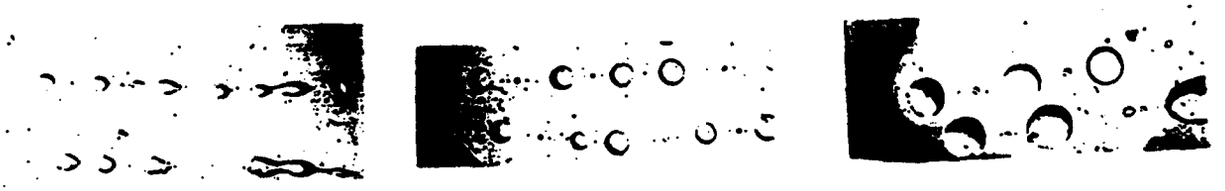

Figure IV.A.9.6 Effect of separation distance on final morphology PSF/PEI system.

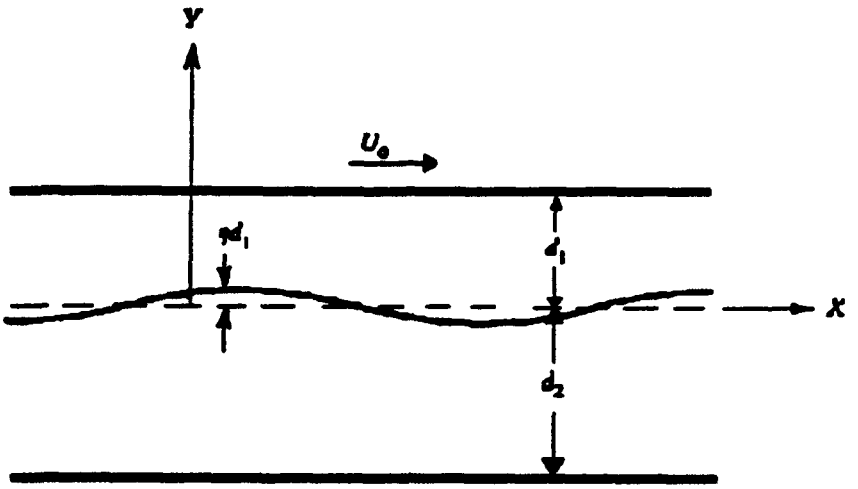

Figure IV.A.9.7 Definition sketch:two layer flow.

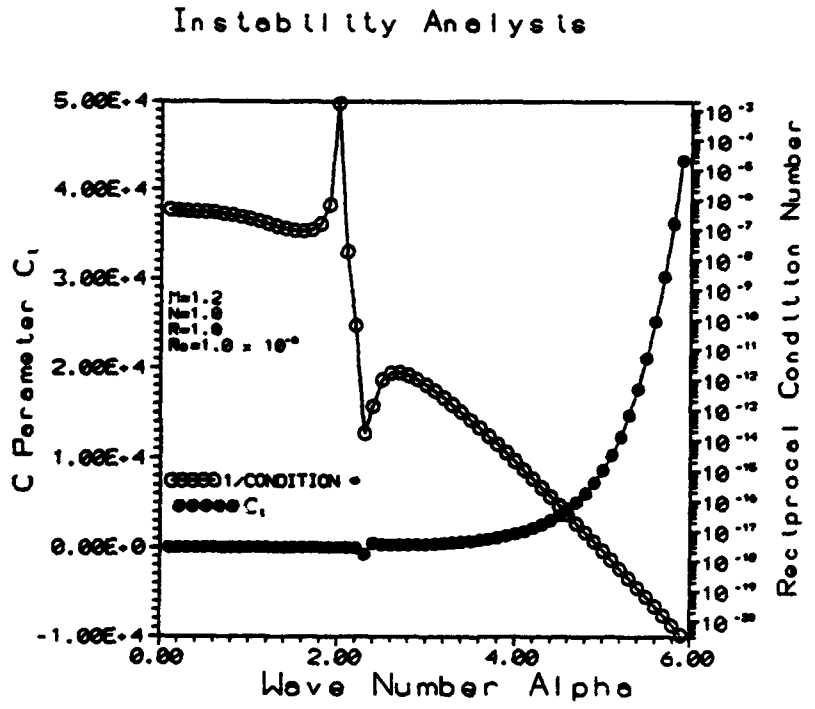

Figure IV.A.9.8 Plot of stability parameter C_i and reciprocal condition number for the solution for a two layer pressure flow.

IV.B OPTOELECTRONICS

IV.B.1 Development of Submicron Periodicities for Optical Diffraction Devices

Principal Investigator:	Professor Sanford A. Asher Department of Chemistry University of Pittsburgh
Other Faculty Participant:	Professor Rob Coalson Department of Chemistry University of Pittsburgh
Students:	Dr. Sesh Jagannathan Dr. Song-yuan Chang Mr. Guisheng Pan

IV.B.1.1 INTRODUCTION

We recently created a new optical-filtering device fabricated through the self-assembly of colloidal spherical particles. These spherical particles self-assemble in solution into a cubic crystalline array with a lattice spacing comparable to visible light (Fig.IV.B.1.1). Intense Bragg diffraction from the array prevents transmission (T) of light meeting the Bragg diffraction condition ($T < 10^{-6}$). Thin films of these arrays diffract light throughout the UV, visible and IR spectral regions with high rejection efficiencies within a well defined rejection band, and with high transmission off this band.

We developed fabrication techniques to prepare solid Bragg diffraction devices and have developed new materials for construction of nonlinear and wavelength-agile Bragg diffraction devices. The devices have been created from ca 100 nm highly charged monodisperse polymer and inorganic spheres synthesized using new methods which attach greater than 25,000 sulfonate groups to the sphere surfaces. The sulfonates ionize in solution; the spheres become highly charged and repel one another. This electrostatic repulsion is responsible for the self-assembly of the spherical particles in the cubic array; this is the minimum energy configuration of the system.

IV.B.1.2 OBJECTIVES

The objective of this work has been to develop new materials with submicron periodicities which will be used to create new devices in the field of optics and spectroscopy. We will create the submicron periodicities by utilizing self-assembly processes in monodisperse charged colloids; the charged colloids self-assemble in solution to form BCC or FCC crystalline arrays. We will rigidize the arrays by polymerizing the surrounding medium with substances with appropriate properties for the applications desired.

The colloidal sphere arrays Bragg diffract light in the "Dynamical Diffraction" regime. Thus, thin films of these arrays diffract essentially all light meeting the Bragg condition; the films will be fabricated as highly efficient optical rejection filters since they transmit less than 10^{-6} of the light meeting the Bragg condition, but freely transmit adjacent wavelengths.

The work focuses upon new optical materials with submicron periodicities which can be used for optical Bragg diffraction. The end use will include optical filters for laser eye protection and for coating of window and canopies to protect against laser threats. In addition, we will develop new fabrication strategies for creating submicron periodicities which will be of utility in other areas of technology such as preparation of semi-porous membranes. In addition, we will develop novel wavelength agile diffraction films in which the wavelengths diffracted can be easily and continuously altered. These devices will be useful for spectroscopic instrumentation and laser spectroscopy, in addition to being useful for laser eye protection.

IV.B.1.3 ACCOMPLISHMENTS AND SIGNIFICANCE

We have concentrated in this period on developing synthetic methods to create new monodisperse colloids with increased charge. We have developed a number of methods to prepare novel colloids from polymethylmethacrylate (PMMA), fluorinated methacrylates and SiO_2 colloids and SiO_2-CdS quantum dot composites and have developed methods to solidify these arrays:

A. Cystalline Colloidal Arrays Made of Low Refractive Index Highly Fluorinated Polymers

The purpose of the work is to devise a synthetic method to prepare monodisperse highly charged colloids of fluorinated polymers. We expect these colloids to have very small refractive indices and be easy to refractive index match for the nonlinear optical devices.

Figure IV.B.1.2 shows the molecular structures of the monomers used for the emulsion polymerization of the fluorinated colloids, while Figure IV.B.1.3 shows TEM micrographs of the resulting colloids and indicates that the particles are monodisperse and spherical (some damage is evident from the electron beam). Figure IV.B.1.4 shows a conductometric titration that indicates that approximately 900 charges reside on each sphere. Figure IV.B.1.5 shows a turbidity plot that shows the particle refractive index is 1.393.

We have successfully prepared crystalline colloidal arrays (CCA) from these spheres as illustrated in Figures IV.B.1.6 and IV.B.1.7 which show diffraction from these CCA.

B. Polymethylmethacrylate Colloidal Crystals for Passive and Active Optical Notch Filters

This work successfully developed synthetic techniques to synthesize monodisperse polymethylmethacrylate (PMMA) colloidal spheres of high charge which self-assemble into crystalline colloidal arrays (CCA). We also incorporated dye into these spheres and polymerized them into a gel using the techniques of Holtz et al. We chose PMMA because its refractive index of ca 1.5, which is much easier to refractive index match with the medium than are colloids prepared from polystyrene.

Figure IV.B.1.8 shows a preferred recipe we have developed to create highly charged PMMA spheres with covalently attached uniblue A dye, while Figure IV.B.1.9 shows the molecular structure of the monomers used. Figure IV.B.1.10 shows a TEM micrograph of these spheres. Although some damage occurs to the colloid due to the beam current, the spheres appear to be spherical and monodisperse in size.

These colloids are highly charged and can form highly ordered CCA; Figure IV.B.1.11 shows a transmission spectrum of the CCA prepared from the dyed PMMA sphere. The excellent ordering is evident from the high, narrow Bragg diffraction peak. We have polymerized these colloids into a hydrogel matrix schematically illustrated in Figure IV.B.1.12. Figure IV.B.1.13 illustrates the polymerizable monomers and recipes used while Figure IV.B.1.14 illustrates the impact of the polymerization on the Bragg diffraction peak.

Figure IV.B.1.15 illustrates that as the refractive index of the spheres is matched to the medium by the addition of MPSO the diffraction peak almost disappears. These dyed PMMA colloids should work well as the nonlinear elements in our thermally controlled nonlinear optical diffraction devices.

C. Polymerization of Crystalline Colloidal Arrays in Irreversible Hydrogels

The purpose of this work was to develop techniques to polymerize the CCA into a solid material containing submicron periodic structures. We have developed a motif for creating complex materials which can be tailored for use as smart materials. We polymerize the CCA initially into an elastic gel. We can then either directly utilize this gel or to further chemically alter the gel. For example, we can further rigidize it by adding additional species to be polymerized.

Figure IV.B.1.16 schematically illustrates our objective to polymerize the array by introducing polymerizable monomers into the medium surrounding the CCA spheres. Figure IV.B.1.17 illustrates the chemical structures of the polymerizable monomers used and of the UV photochemical free radical initiator, benzoin methyl ether.

Figure IV.B.1.18 shows the light diffraction properties of crystalline colloidal array prior to and after polymerization. The modest changes in the Bragg diffraction peak shows that the array ordering is maintained as the matrix polymerizes around the spheres.

D. Periodic Arrays of Nothing in Irreversible Hydrogel Networks

We have developed a novel material composed of ca 100 nm diameter spherical holes in a hydrogel membrane. This system was synthesized by polymerizing 100 nm SiO_2 spheres in a CCA array in a hydrogel. We then etched away the SiO_2 spheres with HF. The array of spherical voids diffract light well. We are examining applications of this material in separation science.

IV.B.1.4 SUMMARY

1. Development of novel general technique for synthesizing monodisperse SiO_2 spheres and SiO_2-CdS composites.

2. Development of new emulsion polymerization method for synthesizing monodisperse fluorinated colloids.

3. Developed method for synthesizing monodisperse highly charged PMMA colloids containing dyes.

4. Developed methods to polymerize arrays of these colloids in hydrogel arrays.

5. Characterized the diffraction properties in order to optimize the optical diffraction properties and the ruggedness of the gels.

6. Developed and published model for utility and prediction of phases of crystals.

7. Demonstrated and published results which show that nucleation of crystals occurs at dielectric surfaces.

8. Developed model that demonstrates that nucleation results from image charge effects.

Publications in Reviewed Journals:

"Melting of Colloidal Crystals: A Monte Carlo Study",
J. C. Zahorchak, R. Kesavamoorthy, R. D. Coalson, and S. A. Asher, J. Chem. Phys. 96, 6873-6879 (1992).

"Self-Assembly and Ordering of Electrostatically Stabilized Silica Suspensions",
R. Kesavamoorthy, S. Tandon, S. Xu, S. Jagannathan, and S. A. Asher, J. Coll. Int. Sci. 153, 188-198 (1992).

"A Self Assembly Motif for Creating Submicron Periodic Materials. Polymerized Crystalline Colloidal Arrays",
S. A. Asher, J. Holtz, L. Liu, and Z. Wu, J. Am. Chem. Soc., submitted (1994).

Patents:

S. A. Asher and S. Jagannathan, "Method of Making Solid Crystalline Narrow Band Radiation Filters", U.S. Patent Number 5,281,370.

We also filed patent applications for a "Method of Making an Optically Nonlinear Switched Optical Device and Related Devices" (serial number 07/999,487) and a "Method of Filtering Submicron Particles and Associated Product".

Crystalline Colloidal Arrays

1. Fabricated From Colloidal Particles

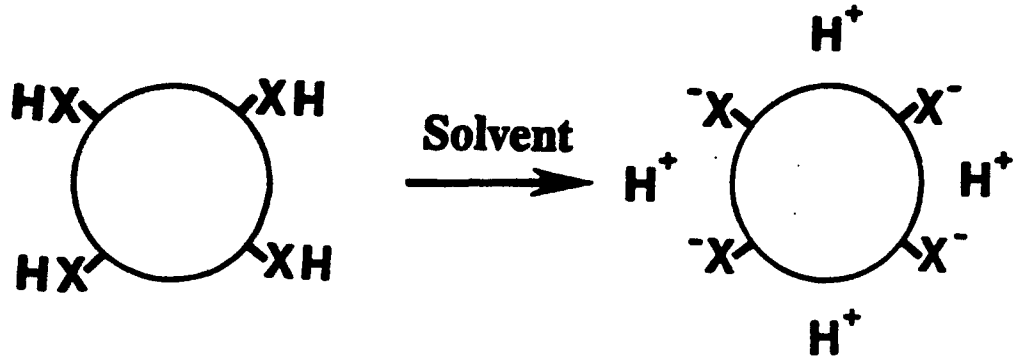

2. Particles Self Assemble Into 3-D Ordered Crystal Structure

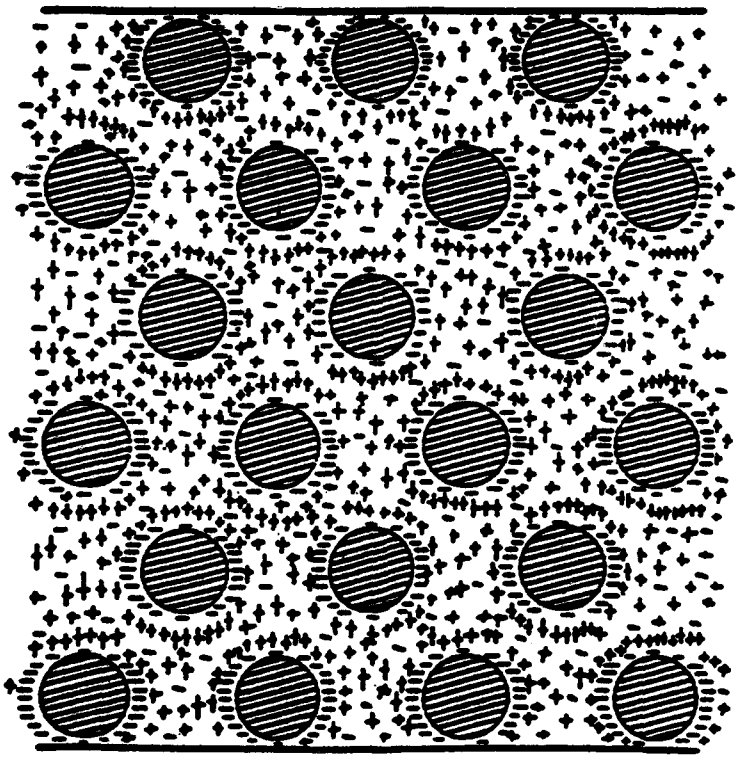

Figure IV.B.1.1

Free-Radical Emulsion Polymerization

Reagents	Abbreviated Names
$CH_2=C(CH_3)COOCH_2CF_2CF_2CF_3$	FBMA
$CH_2=C(CH_3)COOCH_2CH_2OOC(CH_3)=CH_2$	EGDMA
$CH_2=CHCH_2OCH_2CH(OH)CH_2SO_3Na$	COPS-1
$C_{12}H_{25}SO_4Na$	SDS
$Na_2S_2O_8$	
H_2O	

Reaction Temperature: 50 C

Reaction Time : 2.0 hrs

Figure IV.B.1.2

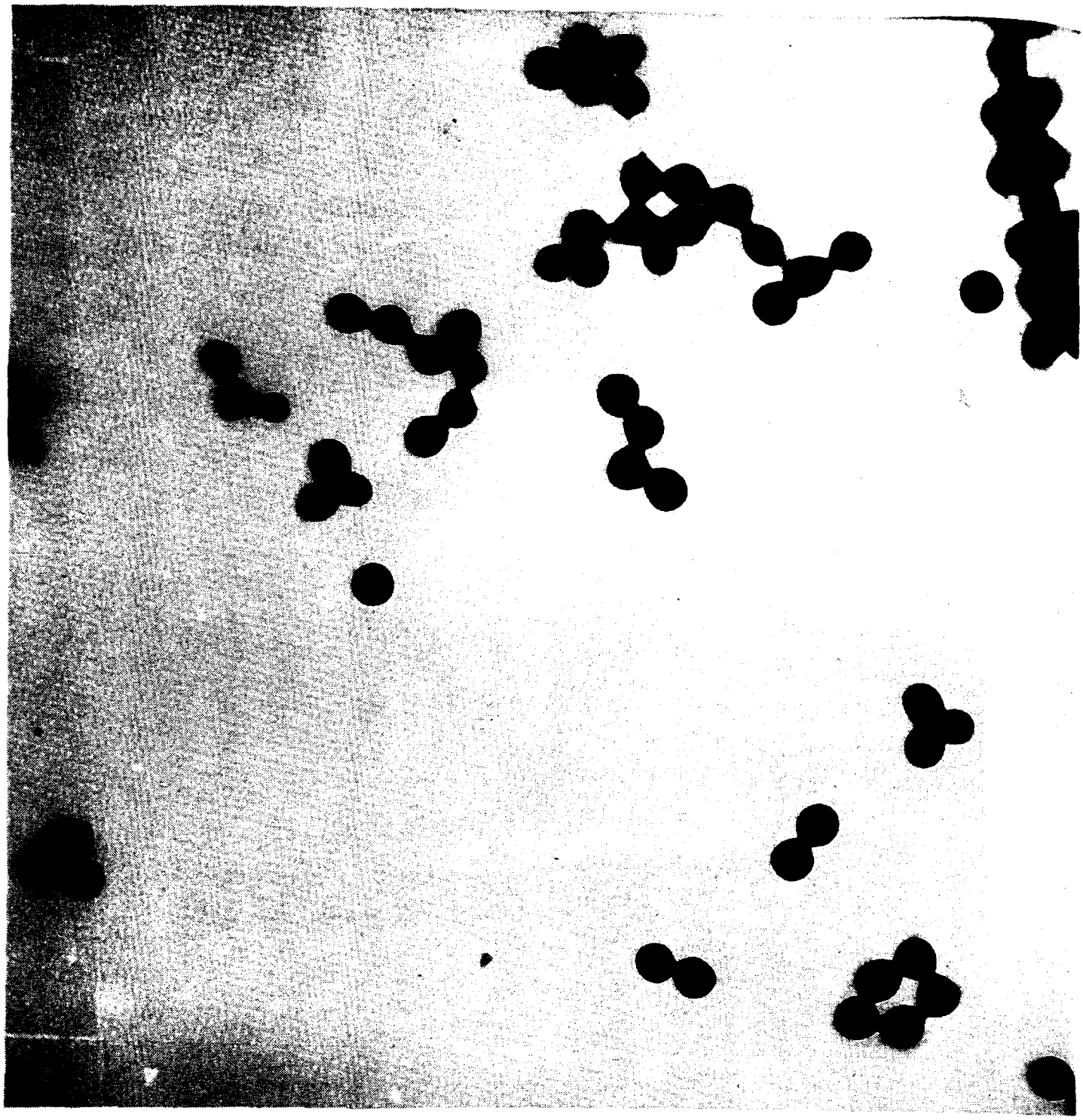

Particle Size: 60 to 250 nm

Figure IV.B.1.3 Shape and Size of Colloidal Particles (TEM)

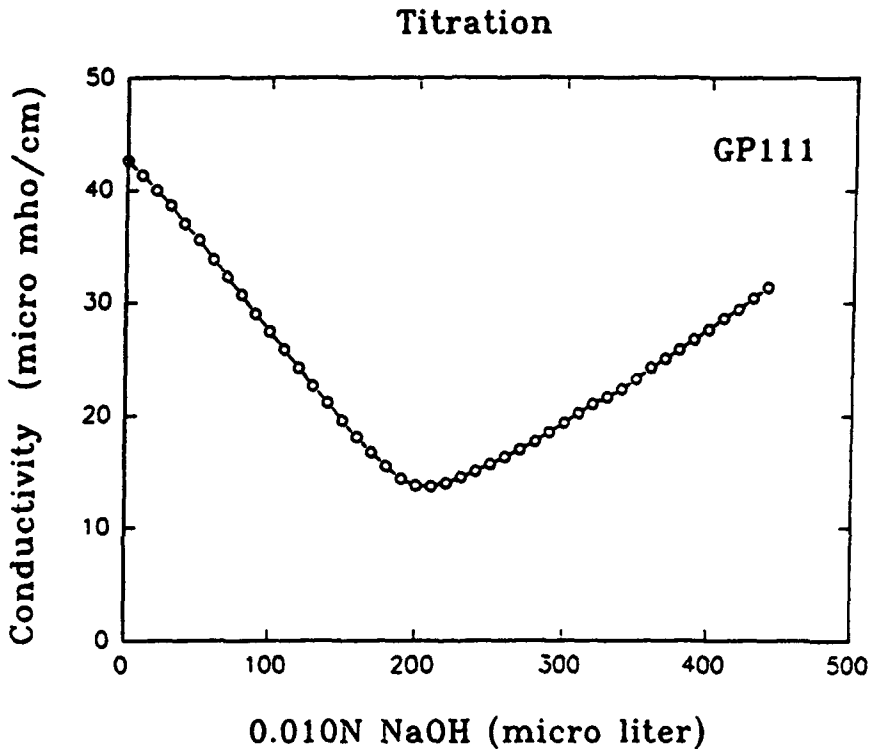

Charge density: **300~900 e^-/particle**
(0.2~0.6 $\mu C/cm^2$)

Figure IV.B.1.4 Charge Density Measurement

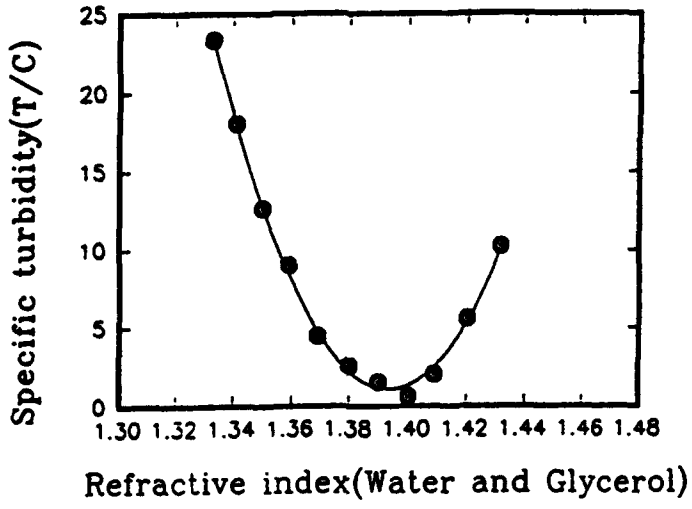

Turbidity: $T = (1/b) \ln(I_0/I_t)$

Specific Turbidity: $T/C \propto (n_p - n_m)^2$

Model: $T/C = a \bullet n_m^2 + b \bullet n_m + c$

Derivative: $d(T/C)/dn_m \Big|_{n_m=n_p} = 0$

$n_p = 1.393$

Figure IV.B.1.5 Measurement of Refractive Index

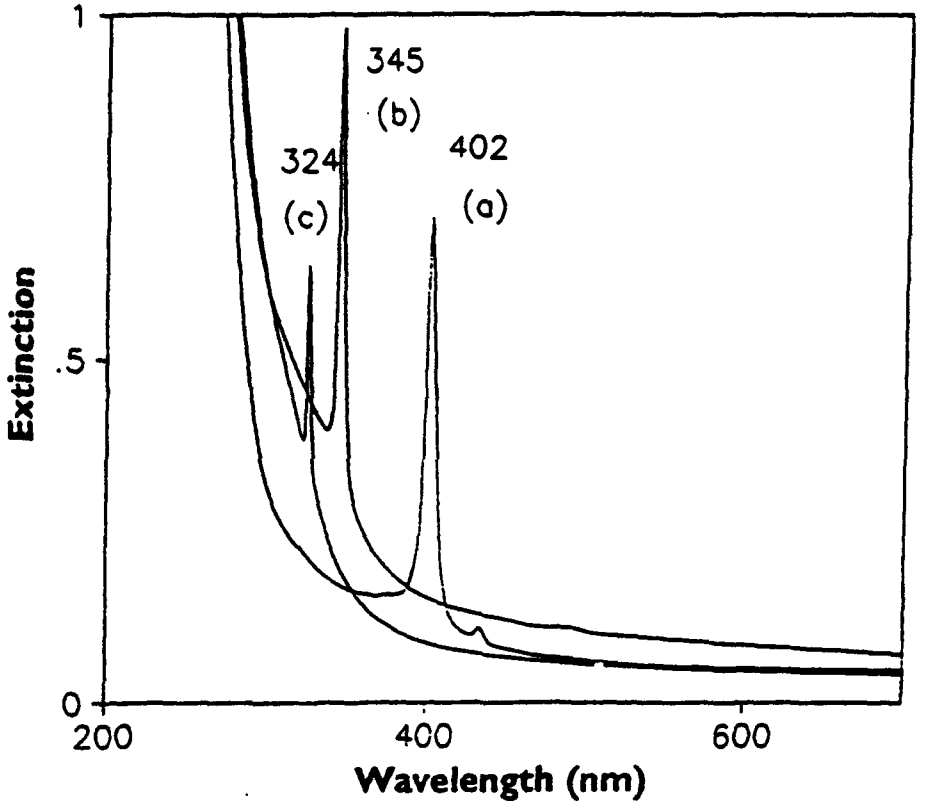

Samples I.D.	a (GP73)	b (GP72)	c (GP74)
Particle size (nm)	91.1	95.6	87.9
Volume%	14.2%	12.0%	11.3%
Cell thickness (mm)	0.40	0.40	0.40

Figure IV.B.1.6 Transmission Spectra of Small Particle Samples

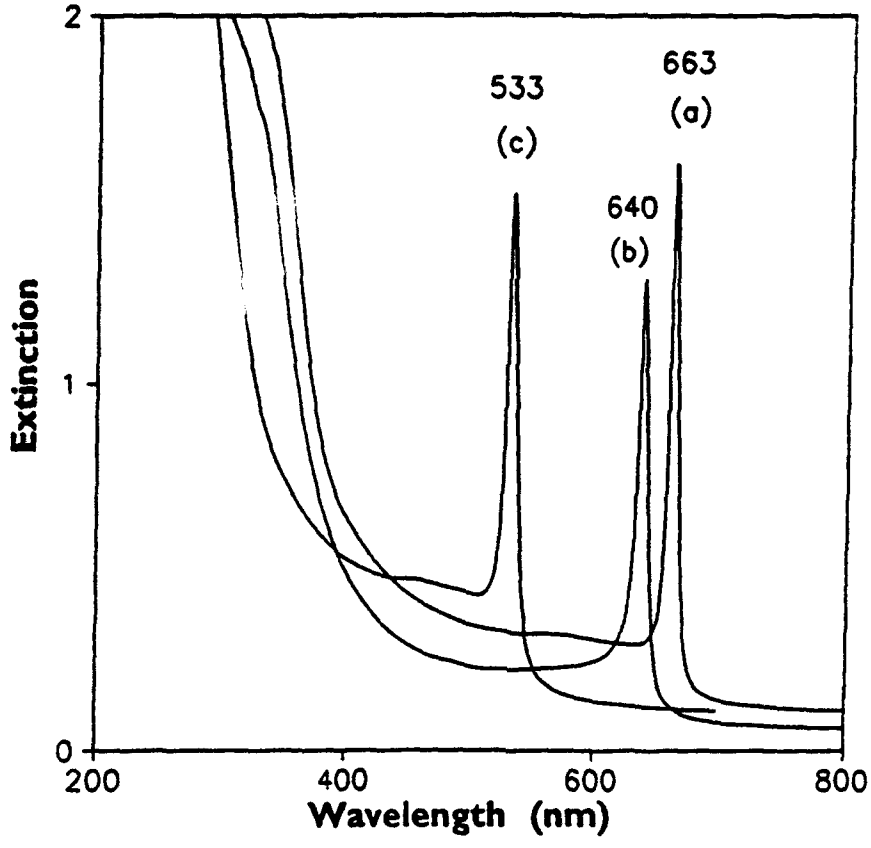

Samples I.D.	a (GP153)	b (GP159)	c (GP158)
Particle size (nm)	174.6	163.8	152.6
Volume%	8.5%	10.5%	11.0%
Cell thickness (mm)	0.40	0.40	0.40

Figure IV.B.1.7 Transmission Spectra of Large Particle Samples

Synthesis

Free-radical Emulsion Polymerization

Recipe of PM72 (in mole ratio)

Methyl Methacrylate (MMA)	:	1
Divinylbenzene (DVB)	:	0.0073
Lauryl Sulfate (SDS)	:	0.0011
COPS-1	:	0.0041
Sodium Persulfate	:	0.00051
Water	:	25.3
Uniblue A	:	0.0002

T = 84 °C
Stirring Speed : ~350 rpm
Reaction Time : ~ 4 hours

Figure IV.B.1.8 Synthesis: Free-radical Emulsion Polymerization

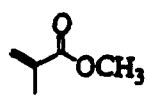

MMA

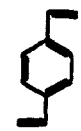

DVB

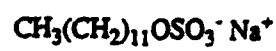

SDS

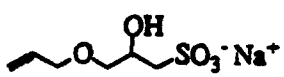

COPS-1

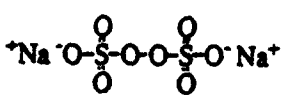

Sodium Persulfate

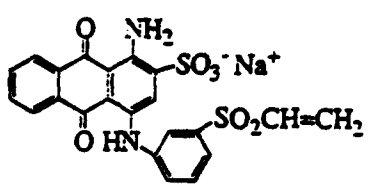

Uniblue A

Figure IV.B.1.9 Structure of the Reagents

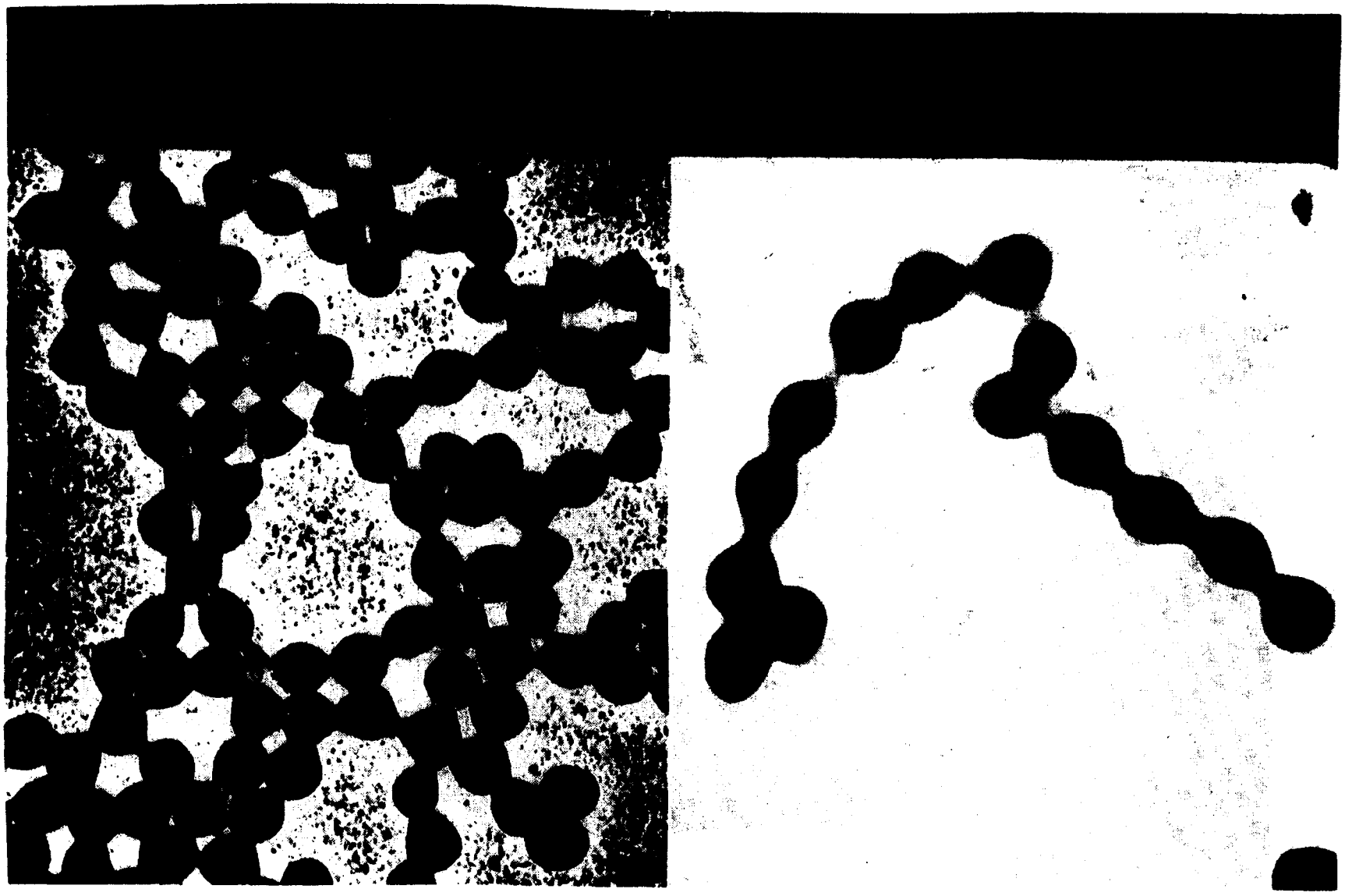

Figure IV.B.1.10 TEM Micrographs of PMMA Spheres

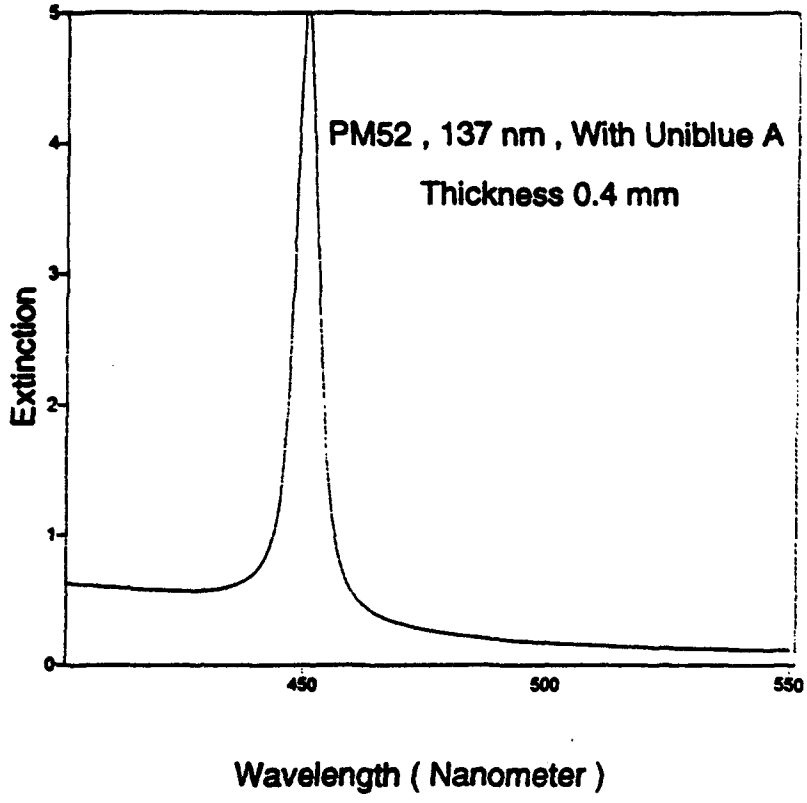

Figure IV.B.1.11 Crystal Formation: Colloids + Ion Exchange Resin + Water

Fix the Particles in Hydrogel Matrix

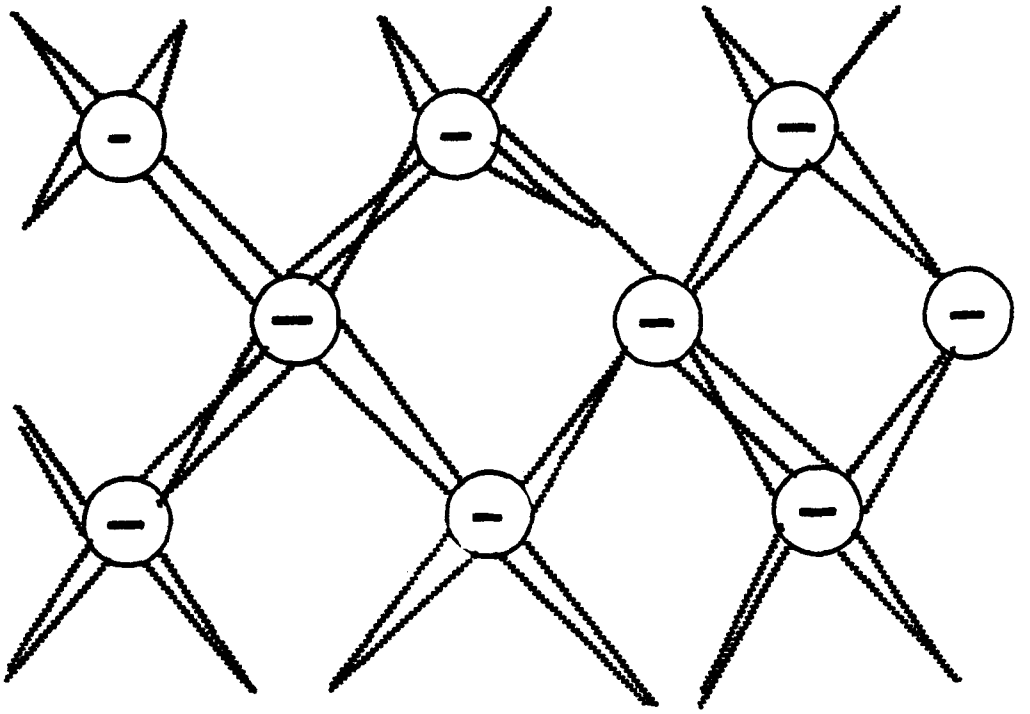

Figure IV.B.1.12 Solidification of PMMA Colloidal Crystals

Monomers in Hydrogels

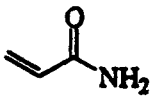

Acrylamide (AMD)

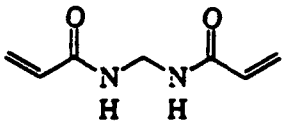

Methylene - bis - acrylamide (MBA)

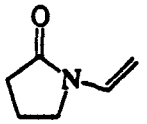

N - vinylpyrrolidone (NVP)

PMMA colloids: ~6%
AMD + MBA (~6:1): 3%
NVP: ~15%

Figure IV.B.1.13 Monomers in Hydrogels

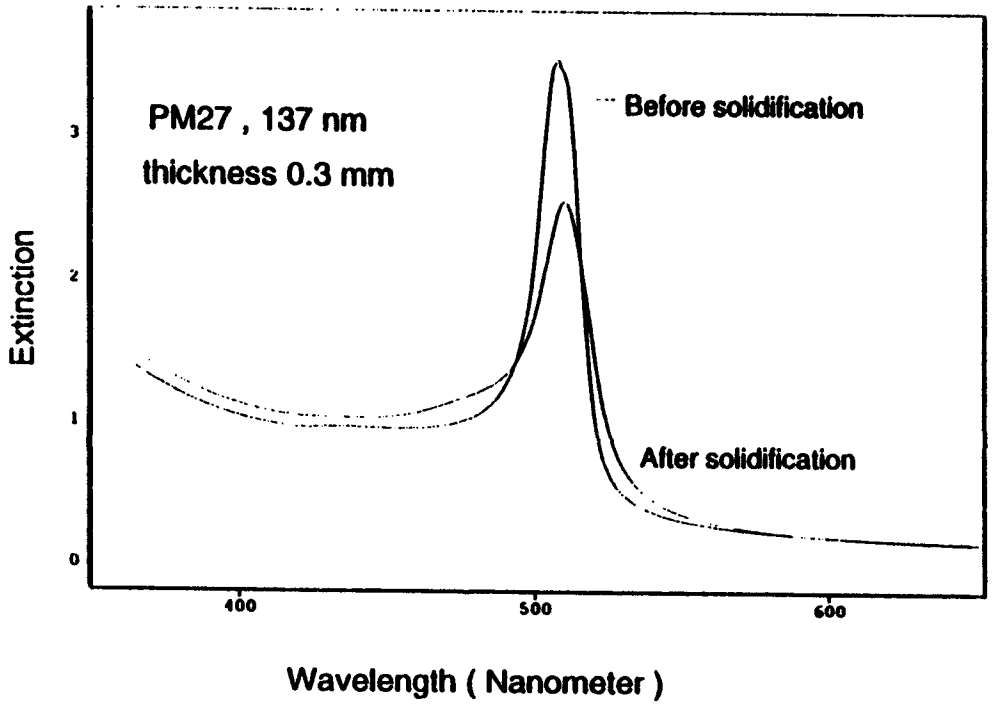

Figure IV.B.1.14 Solidification of PM-27

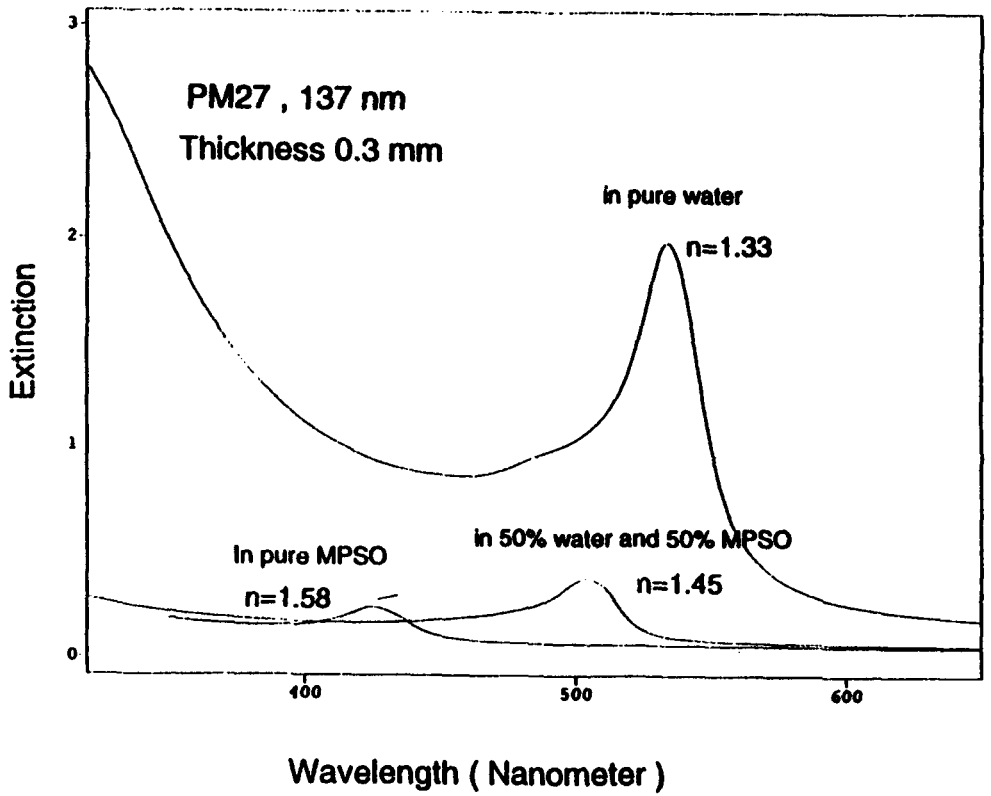

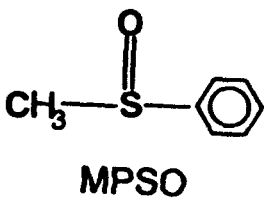

Figure IV.B.1.15 Transmission Spectra of Spheres with MPSO

Colloidal Array with Polymerizable Agent 'R'

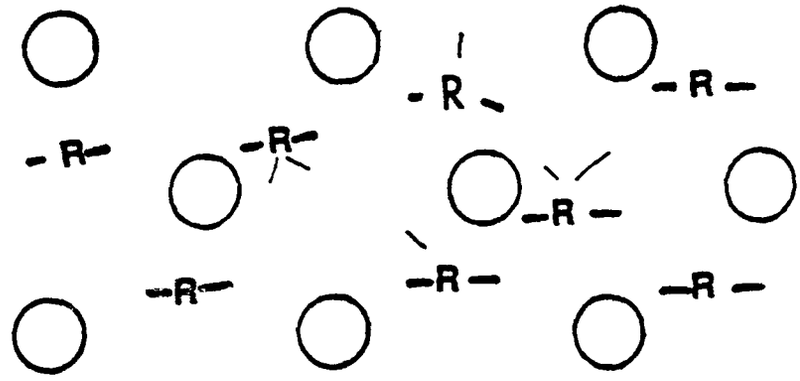

initiate polymerization

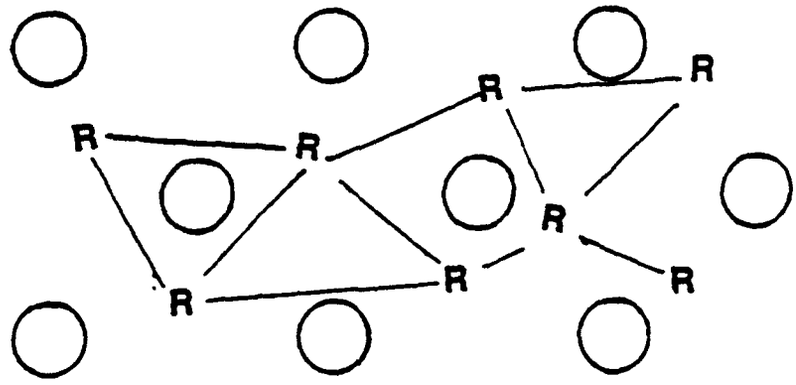

Figure IV.B.1.16 Polymerization Scheme

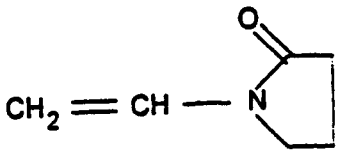

N - Vinylpyrrolidone

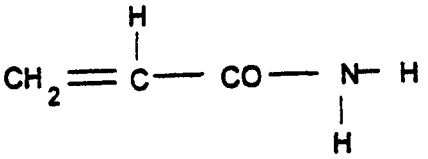

Acrylamide

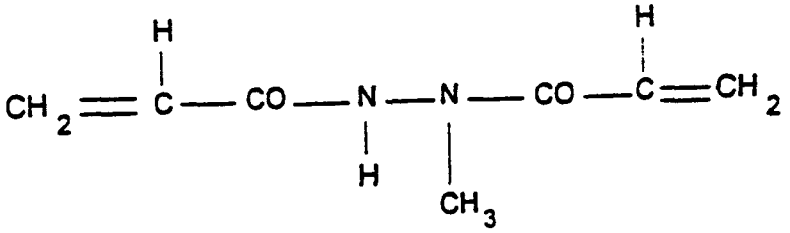

N,N'-methylene bis acrylamide

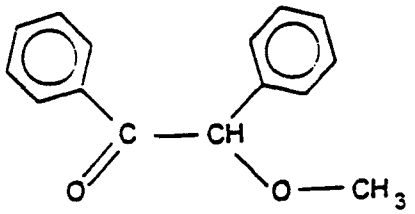

Benzoin methyl ether

Figure IV.B.1.17 Chemical Structures of Monomers and Initiator

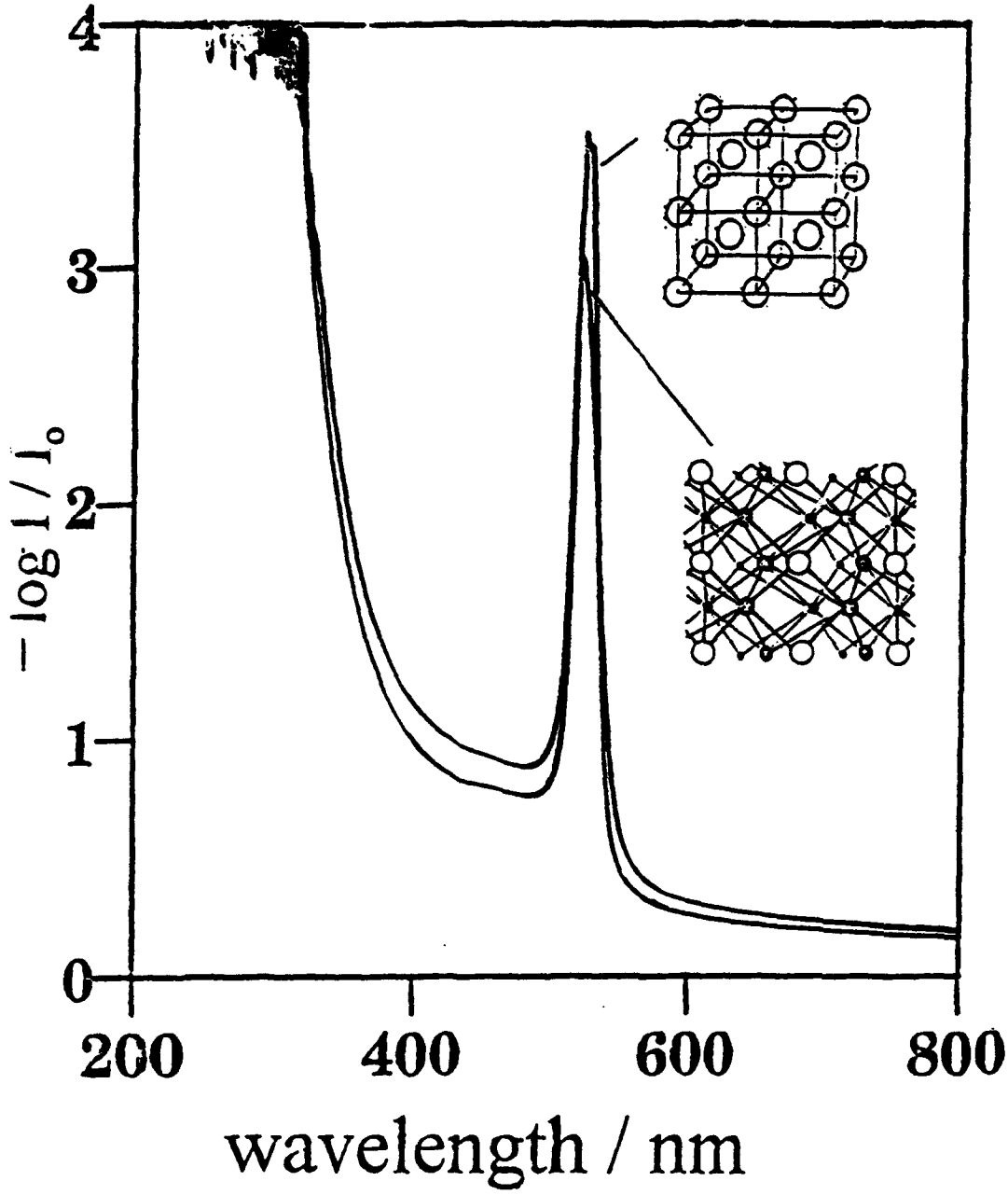

Figure IV.B.1.18 Light Diffraction Properties of Crystalline Colloidal Arrays Before and After Polymerization

IV.B.2. Nonlinear Selective Diffraction Devices Based on Crystalline Colloidal Array Submicron Periodicities

Principal Investigator:	Professor Sanford A. Asher Department of Chemistry University of Pittsburgh
Other Faculty Participants:	Dr. Rob Coalson Department of Chemistry University of Pittsburgh
Students:	Dr. Albert Tse Dr. Song-yuan Chang Dr. Sesh Jagannathan Mr. John Holtz

IV.B.2.1 INTRODUCTION

We recently created a new optical-filtering device fabricated through the self-assembly of colloidal spherical particles. These spherical particles self-assemble in solution into cubic crystalline arrays with lattice spacings comparable to visible light (Fig. IV.B.2.1). Intense Bragg diffraction from the array prevents transmission (T) of light meeting the Bragg diffraction condition ($T < 10^{-6}$). Thin films of these arrays diffract light throughout the UV, visible and IR spectral regions with high rejection efficiencies within a well defined rejection band, and with high transmission off this band.

We developed fabrication techniques to prepare solid Bragg diffraction devices and have developed new materials for construction of nonlinear and wavelength-agile Bragg diffraction devices. The devices have been created from ca 100 nm highly charged monodisperse polymer and inorganic spheres synthesized using new methods which attach greater than 25,000 sulfonate groups to the sphere surfaces. The sulfonates ionize in solution; the spheres become highly charged and repel one another. This electrostatic repulsion is responsible for the self-assembly of the spherical particles in the cubic array; this is the minimum energy configuration of the system.

IV.B.2.2 OBJECTIVES

It has been the intent to prepare nonlinear crystalline-colloidal arrays that operate via the nonlinear component of the sphere refractive index. The refractive index, n of a material can be expressed as:

$$n = n_o + (n_2 / 238.7\, n_o\, I_o + \ldots,$$

where n_o is the refractive index at low intensities and n_2 is the largest nonlinear

term. We create transparent nonlinear selective diffraction devices by making the refractive index of the spheres identical to that of the medium at low light intensities. However, at high light intensities n_2 causes the sphere refractive index to diverge from the medium. Thus, the array diffracts light meeting the Bragg condition and prevents light transmission ($T < 10^{-10}$). This "pop up" grating diffracts a band of light specified by the grating periodicity and the wavelength of light in the material. Since the Δn is confined to the spheres, there is only a small change in the average n of the device; thus, alterations of the wavelength of light are less than the diffracted bandwidth.

The work develops nonlinear optical diffraction devices useful for laser eye protection as well as for optical switching and computer applications. We will develop a new technology for optical limiters and optical switches which operate at much lower thresholds than any previous technology. The nonlinear materials we develop will serve as the basis for entirely new optical materials.

IV.B.2.3 ACCOMPLISHMENTS AND SIGNIFICANCE

A. Preparation and Processing of Monodisperse Colloidal Silica-CdS Nanocomposites

The purpose of this work was to develop methods for preparing SiO_2 spheres with CdS quantum dot inclusions. These silica spheres would be functionalized with sulfonate groups such that they would self-assemble into crystalline colloidal arrays (CCA). The CdS quantum dots are reported to have extraordinarily high nonlinear coefficients and, thus these CCA would be nonlinear and capable of being optically switched. We are proud to have accomplished the synthesis of these nanocomposites.

We have developed new methods for preparing silica-CdS quantum dot composite spheres. Figure IV.B.2.2 compares the standard Stöber process to the new approach we used to synthesize these spheres in water-in-oil microemulsions while Figure IV.B.2.3 illustrates the synthetic procedure. Figures IV.B.2.4-IV.B.2.6 show TEM micrographs illustrating the success of this microphase preparation technique for synthesizing monodisperse silica spheres.

Coaddition of microemulsions containing Cd^{+2} and S^{-2} results in the coprecipitation of CdS. Careful timing of the addition of Cd^{+2} and S^{-2} successfully incorporates quantum dots within the silica spheres as shown in Figure IV.B.2.7.

Elemental analysis using SEM/EDX (energy dispersive x-ray analysis) shows the existence of 4-8 mole % CdS, which is identical to the amount initially added. X-ray diffraction measurements (Fig. IV.B.2.8) show a broad peak from the amorphous silica, while we see moderately sharp peaks for the CdS quantum dots. The diffraction widths indicate that the CdS colloids are ca. 2.4 nm in diameter. This size is consistent with that calculated from the Figure IV.B.2.9 absorption

spectrum of the CdS-silica sphere nanocomposite; the absorption spectral features around 430 nm derive from quantum confinement effects of ca. 2.4 nm CdS quantum dots. As schematically indicated in Figure IV.B.2.10 the microphase synthesis methodology can be modified to form different types of silica particles containing CdS quantum dots. These morphologies can be visualized using TEM by etching out the CdS with nitric acid. The etching will leave holes in the silica spheres. Figs. IV.B.2.11-IV.B.2.14 show the differently prepared, etched silica sphere-CdS composites.

B. Preparation and Characterization of Cationic Polystyrene Latexes

The objective of this work was to develop a synthetic route to prepare highly cationically charged colloid. This would complement our work with the more common anionically charged colloids. We developed this synthesis by modifying recipes that exist in the literature. We intend to use these cationically charged spheres to make crystalline colloidal arrays (CCA) analogous to Na^+Cl^- crystals.

Figures IV.B.2.15 and IV.B.2.16 list the chemical species used, while Figures IV.B.2.17-IV.B.2.19 relate the reaction conditions to the colloid size and to whether the spheres self assemble to form crystalline colloidal arrays that Bragg diffract and thus, show iridescence. Figure IV.B.2.20 shows a preferred recipe, while Figure IV.B.2.21 shows a TEM micrograph which illustrates the excellent particle monodispersity we have obtained.

Figure IV.B.2.22 shows the diffraction attenuation spectrum of a CCA prepared from cationic colloids prepared using these synthetic methods. In this case the colloidal spheres had a diameter of 111 nm. This indicates a high level of surface charge.

IV.B.2.4 SUMMARY

- Developed theoretical model for operation of nonlinear thermal CCA.
- Synthesized SiO_2-CdS composite spheres with CdS quantum dots
- Polymerized dyed PMMA colloids in hydrogel network
- Refractive indexed matched network

Publications in Reviewed Journals:

"Nanosecond Photothermal Dynamics in Colloidal Suspension",
R. Kesavamoorthy, M. S. Super, and S. A. Asher, J. Appl. Phys. 71, 1116-1123 (1992).

"New Nonlinear Bragg Diffraction Devices",
S. A. Asher, R. Kesavamoorthy, S. Jagannathan, P. Rundquist, SPIE Vol. 1626 Nonlinear Optics III, 238-241 (1992).

"Preparation and Properties of Tailored Morphology, Monodisperse Colloidal Silica-Cadmium Sulfide Nanocomposites",
S.-Y. Chang, L. Liu, and S. A. Asher, J. Am. Chem. Soc., submitted (1994).

"Creation of Complex Topological Morphologies in Colloidal Silica",
S.-Y. Chang, L. Liu, and S. A. Asher, J. Am. Chem. Soc., submitted (1994).

Patents:

S. A. Asher and S. Jagannathan, "Method of Making Solid Crystalline Narrow Band Radiation Filters", U.S. Patent Number 5,281,370.

We also filed patent applications for a "Method of Making an Optically Nonlinear Switched Optical Device and Related Devices" (serial number 07/999,487) and a "Method of Filtering Submicron Particles and Associated Product".

1. Fabricated From Colloidal Particles

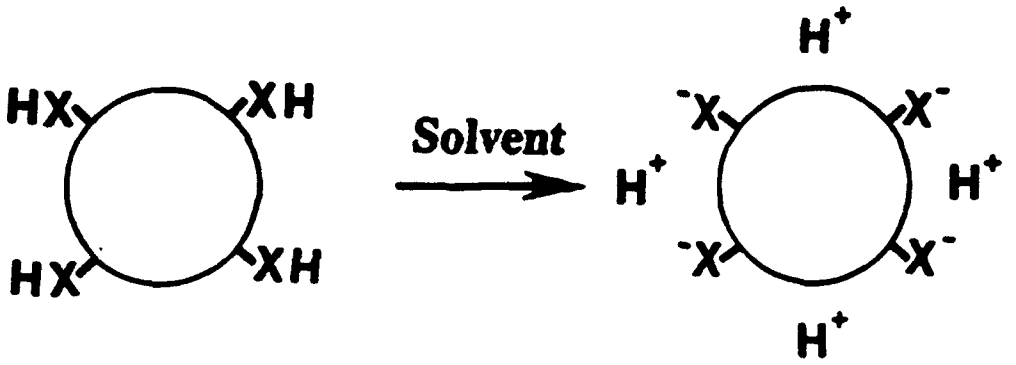

2. Particles Self Assemble Into 3-D Ordered Crystal Structure

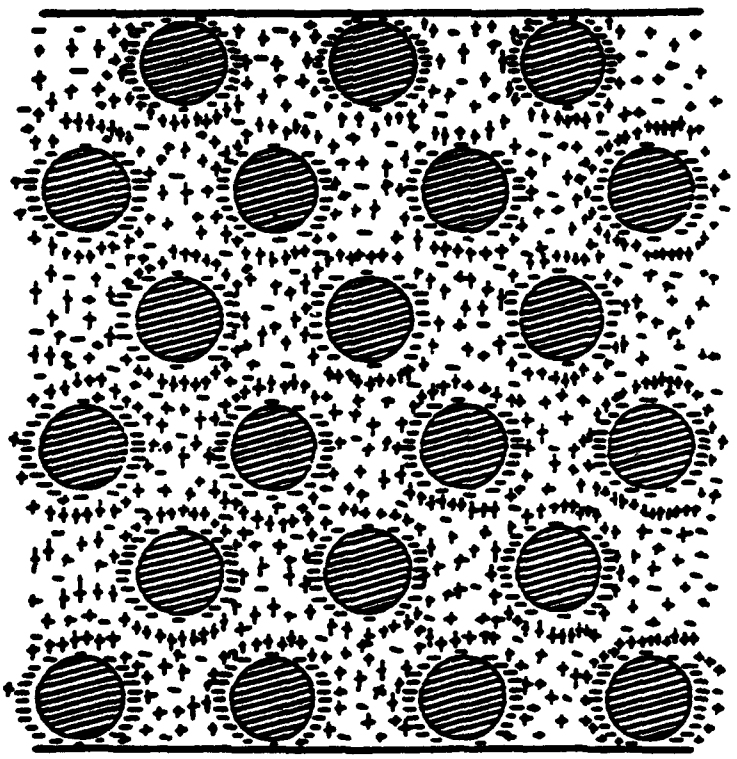

Figure IV.B.2.1 Crystalline Colloidal Arrays

● Stöber Process

$$Si(OR)_4 + 4H_2O \xrightarrow{NH_3, ROH} Si(OH)_4 + 4ROH$$

$$n Si(OH)_4 \longrightarrow nSiO_2 + 2nH_2O$$

● Microemulsion Route

- ◆ Igepal/ammonia/water/cyclohexane

  K. Osseo-Asare and F.J. Arrigada, *Colloids and Surfaces*, **50** (1990) 321.

- ◆ Triton N-101/ammonia/water/cyclohexane/hexanol

● Controlling Factors

factor	Stöber process[1]	microemulsion route
h=[water]/[alkoxide]	h↑, d↑	no significant effect
[NH_3]	[NH_3], d↑	no significant effect
w=[water]/[surfactant]	-	w↑, d↓
ROH	R↑, d↑ polydispersity ↑	ROH↑, polydispersity ↑

1 general rule for condition where [water]<8M and [NH3]>2M.

Figure IV.B.2.2 Synthesis of Silica Colloids

❶ Igepal/ammonia/water/cyclohexane

❷ Triton N-101/ammonia/water/cyclohexane/hexanol

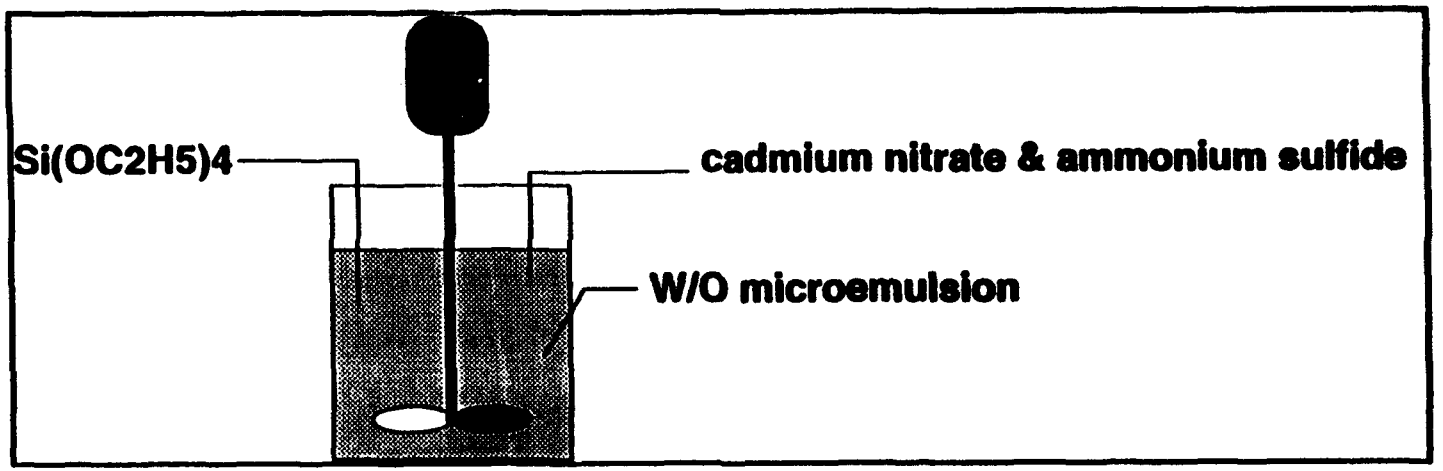

Figure IV.B.2.3 Colloidal Synthesis via Microemulsion Route

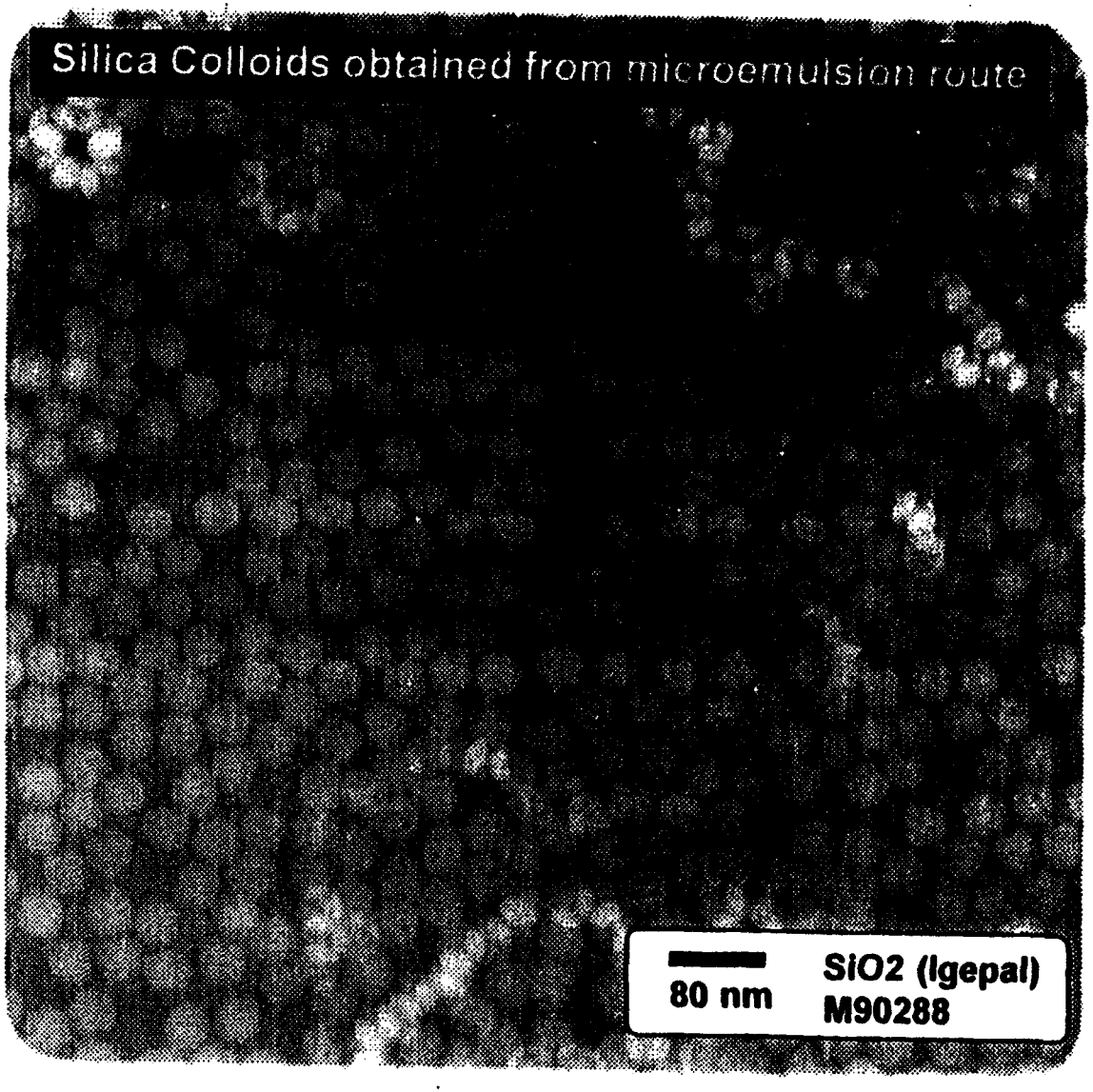

Figure IV.B.2.4 Silica Colloids by Microphase Separation

Figure IV.B.2.5 Silica Colloids by Microphase Separation

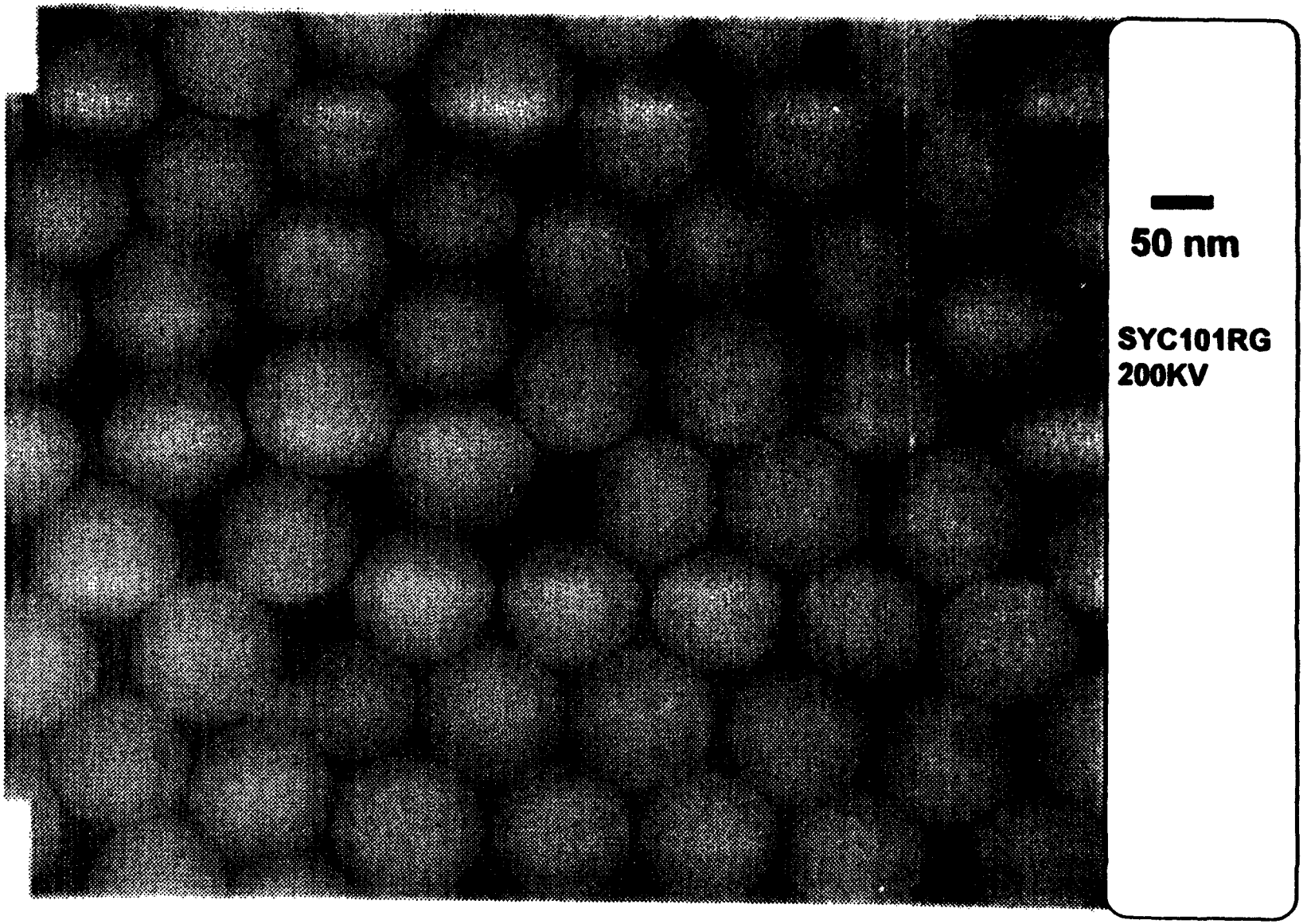

Figure IV.B.2.6 Phase Separated Silica Colloids at High Magnification

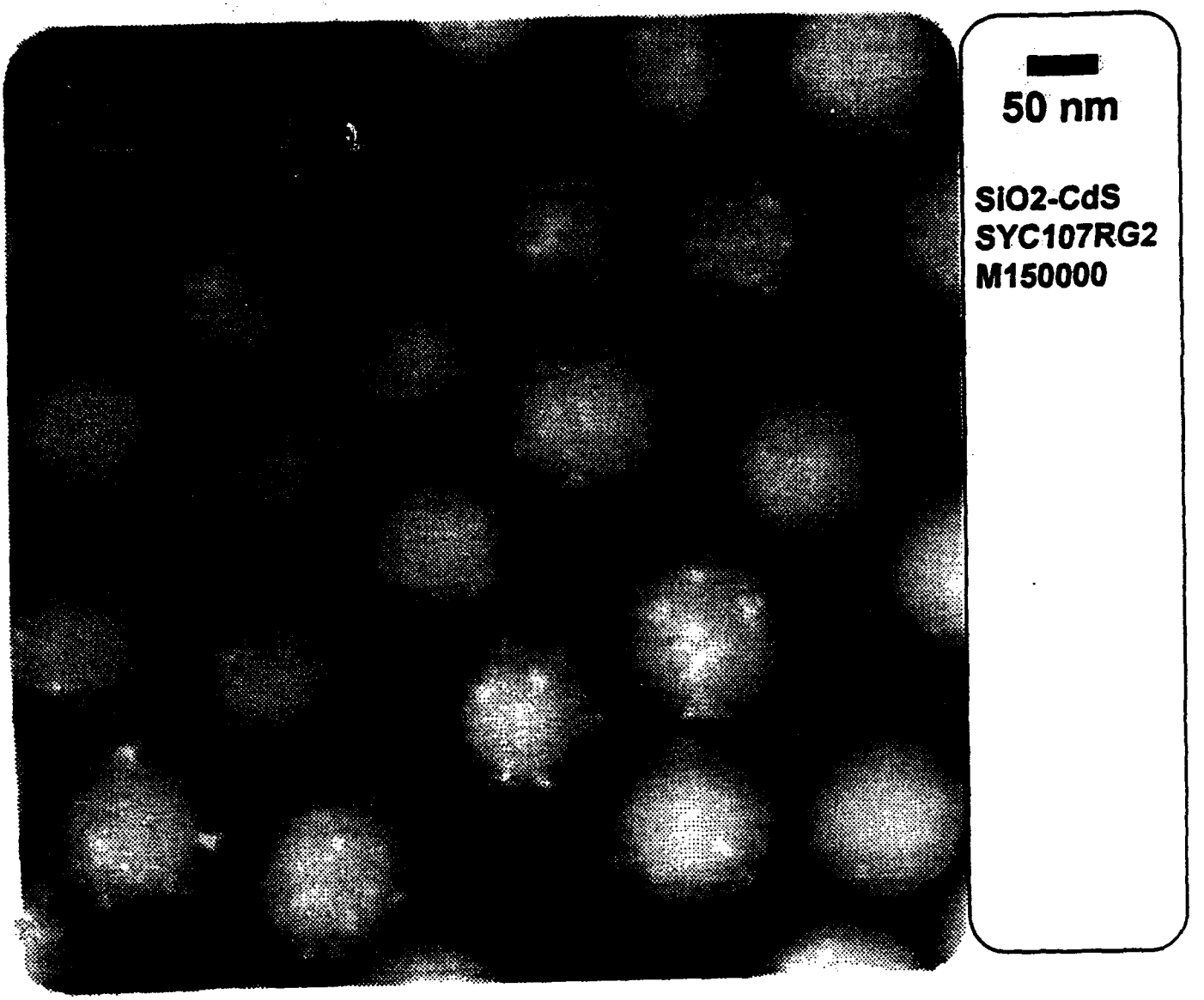

Figure IV.B.2.7 Quantum Dots within Silica Spheres

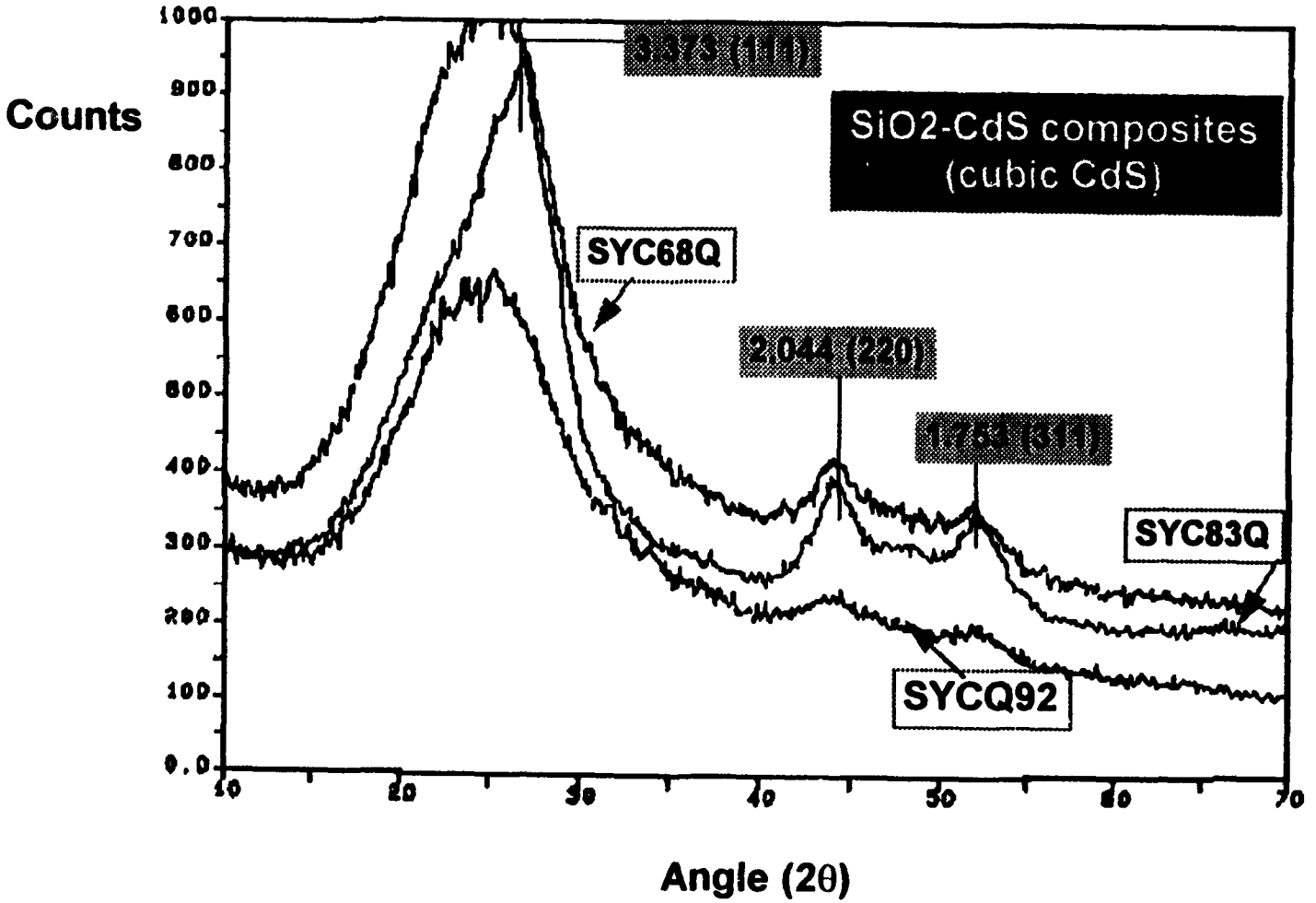

Figure IV.B.2.8 X-Ray Diffraction of SiO_2 - cdS Composites

● Quantum Confinement Effect

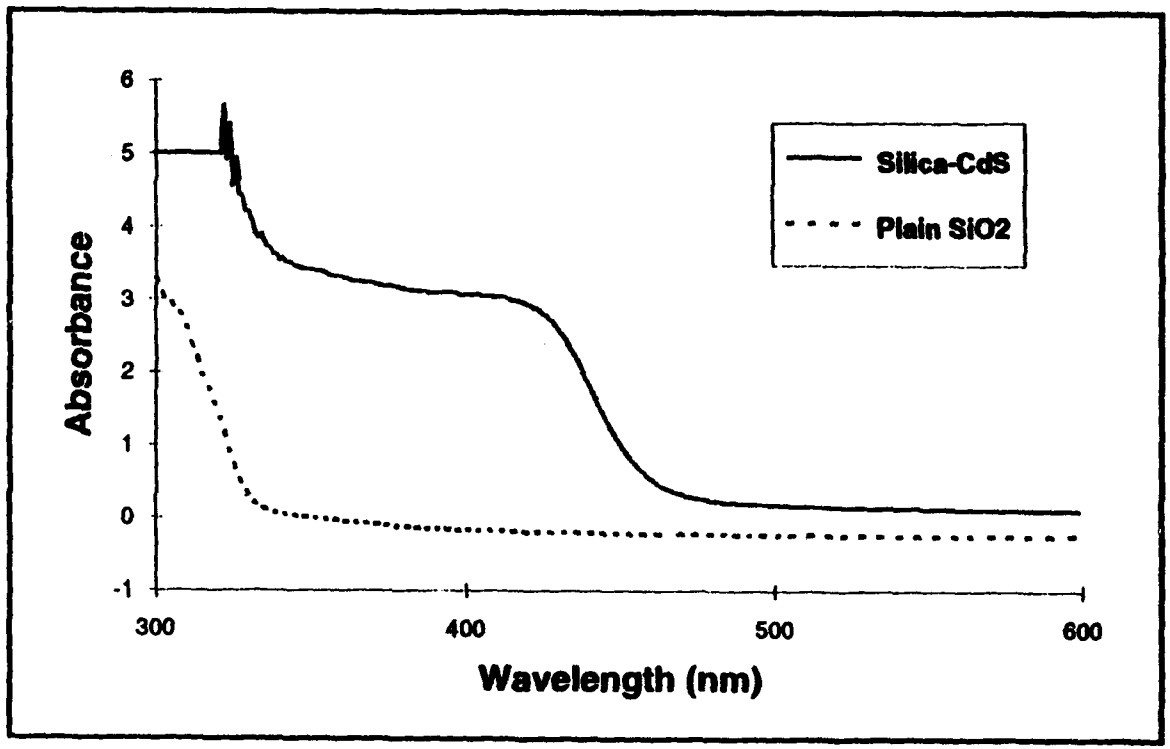

Figure IV.B.2.9 Absorption Spectra of SiO_2 and CdS - SiO_2 Nanocomposites

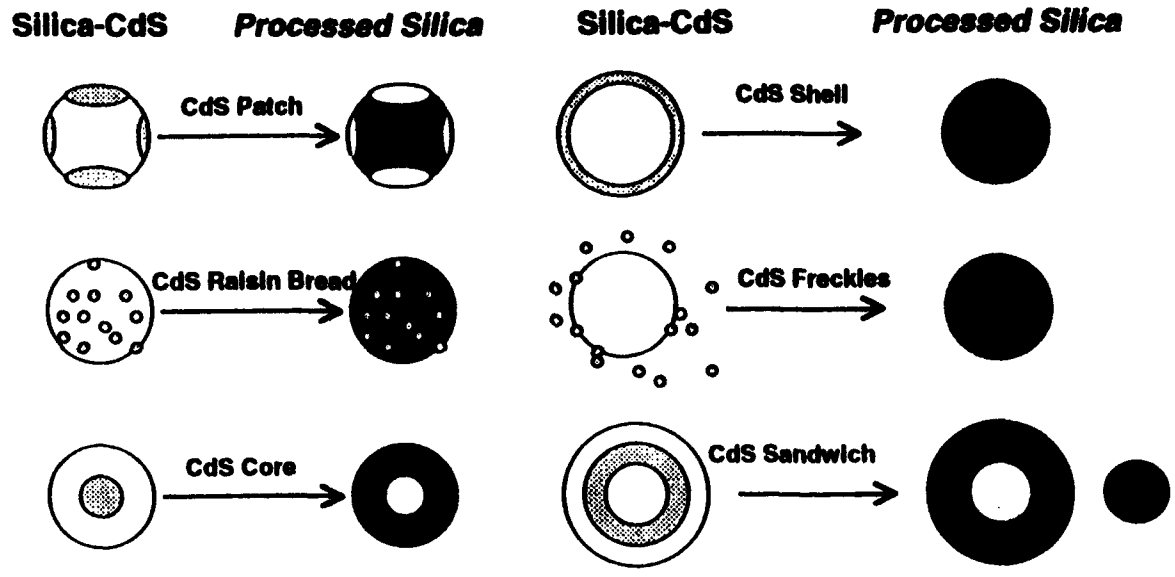

Figure IV.B.2.10 Processing of SiO_2 - CdS Nanoparticles

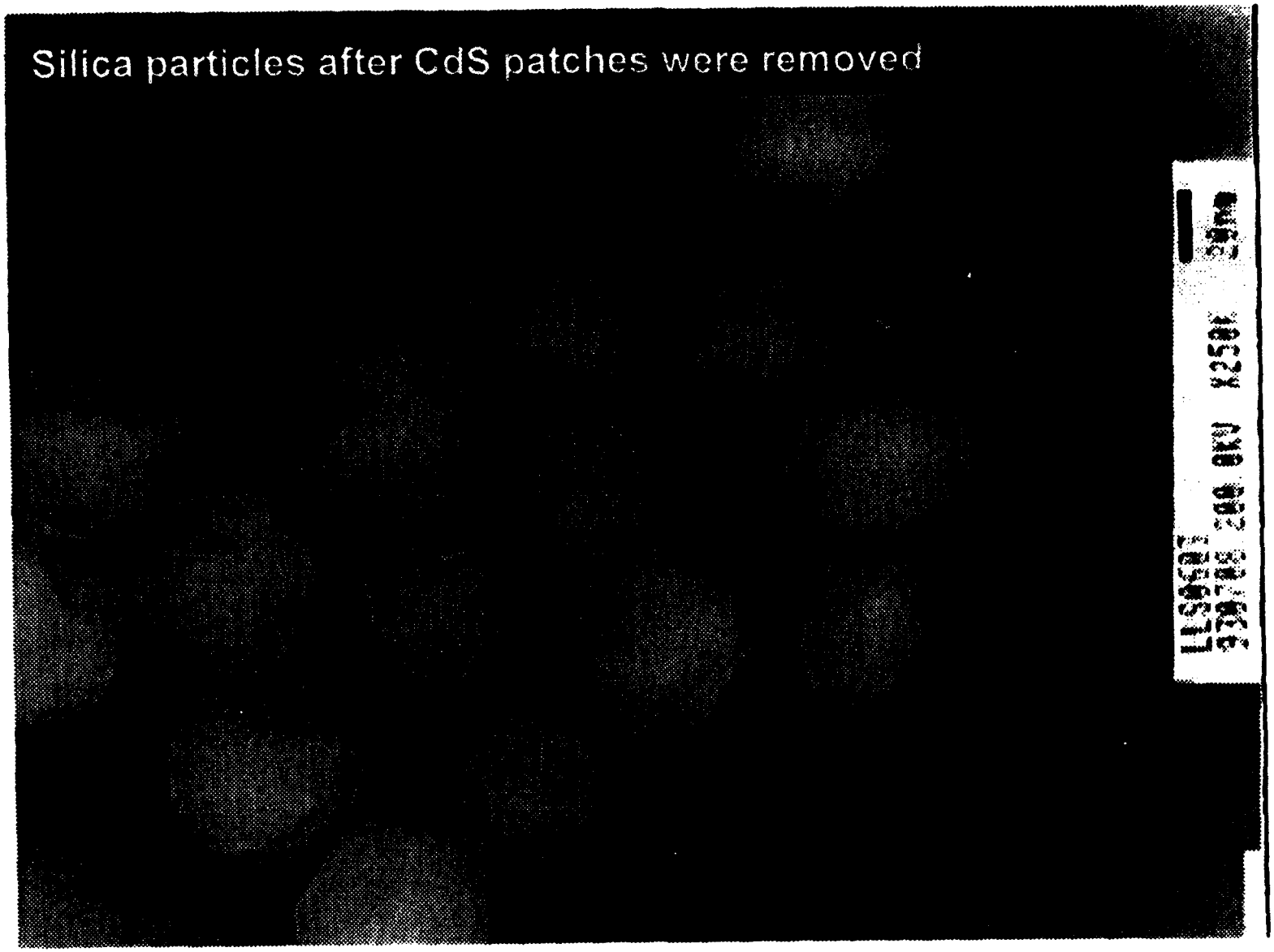

Figure IV.B.2.11 SiO_2 Particles After Removal of CdS

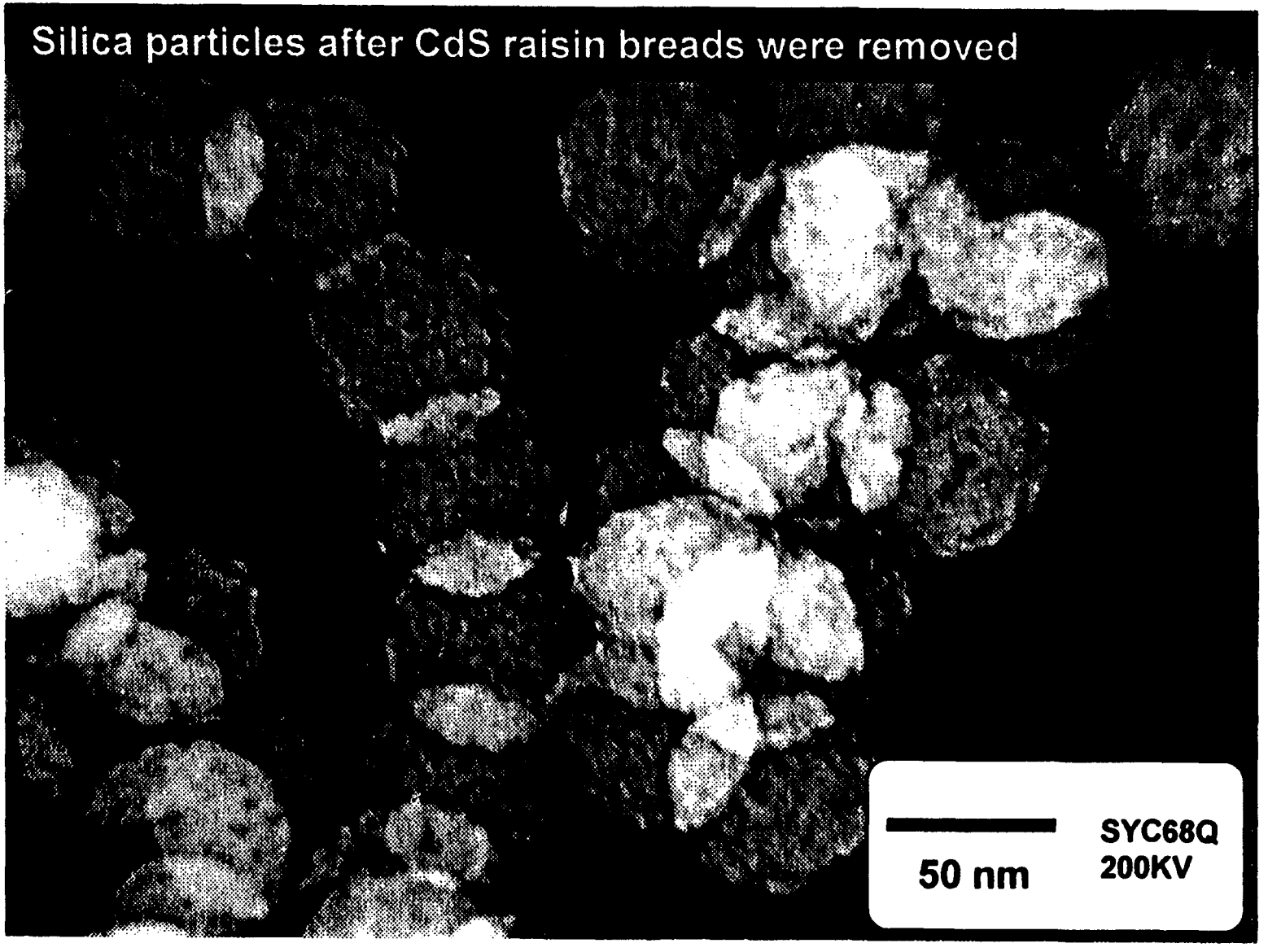

Figure IV.B.2.12 SiO_2 Particles After Removal of CdS

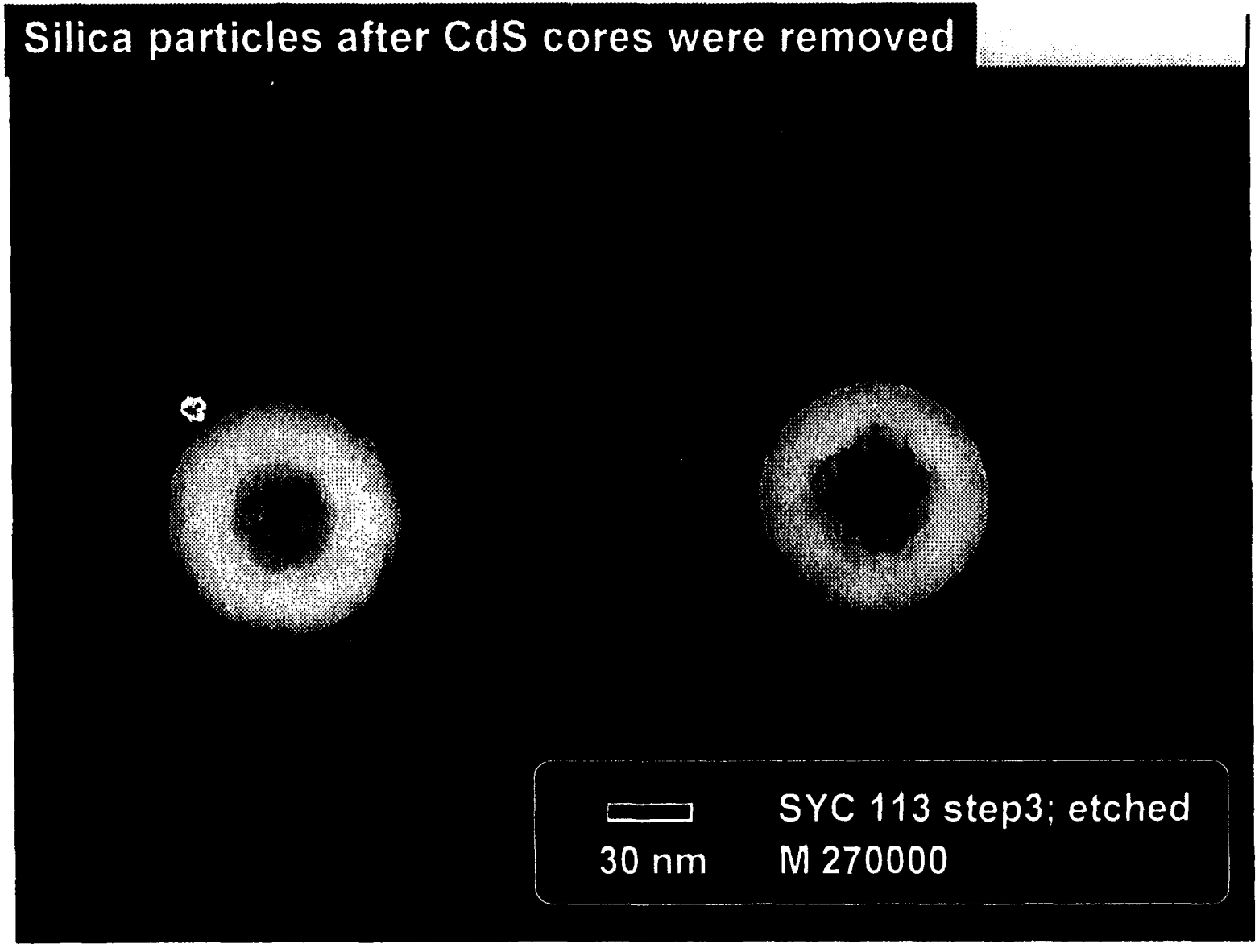

Figure IV.B.2.13 SiO_2 Particles after CdS Core Removal

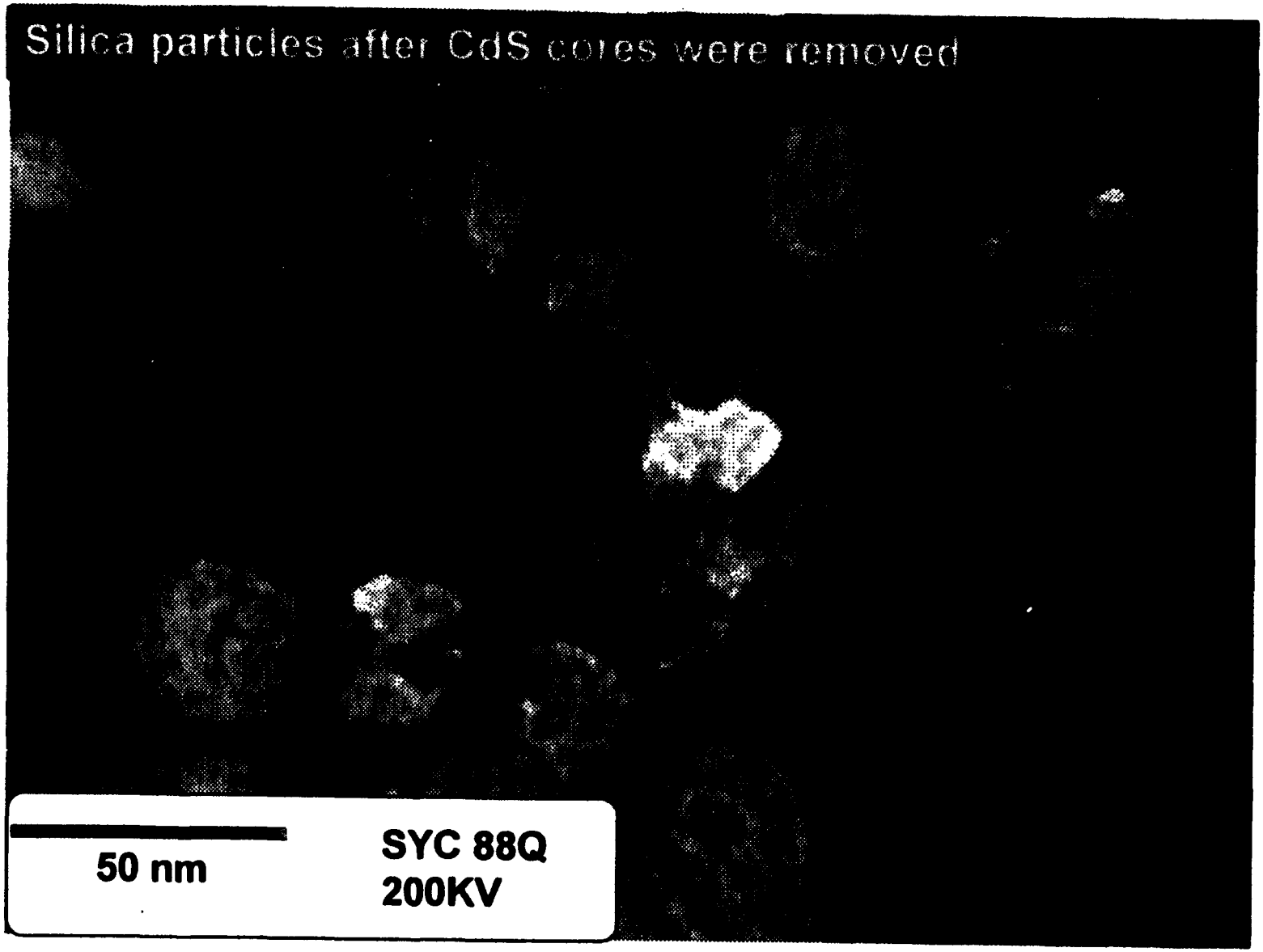

Figure IV.B.2.14 SiO_2 Particles After CdS Core Removal

Experimental

Monomer: Styrene (S)

Crosslinker: Divinylbenzene (DVB)

Comonomer: Diallyldimethylammonium chloride (DADMAC)

$(CH_2=CHCH_2)_2N^+(CH_3)_2\ Cl^-$

Surfactant: Hexadecyltrimethylammonium chloride (HTAB)

$C_{16}H_{33}N^+(CH_3)_3\ Br^-$

Initiator: Azo-bis(butyramidine hydrochloride) (AIBA)

$Cl^-\ ^+(NH_2)_2C(CH_3)_2CN=NC(CH_3)_2C(NH_2)_2^+\ Cl^-$

Figure IV.B.2.15 - Preparation of Cationic Polystyrene Latexes

Other Cationic Comonomers

1. 3-(Methacrylamidinopropyl)trimethylammonium chloride (MAPTAC)

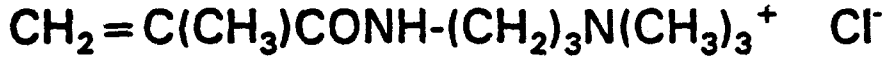

2. Mthacryloxyethyltrimethylammonium chloride (MADQUAT)

3. 2-(Dimethylamino)ethyl methacrylate (DM)

Figure IV.B.2.16 - Preparation of Cationic Polystyrene Latexes

Run #	HTAB conc. (mM)	Size (nm)	Iridescence
ps185	0.27	----	No
ps145	0.54	180	Strong
ps176	1.08	111	Strong
ps144	2.70	89	No

S = 27.25g., DVB = 1.10g., no comonomer, AIBA = 0.15g.

Critical micelle concentration of HTAB = 0.026 mM

cmc of SDS (anionic) = 8.3 mM
cmc of Triton X-100 (nonionic) = 0.24 mM

Other cationic surfactants :

	cmc (mM)
Tetradecyltrimethylammonium chloride(TTAB)	0.28
Cetylpyridinium chloride (CPC)	0.90

Figure IV.B.2.17 - Effect of Surfactant Concentration on Colloidal Particles

Run #	AIBA (mole % S)	Size (nm)	Iridescence
ps184	0.070	119	Strong
ps177	0.14	108	Strong
ps156	0.21	105	V. Strong
ps165	0.42	99	Weak
ps151	0.63	100	Weak

S = 27.25g., DVB = 1.10g., no comonomer, HTAB = 0.10g..

Another initiator:

The neutral initiator azo-bisisobutyronitrile

(AIBN) gave colloids with weak or no iridescence.

Figure IV.B.2.18 - Effect of Initiator Concentration on Colloidal Particles

Run #	Temp. (°C)	Size (nm)	Iridescence
ps183	60	94	No
ps146	70	111	Strong
ps178	75	100	Weak
ps180	80	99	No

S = 27.25g., DVB = 1.10g., no comonomer, HTAB = 0.10g., AIBA = 0.15g.

Figure IV.B.2.19 - Effect of Temperature on Colloidal Particles

Water	250ml
S	27.25 g. (0.262 mole)
DVB	1.10g. (3.22 mole % styrene)
DADMAC	0g. (no comonomer)
HTAB	0.10g. (0.10 mole % S)
AIBA	0.15g. (0.21 mole % S)

Temperature = 70 °C
Time = 3 hours
% solids = 8 to 9 %

Figure IV.B.2.20 - A Prepared Recipe for Cationically Charged Colloids

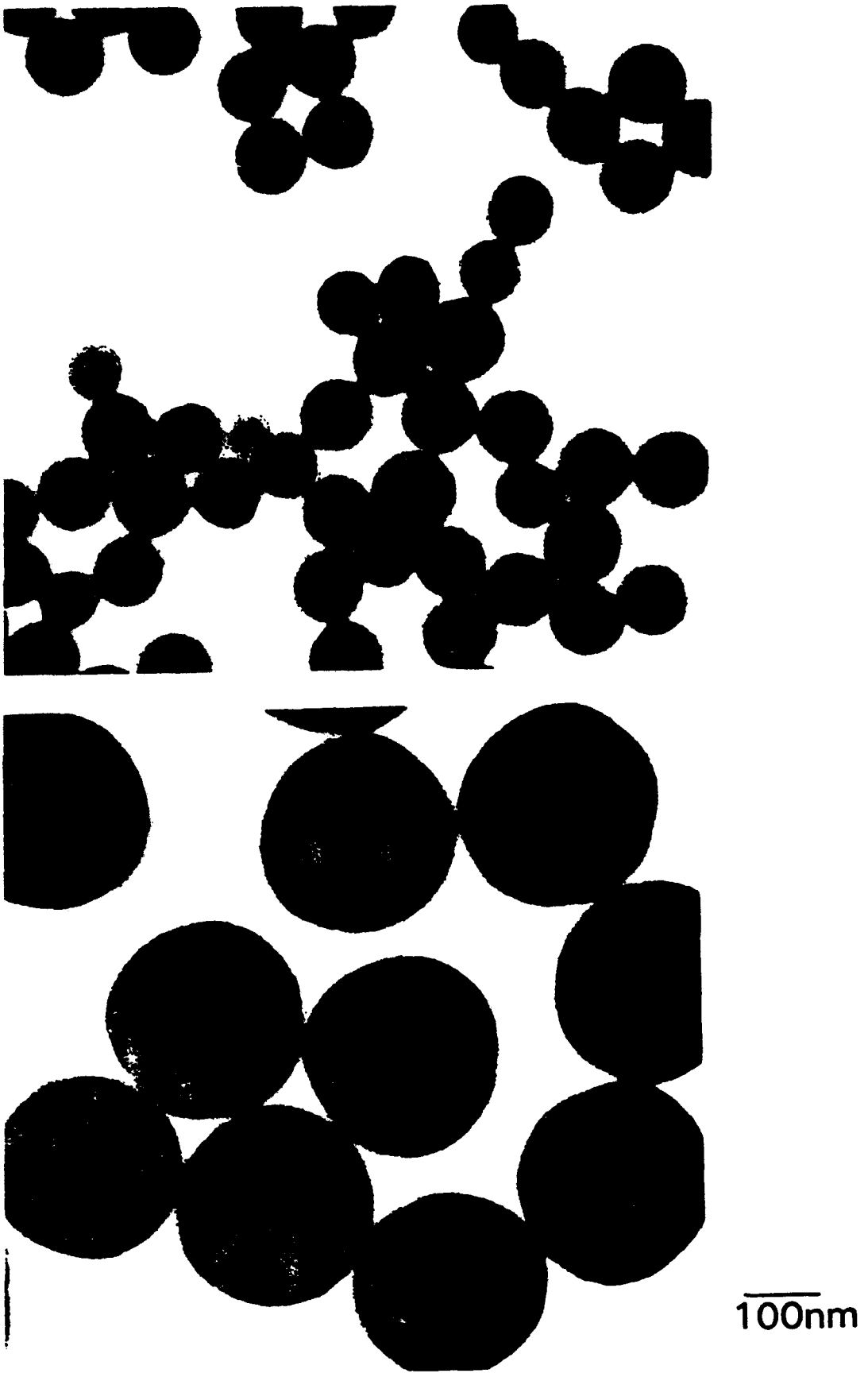

Figure IV.B.2.21 - Transmission Electron Micrographs of Polystyrene Particles

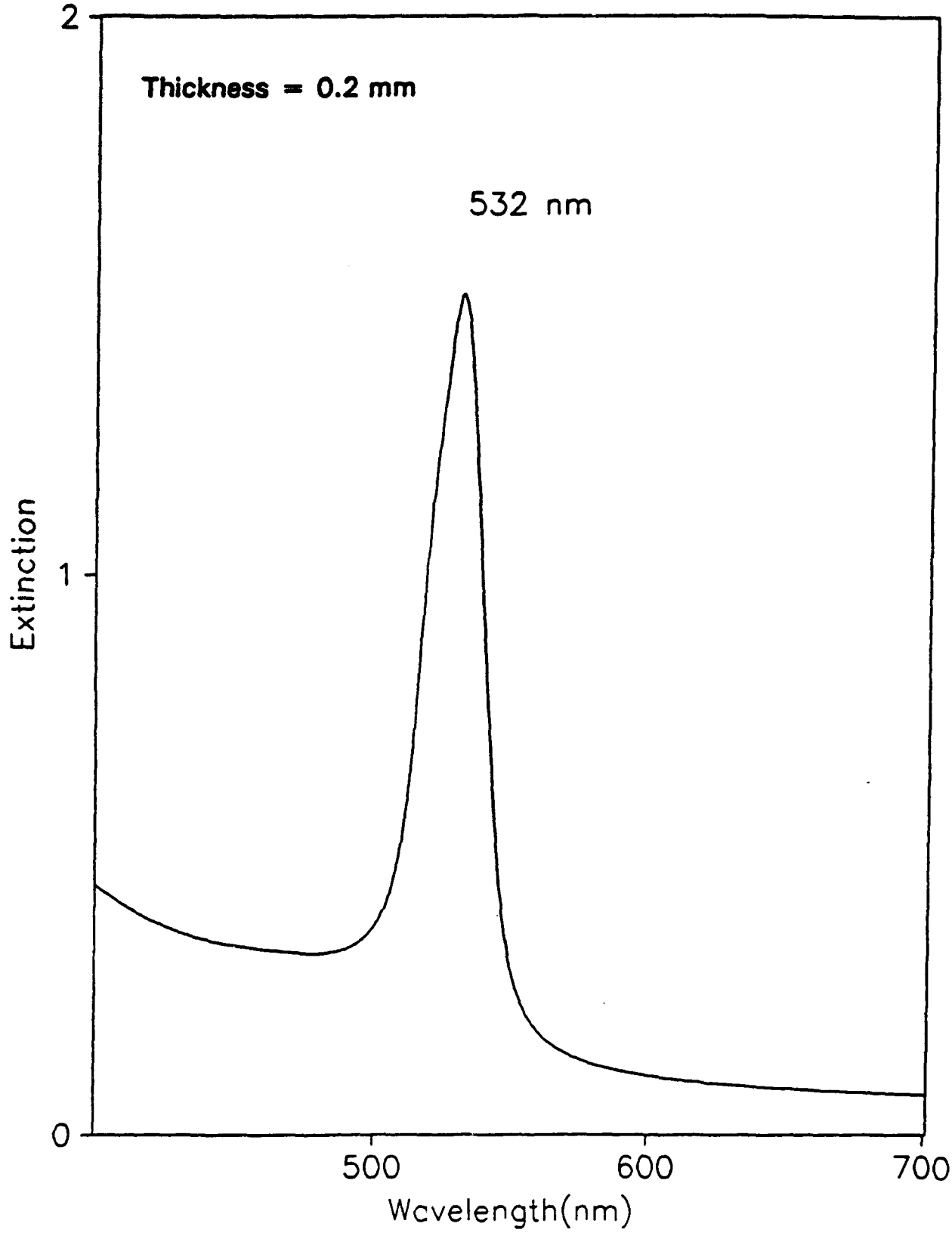

Figure IV.B.2.22 Diffraction Attenuation Spectrum of Polystyrene CCA - Sample PS146L

IV.B.3 Material Research and Design of Ultra-Stable Frequency Light Emitters

Principal Investigator:	Professor D.W. Langer Electrical Engineering Department University of Pittsburgh
Other Faculty Participants:	Professor N.J. Cooper Chemistry Department University of Pittsburgh
	Professor H. K. Kim Electrical Engineering Department University of Pittsburgh
Students:	Mr. Yabo Li Mr. Xiao Fang

IV.B.3.1 INTRODUCTION:

The peak emission of presently used injection laser e.g. InGaAs shifts by 50 nm for a temperature variation of 100 K and also significantly with the level of injection, i.e. depth of modulation. The corresponding wavelength shift for emission from rare earth ions in suitable hosts, e.g. Erbium in GaAs, is less than 0.1 nm [1]. In the rare earths the light emission originates from electron transitions between the well-shielded inneratomic 4f orbitals. Neither crystal fields nor lattice vibrations strongly influence any of the transition wavelengths.

Several rare earth doped semiconductor systems have been made to lase by photon or by electron beam excitation. Unfortunately, lasing action pumped by electron injection has not been accomplished. Recent observations of luminescence at emission wavelengths of several rare-earths [2] has renewed interest in pursuing lasing in doped III-V compound semiconductors. Erbium has been incorporated as Er^{3+} in a variety of III-V compounds by ion implantation, doping during MOCVD [3] or MBE [4] growth. The presence of Er^{3+} in these systems is indicated by the narrow band, 1.54 μm emission observed in most binary III-V compounds.

While transitions in some rare-earth doped semiconductors, e.g. Ytterbium, can be excited only by being pumped optically from the host semiconductor, excitation of Er^{+3} can be accomplished not only via free carriers, but also by the resonant energy transfer from excited deep levels or Donor-Acceptor pair transitions [5]. The successful injection of carriers to produce Er emission in MBE grown GaAs diodes has been recently reported by two groups [6,7]. The Er emission dominates over the GaAs band edge emission at low injection levels,

while the opposite is true at higher levels. Very similar results have been obtained by a Japanese group, using MOCVD grown GaAs. Tsang and Logan had reported lasing in a current injection pumped Er-doped GaInAsP but in a later publication speculated that lasing might not have been observed and the emission recorded might have been due to Er clusters [8]. To summarize:

* Rare Earth Ions, when in a solid, have 4f-4f transitions which are well shielded by from surrounding crystalline field; i.e. the correspondingly emitted light is in a narrow frequency band (not influenced by crystal field variations) and is not influenced by temperature variations.

* Especially of interest are emission frequencies which correspond to applications in the opto-electronic environment, e.g. fiber communication. Erbium 3+ ions exhibit a strong emission at 1.54 μm, which corresponds to the wavelength of lowest absorption in silica fibers. Er-doped fibers of several meter length have been used as light amplifiers for 1.54 μm, when pumped by suitable excitation wavelengths.

The objective of this work is the development of materials for efficient, narrow band and ultra-stable LEDs or lasers. Ultra-stable injection and surface emitting lasers emit in a narrow range, but variations in temperature and in the electron injection level cause frequency instabilities (mode hopping). Efficient narrow band emitters with good frequency stability are a fundamental requirement not only for fiber optic communication but also for important new optoelectronic devices and systems, such as light broadcasters for optical computing, laser gyros or image comparitors [9].

Research goals are to produce efficient Er^{3+} emitting semiconductor device by 1) finding the suitable Erbium metal-organic and growth conditions to incorporate Er in GaAs, 2)controlling the percentage of the Er dopant which is incorporated substitutionally, i.e. in the 3+ state. Growth conditions, such as V/III ratio, temperature and codopants have an influence. 3) optimizing the total Erbium dopant concentration; (too high a concentration may lead to defective crystal growth or concentration quenching). 4) maximizing the transfer of energy to the Er^{+3} ion from the excited semiconductor by resonant energy transfer (radiant or via the Auger process) and impact excitation.

IV.B.3.2 ACCOMPLISHMENTS AND SIGNIFICANCE:

* Growth of Erbium doped epitaxial GaAs was accomplished by MOCVD. Several Erbium precursors were used, among them Tris(isopropyl-cyclopentadienyl)-erbium and Tris-(n-butylcyclopentadienyl)-erbium. The characteristics of incorporation and their dependance on source temperature, growth temperature and flow ratios were established by luminescence and SIMS measurements. (cf. Figure IV.B.3.1)

* The photoluminescence spectrum which corresponds to inneratomic Erbium transitions was observed at various temperatures (cf. Figure IV.B.3.2). An analysis of the functional behavior of the intensity vs.temperature resulted in the quantitative identification of two quenching levels: $E_1 = 74 \pm 2$ meV and $E_2 = 11 \pm 2$ meV.

* Investigations of the photoluminescence intensity as function of the excitation power showed that Auger transitions play a dominant role in the deexcitation of the photoexcited carriers (cf. Figure IV.B.3.3). A quantitative fit showed that the recombination channel via Auger transitions is about 4.6 times higher than the channel resulting in the excitation of Erbium ions.

Of significance is the fact that we identified a novel Erbium containing precursor suitable for epitaxial crystal growth by MOCVD. This precursor, Tris-n-butylcyclopentadienyl-erbium, having a relatively high vapor pressure, contains in addition to Erbium only Hydrogen and Carbon, i.e. elements which are anyway present in the growth process. In particular it is free of Oxygen, Chlorine or Fluorine which are contained in other often used precursors. Thus the probability is eliminated that Erbium is incorporated in form of complexes containing Oxygen, Chlorine or Fluorine -although the possibility of a Carbon containing complex still exists.

Both temperature induced quenching and competing Auger deexciting transitions are reducing the overall efficiency of the material for LEDs or LDs. The quantitative identification of these competing deexcitation processes, which we carried out for the first time for GaAs:Er, is a necessary tool for the comparison of differently prepared materials and for gauging improvements. E.g. the effect of Carbon containing complexes is not known and a comparison with e.g. MBE grown samples should illustrate whether the indicated deexcitation processes are related to Carbon complexes.

IV.B.3.3 SUMMARY:

* Identified and used novel Erbium-precursor (free of O, Cl and F) for MOCVD growth.

* Established growth parameter space for epitaxial growth of GaAs:Er epilayers with mirror like surfaces.

* Characterized quantitatively competing processes (quenching levels and Auger transitions) which degrade the Er-related (1.54 μm) light emission process.

IV.B.3.4 REFERENCES

1. K. Takahei, P.S. Whitney, H. Nagagome and K. Uwai, *"Temperature dependence of intra-4f-shell photo-and electroluminescence spectra for erbium-doped GaAs"*, J. Appl. Phys. 65, 1257 (1989).

2. cf., H. Ennen et al.: *Rare Earth activated luminescence in InP, GaP and GaAs*, J. Cryst, Growt, 64, 165 (1983). H. Ennen and J. Schneider: Luminescence of rare earth ions in III-V semiconductors, in L.C. Kimerling and J.M. Parsey (Eds.): Defects in Semiconductors, (AIME, New York, 1985) p. 115.

3. H. Nakagome, K. Uwai and K. Takhei: *Extremely sharp erbium-related intra-4f-shell photoluminescence of erbium-doped GaAs grown by MOCVD*, Appl. Phys. Lett. 53, 1726 (1988).

4. H. Ennen et al.: *Photoluminescence excitation measurements on GaAs: Er grown by molecular-beam epitaxy*, J. Appl. Phys., 61, 4877 (1987).

5. G. Pomerenke, R.Hengehold and Y.K. Yeo: *Excitation Mechanism of Rare Earth Emissions (Yb, Tm, Er, Pr) in GaAs and InP*, Proceedings, 16th Int. Conference on GaAs and Related Compounds, (Kyoto, 1989).

6. A. Rolland et al.: *Erbium-doped GaAs Light-emitting Diode at 1.54 μm, Electron*. Lett. 24, 956 (1988).

7. P.S. Witney et al.: *Erbium-doped GaAs Light-Emitting Diodes Emitting Erbium f-shell Luminescence at 1.54 μm*, Electron. Lett. 24, 740 (1988).

8. J.P. van der Ziel, M.G. Oberg and R.A. Logan: *Single longitudinal mode operation of Er-doped 1.5 μm InGaAsp lasers*, Appl. Phys. Lett., 50, 1313 (1987). (The authors attribute the origin of lasing action to Er-caused inhomogeneities).

9. cf. solicitations PRDA #89-18 and #90-15 from ASD/PMREA,WPAFB,OH.

Published Papers:

"Radiative and Nonradiative Transitions in GaAs:Er", X.M. Fang, Y. Li and D.W. Langer, J. Appl.Phys. 74, 6993 (1993).

"Photoluminescence of Highly Er-Doped Silica Films and Er-Doped GaAs", H.K.Kim, C.C. Li, X.M. Fang, Y. Li, D.W. Langer and J. Solomon, accepted J. Luminescence (1993).

"MOCVD Growth of GaAs:Er Using $Er(C_4H_9C_5H_4)_3$", X. M. Fang, Y. Li, D.W. Langer and J. Solomon, J. Electron. Mater. submitted (1993).

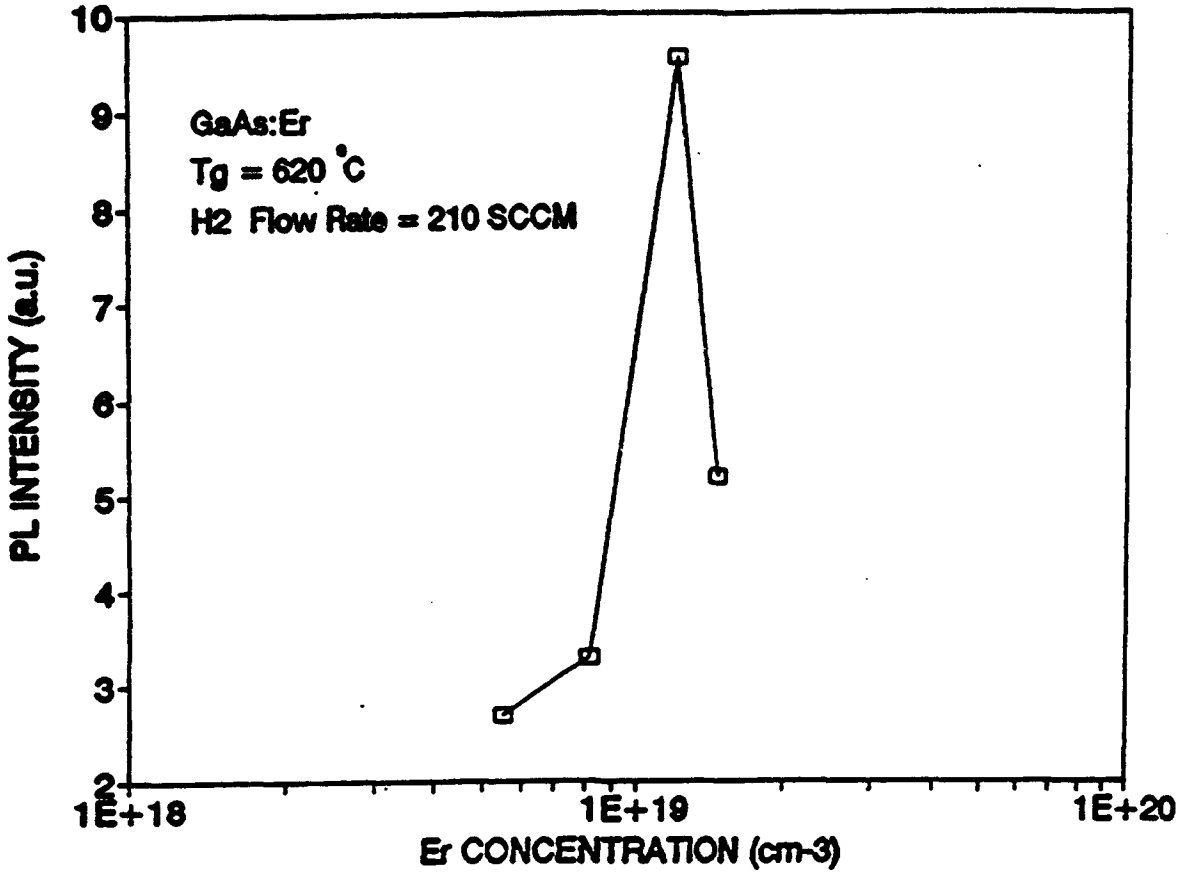

Figure IV.B.3.1: Example of grow[illegible]ameter studies: Photoluminescence [illegible]e to the trivalent Erbium as function of the maximum Erbium concentration, as determined by SIMS measurements at an epilayer growth temperature of 620 °C and constant V/III vapor flow ratio of 20 to 1. The temperature of the Erbium source was changed from 180 to 220°C, resulting in higher Er concentrations. The light emission, however, reaches a maximum because too high an Er concentration results in inferior morphology and concentration quenching.

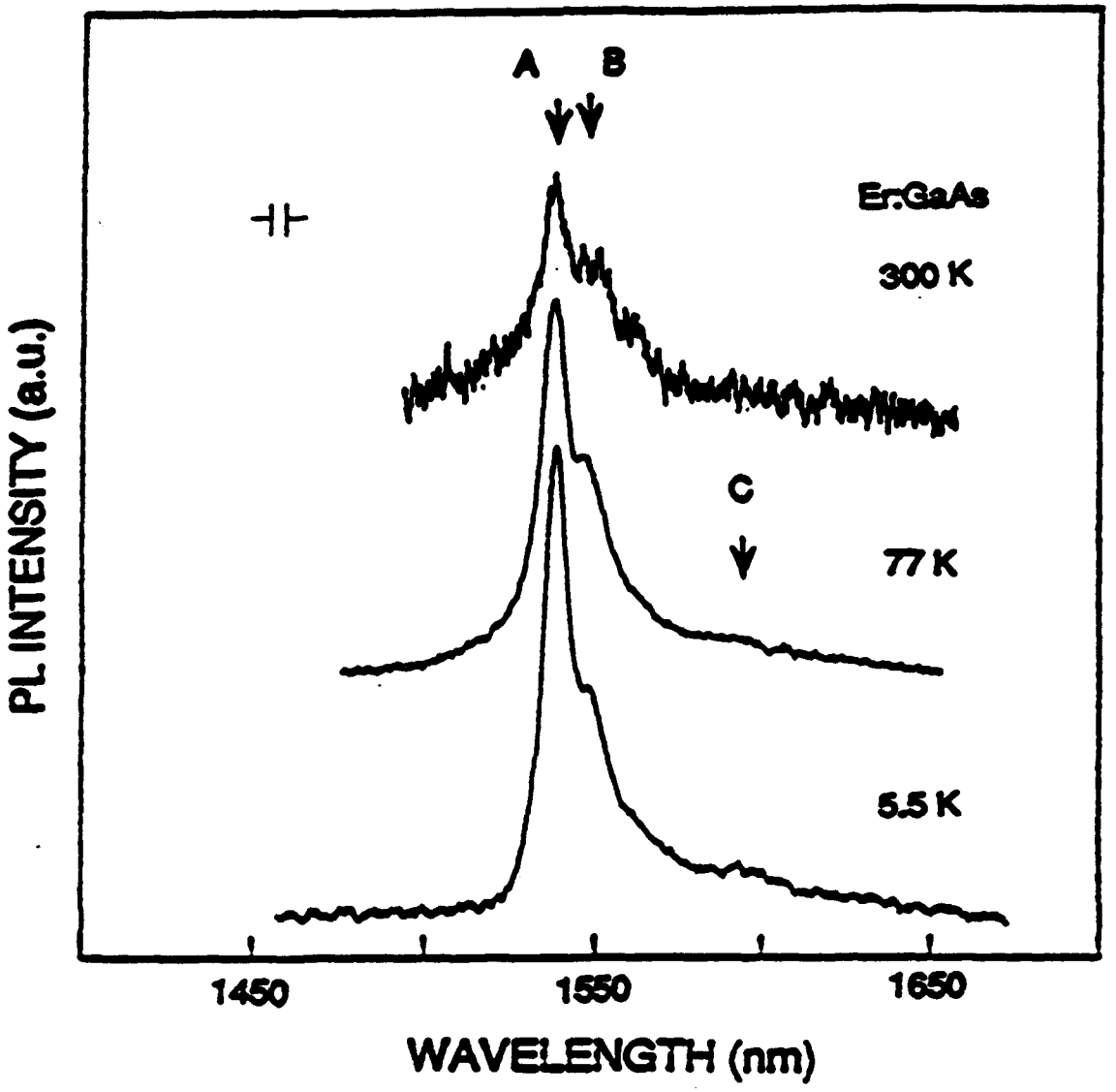

Figure IV.B.3.2: Spectrum of Erbium related photoluminescence at different temperatures. The analysis of the integrated intensity as function of temperature results in the identification of two dominant quenching levels and their relative contributions. The origin of these quenching levels is presently unknown.

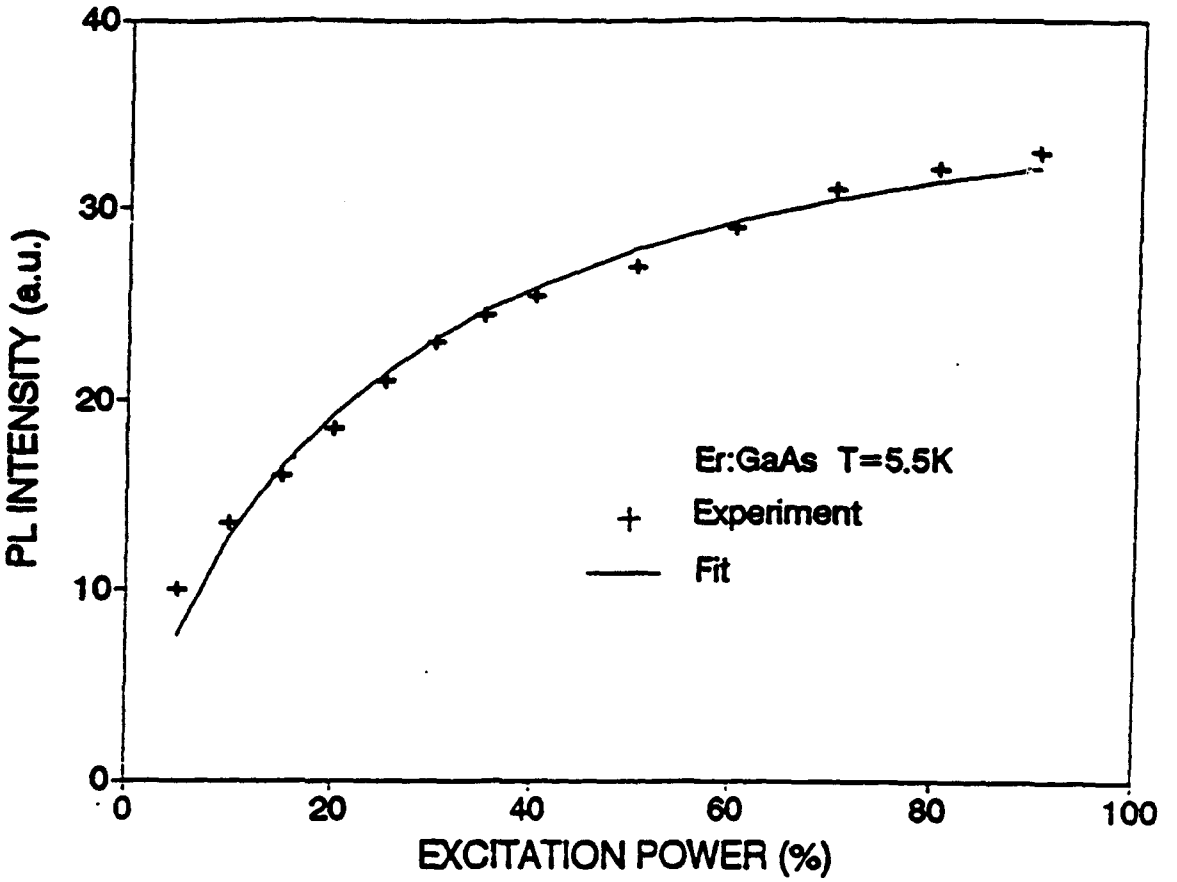

Figure IV.B.3.3: Erbium related photoluminescence intensity as function of the excitation power. An analysis results in an identification of an Auger process which competes with the excitation of the Erbium ions. It is about 4.6 times more efficient than the excitation of Erbium ions. The nature of this Auger process is presently unknown.

IV.B.4 Quantum Well Structures For Integrated Optoelectronics

Principal Investigator:	Professor D.W. Langer Electrical Engineering Department University of Pittsburgh
Other Faculty Participants:	Dr. J.R. Blachere Materials Science and Engineering Department University of Pittsburgh
	Dr. R. D. Coalson Department of Chemistry University of Pittsburgh
	Dr. J. Hurley Hampton College, Virginia (Visiting Professor)
Students:	Mr. H. Rahman Mr. A. Ali Mr. X. Fang Mr. H.S. Chu

IV.B.4.1 INTRODUCTION:

Integrated optoelectronic devices will revolutionize communications, networking, signal processing and optical computing. This integration will involve, for example, the coupling, at the fabrication stage, of lasers with waveguides, modulators and detectors. The cost and reliability advantages of this optoelectronic integrated circuit (OEIC) technology is abundantly clear as is the increased performance of such devices. The most promising systems for development involve GaAs-based hetero- and quantum well structures.

Recently, Langer and Chmielowski patented the idea of a novel waveguide coupler/switch that uses multiple quantum wells (MQW) to couple monochromatic light between waveguides. The operation of this device depends on the high electrorefractive coefficient which occurs near the confined exciton transition of the MQW. [1] This coupler is ideal for integration because of its modest voltage needs (6 V) and its short coupler lengths (100μm). The concept this device can be generalized to construct "field induced waveguides". These light guides can switch from "guiding" to "nonguiding" (or vice versa) by the application of an electric field. This allows changing the optical structure by the application of appropriate voltages. The original fabrication process does not permanently determine the optical path. This type of device was recently demonstrated [2] experimentally by Huang et al. [3] and a vertical MQW coupler, exhibiting these

properties, was demonstrated by Cavailles et al. [4] A major difficulty, however, with these devices is the strong absorption of the MQW waveguide near the exciton transition.

The physical principles on which such operation depends are:

* The confinement of an exciton in a quantum well increases its binding energy.

* The electric field induced shift of the exciton energy in a quantum well is larger than the shift induced by the same field in a bulk crystal.

* For a wavelength near the long wavelength edge of the exciton absorption, the refractive index change due to an applied electric field is up to 100 times larger than the change found for the same wavelength in the corresponding bulk material.

We proposed a solution to the problem of high absorption within the guide; reducing it theoretically by 95% as follows: we will build a device where the light does not propagate inside the MQW, but propagates adjacent to it within an $Al_xGa_{1-x}As$ guiding layer. Figure IV.B.4.1 shows the proposed concept: confinement in the plane of growth (y) occurs due to the ingrown difference of refractive indices and confinement perpendicular to it (x) occurs due to an applied electric field which dramatically changes the index in the MQW-confinement layer. We demonstrated previously that we are capable of producing similar GaAlAs/GaAs MWQ structures with defined wells and barriers of 10 nm widths. [5]

The objective of this work was to create new materials structures with well determined and reproducible indices of refraction in different layers, such that they correspond to design parameter for a new class of integratable optoelectronic devices. We will propose new devices based on the electric field induced change of the index of refraction in MQWs for the purpose of "field induced waveguides".

The initial development work involved the critical adjustment of the index of the guiding layer relative to that of the MQW, by varying the Al content in the ternary epilayer. We monitored the confinement and the waveguide absorption properties. Several structures were modelled by our effective index method of calculation. Additional corroborating calculations originated from Dr. Robert Coalson's group. Material was grown in accordance with modelled thicknesses and indices of refraction (i.e. Aluminum content) and it was evaluated in terms of actual thicknesses, electric properties (can a field be applied) and optical properties.

IV.B.4.2 ACCOMPLISHMENTS AND SIGNIFICANCE:

* **Waveguide design with propagation in the MQW is investigated.** An experimental set-up is expanded for two types of measurements: 1) using the Avalanche Photo Diode (APD) for modulative "on-off" measurements, i.e without an additional electric field applied perpendicular to the MQWs and with such field applied and 2) using the Beam Shape Analysis (BSA) the variation of the beam confinement was measured directly.

The set up is schematically shown in Fig.IV.B.4.2: The light of the Titanium Sapphire laser, which is excited by an Argon laser is modulated by an Acousto-Optic Modulator (AOM) capable of delivering pulses of a few hundred nanoseconds or longer. The light was endfire coupled into the waveguide with a 40 power microscope objective. The beam was linearly polarized perpendicular to the growth direction. The light transmitted through the rear facet of the waveguide was imaged by a 20 power microscope objective onto a silicon Avalanche Photo Diode (APD). The output of the APD was passed to a computer through an A/D converter. Part of the light in front of the ADP was reflected using a beam splitter to an infrared sensitive television camera, which was first used for alignment purposes. The camera was also equipped with a beam shape analyzer (BSA) allowing the measurement of the optical beam profile in any horizontal or vertical position. Encoder mikes and microprocessor controlled stepping motors were used for the alignment of the samples. A provision was provided in the sample mount so that a Voltage could be applied to the sample. A pulse generator triggered by the AOM was used to apply the electric field only for time when the sample was illuminated. The duty cycle of the pulses was less than 10% in order to avoid any sample heating effects.

* These measurements resulted in the determination of the **variation of the index of refraction as a function of the applied Voltage.** 1) by analysis of the induced absorption via a Kramers-Kronig transformation and 2) by analysis of the change of the confinement profile with Voltage using the effective index method. Both methods' results agreed to within 15%. Previously, the variations of the index in MQWs had never been measured over such an extended wavelength range and never been verified by two independent methods. These results were published by us in detail. [6]

* With reference to our proposal to create field induced waveguides with much reduced absorption for the propagating wavelengths, we **demonstrated the reduction of absorption (increase of attenuation length) by more than an order of magnitude** in waveguides with light propagation adjacent to MQW layers. Figure IV.B.4.3 shows the measured attenuation length in a wavelength region from 865 to 880 nm of such structure (solid line) and compares it to calculated values for this structure (squares) and for one where light propagation occurs inside a similar MQW layer (triangles).

The properties of these waveguides with reduced absorptions were calculated in collaboration with Prof. Coalson. It was found that field induced MQW single mode waveguides can be designed which should not have a loss of more then 1db over 150 μm, a length which is still practical in integrated opto-electronic designs. The details of this model and the results of the calculations are accepted for publication. [7]

IV.B.4.3 SUMMARY:

* Experimental Automated Analyses of Waveguide Transmission Characteristics using Pulsed Absorption and Beam Confinement Measurements

* Determination of Field Induced Index of Refraction Change of MQW Waveguide Layers over a Wide Wavelength region

* Fabrication of Multi-Quantum Wells with Improved Interface Sharpness

* Demonstrated Reduced Absorption in Waveguide with MQW Cladding Layer for Field-Induced Waveguides

IV.B.4.4 REFERENCES:

1. D.W. Langer and M. Chmielowski, "Quantum-Well Wave Guide Coupler", Superlattices and Microstructures 6, 17 (1989); M. Chmielowski and D.W. Langer, "Multiple-Quantum-Well Vertical Light Guide Switch", J. Appl. Phys., 65, 927 (1989); Also U.S. Patent: *Vertical Multiple-Quantum-Well Light Guide Switch* No. 4, 923,264 (May 8, 1990).

2. D.W. Langer et.al., Quantum Well Structures for Integrated Opto-electronics", SPIE vol. 1215 Digital Optical Computing, p. 243-251, (Jan. 1990).

3. T.C. Huang, Y. Chung, N. Dagli and L.A. Coldren, GaAs/AlGaAs multiple quantum well field-induced optical waveguide", Appl. Phys. Lett., 57, 114 (1990).

4. J.A. Cavailles and M. Erman, "Very Low Power Nonlinear Directional Coupling in a p-i (MQW)-n Vertical Coupler Using Electrooptic Feedback" IEEE Photo. Techn. Lett., 2,343-345, (1990).

5. H.G. Lee, H.K. Kim,S.H. Park and D.W. Langer, "Study of GaAs/AlGaAs Quantum Well Structures Grown by MOVPE using Tertiarybutylarsine", SPIE Physical Concepts of Materials for Novel Optoelectronic Device Applications I, SPIE, vol. 1361, pp. 893-900 (1990).

6. H.U. Rahman, D.W. Langer, J.Falk and S.H. Park,"Measurement of Electric Field Dependent Refractive Index Variations in GaAs/AlGaAs Quantum Well

Waveguides", Intern. J. Optoelectron. 8, 259-266 (1993).

7. R.D. Coalson, D.K. Pant, A. Ali and D.W. Langer, "Computing the Eigenmodes of Lossy Field-Induced Optical Waveguides", J. Lightwave Techn., accepted (Jan. 1994).

Published Papers:

"Measurement of Electric Field Dependent Refractive Index Variations in GaAs/AlGaAs Quantum Well Waveguides", H.U. Rahman, D.W. Langer, J. Falk and S.H. Park, Intern. J. Optoelectron., 8, 259-266 (1993).

"Computing the Eigenmodes of Lossy Field-Induced Optical Waveguides", R.D. Coalson, D.K. Pant, A. Ali and D.W. Langer, IEEE J. Lightwavetechn., accepted (Jan.1994)

Field Induced Waveguide with Reduced Absorption

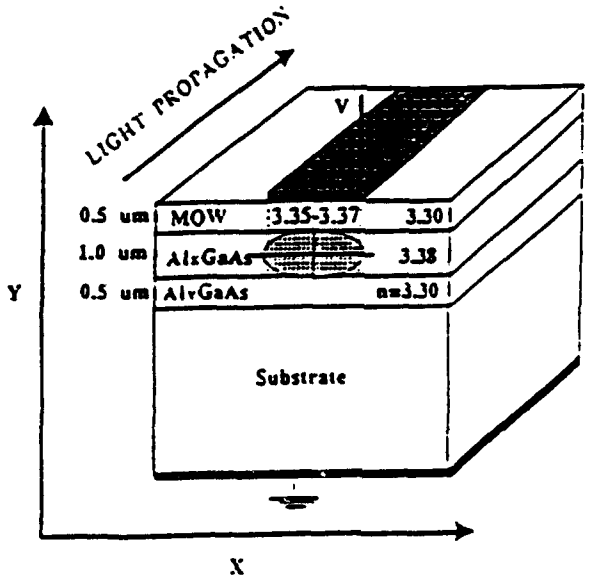

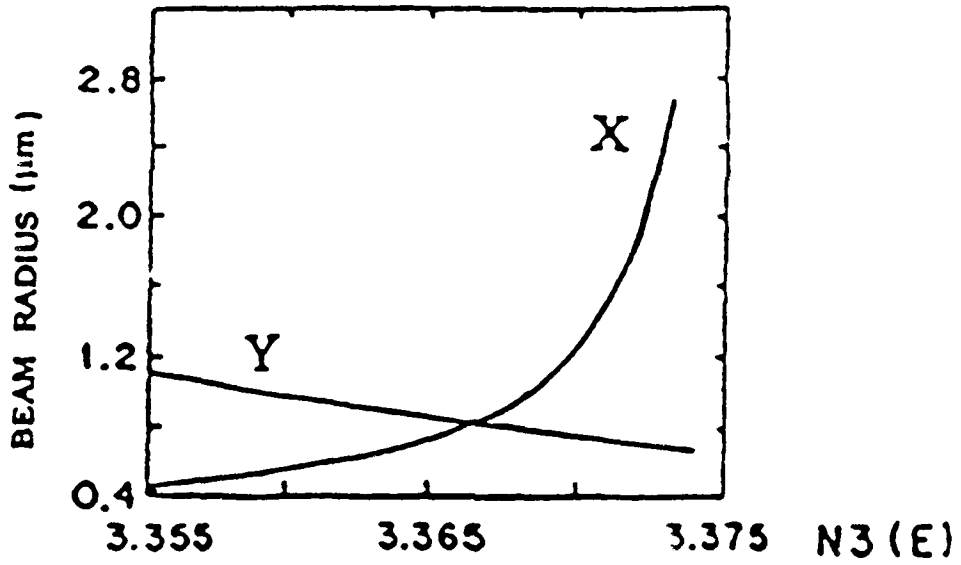

ELECTRIC FIELD INDUCED VARIATION OF
REFRACTIVE INDEX IN M Q W

Figure IV.B.4.1 Confinement of light beam (shaded region) propagating in z-direction. The values of the refractive index of the middle guiding region and the adjacent cladding regions are indicated. The refractive index of the MQW-cladding layer may vary due to the strength of a perpendicularly applied electric field - and thus determine the degree of confinement of the propagating beam.

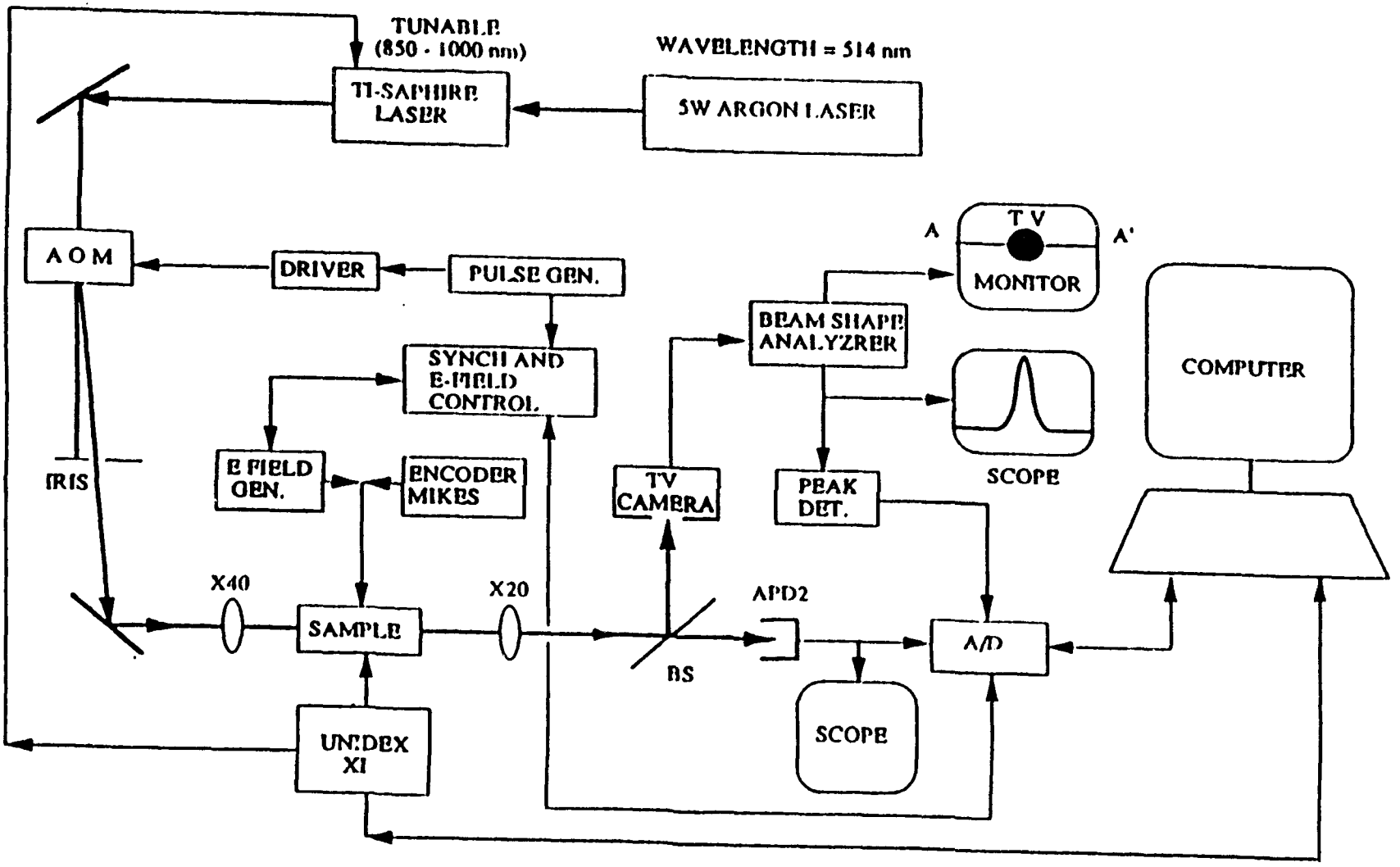

Figure IV.B.4.2 Experimental setup to measure beam propagation parameter, i.e shape and intensity of transmitted beam.

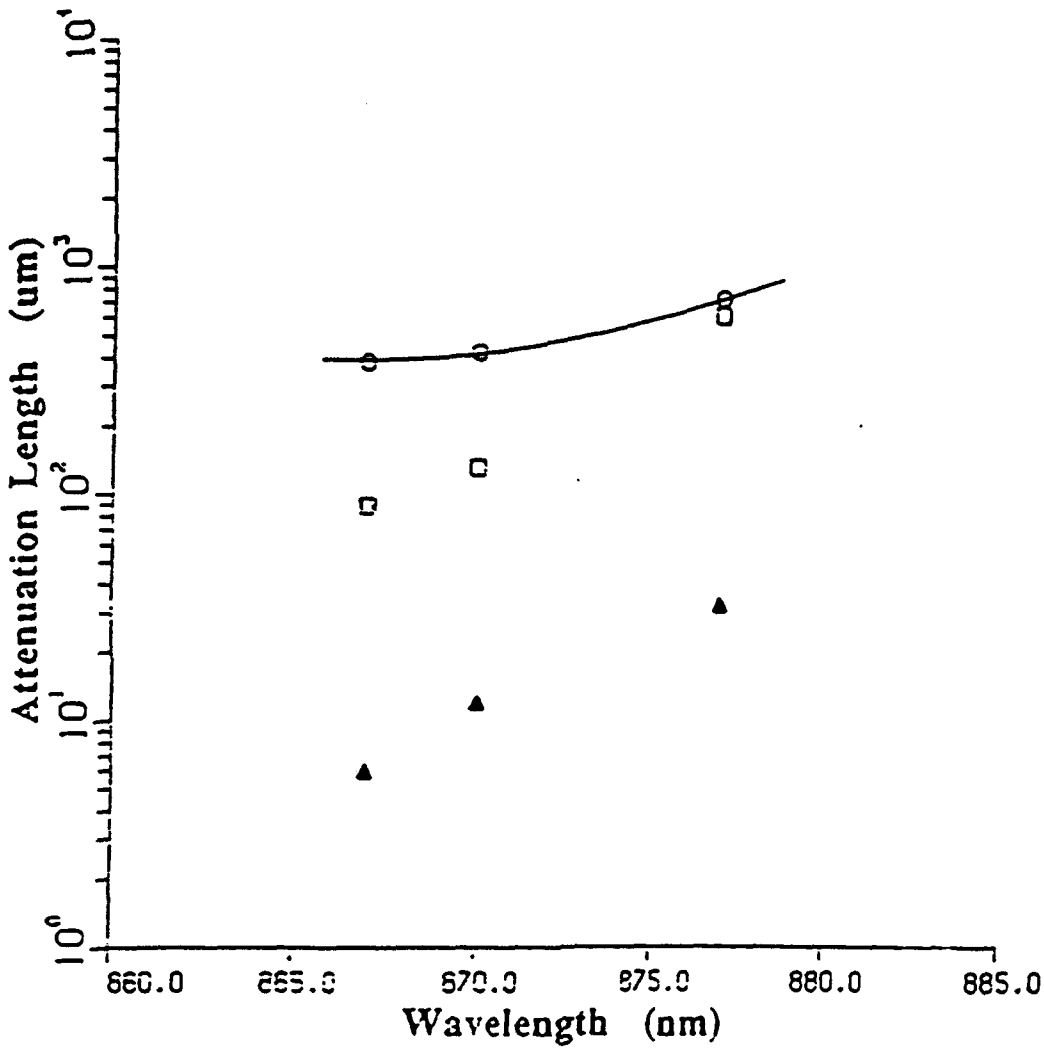

Figure IV.B.4.3 Solid line shows measured attenuation length of "MQW-waveguide with reduced absorption" (as shown in Fig. 1) for a 66 kV/cm field. Open squares are calculated points for this waveguide. Triangles are calculated values for a comparable waveguide with propagation in the MQW layers. Comparison indicates that the new waveguide structure has an increased attenuation length by a factor between 12 and 20.

IV.B.5 Highly Nonlinear Semiconductor-Metal Composites

Principle Investigator: Professor Joel Falk
Department of Electrical Engineering
University of Pittsburgh

Other Faculty Participants: Dr. Ramesh Patel
Department of Chemistry
Clarkson University

Dr. Sanford Asher
Department of Chemistry
University of Pittsburgh

Students: Ms. X. Hua
Mr. Y. Shi
Mr. G. Bijak

IV.B.5.1 INTRODUCTION

Nonlinear optical coefficients of materials currently available are approximately an order of magnitude too small to be useful with low power, large-scale-integratable, cw sources such as laser diodes. Large nonlinear optical responses result from either large nonlinear coefficients or high electric field strengths. Enhanced fields are available in the vicinity of a metal-semiconductor interface. We are preparing thin, smooth coatings of metals, e.g. silver at the surface of semiconductors e.g. CdSe. The presence of the metal will greatly enhance the local electromagnetic field strengths near the metal-semiconductor. The enhanced electromagnetic field strength will extend into the semiconductor material and increase the material's nonlinear response and its usefulness for device applications. [1]

IV.B.5.2 OBJECTIVES

Our objectives for the second year of this program were 1) the preparation and 2) the evaluation of semiconductor-metal composites. We are preparing semiconductor metal composites in ways detailed below. We are evaluating them physically and optically. Our aim is to produce materials with strong optical nonlinearities that are useful for optical switches and couplers.

The preparation of the composite nanoparticles consists of two major objectives:

1) Preparation of monosized semiconductor materials. A typical diameter of the material produced is 150 nm. The monosized particles, having large nonlinear susceptibilities $\chi^{(3)}$, were prepared using a controlled precipitation technique. One

semiconductor material studied is CdSe. Further details are given below.

2) Application of a metallic (silver) coating to the semiconductor (CdSe) nanoparticle and the determination of the experimental parameters required to generate thin (a few nm), smooth coats of silver on the semiconductor nanoparticles.

The evaluation of the composite particles was directed toward characterizing them physically and optically. Electron micrographs were taken of all samples produced. Linear optical (absorption) and nonlinear (third order susceptibilities) optical properties were obtained.

IV.B.5.3 ACCOMPLISHMENTS AND SIGNIFICANCE

Work during the second year of this project has focused on two areas:

A. Preparation of Samples. In the last sixteen months of the program, the following samples, prepared at Clarkson University were sent to Pitt for investigation :

Ag
Ag shell/Ag_2S core
Ag shell/Ag_2Se core
CdSe
Ag shell/CdSe core

The samples of greatest technical interest are the CdSe/Ag composites. The other samples are of interest primarily for the development of growth techniques. Samples prepared during the first year of the program included silver nanoparticles and CdSe nanoparticles but not metal (e.g. silver) coated semiconductors (e.g. CdSe). Most of the samples prepared during the last year were silver coated CdSe. The thin (a few nm) smooth coats of silver on the semiconductor cores were achieved by controlled photochemical methods based on the generation of highly reducing organic free radicals (in addition to direct photochemical reduction of the complexed metal ion). Details of this method were given in the Material Research Center's first annual report (November 23, 1992). [2] Details concerning the application of these silver coatings to CdSe are given below.

All semiconductor samples prepared during the past year show a much better size uniformity than those prepared during the previous year. Size distribution was restricted by careful control of the growth of semiconductor core particles as described below.

<u>CdSe Preparation</u>:

A .001 TO .0001 M cadmium sulfate solution was made by dissolving

reagent grade powder (Aldrich) in triply distilled water using an all glass still. All glass vessels used for particle preparation were made thoroughly dust free by steam cleaning for approximately one half hour prior to use. Two growth modifiers, hexametaphosphate or polyvinylalcohol (PVA) were added at a level of 0.1% by weight. The concentration ranges specified are very critical, and were established by experimentation. Although both growth modifiers worked well (based on spectral absorption results), PVA was preferred because of better reproducibility and all samples evaluated optically were made using PVA.

Between 1-5 ml of hydrogen selenide was injected above 100 ml of the cadmium sulfate solution in a closed three neck flask with a magnetic stirrer. The hydrogen selenide was generated in a separate flask with a serum cap, by the hydrolysis reaction of aluminum selenide with distilled water. The experimental [3] procedure is very similar to that used in preparation of quantum-dot- sized PbS. In general, aging of the samples (aqueous suspensions) over periods of days results in larger, 50-200 nm size, uniform particles. This process can be retarded by refrigeration of the samples, and the growth process arrested at a given stage by incorporating the particles in a solid matrix, e.g. low temperature silicate glass, or polymer thin films. The CdSe particles are cleaned thoroughly five times by repeated centrifugation and resuspension in triply distilled water (TDW). The cleaned particles were resuspended in 100 ml of TDW, followed by sonication for one minute to eliminate agglomeration.

Silver Coating of CdSe Particles:

The thin (a few nm) smooth coats of silver on dielectric cores are achieved by controlled photochemical methods. [2] The CdSe suspension containing acetone and propanol-2 was exposed to low intensity UV radiation for a period of four hours. Stirring of the sample, and exclusion of oxygen by bubbling nitrogen in the UV reaction vessel, was critical. A visible change in the color of the sample could be noticed. This color change was confirmed by absorption spectroscopy.

B. Evaluation of Samples. Evaluation of samples consisted of electron microscopy for physical properties, optical absorption for linear optical properties and four-wave-mixing for nonlinear optical properties. Evaluation facilities were improved during the past year so that degenerate-four-wave-mixing could be performed on all samples. This technique measures the nonlinear susceptibility $\chi^{(3)}$. The use of a pulsed dye laser permitted the measurement of the frequency dependence of the nonlinear response. Particle size distributions and particle constituents were determined using electron microscopy done in the Department of Material Science and Engineering at Pitt. Theoretical (computer) extensions to the theory of metal-semiconductor composites were used along with the STEM and linear absorption data to infer the thickness of the silver coating on the CdSe core.[1]

Some typical measurements on a silver coated CdSe sample are shown in

Figures IV.B.5.1 and IV.B.5.2. Figure IV.B.5.1 shows a STEM photo of the composite particles. The average particle diameter is approximately 150 nm. The distribution of sizes is small. A comparison with similar STEM photos in the first Material Research Center's annual report shows that the growth process has been much improved.[2] The thickness of the silver coating cannot be determined from electron microscope data but can be inferred from the sample's optical absorption spectrum. Optical absorption of a typical sample is shown in Figure IV.B.5.2. The locations of the absorption peaks indicate the value of the ratio of core/shell radii (r1/r2). Figure IV.B.5.3 shows the results of theoretical calculations of absorption spectra for several values of this ratio and shows that the experimentally observed absorption peaks (near 350 and 585 nm) are indicative of a ratio r1/r2 = 0.68. Fig. IV.B.5.4 shows the expected electric field enhancement as a function of wavelength for a CdSe/Ag composite having r1/r2 = 0.68. Figure IV.B.5.5 shows an electric field enhancement of approximately 4 at a wavelength near 600 nm.

Our experimental four-wave-mixing apparatus was designed to verify this electric field enhancement. The apparatus employed was a standard degenerate four-wave-mixing apparatus. [4] Two pump waves and a probe wave, all with the same wavelength, interact to produce a signal wave. The strength of the signal wave indicates the size of the third order optical nonlinearity $\chi^{(3)}$. Degenerate four-wave-mixing measurements were made with each of the samples received from Clarkson University. The laser source for the input pump and probe waves was either a frequency doubled Nd:YAG laser (wavelength = 532 nm) or a tunable dye laser pumped by the frequency doubled laser.

Third order nonlinearities recorded are due to two possible physical mechanisms: a) absorption of the pump and probe beams causes heating which perturbs the refractive index of the composite material and its solvent. This thermal nonlinearity is characterized by a relatively slow (nsec) response and a signal dependence of the absorption coefficient of the composite material but not on the electric field enhancement at the interface between silver and semiconductors. In addition, the output signal obtained from a thermal nonlinearity depends on a precise arrangement of pump and probe polarizations. [5] b) a third order polarization generated by the simultaneous application of two pump fields and a probe field. This electronic nonlinearity has a fast (subpicosecond) response time and should exist for most combinations of pump and probe polarizations. The signal intensity due to the electronic nonlinearity is proportional to the cube of the applied electric field and is thus is a direct indicator of electric field enhancement within the composite particle.

Figures IV.B.5.5 and IV.B.5.6 show representative experimental four-wave-mixing data. Figure IV.B.5.5 shows the variation in four-wave mixing reflectivity with input laser power. Figure IV.B.5.6 shows the measured variation of nonlinearity with wavelength (nonlinearity is proportional to the square root of four-wave-mixing reflectivity). Note that Figure IV.B.5.6 does not show a substantial variation of mixing signal with wavelength and consequently does not show the

electric field enhancement indicative of an electronic nonlinearity. Further verification that the nonlinearity obtained was thermal in nature came from two related experiments. In the first, an aqueous solution containing the composite CdSe/Ag particle was circulated through a cell which had transparent windows, so that the volume of composite material illuminated by the laser beams was rapidly replaced. This prevented heating of the material in the active volume and resulted in the disappearance of the four-wave-mixing signal. In a second experiment, the polarizations of the two pump beams and the probe beam were arranged so that a thermal signal was impossible but an electronic signal could exist. No output signal was observed. [5] We note that the size of the signals recorded in Figures IV.B.5.5 and IV.B.5.6 are roughly the size of signals recorded for four-wave-mixing from a reference sample of CS_2. (Carbon disulfide has been widely investigated as a nonlinear material and its nonlinear coefficients are well known.) The nonlinearity recorded in Figures IV.B.5.5 and IV.B.5.6 is about an order of magnitude smaller than that which might be useful for optical limiting. [6]

The four-wave-mixing signal caused by the thermal nonlinearity must be reduced and any signal due to an electronic nonlinearity enhanced if the effects of electric field enhancement are to be observed. This can be accomplished by maintaining or slightly reducing the energy in the pump and probe beams while increasing peak powers. Replacing the 5 nanosecond pulse-duration laser with a 5 psec pulse-duration laser would accomplish this. Thermal nonlinearities are too slow to respond to psec duration pulses. Furthermore a reduction of pulse duration by a factor of 100 (at constant energy) results in a 1000 fold increase in peak power and a 10^9 increase in the (electronic) four-wave-mixing signal. We note that a recently published report of four-wave-mixing in a composite material (Cu:silica) employed a psec duration dye laser. [7] Experiments are currently being planned that will replace our nsec pulse-duration laser with a psesc laser.

IV.B.5.4 SUMMARY

Theory of nonlinear optics in composite materials extended to systems of experimental interest.

a) enhancement of electronic nonlinear effects calculated for wide variety of composite materials.

Variety of Samples Prepared:

a) To study growth techniques: nanosized silver, CdSe, Ag_2S shell and silver core.

b) Technologically interesting composite: CdSe core and silver shell.

Evaluation of samples.

a) linear absorption
b) electron microscopy
c) four-wave mixing

Thermal nonlinearities observed; thermal signals obscured the measurements of electronic nonlinearity. A psec duration laser is required to observed electronic nonlinearities and electric field enhancement.

IV.B.5.5 REFERENCES

1a. "Composite Structures for the enhancement of nonlinear-optical usceptibility", A.E. Neeves and H.H. Birnboim, Jour. Opt. Soc. Am. B. 6, 787 (1989).

b. "Highly Nonlinear Semi-conductor-Metal Composites", Yan Shi and Joel Falk, and R.Patel, paper presented at the March 1994 meeting of the American Physical Society, Pittsburgh, PA.

2. First Annual Progress Report, Materials Research Center, University of Pittsburgh, pp. 147-148, Pittsburgh, PA., November 23, 1992.

3. "Synthesis and Optical Properties of Quantum-Size Metal Sulfide Particles in Aqueous Solution", J.M. Nedeljkovic, P. Kaufman, R.C. Patel, C. Joyce-Pruden, and N. O'Leary, J. Chem. Education, 70, 342 (1993).

4. "Conjugate waveform generation and image reconstruction by four-wave mixing", D. Bloom and G.C. Bjorklund, Appl. Phys. Lett. 31, 592 (1977).

5. "Picosecond degenerate four-wave mixing in soluble polydiacetylenes", W.M. Dennis, W. Blau and D.J. Bradley, Appl. Phys. Lett. 47, pp. 200, 1985.

6. Private communication, S. Guha, Martin Marietta Research Labs, Baltimore, MD. (1993).

7. "Picosecond nonlinear optical response of a Cu:silica nanocluster composite", R.F. Haglund, Jr., L. Yang, R.H. Magruder III and J.E. Wittig, K. Becker, R.A. Zuhr, Optics Letter, 18, pp. 373, March 1, 1993.

Figure IV.B.5.1 Sample CdSe025-Ag2. Silver Coated CdSe Composite Particles.

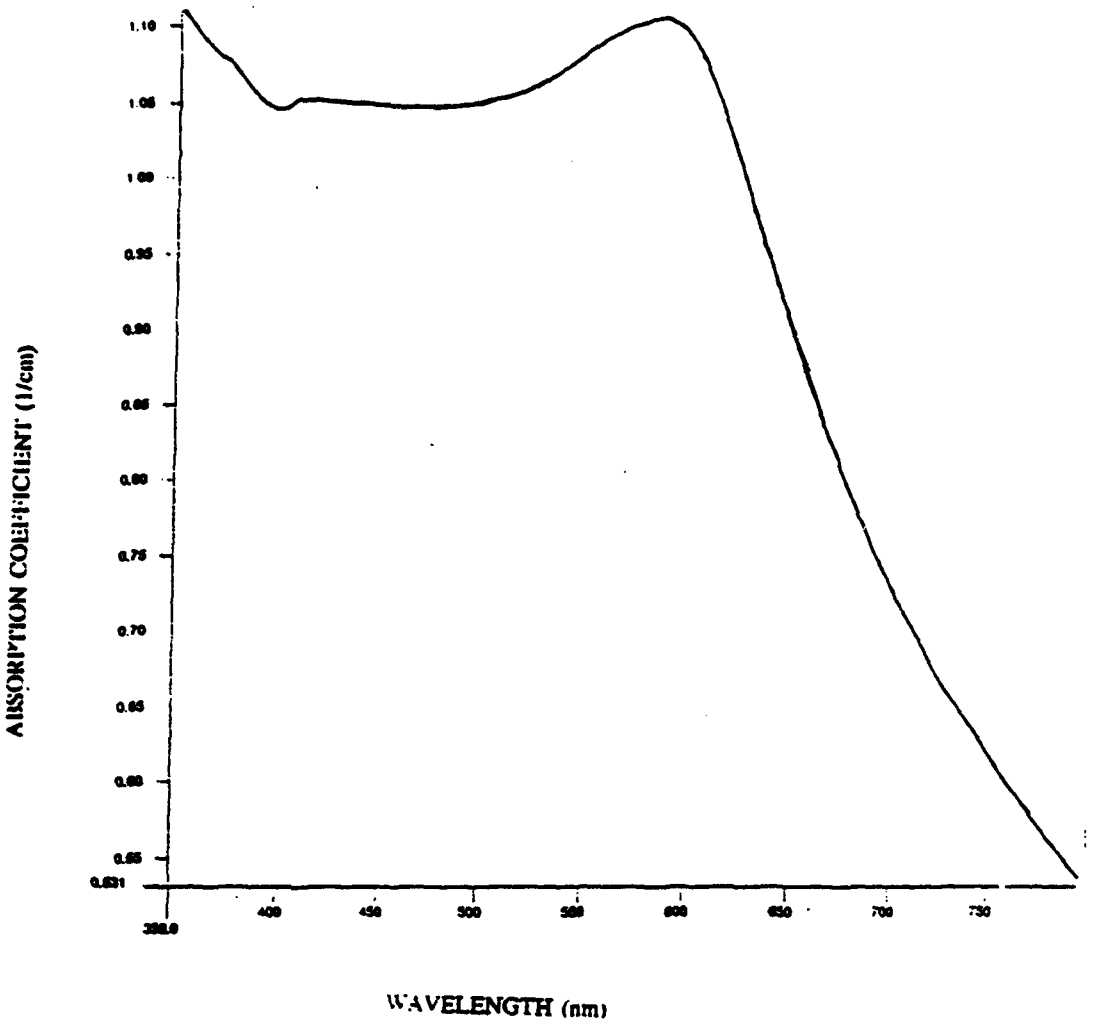

Figure IV.B.5.2 Sample CdSe025-Ag2. Silver Coated CdSe Composite Particles Absorption Versus Wavelength (experimental).

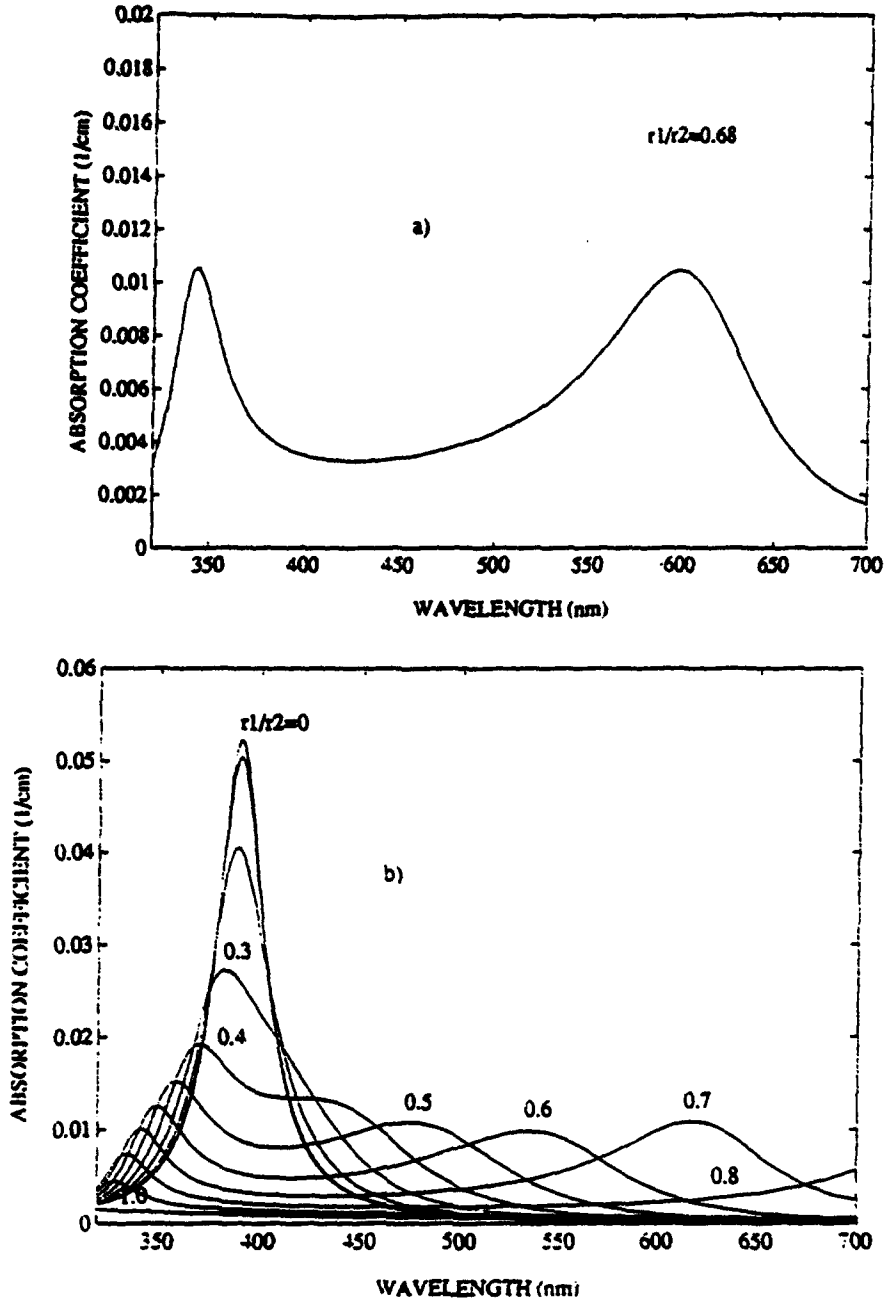

Figure IV.B.5.3 Sample CdSe025-Ag2. Silver coated CdSe composite particles absorption versus wavelength (theoretical). a) Ratio of CdSe core radii/Ag shell = r1/r2 = 0.68 b) r1/r2 = 0.5, 0.6, 0.7, 0.8.

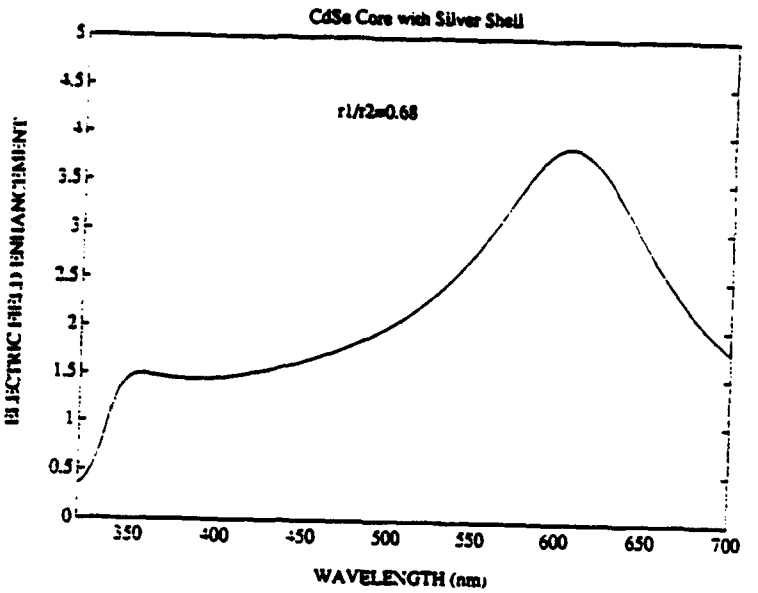

Figure IV.B.5.4 CdSe Core, Silver Shell (rl/r2 = 0.68). Expected field enhancement in the semiconductor core versus wavelength. Field enhancement is relative to the applied field.

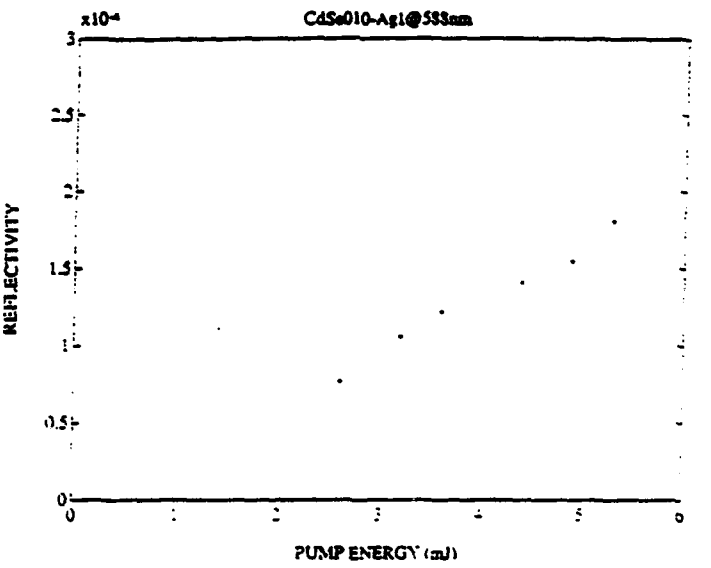

Figure IV.B.5.5 Sample CdSe025-Agl. CdSecore, siiver shell. Four-wave mixing reflectivity versus pump energy (wavelength = 588 nm). Reflectivity is defined as the ratio of output signal energy to input probe energy.

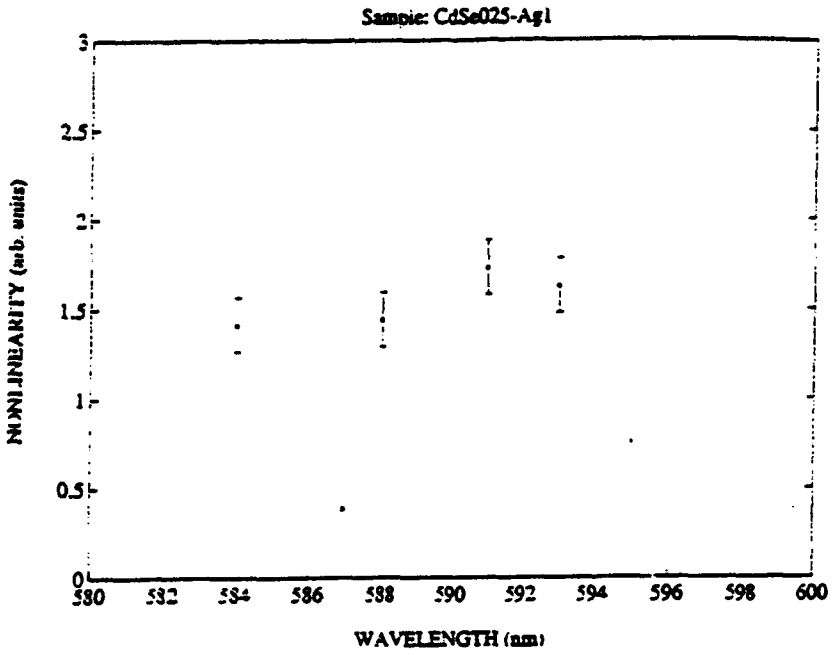

Figure IV.B.5.6 Sample CdSe025-Agl. CdSe Core, Silver Shell. Third-Order Nonlinearity Versus Wavelength. The nonlinearity is approximately proportional to the square root of the four-wave mixing reflectivity (ratio of output signal energy to input probe energy).

IV.B.6 New Laser Systems Featuring Ultra High Resolution Capabilities

Principal Investigator:	Professor David W. Pratt Department of Chemistry University of Pittsburgh
Other Faculty Participants:	Dr. Richard Ulsh University of Pittsburgh Johnstown, PA
Students:	Dr. J. Go Dr. A. Held Dr. S. Humphrey Mr. J. Pfanstiel Mr. B. Champagne Ms. M. McKernan

IV.B.6.1 INTRODUCTION

Intense interest has recently been generated in understanding the size dependence of bulk structural and electronic properties in a variety of materials [1]. This is because submicron, or "nanoscale" structures are likely to play a major role in the development of new electro-optic devices. Such intermediate-sized clusters can have unique properties, characteristic of neither the molecular nor the solid state limits. Examples include a new allotrope of carbon, C_{60}, magic numbers in simple metal clusters, and the existence of semiconductor crystallites that exhibit the bulk unit cell but have only partial band structure development. These "nanoclusters" have optical spectra that can be tuned in wavelength simply by varying the crystallite size.

The purpose of the proposed research is to develop high resolution laser systems that may be employed to obtain the fully resolved optical spectra of such structures, and to examine the dependence of such spectra on sample size. Assessing the size-dependent physical and chemical properties of a wide variety of optical materials will assist in developing methods for their synthesis, and for their controlled assembly into new materials with novel electronic, photonic, and biomolecular properties.

The principal laser system being developed is a tunable CW ring Ti:sapphire laser system. Hole burning and fluorescence line narrowing are two of the experimental techniques that will be used to obtain the desired optical spectra. Additionally, we are extending the operating frequency range of an existing tunable CW ring dye laser, so that the two lasers together can be operated at any wavelength between 260 and 1050 nm, with a single frequency linewidth of less than 1 MHz. Both lasers also will be used in continuing studies of the structural and dynamical properties of large organic molecules in the collision-free

environment of a molecular beam [2]. Finally, we will develop new methods for detecting and analyzing the optical spectra of single impurity molecules in small particles and crystals [3].

Our objective is to construct a frequency-stabilized Ti:sapphire laser for high resolution spectroscopy in the gas phase and in the condensed phase. The laser will operate over the wavelength range 680-1050 nm and, with frequency doubling, over the wavelength range 340-525 nm. It will be tunable in a single scan over widths up to 10 cm^{-1} in the UV. The anticipated single-frequency linewidth will be less than 1 MHz, with power levels greater than 10 mW at all wavelengths. We will develop new methods of detection of high resolution optical spectra that may be used for isolated molecules, small clusters, and samples in the condensed phase at low temperatures. We will use these methods to measure the linear, homogeneously broadened optical spectra of isolated large molecules of both pure and open semiconductors, of thin films and layered structures, of polymeric one-dimensional chains, and of self-assembling periodic structures, as a function of temperature and sample size.

IV.B.6.2 ACCOMPLISHMENTS AND SIGNIFICANCE

We have purchased the optical components for wavelength extension of the dye laser. Currently, one student (MRC Fellow Fujita) is working to obtain laser action at wavelengths shorter than 300 nm, using a BBO doubling crystal. If successful, he will use the shorter wavelength radiation to examine the fully resolved optical spectra of aniline, benzonitrile, and their devrivatives in the gas phase. Information obtained from these experiments will be used to design new NLO materials for second-harmonic generation.

We have designed and are building the new ring laser cavity for the CW Ti:sapphire laser, using the purchased (used) S/P 380A laser as a frame. The NLO equations pertinent to laser action in this system have been solved by Dr. Go. These solutions have been used to specify the characteristics of the Ti:sapphire crystal and the crystal has been ordered. Following extensive negotiations with laser companies, a large frame argon-ion laser has been ordered. This laser will provide power that is sufficient to produce up to 100 mW of single-frequency UV, *via* intracavity SHG. Lindwidths of less than 1 MHz are predicted. Additionally, we have designed and ordered the mirrors and doubling crystals necessary to achieve operation of the laser over the wavelength range 680-810 nm (fundamental) and 340-405 nm (frequency doubled). Other key parts also have been ordered. Currently, we are designing the frequency locking and scanning electronics, the calibration system, and methods for producing and detecting the high resolution spectra. Discussions with potential collaborators (*e.g.* Dr. S. Asher) are continuing. The necessary space renovations for this new project were discussed in our earlier report.

We are encouraged by a recent report [4] which shows that single frequency

Ti:sapphire lasers can be stabilized to ± 1 kHz r.m.s. with respect to a locking etalon.

While these laboratory plans were being developed, we also have been very active in the molecular beam laboratory. Of particular interest are experiments on hydrogen bonding systems, which have been shown to form the acentric crystal structures necessary for nonlinear optical materials [5]; Hydrogen bonds also are important in molecular recognition [6]; In the MRC research, we model such interactions with monomers linked together to form dimers in an otherwise non-interactive environment. We determine the structures of these dimers by measuring their rotationally resolved electronic spectra, from which the moments of inertia can be obtained with high precision. Systems studied to date include the 2-pyridone dimer [7], dimers of 4-methyl-2-pyridone and 6-methyl-2-pyridone [8], the *cis* and *trans* NH_3 complexes of 2-naphthol [9,10], 2-pyridone-H_2O and -$(H_2O)_2$ [11], 2-pyridone-NH_3 and -$(NH_3)_2$ [12], and the *cis* and *trans* NH_3 complexes of hydroquinone [13]. Additionally, we have recently detected the electronic spectra of two intriguing CH_4 complexes of fluoronaphthalene [14]. These complexes, held together by weak van der Waals forces, will provide important information about the potential energy surfaces that govern gas-surface dynamics.

A review of our recent high resolution work is in preparation [15].

IV.B.6.3 FUTURE WORK

The key to the success of our experiments is the spectroscopic resolution. Like molecules, many advanced electro-optic materials require minimum homogeneous linewidths for their optimal performance. And some materials exhibit extraordinarily narrow lines, some as narrow as 1 MHz at very low temperatures. But the typical nanoscale cluster exhibits very broad lines, of the order of 100 cm^{-1} (3×10^6 MHz) even at 15 K. It is believed that this width is caused by rapid dephasing of the purely electronic transition, *via* coupling with either low frequency phonons and/or surface states. In the research to be performed in the near future, we will examine the possibility that this dephasing can be reduced or eliminated by growing some inert material around the chromophore. We also will attempt to control other properties of the sample, such as its monodispersity, order parameter, and bandgap, thereby further reducing the inhomogeneous width. Using our new laser, we will then determine the homogeneous widths of the optical transitions directly, and how these widths depend upon the physical and chemical characteristics of the sample. Learning how to control these widths will enhance the value of these new materials in potential applications.

IV.B.6.4 SUMMARY

A new high resolution CW laser system has been designed and is being constructed. The active medium in the laser will be Ti:sapphire. Starting with a

commercially available system, we will actively stabilize the resonator length to achieve tunable, single-mode operation over the wavelength range 680-1050 nm. The anticipated single-frequency linewidth will be less than 1 MHz. Additionally, we will mount an intracavity doubling crystal at the second beam waist of the resonator, and use it to generate tunable narrowband radiation (< 1 MHz) at the SHG wavelengths 340-525 nm. Power levels in excess of 10 mW are anticipated over the entire wavelength range. When combined with an existing single-frequency ring dye laser, we will provide continuous wavelength coverage from 260-1050 nm at a resolution of better than 1 MHz.

The operating characteristics of the proposed Ti:sapphire ring laser exceed the state-of-the-art in all existing commercial lasers. Specifically, the new laser will

- be capable of single frequency operation at powers ≥ 10 mW over the wavelength ranges 340-525 nm and 680-1050 nm,
- exhibit linewidths narrower than 1 MHz at all wavelengths, with less than 1 MHz drift/hr,
- and be tunable in single scans over widths up to 10 cm^{-1}, with a relative frequency stability during the scan of 0.1 MHz.

A block diagram of the proposed laser system is enclosed (Figure IV.B.6.1).

We will use the new laser system in hole burning and fluorescence line narrowing experiments on samples of interest to (and prepared by) Materials Research Center personnel. We will separate the homogeneous and inhomogeneous contributions to their optical spectra, and thus obtain the spectra of "single-size" absorbers. We will investigate the dependence of hole shape and position on pump wavelength. We will observe both the electronic origins and the phonon sidebands, and from their relative intensities deduce electron-phonon couplings, which will be used to model the surface state dynamic relaxation behavior. And we will examine the temperature dependencies of the spectra in order to assess the role of lattice modes in promoting bulk surface relaxation.

IV.B.6.5 REFERENCES

1. For a review, see M. L. Steigerwald and L. E. Brus, *Ann. Rev. Mater. Sci.* **19**, 471 (1989).
2. See, for example, W. A. Majewski, D. F. Plusquellic and D. W. Pratt, *J. Chem. Phys.*, **90**, 1362 (1989).
3. See, for example, W. P. Ambrose and W. E. Moerner, *Nature* **349**, 225 (1991).

4. W. Vassen, C. Zimmermann, R. Kallenbach, and T. W. Hänsch, *Opt. Commun.* **75**, 435 (1990).

5. See, for example, G. M. Frankenbach and M. C. Etter, *Chem. Mater.* **4**, 272 (1992).

6. For a review, see *Molecular Recognition Mechanisms*, ed. M. Delaage (VCH Publishers, Inc., New York, 1991).

7. A. Held and D. W. Pratt, *J. Chem. Phys.* **96**, 4869 (1992).

8. A. Held, M. McKernan, and D. W. Pratt, in preparation.

9. D. F. Plusquellic, X.-Q. Tan, and D. W. Pratt, *J. Chem. Phys.* **96**, 8026 (1992).

10. D. F. Plusquellic and D. W. Pratt, *J. Chem. Phys.* **97**, 8970 (1992).

11. A. Held and D. W. Pratt, *J. Am. Chem. Soc.* **115**, 9708 (1993).

12. A. Held and D. W. Pratt, *J. Am. Chem. Soc.* **115**, 9718 (1993).

13. S. Humphrey and D. W. Pratt, in preparation.

14. B. B. Champagne and D. W. Pratt, in preparation.

15. W. A. Majewski, D. F. Plusquellic, and D. W. Pratt, in *Techniques in Laser Chemistry*, ed. T. Rizzo and A. Myers, Wiley-Interscience, in press.

LIST OF PUBLICATIONS (1992 - Present)

"Exploiting Quantum Interference Effects for the Determination of the Absolute Orientation of an Electronic Transition Moment Vector in an Isolated Molecule", with D. F. Plusquellic, Journal of Chemical Physics ***97***, 8970 (1992).

"High Resolution $S_1 \leftarrow S_0$ Fluorescence Excitation Spectra of Hydroquinone. Distinguishing the *cis* and *trans* Rotamers by Their Nuclear Spin Statistical Weights", with S. J. Humphrey, Journal of Chemical Physics ***99***, 5078 (1993).

"Hydrogen Bonding in Water Complexes. Structures of 2-Pyridone-H_2O and 2-Pyridone-$(H_2O)_2$ in Their S_0 and S_1 Electronic States", with A. Held, Journal of the American Chemical Society ***115***, 9708 (1993).

"Ammonia as a Hydrogen Bond Donor and Acceptor in the Gas Phase. Structures of 2-Pyridone-NH_3 and 2-Pyridone-$(NH_3)_2$ Complexes in Their S_0 and S_1 Electronic States", with A. Held, Journal of the American Chemical Society ***115***, 9718 (1993).

"Internal Rotation Dynamics from Electronic Spectroscopy in Supersonic Jets and Beams", with L. H. Spangler, in *Jet Spectroscopy and Molecular Dynamics*, ed. J. M. Hollas and D. Phillips, Chapman and Hall, Ltd., 1994.

APPROACH. Ti^{3+}: sapphire CW ring laser with frequency doubling.

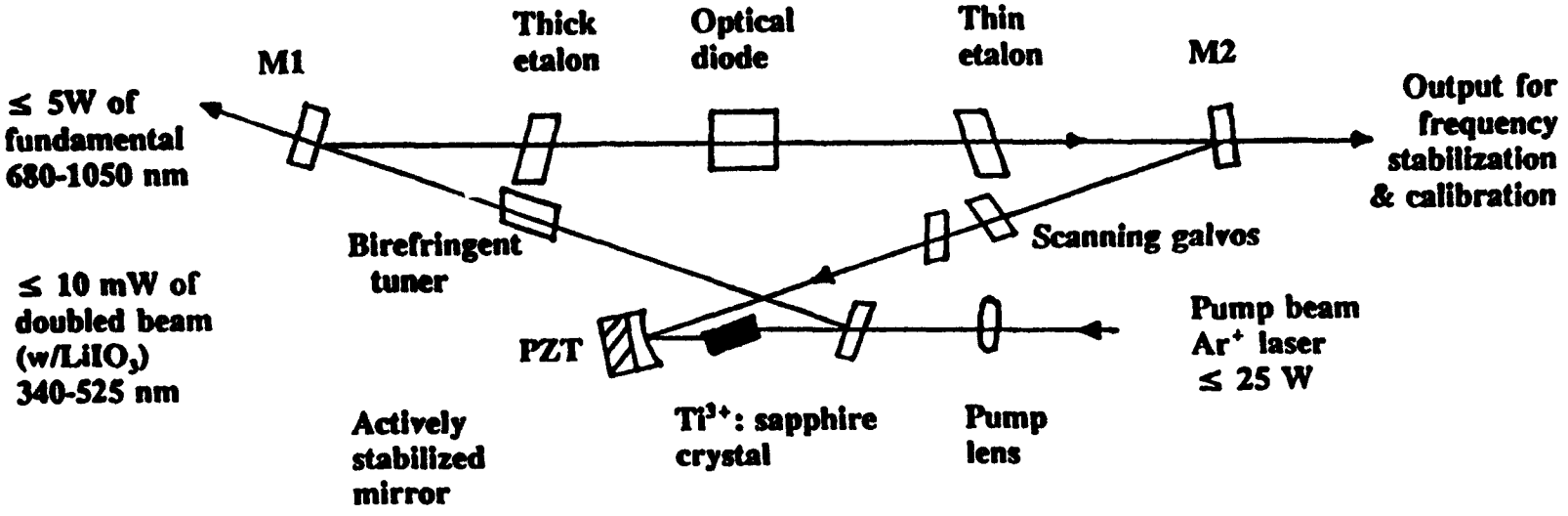

- single longitudinal mode (TEM_{00}) operation
- less than 1 MHz frequency width
- w/existing CW ring dye laser, cover λ range 260-1050 nm

Figure IV.B.6.1 Block Diagram of Laser System

IV.B.7 Thin Film Ferroelectric and Electro-Optic Ceramics

Principal Investigator: Professor Pradeep Phule'
Materials Science and Engineering
Department
University of Pittsburgh

Students: Mr. T. Deis, Ms. Y. Liu, Mr. R. Russell, Mr. I. Bjorhovde, Mr. M. Carper, Mr. J. Chronister

IV.B.7.1 INTRODUCTION

Ferroelectric, electro-optic and pyroelectric ceramic thin films, integrated into miniaturized advanced electronic circuitry, offer unique opportunities with respect to the development of non-volatile, radiation hard memories, alternative high dielectric materials for DRAM applications, micro-sensors and actuators, and uncooled infrared imaging arrays for detection and imaging of infrared radiation. The primary objective of our research program was to develop a scientific basis for sol-gel thin deposition process, based on transition metal alkoxides modified at a molecular level, for the integration of ferroelectric, electro-optic and pyroelectric ceramic thin films on to semiconductor substrates such as silicon (Si). Some of the pyroelectric and electro-optic ceramic materials investigated in the first year of the program were Lithium tantalate ($LiTaO_3$) and lead titanate ($PbTiO_3$). In the second year, the experimental work was focused on the synthesis, processing, and electrical characterization of lead zirconium titanate (PZT) thin films.

IV.B.7.2 ACCOMPLISHMENTS AND SIGNIFICANCE

A. Sol-gel preparation and characterization of PZT thin films

Sols for PZT 53.5/46.5 thin films were prepared using the following procedure. All sol preparation steps were performed in a glove box with a dry argon atmosphere. In a typical experiment, 0.66 g of titanium isopropoxide was added to 14.3 ml of isopropanol and stirred. While stirring, 4.6 ml of glacial acetic acid was slowly added to the sol for a CH_3COOH/Ti molar ratio of 34/1. In a separate beaker, 2.086 g of *hydrated* lead acetate (Pb/(Ti+Zr) molar ratio of 1.1, or 10% excess lead) was dissolved in 2.0 ml of glacial acetic acid. After stirring for 1 hour, 1.304 g of zirconium acetylacetonate ($Zr[CH_3COCHCOCH_3]_4$, Aldrich) was added to the Ti-precursor sol for a Zr/Ti molar ratio of 53.5/46.5. After another hour of stirring, the precursor sols were combined and mixed for 1 hour.

Thin films were prepared by spin coating substrates with the prepared sols using a photo-resist spinner (Headway Research Inc. 1-EC101D-R485). The as-received substrates were ultrasonically cleaned in an acetone bath for 5 minutes

and rinsed with deionized water prior to use. The sol was applied through a syringe with a 0.22 mm filter (Micron Separations, Inc.). After completely covering the substrate (~ 3 ml of sol), it was spun for 10 seconds at 4000 rpm and placed on a hot plate at 300°C for 2 minutes for densification and partial removal of organics. Deposition and densification was repeated until the desired film thickness was obtained. Films were then further heat treated at 400°C for 10 minutes in a preheated furnace (Thermolyne Model 48000 Box Furnace) with an oxygen atmosphere to further promote pyrolysis of any residual organics. PZT 53.5/46.5 films were crystallized at temperatures ranging from 550-700°C for 30 minutes in an oxygen atmosphere. Heat treatments included an initial 550°C step with further treatment at 600-700°C for some samples, while other samples were heat treated directly (i.e. without a 550°C step) at temperatures of 600-700°C. In all cases, the furnace was preheated and samples were inserted directly at the higher temperatures for a simple rapid ramping treatment.

The crystal structure and grain orientation of these thin films were studied using x-ray diffraction (Phillips X-pert System), scanning electron microscopy (SEM, JEOL JSM-35CF), and transmission electron microscopy (TEM, JEOL 200 CX). Dielectric properties were obtained using a LF Impedance Analyzer (HP 4192A) and a computer interfaced ferroelectric test system (Radiant Technologies RT-66A). Two types of x-ray diffraction were used to characterize the thin film microstructures. A parallel beam geometry is used to collimate the diffracted beams with respect to the desired 2θ. An incidence angle of $\delta = 8^\circ$ was determined by finding the highest δ at which the intensity of the strongest Pt peak (Pt(111), ~ 40° 2θ) was below 150 counts/sec. The θ-2θ diffraction was done at 30 kV and 20 mA settings, while glancing angle diffraction was done at 40 kV and 30 mA in order to increase the measurable signal sent to the detector. In all θ-2θ scans Cu Kα (λ = 1.541 Å) radiation was used. In order to characterize the preferred grain orientation of the thin films, pole figure analysis was utilized.

B. PZT Sol Preparation

One of the most important accomplishments was that using the process chemistry we developed, moisture-tolerant sols, with significant flexibility with respect to composition, could be easily prepared. The PZT 53.5/46.5 precursor sols prepared using the procedure outlined above were clear and did not show precipitate formation for several months after preparation. This stability was due to the *molecular modification* of the titanium isopropoxide precursor. Owing to the stability of the acetate groups, hydrolysis of the modified titanium precursor remains incomplete, even upon exposure to air. Another key advantage to our approach was that *hydrated* lead acetate could be used as a precursor. Once prepared, sols could be easily handled in air. This is an important achievement since sols prepared using common processing routes (such as the methoxyethanol process) tend to be moisture sensitive. The significance of all this is that the process we developed will be much better suited for larger scale applications.

C. PZT 53.5/46.5 Thin Film Microstructure

Films heat treated at temperatures below 600°C appeared smooth and any grain structure present was below the SEM resolution. Single layer films heat treated at 600°C showed a fine-grained structure (~ 100 nm grain size) with some porosity present Micrographs of single layer films heat treated to 700°C indicated that the pore density decreased with increasing crystallization temperatures. SEM cross sectional views of three layer PZT films indicated an overall thickness of 300 nm (Figure IV.B.7.1).

The important goal that was achieved here was that a protocol for the reproducible preparation of high resistivity PZT thin films was developed. The significance of high resistivity (i.e. films with very small or no interconnected porosity) is that such films will not show electrical breakdown during DRAM or non-volatile applications and for electro-optic applications minimum porosity will assure highest optical properties.

D. Phase Evolution and Orientation of PZT 53.5/46.5 Thin Films

Glancing angle diffraction of these films indicated that for heat treatment temperatures below 550°C, the films were mostly amorphous (Figure IV.B.7.2). The peak at ~ 29° 2θ indicates the presence of oxygen-deficient pyrochlore, non-stoichiometric PbO, or a combination of the two. Upon heat treatment at 550°C, enhanced pyrochlore formation is observed from the diffraction pattern (Figure IV.B.7.2). Perovskite PZT was observed with heat treatment temperatures above 600°C using standard diffraction geometry (Figures IV.B.7.3 & IV.B.7.4). In order to observe the film orientations as a function of heat treatment, two different film heat treatment routes were used. Half of the samples were exposed to a 550°C heat treatment for 30 minutes before subsequent treatment at 600-700°C, while the 550°C step was bypassed for the others, and films were heat treated directly at 600-700°C. Figure IV.B.7.3 shows a comparison of PZT films heat treated to 600°C with and without an intermediate 550°C treatment. Both films display (111) preferred orientation, although the film heat treated directly to 600°C exhibits a lower degree of (111) orientation and a higher degree of (100) orientation than the film with the 550°C treatment. Figure IV.B.7.4 shows a comparison of PZT films heat treated to 700°C with and without an intermediate 550°C treatment. With a 550°C step the thin film is (111) oriented. However, if the 550°C step is bypassed, a strong (100) orientation is observed.

In order to confirm the orientation relationships obtained from θ-2θ diffraction patterns, modified pole figure measurements were made. The pole figure analysis showed that the films had a fiber texture. The pole figure analysis also confirmed that a strong (111) and a weak (100) orientation was observed for films heat treated at 600°C, while for films heat treated at 700°C the (100) orientation was dominant.

Another interesting result was that for films heat treated at 700°C there was a significant presence of (111) orientation. This PZT (111) orientation is the epitaxial orientation since the lattice mismatch between the Pt (111) and the PZT (111) is small (d = 2.26 Å and 2.35 Å, respectively). According to analysis of epitaxial growth, epitaxy is favored when growth rates are slow and adatoms have more time to occupy equilibrium positions. The enhancement of the pyrochlore phase at 550°C would slow the perovskite structure growth kinetics because the perovskite phase will form by a structural phase transformation from the pyrochlore phase. Since these two phases have very different crystal structures such a transformation may be reconstructive in nature. This would explain the difference in orientation between the 700°C films with and without the 550°C step. Also, since films are inserted into the furnace at the desired temperature with no ramping, then higher temperature treatments will result in higher sample heating rates. This would explain the difference between the 600°C and 700°C film orientations. The strong (100) orientation evident in the films heat treated at high temperature may be because the (100) faces are the lowest surface energy faces, as noted by other researchers. Because of the higher temperature, the driving force for nucleation would be higher, allowing nucleation to begin at the film surface instead of the film-substrate interface and introducing the non-epitaxial (100) orientation.

Experiments with three layer films (**Figure IV.B.7.5**) showed that the initial layer orientation is propagated through additional film layers, regardless of the heat treatment temperature of these layers. Films initially heat treated at 600°C, with strong (111) orientations, show an increase only in the (111) orientation with additional layers and crystallization temperatures of 700°C (no 550°C step). Similarly, films heat treated at 700°C and displaying strong (100) orientation show an increase only in the (100) orientation with additional layers and 700°C heat treatments (**Figure IV.B.7.6**). This effect may be due to the nature of the nucleation surface present in the thin films. The first layer is directly deposited on the platinum layer, and so nucleation at the interface would be by heteroepitaxy, and would involve some strain due to the difference in lattice dimensions. However, subsequent layers were deposited directly onto the crystallized PZT layer, and nucleation at the interface would be by homoepitaxy, with no significant strain. Thus, based on these data, it is clear that PZT films with either (100) or (111) orientations can be prepared using a ***"seed layer"*** formed under controlled conditions.

Thus, one of the most important **accomplishments**, with respect to microstructure evolution, was that it was established that PZT films with either predominantly (111) or (100) orientation could be reproducibly prepared. The significance of this is that for different applications different processing time-temperature windows and substrates could be chosen so as to obtain desired orientation. This is, for example, particularly important for the uncooled IR detection and imaging arrays applications where pre-poled individual elements can be prepared directly.

E. TEM Analysis of PZT 53.5/46.5 Thin Films

Figure IV.B.7.7 shows a bright field (BF) image of a three layer PZT cross section using TEM. On closer inspection the three individual layers of the film were visible. Each single layer thickness is ~ 100 nm. The interface between the platinum and the PZT films is quite sharp and showed no evidence of any second phases present. Dark field (DF) imaging of the same area revealed that the PZT grains are columnar through all three layers, suggesting that grain growth of multiple layers is influenced by the initial PZT layer. The significance of this is that it reinforces the XRD results for three layer films in which subsequent layers form the same preferred orientations as the initial layer regardless of their crystallization temperatures. Evidence of an ultrafine-grained phase was observed for planar samples. The d-spacings calculated from the diffracted ring pattern matched those for oxygen deficient pyrochlore, and the estimated grain size was 10-15 nm. Note that this phase was *not* always detected using XRD (particularly for samples heat treated above 600°C).

F. Dielectric and Ferroelectric Properties of PZT 53.5/46.5 Thin Films

Dielectric and ferroelectric measurements were performed on samples crystallized at 550°C and confirmed by XRD to have the oxygen-deficient pyrochlore structure. The measured dielectric constant was 40, with a dielectric loss of 0.02 and a resistivity of ~ 10^9 Ω-cm. Ferroelectric hysteresis measurements showed a linear relationship of polarization with electric field, confirming the non-ferroelectric nature of oxygen-deficient pyrochlore structure. A marked difference was observed for the dielectric and ferroelectric properties of (100) and (111) oriented perovskite phase thin films. In general the polarizations and dielectric constants were higher for (111) oriented films, while coercive voltages, resistivities, and dielectric losses were similar for both orientations (**Table IV.B.7.I**). A comparison of the hysteresis loops associated with both orientations is shown in **Figure IV.B.7.8.** The trends observed for polarization with preferred orientation may be explained in terms of the film microstructure. Since at room temperature PZT 53.5/46.5 is slightly on the rhombohedral side of the morphotropic phase boundary, the expected crystal structure is rhombohedral. For this crystal structure the polar axis is the [111]. For (111) oriented thin films the [111] is oriented perpendicular to the plane of the film and therefore perpendicular to the electrodes, which is the optimum configuration for polarization of the film. For this reason then (111) oriented PZT 53.5/46.5 films would be expected to have higher values of polarization than (100) oriented thin films.

The asymmetry of the hysteresis loops with respect to $\pm P_r$ and $\pm E_c$ could be due to stresses caused by "clamping" of the film to the substrate. The clamping in this case could be the result of the epitaxial growth of the film on the substrate. Since there is some mismatch between the PZT (111) and Pt (111) lattice sites (the PZT (111) dimensions are 3% larger) then the PZT film will be constricted at the film/substrate interface. Since the constricted PZT plane is the (111), the Ti^{4+}

(or the Zr^{4+}) would be forced away from the substrate along the [111] by the constriction, thus resulting in a localized charge displacement at the interface. This charge displacement would act like an internal bias field, resisting an oppositely applied electric field and resulting in lower polarizations, and lowering the necessary applied field in the same direction as the bias, resulting in higher measured polarizations. Our results so far indicate that the variation in the polarization values between (111) and (100) oriented films may only be due to the orientation of the polar axis, and not clamping differences.

G. Ferroelectric Fatigue of PZT 53.5/46.5 Thin Films

Figure IV.B.7.9 shows a typical ferroelectric fatigue test on a PZT 53.5/46.5 thin film. The quantity plotted is the total polarization switched in changing the applied field from -167 kV/cm to +167 kV/cm. The plot shows that the film's switched polarization is not reduced below 50% of the original value after 10^{10} cycles. The decrease in polarization at ~ 10^8 cycles may signal an accumulation of space charges to neutralize the polarizations of the PZT domains. A comparison of film properties before and after fatigue testing was made. In general, polarizations decreased with fatiguing to 10^{10} cycles. These results further support the idea that space charges are responsible for decreasing polarizations with increased cycling. However, further examination of our PZT thin films under fatigue conditions is required before any conclusive statements can be made as to the origin of their fatigue behavior.

IV.B.7.3 SUMMARY OF MAJOR FINDINGS AND CONCLUSIONS

1. A successful and simple process based on inexpensive and moisture-tolerant precursors was developed for the chemical deposition of thin films of ferroelectric and electro-optic materials.

2. Two distinctly different fundamental mechanisms were found to control the grain orientation of the PZT thin films. Specifically, PZT thin films with (111) orientation were prepared by a molecularly modified alkoxide precursor process and heat treatment at 600°C or at higher temperatures with an additional 550°C step. This orientation was due to the epitaxial matching with the bottom electrode. PZT thin films with (100) orientation were grown by heat treatment at 700°C with no intermediate 550°C step. This orientation may form preferentially since the (100) is the lowest energy face.

3. Columnar grain morphology was observed for PZT thin films using electron microscopy, indicating that the initial layer orientation can be propagated through all subsequent layers. Grain size was ~ 0.10 μm and the single layer thickness was ~ 0.10 μm.

4. Polarization values and dielectric constant were observed to be higher for (111) oriented PZT 53.5/46.5 thin films than those for (100) oriented thin

films. No significant variation with orientation was seen for coercive fields and dielectric losses. The higher polarizations may be the result of orientation of the polar axis parallel to the applied electric field.

5. Hysteresis loops were asymmetric with respect to the coercive fields. This may be due to stresses at the interface causing a net "internal bias field" effect.

6. Ferroelectric PZT thin films retained more than 50% of their original polarization after 10^{10} fatigue cycles.

PUBLICATIONS FOR THE SECOND YEAR

1. P. P. Phulé, " Molecularly Modified Alkoxide Approach for Thin film Ferroelectrics", Integrated Ferroelectrics. 1994 (in press).

2. P. P. Phulé, "Sol-gel Processing of Ceramic Thin Films", in **Encyclopedia of Advanced Materials** (Eds. S. Mahajan et al.) Elsevier Press (UK) 1994 (in press).

3. P. P. Phulé, R.A. Russell, and M. Carper, " Preparation of PZT Films and Tantalum Zirconate Powders Using Chemical Techniques", Ceramic Transactions, Vol.32, Dielectric Ceramics (Ed. by K.M. Nair and A.S. Bhalla), 1993, p. 333-338.

4. M.D. Carper and P. P. Phulé, Preparation of oriented $PbTiO_3$ Thin Films Using a Spin-On Sol-Gel Process", Applied Physics Letters, 1993, 63 (2), 153.

5. M.D. Carper, Yimin Liu and P. P. Phulé, Chemical Processing, Microstructure Evolution and Dielectric Properties of oriented PZT Thin Films", 1994, to be submitted to J. American Ceramic Society.

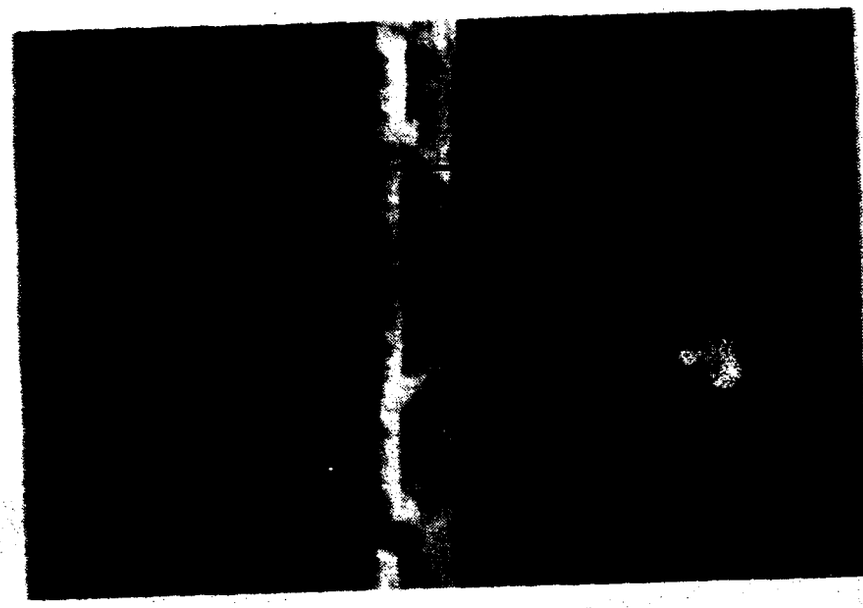

Figure IV.B.7.1 SEM cross section of a triple layer PZT 53.5/46.5 thin film heat treated at 700°C, showing a PZT film thickness ~ 0.3 μm.

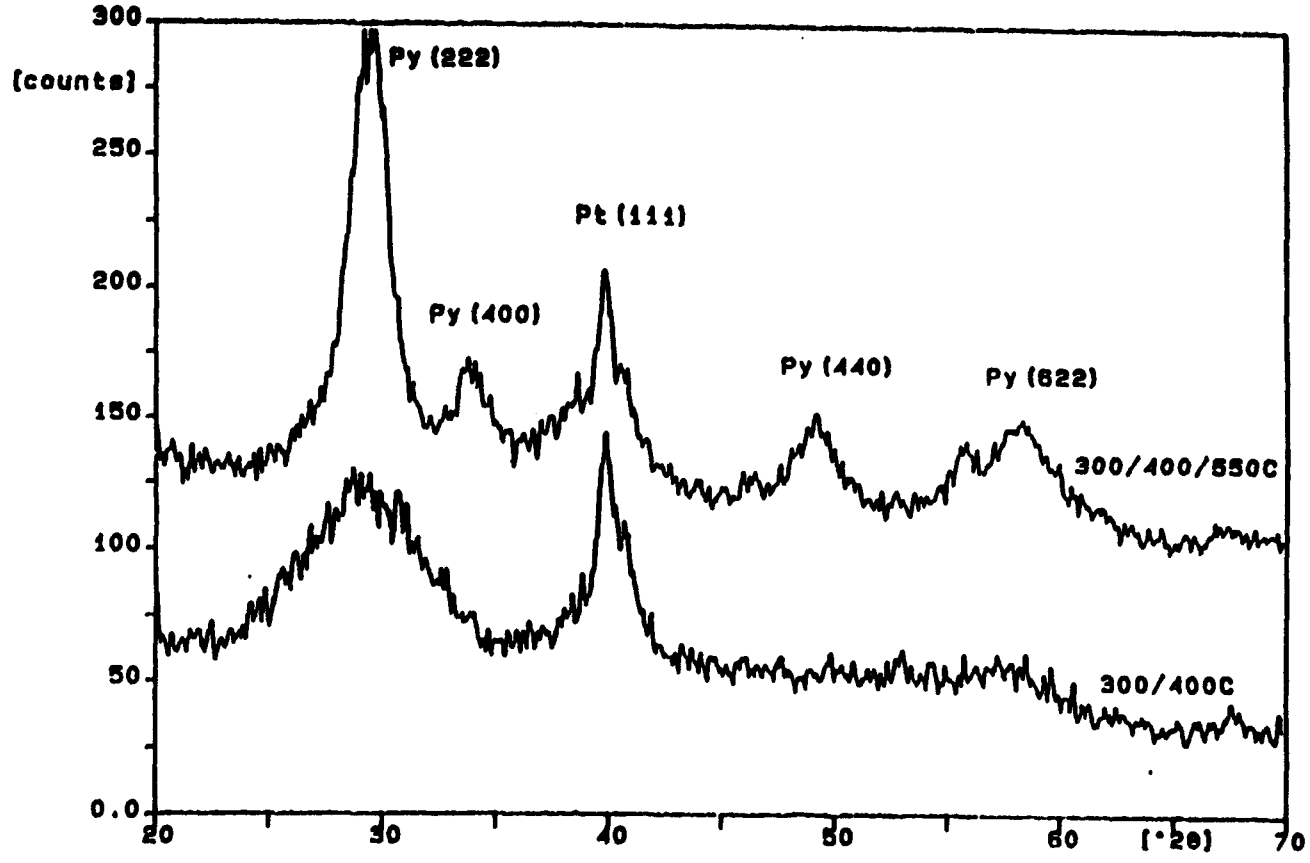

Figure IV.B.7.2 Fixed incidence angle ($\theta = 8°$) diffraction patterns of a single layer PZT 53.5/46.5 thin film showing the enhanced crystallization of the oxygen-deficient pyrochlore structure at 550°C. Py = Pyrochlore, Pt = Platinum.

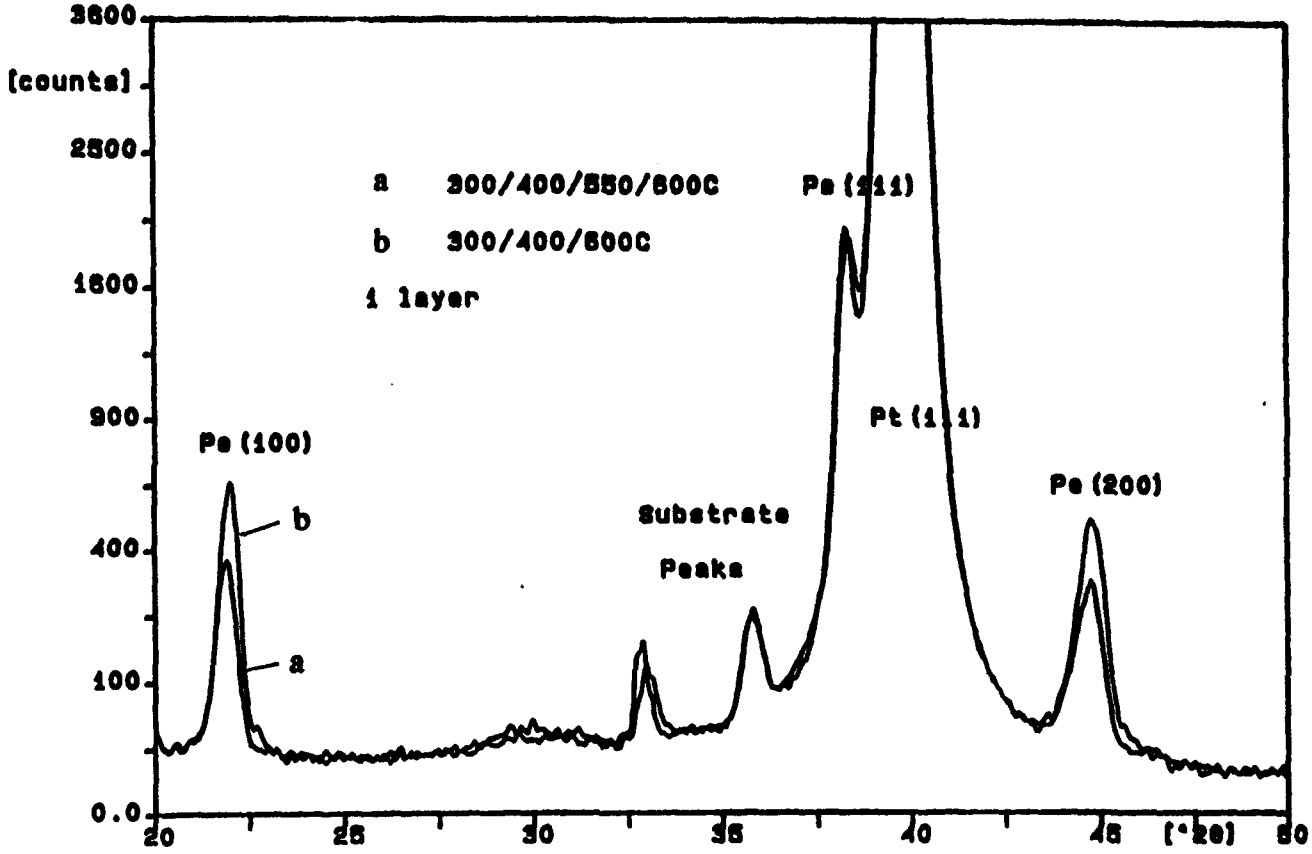

Figure IV.B.7.3 *θ-2θ* diffraction pattern of two single layer PZT thin films heat treated to 600°C with (a) and without (b) an intermediate 550°C step. Note the development of (111) orientation in both films.

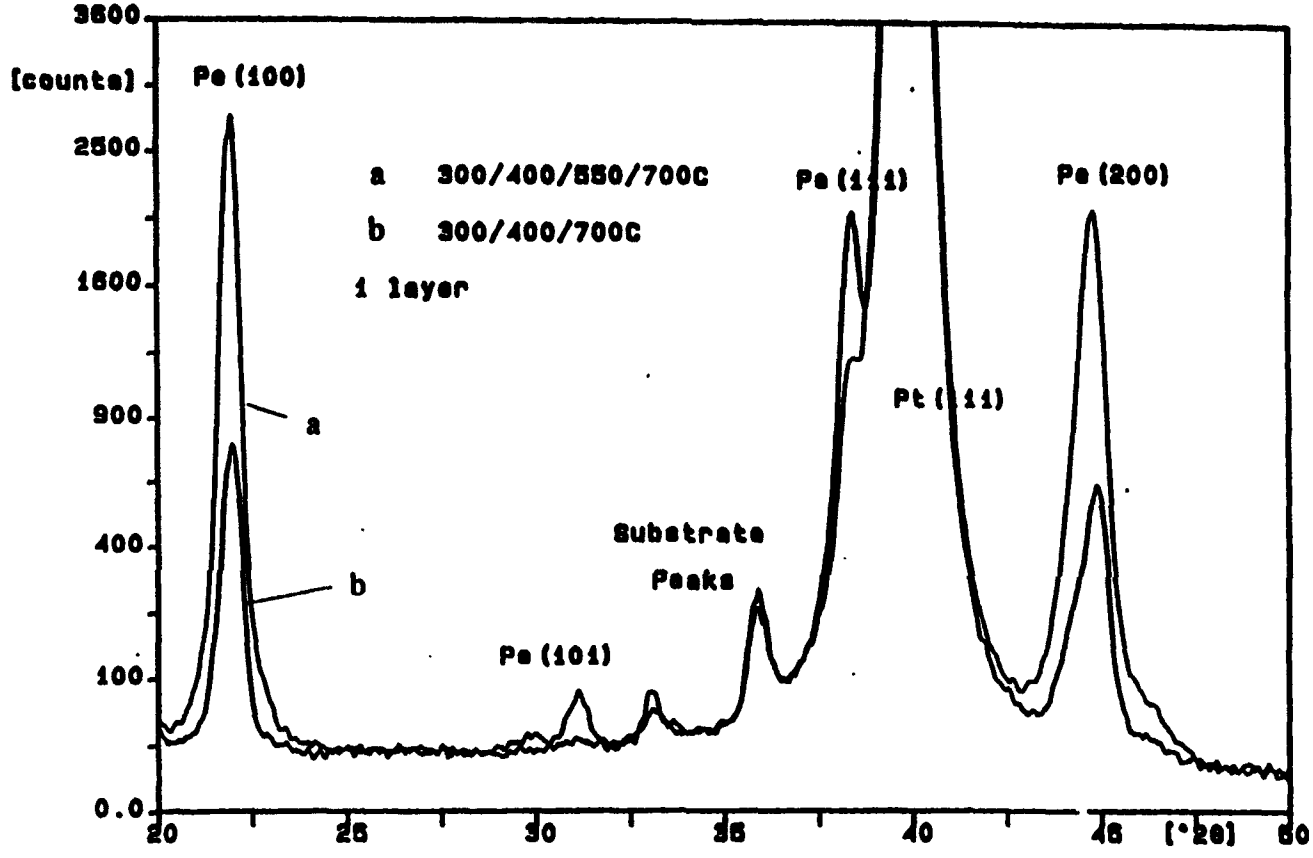

Figure IV.B.7.4 θ-2θ diffraction pattern of two single layer PZT thin films heat treated to 700°C with (a) and without (b) an intaermediate 550°C step. Note the development of different orientations with different heat treatments.

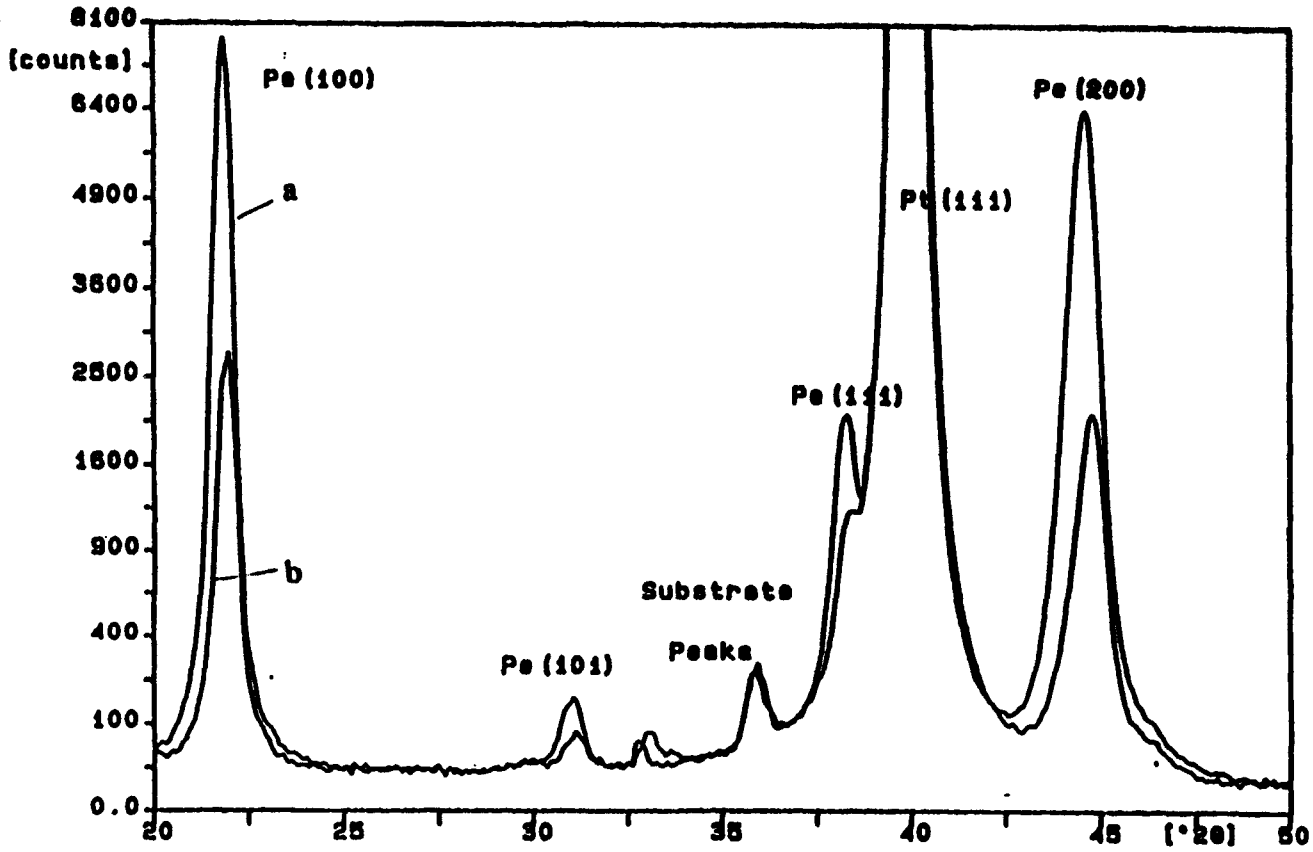

Figure IV.B.7.5 θ-2Θ diffraction pattern of a PZT thin film with one deposited layer (b) and three deposited layers (a) showing the propogation of the initial (100) orientation through the layers.

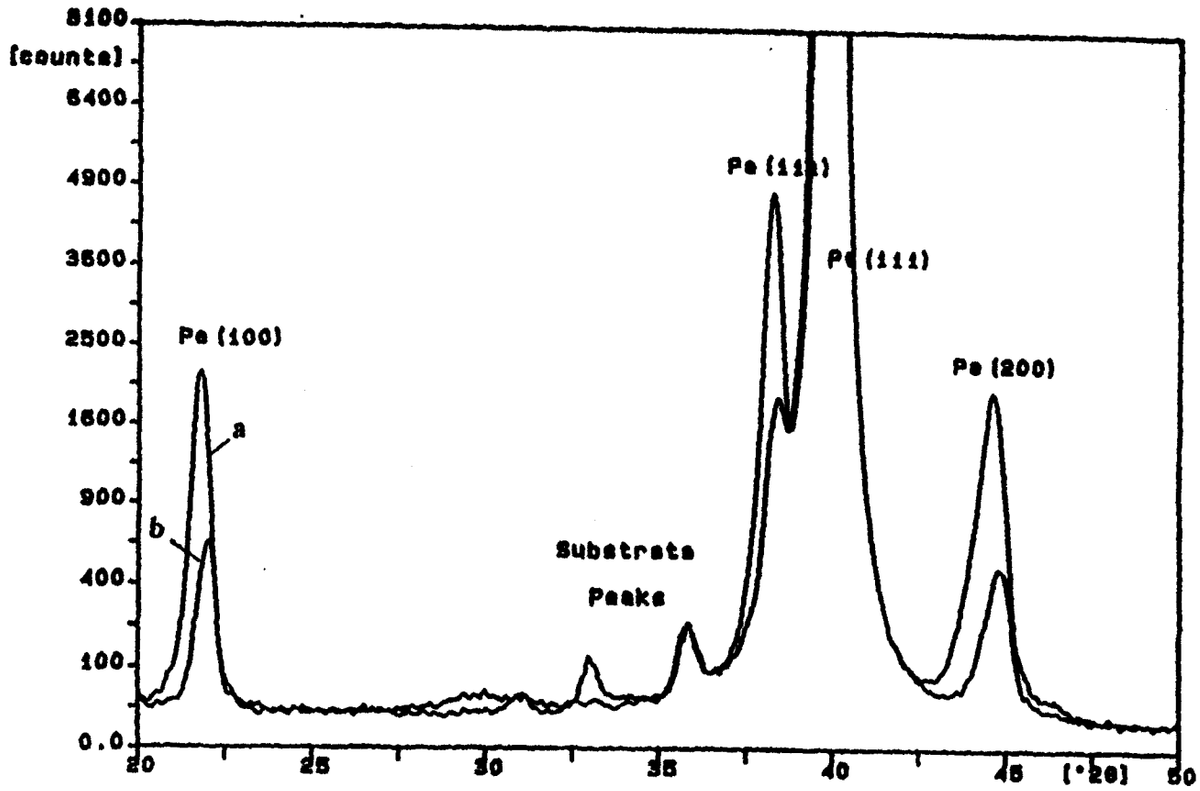

Figure IV.B.7.6 θ-2θ diffraction patterns of a PZT thin film with one deposited layer (b) and three deposited layers (a) showing the propogation of the initial (111) orientation through the layers.

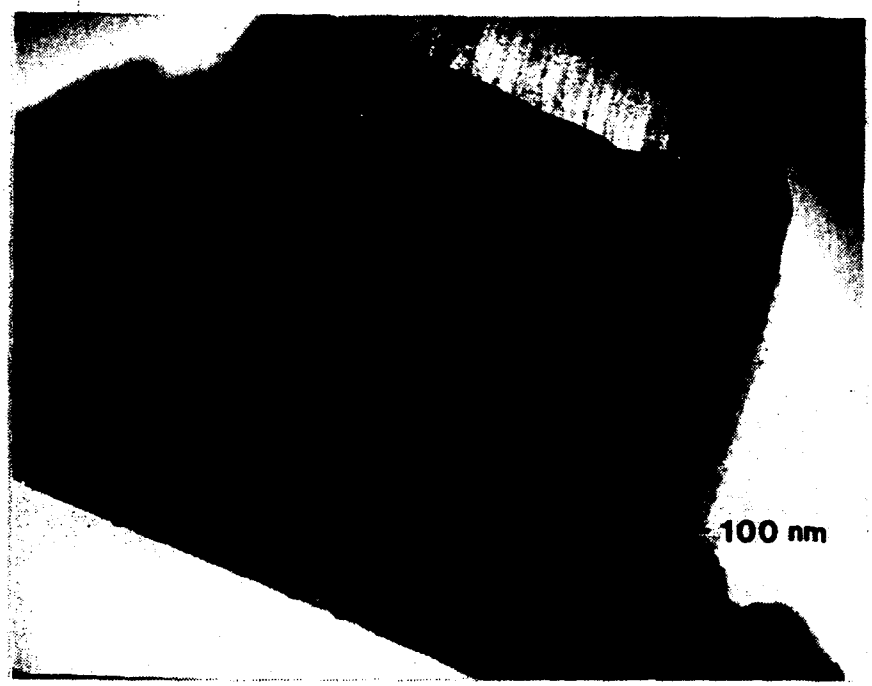

Figure IV.B.7.7 TEM cross sectional view (bright field) of a three layer PZT thin film. The arrows indicate the layer boundaries in the film, confirming the single layer thickness to be ~ 0.1μm.

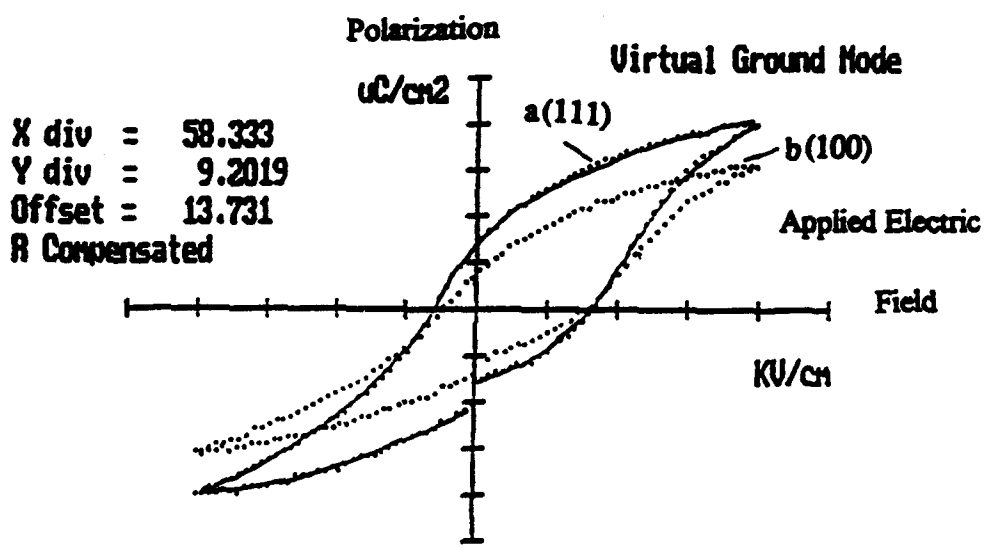

Figure IV.B.7.8 Ferroelectric hysteresis loops of three layer PZT 53.5/46.5 thin films with (111) orientation (a) and (100) orientation (b) Note that the (111) oriented film displays higher polarization values but similar coercive voltages.

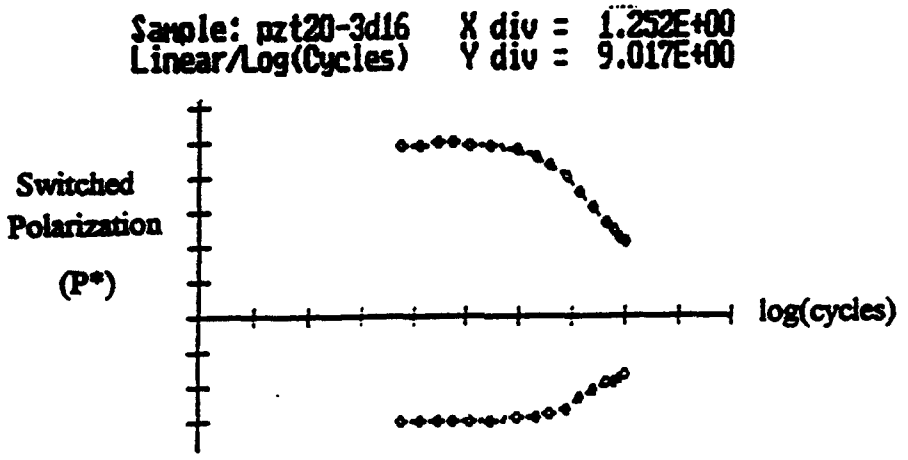

Figure IV.B.7.9 Ferroelectric fatigue behavior of a three layer PZT 53.5/46.5 thin film, showing retention of over 50% of the original polarization after 10^{10} cycles.

Table IV.B.7.1 Dielectric and Ferroelectric Properties of (111) and (100) Oriented PZT 53.5/46.5 Thin Films.

Sample	P_s(μC/cm^2)	+P_r(μC/cm^2)	-P_r(μC/cm^2)	+E_c(kV/cm)	-E_c(kV/cm)	R_v(Ω-cm)	K'	tanδ	orientation
14-5	38	16	22	84	50	10^{10}	561	0.021	(111)
20-3	39	14	22	82	31	10^{10}	570	0.020	(111)
26-4	32	12	15	71	42	10^{11}	713	0.028	(111)
26-5	33	14	16	70	45	10^{11}	730	0.031	(111)
26-6	34	13	16	66	44	10^{11}	751	0.033	(111)
average	35	14	18	74	42	10^{10}	665	0.027	
14-6	28	9	13	77	42	10^{10}	525	0.020	(100)
17-1	28	10	13	75	44	10^{9}	525	0.019	(100)
17-2	28	10	14	81	42	10^{10}	545	0.023	(100)
20-1	30	7	14	72	23	10^{11}	498	0.018	(100)
average	28	9	14	76	38	10^{10}	523	0.020	

Each value is an average of at least 20 different capacitors from each sample.

IV.B.8 Optoelectronic Supercomputer Modeling of Electro-optical Devices

Principal Investigator: Professor Rob Coalson
Department of Chemistry
University of Pittsburgh

Other Faculty Participants: Dr. Sanford Asher
Dr. Rasu Kesavamoorthy
Department of Chemistry
University of Pittsburgh

Dr. Dietrich Langer
Department of Electrical Engineering
University of Pittsburgh

Dr. Anthony Duncan
Department of Physics
University of Pittsburgh

Dr. John Hurley
Hampton College, VA
(Visiting Professor)

Students: Dr. Alan Walsh
Mr. James Zahorchak
Mr. Dhruv Pant

IV.B.8.1 INTRODUCTION:

The development and perfection of small scale (micron and submicron) electro-optical devices is a powerful driving force in current materials science research. Over the past two years my group has applied its expertise in theoretical chemistry (quantum mechanics, statistical mechanics, molecular dynamics and Monte-Carlo simulation) to several forefront areas, including:

(1) Design of Dielectric Waveguides

(2) Static and Dynamic Properties of Colloidal suspensions, with application to colloidal crystalline arrays.

IV.B.8.2 ACCOMPLISHMENTS AND SIGNIFICANCE:

A. Optics

In Prof. D.W. Langer's lab in the Electrical Engineering Dept. at Pitt, novel dielectric waveguides are synthesized from micron-thick layers of semiconductor materials [1]. The upper cladding layer consists of a Multi-Quantum Well structure, whose index of refraction can be substantially altered by application of a DC electric field. A typical Field-induced Waveguide is shown in Fig. IV.B.8.1. By proper choice of geometry, materials and applied voltages, the device can confine an induced light beam and "guide" it underneath the indicated electrical contact.

Questions concerning the size of the confined spot and power loss along the propagation direction are critical to the practical success of such technology. We adapted quantum mechanical basis set techniques familiar in electronic structure theory and molecular spectroscopy in order to compute the eigenmodes of Lossy Dielectric Waveguides. In collaboration with Prof. Langer's group, we applied these numerical algorithms to the case of Field Induced Waveguides synthesized in the Langer lab [2]. We showed that our numerical method was convergent and efficient. We found a confined mode in the operating wavelength and device spec regime of Langer's waveguides (cf. Fig. IV.B.8.1). We studied the effect of applying a voltage across the waveguide, and probed the power loss expected to increased absorption in the MQW layer. Our attenuation lengths (ca. 150 microns) are consistent with experimental observations in these structures. We also found, unexpectedly, that the guided mode can become unconfined along the lateral direction of the guiding layer if the applied voltage is too large. Through this work we have demonstrated the power of computer-assisted design of dielectric waveguides.

Work in progress includes:

(1) Eigenmode Characterization in complex structures, including bending waveguides, multiple waveguides in series. The simplest way to model these phenomena is via scalar optics (essentially, the route taken in the completed work taken above), and we are currently pursuing this route.

(2) Exact space-time evolution of the electro-magnetic field according to Maxwell's equations.

(3) Analysis of the effect of surface roughness and other defects on the efficiency of waveguide operation.

B. Polyballs

(1) Phase Diagram

Suspensions of ca. 100nm charged polystyrene sphere balls ("polyballs") self-assemble under appropriate conditions (polyball charge, polyball concentration, counterion concentration, etc.) into periodic arrays. These arrays scatter visible light efficiently. Hence, by controlling the composition and structure of the polyball suspensions, sensitive diffraction-based filters can be synthesized. We have developed Monte-Carlo (MC) based algorithms for studying the equilibrium state of these systems. In collaboration with Prof. S.A. Asher and his associate Dr. R. Kesavamoorthy, we used this methodology to determine the critical impurity ion concentration at which crystalline polyball arrays "melt", for several systems of experimental interest [3]. Complete consistency with available experimental data was found.

(2) Theory of the Interpolyball Potential

An essential ingredient in any microscopically based theory of both equilibrium and nonequilibrium behavior of polyball systems is the interpolyball force field. Determining this dependence from "first principles", i.e. by computing the statistical mechanics of a 3D Coulomb gas interacting with fixed polyball charge distributions, is difficult. Historically, a number of simpler approximations have been used. Although some empirical calibration can be obtained by comparison to experimental data, the question of the correct interpolyball potential is still hotly debated in the literature.

With Prof. A. Duncan of the Dept. of Physics at Pitt, we provided an algorithm which solves the three dimensional Coulomb gas problem for the motion of simple ions in the presence of (fixed) charged polyballs. Our formulation and numerical methods derive from elementary particle physics, in particular the Lattice Gauge Field Theory of quark confinement [4]. The foundations of our Lattice Field Theory (LFT) approach as well as initial numerical tests are presented in Ref. 5. Recently, the PI and post-doc Alan Walsh utilized LFT to study equilibrium properties of a polyball fluid [6]. The inter-polyball interaction potential was computed using LFT "on the fly" in the course of sampling many polyball configurations via standard Monte-Carlo techniques. This is, to our knowledge, the first time that "ab initio" interpolyballs have been utilized in Monte-Carlo simulations of the equilibrium properties of colloidal suspensions.

Two more polyball projects are in the process of being written up for publication, namely

(i) A molecular dynamics study of the effects of intense laser heating of a small spot in a colloidal crystal, in particular the dynamics of relaxation

back to equilibrium. [This work has been performed in the PI's lab by graduate student J. Zahorchak.] Under certain conditions the lattice planes of the crystal compress (rather than expand, as would be expected upon heating). This effect has been seen experimentally, and our computations help to explain its occurrence.

(ii) Inclusion of spatial dependence in the dielectric constant into the LFT formalism. The dielectric inside the colloid is generally much lower than that of the water solvent. This is also the case for biological macroions like DNA, enzymes, etc. The LFT formulation has been generalized to treat systems with arbitrary dielectric constants by the PI and Dr. Nir Ben-Tal of Columbia University. Applications have been carried out on systems consisting of +/- macroion pairs (a situation that is currently of great interest to the Asher group).

IV.B.8.3 SUMMARY:

We have made substantial progress in understanding several micron and submicron optical devices. We have successfully modelled the properties of Field Induced Dielectric waveguides, in close collaboration with the Langer group in Electrical Engineering. We have even predicted some unusual and technologically important effects such as a transition from confined to unconfined eigenmodes of the electromagnetic field in these structures at high applied voltage strengths. In a different area, we have applied MC and MD simulation techniques to better understand the equilibrium properties of colloidal crystals synthesized in the Prof. S.A. Asher's lab in the Chemistry Dept. at Pitt [3]. Our work helps to determine the impurity ion concentration range in which crystalline stability will be enhanced. This property is critical to the commercial success of such structures in the role of visible light filters. At a more fundamental level, we developed a methodology to rigorously evaluate the Grand Canonical Partition function for the classical Coulomb gas in an environment of fixed charged polyballs. This represents a potentially important breakthrough in colloid science and biophysics, since it enables "ab initio" evaluation of the interactions of an arbitrary suspension of charged macroions in an ionic aqueous solution.

Strong collaborations have been fostered between faculty in Chemistry, Physics and Electrical Engineering Departments at Pitt.

IV.B.8.4 REFERENCES:

[1] D.W. Langer, M. Chen, H. Lee and M. Chemielowski, "Quantum Well Structures for Integrated Opto-electronics", SPIE vol. 1215 Digital Optical Computing II, pp. 243-251, 1990.

[2] "Computing the Eigenmodes of Lossy Field-Induced Optical Waveguides", R.D. Coalson, A. Ali, and D.W. Langer, Journal of Lightwave Technology, in press.

[3] "Melting of Colloidal Crystals: A Monte Carlo Study", J.C. Zahorchak, R. Kesavamoorthy, R.D. Coalson and S.A. Asher, J. Chem. Phys. 96, 6873 (1992).

[5] A. Duncan and R. Mawhinney, Phys. Rev. D 43, 544 (1991).

[6] R.D. Coalson and A. Duncan, J. Chem. Phys. 97, 5081 (1992).

[7] A.M. Walsh and R.D. Coalson, J. Chem. Phys. 100,1559 (1994).

PUBLICATIONS

In the two year period, MRC supported projects have culminated in five (refereed) papers: two have appeared in the Journal of Chemical Physics, a fourth in Chemical Physics Letters, and the fifth has been accepted for publication in the Journal of Lightwave Technology. (In addition, two more papers are being readied for publication, as described below.) The titles and author lists for the published articles are:

(1) "Melting of Colloidal Crystals: A Monte Carlo Study", J.C. Zahorchak, R. Kesavamoorthy, R.D. Coalson and S.A. Asher, J. Chem. Phys. 96, 6873 (1992).

(2) "Systematic Ionic Screening Theory of Macroions", R.D. Coalson and A. Duncan, J. Chem. Phys., 97, 5081 (1992).

(3) "Redfield Theory is Quantitative for Coupled Harmonic Oscillators", A.M. Walsh and R.D. Coalson, Chem. Phys. Lett, 198,293(1992).

(4) "Lattice Field Theory for Spherical Macroions in Solution: Calculation of Equilibrium Pair Correlation Functions", A.M. Walsh and R.D. Coalson, J. Chem. Phys. 100, 1559 (1994).

(5) "Computing the Eigenmodes of Lossy Field-Induced Optical Waveguides", R.D. Coalson, D.K. Pant, A. Ali, and D.W. Langer, Journal of Lightwave Technology, in press.

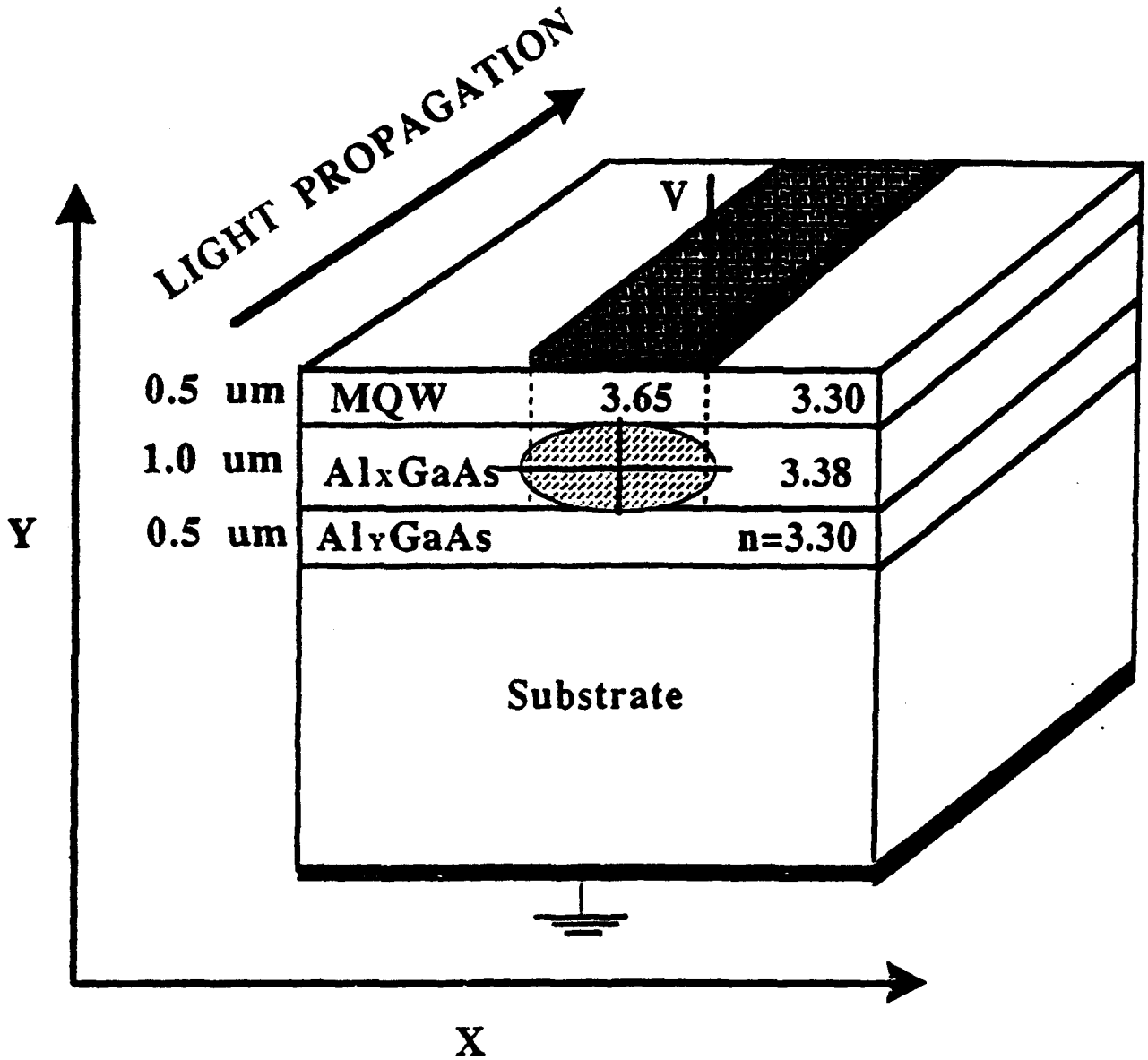

Figure IV.B.8.1 Schematic of a field-induced waveguide with reduced spatial dimensions. The real part of refractive indices are indicated. Application of an electric field induces an imaginary part into the index of refraction as well. In the calculations described in the text the imaginary part of the refractive index is taken to be non-zero only in the top central region directly under the metal cladding layer.

IV.B.9 Novel Nonlinear-Optical Materials

Principal Investigator: Professor Michael D. Hopkins
Chemistry Department
University of Pittsburgh

Other Faculty Participants: Dr. Kenneth D. Jordan
Dr. N. John Cooper
Dr. Andrew D. Hamilton
Department of Chemistry
University of Pittsburgh

Dr. Vincent M. Miskowski
California Institute of Technology (Visiting Professor)

Students: Mr. Timothy C. Stoner
Mr. Timothy P. Pollagi
Mr. Bradley A. Lewis
Dr. Jie Yu

IV.B.9.1 INTRODUCTION

Our research has been directed at developing new design and synthetic strategies for molecular and polymeric nonlinear-optical (NLO) materials.[1] The main emphasis of our efforts has been to extend the building blocks for these traditionally organic materials to include complexes of the transition elements, thereby improving their structural and electronic tunability. Our approach has integrated all key aspects of materials design: the synthesis of new NLO chromophores has been supported by separate programs directed at advancing the state of the art in the measurement of NLO properties; the use of electronic-structure calculations to lay the groundwork for deriving detailed structure/property relationships; and the development of new bulk phases for the efficient expression of molecular hyperpolarizabilities.

The general objectives of our research have been to develop novel, highly efficient classes of NLO materials and to fashion these (and existing) molecular materials into bulk phases that allow the tuning of optical nonlinearities. We have pursued four specific projects along these lines:

(1) The design, synthesis, and structural, electronic, second-harmonic generation (SHG: $\chi^{(2)}$, β) and third-harmonic generation (THG: $\chi^{(3)}$, γ) characterization of transition-metal analogues of conjugated organic compounds and polymers.

(2) The evaluation of ab initio quantum mechanical calculations as a means to predict the structures and properties of theoretically challenging NLO materials. This was undertaken in collaboration with Prof. K. D. Jordan.

(3) The development of chiral metal complexes as NLO materials with desirable noncentrosymmetric bulk structures. Part of this work was carried out in collaboration with Prof. N. J. Cooper.

(4) The design of new bulk phases designed from molecular-recognition principles. (During the first year of the grant, this work was a joint effort between our research group and that of Prof. A. D. Hamilton.)

IV.B.9.2 ACCOMPLISHMENTS AND SIGNIFICANCE

A. *Conjugated Transition-Metal Complexes and Polymers*

Our efforts to prepare transition-metal complexes that are analogues of conjugated organic compounds and polymers have resulted in the discovery of four new classes of materials: alkynyl-substituted, quadruply metal-metal bonded dimetallapolyynes of the type $M_2(CCR)_4(PMe_3)_4$ (1; M = Mo, W; R = H, alkyl, aryl, silyl) [2]; internally metal-substituted diacetylenes (metallabutadiynes) with formulae $HC{\equiv}WL_4(C{\equiv}CR)$ (2; R = H, alkyl, aryl, silyl, alkynyl, metal-carbynyl; L = phosphine) [3]; alternate bond-order, extended-chain metal-alkylidyne polymers (3; $[W(\equiv CR)(OR')_3]_n$: R = conjugated N-heterocycle, R' = alkyl) [4]; and metal-substituted donor-acceptor arene complexes of the type *p*-$((R'O)_3W{\equiv}C)$-C_6H_4-X (4; X = NR_2, OR, SR, NO_2). [5] Each class of compounds is patterned after an archetypal organic NLO material. The molecular and electronic-structural characterization of all compounds, using X-ray crystallography and IR, Raman, multinuclear NMR, and electronic-absorption and emission spectroscopy has been thorough, such that the electronic perturbation due to the metal center(s) has been evaluated. In all cases, the self-consistent picture that has emerged from these

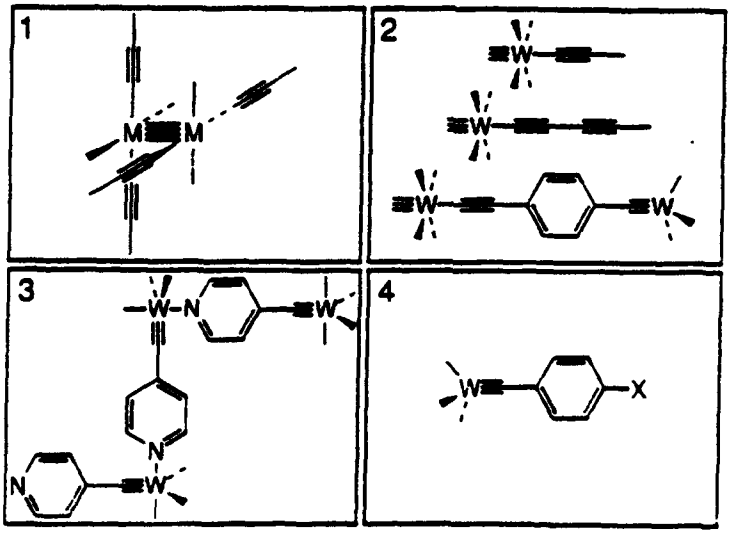

data is that the these compounds are highly conjugated. For example, the optical absorption bands of 1 and 2 red-shift and intensify with increasing chain length; the photophysical properties of 3 are strongly sensitive to the metal geometry and the specifics of polymer folding; and 4 structurally and electronically manifests donor-acceptor interactions across the arene ring. [2-5] Preliminary measurements, undertaken both here and in collaboration with workers at JPL, [6] indicate that the optical nonlinearities of these materials should be an order of magnitude or more larger than those of traditional all-organic materials, thus validating the central thesis of our approach, outlined in the MRC proposal, to optimizing the properties of molecular NLO materials.

In conjunction with this experimental program, we have collaborated with Prof. K. D. Jordan in the evaluation of ab initio quantum mechanical calculations as a means to predict the structures and properties of potential NLO chromophores. [7] The details of this effort are provided in Prof. Jordan's MRC final report; our major accomplishments have been the successful quantitative predictions of both the ground-state molecular structure and the vibrational frequencies of complexes of the type $W(\equiv CH)L_4X$, which are building-blocks for organometallic polymers with applications toward nonlinear optics and electrical conduction. This effort has been supported in tandem by extensive experimental studies of these properties, with this work having provided the first accurate determinations of the molecular and electronic structures, force constants, excited-state dynamics, and diamagnetic anisotropies of these compounds. Having determined the computational approaches that reproduce experimental results, we are now in a position to predict the NLO properties of potential conjugated transition-metal chromophores prior to their synthesis.

B. *Noncentrosymmetric Bulk Phases*

The utility of molecules with large β as SHG materials is greatly enhanced if they either naturally possess a noncentrosymmetric bulk phase, or if they can be induced to form one. Our initial approach, undertaken with Prof. A. D. Hamilton, to enforcing noncentrosymmetric structures utilized hydrogen bonding strategies. This led to the discovery that glutaramides self-assemble to form molecular rods, and exhibit SHG properties similar to the archetypal urea. [9] We also found that alkynyl pyridine models of 3 form noncentrosymmetric structures driven by hydrogen bonding. [10]

Other workers have established that conjugated organic donor-acceptor compounds whose principal resonance structures differ little in energy possess larger hyperpolarizabilities than do compounds with high-energy resonance forms. [11] In view of this, we set out to equalize the energies of otherwise nonisoenergetic resonance forms of potential NLO chromophores through the introduction of hydrogen bonding, which could simultaneously introduce a noncentrosymmetric structure. The charge-transfer form ($5^{+/-}$) of ylide 5 lies to

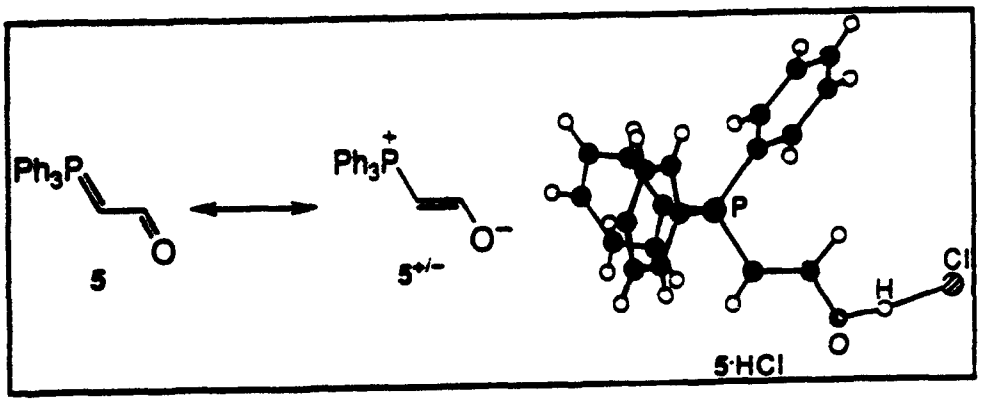

considerably higher energy of the ground state, limiting the NLO utility of this compound. Introduction of HCl results in the formation of a hydrogen-bonded, molecular HCl complex (**5**·HCl) with a delocalized structure ideal for optimizing the molecular hyperpolarizability. Characterization of the SHG properties of this material is underway. Efforts to extend this strategy to other potential NLO chromophores are in progress.

A second breakthrough in the area of designed bulk phases resulted from our discovery that the inorganic acetylene analogues that are the building blocks of our conjugated organometallic NLO polymers can, through ligand design, possess chiral metal centers. The crystal structure of the first such material, $W(\equiv C\text{-}Bu^t)(CH_2Ph)_3$, is shown below (viewed down the crystallographic *c* axis). Chirality at the metal center results from the propellane-like structure enforced by the η^2-benzyl ligands. The space group of the material is *P*31*c*; its SHG efficiency (λ_{ex} = 1907 nm) is 0.5 x urea, even without our having introduced donor-acceptor character to the W≡C

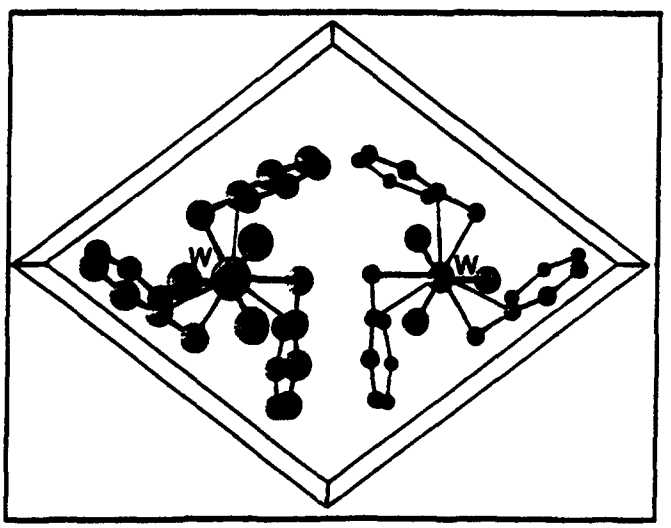

fragment. A rational strategy for enforcing noncentrosymmetric structures on compounds and polymers of types **2**, **3**, and **4** is now at hand.

We have also carried out the first SHG measurements on chiral, differentially substituted metallocene complexes, which were prepared and supplied by Prof. N. J. Cooper. The details of these experiments are described in his section of the MRC final report.

IV.B.9.3 SUMMARY

Our most significant accomplishments over the two-year MRC grant period include:

- Synthesis, structural, and electronic characterization of four new classes of materials based on conjugated transition-metal complexes and polymers: dimetallapolyyne complexes, metallabutadiyne complexes, extended-chain metal-alkylidyne polymers, and conjugated donor-acceptor arenes with metal substituents.
  - First $\chi^{(3)}$ measurement of an unsaturated transition-metal NLO chromophore. The second hyperpolarizability (γ) of this material is 10 times larger than that of its closest organic analogue.
  - Discovery of the first chiral inorganic acetylene, and evaluation of its SHG efficiency.
  - Development of new anaerobic cells for γ and $\chi^{(3)}$ measurements.
  - Demonstration, in collaboration with Prof. K. D. Jordan, of the utility of ab initio quantum mechanical calculations toward the prediction of the molecular structures and electronic properties of potential NLO chromophores.
  - Discovery that hydrogen bonding can stabilize high-energy resonance forms of conjugated materials.
  - Study of the structures and NLO properties of noncentrosymmetric solids based on hydrogen bonding (in part with Prof. A. D. Hamilton).

IV.B.9.4 REFERENCES

1. S. R. Marder, J. E. Sohn, G. D. Stucky, Eds., *Materials for Nonlinear Optics: Chemical Perspectives*, American Chemical Society: Washington, D.C., 1991.

2. (a) T. C. Stoner, R. F. Dallinger, M. D. Hopkins, *J. Am. Chem. Soc.* **1990**, *112*, 5651. (b) T. C. Stoner, S. J. Geib, M. D. Hopkins, *ibid.* **1992**, *114*,

4201. (c) T. C. Stoner, S. J. Geib, M. D. Hopkins, *Angew. Chem. Int. Ed. Engl.* **1993**, *32*, 409. (d) T. C. Stoner, W. P. Schaefer, R. E. Marsh, M. D. Hopkins, *J. Cluster Sci.* **1994**, *5*, 107.

3. J. Manna, S. J. Geib, M. D. Hopkins, *J. Am. Chem. Soc.* **1992**, *114*, 9199.

4. (a) T. P. Pollagi, J. Manna, T. C. Stoner, S. J. Geib, M. D. Hopkins, in *Transition Metal Carbyne Complexes*, F. R. Kreissl, Ed.; Kluwer Academic Publishers:Dordrecht, The Netherlands, **1993**, p. 71. (b) T. P. Pollagi, S. J. Geib, M. D. Hopkins, *Division of Polymeric Materials: Science and Engineering Proceedings* **1993**, *69*, 157. (c) T. P. Pollagi, S. J. Geib, M. D. Hopkins, *J. Am. Chem. Soc.* **1994**, *116*, accepted for publication.

5. T. P. Pollagi, S. J. Geib, M. D. Hopkins, manuscript in preparation.

6. T. C. Stoner, J. Perry, M. D. Hopkins, work in progress.

7. R. Feldman, P. Nachtigall, M. D. Hopkins, K. D. Jordan, manuscript in preparation.

8. (a) J. Manna, T. M. Gilbert, R. F. Dallinger, S. J. Geib, M. D. Hopkins, *J. Am. Chem. Soc.* **1992**, *114*, 5870. (b) J. Manna, S. J. Geib, M. D. Hopkins, *Angew. Chem. Int. Ed. Engl.* **1993**, *32*, 858. (c) J. Manna, L. A. Mlinar, R. J. Kuk, R. F. Dallinger, S. J. Geib, M. D. Hopkins, in *Transition Metal Carbyne Complexes*, F. R. Kreissl, Ed.; Kluwer Academic Publishers: Dordrecht, The Netherlands **1993**, p. 75. (d) J. Manna, R. J. Kuk, R. F. Dallinger, M. D. Hopkins, *J. Am. Chem. Soc.*, submitted for publication.

9. E. Fan, T. C. Stoner, S. J. Geib, M. D. Hopkins, A. D. Hamilton, manuscript in preparation.

10. T. P. Pollagi, S. J. Geib, M. D. Hopkins, *Acta Crystallogr.* **1994**, *C50*, in press.

11. S. R. Marder, D. N. Beratan, L.-T. Cheng, *Science* **1991**, *252*, 103.

12. T. P. Pollagi, S. J. Geib, M. D. Hopkins, unpublished results.

Michael D. Hopkins

MRC Publications

This list does not include manuscripts that are in preparation.

1. ***p-Conjugated Metallabutadiyne Complexes: Synthesis, Structure, and Bonding***
   J. Manna, S. J. Geib, M. D. Hopkins, *J. Am. Chem. Soc.* **1992**, *114*, 9199.

2. ***Conjugated Complexes and Polymers Derived from Metal–Alkylidyne Building Blocks***
   T. P. Pollagi, J. Manna, T. C. Stoner, S. J. Geib, M. D. Hopkins, in *Transition Metal Carbyne Complexes*, F. R. Kreissl, Ed.; Kluwer Academic Publishers: Dordrecht, The Netherlands, **1993**, p. 71.

3. ***Methylidyne Complexes: Structures, Spectra, and Bonding***
   J. Manna, L. A. Mlinar, R. J. Kuk, R. F. Dallinger, S. J. Geib, M. D. Hopkins, in *Transition Metal Carbyne Complexes*, F. R. Kreissl, Ed.; Kluwer Academic Publishers: Dordrecht, The Netherlands **1993**, p. 75.

4. ***Molecular and Electronic Structures of Conjugated Metal-Alkylidyne Polymers***
   T. P. Pollagi, S. J. Geib, M. D. Hopkins, *Division of Polymeric Materials: Science and Engineering Proceedings* **1993**, *69*, 157.

5. ***Synthesis and Characterization of $M_2(CCR)_4(PMe_3)_4$ Dimetallapolyynes***
   T. C. Stoner, W. P. Schaefer, R. E. Marsh, M. D. Hopkins, *J. Cluster Sci.* **1994**, *5*, 107.

6. ***Structure of 2-Methyl-4-(4-pyridyl)-3-butyn-2-ol, a Two-Dimensional Hydrogen-Bond Network***
   T. P. Pollagi, S. J. Geib, M. D. Hopkins, *Acta Crystallogr.* **1994**, *C50*, in press.

7. ***Synthesis and Structures of Extended-Chain Metal-Alkylidyne Complexes: Conjugated Polymers Composed of Alternating Organic and Transition-Metal Subunits***
   T. P. Pollagi, S. J. Geib, M. D. Hopkins, *J. Am. Chem. Soc.* **1994**, *116*, accepted for publication.

8. ***Nature of the Metal-Carbon Triple Bond. Reevaluation of the M≡C Stretching Frequency and Force Constant***
   J. Manna, R. J. Kuk, R. F. Dallinger, M. D. Hopkins, *J. Am. Chem. Soc.*, submitted for publication.

IV.B.10 Non-Linear Optical Properties of Chiral Tungstenocene Complexes

Principal Investigator:	Professor N. John Cooper Department of Chemistry University of Pittsburgh
Other Faculty Participants:	Dr. Michael Hopkins Department of Chemistry University of Pittsburgh
	Dr. Peter Konidaris Department of Chemistry University of Pittsburgh
Students:	Mr. Sijoon Lee Ms. Sherri Lovelace Ms. Inkyung Lee

IV.B.10.1 INTRODUCTION

Our research under the sponsorship of the MRC has been targeted at using the window of opportunity opened by the increasing sophistication of synthetic inorganic and organometallic chemistry to prepare molecular materials which have been specifically designed to have bulk properties with potentially valuable applications in materials chemistry. Nonlinear optical properties are attractive in this context, partly because of their well established molecular basis, and partly because of the broad potential range of new technological applications in the area of optical signal processing and, ultimately, optical computing, which would become feasible with a new generation of materials with enhanced optical nonlinearities. [1,2]

The χ^2 coefficients for transition metal complexes can be markedly larger than those of typical organic systems. [1,2] They may, therefore, have technologically useful NLO properties, but to determine this we must examine the ways in which the properties of systems with the basic elements required for second order NLO behavior vary with the electronic nature of the metal center and with the coordinated ligands. Those basic elements are a large molecular hyperpolarizability β (which, in donor-acceptor systems in which the CT term dominates the excited state, is thought to vary as $(\mu_{ee} - \mu_{gg})\mu ge^2/Ege^2$) [3] together with an acentric distribution of molecular orientations. [1,2]

Differentially substituted tungstenocene complexes constitute an ideal system in which to explore the design and synthesis of molecular organotransition metal compounds with useful χ^2 properties — the oxidation state of the metal and the nature of other ligands at the metal center can be readily and systematically varied, and our recent report that heteroanionic nucleophiles add to a cyclopentadienyl

ligand within $[W(\eta 5\text{-}C_5H_5)_2(SMe_2)Br]^+$ should provide a convenient approach to the introduction of an enantiomeric substituent which will ensure that the molecules crystallize in a non-centrosymmetric space group. [4]

IV.B.10.2 OBJECTIVE

The object of our work within the Materials Research Center has been to use our expertise in this system to prepare a range of promising chirally substituted tungstenocene complexes and to study their NLO properties.

SPECIFIC AIMS

- Use our expertise in the synthesis of differentially substituted tungstenocene complexes to prepare and isolate single enantiomers of chiral tungstenocene complexes.
- Determine the χ^2 coefficients of the enantiomers in collaboration with Professor Hopkins.
- Devise synthetic strategies to chiral tungstenocene complexes in which some of the ligands are powerful donors while others are powerful acceptors, and determine the χ^2 properties of enantiomeric complexes in such systems.
- Correlate the NLO properties of differentially substituted tungstenocene complexes with their structures to determine the features which are most effective in enhancing χ^2 coefficients.

IV.B.10.3 ACCOMPLISHMENTS AND SIGNIFICANCE

We had established through the addition of KO-1-menthyl to $[W(\eta^5\text{-}C_5H_5)_2(SMe_2)Br]^+$ that our methodology for the preparation of differentially substituted bent tungstenocene complexes could be used to introduce a chiral substituent which is cheaply available as a single enantiomer (Scheme I), and in the second year of this project we have established that the oxidation state of the metal and of the ligands attached to the metal can be varied dramatically as shown in Scheme II.

Scheme I

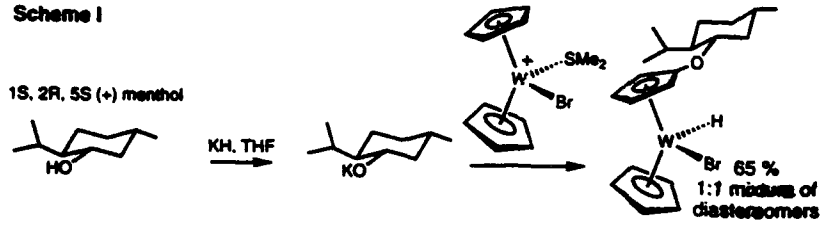

Scheme II

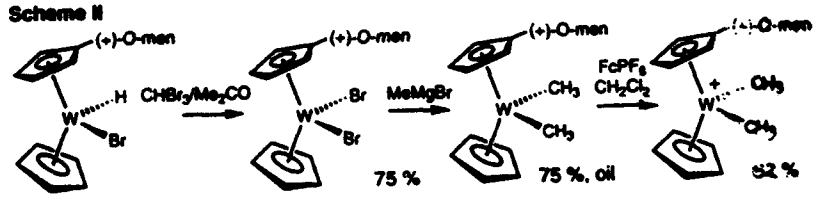

One of the most attractive features of our approach to the synthesis of differentially substituted tungstenocene complexes is the facility with which we can vary the substituent added to the cyclopentadienyl ligand, and the power of our approach is illustrated by the related series of thiomentholate and neomenthanethiolate complexes prepared this year (Scheme III) by variations on the reactions in Schemes I and II using ligands prepared as shown in Scheme IV

Scheme III

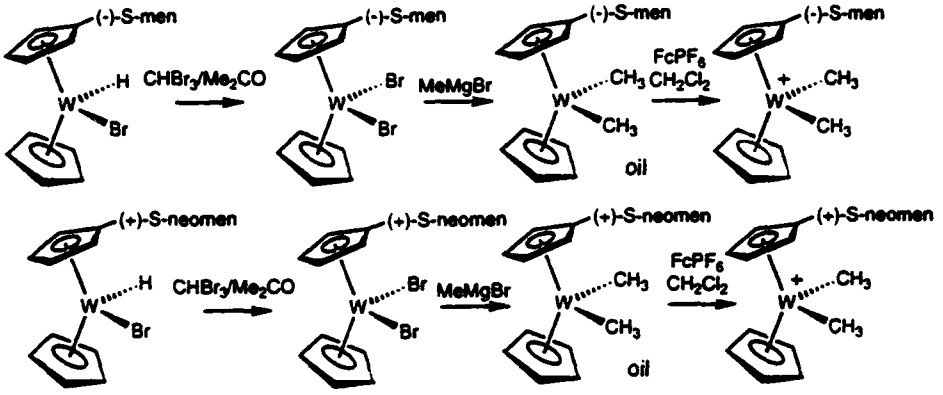

Scheme IV

Thiomentholate Synthesis

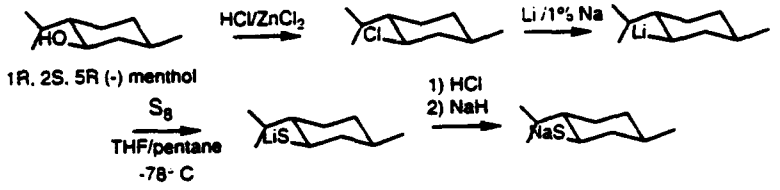

Neomenthanethiolate Synthesis

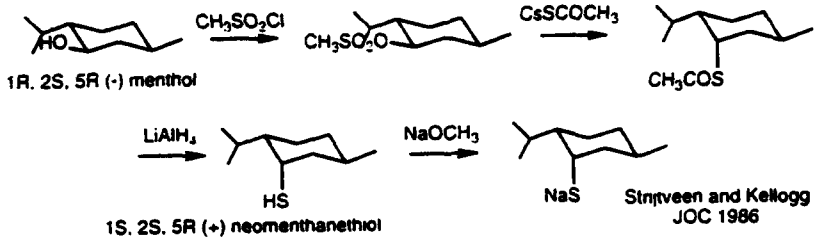

The mentholate, thiomentholate and neomenthanethiolate substituents are all donor substituents, and since large β values arise from interacting donor and acceptor centers tungstenocene derivatives with these substituents in which the metal is also an acceptor center (as in the cationic W(V) complexes) are likely to have significant β values. Complexes in which the *metal* would be expected to act as the donor (as in the neutral W(IV) complexes) are, however, even more interesting prospective NLO substrates since such metal centers are more electron rich than typical organic donors. To obtain a donor-acceptor combination we then require a chiral acceptor substituent on the ligand, and we had initially assumed (see last year's report) that this would require that we add carbon centered nucleophiles (such as derivatives of the $O_2NC_6H5^-$ carbanion) to the cyclopentadienyl ligand of $[W(\eta5\text{-}C_5H_5)_2(SMe_2)Br]^+$. This has not, however, been feasible to date.

One of the most exciting advances in the second year of this project has been the discovery of an elegant alternate approach to acceptor substituents via oxidation of thiomentholate and neomenthanethiolate ligands as shown in Scheme V — this allows a systematic approach to the preparation of materials in which the metal is the donor and the ligand is the acceptor.

Scheme V

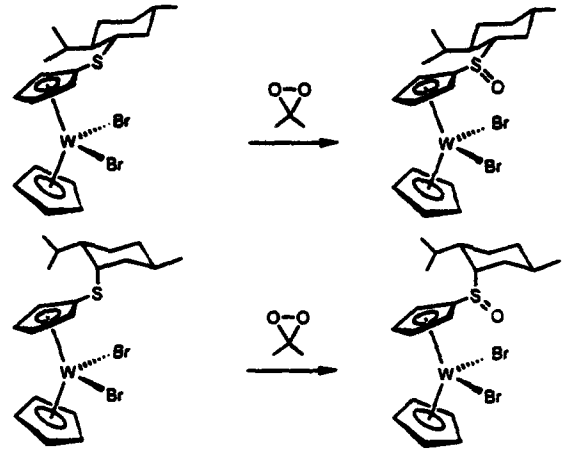

X-ray diffraction studies of two of the compounds prepared to date have confirmed that the materials crystallize in non-centrosymmetric space groups as anticipated. About half have also been examined for second order NLO effects, and although none have exhibited strong effects to date it is clear from the diffraction studies that this is probably because the molecules pack together so that the molecular hyperpolarizabilities are likely to cancel (rather than reinforce) each other in the solid state. This suggests that the next step should be to determine the molecular hyperpolarizabilities directly in solution, and then to explore ways, such as the use of a host lattice, to control the solid state packing of the molecules.

IV.B.10.4 SUMMARY

- Primary objective is to prepare new second order molecular NLO materials based on organotransition metal complexes.
- Secondary objective is to determine how the unique electronic properties of transition metal centers influence the NLO characteristics of organotransition metal complexes.
- First year accomplishments:
  - The adaption of our unique route to the synthesis of chiral tungstenocene complexes with differentially substituted cyclopentadienyl rings to the preparation of complexes containing a chiral auxiliary which is cheaply available as a single enantiomer.
  - The discovery of an oxidative addition reaction of a d^4 tungstenocene complex which results in the addition of a reactive CCl_3 substituent to a cyclopentadienyl ligand.
- Second year accomplishments:
  - The demonstration that the oxidation state of the metal and the non-cyclopentadienyl ligands attached to the metal can be varied dramatically in tungstenocene complexes with a mentholate substituted cyclopentadienyl ligand.
  - The preparation of a related series of tungstenocene derivatives containing thiomentholate and neomenthanethiolate substituted cyclopentadienyl ligands.
  - The discovery of an elegant approach to tungstenocene complexes with acceptor substituents on a cyclopentadienyl ligand via oxidation of thiomentholate and neomenthanethiolate groups.

IV.B.10.5 REFERENCES

1. S. R. Marder, J. E. Sohn, and G. D. Stucky Materials for Nonlinear Optics - Chemical Perspectives American Chemical Society, Washington, D.C., 1991.
2. D. W. Bruce, D. O'Hare Inorganic Materials John Wiley and Sons, New York, 1991.
3. S. R. Marder, D. N. Beratan, and L.-T. Cheng, Science, 1991, 252, 103.
4. J. P. McNally, D. Glueck, and N. J. Cooper, J. Am. Chem. Soc. 1988, 110, 4838.

Publications Supported in part by MRC

"Electrophilic Modification of a Cyclopentadienyl Ligand in a Tungstenocene Complex: Oxidative Addition of CCl_4 to $[W(\eta^5\text{-}C_5H_5)_2(CO)]$ to give $[W(\eta^5\text{-}C_5H_5)_2(CO)(\eta^5\text{-}C_5H_5\text{-exo-}CCl_3)(CO)Cl]$" Lee, S.; Jernakoff, P.; Cooper, N. J. in preparation for J. Am. Chem. Soc.

"The Addition of Heteroanionic Nucleophiles to an Electrophilic Cyclopentadienyl Ligand in $[W(\eta^5\text{-}C_5H_5(SMe_2)Br]^+$ as a Route to Chiral Tungstenocene Complexes" McNally, J. P.; Lee, S.; Cooper, N. J. in preparation for Organometallics.

"The Synthesis of Tungstenocene Compounds Constrained to Non-Centrosymmetric Space Groups by the Addition of Enantiomeric Mentholate Substituents to a Cyclopentadienyl Ligand" Lee, S.; Cooper, N. J. in preparation for Organometallics.

"The Synthesis and Second Order NLO Properties of Acentric Tungstenocene Compounds with Thiomentholate and NeomenthanethiolateSubstituents on Cyclopentadienyl Ligands" Konidaris, P; Cooper, N. J. in preparation for Organometallics.

"Modification of the Donor/Acceptor Characteristics of Substituted Tungstenocene Compounds through Oxidation of the Thiomentholate and Neomenthanethiolate Substituents on the Cyclopentadienyl Ligands " Konidaris, P; Cooper, N. J. in preparation for Organometallics.

IV.B.11 Supercomputing Applications in Materials Design and Characterization

Principal Investigator: Professor K.D. Jordan
Department of Chemistry
University of Pittsburgh

Students: Ms. D. Nachtigallova
Mr. R. Feldman
Dr. K. Kim

IV.B.11.1 INTRODUCTION

During the second year of the MRC grant, we have pursued research in four separate areas: (1) characterization of donor-bridge-acceptor systems of interest for use as electronic and non-linear optical materials; (2) understanding the factors that determine the multiplicity of the ground state of organic diradicals (with the ultimate goal of designing organic ferromagnets); (3) the characterization of novel organometallic molecules being synthesized in Mike Hopkins' group; and (4) the calculation of the OH rotational barrier in phenol.

IV.B.11.2 ACCOMPLISHMENTS AND SIGNIFICANCE

A. Electronic Coupling through Saturated Bridges

We have tested the utility of density functional theory (DFT) for calculating the electronic coupling in a series of polynorbornyl dienes. For the shorter members of the series, the results of the DFT calculations closely reproduce those from much more computationally demanding perturbational theoretical (MP2) calculations. However, for the systems with longer polynorbornyl bridges, we encountered severe convergence difficulties in the solution of the Kohn-Sham equations. This problem was traced to the existence of near degeneracies in the π and σ Kohn-Sham orbitals for the longer bridges.

B. Multiplicities of the Ground States of Diradicals

We have investigated the use of the multi-reference MP2 procedure for determining the relative energies of the low-lying singlet and triplet states of tetramethyleneethane (TME), a prototypical diradical. Comparison of the results of the MP2 calculations and those of more sophisticated multi-reference configuration interaction (CI) calculations reveals that the former method is not sufficiently reliable for correctly predicting the state ordering. We have initiated a new set of multi-reference CI calculations on TME in order to obtain a more reliable estimate of the singlet/triplet gap in this molecule.

C. Structure of Novel Organometallic Compounds

We have completed an MP2 geometry optimization of the W-containing acetylene analog shown below. The calculated geometrical parameters are found to be in excellent agreement with those determined by means of X-ray diffraction measurements. (The two sets of bond lengths agree to within 0.01 Å!) This indicates that this level of theory will be a very useful tool for establishing the geometries of related molecules for which crystal structures are not available (*e.g.*, due to difficulties in obtaining suitable crystals).

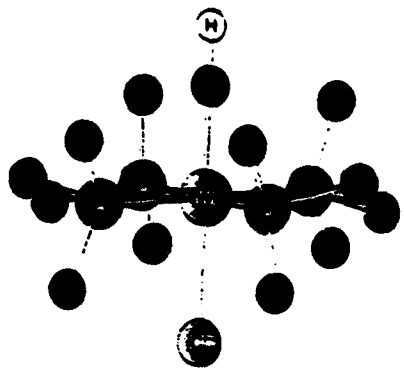

Figure IV.B.11.1 - MP2 Geometry Optimization of W-Containing Acetylene analog

D. Rotational Barrier in Phenol

Molecules such as 1- and 2-hydroxynaphthalene can exist in two conformational forms, which differ slightly in their electronic properties. Of fundamental importance is the height of the barrier separating different conformers. As a calibration of various theoretical methods for calculating rotational barriers in such molecules, detailed calculations have been carried out on phenol. It is shown that the quadratic CI (QCISDT) method used with flexible basis sets gives a value of the barrier height about 240 cm^{-1} lower than the most recent (1207 cm^{-1})value deduced from experiment. We believe that assumptions made in the analysis of the experimental data led to too high a value for the experimental barrier height.

Density functional theory, even with non-local corrections, is found to yield much too large a value of the barrier height of phenol. These calculations were carried out with the Becke-Perdew form for the nonlocal exchange-correlation potential. It is possible that other choices of the exchange-correlation potential

might prove to be superior for purposes of calculating rotational barriers. This will be explored in future studies.

IV.B.11.3 SUMMARY

During the second year of the MRC grant we made significant progress on four separate projects. The MRC support was pivotal to our studies of the utility of density functional theory for studying long-range electronic coupling in molecules and for calculating the rotational barriers in substituted aromatic molecules. The MRC support also enabled us to initiate theoretical studies of W containing acetylene analogs synthesized in Mike Hopkins' group.

Publications

1. P. Nachtigall and K.D. Jordan, "Theoretical Study of the Low-lying Triplet and Singlet States of Tetramethyleneethane at the Triplet Equilibrium Geometry", *J. Am. Chem. Soc.* 115, 270 (1993).

2. J. Nash, P. Dowd, and K.D. Jordan,"Theoretical Study of the Low-lying Triplet and Singlet States of Diradicals: Prediction of Ground State Multiplicities in Cyclic Analogs of TME", *J. Am. Chem. Soc.* 114, 10071 (1993).

3. K.D. Jordan, K. Kim, and M.N. Paddon-Row, "Long-range Interactions in a Series of Rigid Non-conjugated Dienes: 2. Role of Electron Correlation in Determining the Distance Dependence of the π_+,π_- and π_+^*,π_-^* Splittings", *J. Phys. Chem.*, submitted.

4. K. Kim, and K.D. Jordan, "Theoretical Calculation of the OH Rotational Barrier in Phenol", *Chem. Phys. Lett.*, in press.

IV.B.12 Ultrahigh Vacuum Low Temperature Cathodoluminescence Studies of Diamond and Other Large Band Gap Semiconductors

Principal Investigator: Professor W.J. Choyke
Professor R.P. Devaty
Department of Physics and Astronomy
University of Pittsburgh

Students: Mr. Michael F. MacMillan
Mr. Igor Linkov
Mr. M. Yoganathan

IV.B.12.1 INTRODUCTION

The wide band gap semiconductors diamond and the III-V nitrides, including AlN, GaN, and the AlGaN alloy system, show considerable promise for applications in opto-electronics. We proposed studies of state of the art epitaxial films of these materials, obtained from collaborators representing a substantial fraction of the growth effort in this area, using ultra-high vacuum low temperature cathodoluminescence. Rapid feedback of diagnostic information to the growers is essential to progress. Here we summarize our work over the past year on low temperature cathodoluminescence applied to wide band gap semiconductors and examine a few representative examples [1] of our results. We describe measurements and analysis of room temperature FTIR reflectance of III-V nitrides, which can provide diagnostic information that is complementary to luminescence. We have also performed an exhaustive search of the literature on the III-V nitrides of interest and compiled an atlas of reported luminescence lines [2].

IV.B.12.2 ACCOMPLISHMENTS

A. Low Temperature Cathodoluminescence

For luminescence studies of wide band gap materials, there are significant advantages of electron beam over optical excitation [3]. The penetration depth of the electron beam, which can be adjusted over the range 0.1 - 2.5 μm, is determined by selecting the accelerating voltage. Electron beams produce no stray light. However, extreme care must be taken to control the vacuum, especially for measurements at cryogenic temperatures, to eliminate any condensation.

Cathodoluminescence spectra are collected at 6K, 77K, and 300K on an instrument described in detail by Ruan [3]. The samples are mounted on a cold finger in an ultrahigh vacuum chamber (5 x 10^{-11} torr). The six-position rotatable sample turret, which makes use of a turbo-pumped rotating seal, enables a number of samples to be examined without breaking vacuum. The sample is excited by an

Ebert vacuum monochromator to a liquid nitrogen cooled photomultiplier tube connected to either a photon counter or a lock-in amplifier. One of two 1200 //mm gratings, blazed at 3000 Å and 5000 Å, respectively, is used. The spectral range of the system as presently configured is 1600 Å to 9000 Å.

Fifteen cathodoluminescence runs were performed during the period of MRC support. At least six samples are examined in a typical run, which is usually two to three weeks in duration. A total of 54 samples of III-V nitride or diamond films were studied. These sample were provided through collaborations with APA Optics, Inc., the Coordinated Science Laboratory at Johns Hopkins University, Cree Research, Inc., Howard University, Crystallume, and Kansas State University. We discuss a few representative spectra in the following paragraphs.

Figure IV.B.12.1 shows the low temperature (77K) cathodoluminescence spectrum of a 4.48 μm thick GaN film deposited on a sapphire substrate. There is a GaN buffer layer between the film and substrate. At this temperature the band gap of GaN is 3.5 eV [4]. The dominant emission peak at 3567 Å is probably due to recombination of bound excitons [5]. The shoulder lying on the high energy side of the main emission peak at 3548 Å has been attributed to recombination of full excitons [6]. The two side bands at 3546 Å and 3751 Å may be longitudinal optical (LO) phonon replicas of the free exciton. This assignment is based on the LO phonon energy of 91.3 meV (737 cm^{-1}) obtained from the infrared reflectance spectrum of this sample.

Figure IV.B.12.2 shows the low temperature (77K) cathodoluminescence spectrum of a 0.5 μm thick GaN film deposited on a 6H SiC substrate. This film was intentionally doped with Si to a level of $1.2 \times 10^{18} cm^{-3}$. Silicon acts as an acceptor in GaN with an estimated binding energy of 225 meV [7]. The peak at 3775 Å is associated with Si, but the mechanism for luminescence has not yet been established.

Figure IV.B.12.3 shows low temperature (6K) and room temperature cathodoluminescence spectra of a 0.58 μm thick AlN film deposited on a sapphire substrate in a UHV chamber. The peak centered at 3260 Å is broad and does not shift with temperature. A similar peak was observed in polycrystalline AlN ceramics as well as a single crystal by Youngman and Harris [8], who attributed the feature of oxygen in the AlN.

B. FTIR Reflectance

We have shown [9] that room temperature infrared reflectance obtained by Fourier transform spectroscopy, when interpreted using simple models based on measured bulk parameters, can provide useful information on the identify and quality of III-V nitride films on various substrates. The contribution of the nitride

layer can be extracted from a complicated spectrum even when the substrate has overlapping reststrahl bands.

Room temperature reflectance spectra were measured at 1 cm^{-1} resolution on a Nicolet System 740 Fourier transform infrared spectrometer using a KBr beamsplitter and a deuterated triglycine sulfate (DTGS) detector. The commercial reflectometer was set at 5°, near normal incidence. The reflectometer makes use of a converging incident beam. The effect of the solid angle was estimated by calculating an rms average angle of incidence, 7.2°. A Pt film deposited on a polished sapphire substrate [10] served as a reflectance standard. The spectra were not corrected for the reflectivity of Pt.

AlN, GaN, and many of the substrate crystals are uniaxial so that the infrared properties are anisotropic. We model the infrared properties of the films and substrates using Lorentz oscillators. The treatment follows the method of Piro [11]. All uniaxial media are assumed to be oriented with their axes of symmetry perpendicular to the surfaces and interfaces. In this case, the solution separates into components with electric field vectors polarized either parallel (p) or perpendicular (s) to the plane of incidence. Both s and p polarizations are included, corresponding to unpolarized radiation. The non-normal angle of incidence is included, which is essential to the interpretation of the measured spectra. Complete account is taken of interference effects in the films. The best results are usually obtained when multiple reflections within the substrates are neglected. Usually, the back sides of the substrates are not polished.

Figure IV.B.12.4 shows the room temperature reflectance spectrum in the reststrahl region of a 0.96 μm thick GaN film deposited on a 6H SiC substrate. The complicated structure arises because the thin film and substrate have reststrahl bands in the same region. The perhaps unfamiliar triangular shape of the GaN reststrahl band is due to the thinness of the film. The sharp dip at 733 cm^{-1} indicates the LO (A_1) vibrational frequency of GaN. This value does not agree with the value 744 cm^{-1} obtained by Barker and Ilegems [12]. However, their measurements were performed on thin GaN films deposited on (0001) sapphire, which has a significant lattice mismatch with GaN. The lattice constant of 6H SiC is much closer to that of GaN, so that strain effects should be reduced [13]. Sharp dips associated with LO modes, discussed by Berremen [14], are only observable at non-normal incidence.

Figure IV.B.12.5 shows the room temperature reflectance spectrum of a 4.52 μm thick GaN film deposited on a sapphire substrate. Sapphire has several reststrahl bands in this region, giving rise to many of the peaks observed in this spectrum. For this film, the LO(A1) frequency is 743 cm^{-1}, which agrees quite well with the result of Barker and Ilegems [12].

Figures IV.B.12.6 and IV.B.12.7 show measured and calculated reflectance spectra for an AlN film deposited on a 0.02 cm thick Si substrate oriented 4° from

(001). The film is polycrystalline, with a high degree of orientation. The Fabry-Perot oscillations due to multiple reflections within the film are clearly visible in the region of transparency above 1000 cm^{-1} (Fig. IV.B.12.6). These data can be used to obtain the film thickness, given the index of refraction of AlN. The calculated curves in Fig. IV.B.12.6 were obtained by adjusting the thickness of the AlN film to 0.92 μm, which is in reasonable agreement with the 1.1 μm thickness measured by profilometry. Comparison of the calculated curves shows that neglect of multiple reflections within the substrate provides a better description of the data.

Figure IV.B.12.7 shows an expanded view of the AlN reststrahl region. The model lead to the following interpretation. The large maximum is associated with the reststrahl of AlN. The two dips near 650 cm^{-1} are associated with absorption by the AlN TO(E_1) mode combined with interference effects. The dip at 894.5 cm^{-1} is associated with the AlN LO(A_1) mode, observed at non-normal incidence for p-polarized radiation. Further interpretation is provided in a recent publication [9].

Figure IV.B.12.8 shows the infrared reflectance for an AlN film on a (0001) face of a Lely grown 6H SiC substrate. Films prepared under similar growth conditions are known to be single crystal by electron channeling. The film thickness determined by comparing measured and calculated Fary-Perot oscillations (not shown) is 0.98 μm, which agrees very well with the value 1 μm obtained by profilometry. Except for the difference in magnitude, the agreement between the measured and calculated spectra is good. Multiple reflections within the substrate are neglected. Also shown on Fig. IV.B.12.8 is the calculated spectrum for a bare 6H SiC substrate. The high reflectance between 800 and 990 cm^{-1} are associated with the reststrahl of the SiC substrate. The remaining features are associated with the AlN layer. The behavior between 550 and 800 cm^{-1} is due to the TO (E_1) mode plus interference effects in the AlN film. The dip near 890 cm^{-1} is associated with the LO(A_1) mode of AlN, observable due to non-normal incidence.

IV.B.12.3 REFERENCES

1. M.F. MacMillan, R.P. Devaty, W.J. Choyke, A. Khan, M.E. Lin, H. Morkoc, W.A.. Bryden, T.J. Kistenmacher, and S. Nakamura, to be presented at ICSCRM-93, Washington, DC, Nov 1, 1993.

2. W.J. Choyke and I. Linkov, to be presented at ICSCRM-93, Washington, DC, Nov. 1, 1993.

3. Ju-Ai Ruan, Ph.D. Thesis, University of Pittsburgh, 1991.

4. B. Monemar, Phys. Rev. B 10, 676 (1974).

5. R. Dingle, D.D. Sell, S.E. Stokowski, and M. Ilegems, Phys. Rev. B 4, 1211 (1971).

6. R. Dai, S. Fu, J. Xie, G. Fan, G. Hu, H. Schrey, and C. Klingshirn, J. Phys. C: Solid State Physics 15, 393 (1982).

7. M.R.H. Khan, Y. Oshita, N. Sawaki, and I. Akasaki, Solid State Commun. 57, 405 (1986).

8. R.A. Youngman and J.H. Harris, J. Am. Ceram. Soc. 73, 3238 (1990).

9. M.F. MacMillan, R.P. Devaty, and W.J. Choyke, Appl. Phys. Lett. 62, 750 (1993).

10. J.V. Mantese, W.A. Curtin, and W.W. Webb, Phys. Rev. B 33, 9897 (1986).

11. P. Piro, Phys. Rev. B 36, 3427 (1987).

12. A.S. Barker, Jr., and M. Ilegems, Phys. Rev. B 7, 743 (1973).

13. S. Strite and H. Morkoc, J. Vac. Sci. Technol. B 10, 1247 (1992).

14. D.W. Berreman, Phys. Rev. 130, 2193 (1963).

PUBLICATIONS

1. "Low pressure metalorganic chemical vapor deposition of AlN over sapphire substrates," M. Asif Khan, J.N. Kuznia, R.A. Skogman, D.T. Olsen, M.F. MacMillan, and W.J. Choyke, Appl. Phys. Lett. 61, 2539 (1993) (1993).

2. "Infrared reflectance of thin aluminum nitride films on various substrates," M.F. MacMillan, R.P. Devaty, and W.J. Choyke, Appl. Phys. Lett. 62, 750 (1993).

3. "Cathodoluminescence and FTIR reflectance of thin A1N and GaN films on various substrates," M.F. MacMillan, R.P. Devaty, W.J. Choyke, M. Asif Khan, M.E. Lin, H. Morkoc, W.A. Bryden, T.J. Kistenmacher, and S. Nakamura, to be published in the proceedings of ICSCRM-93.

4. "Atomic layer chemical vapor deposition of single layers, quantum wells and (AlN-GaN) short period superlattices," M. Asif Khan, J.N. Kuznia, D.T. Olsen, W.J. Choyke, M.F. MacMillan, and T. George, to be published in the proceedings of ICSCRM-93.

5. "A short atlas of luminescence and absorption lines and bands in SiC, GaN, AlGaN and AlN," W.J. Choyke and I. Linkov, to be published in the proceeding of ICSCRM-93.

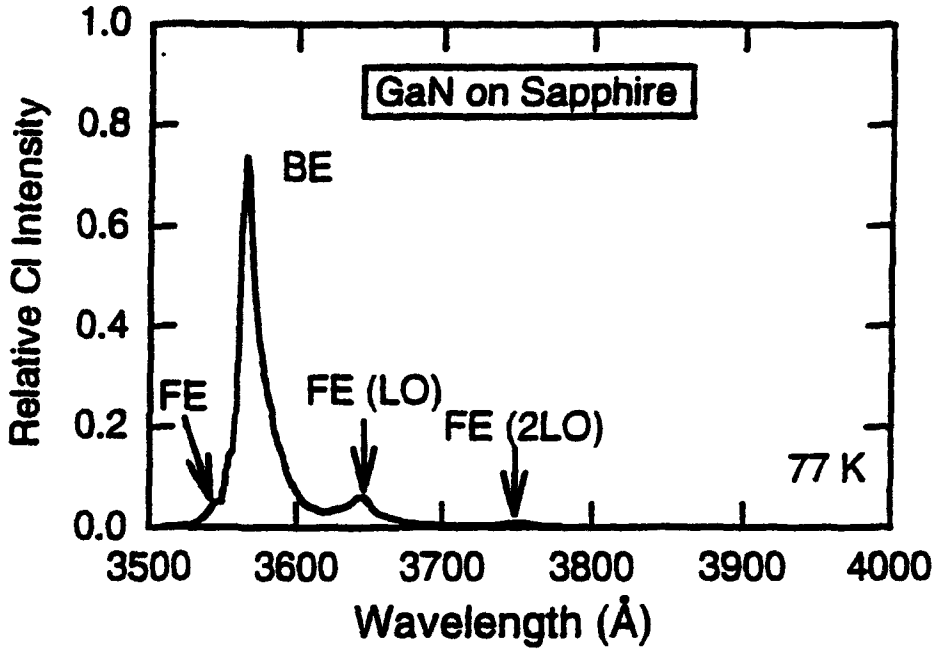

Figure IV.B.12.1 Cathodoluminescence of a 4.48 μ thick GaN film deposited on a sapphire substrate with a GaN buffer layer

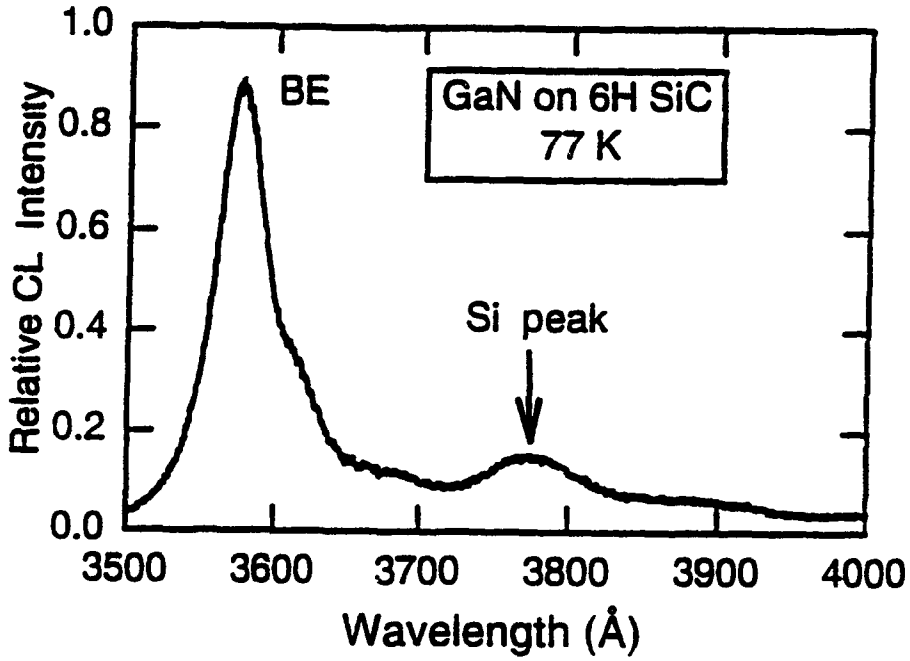

Figure IV.B.12.2 Cathodoluminescence of a 0.5 μ thick GaN film doped with silicon deposited on a (0001) 6H SiC substrate.

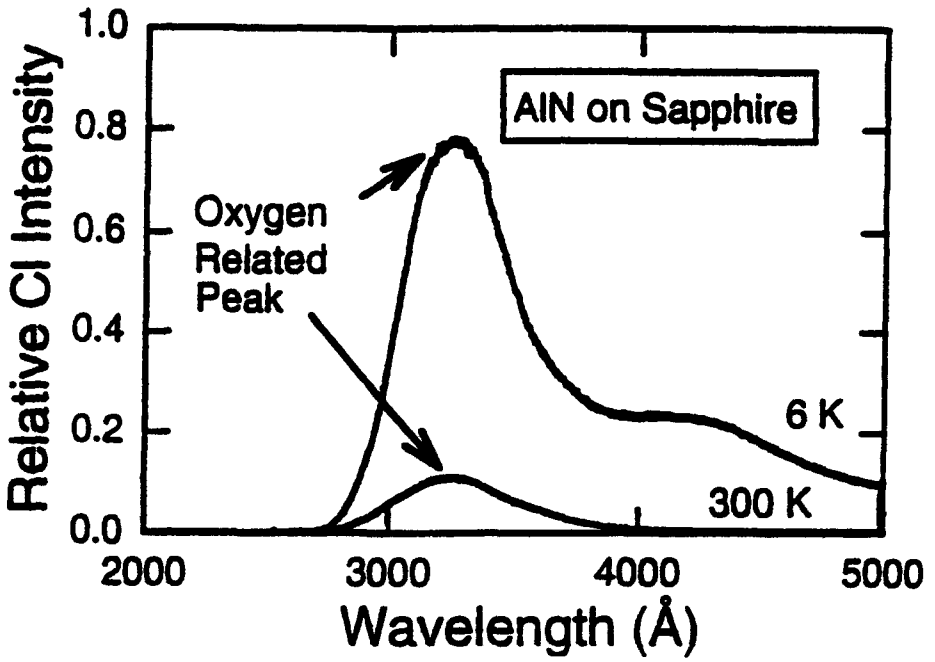

Figure IV.B.12.3 Cathodoluminescence of a 0.58 μ thick AlN film deposited on a sapphire substrate.

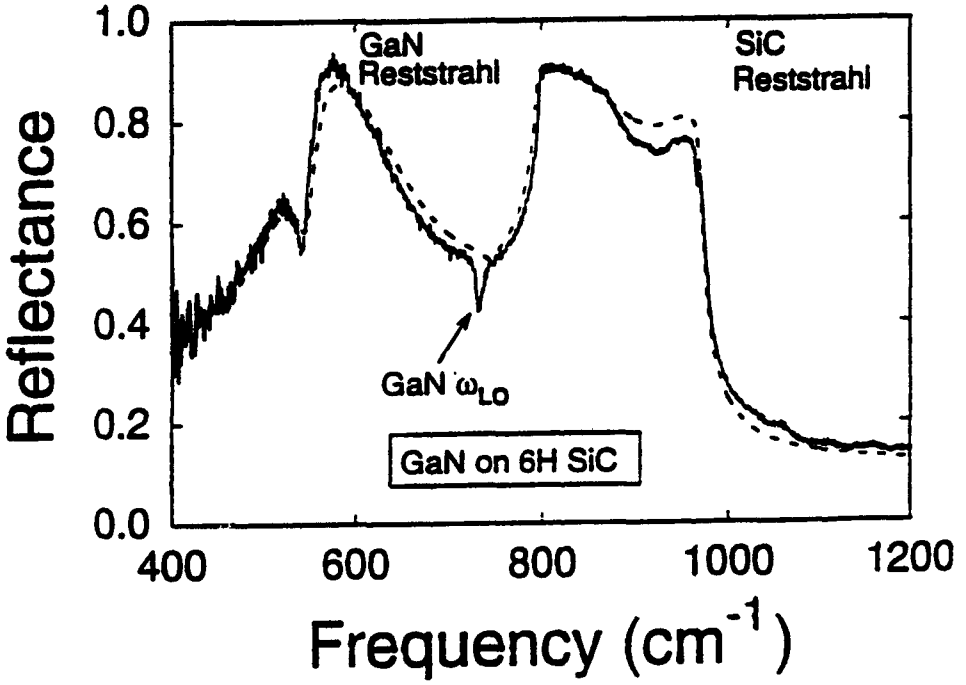

Figure IV.B.12.4 Relative reflectance of a 0.96 μm thick GaN film on a (0001) 6H SiC substrate. The solid line represents the data and the dashed line the calculated spectrum.

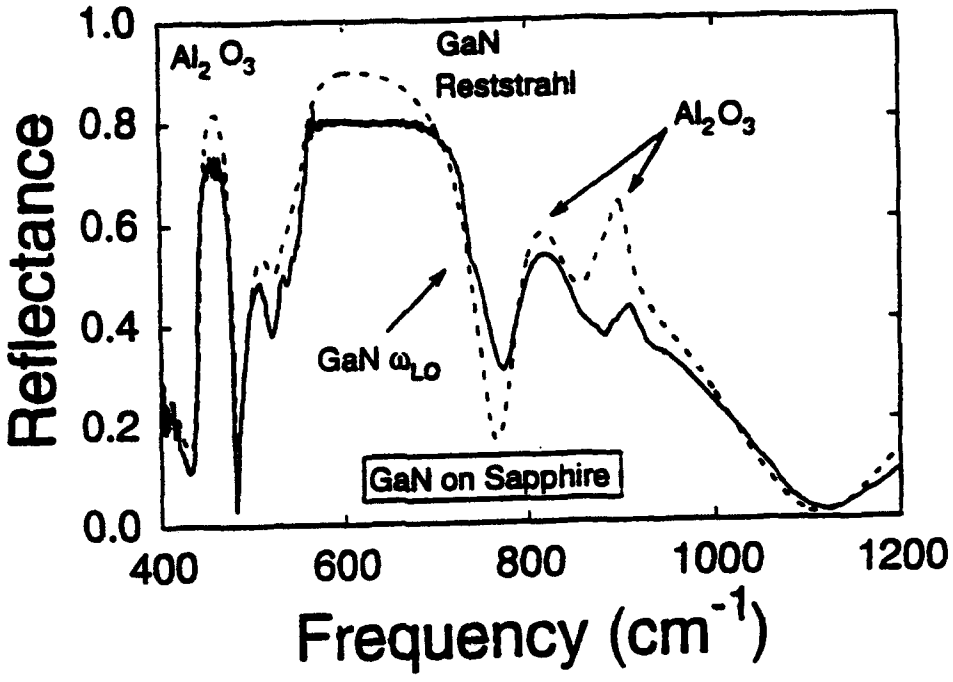

Figure IV.B.12.5 **Reflectance ofa 4.52 μm thick GaN film on a sapphire substrate. The solid line represents the data and the dashed line the calculated spectrum.**

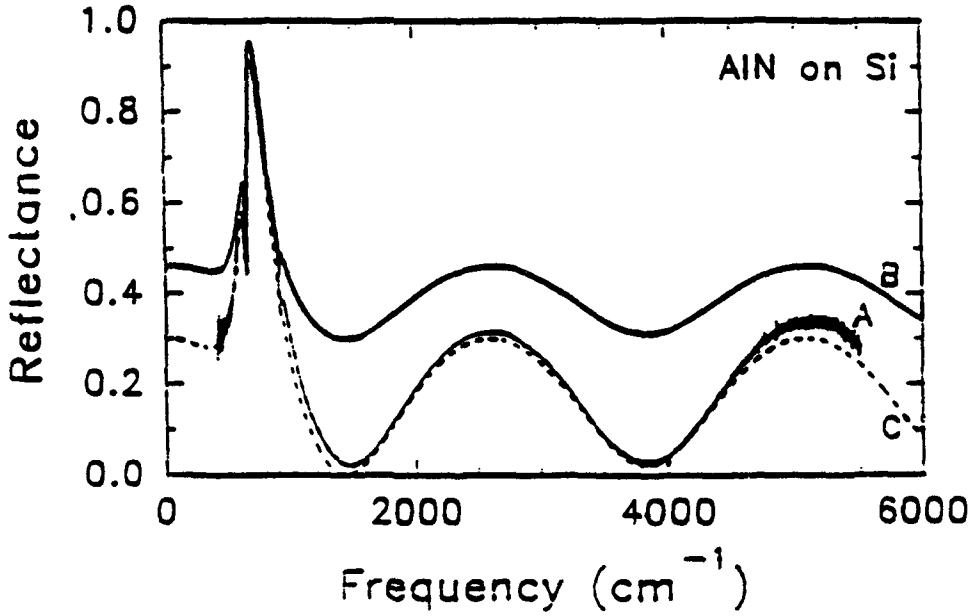

Figure IV.B.12.6 **Reflectance of a 0.92 μm thick AlN film on a Si substrate. A (thin solid line) - data; B (heavy solid line) - calculated spectrum, including multiple reflections within the substrate; C (dashed line) - calculated spectrum, neglecting multiple reflections within the substrate.**

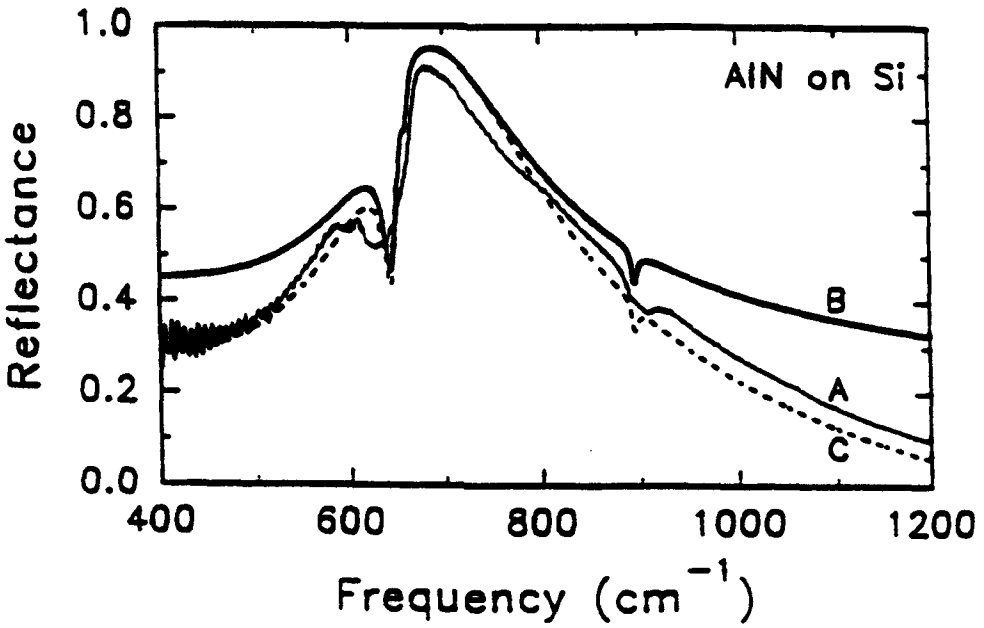

Figure IV.B.12.7 **Same as Figure IV.B.12.6, expanded view of low frequency region.**

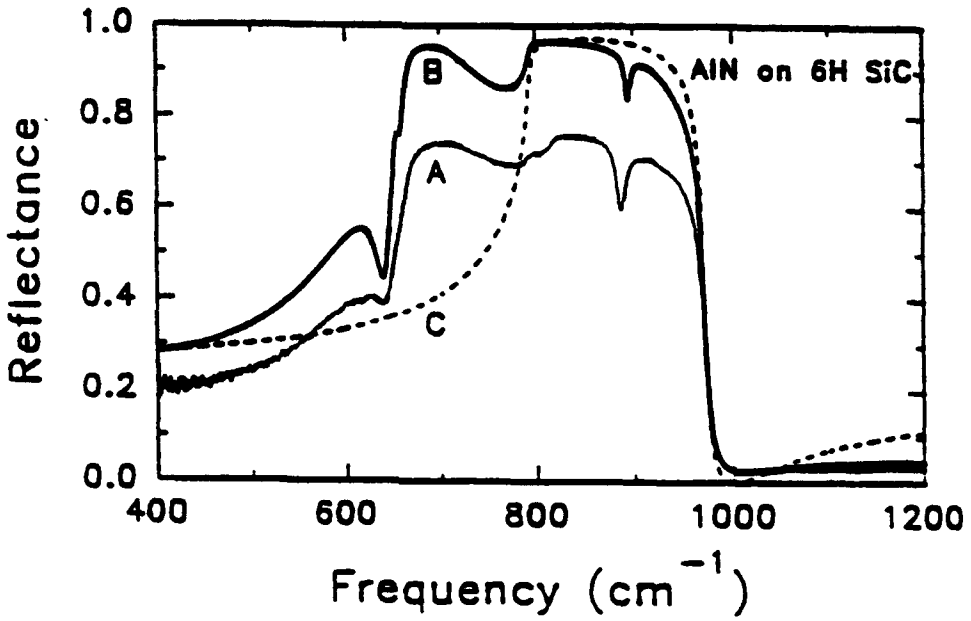

Figure IV.B.12.8 **Reflectance of a 0.98 μm thick AlN film on a (0001) 6H SiC substrate. A (thin solid line) - data; B (heavy solid line) - calculated spectrum, neglecting multiple reflections wihtin the substrate; C (dashed line) - calculated spectrum, SiC substrate only**

IV.C CATALYSIS

IV.C.1 Catalysts for Destruction of Nerve Gas, and Catalysts for Alternative Fuels, and Other Surface Dependent Processes

Principal Investigator: Professor David M. Hercules
Department of Chemistry
University of Pittsburgh

Other Faculty Participants: Dr. N. John Cooper
Dr. W. Keith Hall
Dr. Marwan Houalla
Dr. Andrew Proctor
Department of Chemistry
University of Pittsburgh

Dr. Nicholas Eror
Materials Science and Engineering Department
University of Pittsburgh

Students: Dr. Vadim Kazansky
Dr. Kwan Young Lee
Ms. Jane Aigler
Ms. Mary Eberhardt
Ms. Patricia A. Leach

IV.C.1.1 INTRODUCTION

Goals - We are developing a systematic approach for synthesis, characterization and testing of new catalytic materials for use in nerve gas destruction and a variety of other catalytic processes. For the first time, the preparation of catalysts is being approached as a materials problem, rather than from the perspective of catalytic reaction kinetics. We seek to achieve better performance than the currently-used catalyst. We address fundamental questions in catalysis while developing practical catalysts.

Approach - Several approaches are being tried in parallel. Synthesis of catalysts containing well-defined species provides the possibility of high selectivity. Catalysts with an adjustable functionality allow changing catalytic properties without grossly modifying catalyst structure. Use of probe reactions allows evaluation of catalytic functions important for nerve gas destruction. Part of the program involves identification of surface species and how they relate to catalytic function.

Selection of Catalytic Systems - Catalysts useful for nerve gas destruction should be active for one or more of the following reactions: oxidation; dealkylation;

hydrolysis; and dehalogenation. The catalyst support must be stable in the presence of decomposition products. Transition metals are being evaluated because of their known efficacy as oxidation catalysts. Specifically, Mo, Cr and V based catalysts are being investigated. A novel support being investigated is calcium phosphate because of its adjustable functionality and potential stability in the presence of phosphorus compounds produced by nerve gas decomposition. Model catalyst systems are used for study because one can: 1) identify the chemical nature of surface species; 2) determine distribution(s) of surface species; and 3) correlate abundance of a given species with catalytic activity.

IV.C.1.2 OBJECTIVES

1. To prepare catalysts containing a single species by reaction of Mo allyls with conventional supports such as silica.

2. To react such catalysts to produce single oxidation states on the surface. To characterize these catalysts spectroscopically.

3. To prepare catalysts having a single oxidation state by photoreduction. To characterize such catalysts with spectroscopic methods.

4. To prepare phosphate-based catalysts having different properties by synthesis of hydroxyapatites.

5. To incorporate metals into the catalysts and to test such catalysts for activity using probe reactions.

6. To develop catalysts for the destruction of nerve gas using the above preparation methods.

IV.C.1.3 ACCOMPLISHMENTS AND SIGNIFICANCE

A. Model Catalysts

Allyl-based Mo dimer/SiO_2 catalysts were synthesized for the purpose of comparison with monomeric and trimeric materials.

The methodology previously used for the synthesis of allyl-based Mo catalysts was applied to the preparation of model Cr/Al_2O_3 system from Cr allyl dimer. This was done in collaboration with John Cooper's group.

Model Mo/SiO_2 catalysts containing a single oxidation state were successfully prepared by photoreduction in CO atmosphere. The results were authenticated by XPS. This approach for the synthesis of catalysts containing a single oxidation state is been currently applied to other catalyst systems (W/TiO_2, V/Al_2O_3).

B. Calcium Phosphates-Based Catalysts

Synthesis, characterization and testing of Cu hydroxyapatites (Cu-HA) as catalysts for the decomposition of nerve gas simulants have been completed. The results are already published [1,2].

As a follow up of the Cu-HA work, hydroxyapatites have been evaluated as supports for other transition metals known to be active as oxidation catalysts (ex: Mo). In particular, the adsorptive properties of HA have been examined and compared with those of a conventional support such as alumina.

The Zero Point Charge (ZPC, the pH at which the net surface charge is zero) for the hydroxyapatite used as a support for Cu-HA catalysts was determined. The measured value (ca. 8) was identical to that reported for most alumina supports.

Adsorption of Mo from aqueous solutions on HA was examined. The variation of Mo uptake by the HA support was measured as a function of the pH of preparation. The results were comparable to those measured for the corresponding Mo/Al_2O_3 system. Specifically, Mo uptake is low for pH's higher than the ZPC of the support and increases with decreasing the pH of preparation. However, in the case of the Mo-HA system, a significant part of the increase in Mo uptake with decreasing pH is due to increased formation of $CaMoO_4$.

The surface and bulk composition of Mo-HA catalysts, obtained by equilibrium adsorption (EA) as described above, were determined. Two Mo phases were identified and quantified in all catalysts: a Mo surface phase and $CaMoO_4$.

The presence of $CaMoO_4$ in all catalysts was attributed to the long contact time in equilibrium adsorption (EA) preparations between Mo solutions and the HA support. This hypothesis appears to be substantiated by quantitative analysis of Mo-HA catalysts prepared by incipient wetness impregnation (i.e. short contact time between the Mo solution and the HA support) which indicates a drastic decrease in $CaMoO_4$ formation as compared to those obtained by the EA method.

IV.C.1.4 SUMMARY

A. Model Catalysts

- Model Mo dimer/SiO_2 and Cr dimer/Al_2O_3 were synthesized from their respective allyl precursors.

- Model Mo catalysts containing a discrete Mo oxidation state were successfully prepared by CO photoreduction of the oxidic catalysts.

B. Calcium Phosphate-Based Catalysts

- Hydroxyapetite HA was evaluated as a support, and was found to exhibit adsorptive properties similar to those of a conventional support such as alumina.
- HA and Al_2O_3 have identical point of zero charge PZC's (~8).
- The adsorption behavior of Mo on HA from aqueous solutions as a function of pH of preparation was similar to that obtained for the Mo/Al_2O_3 system.
- Mo-HA catalysts prepared by equilibrium adsorption (EA) contain two Mo phases: $CaMoO_4$ and a surface interaction species, the distribution of these phases was estimated from Raman results.
- The formation of $CaMoO_4$ in EA preparation was attributed to the long contact time between the Mo solution and the HA.
- Consistent with the above hypothesis, Mo HA catalysts prepared by incipient wetness impregnation contain a significantly lower amount of $CaMoO_4$.

PUBLICATIONS

1. "ESCA Study of "Model" Allyl-Based Mo/SiO_2 Catalysts", J. M. Aigler, J. L. Brito, P. A. Leach, M. Houalla, A. Proctor, N. J. Cooper, W. K. Hall and D. M. Hercules, J. Phys. Chem., ***97***, 5699 (1993).

2. "Catalytic Oxidative Decomposition of Dimethyl Methylphosphonate over Cu-Substituted Hydroxyapatite", K. Y. Lee, M. Houalla, D. M. Hercules and W. K. Hall, J. Catal. ***145***, 223 (1994).

IV.C.2 New Catalytic Materials for the Synthesis of Alternative Fuels

Principal Investigator: Professor James G. Goodwin, Jr.
Department of Chemical Engineering
University of Pittsburgh

Other Faculty Participants: Dr. Rachid Oukaci
Dr. George Marcelin
Department of Chemical Engineering
University of Pittsburgh

Dr. Marwan Houalla
Department of Chemistry
University of Pittsburgh
Dr. Ayse Senatalar
Technical University of Istanbul

Dr. Johannes Lercher
Technical University of Vienna

Students: Dr. Andreas Kogelbauer
Mr. Apostolos A. Nikolopoulos

IV.C.2.1 INTRODUCTION

The quality standards imposed upon gasoline by the Clean Air Act Amendments [1] have made MTBE (methyl tertiary-butyl ether) the additive of choice for gasoline improvement because of its high mixing octane value [2], advantageous properties with respect to environmental concerns during the engine combustion process [3,4] and outstanding physico-chemical properties compared to alcohols [4]. During the last few years MTBE has become one of the fastest growing commodity chemicals [5,6].

The commercial process currently in application (liquid phase reaction of methanol and isobutene at temperatures below 100°C and at pressures of up to 20 bar) uses a sulfonated ion-exchange resin catalyst whose lack of thermal stability and corrosive properties are considered to be major drawbacks. Because of these and other restrictions in the applicability of the resin catalyst [7], a suitable alternative catalyst is of great interest.

Zeolites seem to be very promising because they not only exhibit excellent stability at elevated temperatures but also high selectivity towards MTBE, even at

methanol-to-isobutene ratios smaller than unity [8]. This is of substantial interest for the commercial synthesis process where the currently required high ratios increase the costs due to separation and recycling of the excess methanol [9]. Another outstanding advantage of zeolites is their alterable acidity which could permit MTBE synthesis, a strongly exothermic reaction, at considerably lower temperatures, away from reaction equilibrium [10].

IV.C.2.2 OBJECTIVES

The research performed under this project has three major objectives. The first objective aims towards a better understanding of the etherification reaction on solid acid catalysts, especially zeolites. Questions like the influence of the overall acidity, the acid strength of the sites, the composition of the catalyst, and the catalyst geometry upon activity and selectivity during the MTBE synthesis reaction have been addressed. In addition, fundamental aspects such as adsorption behavior, possible transport limitations, and dissipation of the heat of reaction have been investigated.

The second objective involves the development and preparation of novel solid acid catalysts, especially strongly acidic zeolites, having unique properties for low temperature organic reactions such as etherification. Since the MTBE formation is strongly exothermic and, thus, exhibits substantial thermodynamic limitations at high temperatures, a catalyst which operates at low temperatures (around 60°C) with reasonable reaction rates would be preferable.

The third objective is concerned with the determination of the nature of the active sites, especially in strongly acidic catalysts. By determining the structure of the active sites we could develop new insights leading to the formulation of unique strongly acidic zeolites.

IV.C.2.3 EXPERIMENTAL

Various types of acidic zeolites have been selected and examined in terms of their catalytic behavior (activity, selectivity, deactivation) for the formation of MTBE, along with the commercially used MTBE synthesis catalyst, Amberlyst-15 ion exchange resin. Two series of partially dealuminated HY zeolites and a series of partially cation-exchanged HY zeolites were selected for investigating the influence of acidity on MTBE synthesis. For the investigation of the influence of post-synthesis modification on acidity and, thus, catalytic activity towards MTBE formation, post-synthesis modified zeolites have been prepared and examined, the modification of which was performed by impregnation with triflic acid (TFA), and by ion exchange with ammonium fluoride (NH_4F).

Catalyst activity studies were performed in a fixed-bed reaction system with on-line GC-FID analysis. The flow system was designed so as to offer accurate control of the flow and partial pressure of each of the reaction gases. The reaction

temperature was continuously monitored by a thermocouple inserted in the catalyst bed. Product analysis calibration was based on literature reported relative sensitivities and experimentally verified. Products were identified using an off-line mass spectrometer. Prior to reaction, all catalysts were pretreated *in-situ* by heating under helium flow. The reaction conditions used were: reaction pressure of 156±7 kPa, temperature of 60-90°C, methanol-to-isobutene feed ratio of 1.0, and reactant partial pressure of 6.9 kPa. These conditions were chosen so as to minimize the influence of possible mass/heat transport limitations.

IV.C.2.4 RESULTS FOR YEAR 2

A. Effect of Acid Strength Variation on MTBE Synthesis

In order to investigate the influence of acid strength upon the catalytic activity for MTBE formation while maintaining the acid site concentration constant, a series of partially cation-exchanged HY zeolites was used, the cations being Li, Na, and Rb. The exchange of alkali cations is known to lead to more acidic zeolites in the order Li > Na > Rb due to the higher electrostatic potential of the smaller cations [11,12]. The catalysts used in this study have been previously found to exhibit different activities for typical acid-catalyzed reactions, something suggested to be due to an increase in the acid strength of the sites [18]. The chemical composition of these samples was determined by AAS and solid state NMR. TPD of ammonia and pyridine was used for a measurement of the acid site density.

The MTBE synthesis reaction on the cation-exchanged zeolites was performed at 60-90°C with a MeOH/IB ratio of unity. Arrhenius type rate results were obtained in this temperature range which were verified to be reaction-controlled. The activities of the cation-exchanged zeolites for MTBE formation versus the partial charge of proton (an indication of increased acid strength) are shown in Figure IV.C.2.1. The steady-state activity profile obtained was similar to that for other acid-catalyzed reactions [13], whereas the initial activities were found to be very similar. A time-on-stream study and the determination of the extent of coke formation on these samples indicated that the variation in steady-state activities was due to differences in deactivation behavior, especially for RbHY, where a complete blockage of sites caused reduced activity. The similar initial activities observed (contrary to the expected effect of acidity enhancement on activity) can be attributed to the formation of clusters of adsorbed methanol molecules. Such formation would act to reduce the acid strength of the sites, as has been observed in the case of the resin catalyst [14], and, thus, to decrease their activity for MTBE synthesis.

B. Adsorption Study of Methanol and Isobutene on MTBE Synthesis Catalysts

The adsorption behavior of each of the MTBE synthesis reactants on various acid catalysts was examined, in order to obtain some information about the extent

and the type of interaction between the adsorbed molecules and the acid sites. The catalysts studied were a series of HY zeolites, ZSM-5, and Amberlyst-15 resin for comparison. The catalysts were pretreated in a manner similar to that applied for reaction experiments. Typical sigmoidal response curves were obtained, which by normalization and integration gave the residence times for each of the adsorbed compounds. In addition, by performing a cycle of adsorption-desorption steps so as to remove all weakly adsorbed molecules, we were able to differentiate between reversibly and irreversibly adsorbed molecules.

The results for the extent of irreversible adsorption of methanol and isobutene on all the catalysts studied are presented in Figure IV.C.2.2, expressed in molecules adsorbed per acid site. These results indicate that the extent of adsorption on Amberlyst-15 resin was similar for methanol and isobutene, and it also was relatively low on a site basis. On the other hand, all the zeolites exhibited a one-to-one adsorption pattern for isobutene but a two-to-one pattern for methanol, indicating an enhanced affinity for the latter, under the conditions applied. Although based on these experiments we cannot predict the adsorption behavior of each of the reactants in the presence of the other one, we can assume that the coverage of the active sites could be different (and, possibly, in favor of methanol) from that implied by the gas feed ratio. This hypothesis can explain the decreased selectivity of the zeolites to the isobutene dimer as compared to the resin, along with the shape selectivity effect, which has been proposed in the literature [15,16].

C. Effect of Post-Synthesis Modification on MTBE Synthesis

Modification of the acidity of solid acids by incorporation of strong electron withdrawing compounds like triflic acid [16] or ammonium sulfate [17] has been found to result in enhanced etherification. However, no systematic investigation of the parameters influencing the behavior of modified solid acids and the mechanism by which modification affects acidity has been reported. In order to investigate the impact of post-synthesis modification with strongly acidic compounds on the catalytic activity for MTBE synthesis, several series of modified HY, H-ZSM-5, and H-mordenite zeolites were produced and examined. Two modification processes were applied, i.e., impregnation with triflic acid, and ion exchange with ammonium fluoride. Extensive characterization of these samples has been performed for determining their acidic parameters and the extent of modification, and the results are presented in Tables IV.C.2.1 and IV.C.2.2.

The MTBE synthesis reaction was performed under the conditions previously mentioned. The pretreatment process was also the same, except for the TFA modified samples, which were treated only up to 180°C, due to decomposition of TFA for T > 200°C [16]. The steady-state MTBE formation rates at 90°C on the TFA and F^- modified zeolites plotted as a function of the extent of modification are presented in Figures IV.C.2.3 and IV.C.2.4, respectively. In the case of the TFA modified HY zeolites, a low level of TFA modification (up to ca. 3 wt%) was found

to increase the MTBE formation rate, but further incorporation of TFA resulted in a decrease in activity. A reduction in activity was also observed for the H-ZSM-5 and H-mordenite TFA modified samples. These results are in agreement with other TFA-modification studies [16] and seem to support the hypothesis of activity loss due to site blocking caused by excess of TFA. A site blockage phenomenon would be expected to be more severe for medium pore-opening zeolites (such as ZSM-5) and zeolites having a unidimensional channel system (like mordenite).

Two possible models of acidity enhancement by TFA modification have been proposed [18] and are shown in Figure IV.C.2.5. These are (a) formation of Lewis sites by reactive adsorption (dehydration) of TFA, and (b) formation of new Brønsted sites of high acid strength by dissociative adsorption of TFA. In contrast to pervious reports [16,18], our characterization results indicate the formation of extra-lattice Al during TFA impregnation (Table IV.C.2.1), thus suggesting that the formation of extra-lattice Al may be responsible for the observed activity increase. A schematic of the model of acidity enhancement by TFA modification that is in agreement with our observations is shown in Figure IV.C.2.6.

In terms of F^- modification, an increase in the MTBE formation rate with increasing F^- content was observed, covering a wide range of F concentration (up to 20% of lattice Al). The activity curves obtained for the HY and H-ZSM-5 modified zeolites appear to reach a saturation level, thus indicating that a maximum in the acidity function can be attained by this method. A significant activity increase was also observed for the F^- modified H-mordenite samples, however, the unmodified mordenite was much less active for MTBE formation compared to the other two types of zeolites examined. It should be noted that by performing ^{27}Al MAS-NMR on one F^- modified sample after activation to 400°C under He flow, a measurable formation of extra-lattice Al was observed. It is thus quite possible that the activity enhancement of the F^- modified samples can be related to the formation of extra-lattice Al upon activation.

The results presented above indicate that TFA modification can cause a substantial enhancement in MTBE synthesis activity only in the case of relatively large pore zeolites (like Y, with critical opening of 7.4Å) and only for a limited extent of TFA incorporation. On the other hand, F^- modification was found to result in an activity increase for all the zeolite types studied, and thus it appears to be a more attractive method for acidity variation than TFA modification.

IV.C.2.5 SUMMARY OF OVERALL RESULTS

- Under our reaction conditions, the gas phase synthesis of MTBE is equilibrium limited at temperatures above 100°C for the zeolites examined and at temperatures above 60°C for Amberlyst-15 resin. There are no indications for the presence of heat/mass transport limitations below 100°C on the zeolites studied.

- Dealumination of HY zeolites resulted in a substantial increase in MTBE synthesis activity. The ratio of extra-lattice to lattice Al appears to be an important parameter for determining the catalytic behavior of zeolites for MTBE formation.

- The similar activities exhibited by cation-exchanged zeolites having moderate differences in acid strength can be attributed to the protonation of the adsorbed methanol molecules and the possible dissipation of the charge through methanol clusters, causing a decrease in the acid strength of the sites.

- The high selectivity of zeolites towards MTBE, especially the large pore zeolite HY, can be explained by the protecting function of excess methanol adsorbed in the zeolite pores.

- A high affinity of the zeolites towards methanol compared to isobutene was observed, indicating a possible excess of methanol above the acid sites, apparently in a cluster configuration, for a given reactant feed ratio.

- Post-synthesis modification of various types of zeolites with strong electron with-drawing compounds like triflic acid (TFA) and ammonium fluoride (NH_4F) resulted in a significant variation in zeolite activity for MTBE formation.

- TFA modification was found to enhance the MTBE synthesis activity only for large pore zeolites (like Y) and only within a certain extent of modification (ca. 3 wt%).

- A high level of TFA modification was found to cause a reduction in MTBE synthesis activity due to blockage of the acid sites by the bulky TFA molecules, in particular for medium pore (ZSM-5) and unidimensional channel (mordenite) zeolites.

- F^- modification was found to enhance the activity for MTBE formation for all the zeolite types examined, indicating the absence of pore restriction/blockage phenomena.

- The mechanism of acidity enhancement by TFA-modification appears to be related to the formation of extra-lattice Al. It is quite possible that the formation of extra-lattice Al upon high temperature activation of the F^- modified zeolites may also be influencing the activity of these catalysts for the formation of MTBE.

IV.C.2.6 REFERENCES

1. F. L. Potter, Fuel Reformulation, 1 (1), 22 (1991).

J. E. Peeples, Fuel Reformulation, 1 (1), 27 (1991).

2. B. Taniguchi and R. T. Johnson, CHEMTECH, Aug. 1989, 502.

3. G. H. Unzelman, Fuel Reformulation, 1 (2), 50 (1991).

4. W. J. Piel and R. X. Thomas, Hydrocarbon Processing, 69 (7), 68 (1990).

5. M. S. Reisch, Chemical & Engineering News, Apr. 13, 16 (1992).

6. M. B. Haigwood, Fuel Reformulation, 1 (1), 52 (1991).

7. T. Takesono and Y. Fujiwara, US Patent 4 182 913, (1980).

8. P. Chu and G. H. Kühl, Ind. Eng. Chem. Res., 26, 366 (1987).

9. H. L. Brockwell, R. R. Sarathy and R. Trotta, Hydrocarbon Processing, 70 (9), 133 (1991).

10. F. Colombo, L. Cori, L. Dalloro and P. Delogu, Ind. Eng. Chem. Fundam., 22, 219 (1983).

11. E. O'Donoghue and D. Barthomeuf, Zeolites, 6, 267 (1986).

12. J. W. Ward, J. Catal., 10, 34 (1968).

13. R. Oukaci, J. C. S. Wu and J. G. Goodwin, Jr., J. Catal., 107, 471 (1987).

14. F. Ancillotti, M. M. Mauri, E. Pescarollo and L. Romagnoni, J. Molec. Catal., 4, 37 (1978).

15. P. Chu and G. H. Kuhl, Ind. Eng. Chem. Res., 26, 365 (1987).

16. R. Le van Mao, R. Carli, H. Ahlafi and V. Ragaini, Catal. Lett., 6, 321 (1990).

17. I. Rodriguez-Ramos, A. Guerrero-Ruiz and J. L. C. Fierro, Prepr.-Div. Petr. Chem., A.C.S., 36 (4), 804 (1990).

18. R. Le van Mao, T. M. Nguyen and G. P. McLaughlin, Appl. Catal., 48, 265 (1989).

PRESENTATIONS AND PAPERS BASED ON MRC FUNDED WORK

Presentations

1. "Influence of Catalyst Acidity on MTBE Synthesis Reaction", A. A. Nikolopoulos, M. Öcal, A. Kogelbauer, J. G. Goodwin, Jr., and G. Marcelin, "13th North American Meeting of the Catalysis Society", Pittsburgh, May 1993.

2. "Synthesis of MTBE and Other Ethers", J. G. Goodwin, Jr.; invited paper at the "11th International Symposium on C1 Reactions", Vienna, Austria, July 1992.

3. "Adsorption Behavior of Methanol and Isobutene on MTBE Synthesis Catalysts", A. A. Nikolopoulos, A. Kogelbauer, J. G. Goodwin, Jr., and G. Marcelin, "31st Annual Spring Symposium of the Pittsburgh-Cleveland Catalysis Society", Cleveland, May 1992.
4. "Gas Phase Synthesis of MTBE over Acid Zeolites", A. A. Nikolopoulos, R. Oukaci, J. G. Goodwin, Jr., and G. Marcelin, "203rd ACS National Meeting, San Francisco, CA, April 1992.

Publications

1. "MTBE Synthesis on Partially Alkali-Exchanged HY Zeolites", A. Kogelbauer, M. Öcal, A. A. Nikolopoulos, J. G. Goodwin, Jr., and G. Marcelin, accepted for publication in *J. Catal.*

2. "Effect of Dealumination on the Catalytic Activity of Acid Zeolites for the Gas Phase Synthesis of MTBE", A. A. Nikolopoulos, A. Kogelbauer, J. G. Goodwin, Jr., and G. Marcelin, submitted for publication in *Applied Catalysis*.

3. "Selectivity Behavior During the Equilibrium-Limited High Temperature Formation of MTBE on Acid Zeolites", A. A. Nikolopoulos, R. Oukaci, J. G. Goodwin, Jr., and G. Marcelin, submitted for publication in *Catal. Letters*.

4. "Impact of Reactant Adsorption on MTBE Synthesis over Zeolites", A. Kogelbauer, A. A. Nikolopoulos, J. G. Goodwin, Jr., and G. Marcelin, to be submitted for publication.

5. "Synthesis of MTBE on Triflic Acid Post-Synthesis Modified Zeolites", A. A. Nikolopoulos, A. Kogelbauer, J.G. Goodwin, Jr., and G. Marcelin, to be submitted for publication.

6. "Synthesis of MTBE on Ammonium Fluoride Post-Synthesis Modified Zeolites", A. A. Nikolopoulos, A. Kogelbauer, J.G. Goodwin, Jr., and G.

Marcelin, to be submitted for publication.

Table IV.C.2.1 CHARACTERISTICS OF TFA POST-SYNTHESIS MODIFIED ZEOLITES

Zeolite	Modif. Extent[a]		Al_L[b] (mmol/g)	Al_E[c] (mmol/g)	Lattice Si/Al[d]	Mod./Al[e] (%)
	(wt%)	(mmol/g)				
Mordenite	0	0	1.35	0.25	9.5	0
M(T-1.2)	1.2	0.08	1.30	0.30	9.9	5.9
M(T-1.7)	1.7	0.11	1.25	0.35	10.3	8.1
LZ210-12	0	0	2.20	0	6.0	0
L(T-1.4)	1.4	0.09	1.95	0.25	6.4	4.1
L(T-2.0)	2.0	0.13	1.80	0.40	7.3	5.9
L(T-2.8)	2.8	0.19	1.75	0.45	7.5	8.6
L(T-3.6)	3.6	0.24	1.70	0.50	7.8	10.9
L(T-11.5)	11.5	0.77	1.50	0.70	8.8	35.0
L(T-16.4)	16.4	1.09	1.30	0.90	10.2	49.5
ZSM-5	0	0	1.20	0	12.0	0
Z(T-1.3)	1.3	0.09	1.10	0.10	13.1	7.5
Z(T-2.3)	2.3	0.15	1.00	0.20	14.4	12.5

Table IV.C.2.2 CHARACTERISTICS OF NH_4F POST-SYNTHESIS MODIFIED ZEOLITES

Zeolite	Modif. Extent[a]		Al_L[b] (mmol/g)	Al_E[c] (mmol/g)	Lattice Si/Al[d]	Mod./Al[e] (%)
	(wt%)	(mmol/g)				
Mordenite	0	0	1.35	0.25	9.5	0
M(F-0.12)	0.12	0.06	1.35	0	9.5	4.4
M(F-0.37)	0.37	0.20	1.35	0	9.5	14.8
M(F-1.53)	1.53	0.81	1.35	0	9.5	60.0
LZ210-12	0	0	2.20	0	6.0	0
L(F-0.12)	0.12	0.06	2.20	0	6.0	2.7
L(F-0.43)	0.43	0.23	2.20	0	6.0	10.5
L(F-0.85)	0.85	0.45	2.20	0	6.0	20.5
ZSM-5	0	0	1.20	0	12.0	0
Z(F-0.08)	0.08	0.04	1.20	0	12.0	3.3
Z(F-0.13)	0.13	0.07	1.20	0	12.0	5.8
Z(F-0.54)	0.54	0.28	1.20	0	12.0	23.3

a : from measured TFA (by TGA) and F^- (by AAS) addition.
b : from ^{27}Al MAS NMR and Al elemental analysis (AAS).
c : from ^{27}Al MAS NMR.
d : from ^{27}Al MAS NMR and Al, Si elemental analysis (AAS).
e : ratio of modifying compound to initial Al content of zeolites.

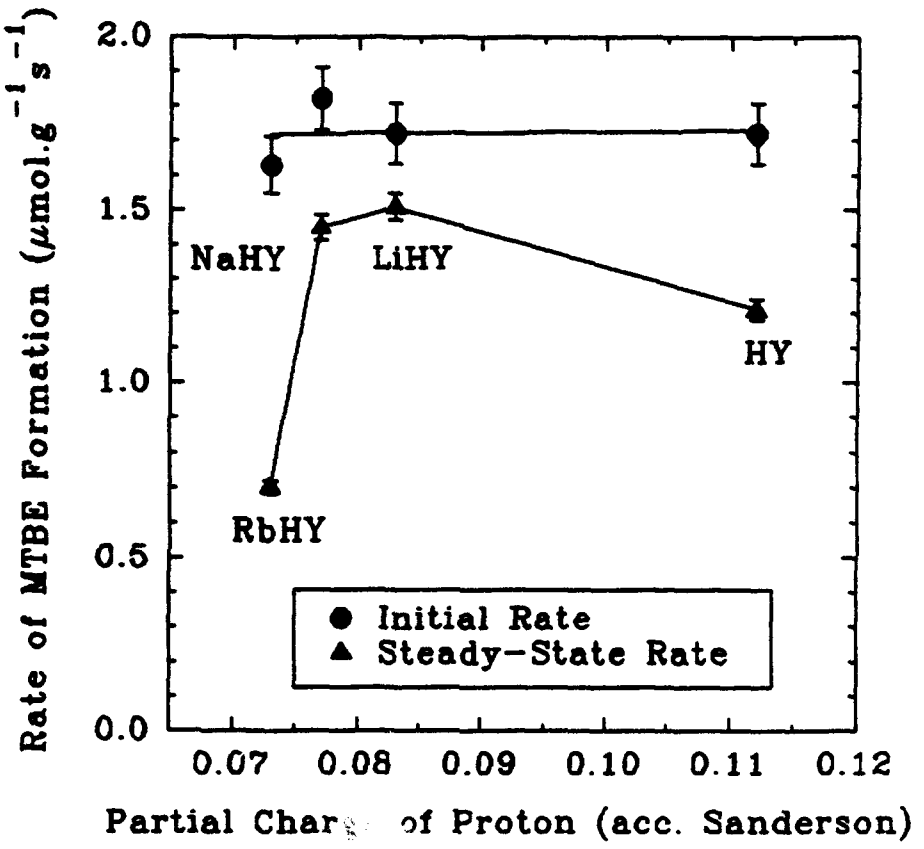

Figure IV.C.2.1 Comparison of Catalytic Activities of the Alkali-HY Zeolites at 90°C MeOH/IB = 1.0

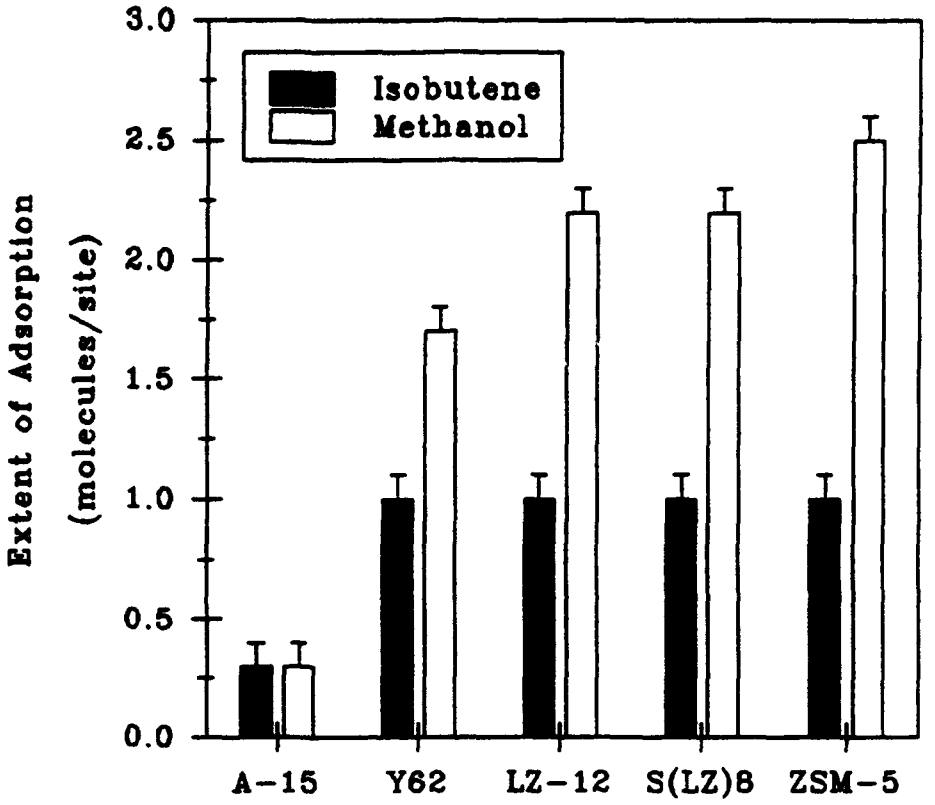

Figure IV.C.2.2 Adsorption of Methanol and Isobutene on MTBE Synthesis Catalysts

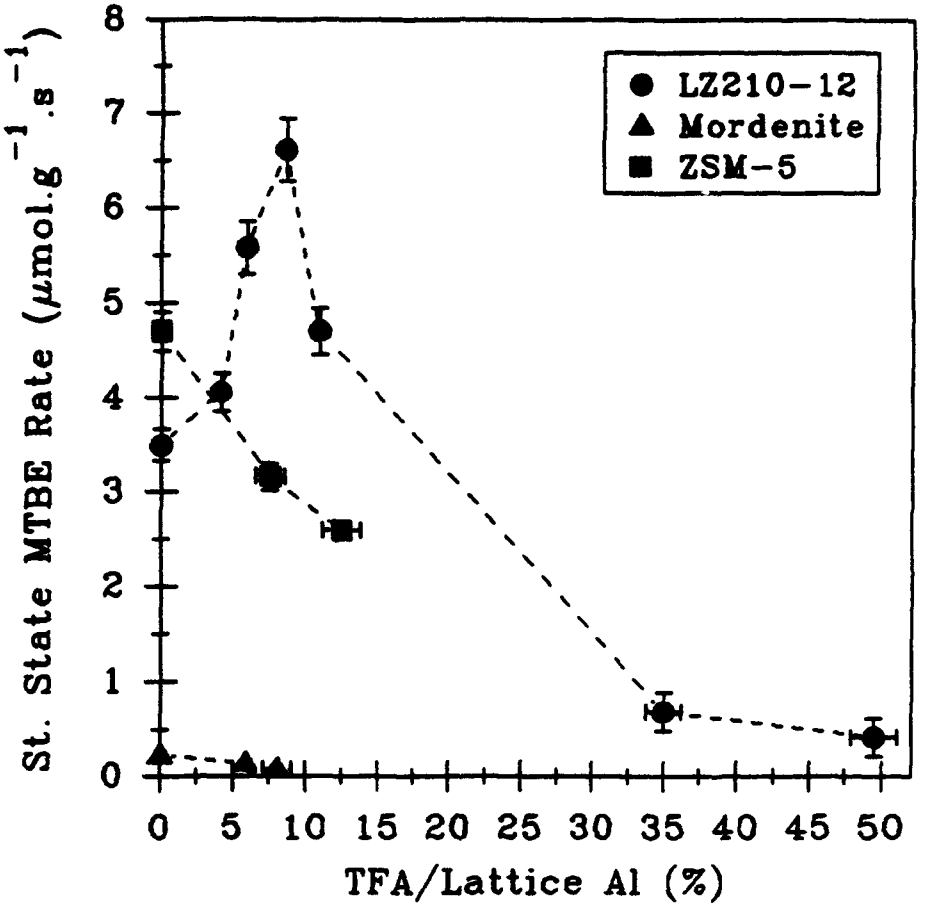

Figure IV.C.2.3 Influence of TFA-Modification upon Zeolite Activity T = 90°C ; MeOH/IB = 1.0

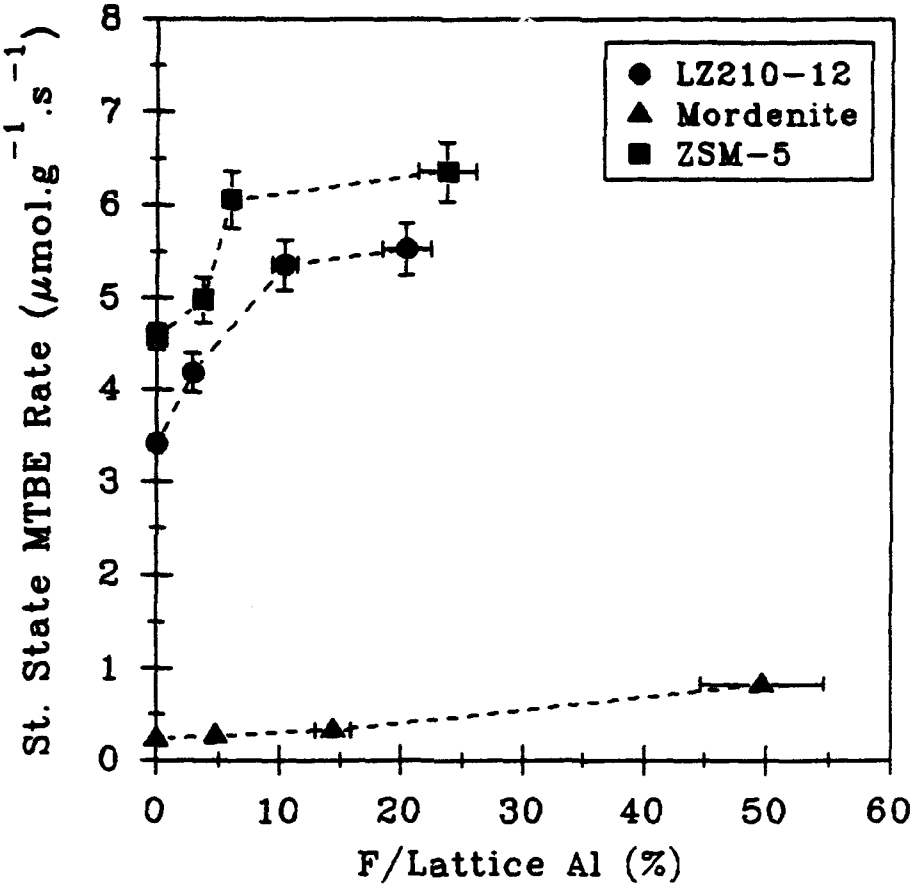

Figure IV.C.2.4 Influence of F-Modification upon Zeolite Activity T = 90°C ; MeOH/IB = 1.0

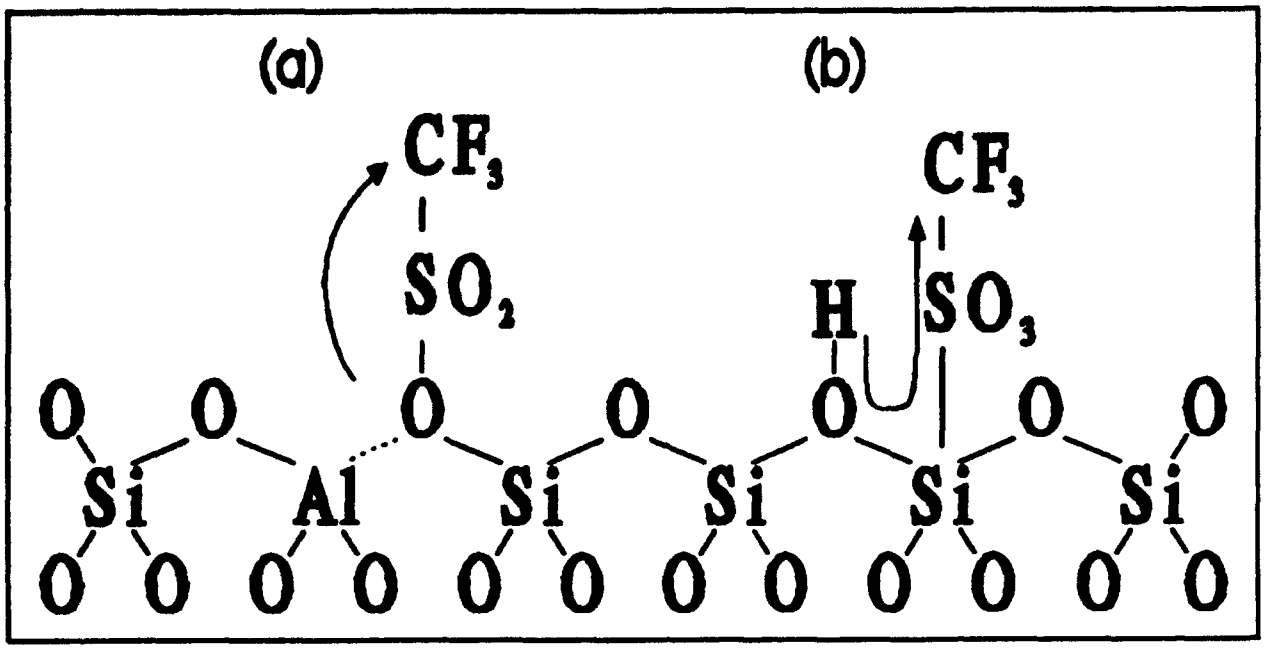

Figure IV.C.2.5 Possible Models for Acidity Enhancement by TFA-Modification (a): Reactive adsorption (dehydration) ; (b): Dissociative adsorption Le Van Mao et. al., *Appl. Catal.*, 48 (1989)

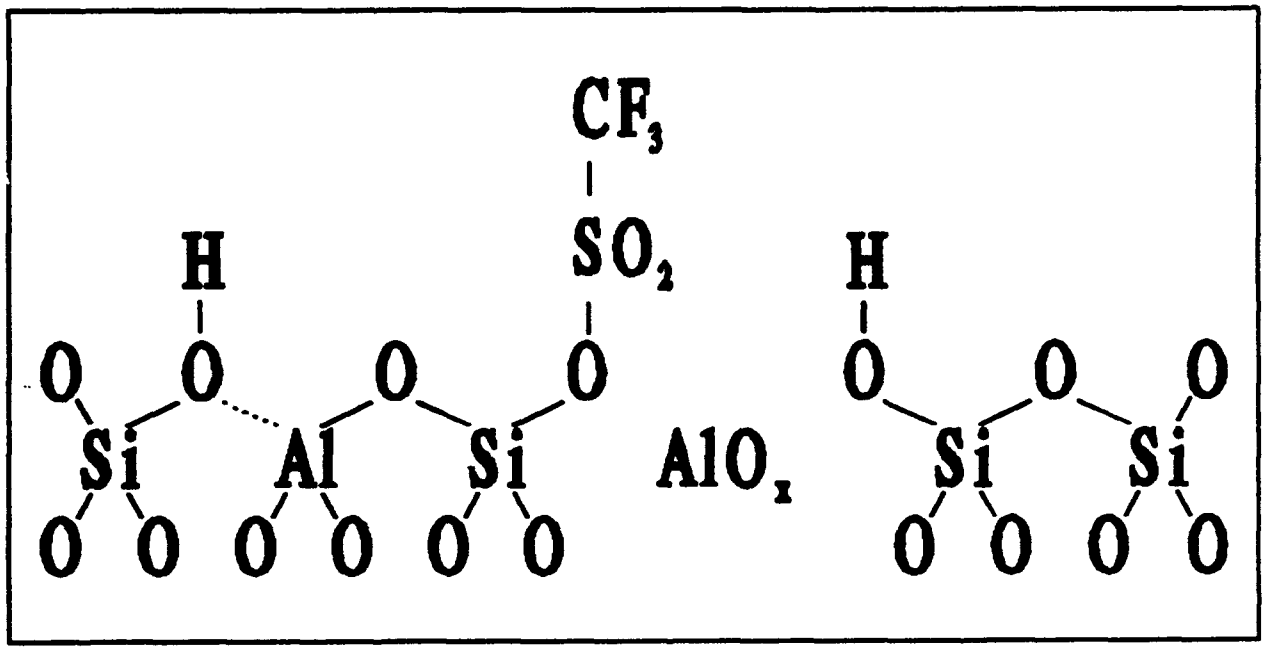

Figure IV.C.2.6 Proposed Model for Acidity Enhancement by TFA-Modification (reactive adsorption with dealumination)

IV.C.3 Synthesis, Structure and Properties of Hydroxyapatities Fluorapatities, Alumina and Titania for Oxidative Catalytic Decomposition of Toxic Nerve Gas Agents

Principal Investigator: Professor N.G. Eror
Materials Science and Engineering Department
University of Pittsburgh

Other Faculty Participants: Dr. V.L. Richards
Materials Science and Engineering Department
University of Pittsburgh

Dr. M. Houalla
Dr. W.K. Hall
Dr. D.M. Hercules
Department of Chemistry
University of Pittsburgh

Students: Mr. T. McNamara
Mr. T. Palucka
Dr. K.Y. Lee
Mr. J. Huey

IV.C.3.1 INTRODUCTION

Toxic nerve agents are comprised of organic esters of substituted phosphoric acid. Any decomposition by oxidation of these highly toxic compounds will result in a non-volatile phosphorous compound in addition to the gaseous products; CH_4, CO_2, CO, CH_3, CH_3OH, and H_2O. In order to develop a catalyst to safely decompose nerve gas agents the issue of catalyst stability along with activity and selectivity is very important. Because of the reactivity of the phosphorous containing decomposition fragments in the presence of oxygen or water, the active catalytic phase and/or the support can be adversely affected. The structure and/or activity of the catalyst can be deleteriously affected and result in catalyst deactivation. For this reason there is a significant potential advantage in using phosphates as supports and/or catalysts for the decomposition of nerve gas agents in order to minimize the effect of the produced phosphorous compounds on the catalyst and/or support and maximize the facility by which the catalyst and/or support is reactivated.

Dimethyl-methyl phosphonate (DMMP) was used as a stimulant molecule for nerve gas agent GB. The catalytic oxidation was carried out at 300° C at atmospheric pressure with a DMMP partial pressure of 0.065 Torr and a nitrogen/oxygen carrier gas with $N_2/O_2 = 4$ to simulate air.

IV.C.3.2 OBJECTIVES

The objectives of this research project were to synthesize and determine the structure and properties of calcium hydroxyapatites and fluorapatites for the effective oxidative catalytic decomposition of toxic nerve gas agents. Platinum, palladium and copper metal impregnation techniques were also developed and utilized to enhance the catalytic properties. Success can be measured by the creation of a catalyst that will operate at 300° C, be easily regenerated and have a lifetime that is substantially better (factor of two) than the current catalyst of choice by the Army.

IV.C.3.3 ACCOMPLISHMENTS AND SIGNIFICANCE

We synthesized calcium hydroxyapatites (HAp) of various stoichiometries and metal substitutions for calcium. We were able to determine variations in lattice parameter as a function of both stoichiometry and concentration of metal substitution for calcium. We were also able to synthesize both calcium fluorapatite and predetermined substitution of fluorine for the hydroxyl groups. It was also possible to determine the continuous change in lattice parameter as the composition was varied from calcium hydroxyapatite to calcium fluorapatite. We have been able to significantly increase the surface area of the both the hydroxyapatites and fluorapatites to nearly 250 m^2/g.

A method was developed, using metal acetylacetonates, to impregnate the catalyst substrate with platinum, palladium or copper. The finest dispersion was obtained with platinum where the metal particle size was on the order of 5-15 Å (see Figure IV.C.3.1). For the cases of palladium and copper the dispersions were 50-100 Å and 200 Å, respectively.

The DMMP conversion rates for a number of metal impregnated catalysts are given in Figure IV.C.3.2. The Cu-HA is the 1.3 wt% copper impregnated HAp. The Cu2 refers to the coprecipitated copper HAp having 0.2 molar copper substitution. The Pt-Cu2 is a 1.2 wt% Pt impregnated sample using coprecipitated copper (2) HAp as the substrate. The Pt-TiO_2 is a commercially prepared cordierite monolith catalyst obtained from Dr. C. Hsu [1]. The monolith was crushed into 40-80 mesh particles and 0.3 g was run in the reactor. This material has been reported [1] as the best oxidative catalyst for the oxidative decomposition of DMMP. The Pt/TiO_2 sample came unanalyzed, but typical catalysts of this type have 0.5-1.5 wt% Pt. The Pt-HA is the standard 1.2 wt% Pt impregnated HAp (Aldrich). The (I) and (II) are independently prepared samples shown for reproducibility.

The Cu-HA sample has a lifetime on the order of that of a pure HAp sample which demonstrated that just having the copper present in the system was not sufficient to increase the lifetime of the catalyst. In contrast, the Pt-HA sample extends the lifetime of the catalyst to beyond 8 hours with the addition of 1.2

that of copper [2] HAp without the addition of platinum.

A useful sample for comparing lifetimes is the Pt-TiO_2 catalyst. Hsu et al [1] determined that the Pt-TiO_2 was an efficient oxidative catalyst in the decomposition of DMMP. The lifetime of this sample was 1.8 hours.

The two primary catalysts that have been previously studied to date in the oxidative decomposition of DMMP in a flow system are γ-alumina and titania. We, therefore, evaluated these two compounds as catalysts. The surface area of the alumina was ~ 200 m^2/g while the titania had a surface area of 40 m^2/g and was approximately 78% anatase and 22% rutile.

The pure substrates were tested for catalytic activity and the DMMP conversion rates are given in Figure IV.C.3.3. The titania and hydroxyapatite (HA) lifetimes are similar (0.25 hours) while the alumina has a lifetime of 1.75 hours. In this case, the influence of surface area is critical, so the data should be normalized. Listed in Table IV.C.3.I are the pure substrate lifetimes along with the lifetimes normalized for surface area.

Table IV.C.3.I Lifetimes of Pure Alumina, Titania and Hydroxyapatite Catalysts and the Normalized Lifetimes with Respect to Surface Area.

Catalyst	Surface Area (m^2/g)	Lifetime of .3g of sample (Hr)	Lifetime normalized for surface area (Hr)
HAp	80	0.25	.63
TiO_2	40	0.25	1.25
Al_2O_3	200	1.75	1.75

Each of the substrates were impregnated with equal moles of platinum and the DMMP conversion tests were repeated. The DMMP conversion data is given in Figure IV.C.3.4. The -Al_2O_3as a remarkable lifetime of beyond 15 hours while the TiO_2 has a respectable lifetime, similar to the Pt-HAp, of ~ 8 hours.

In this case, the normalization for surface area is less critical since the active sites are the platinum and each catalyst is impregnated with equal molar quantities. For the case of Pt-HAp, there was no difference in catalyst lifetime when the surface area was increased

to 100 m_2/g from a value of 50 m_2/g. The surface area will play a role in determining the amount of by-products that can be accommodated at the surface before poisoning the platinum sites. If normalized with respect to surface area, the Pt-Al_2O_3 sample still had the longest lifetime when compared to both the Pt-HAp and Pt-TiO_2 catalysts.

For the cases of very high surface area (> 200 m^2/g) calcium hydroxyapatite and fluorapatite it was found that the catalytic properties improved for the hydroxyapatite and that the fluorapatite had a lifetime that was approximately 50% greater than for the hydroxyapatite. See Figure IV.C.3.5.

It was only possible to regenerate catalysts that had seen a modest amount of conversion of DMMP. Lee, in another part of this study, showed that methylphosonate forms at 573 K on the surface of the catalyst. The deactivation data are consistent with the effect of surface area and the maximum number of available calcium sites on catalyst lifetime for undoped calcium hydroxyapatite. It was not possible to reactivate the spent catalysts after more than ~ $3x10^{-4}$ moles of DMMP decomposition for 0.3 grams of ~ 100 m^2/g calcium hydroxyapatite catalyst. Larger amounts of conversion together with longer lifetimes resulted in degradation of the hydroxyapatite structure and for all catalysts, a drastic lowering of the surface area to ~ 1 m^2/g.

IV.C.3.4 SUMMARY

Significant accomplishments:

- Extended the processes developed for reliably synthesizing pure and doped calcium hydroxyapatites to the fluorapatites with controlled [F].
- Developed processes for synthesizing very high surface area (> 200 m_2/g) calcium hydroxyapatites and fluorapatites with controlled [F].
- Extended the method developed to deposit Pt as an active and stable catalyst on the surface of calcium hydroxyapatite to fluorapatite, alumina, and titania.
- Extended the major breakthrough by an additional factor of two in developing a catalyst that far exceeds the lifetime (factor of 6 - 8) of the current catalyst of choice by the Army for the oxidative catalytic decomposition of toxic nerve gas agents.

IV.C.3.5 REFERENCES

1. Hsu, C.C., Dulacey, C.S., Horwitz, J.S., and Lin, M.C., "Mass Spectrometric Characterization of Performance of a Low-Temperature Oxidation Catalyst", Journal of Molecular Catalysis, Vol. 60 (1990), 389 p.

2. Lee, K.Y., Houalla, M., Hercules, D.M., and Hall, W.K., "Catalytic Oxidative Decomposition of Dimethyl Methylphosphonate over Cu-substituted Hydroxyapatite", (University of Pittsburgh, 1993), to be published.

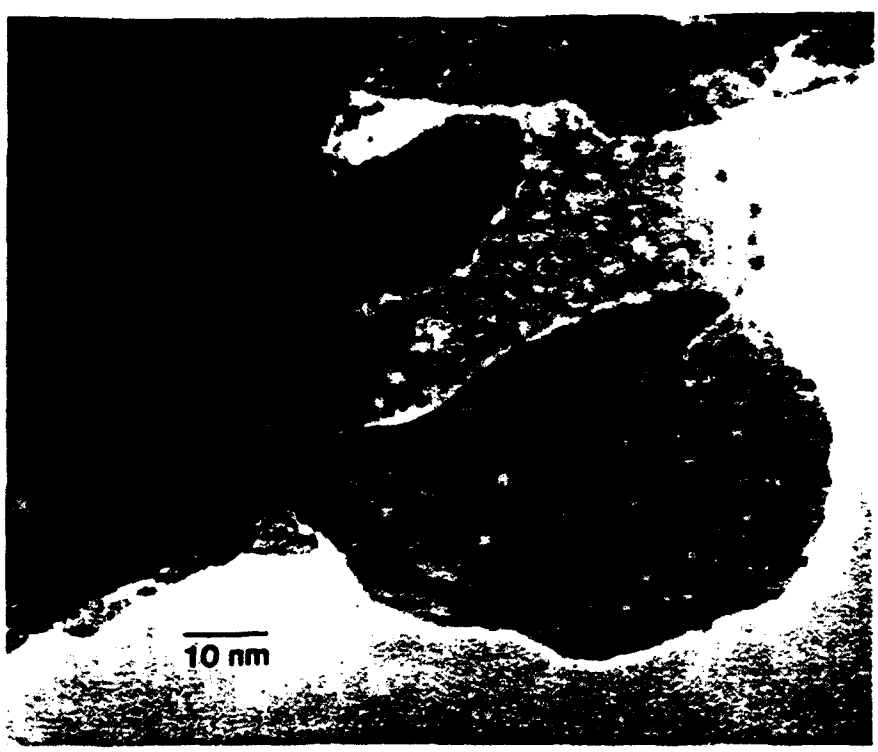

Figure IV.C.3.1 STEM bright field image of the 1.2 wt% Pt-HAp depicting the isolated platinum regions as small dark dots (5-15 Å in size) on the hydroxyapatite surface.

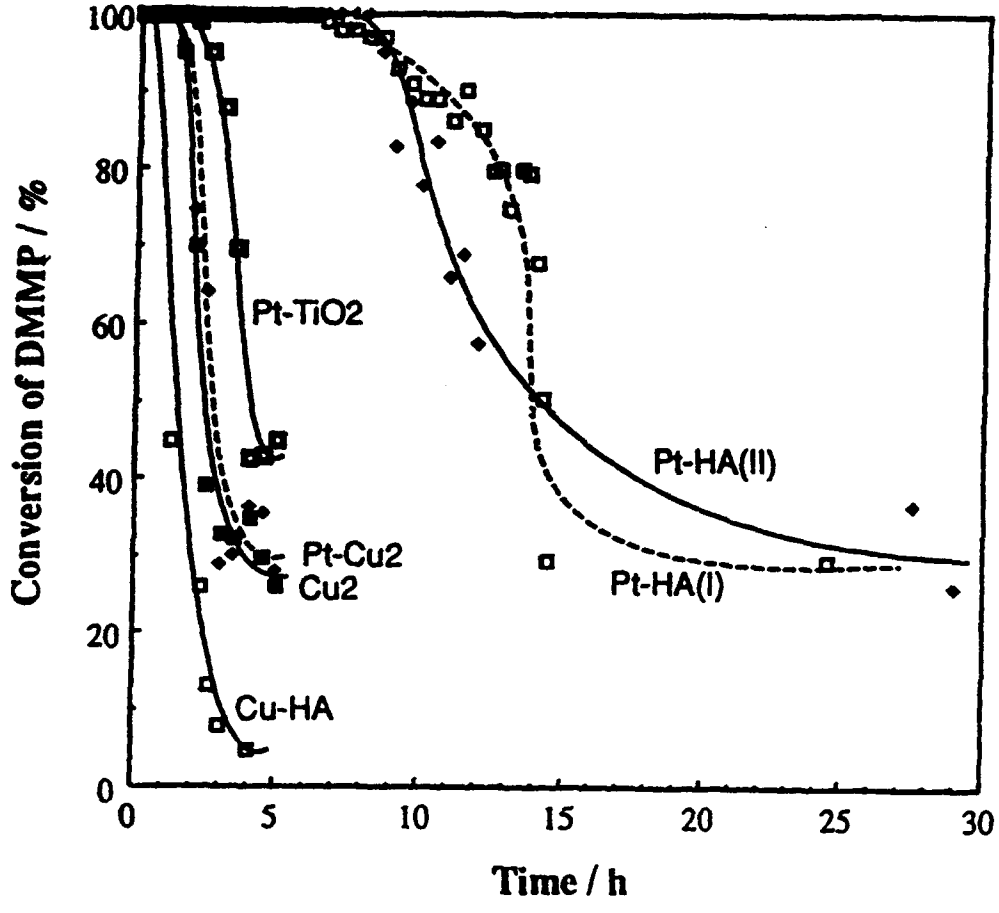

Figure IV.C.3.2 DMMP conversion curves of metal impregnated catalysts.
Cu-HA - copper impregnated hydroxyapatite.
Cu2 -coprecipitated copper (x = 2) HAp.
Pt-Cu2 - platinum impregnated Cu2 sample.
Pt-TiO2 - commercial monolith catalyst with a washcoated platinum/titania catalyst.
Pt-HA - platinum impregnated hydroxyapatite.

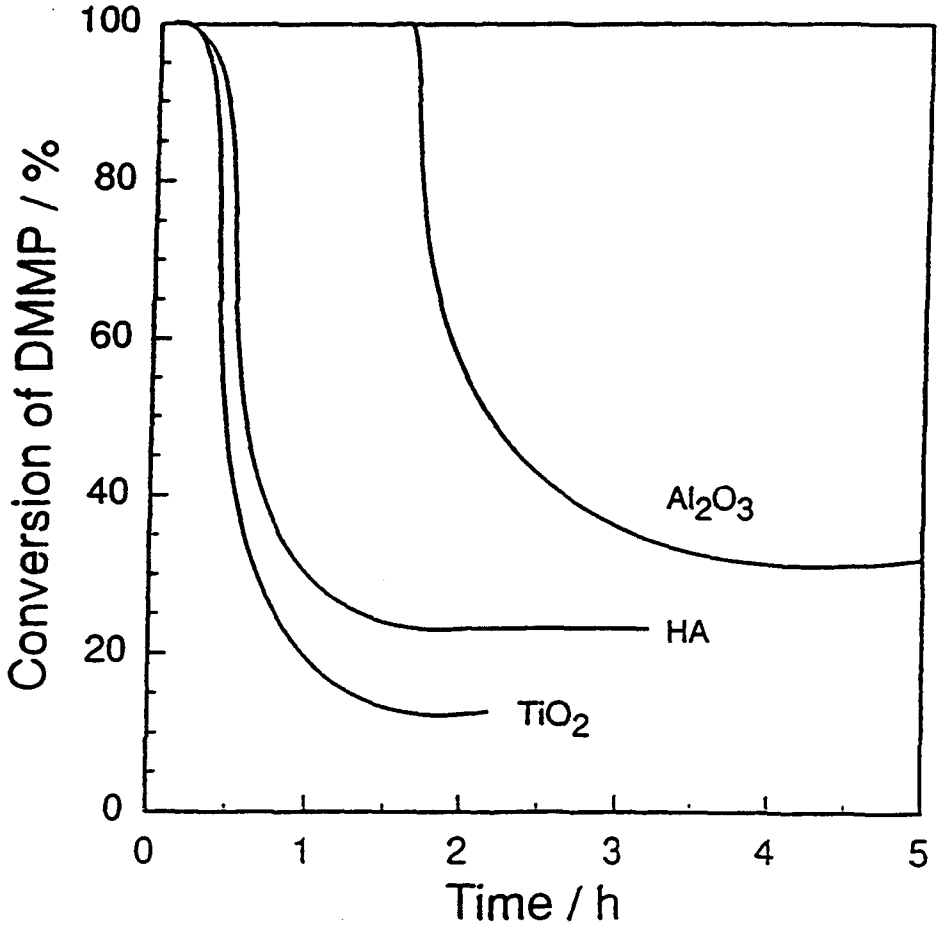

Figure IV.C.3.3 **DMMP conversion curves of the pure alumina, titania and hydroxyapatite catalysts.**

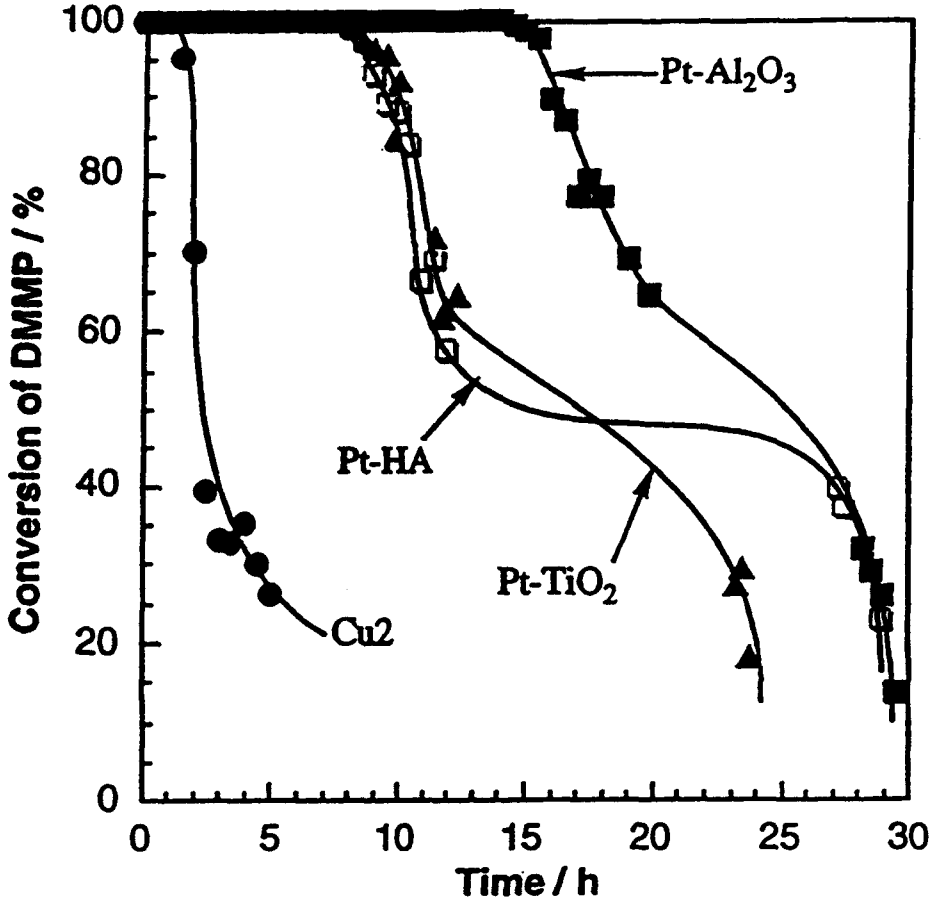

Figure IV.C.3.4 DMMP conversion curves of platinum impregnated catalysts of alumina, titania and hydroxyapatite.

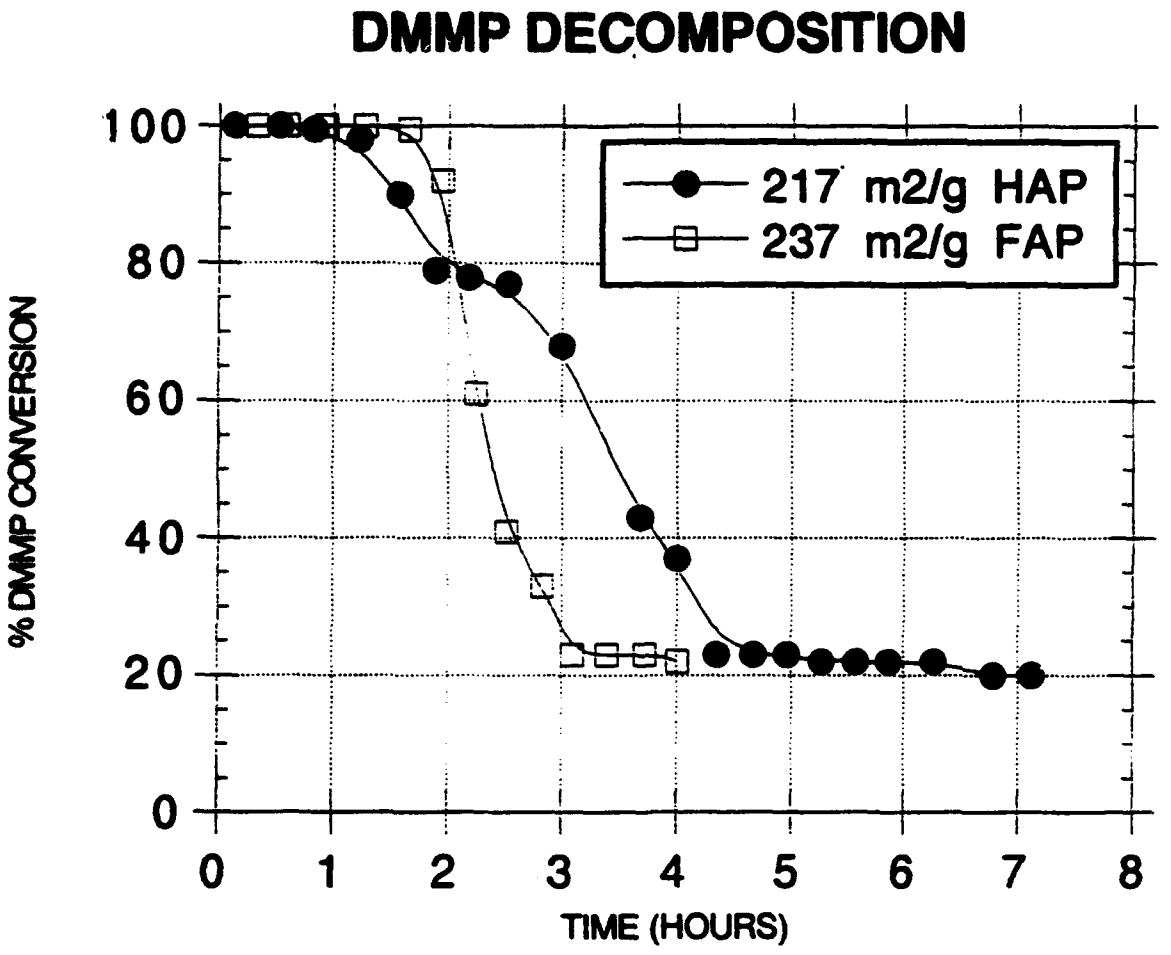

Figure IV.C.3.5 DMMP conversion curves of > 200 m^2/g hydroxyapatite (HAP) and fluorapatite (FAP).

IV.D BIOTECHNOLOGY

IV.D.1 Acetylcholine Biosensor Manufacture

Principal Investigator:	Professor Jerome S. Schultz Department of Chemical Engineering Center for Biotechnology and Bioengineering University of Pittsburgh
Other Faculty Participants:	Dr. Alan Russell Department of Chemical Engineering University of Pittsburgh
	Dr. David Rohrbach Department of Dental Medicine University of Pittsburgh
	Dr. Satish Arora Department of Crystallography University of Pittsburgh
	Dr. Jane Schultz Department of Pathology University of Pittsburgh
Students:	Mr. Kevin Vaughan

IV.D.1.1 INTRODUCTION

The goal of this project was to develop an approach to for constructing biosensors to respond to toxic materials. The prototype system selected was to design a sensor that would respond to toxic chemicals that affected the acetylcholine receptor in biological cells. The natural acetylcholine receptor is a very unstable protein that resides in biological membranes. Instead of using this protein as the biological recognition element of the prototype biosensor, we opted for using the polypeptide region of acetylcholine receptor that actually binds natural and toxic ligand. This segment, often referred to as the a-bungarotoxin binding site, was identified by Neuman et al. [1]

The essential components of the biosensor are:

a. An immobilized acetylcholine-like receptor selective for the natural ligand and toxic chemicals for the natural receptor.

b. A reporter system that provides a signal that is related to the concentration of the toxic chemical.

A scheme having these characteristics is shown in Figure IV.D.1.1.

IV.D.1.2 RESULTS

A. Immobilized Acetylcholine-like Receptor

The duodecapeptide, Lys-His-Trp-Val-Try-Try-Thr-Cys-Cys-Pro-Asp-Thr-Arg, was synthesized with an automated peptide synthesizer. It was analyzed by reverse-phase column chromatography and found to be 92% pure. The duodecapeptide was then immobilized on derivatized sepharose beads, and the binding behavior measured by an inhibition assay. The assay consisted of incubating a fixed amount of the sepharose-receptor beads with a fixed amount of radioactive bungarotoxin and various amounts of the competing ligand. The results, given in Figure IV.D.1.2, show that the immobilized synthetic receptor behaves very similarly to the natural acetylcholine membrane receptor.

B. Reporter System

As shown in Figure IV.D.1.1, we decided to use the luciferase enzyme system to quantitate the amount of binding of the toxic material to the immobilized-duodecapeptide-bioreceptor.

Luciferase is an example of a bioluminescence system, which are well known to provide a high level of sensitivity, because for each molecule of enzyme activated hundreds of photons of light are emitted. Thus there is a high level of amplification of the binding event. Also, since in the null state no light generated, the signal to noise ratio is very large in luminescence systems of this type.

Luciferase is a very unstable enzyme and reports in the literature show that its activity diminishes significantly over a period of hours. We immobilized luciferase to the same type of derivatized sepharose beads as used for the duodecapeptide. After many trials of attempting to develop a stable enzyme system, we finally found conditions to where the enzyme catalyzed bioluminescence for a period of days. An example of the results is given in Figure IV.D.1.3. Two cuvettes were placed in a recording fluorometer. Luciferase-beads were placed in one cuvette, and fresh soluble luciferase enzyme was periodically placed in the control cuvette. Panel A shows the light emitted by luciferase-beads when the substrate was added. The light intensity is about 10 times background, and fairly constant over the period of measurement. Panel B shows the behavior of soluble luciferase. There is a burst of light emission when substrate is added, and eventually exhaustion of the substrate with termination of the signal. For approximately the same amount of enzyme, the immobilized preparation shows a lower level of bioluminescence but for a longer time span. Fortunately,

the immobilized-luciferase has properties more suitable for use in a biosensor. The same experiment was repeated about 5 hours later, and the results shown in Panels C and D indicate that the system is reproducible and stable over this time period.

C. Combinatorial Peptide Libraries

The success of this approach for developing biosensors for toxic materials depends on the availability of suitable bioreceptors for the target toxic chemical of interest. In general finding the appropriate natural bioreceptor for an arbitrary toxic chemical of interest would be very difficult and time consuming. Because of this we investigated the possibility of using some new technologies for making libraries (containing millions of different proteins or peptides) as a resource to isolate a bioreceptor surrogate for a particular toxic compound of interest. Our survey of the literature showed that this is a very viable approach. For example, a bacteriophage can be used as host to biosynthesize a library of antibodies which can be screened to find an appropriate bioreceptor for biosensor development. We have discussed this approach at several international meetings.

IV.D.1.3 ACCOMPLISHMENTS AND SIGNIFICANCE

During the course of this research project we demonstrated that:

a. A synthetic polypeptide can be used as a surrogate for a natural bioreceptor for the development of a biosensor.

b. The synthetic receptor polypeptide can be immobilized on a solid matrix and maintain normal binding function.

c. Luciferase can be immobilized on a solid matrix and maintain its catalytic activity for an extended period of time. Thus luciferase can be used as a very sensitive reporter system for biosensors.

d. The approach of using polypeptide surrogates as bioreceptors can be generalized by using combinatorial peptide libraries made with bacteriophage.

IV.D.1.4 SUMMARY

We have demonstrated an approach to producing two of the key elements of biosensor for toxic materials, namely the receptor element and the reporter chemistry.

The next step in this project would be to combine these two elements to make a prototype biosensor. We believe that this can be readily accomplished in a follow-up research program.

IV.D.6 REFERENCES

1. Neuman, D., Barchan, D., Horowitz, M., Kochva, E., and Fuchs, S. Proc. Natl. Acad. Sci. 86: 7255-7259 (1989).

Publications/Presentations

1. Schultz, J.S. Fiber optical methods for bioprocess monitoring - promises and problems. Proceedings 9th International biotechnology Symposium. Harnessing Biotechnology for the 21st Century. Ed M. Ladish and A. Bose. Amer. Chem. Soc. pp 334-336 (1992).

2. Schultz, J.S. The use of recognition molecules in biosensors. BioJapan '92, Yokohama. Symposium Proceedings. pp 339-347 (1992)

3. Schultz, J.S. and J.S. Schultz. Applications of combinatorial libraries in cellular engineering. Proceedings of the 1st International Conference on Cellular Engineering. pp 73-74 (1992)

4. Schultz, J.S. and J.S. Schultz. Sources of biorecognition molecules for biosensors. 20th Annual Meeting Federation of Analytical Chemistry and Spectroscopy Societies. Detroit. Abs. 120 p.71 (1993)

5. Schultz, J.S. The challenge of maintaining biosensor functionality at material interfaces. 40th National Symposium of American Vacuum Society. Orlando. Abs. TC2-TuA1 p. 194 (1993)

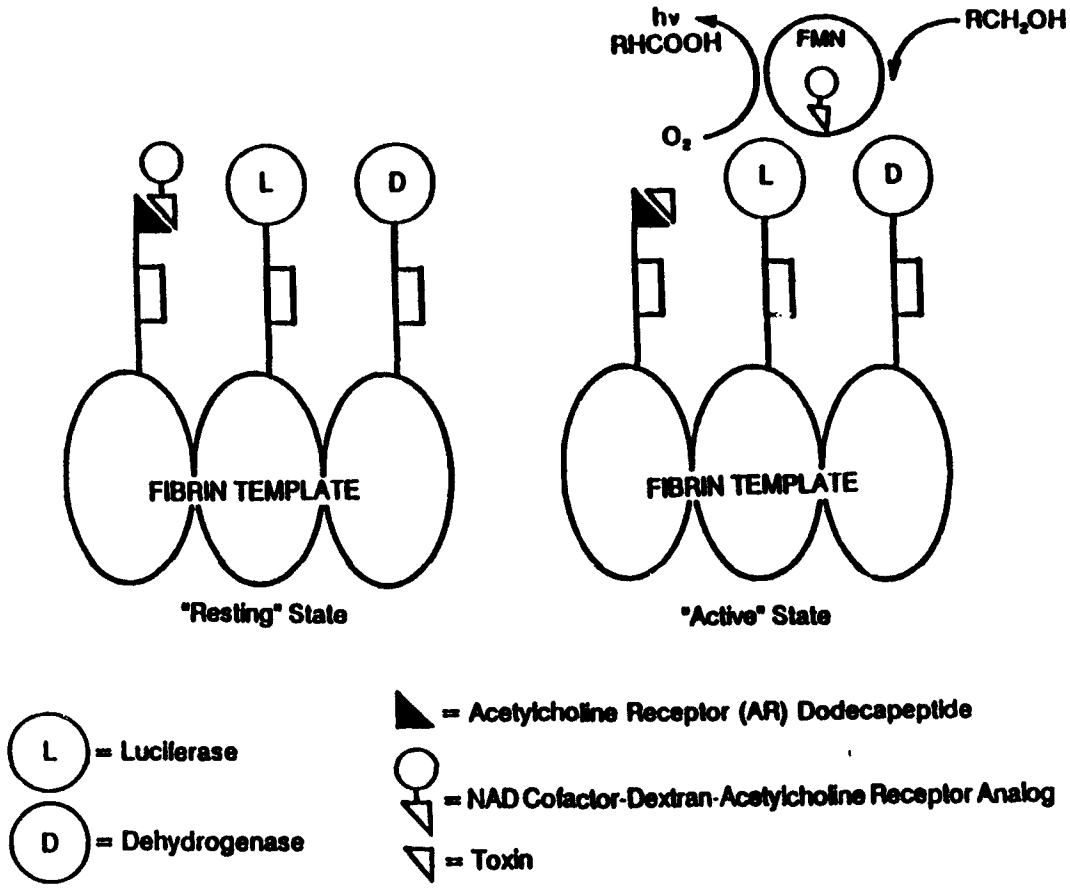

Figure IV.D.1.1 Conceptual design of a biosensor for a toxic material (toxin) that inhibits, by binding, the normal functioning of a biological receptor site (Acetylcholine Receptor). In the "active" state of the biosensor, i.e. in the presence of a toxin, the cofactor NAD is released and allows the luciferase enzyme system to produce light.

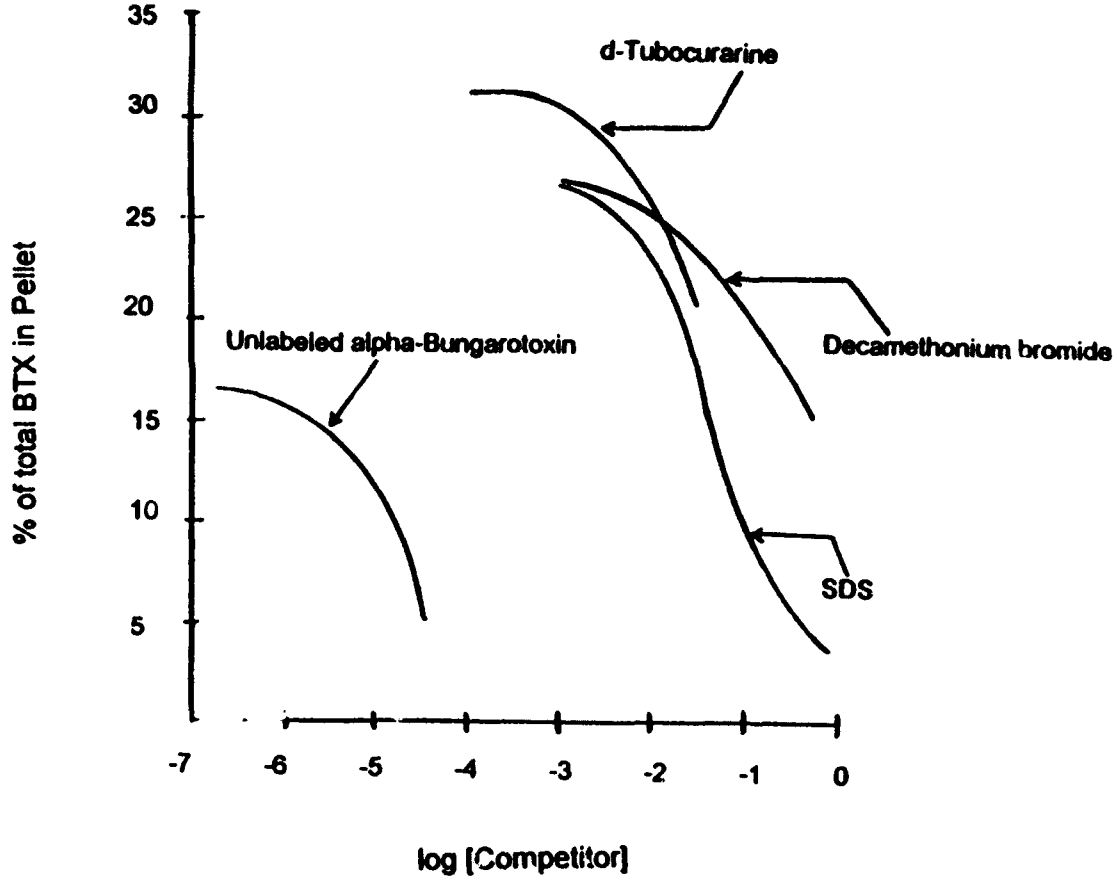

Figure IV.D.1.2 Binding behavior ofa duodecapeptide which has been identified as a part of the normal binding site of the natural acetylcholine bioreceptor that resides in membranes

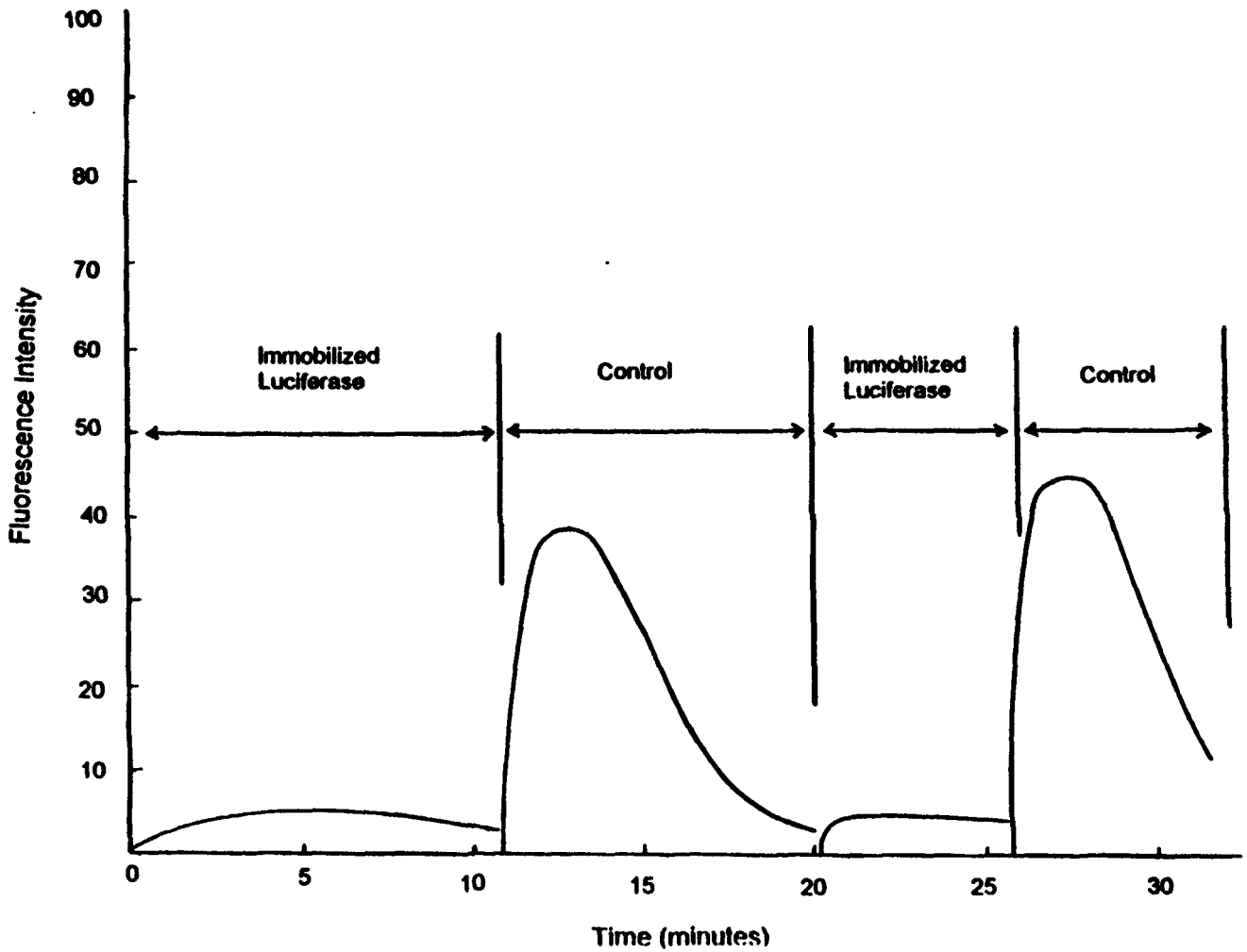

Figure IV.D.1.3 Demonstration of the successful immobilization of luciferase (normally a very unstable enzyme). A constant fluorescence response was obtained over a period of about 6 hours.

IV.D.2 Materials and Sensors Based on Molecular Recognition

Principal Investigator:	Professor Stephen G. Weber Department of Chemistry University of Pittsburgh
Other Faculty Participants:	Dr. Andrew Hamilton Department of Chemistry University of Pittsburgh
Students:	Mr. Chris Switala Ms. Jane Valenta Ms. Beth Wise Dr. Yuanhua Shao

IV.D.2.1 INTRODUCTION

Our goals are the preparation and understanding of materials that respond in a predetermined way to a restricted set of chemical species. Chemical sensors are based on a subset of those materials. The materials on which sensors are based respond electrically to a species. Our thesis is that sensors are but a small part of the many possible functional, chemically sensitive materials that can be envisioned.

Work on chemically "smart materials" is new. It is essential, therefore, to establish very clearly the fundamental basis for the functioning of such materials. We have expended a great deal of effort to determine the rules governing each material's behavior. In each case, the chemical selectivity is inherent in a molecular recognition process that occurs between pairs of chemically complementary species. The chemical complementarity leads to association, or binding, between the species involved. Such binding processes are described formally in thermodynamics. In each of the cases studied, we have attempted to understand how well a simple thermodynamic picture describes the material.

The three sorts of materials that we have studied, and a brief resume of the results that we have obtained, and their significance, follow.

1. Sensor for carboxylates. We can prepare sensors for glutarate with a high degree of selectivity over succinate. The sensors, however, do not behave ideally. The largest factor in the nonideal behavior is the high degree of water solubility of the analyte.

2. Selectively enhanced extraction of phenobarbital. In the standard procedure for this often prescribed drug, an extraction with an organic solvent is used during sample preparation. The volume of organic solvent is ten times the volume of serum. Using a complementary binding species, we can extract the same amount of drug with a volume of organic solvent that is one

quarter of the volume of serum. The significance of this is in the minimization of the volume of organic solvents that must be discarded or recycled.

3. Reversible polymer gels. Certain polymer solutions can be made to gel by the addition of an agent that associates with the polymer, forming reversible crosslinks. When such a gel is exposed to a chemical agent that reacts with the crosslinker, lowering its activity, the gel becomes fluid. We have developed the first quantitative model to describe such smart materials, and we have applied it the system poly (vinyl alcohol)/borate/sugar. The formation of a polymer-cross linker-polymer complex is not described by the same sort of equilibria as the formation of a complex consisting of only small molecules, i.e., sugar-borate-sugar.

IV.D.2.2 OBJECTIVES

1. Glutarate sensors. Improve performance, as of the last report, sensors could be prepared based on artificial receptors, but the results did not correlate with our understanding of the binding as studied by NMR. Set up and apply the ITIIES experiment, Ion Transfer at the Interface of Immiscible Electrolyte Solutions, in order to investigate the thermodynamics of analyte ion transfer in the presence and absence of artificial receptor.

2. Barbiturate extraction. Test quantitative theory and apply to human blood serum. Investigate the solvent properties of plasticized polymers with the intent to create reusable, solvent-free, selective organic extraction media.

3. Smart materials. Develop quantitative model of crosslinker binding to polymer as a function of concentrations of the species involved. Test against experiments with atactic poly (vinyl alcohol)/borate. Determine material's sensitivity to a chemical species such as fructose.

IV.D.2.3 ACCOMPLISHMENTS AND SIGNIFICANCE

1. Glutarate sensors. The experiment is illustrated in Fig. IV.D.2.1, and illustrative data are shown in Fig. IV.D.2.2. The bis-urea shown in Fig. IV.D.2.1 yields a membrane that generates a glutarate-dependent potential as shown in Fig. IV.D.2.2. The selectivity of the sensor mirrors the binding constants for dicarboxylates with the receptor as determined by NMR. Both the sensitivity of the sensor and the selectivity are better than any in the literature. However the sensitivity is not ideal (30 mV per decade of concentration), and the sensors do not last long. Studies with the ITIIES have shown (Fig. IV.D.2.3) that an organic solvent containing a bis-imidazolinium receptor and glutarate loses the glutarate to the aqueous solution over time. Current investigations are designed to improve the H-bond donating properties of the membrane material so that the glutarate ion

is less prone to partition to water. We have determined in related experiments that the presence of large quantities of strongly H-bonding solvents leads to weaker binding with the analyte. There is therefore an optimum solvent environment for H-bonding based sensors.

Significance. We have shown very clearly that the application of the tremendous power in H-bond-based molecular recognition towards chemical sensors is essentially a materials problem. We have defined the material properties required to determine organic anions. This is the first such understanding to be developed in the two decades or so during which the general difficulties of making anion sensors have been discussed.

2. Barbiturate extraction. Fig. IV.D.2.4 shows the chemical process studied. We have determined all of the equilibrium constants for the reactions shown in Fig. IV.D.2.4. Figure IV.D.2.5 shows experimental and theoretical predictions for the fraction of phenobarbital extracted from aqueous solution as a function of pH and amount of artificial receptor. There are no adjustable parameters in the theory.

The amount of phenobarbital extracted as a function of quantity of solvent is shown in Fig. IV.D.2.6. Figure IV.D.2.6a is for aqueous buffer and serum without receptor. Note that to extract 90% of the barbiturate requires 10 times the volume of chloroform as serum. With the receptor in chloroform, 1mM, a solvent volume that is 1/4 of the serum volume extracts 90% of the barbiturate.

Work continues, in conjunction with similar work described above, to find extraction systems that are free of disposable solvents. Any material that is used for this application must be fluid enough to allow rapid molecular diffusion, but it must be dimensionally stable as well. Plasticized polymers are a good candidate base material. We have explored several common and uncommon plasticizers for their effect on the association of phenobarbital for its receptor. The spectrum of the receptor-barbiturate complex is determined as a function of the volume percent of plasticizer. Data are shown in Fig. IV.D.2.7. Clearly there are several plasticizers, typically hydrogen bond donors, that destroy the complex. At the same time, there are several whose presence does not upset the binding. Materials based on these plasticizers will be used to make the first chemically selective, synthetic extraction materials.

Significance. In less than 20 years, the use of organic solvents in analytical laboratories will be a minute fraction of what it is today. The biggest use of solvents is in extraction. Materials developed in this program will help to reduce dramatically the use of disposable solvents in routine analytical labs.

The same materials can be used to extract with preconcentration into a solid-like polymer-based material. Such materials can be used to extract samples in the field and transport them to the laboratory without the hazards and

difficulties of organic solvents. Further, by concentrating into a dimensionally stable material, injection into microseparations devices will be facilitated.

3. Smart materials. The phases displayed by an atactic poly (vinyl alcohol) (aPVA) with borate are shown in Fig. IV.D.2.8. Also shown is the theoretical prediction of our model. The model for the crosslinking of aPVa with borate differs from the analogous small molecule "crosslinking". The formation of, for example, a mannitol-borate-mannitol complex from mannitol and borate has a linear dependence on borate and a quadratic dependence on mannitol. The ratio of the amount of mannitol-borate-mannitol (so-called "didiol") to mannitol-borate (so-called "monodiol") increases linearly with mannitol concentration. For polymeric diols, however, we have found no quadratic dependence of didiol formation with diol concentration. Furthermore, although we cannot distinguish the monodiol from the didiol by NMR, a French group has recently determined each one quantitatively in a very similar system in which the polymer was a poly (glycerylacrylate). The didiol-monodiol ratio is constant below a particular diol concentration, then it increased slowly (Fig. IV.D.2.9). We have a model that fits both our data and the French data (Fig. IV.D.2.10).

Significance. Chemically smart materials are rare. They must be based on some sort of molecular recognition process, and will often use polymers as a mechanical basis. A sound understanding of the way binding operates in such systems is essential for their design and application. We have developed, and partly tested, the first and only general model for reversible crosslinking of polymers in solution. Although the work clearly needs to be extended and tested more severely, it is an important foundation.

IV.D.2.4 SUMMARY

We have developed a carboxylate sensor of unsurpassed sensitivity and selectivity. We have developed a barbiturate extraction medium with which a 40-fold reduction in the use of organic solvents can be realized. We have developed and tested a model for the reversible crosslinking of polymers in solution, which is the first important step in the development of polymer-based smart materials. Finally, taking the subprojects together, we have now developed a significant understanding of the thermodynamic requirements for the successful application of synthetic receptor-based materials.

Publications and Abstracts

E.T. Wise and S.G. Weber, Quantitative Evaluation of a Smart Material: PVA-Borate Gelation and the Gel's Response to Diols, Symposium on New Macromolecular Architecture and Supramolecular Polymers, 205th ACS National Meeting, Denver, CO, April 1993.

J.N. Valenta, R.P. Dixon, A.D. Hamilton, and S.G. Weber, Enhanced Extraction of Phenobarbital Using Synthetic Receptor, Baltimore, April, 1993.

S.G. Weber, Sensors Based on Molecular Recognition, FACSS, Detroit, October 1993.

J.N. Valenta, S.G.Weber, A.D. Hamilton, and R.P. Dixon, Further Investigations of the Enhanced Extraction of Phenobarbital from Serum, Pittsburgh Conference, March 1994.

J.N. Valenta, R.P. Dixon, A.D. Hamilton, and S.G. Weber, Enhanced Extraction of Phenobarbital from Serum with a Designed Artificial Receptor, submitted, Analytical Chemistry.

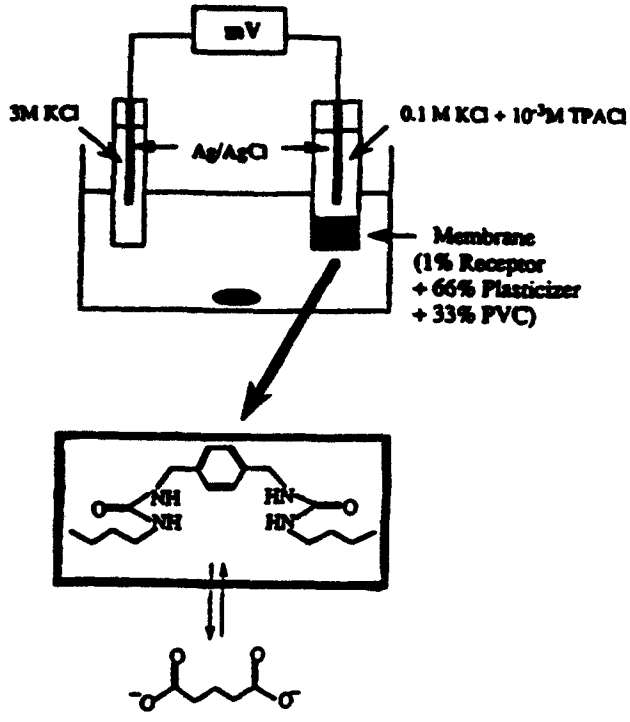

Figure IV.D.2.1 Membranes containing artificial receptor are fitted with a reference electrode. The potential across the membrane is determined as a function of the concentration of dicarboxylate in the aqueous solution.

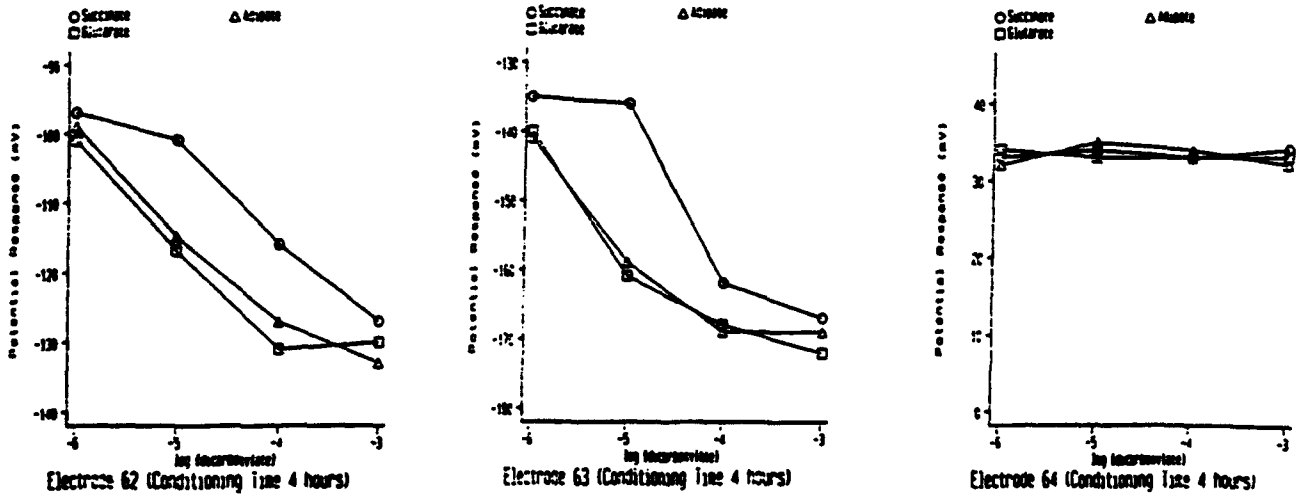

Figure IV.D.2.2 Calibration curves for membranes containing a bis-thiourea. Electrodes 62 and 63 contain the receptor and electrode 64 does not. Note the higher sensitivity to adipate and glutarate over succinate, as anticipated by the NMR studies of the binding selectivity.

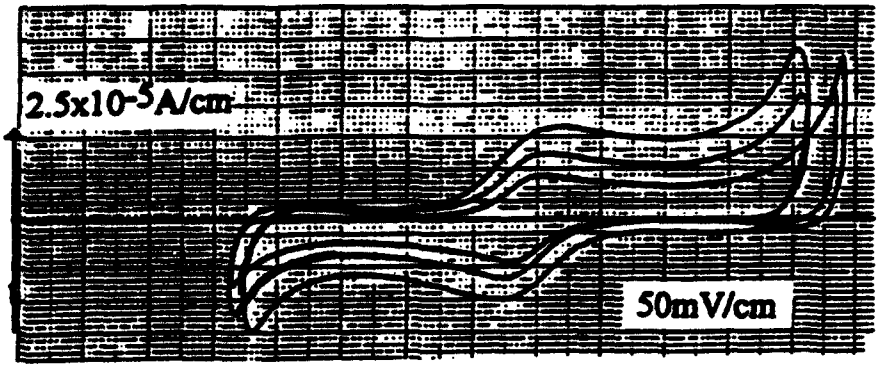

a

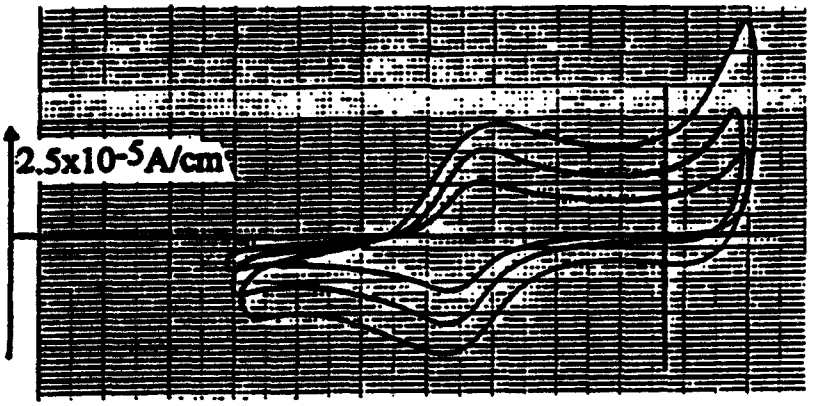

b

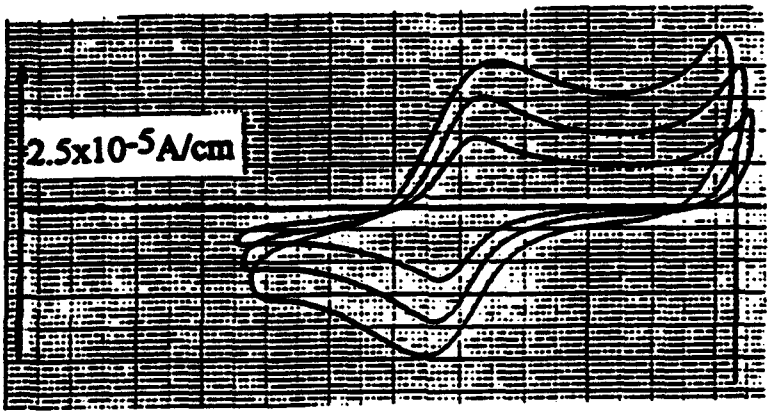

c

Figure IV.D.2.3 The variations of the cyclic voltammograms with the waiting times for the following system:

Ag/AgCl/1mMNaCl//0.15mMp-XDI + 0.1mM$(TBA)_2$Glutarate.$3H_20$/0.01MTBACl/AgCl/Ag
a. 2 mins b. 122 mins c. 242 mins.

The vertical arrow at the left defines zero volts on the abscissar, and the horizontal line defines zero current on the ordinate. Scales are shown on the voltammograms.

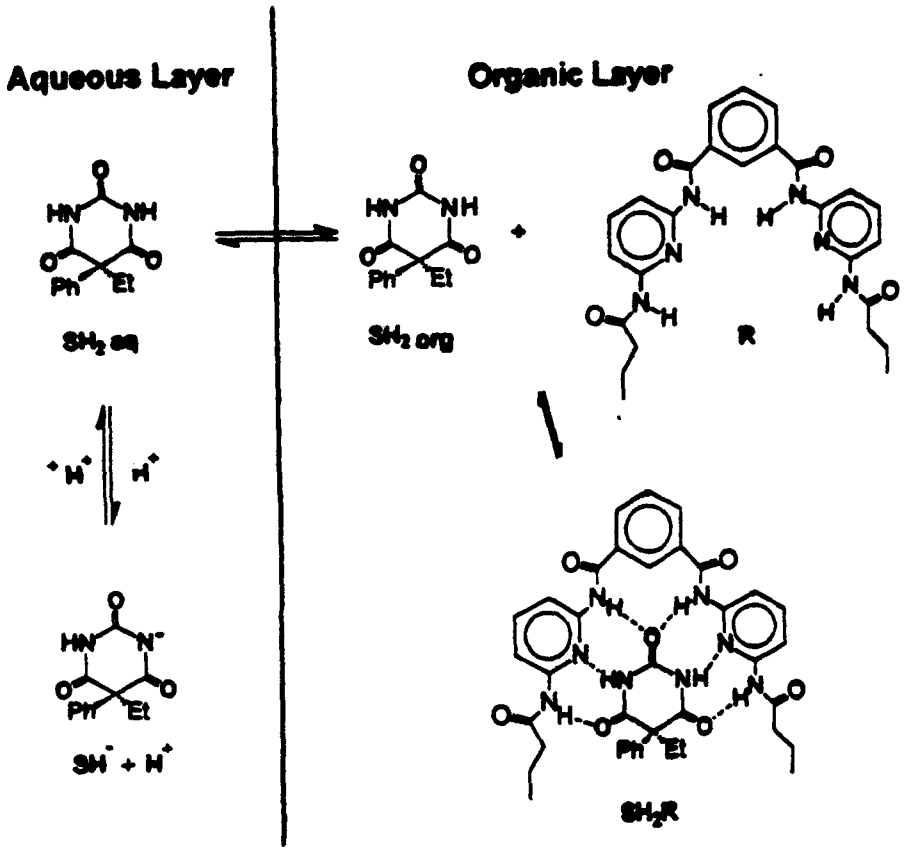

Figure IV.D.2.4 Scheme for the enhanced extraction of phenobarbital.

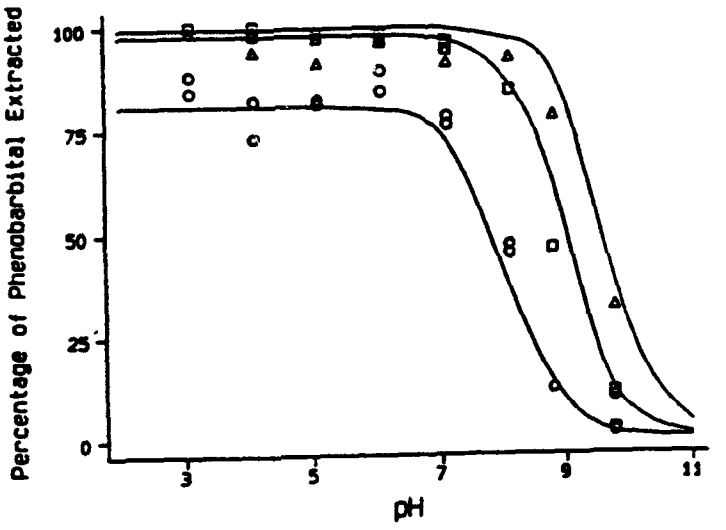

Figure IV.D.2.5 Fraction of phenobarbital extracted from an aqueous solution as a function of pH and concentration of artificial receptor in the chloroform. (○) no receptor, (□) 0.2 mM receptor, (△) 1mM receptor. Solid lines are theoretical with no adjustable parameters.

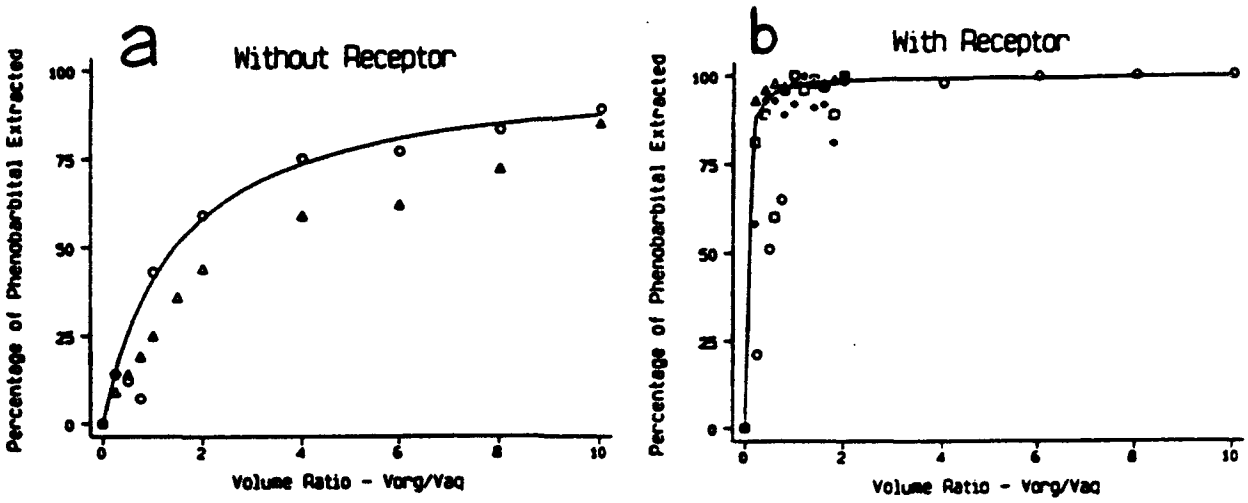

Figure IV.D.2.6 Fraction of phenobarbital extracted from buffer (○) and serum (△) without receptor (left, panel a) and from buffer (○, □, and △) and serum (◇) with 1mM receptor (right, panel b). Solid lines are theory with no adjustable parameters.

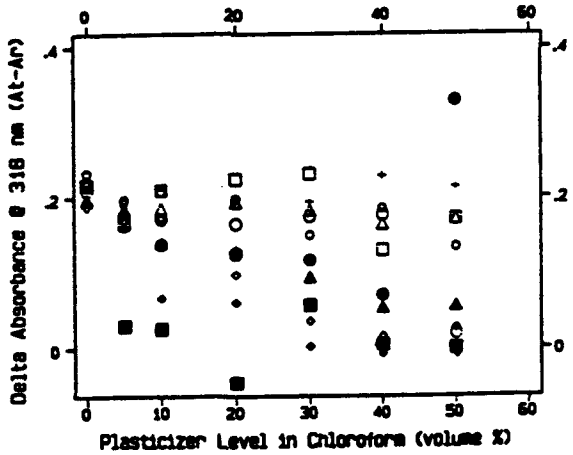

Figure IV.D.2.7 The Effect of Plasticizer Level on Phenobarbital-Receptor Complex Formation: At - total absorbance (receptor plus phenobarbital), Ar-absorbance of receptor only,O - Dioctyl Sebacate, □ - Dioctyl Phthalate/Chloroparaffin (3:1 by weight), Δ - Dioctyl Phthalate, o - Dioctyl Phthalate/ n-ethyl-p-sulfonamide (9:1 by weight), + - Chloroparaffin ◇ - Tributyl Phosphate, ● Tributyl Phosphate/Chloroparaffin (3:1 by weight), Δ - Epoxidized Soya Oil, ■ - Tributyl Citrate, and ◆ Decanol.

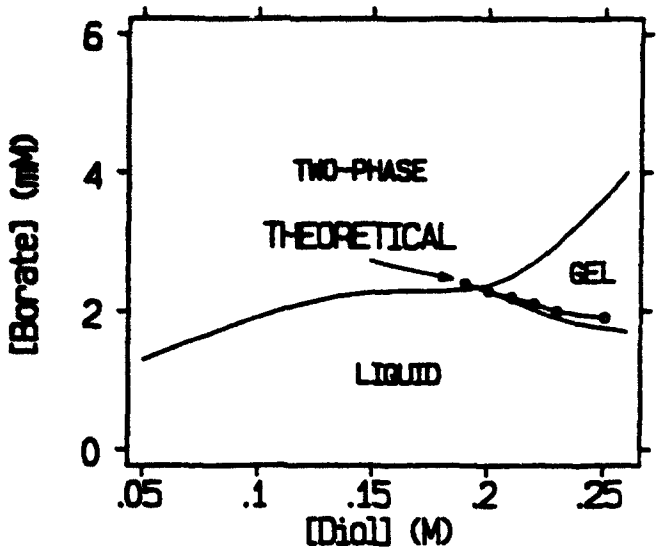

Figure IV.D.2.8 Composition diagram for the PVA-borate system. PVA is number average molecular weight 54,000, but the units of its concentration axis are in molar of diol.

Figure IV.D.2.9 Data from Pezron et al. in which the ratio of the monodiol to the free borate, and of didiol to monodiol, are plotted as a function of the diol concentration. These are the only definitive data on this distribution in the literature. For a low molecular weight diol, both ratios are straight lines passing through the origin.

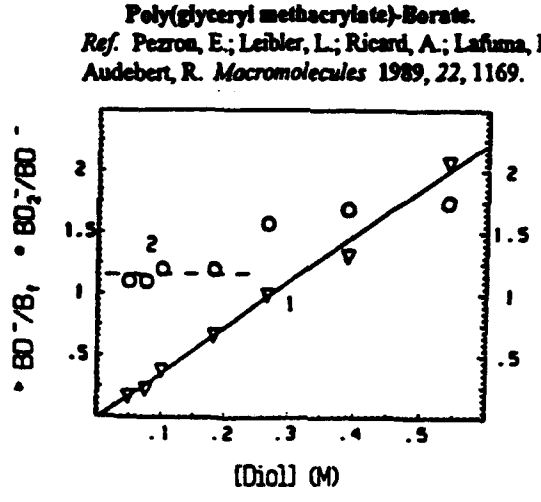

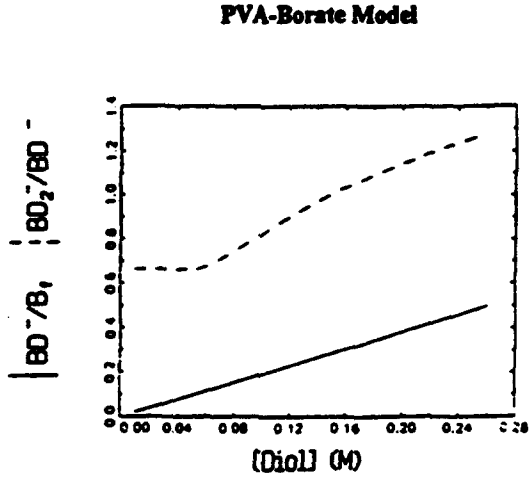

Figure IV.D.2.10 Predicted borate complex ratios as a function of diol concentration. There is not enough data in the Pezron paper to make a quantitative comparison. The theoretical result in the figure is intended to show the qualitative similarity.

IV.D.3 Incorporation of Proteins into Acrylic Polymers

Principal Investigator: Professor Alan J. Russell
Department of Chemical Engineering
University of Pittsburgh

Students: Dr. Zhen Yang
Mr. Darrell Williams

IV.D.3.1 INTRODUCTION

The covalent attachment of proteins to polymers has been the subject of intensive research for many decades. Immobilized proteins have been used in the food, chemical, pharmaceutical, and agricultural industries. Nevertheless, the variety of polymers which can serve as suitable hosts for biological molecules are limited by the conditions under which proteins are typically incorporated into polymers. The predominant reason for this apparent limitation is related to the sensitivity of most proteins to their environment. For instance, a protein which is unstable at pH 9.0 is unlikely to be successfully immobilized using a strategy which is dependent on alkaline pH's during attachment. Further, the development of a wide variety of classes of protein-containing polymers depends not only on the availability of immobilization strategies, but also on the stability of proteins in environments which are best suited to rational polymer design. Indeed, potential applications of biomaterials would be enhanced by redirecting our focus on choosing a given set of polymer properties, and having a general method for incorporating a protein in the favored polymer matrix.

A commonly-used strategy for tuning the physical properties of polymers is to vary the proportion of solvent and non-solvent in the polymerization reaction mixture. The ability of the protein to both withstand the solvents utilized, and to also be used as a co-monomer, would enable the synthesis of many different types of protein containing polymers (for instance, beads, fibers, and membranes) from the same starting materials. The resulting polymers will have properties which are most useful for a given application, and will also contain active biological molecules. Clearly, achieving such a goal is dependent on the solubilization of proteins in organic solvents.

Proteins which have been covalently modified with polyethylene glycol can be solubilized in a variety of organic solvents. Figure IV.D.3.1 outlines how a modified polyethylene glycol, which has a monomeric functional group at one end, can be used to modify a protein. The resulting "bio-monomer" would be soluble and active in water, organic solvents, and mixtures of the two. The protein co-monomer can then be simply incorporated into a polymer during a polymerization in the presence of solvents necessary to synthesize a polymer of

desired properties. Maintaining the protein at low (<2%) weight percent will result in polymers which have the same properties as those in the absence of proteins. It should be noted that the strategy we have outlined above does not address the issue of diffusion of substrates within immobilized enzyme preparations. The concept we describe would enable the physical properties of a polymer to be selected prior to immobilization of the protein, and thus, if necessary, materials with high porosities could be synthesized with active protein contained within the material.

The incorporation of proteins into polyacrylates serves as a model system to test this strategy. Acrylic polymers can be synthesized from, for instance, methyl methacrylate in organic solvents. By varying the ratio of solvent (chloroform) and non-solvent (carbon tetrachloride) during the free-radical initiated polymerization polymers of varying molecular weight, porosities, and other properties can be synthesized. We have used the serine protease subtilisin Carlsberg to demonstrate a general strategy to modify an enzyme with PEG and incorporate the modified enzyme into polyacrylates (Figure IV.D.3.1). The activity and stability of the functionalized enzyme have been investigated, as have the activity and stability of the enzyme once incorporated into the polymer.

IV.D.3.2 EXPERIMENTAL PROCEDURES

A. Reagents:

Subtilisin Carlsberg was obtained from Sigma Chemical Co. Polyethylene glycol monomethacrylate (MW 8000) was purchased from MTM Research Chemicals, Inc. All other reagents were from either Sigma or Aldrich and were of the highest purity available.

B. PEG-Aldehyde Synthesis:

Aldehydes were produced from PEG monomethacrylate (MW = 8,000) using a method adapted from Wirth et al.(8). The presence of aldehyde was determined using the 2,4-dinitrophenylhydrazine test and peak detection with infrared spectroscopy.

C. Modification of subtilisin with the PEG-aldehyde:

Subtilisin (9.1 μmol) was dissolved in 8.0 ml of 0.1 M borate buffer (pH 9.0). The aldehyde (0.25 mmol) was added, along with sodium cyanoborohydride (0.2 mmol), while shaking the solution. After incubating at 18 °C for 4 hours, the solution was passed through a Sephadex G-25 gel filtration column, with protein being detected spectrophotometrically as fractions were collected. Fractions containing the modified protein were lyophilized.

D. Characterization of modified protein:

Modification was verified with electrospray mass spectrometry (Fisons, VG Quattro), amino acid analysis (University of Pittsburgh Peptide Analysis Facility), and high pressure liquid chromatography by passing the sample through a Protein Pak 200SW column (Waters) using a Waters HPLC (model 600E, 490E detector). Protein contents were estimated by measuring the absorbance at 280 nm.

E. Activity of Modified Subtilisin:

Kinetic studies of the modified protein were performed by following the hydrolysis of N-succinyl-L-alanyl-L-alanyl-L-prolyl-L-phenylalanyl p-nitroanilide at 20°C in Tris-HCl buffer (0.01 M, pH 8.6), dioxane or a mixture of the two. Prior to reactions, the samples of modified enzymes were dissolved in tetrahydrofuran and filtered through a solvent resistant 0.22 μm filter (from Fischer) in order to remove the insoluble native protein, then the modified enzymes were obtained by evaporating the solvent. 10 μl enzyme solution (5 mg/ml) in phosphate buffer (0.01 M, pH 7.0) was added to a cuvette containing 1 ml substrate solution (0.01-0.7 mM) to initiate the reaction. The increase in absorbance at 412 nm on the release of the product p-nitroaniline was monitored to calculate the initial reaction rate. Substrate concentration versus rate was plotted to determine V_{max} and K_m using non-linear regression analysis. A standard of native subtilisin (3 μg/ml) was analyzed as a control.

F. Stability of Modified Subtilisin:

The modified (0.4 mg/ml) and unmodified (0.01 mg/ml) subtilisin were separately incubated at 30°C in either aqueous buffer (pH 8.6, 0.01 M Tris-HCl), organic solvent (dioxane), or a mixture of the two. Periodically, 10 μl aliquots were removed and added to 1 ml substrate solution (0.4 mM), assessing for enzyme activity as described above.

G. Polymerization of the Protein with Methyl Methacrylate:

Prior to reaction, methyl methacrylate (MMA) was passed through a column filled with CG-20 alumina beads to remove the inhibitor. Typically, 102 mg of PEG-modified subtilisin, 1 ml of treated MMA, 0.04 ml of trimethylolpropane trimethacrylate solution (TMA) (50/50 TMA/chloroform as crosslinker), and 20 ml carbon tetrachloride were placed in a 25 ml reaction vial capped with a septum. After degassing with nitrogen for 30 minutes, 0.1 ml of initiator solution (1 g AIBN in 100 ml chloroform) was added and the polymerization was initiated by UV light at 365 nm. 24 hours later, the polymer beads were obtained by evaporating the solvent and washing with water.

H. Flow cell apparatus: A flow cell apparatus (Figure IV.D.3.2) was designed and constructed for testing of protein-polymer activity and stability. 0.1 mM substrate solution in Tris-HCl buffer (0.01 M, pH 8.6) was incubated in ice in order to minimize the auto-hydrolysis of the substrate, 46.5 mg of enzyme-containing polymer beads was added in the reactor, and the flow rate was set to 0.5 ml/min. The absorbance at 412 nm was followed continuously with a spectrophotometer.

IV.D.3.3 RESULTS AND DISCUSSION

A. Modification with PEG

PEG monomethacrylate was oxidized to the corresponding aldehyde. The product was a solid after evaporation of the solvent. A precipitate was formed with the 2,4-dinitrophenylhydrazine test, indicating the presence of an aldehyde. Fourier transform infrared spectroscopy was used to confirm the results. The PEG-aldehyde was not separated from the starting material, since the reactant impurities do not interfere with the subsequent modification of the protein. In addition the separation of PEG monomethacrylate from PEG aldehyde monomethacrylate would be extremely difficult. The approximate yield of aldehyde, according to a quantitative assay based on the 2,4-dinitrophenylhydrazine test, was 75 ± 5%. We note, for those interested in repeating this procedure, that the stench associated with the aldehyde synthesis is considerable, and we advise the use of a fume hood throughout the handling of the aldehyde, and any contaminated glassware prior to cleaning.

The addition of PEG aldehyde to subtilisin, in the presence of either sodium cyanoborohydride or sodium borohydride, resulted in the covalent linkage of PEG to the protein. Adsorption of the protein fractions at 280 nm after gel filtration chromatography showed three peaks, one with a slight shoulder, which was confirmed by HPLC. Electrospray mass spectroscopy (Figure IV.D.3.3) on the neat and fractionated samples clearly indicated that they are unmodified, singly- and doubly-modified subtilisin. The molecular weight of the first peak (28,109.6) corresponds to that of native subtilisin, and the differences between the two subsequent peaks are approximately 8,000, which is the average molecular weight of the PEG used in our study. This result was further confirmed by amino acid analysis. Therefore, under the conditions we used, one or two lysine groups out of 9 from subtilisin can be covalently modified with PEG monomethacrylate, and the singly- and doubly-modified proteins can be separated easily and effectively using gel filtration chromatography. PEG-modification of proteins has been reported many times previously [6], and it is not surprising that it is straightforward to synthesize a modified subtilisin. The properties of subtilisin modified with PEG monomethacrylate have not been reported previously.

The modified subtilisin is soluble in a variety of organic solvents, up to 5 mg powder/ml, including: chloroform, methylene chloride, 1,1,1-trichloroethane,

carbon tetrachloride, toluene, benzene, dimethyl sulfoxide, tetrahydrofuran, dioxane, and acetonitrile. For modified subtilisin to remain in solution in tetrahydrofuran and acetonitrile, slight heating is required. The powder is not soluble in solvents such as hexane, acetone, ethyl ether and isoamyl alcohol. The solubility data is another confirmation of modification, since native subtilisin is not soluble in any of the above solvents. The data also indicate that the presence of the methacrylate group on the PEG does not alter the well known ability of PEG-modified proteins to be solubilized in organic media.

The solubility of PEG-subtilisin in organic solvents can be used to purify the modified protein from unmodified protein. It is important that this is achieved since future use of the modified protein will depend on low contaminating levels of native subtilisin. The solubilization of PEG modified proteins in organic solvents has been questioned by Khan et al. [7], who have suggested that PEG-proteins are not soluble in organic solvents, but instead, form aggregates which can give rise to an optically transparent solution. This distinction is not important when considering the use of a PEG-modified protein for polymer synthesis.

B. Activity and Stability of PEG-Modified Protein

Before reacting PEG-subtilisin with other materials it is necessary to fully characterize the activity and stability of the "bio-monomer". Using a gel filtration column, we have separated the modified protein into predominantly singly or doubly modified protein fractions. The subtilisin fractions were of course contaminated to some degree with each other, and our data does not indicate that all the enzyme molecules have been modified in the same position. Thus, the activities and stabilities noted are average properties for the sample being studied.

The activities of the modified enzymes were assessed with the artificial peptide substrate succinyl-L-alanyl-L-alanyl-L-prolyl-L-phenylalanyl*p*-nitroanilide. The kinetic constants, V_{max} and K_m, for the native, and singly or doubly modified fractions in both aqueous buffer and buffer/solvent mixtures are listed in Table IV.D.3.1. The K_m values in aqueous solution increased slightly after modification, while those for PEG-subtilisin in the aqueous/organic mixture were obviously higher versus the native enzyme. Also, for all the proteins involved, the K_m values in organic media were always much greater than those in aqueous buffer. The V_{max} data for both modified enzyme fractions were increased when dioxane/buffer was used instead of buffer only, but V_{max} decreased for the native subtilisin. The specificity constants were all lower when organic solvent was introduced, mainly due to the increase in K_m. In both reaction media, the modified enzymes were less active than native subtilisin, but the singly-modified enzyme showed higher activity than the doubly-modified protein fraction.

It is not surprising that K_ms for the enzyme in aqueous solution are not significantly altered after modification, since modification involves the covalent linkage of PEG to the lysine groups, which are not involved in the hydrophobic

binding site of subtilisin [3]. The increased K_ms in dioxane/buffer mixture are simply the result of altered substrate partitioning into the enzyme active site after the addition of solvent [2]. The V_{max}s of both modified enzymes in aqueous buffer and the mixture of dioxane and buffer are presumably reduced because of exposure of the protein to high pH, and contact with reductants, during modification. The effect of treatment with tetrahydrofuran, for removal of the unmodified protein, may also have caused the changes in V_{max}.

A specific interest in our group is the activity of proteins in anhydrous media, and materials incorporating organic-stable and -active proteins could form the basis of a first generation of organic solvent resistant biosensors. The activity of PEG-modified subtilisin was further investigated by solubilizing the enzyme in tetrahydrofuran (THF), following the catalysis of transesterification rather than hydrolysis. The kinetic constants for the methanolysis of N-acetyl-L-phenylalanyl ethyl ester in THF were determined as described previously [2]. At 32_C, 1 mg/ml protein, and 100 mM methanol, the values for V_{max} and K_m in THF were found to be 0.071 mM/sec and 81 mM respectively, thus V_{max}/K_m for PEG-subtilisin in THF is 5.3×10^{-2} min^{-1}. Since subtilisin is not soluble in THF, these values must be compared to those of insoluble subtilisin. V_{max} and K_m in THF for native subtilisin under the same conditions are 1.78×10^{-3} mM/sec and 275 mM respectively. Thus, the activity of the modified, solubilized protein is 136 times that of the native protein. This effect is not the result of diffusional limitations in the powdered enzyme preparation since this reaction has been shown not to be diffusionally limited [2]. Without question, PEG-subtilisin is active in organic solvents, and should thus remain active when solubilized in organic solvents, and covalently incorporated into a growing polymer.

The stability of PEG-subtilisin is also of importance, since the stability of the polymerized protein will probably resemble more closely the modified protein rather than the native protein. We determined the half lives of subtilisin and PEG-subtilisin (singly and doubly modified) in buffer, organic solvents, and mixtures of the two. The results are shown in Figure IV.D.3.4. Clearly, PEG-subtilisin is remarkably stable in buffer. The half-life increases from 3 hours, for native subtilisin, to 700 hours as a result of single modification, and to over 1500 hours as a result of double modification. This effect is probably the result of decreased autolysis of subtilisin given the steric hindrance that the large PEG chain must create. For both modified subtilisins, the half-lives decreased with increasing dioxane concentration. However, introduction of dioxane into the buffer results in an apparent stabilization of the unmodified protein. While the decreased stability of the PEG-enzyme upon addition of dioxane can be explained by variations in the flexibility of the protein after exposure to organic solvents [1], the increased stability of the native protein is more likely related to the known reduction in the rate of amide hydrolysis, and thus the rate of inactivation via autolysis, in the presence of organic solvents.

C. Polymerization

We have shown that subtilisin modified with PEG-monomethacrylate is active in both aqueous and organic media. Since the stability of the modified protein monomer is significant, and immobilization usually stabilizes proteins, it is reasonable to expect that the protein-containing polymers will be particularly stable in terms of protein activity. In order to demonstrate this, we have proceeded to incorporate the singly, and doubly modified subtilisin samples into acrylic polymers which are synthesized in organic media. An important distinction exists between these studies and more conventional approaches to forming protein containing polymers. We are not intending to synthesize a hydrogel by cross-linking the acrylic groups attached to the proteins as others have described previously [4,5]. Instead we have incorporated a low weight per cent of protein into a polymer and assessed some of the gross properties of the polymer, and the enzyme. Further, the incorporation step itself takes place in non-aqueous media, thus expanding the range of polymers which can be synthesized.

To demonstrate the formation of PEG-acrylic polymers, five different acrylic polymers, varying in their PEG percentages, were synthesized using the conditions described in Table IV.D.3.2. Scanning electron microscopy showed that there was no significant difference in their particle size and shape. The surface area, determined by BET analysis, varied from 27 m^2/g for 1.4% PEG to 39 m^2/g for 7.6% PEG, to some degree dependent on the amount of PEG in the preparation. Examples of electron micrographs of the porous polymers in the absence and presence of protein are shown in Figure IV.D.3.5. As expected, no difference was observed in the morphology of the polymer when PEG was incorporated at a low percentage. It is thus reasonable to expect that the incorporation of low-percentage PEG and protein will not affect the properties of the polymers formed.

A subtilisin-containing PEG-acrylic polymer was then synthesized, as described above, to demonstrate the feasibility of producing active subtilisin incorporated into polymethylmethacrylate. The polymer beads remained active after sonication and washing with water overnight. No absorbance at 280 nm was observed in the final wash, indicating that at least some of the enzyme was covalently attached to the polymer. The activity and stability of the enzyme were assessed in both batch experiments and a simple continuous flow reactor. In the continuous flow system, the "biopolymer" retained activity over 35 hours (Figure IV.D.3.6), indicating that the enzyme was both active and stable. The shape of the curve in Figure IV.D.3.6 can be explained in two ways. First, any unbound PEG-subtilisin will be washed out of the reactor after initiating the reaction since there is a continuous flow and the enzyme will be soluble in the buffer. This enzyme will catalyze hydrolysis of the substrate, but the absorbance of the reactor output will decrease after an initial burst since the unattached enzyme will eventually be completely removed from the system. An alternative explanation is that the reaction catalyzed by the immobilized enzyme is diffusionally limited.

Under such conditions one would also expect an initial burst of activity followed by a slow decrease to a steady rate. The protein-polymer activity profile can probably be explained by a combination of these explanations since enzyme can be detected in the initial flow through, and yet "bursts" of activity are observed during re-filling of the substrate reservoir (an effect which would be predicted if the reaction were diffusionally limited).

IV.D.3.4 CONCLUSIONS

Our results have shown that attachment of PEG to subtilisin is sufficient to enable solubilization and stability of the enzyme in water and organic solvents. The activity of the enzyme is maintained after modification. It is then possible to incorporate the PEG-protein into a polyacrylate polymer. By varying the ratio of solvent (chloroform) and non-solvent (carbon tetrachloride) during the free-radical initiated polymerization, polymers of varying molecular weight, porosities, and other properties can be synthesized. Also, formation of different types of protein-containing polymers, such as beads, fibers, or membranes, will shed light on applications of enzyme-containing polymers. Further studies in this area are being conducted in our group.

IV.D.3.5 SUMMARY

1. Synthesis and characterization of PEGA*-protein conjugates. Have been achieved.

2. Synthesis of acrylic polymers incorporating PEGA*-protein conjugates. Have been completed.

3. Demonstration of stability of protein polymers.

IV.D.3.6 BIBLIOGRAPHY

1. Baillargeon, M.W., Sonnet, P.E. 1988. Lipase modified for solubility in organic solvents. Ann. N.Y. Acad. Sci. **542**: 244-249.

2. Chatterjee, S., Russell, A.J. 1993. Kinetics analysis of the mechanism for subtilisin in essentially anhydrous organic solvents. Enzyme Microb. Technol. **15**: 1022-1029.

3. Fersht, A.R. 1985. Enzyme Structure and Mechanism. W.H. Freeman and Co., New York.

4. Fulcrand, V., Jacquier, R., Lazaro, R., Viallefont, P. 1990. New biocatalysts for peptide synthesis: gels of copolymerized acrylic derivatives of a-chymotrypsin and polyoxyethylene. Tetrahedron. **46**: 3909-3920.

5. Fulcrand, V., Jacquier, R., Lazaro, R., Viallefont, P. 1991. Enzymatic peptide synthesis in organic solvent mediated by gels of copolymerized acrylic derivatives of a-chymotrypsin and polyoxyethylene. Int. J. Peptide Protein Res. 38: 273-277.

6. Inada, Y., Takahashi, K., Yoshimoto, T., Ajima, A., Matsushima, A., Saito, Y. 1986. Application of polyethylene glycol-modified enzymes in biotechnological processes: organic solvent-soluble enzymes. TIBTECH 7: 190-194.

7. Khan, S.A., Halling, P.J., Bosley, J.A., Clark, A.H., Pellow, A.D., Pelan, E.G., Rowlands, D.W. 1992. Polyethylene glycol-modified subtilisin forms microparticulate suspensions in organic solvents. Enzyme Microb. Technol. 14: 96-100.

8. Wirth, P., Souppe, J., Tritsch, D., Biellmann, J.-F. 1991. Chemical modification of horseradish peroxidase with ethanal-methoxypolyethylene glycol: solubility in organic solvents, activity, and properties. Bioorg. Chem. 19: 133-142.

Publications acknowledging MRC support

In Print

Kamat, S., Barrera, J., Beckman, E.J. and Russell, A.J. (1992) Biotechnol. Bioengin., 40, 158-166. Biocatalytic synthesis of acrylates in organic solvents and supercritical fluids.

Chatterjee, S. and Russell, A.J. (1992) Biotechnol. Bioengin., *40,* 1069-1077. Determination of microscopic rate constants for subtilisin catalyzed transesterification in anhydrous environments.

Ayala, G.A., Kamat, S., Komives, C., Beckman, E.J. and Russell, A.J. (1992) Annals New York Acad. Sci., *672.* 283-293. Solubilization and activity of proteins in supercritical fluids.

In Press

Yang, Z., Williams, D. and Russell, A.J., (1994) Biotechnol. Bioengin. Synthesis of protein-containing polymers in organic solvents.

Yang, Z., Chaudhray A., and Russell, A.J. (1994) Biotechnol. Bioengin. Synthesis, activity, and solubility of PEG-modified subtilisin

Abstracts & Presentations

Williams, D.L., Beckman, E.J. and Russell, A.J. (1992) abstract from *AIChE, Annual Meeting (November)*, Miami. Synthesis of solvent resistant biosensor materials.

Williams, D. and Russell, A.J. (1993) abstract BIOT 0150 from 205 th *ACS, Annual Meeting (March)*, Denver. Synthesis of solvent-resistant biomaterials.
1994 Advances in Biopolymer Engineering, Palm Coast, FL, January.

"Incorporation of proteins into acrylic polymers.
1993 Procter and Gamble Corporation, Cincinatti, OH, December. *(Invited Seminar)*

Rohm & Haas, Springhouse, PA, July. *"Incorporation of proteins into acrylic polymers".*

Shearwater Polymers, Huntsville, AL, July. *"Incorporation of proteins into acrylic polymers".*

Patents

Russell, A.J. (1992) Patent Disclosure on "Incorporation of proteins into acrylic polymers". (Patent Filed on December 8, 1993). Technology to be licensed to Biotechnology Research and Development Corporation.

Table IV.D.3.1 K_m and V_{max} values for native and PEG-modified subtilisin in Tris-HCl buffer and in 25% dioxane/75% Tris-HCl buffer.

Enzyme	Tris-HCl buffer			25% dioxane/75% buffer		
	K_m (mM)	V_{max} (mM/sec/mg)	V_{max}/K_m $(sec\ mg)^{-1}$	K_m (mM)	V_{max} (mM/sec/mg)	V_{max}/K_m $(sec\ mg)^{-1}$
native	0.12	12.7	106	3.6	7.8	2.2
singly modified	0.17	0.34	2.0	6.0	0.62	0.10
doubly modified	0.16	0.19	1.2	14.2	0.21	0.01

Table IV.D.3.2 Conditions used for synthesis of five PEG-acrylic polymers.

Component	Polymer 1	Polymer 2	Polymer 3	Polymer 4	Polymer 5
MMA (ml)	1	1	1	1	1
TMA (ml)[a]	0.8	0.8	0.8	0.8	0.8
AIBN (ml)[b]	0.15	0.15	0.15	0.15	0.15
$CHCl_3$ (ml)	3	3	3	3	3
CCl_4 (ml)	22	22	22	22	22
PEG (mg)	13.2	27.7	42.1	56.7	71.6
PEG/MMA (%, w/w)	1.4	3.0	4.5	6.0	7.6

a. 50% (v/v) in $CHCl_3$.

b. 1% (w/v) in $CHCl_3$.

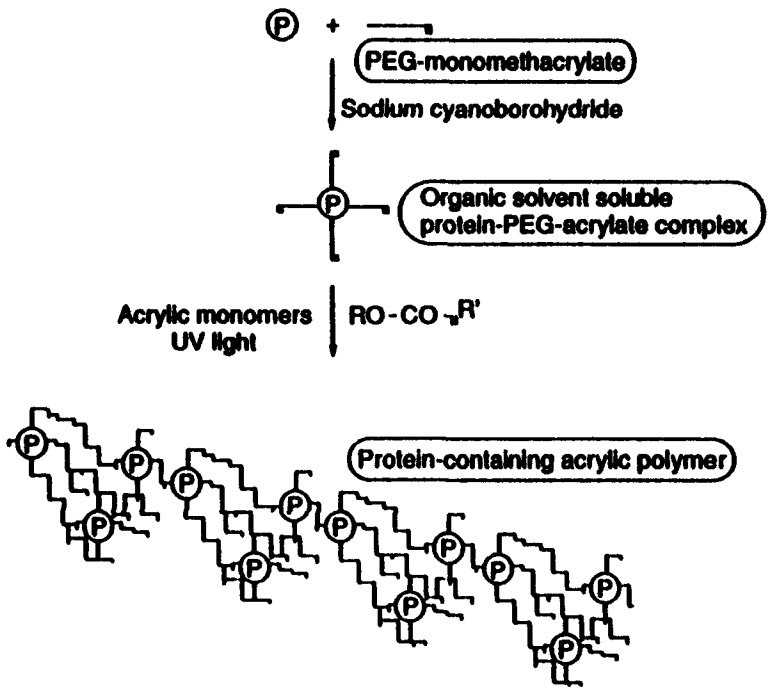

(A)

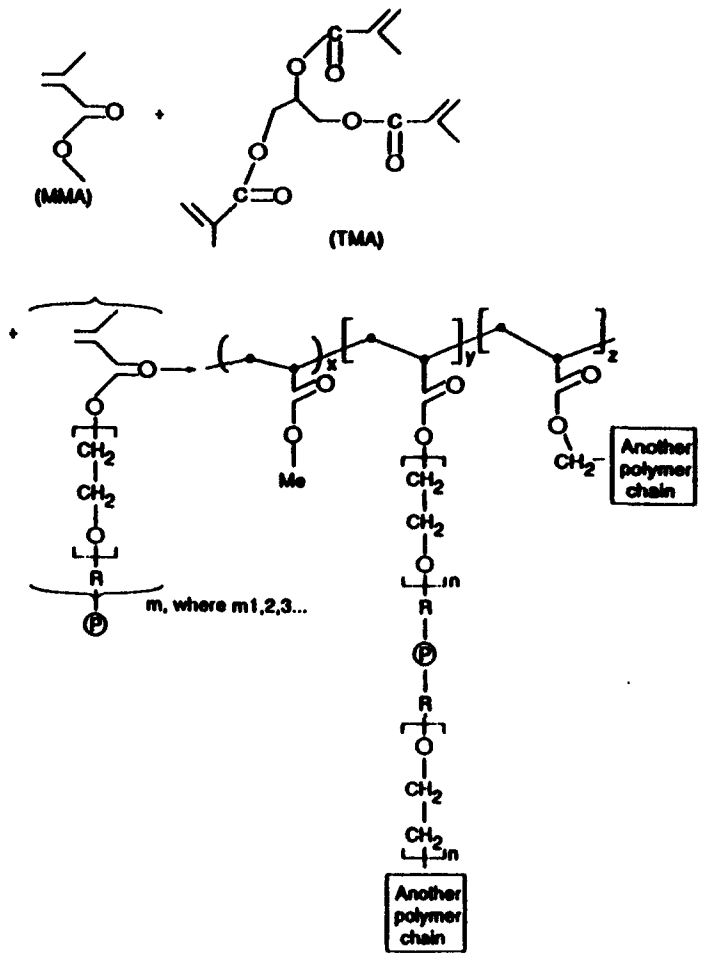

(B)

Figure IV.D.3.1 Overall (A) and detailed (B) schematics representing general method for incorporation of PEG-modified proteins into polymers during polymerization in organic solvents.

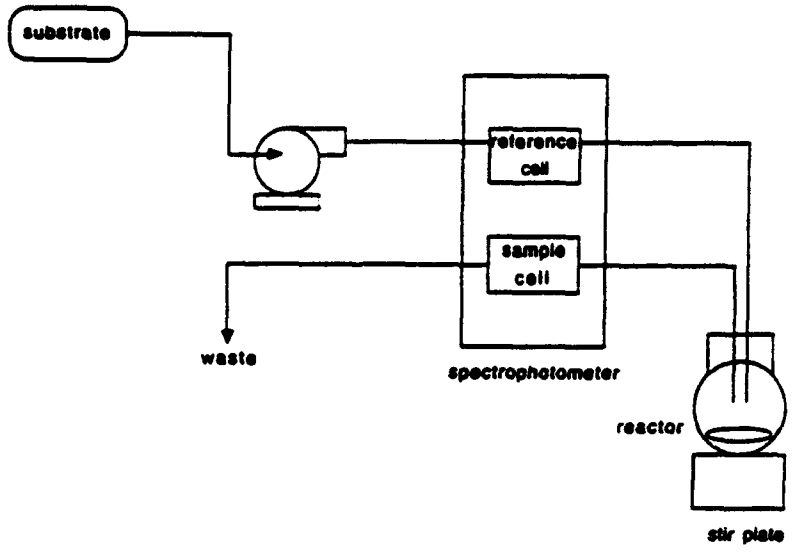

Figure IV.D.3.2 Flow cell apparatus for determination of protein-polymer activity and stability.

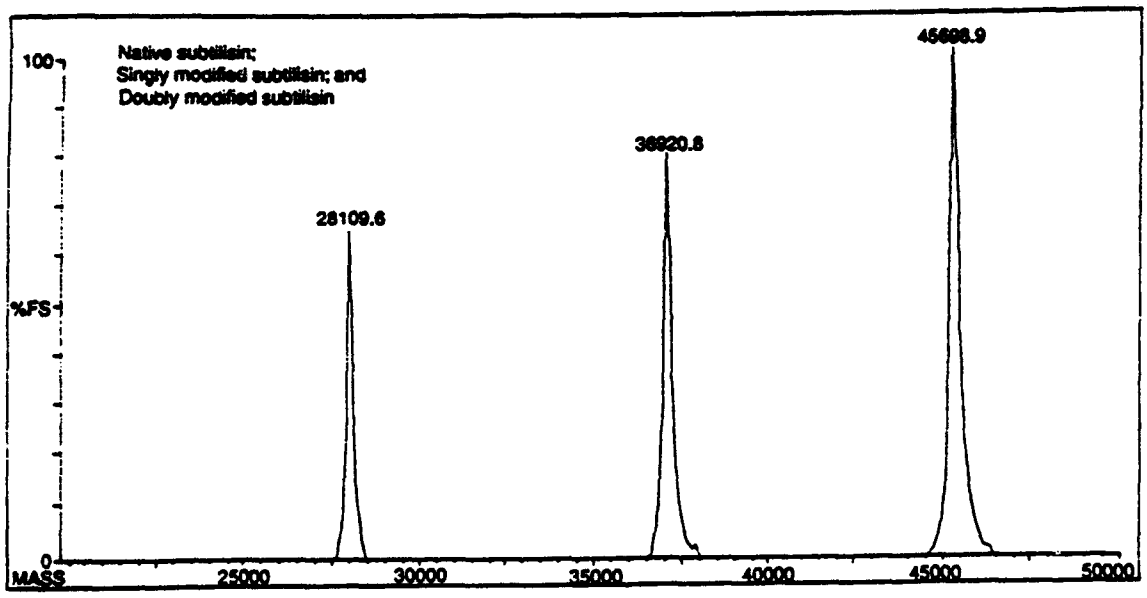

Figure IV.D.3.3 Electrospray mass spectroscopy of PEG-modified subtilisin.

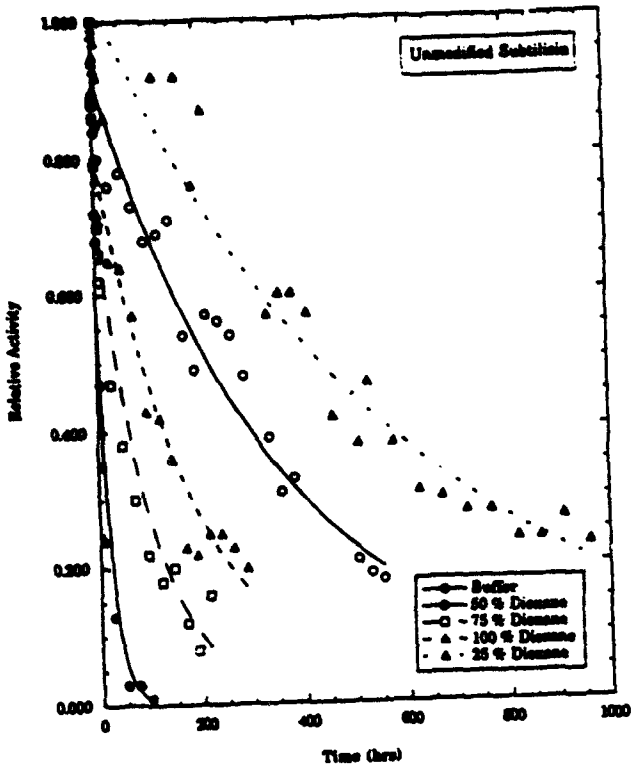

(A)

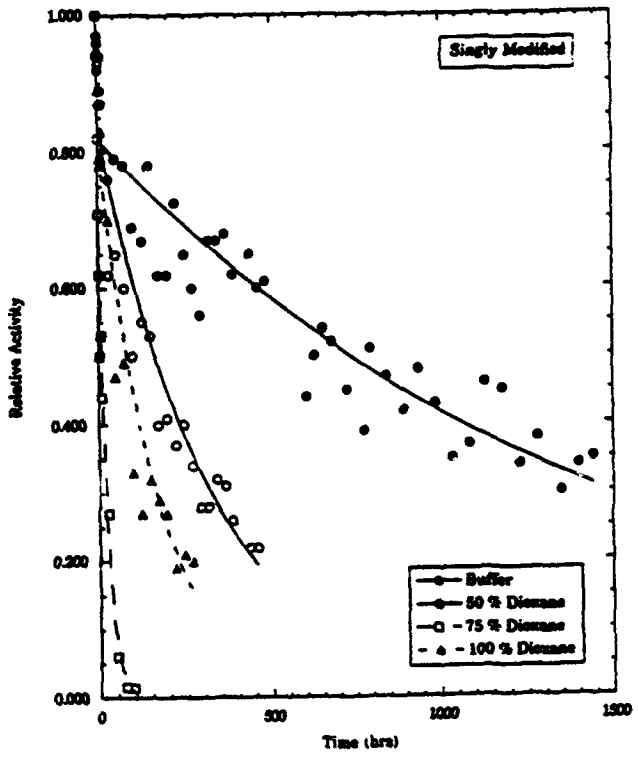

(B)

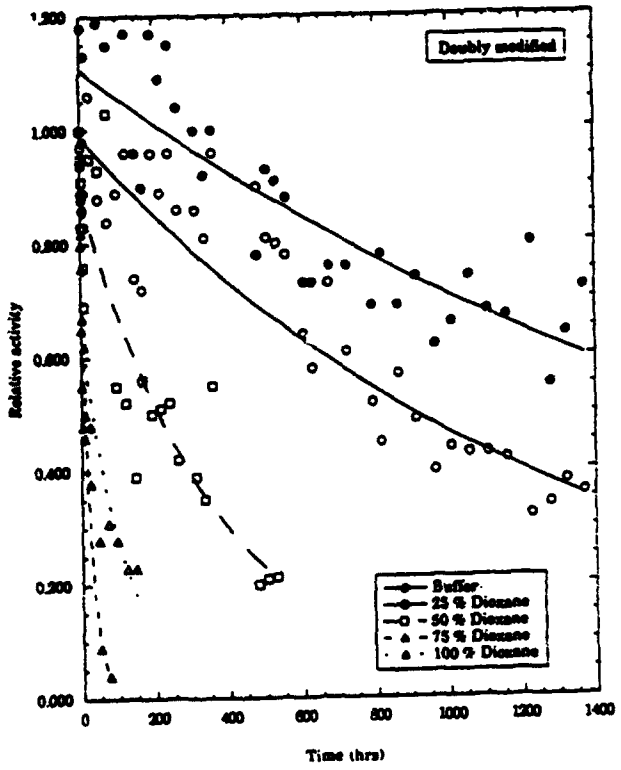

(C)

Figure IV.D.3.4 Stability of (A) unmodified, (B) singly-and (C) doubly-modified subtilisin in aqueous buffer, dioxane and buffer/dioxane mixture.

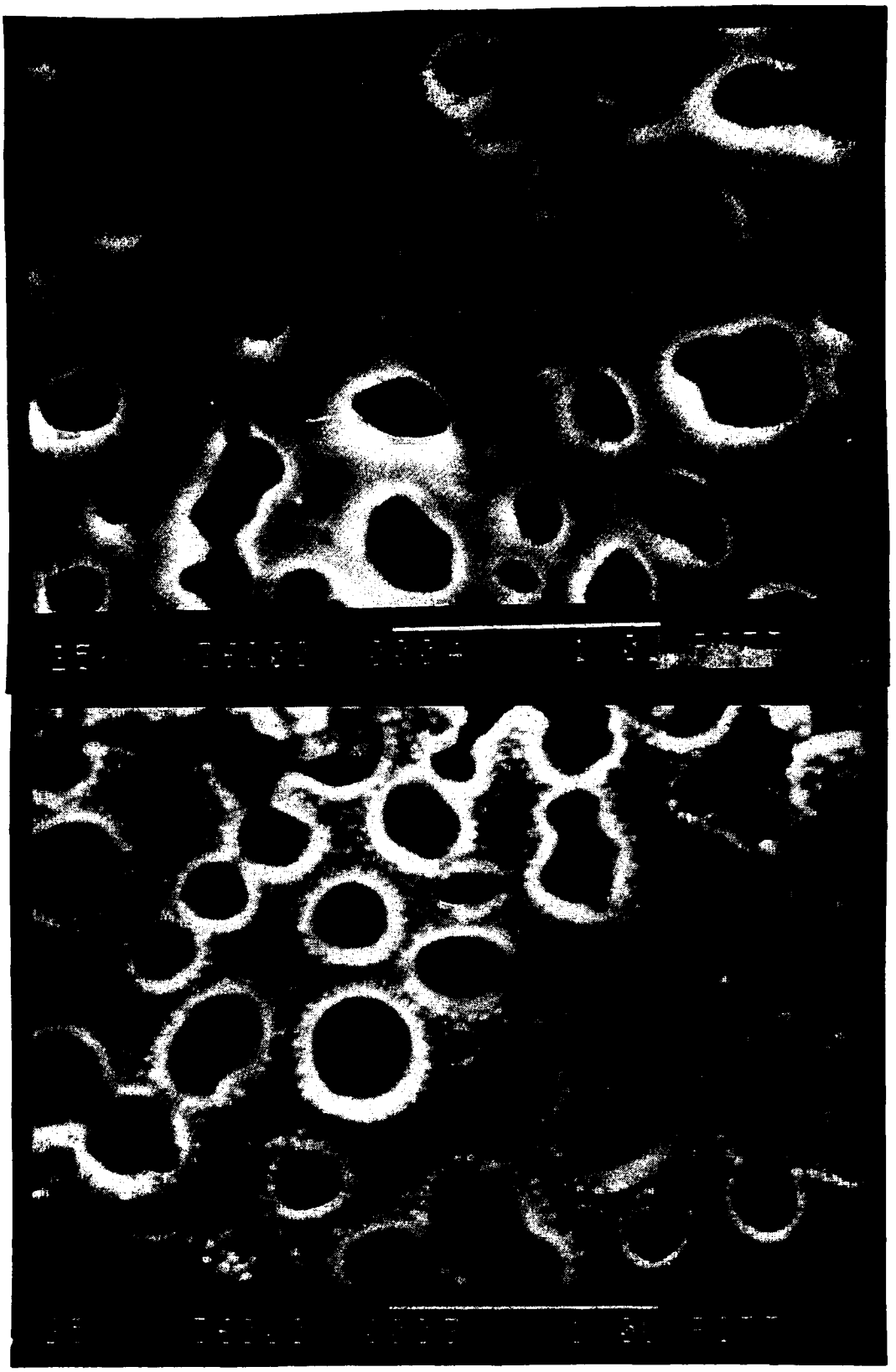

Figure IV.D.3.5 Electron micrographs of A.) acrylic polymers and B.) protein-containing acrylic polymer.

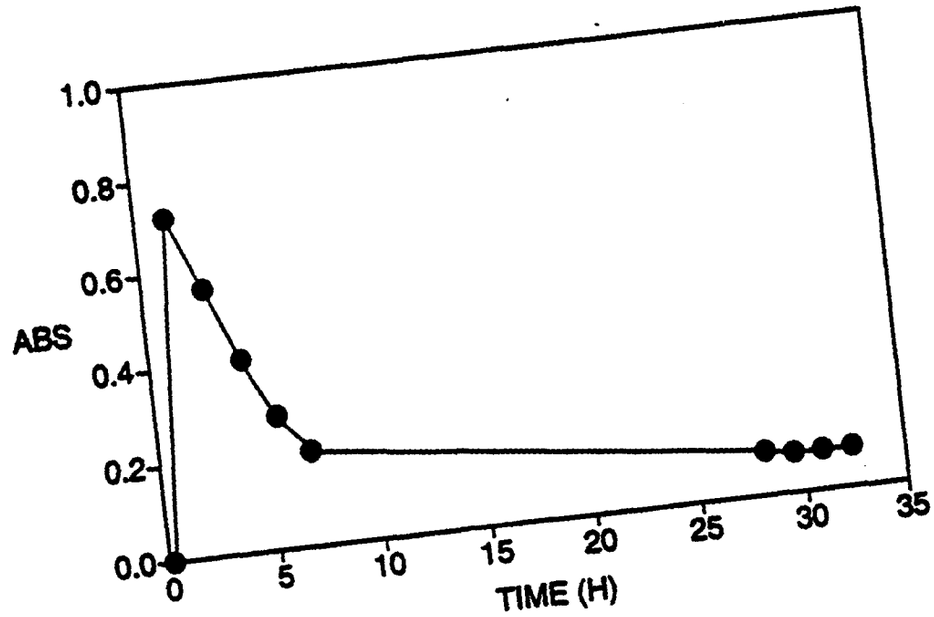

Figure IV.D.3.6 Activity and stability of protein-polymer in continuous reactor.

IV.D.4 Molecular Recognition and Self-Assembly Processes-Applications to New Materials and Chemical Sensors

Principal Investigator: Professor Andrew D.Hamilton
Department of Chemistry
University of Pittsburgh

Students: Dr. Scott Van Arman
Dr. Steve Wathen
Mr. Erkang Fan
Mr. Abdullah Zafar

IV.D.4.1 INTRODUCTION

The primary aims of this project have been to develop new synthetic receptors for the selective complexation of small organic molecules and the construction of monomeric units that self-assemble into oligomeric or polymeric species of well defined structure. Specific goals are the application of the synthetic receptors into membrane based sensors for biologically important molecules and use of the designed monomers in both solid state engineering and in the formation of nanometer scale assemblies. We have had considerable success in both these areas in the past two years. In particular, we have developed a new receptor for dicarboxylate ions (glutarate, glutamate, NMDA etc), have incorporated the receptor into PVC membranes and have used the membrane to construct molecule selective electrodes. We have also demonstrated the use of hydrogen bonding interactions to precisely control the packing in novel materials and have formed a number of self-assembled aggregates with novel structures and properties.

IV.D.4.2 OBJECTIVES

1. To use directed hydrogen bonding interactions to control the binding and aggregation of organic molecules.
2. To construct new hydrogen bonding motifs in the solid state.
3. To develop new receptors for biologically important substrates.
4. To incorporate these receptors into membranes for use as molecule sensitive electrodes.

IV.D.4.3 RESULTS AND DISCUSSION

Key Achievements over the Project Period

A. Receptors for Dicarboxylate Substrates

Simple synthetic receptors for dicarboxylic acids have been developed that function via directed hydrogen bonding interactions in highly competitive solvents.

For example, molecules containing two urea sites (as in 1) or two guanidinium groups (as in 2) bind to glutarate with very high affinity ($K_a > 10^3\ M^{-1}$). Strong binding of this type in polar solvents may be due to a number of factors including favorable secondary hydrogen bonding interactions between the carboxylate and urea, the use of charged H-bond acceptors, an inefficient solvation of the closely spaced H-bond donor sites in the urea, and an entropically favorable release of solvent and/or counterion molecules on complex formation.

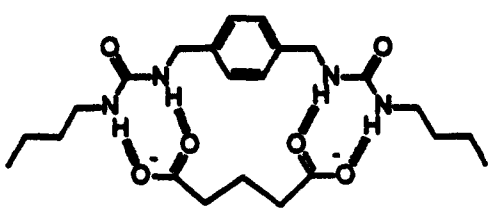

1

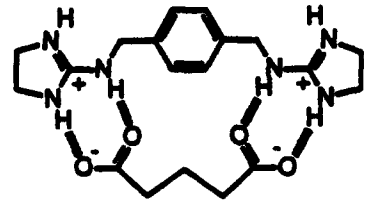

2

In collaboration with Prof. S. Weber we have designed a prototype sensor for glutarate ions (with potential application to the neurotransmitter, glutamate) based on the bis-urea receptor 1. The receptor is immobilized in a PVC membrane and attached to the open end of a standard PVC tube which in turn is fixed to a Ag/AgCl electrode with an internal solution of tetrapentyl ammonium chloride (1mM) and KCl (0.1mM). The sensor (shown schematically in Figure IV.D.4.1) is immersed in a solution of the analyte containing Hepes buffer (5mM) and KCl (0.1mM). A plot of potential change across the membrane vs log. concentration of different dicarboxylates shows a sensitive response that is larger for glutarate than for other homologous dicarboxylates.

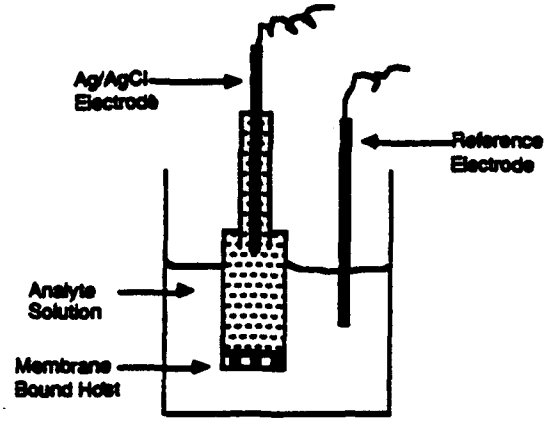

Figure IV.D.4.1. Design of a Recognition based Sensor

B. Hydrogen Bonding Control of Solid State Structure

The design of molecular subunits that self-assemble into predictable structures in the solid state is an area of intense current interest. A key to controlling the shape of the aggregate lies in manipulating the type and orientation of the non-covalent interactions between the subunits. We have recently discovered a simple hydrogen bonding subunit (acylaminopyridine/carboxylic acid pair) that will self-assemble into alternating cocrystals in which the packing in the solid is dictated by the spacer groups. For example the solid state structures of 3 show different packing patterns with glutaric acid (Figure IV.D.4.2) and succinic acid Figure IV.D.4.3), respectively. These two structures show a

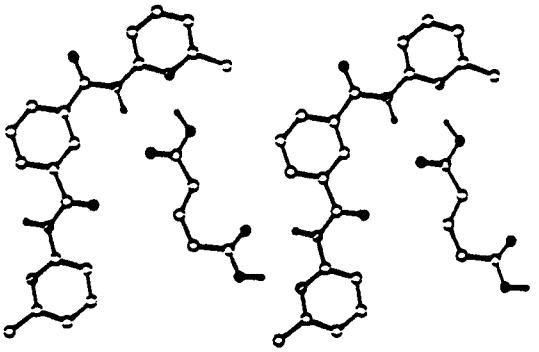

Figure IV.D.4.2 Crystal structure of 3 with glutaric acid

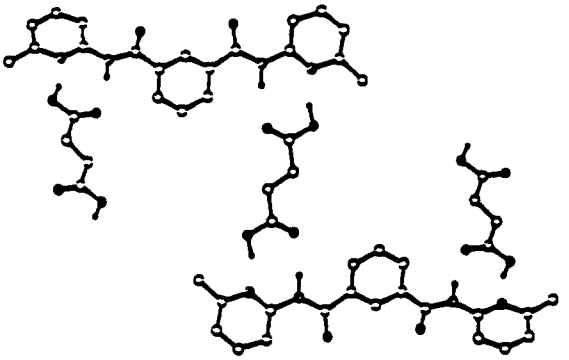

Figure IV.D.4.3 Crystal structure of 3 with succinic acid

complementarity between the curvature present in both the receptor and the diacid that can lead to the tightly packed polymeric complex. However , when receptor 3 takes up the conformation shown then two carboxylic acids could bind with one aminopyridine directed above and the other below the plane of the binding cavity. Propagation of this arrangement with a dicarboxylic acid would lead to an extended helical structure, as shown in Figure IV.D.4.4. X-ray diffraction analysis (Figure IV.D.4.4) of a polymeric cocrystal composed of 3 and pimelic acid units showed a helical structure stabilized by network of hydrogen bonds between the two components.

Figure IV.D.4.4 Stereoview of the X-ray structure between 3 and pimelic acid

C. Self-Assembly of Nanoscale Aggregates

There is great interest material self-assembly where three or more components are induced to form well-defined aggregates. This intermediate molecular weight region (1-20 x 10^3 Daltons) is of considerable importance in the development of nanometer scale structures.

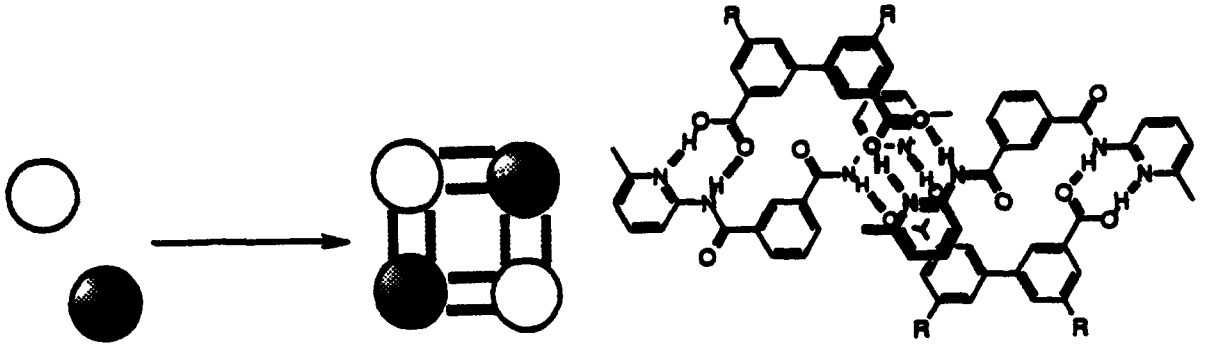

Figure IV.D.4.5 Schematic and Actual Formation of Stable Cyclic Aggregate.

In this project period we have shown that cyclic 2+2 aggregates (as in Figure IV.D.4.5) can be formed in solution and in the solid state by diacid and bis-acylaminopyridine subunits with appropriate spacers between the binding groups. The persistence of the 2+ 2 complex in solution was studied by NMR, gel permeation chromatography and vapor phase osmometry. This is a very general strategy as we have also shown that simple isophthalic acid derivatives can form cyclic hexameric aggregates both in solution and in the solid state (as in Figure IV.D.4.6).

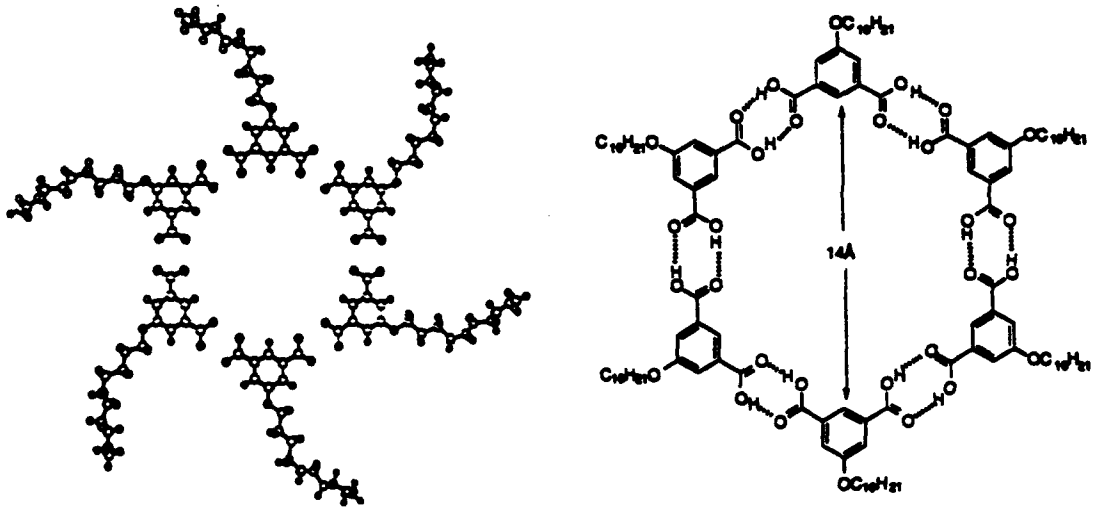

Figure IV.D.4.6 X-Ray and Schematic Structure of Simple Isophthalic Acid Derivatives

IV.D.4.4 SUMMARY

In the past two years we have demonstrated that simple hydrogen bonding structures can be used to achieve impressive selectivities in the binding of dicarboxylate substrates. We have also shown that these receptors can be incorporated into membranes to provide functioning and selective sensors for dicarboxylates. In addition we have discovered a dramatically new hydrogen bonding motif for the formation of self-assembling structures both *in solution* and in the solid state.

PUBLICATIONS

1. S. J. Geib, C. Vicent, E. Fan, A. D. Hamilton, "Selbstorganisation zu einer Helix durch Wasserstoffbrückenbindung" Angew. Chemie, 105, 83 (1993). "A Self-Assembling Hydrogen Bonded Helix" Angew. Chemie, Int. Ed., 32, 119 (1993).

2. E. Fan, S. A. Van Arman, S. Kincaid and Andrew D. Hamilton, "Molecular Recognition: Hydrogen Bonding Receptors that Function in Highly Competitive Solvents" J. Am. Chem. Soc. 115, 369 (1993).

3. S. J. Geib, E. Fan, F. Garcia-Tellado, C. Vicent, and A. D. Hamilton, "Supramolecular Self-Assembly based on Directed Hydrogen Bonding' Polymer Preprints, 34, 106-107 (1993).

4. A. D. Hamilton, E. Fan, S. A. Van Arman, C. Vicent, F. Garcia Tellado, S. J. Geib, "New Synthetic Receptors for Complexation and Catalysis" Supramolecular Chem. 1, 247-252 (1993).

5. J. Yang, E. Fan, S, J. Geib, and A. D. Hamilton, "Hydrogen Bonding Control of Molecular Self-Assembly: Formation of a 2+ 2 Complex in Solution and in the Solid State" J. Am. Chem. Soc. 115, 5314-5315 (1993).

6. E. Fan, J. Yang, S. J. Geib, C. Vicent, F. Garcia-Tellado, P. Tecilla and A. D. Hamilton, "Supramolecular Self-Assembly based on Directed Hydrogen Bonding' Die Macromoleculare Chemie, In press.

7. J. N. Valenta, R. P. Dixon, A. D. Hamilton and S. G. Weber,"Enhanced Extraction of Phenobarbital from Serum with a Designed Artificial Receptor", Analytical Chem. Submitted.

8. J. Yang, J. L. Marendaz, S, J. Geib, and A. D. Hamilton, "Hydrogen Bonding Control of Self-Assembly: Simple Isophthalic Acid Derivatives form Hexameric Aggregates in Solution and in the Solid State" J. Am. Chem. Soc. Submitted.

9. E. Fan, C. Vicent, S. J. Geib and A. D. Hamilton. "Molecular Recognition in the Solid State: Hydrogen Bonding Control of Molecular Aggregation", Chemistry of Materials, Submitted.

IV.D.5 Neurochemical Compounds Capable of Enhancing Memory and Rapid Recall

Principal Investigator: Professor German Barrionuevo, M.D.
Department of Behavioral
Neuroscience
University of Pittsburgh

Students: Dr. Ronald Langdon
Mr. Mark W. Fleck

IV.D.5.1 INTRODUCTION

Glutamate is the principal fast excitatory neurotransmitter utilized by the mammalian central nervous system. Glutamatergic transmission is mediated by several receptor subtypes that can be most clearly divided into N-methyl-D-aspartate (NMDA) receptors and those activated by a variety of other compounds, and specifically by α-amino-3-hydroxy-5-methyl-4-isoxazoleproprionic acid (AMPA). It is widely speculated that the physiological control of glutamatergic mediated synaptic responses is important both physiologically and pathologically. In addition to mediate fast synaptic transmission, glutamate also is involved in long-term modulation of neuronal excitability. For example, protracted changes in glutamatergic synaptic efficacy are the most compelling models in the vertebrate brain for a cellular mechanism underlying memory. This type of synaptic plasticity includes a wide range of short-term and long-term increases or decreases in the efficacy of synaptic transmission are use-dependent because they occur under certain conditions of nerve cell activity. The most widely hypothesized model to explain learning and memory is long-term potentiation (LTP), a phenomenon that depends on persistent changes in glutamate receptors induced by high-frequency (tetanic) stimulation. LTP has been demonstrated in all neocortical areas and has been extensively characterized in the hippocampal formation. Long-term depression (LTD) of glutamatergic synaptic transmission is another example of tetanically-induced synaptic plasticity that relates to memory.

IV.D.5.2 OBJECTIVE

As part of the development of pharmacological means to enhance use-dependent synaptic plasticity, the objective of the present proposal is to examine the factors affecting synaptic plasticity in brain regions known to be involved in memory and learning. These data could serve as a basis for the future development of pharmacological agents that could enhance use-dependent synaptic plasticity through positive modulation of activity of the underlying glutamate receptor/channel complex. Specifically, NMDA receptor activation unambiguously is a critical step in the induction of LTP in various subregions of the hippocampus and neocortex. Thus, enhancement of NMDA receptor activity

through positive allosteric modulation of this receptor complex should facilitate the induction of LTP in those subregions. Our research program on the fundamental principles underlying glutamatergic synaptic plasticity presents some direct tests of this hypothesis and as such, is indispensable for the generation of future proposals that focus on the development of memory enhancers.

IV.D.5.3 ACCOMPLISHMENTS AND SIGNIFICANCE

A. Role of Aspartate in Neurotransmission at the Schaffer Commissural-CA1 Synapse

We examined whether L-aspartate (ASP) and L-glutamate (GLU) both function as endogenous neurotransmitters in area CA1 of the rat hippocampus. Radioligand displacement experiments using [^{3}H]AMPA to label AMPA/kainate receptors and [^{3}H]CGS-19755 to label NMDA receptors confirmed that GLU (Ki ~500 nM) but not ASP (Ki > 1 mM) has high-affintity for AMPA/kainate receptors whereas GLU (Ki ~250 nM) and ASP (Ki ~1.3 μM) both have high-affinity for NMDA receptors. Elevating extracellular potassium concentration (50 mM, 1 min) evoked the calcium-dependent release of both ASP (~50% increase) and GLU (~200% increase) from hippocampal slices and from minislices of area CA1. Reducing extracellular glucose concentration (0.2 mM) reduced GLU release, enhanced ASP release, and reduced AMPA/kainate receptor-mediated responses more than NMDA receptor-mediated responses (to 7% *vs.* 34 % of control, respectively). Fiber volleys, antidromic population spikes, membrane potential, input resistance, ATP content all were not affected by glucose reduction. Unlike low glucose, the inhibitory neuromodulator adenosine (5 μM), which reduces ASP and GLU release to a similar extent, reduced AMPA/kainate- and NMDA receptor-mediated pEPSPs similarly (to 11% *vs.* 12% of control, respectively). AMPA/kainate- and NMDA receptor-mediated pEPSPs were also similarly reduced by 0.4 μM TTX (to 32% *vs.* 22% of control, respectively) and similarly enhanced by 10 μM 4-AP (to 206% *vs.* 248% of control, respectively). Finally, NMDA receptor-mediated EPSCs measured by whole-cell recording decayed faster in low glucose (73 msec *vs.* 54 msec) but not in adenosine (73 msec *vs.* 78 msec). Together, these results confirm that ASP and GLU are both involved in excitatory synaptic transmission at the Schaffer collateral-commissural terminals in area CA1 of the rat hippocampus.

B. Mossy Fiber Asyncronous Activation

During the past year, we discovered one idiosyncratic feature of mossy fiber synaptic responses Specifically, we examined systematically the time-course of EPSCs recorded from CA3 cells. We found that during a typical recording, there were complexities in individual evoked responses that were partly or wholly obscured by response averaging. That is, rising phases of unaveraged EPSCs were often inflected in a way that implied summation of multiple, asynchronous components. The most parsimonious interpretation of these data would be that these EPSCs were evoked by the combined action of mono- and polysynaptic

inputs. To determine whether this was the case, we examined the effects of "suppressing" media upon the shape of response waveforms. The suppression paradigm involves the use of general, but partial block of excitatory transmission, which produces up to 80-90% reduction in EPSC amplitude. This drastic reduction in synaptic transmission is likely to change the relative contributions made by inputs of differing synaptic order. Specifically, removing polysynaptic inputs which contaminate the mossy fiber EPSC with collateral EPSCs would change the shape of the EPSC evoked by stimulation of the dentate gyrus. That is, loss of inflections and/or shortening of a long rising phase of the EPSCs would indicate that the contaminating inputs arriving polysynaptically have been suppressed. By contrast, marked reduction in EPSC amplitude without a change in shape would imply that it was driven by purely monosynaptic inputs, i.e., purely by the mossy fibers. Suppression is performed by either of two methods: application of CNQX (1-4 μM) via the ACSF, or reduction of the ratio of $[Ca^{++}]$ to $[Mg^{++}]$ in the ACSF. In general, suppression had little or no effect on the shape of these complex response waveforms. Thus, we concluded that most long and complex rising phases in this study were not caused by polysynaptic contamination. Instead, asynchrony of mossy fiber input is a major factor determining the shape and duration of the rising phase of mossy fiber EPSCs evoked by bulk stimuli applied to granule cells and/or mossy fibers in the dentate gyrus.

We also examined the mossy fiber volleys (MFVs) that were evoked by dentate gyrus stimulation in the absence of synaptic transmission. MFV negative phases lasted from 2.5 to 4.5 ms and had multiple components. By comparison, negative phases of Schaffer collateral fiber volleys were always simple in shape and lasted 1.5 ms or less. Components of mossy fiber EPSCs and MFVs exhibit "surplus" latency, latency in addition to that expected for conduction of impulses directly to hippocampus along mossy fiber axon trunks. Part of this surplus latency is a consequence of "anti/orthodromic" conduction: Stimulation of the s. granulosum activates collaterals originating from remote granule cells; thus mossy fiber impulses travel to the CA3 region by direct (orthodromic) and indirect (first antidromically and then orthodromically) routes, with the latter involving hilar collaterals of mossy fibers. However, this mechanism due to an "artifactual" activation of mossy fibers accounts for only an small portion of surplus latency (~25%). Additional asynchrony and surplus latency appears to arise by a second mechanism that is inherent in the way mossy fiber axons or boutons function. Specifically, we propose that mossy fiber boutons actively spike to overcome the large impedance mismatch at the junction between a mossy fiber axon and its bouton because diameters of mossy fiber axons and their boutons typically differ by 15 to 20 fold. The bouton spike interposes, in effect, an extra step in the sequence of events by which granule cell activation results in excitatory input to CA3 pyramidal cells. This extra step could serve as a site for modulation of function at the mossy fiber synapse. By analogy with antidromic invasion of cell somata, invasion into mossy fiber boutons should succeed or fail depending upon the balance between the activity of voltage-gated cation channels and shunting conductances. In agreement with this model, unpublished recordings from

Dan Johnston's laboratory obtained by whole-cell clamping mossy fiber boutons do indicate the presence of sodium spiking.

CA3 cells not only are excited by mossy fibers, but also by other CA3 cells via recurrent collaterals. Thus, EPSCs from mossy fibers must be reliably distinguished from collateral EPSCs. It had been assumed that discrimination between mossy fiber EPSCs and collateral EPSCs can be based on the expectation that the former would have a rise time less than <3 msec. However, and because of the asynchronous presynaptic activation of the mossy fibers, it is highly questionable whether the "classic" 3 ms rise-time criterion can provide a valid basis for discrimination between pure mossy fiber EPSCs and EPSCs contaminated by one or more components driven by input from collateral projections of CA3 pyramidal cells. In fact, EPSCs that are driven by collaterals ("collateral EPSCs") often appear as single-component responses that rise in less than 3 ms (for e.g. see Appendix for the time course of fimbrial EPSCs). In fact, as described in our study, many mossy fiber EPSCs appear to be the sum of rapid components with individual rise-times less than 1 ms. Thus, if rise-times are to serve as a useful criterion for identifying authentic mossy fiber EPSCs, the 3 ms rejection threshold must be revised to a new value determined by the lower boundary of the range of collateral EPSC rise-times; this is likely to be near 1 ms.

IV.D.5.4 SUMMARY

- Results from project #1 confirm that ASP is involved in synaptic transmission in area CA1 of the hippocampus. ASP is released in a calcium-dependent manner upon depolarization of terminals in area CA1 and is a potent agonist of hippocampal NMDA- but not AMPA/kainate receptors.

- Low glucose perfusion preferentially reduced the potassium-evoked release of GLU, but not ASP. Likewise, low glucose preferentially reduced AMPA/kainate receptor-mediated pEPSPs for which GLU is a potent agonist more than NMDA receptor-mediated pEPSPs for which ASP is also a potent agonist.

- In contrast, the inhibitory neuromodulator adenosine, which equally reduces ASP and GLU release, equally reduced AMPA/kainate- and NMDA receptor-mediated pEPSPs. NMDA receptor-mediated EPSCs showed significantly faster decay-time constants in low glucose as expected if the lower-affinity agonist, ASP, is preferentially released.

- Therefore, we conclude that ASP release normally underlies a component of excitatory synaptic responses elicited in area CA1, specifically through its action at NMDA receptors.

- The time-course of EPSCs recorded from CA3 cells exhibit complexities in individual evoked responses that were partly or wholly obscured by response averaging.

- Components of mossy fiber EPSCs and MFVs exhibit "surplus" latency, latency in addition to that expected for conduction of impulses directly to hippocampus along mossy fiber axon trunks. Part of this surplus latency is a consequence of "anti/orthodromic" conduction: Stimulation of the s. granulosum activates collaterals originating from remote granule cells; thus mossy fiber impulses travel to the CA3 region by direct (orthodromic) and indirect (first antidromically and then orthodromically) routes, with the latter involving hilar collaterals of mossy fibers.

- We propose that mossy fiber boutons actively spike to overcome the large impedance mismatch at the junction between a mossy fiber axon and its bouton because diameters of mossy fiber axons and their boutons typically differ by 15 to 20 fold. The bouton spike interposes, in effect, an extra step in the sequence of events by which granule cell activation results in excitatory input to CA3 pyramidal cells. This extra step could serve as a site for modulation of function at the mossy fiber synapse.

For the second year of research, this program has generated two publications in peer-reviewed journals.

Publications:

Fleck, M.W., Henze, D.A., Barrionuevo, G. and Palmer A.M. Aspartate and Glutamate Mediate Excitatory Synaptic Transmission in Area CA1 of the Hippocampus. J. Neurosci. 13(9):3944-3955, 1993.

Langdon R. B., Johnson J. W., and Barrionuevo G. Asynchrony of Mossy Fiber Inputs and Excitatory Postsynaptic Currents in Rat Hippocampus. J. Physiol (London), 472:157-176, 1993.

V. NEW INSTRUMENTAL CAPABILITIES

New capabilitites at the MRC include:

- X-ray equipment has been installed and is operational. This equipment includes a computer controlled diffractometer with a solid state detector and the capability of performing some measurements up to 2700°C. An X-ray spectrometer unit, complete with an automated texture goniometer, also is available for the determination of quantitative pole figures and crystallite orientation distribution studies.

- Two new gravimetric microbalances, one with computer recording and programming capabilities, have been installed and are operational.

- A scanning tunneling microscope (STM) has been obtained and has been installed in a laboratory especially renovated for this piece of equipment. It is now in use for studying diamond and other surfaces.

- The atomic force microscope which was originally procured with the STM did not perform satisfactorily, and a new TopoMetrix AFM, which is compatible with the existing STM, is the replacement.

- An existing MTS mechanical test facility has been modified to include elevated temperature high precision tensile, compressive and fatigue testing.

- A chamber to expose specimens at elevated temperatures to controlled gas environments followed by in situ surface analyses using ESCA and SIMS has been constructed.

- A continuous wave UV laser useful for studying crystalline colloidal array ordering and for examining the UV Raman spectra of diamond films has become operational, and is in routine use.

- An electrophoretic light scattering spectrometer for studying colloid size and charge is now available.

- A Nicolet 800 FTIR Spectrometer with microscope and FT Raman accessory for studying molecular structure for use in catalysis research and other programs is operational.

- An experimental set up to measure waveguide propagation in MQW waveguides has been developed.

- A dye laser instrument for determining the wavelength dependence of the optical nonlinear response of a material.
- An anaerobic cell for third harmonic generation measurements has been developed.
- A 100 K detector for monitoring IR light at 8 μm has been developed.
- A new tunable single frequency Ti: sapphire laser has been designed and is under construction.

VI. EXTERNAL AND INTERNAL INTERACTIONS

The MRC has had extensive internal and external interactions during the two years of the grant. Some of these interactions have been as follows:

VI.1 External Interactions

- Complementing earlier efforts on surface characterization of polymeric materials, scientists from Miles, Inc. and the MRC have been exploring the evaluation of borosilicon carbonitride coatings as protective systems in aggressive environments for titanium-based alloys, other metallic alloys, and carbon-carbon. Other coating concepts to be employed at lower temperatures, such as a TiO_2 durable thin layer on polycarbonate base materials are also of joint interest.

- A number of common areas of interest with PPG Industries were found in extended discussions between PPG staff and members of the MRC. One area of MRC activity which may be suitable for cooperative work is sol/gel approaches to new amorphous and non-equilibrium materials with selective design of pore sizes and morphologies for novel optical materials. These approaches may also be employed for new catalysts. Another area is that of self-assembled colloidal materials for optical switching and other optical applications.

- An important future focus of the MRC is the area of materials durability. A major proposal on Materials Durability for Product Design for an Engineering Research Center was prepared with the cooperation of the Alcoa Technical Center. The effort included thrusts in predictive methods, and selected problem areas in the durability of metallic, polymeric, brittle, and high-temperature materials. A wide sector of support for the topic area and the proposal was received from diverse industrial organizations, small and large, including companies such as ALON Processing, Westinghouse Electric Corporation, AT&T, General Electric Aircraft Engines Corp., U.S. Air, and Energy International Corporation.

- We have explored the subject of extended durability of materials for automotive exhaust systems with the Allegheny Ludlum Technical Center and have prepared an initial proposal on the topic.

- We have had on-going interactions with the Westinghouse Science and Technology Center, pursuing joing research efforts and proposals in the area of diamond synthesis and processing, and properties, and materials and processes for environmental applications, including preventive and remediative approaches.

- A number of productive exchanges have been held with the Army Natick Research, Development, and Engineering Center in the areas of smart materials, bioremediation, and bioprocessing.

- Alon, a coatings company in Tarentum, PA., has been visited by MRC personnel. Several technical areas of mutual interest have been defined and are in process of investigation.

- Kennametal, Latrobe, PA., has been visited by MRC personnel and hard surface coatings (e.g. diamond, cubic boron nitride have been discussed. Current interactions have included use of the MRC's FTIR to examine cubic boron nitride prepared at Kennametal. In addition, a major collaborative proposal with Kennametal was prepared, and another with Kennametal and other partners from Diamond-X, Pennsylvania State University, and Northwestern University is in preparation.

- Some of the work on metal matrix composites involves studies on an alloy (X8019) obtained from Alcoa Technical Center. Results from these investigations have been made available to Alcoa.

- Studies of the oxidation resistance of low sulfur nickel base alloys has involved the participation of Dr. James Smialek from NASA Lewis, Cleveland. A paper based on this cooperative effort has been published.

- Investigations of titanium matrix composites have used alloys supplied by Paul Smith, Materials Directorate, WPAFB. A number of technical discussions have transpired about the results obtained in these studies. In order to examine oxygen embrittlement in some of these alloys, measurements using a nanoindenter at Rockwell International Corp., Science Center, are on-going.

- Some of the ceramic-matrix composites (e.g. $MoSi_2$ with SiC, Al_2O_3 or TiB_2) were obtained from Martin Marietta. Results from these studies will be given to Martin Marietta.

VI.2 Internal Collaborations

- Professor Hercules and his associates from the Chemistry Department and Professor Eror of Materials Science and Engineering have collaborated on research into and in the preparation of proposals on Catalysts for the Destruction of Chemical Warfare Agents and Environmental Pollutants.

- Professors Weber and Hamilton of the Department of Chemistry and Professor Beckman of Chemical Engineering have led the preparation of

a proposal on Chemically Activated Smart Polymeric Systems. This effort also had the participation of Professor Hercules (Chemistry) and Professor Balazs (Materials Science and Engineering).

- Collaborative research programs were initiated between:
  - Professors Rob Coalson and Sanford Asher from the Chemistry Department and Anthony Duncan from the Physics Department in the Crystalline Colloidal Array Program.
  - Professors Rob Coalson (Chemistry Department) and Dietrich Langer (Electrical Engineering) and Anthony Duncan (Physics) and John Hurley (Math at Hampton University) on propagation and switching in multiquantum well waveguides.
  - Professor Asher's group has initiated a research program with Mine Safety Appliances Company towards developing laser eye protection equipment for military applications.
  - Professor Asher (Chemistry Department) and Professor Pettit (Materials Science Department) have been collaborating for two years on a joint research program with Westinghouse Corporation, in the investigation of the growth and properties of diamond film. Joint publications have resulted from this effort.
  - Professor Joel Falk (Electrical Engineering Department), Professor Asher (Chemistry Department), and Professor R. Patel (Chemistry Department, Clarkson University) have been collaborating in a program to create enhanced nonlinear materials by the use of metal colloids in contact with CdS and CdSe quantum dots.
  - Professors D. Langer (Electrical Engineering Department) and J. Cooper (Chemistry Department) have collaborated in a program to create volatile Er complexes for CVD.
  - Professors Mike Hopkins and K.Jordan (Chemistry Department) have collaborated on theoretical calculations for determining the structure, optical and nonlinear properties of tungsten acetyleneorganometallics being synthesized.
  - Professor Meier (Materials Science Department) and Professor Hercules (Chemistry Department) have collaborated in investigating surface reactions on $MoSi_2$ and TiAl.

VI.3 Seminars and Workshops

An active program of seminars has been a feature of the two years of the Center's operation. Speakers from industry, government and academia have been brought in to interact with Center scientists, to exchange ideas, and to stimulate new collaborations as well as to open new directions and extensions of on-going research. Several examples of these seminars are on subsequent pages of this report.

In addition to the seminar program, several focussed workshops have been held in areas such as Chalcopyrites and topics dealing with Personnel Protection. Examples of the agendas of such meetings are also appended.

University of Pittsburgh
231 Benedum Engineering Hall
Pittsburgh, PA 15261

MATERIALS RESEARCH CENTER SEMINAR

SPEAKER : **Dr. Joseph Perry**
Technical Group Supervisor
The Jet Propulsion Laboratory
California Institute of Technology
Pasadena, California

DA : **November 3, 1992**

TIME : **3:00 P.M.**

PLACE : **1175 Benedum Engineering Hall**

NONLINEAR POLARIZATION OF SYMMETRIC AND ASYMMETRIC POLYMETHINE DYES

ABSTRACT

Measurements of the nonlinear polarizabilities of polymethine molecules indicate that bond length alternation is a key structural parameter affecting the magnitude and sign of molecular nonlinear polarizabilities. The third-order polarizabilities, g, of polyene, donor-acceptor substituted polyene, and cyanine molecules have been measured using third harmonic generation techniques. Whereas polyenes exhibit positive γ values and symmetric cyanines show negative γ values, donor acceptor substituted polyenes exhibit γ that can vary from positive to negative depending on the degree of charge transfer polarization, which in turn depends on donor-acceptor strength and solvent polarity. Electronic absorption, Raman spectroscopy and x-ray crystallographic studies provide evidence that connects the charge transfer polarization of donor-acceptor polyenes to a reduction in bond length alternation, i.e. their equilibrium structure becomes more cyanine-like upon polarization. These studies provide insight into how to optimize γ in a positive or negative sense for conjugated molecules of a given length. This is of relevance to development of materials with large third-order susceptibilities $\chi^{(3)}$. The results will be related to an interference between various terms of a simple three-state model for nonlinear polarizability.

University of Pittsburgh
231 Benedum Engineering Hall
Pittsburgh, PA 15261

MATERIALS RESEARCH CENTER SEMINAR

SPEAKER : **Dr. John A. Shelnutt**
Fuel Science Dept 6211
Sandia National Laboratories
Albuquerque, NM 87185

DATE : **January 11, 1993**

TIME : **3:00 P.M.**

PLACE : **1175 Benedum Engineering Hall**

CATALYST DESIGN USING MOLECULAR MODELING METHODS

ABSTRACT

Computer-aided molecular design methods are used (1) to tailor catalytic sites that possess a binding site for a small substrate molecule like CO_2 and methane and (2) to engineer the electronic properties of the metal atom at the catalytic site. The goal is to design a cavity, adjacent to a catalytic metal center, into which the substrate will selectively bind through only non-bonding interactions with the groups lining the binding pocket. Molecular orbital calculations are used to determine structural effects on the electronic properties. Porphyrins are used as a basic molecular structure, to which substituents are added to construct the binding pocket. The conformations of these highly-substituted porphyrins are predicted using molecular mechanics calculations that employ a force field that gives accurate predictions for metalloporphyrins (J.Am.Chem. Soc. 1991, 113, 4077; 1992, 114, 9859). In the calculations, the substituents are varied to control the size, shape, and charge-distribution of the groups surrounding the cavity to provide molecular selectivity. Dynamics and energy-minimization calculations of substrate molecules bound to the cavities of several of the designed catalysts indicate enhanced substrate binding affinity. Promising candidate molecular catalysts are then synthesized and characterized. The general catalyst design methodology will be discussed and recent application of the design methods to alkane-oxidation catalysis will be presented, including catalytic activity measurements for a series of iron fluorododecaphenylporphyrins.

Work at Sandia National Laboratories supported by U.S. Department of Energy Contract DE-AC04-76DP00789.

University of Pittsburgh
231 Benedum Engineering Hall
Pittsburgh, PA 15261

REVISED NOTICE

MATERIALS RESEARCH CENTER SEMINAR

PLEASE NOTE REVISED TIME FOR SEMINAR

SPEAKER : **Dr. Theodore Nicholas**
Wright Laboratories Materials Directorate
Wright-Patterson AFB
Dayton, Ohio 45433

DATE : **February 23, 1993**

TIME : **NEW TIME 3:45**

PLACE : **1175 Benedum Engineering Hall**

ELEVATED TEMPERATURE FATIGUE OF METAL MATRIX COMPOSITES

ABSTRACT

Experimental observations of the response of titanium matrix, silicon carbide reinforced composites to thermal, mechanical, and thermomechanical fatigue are presented. Thermal residual stresses developed during cooldown from the processing temperature are shown to be significant in this class of materials, sometimes exceeding the yield stress in the matrix material. The fatigue life is modeled using linear summation concepts based on damage to the fiber or the matrix. The damage, in turn, is based on computations of the micromechanical stresses in the fiber and the matrix. In addition, maximum and minimum strain and stiffness during a fatigue test are considered in models which account for the cumulative damage which occurs under thermomechanical fatigue. The modeling is directly related to observed modes of failure which include creep and plasticity in the matrix, matrix cracking, and fiber breakage. Results are presented for three different play layups, [0], [0/90], and [0/±45/90]. The effect of lateral strain coupling between plies is illustrated through computations involving a fully coupled theory using FEM and an approximate, partially coupled theory referred to as S-CAN, a simplified composites analysis.

University of Pittsburgh
231 Benedum Engineering Hall
Pittsburgh, PA 15261

MATERIALS RESEARCH CENTER SEMINAR

SPEAKER : **Dr. Peter M.A. Sherwood**
Department of Chemistry
Kansas State University
Manhattan, Kansas 66506

DATE : **April 23, 1993**

TIME : **11:00 A.M.**

PLACE : **823 Benedum Engineering Hall**

CARBON FIBER SURFACE OXIDATION - THE KEY TO ADVANCED COMPOSITES

ABSTRACT

Carbon fibers are finding increasing application in making various composites with special properties. It is found that such composites have properties that can be markedly effected by the carbon fiber surface. The effects of surface modification by electrochemical and plasma oxidation will be discussed and the surface chemical changes described. It will be seen that the interaction of the matrix with the fiber surface is a subtle mixture of physical and chemical effects. Surface studies with core and valence band X-ray photoelectron spectroscopy (XPS) and other techniques will be described. Valence band X-ray photoelectron spectroscopy will be shown to have the ability to distinguish some subtle chemical differences, and the combination of XPS data from different regions will be shown to indicate differences in chemical composition with depth into the surface. Evidence will be provided for chemical reactions between treated fibers and a coating of resin or polymer. A special cell for monitoring high temperature carbon oxidation will be described, with examples of oxidation protection by aluminum oxide and magnesium oxide films.

****

Peter Sherwood's research group has been involved in primarily X-ray photoelectron spectroscopy (XPS) of inorganic solids and surfaces with particular interest in electrode surfaces, corrosion systems, and material surface properties (especially carbon fiber surfaces). Professor Sherwood is Director of the "NSF Materials Synthesis and Processing Project" involving 18 faculty at Kansas State University, the University of Kansas and Wichita State University. He has more than 115 publications.

University of Pittsburgh
231 Benedum Engineering Hall
Pittsburgh, PA 15261

MATERIALS RESEARCH CENTER SEMINAR

SPEAKER : Professor Tsuneo Okubo
Department of Polymer Chemistry
Kyoto University
Kyoto, Japan

DATE : August 20, 1993

TIME : 3:30 P.M.

PLACE : Room 132
Chevron Building

GIANT COLLOIDAL CRYSTALS

ABSTRACT

Giant colloidal crystals can be prepared from charged spherical polymer colloids. The crystals self-assemble in cubic arrays where the particles are spaced by many particle diameters. These crystals nucleate at only a few sites and slowly grow to macroscopic dimensions. The properties of this system will be discussed.

University of Pittsburgh
231 Benedum Engineering Hall
Pittsburgh, PA 15261

MATERIALS RESEARCH CENTER SEMINAR

SPEAKER : **Owen Richmond**
Alcoa Technical Center
100 Technical Drive
Alcoa Center, PA 15069

DATE : **February 24, 1994**

TIME : **3:30 P.M.**

PLACE : **823 Benedum Hall**

A FRAMEWORK FOR LIFE CYCLE PRODUCT DESIGN BASED UPON MULTIPLE SCALES OF STRUCTURE AND EVOLVING PRODUCT STATES

ABSTRACT

This talk will describe a framework for designing material products concurrently with their component materials and manufacturing processes. The basis for connecting product performance with material manufacture is the concept of evolving product states which begin during material component manufacture and continue during product use. Product states include accumulating material structure as well as stress and temperature fields. They also include accumulating costs providing a basis for design decisions based on both materials technology and cost. The basis for connecting product and process performance to material composition is the homogenization of material performance models across a hierarchy of dimensional scales from angstroms to meters.

****

****

Dr. Richmond is currently Corporate Fellow and Director of Fundamental Research at Alcoa Technical Center. He received his undergraduate degree in General Engineering, and has graduate degrees in Structural Engineering and Theoretical and Applied Mechanics from the University of Illinois and the Pennsylvania State University respectively. He spent 25 years at the U.S. Steel Research Center performing research on mechanical behavior of materials and materials processing, where he organized and headed the Mechanical Sciences Division. For the past 10 years he has been at Alcoa where he has continued to perform research and organized and directed a fundamental research program. Recent honors include the Frary Award for sustained technical contributions at Alcoa, the Applied Mechanics Award from ASME, Carnegie Lecturer from ASM, Pittsburgh and G.R. Speich Memorial Lecture from ASM, Chicago.

University of Pittsburgh
231 Benedum Engineering Hall
Pittsburgh, PA 15261

MATERIALS RESEARCH CENTER SEMINAR

SPEAKER : **Paul Fleitz**
Systran Corporation
Dayton, Ohio

DATE : **March 23, 1994**

TIME : **4:00 P.M.**

PLACE : **274 Benedum Hall**

CHARACTERIZATION OF NONLINEAR OPTICAL PROPERTIES USING THE DEGENERATE FOUR-WAVE MIXING AND Z-SCAN TECHNIQUES

ABSTRACT

At the Laser Hardened Materials branch of the Materials Directorate at Wright-Patterson Air Force Base, new materials with potential applications for laser eye protection are being studied. One approach involves using materials with large nonlinear optical properties as passive optical limiters. In this presentation, we will introduce optical limiting and describe the techniques that are used to characterize the nonlinear optical properties of materials. The two techniques that will be discussed are Degenerate Four-Wave Mixing and Z-scan.

Nanosecond Degenerate Four-Wave Mixing (DFWM) has been used to investigate the nonlinear optical properties of Buckminsterfullerene and diphenyl polyenes. The Z-scan technique has been used to investigate the nonlinear absorption of a series of conjugated organic materials.

****
****

Paul Fleitz's Ph.D. is in Physical Chemistry from the University of Cincinnati. At a post-doctoral position at Syracuse University he measured the second-order nonlinear optical properties of biological and organic materials. Since 1990 he has been at the Materials Laboratory at Wright-Patterson Air Force Base investigating the nonlinear optical properties of organic materials.

Workshop on Chalcopyrites, Problems and Opportunities

PLACE : University of Pittsburgh, Benedum Engineering Hall (BEH), 3900 O'Hara St.

DATES : June 22-23, 1992

Sponsored by the
Materials Research Center
and
Department of Electrical Engineering
(412-624-9663) Dietrich Langer

Monday, 22 June (room 1175 BEH)

9:00 - 9:15	***Opening Remarks and Introductions*** Dietrich Langer (Dept. of EE, Univ. of Pittsburgh) Melvin Ohmer (Wright Laboratory)
9:15 - 9:30	***Overview of Applications of Chalcopyrites*** Joel Falk (Dept. of EE, Univ. of Pittsburgh)
9:30 - 10:30	***II-IV-V_2 Semiconductors and their Potential Applications*** Yurii V. Rud (A.F. Ioffe Phys. -Techn. Inst., St. Petersburg)
10:30 - 11:00	***LEC Growth and Characterization of $ZnGeP_2$*** H.M. Hobgood (Westinghouse Sci. & Techn. Center)
11:00 - 11:30	***Hetero-Epitaxial Growth by MOCVD of Chalcopyrites*** Michael Timmons (Research Triangle Institute)
11:30 - 12:00	***Photoemission of Polarized Electrons from II-IV-V_2 Chalcopyrite Photocathodes*** Charles Sinclair (CEBAF)
12:00 - 1:00	Lunch
1:00 - 2:00	***Raman Spectroscopy in the Study of II-IV-V_2 Semiconductors*** B. Bairamov (A.F. Ioffe Phys. - Techn. Inst., St. Petersburg)
2:00 - 3:00	***Precise Determination of Stoichiometry and the Effects of Neutral Defects*** Nicholas Eror (Dept. Mat. Sci. & Engin., Univ. of Pittsburgh)
3:00 -	***Discussions*** in Room #240 BEH

Tuesday, June 23 (room 240 BEH)

9:00 -	***Discussions*** (details to be decided: afternoon of June 22)

UNIVERSITY OF PITTSBURGH

MATERIALS RESEARCH CENTER

Agenda for Visit of

DR. MATTHEW HERZ
ASSOCIATE TECHNICAL DIRECTOR
U.S. ARMY NATICK LABORATORIES, NATICK, MASS.

Meeting in Dean's Conference Room
School of Engineering, 240 Benedum Hall

22 July 1992

8:45 A.M.	-	Coffee and Introductions
9:00 A.M.	-	The Soldier Integrated Protective Ensemble (SIPE) Program - Dr. M. Herz, U.S. Army Natick Laboratories
10:00 A.M.	-	Break
10:15 A.M.	-	Catalytic Materials for Nerve Gas Destruction - Professor D.M. Hercules, Department of Chemistry
10:50 A.M.	-	Research Directed Toward Sensors and Smart Materials - Professor S.G. Weber, Department of Chemistry
11:25 A.M.	-	Optical Filtering Devices Based Upon Self-Assembled Colloidal Particles - Professor S.A. Asher, Department of Chemistry
12:00 P.M.	-	Chemical Sensor Development at Westinghouse Science and Technology Center - Dr. R.E. Witkowski, Westinghouse STC
12:20 P.M.	-	Lunch
1:15 P.M.	-	Tour of Research Facilities
3:00 P.M.	-	Departure of Dr. Herz

VII. RESEARCH PERSONNEL, PUBLICATIONS AND PATENTS

Research Personnel

Over the period of the AFOSR Grant, twenty-nine research projects have been led by twenty-seven principal investigators, from the School of Engineering and the Faculty of Arts and Sciences. All told, 54 faculty members took part in the program. They represented nine Departments of the University of Pittsburgh (two from the Medical Center), five from other universities in the United States, four from overseas universities, and two from industry (the latter are also adjunct faculty members).

Seventy-three graduate students have been supported, in whole or in part, by funds from the Center. Of these, nine have completed Ph.D. degrees, and five have finished at the Master's degree level.

Thirty-four post-doctoral scientists have received training through the research program. Twenty-two undergraduate students have been involved in research programs over summer periods as well as during the academic years of the Center's operation.

Among the participants, the MRC support has included a faculty member and an undergraduate students from two historically black colleges. The faculty member still has an active collaboration with an MRC principal investigator in the Chemistry Department, and the student is just completing her freshman year in the graduate program in Electrical Engineering at Pitt.

A listing of faculty, post-doctoral researchers, graduate students, and undergraduate students who have taken part in the research program is provided in Appendix I.

Publications and Patents

Over the two-year period of Air Force Grant Support, 82 publications have appeared in the open literature or are in press. Another twenty papers have been submitted or are in preparation. A member of presentations at professional society meetings are on related occasions have also been made.

Four patent actions have also been instituted, based on MRC support.

VIII. FUTURE PLANS FOR THE MRC

The foregoing sections of this report have detailed important progress, key accomplishments, (some of them have been breakthroughs), significant collaborations, and educational aspects of the approximately two years of operation of the Materials Research Center. It is clear that the individual investigations conducted with Center support have been highly successful. Many follow-on research grants and contracts have been initiated and catalyzed with the help of MRC support. In order for the Center to achieve specific identification for excellence, program focus is being developed. Our focal areas build from some of the critical talents that we have in place within the Center and will incorporate new segments within and outside the University of Pittsburgh. They represent areas of importance that address defense sector, industrial, and societal needs. The Materials Research Center's future plans will focus upon the following areas:

1. High Performance Durable Materials - This area of effort recognizes the needs of all sectors of the national economy for life extension of a wide variety of important assets, ranging from aircraft, to powerplants, to manufacturing equipment, to bridges, and to implants in the human body. We plan to utilize nationally recognized scientific staff of the School of Engineering and the Faculty of Arts and Sciences as well as other sectors of the University of Pittsburgh in collaborative efforts. Those efforts, with outside industrial organizations, government and other laboratories, and other universities will concentrate on problem areas in manufacturing, transportation, power generation, defense, and health care.

2. Catalysis and Other Materials Approaches to Environmental Issues - Both the Faculty of Arts and Sciences and the School of Engineering have strong interests, national reputations, and activities in areas such as the neutralization and destruction of hazardous substances, and materials approaches to prevent introduction of harmful and unacceptable products into the air, land, or ocean environments, including subjects such as catalytic routes, and bioprocessing. Other related topics, e.g., bioremediation, green process design, ultrahigh temperature processing, can be addressed within the Center, or by external partners.

3. Novel Concepts - This area can be considered a concept incubator scheme. It includes subjects such as nanostructural materials for optoelectronic applications (such as extensions of work on the crystalline colloidal arrays) and ceramics with high toughness, and smart materials.

Undergirding these three areas of focus are superb capabilities and world-class facilities within the MRC in characterization of materials, and superb talents in the computation and modelling aspects of materials science.

The future directions of the Center will entail heavy emphasis on outside collaborations, with industries both large and small, with other universities, with outside institutions such as the National Laboratories, Government Laboratories, and with the Commonwealth of Pennsylvania. Joint ventures with all of these sectors have already begun.

APPENDIX I

Faculty, Post-Doctoral, Graduate, and Undergraduate Students

Faculty Investigator	Department
J.S. Schultz*	Chemical Engineering
A.J. Russell*	Chemical Engineering
S.G. Weber*	Chemistry
A.D. Hamilton*	Chemistry
G. Barrioneuvo*	Behavioral Neuroscience
T.W. Berger*	Behavioral Neuroscience
D. Rohrbach	Chemical Engineering
R. Frist	West Virginia University
G.H. Meier*	Materials Science and Engineering
N. Birks	Materials Science and Engineering
F.S. Pettit*	Materials Science and Engineering
S.A. Asher*	Chemistry
J.T. Yates, Jr.*	Chemistry
W.A. Soffa*	Materials Science and Engineering
V. Radmilovic	University of Belgrade
A.J. DeArdo*	Materials Science and Engineering
C.I. Garcia	Materials Science and Engineering
A.K. Lis	Technical University of Czestochowa, Poland
A.C. Balazs*	Materials Science and Engineering
J.T. Lindt*	Materials Science and Engineering
R. Coalson*	Chemistry
S. Jagannathan	Chemistry
R. Kasavamoorty	Chemistry
D.W. Langer*	Electrical Engineering
N.J. Cooper*	Chemistry
R.A. Butera	Chemistry
J.R. Blachere	Materials Science and Engineering
J. Hurley	Hampton College
J. Falk*	Electrical Engineering
R. Patel	Clarkson University
D.W. Pratt*	Chemistry
R. Ulsh	University of Pittsburgh, Johnstown
P.P. Phule*	Materials Science and Engineering
A. Duncan	Physics
V.M. Miskowski	California Institute of Technology
A. Senatalar	Technical University of Istanbul
J. Lercher	Technical University of Vienna
D. Rohrbach	Dental Medicine

M.D. Hopkins*	Chemistry
K.D. Jordan*	Chemistry
A.G.U. Perera*	Physics
R.P. Devaty	Physics
M.H. Hercules*	Chemistry
W.K. Hall	Chemistry
M. Houalla	Chemistry
J.G. Goodwin*	Chemical Engineering
R. Oukaci	Chemical Engineering
G. Marcelin	Chemical Engineering
N. Eror	Materials Science and Engineering
V.A. Richards	Westinghouse S & T Center
W.J. Choyke*	Physics
J.S. Schultz	Pathology
S.K. Arora	Crystallography

Postdoctoral Researchers

Student	US Citizen	MRC Supervisor/Investigator
Douglas Rishel	Yes	G. Meier
Thomas Issaevitch	Yes	A. Balazs
Andreas Kogelbauer	No	J. Goodwin
Alan Walsh	No	R. Coalson
Subramaniam	No	R. Coalson
Kwan Young Lee	No	D. Hercules
Andrew Proctor	No	D. Hercules
Shufang Luo	No	S. Weber
Steve Walthan	Yes	A. Hamilton
Kyungsun Kim	No	K. Jordan
Keija Wan	No	J. Yates
Song-Yuan Chang	No	S. Asher
Hedi Mattorasis	No	S. Asher
Kesavamoorthy Rasu	No	S. Asher
Seshadri Jagannathan	No	S. Asher
Xiao-Ming Fang	No	U. Perera
Xiao-Ping Xie	No	G. Barrioneuvo
D. Monceau	No	G. Meier
V. Ukraintsev	No	J. Yates
P. Pauli	No	A. DeArdo
S. Van Arman	Yes	A. Hamilton
H. Rahman	No	D. Langer
A. Ali	No	D. Langer

*Principal Investigator

Student	US Citizen	MRC Supervisor/Investigator
W. Li	No	A. Balazs
D. Gerasppe	No	A. Balazs
C. Yeung	Yes	A. Balazs
Albert Tse	No	J. Asher
J. Go	No	D. Pratt
Andrew Held	Yes	D. Pratt
Jie Yu	No (Perm Res)	M. Hopkins
Vadim Kazansky	No	D. Hercules
Yuanhua Shao	No	S. Weber
Zhen Yang	No	A. Russell
Ronald Langdon	Yes	G. Barrionuevo

Graduate Students

Student	US Citizen	MRC Supervisor/Investigator
Robert Lizewski	Yes	F. Pettit
Rocco Cerchiara	Yes	F. Pettit
James Rakowski	Yes	G.H. Meier
Ben Lander	Yes	T. Lindt
Tom MacNamara	Yes	N. Eror
Aristolis Nikolopoulos	No	J. Goodwin
Y. Shi	No	J. Falk
X. Hua	No	J. Falk
M. Rao	No	W. Soffa
Tom Fitsoris	Yes	W. Soffa
Patricia Leach	Yes	J. Cooper
Sijoon Lee	No	J. Cooper
Sherri Lovelace	Yes	J. Cooper
Jane Aigler	Yes	D. Hercules
Ralph Mutschler	Yes	A. DeArdo
Nather Dahesh	No	A. DeArdo
Sandeep Betarbet	No	U. Perera
Daphne Curtis	Yes	R. Coalson
Frederick Hann	Yes	R. Coalson
Dhruv Pant	No	R. Coalson
James Zahorchak	Yes	R. Coalson
Deborah Evans	No	R. Coalson
Mary Eberhardt	Yes	D. Hercules
Tamara Radetic	Yes	W. Soffa
Hideyuki Okumura	No	W. Soffa
Erkang Fan	No (Perm.Res.)	D. Hamilton
Abdullah Zafar	No	A. Hamilton
Dana Nachtigallova	No	K. Jordan
Pamela Bolkovac	Yes	K. Jordan
Peter Nachtigall	No	K. Jordan

Student	US Citizen	MRC Supervisor/Investigator
Chung-Jung Tsai	No	K. Jordan
Marc Pedulla	Yes	K. Jordan
Blaise Champagne	Yes	D. Pratt
James Pfanstiel	Yes	D. Pratt
David Plusquellic	Yes	D. Pratt
S. Humphrey	Yes	D. Pratt
Tim Pollagi	Yes	M. Hopkins
Tim Stoner	Yes	M. Hopkins
Xingguo Chen	No	S. Asher
D. Berztiss	Yes	G. Meier
C. Stinner	Yes	G. Meier
M. Stasik	Yes	G. Meier
C. Sarioglu	No	F. Pettit
J.E. Spowart	No	F. Pettit
Richard Bormett	Yes	S. Asher
R. Amata	Yes	J. Yates
K. Xu	No	J. Hercules
M. Hua	No	A. DeArdo
P.K. Harm	Yes	A. Balazs
D.J. Irvine	Yes	A. Balazs
M. Fasolka	Yes	A. Balazs
Yabo Li	No	D. Langer
H.S. Chu	No	D. Langer
Y. Liu	No	P. Phule
Bradley Lewis	Yes	M. Hopkins
Inkyung Lee	No	N.J. Cooper
Ralph Feldman	Yes	K. Jordan
Michael F. MacMillan	Yes	W. Choyke
Igor Linkov	No	W. Choyke
M. Yoganathan	No	W. Choyke
Patricia A. Leach	Yes	D. Hercules
Thomas McNamara	Yes	N. Eror
T. Palucka	Yes	N. Eror
Kevin Vaughan	Yes	J. Schultz
Darrell Williams	Yes	A. Russell
Mark W. Fleck	Yes	G. Barrionuevo
Shalabh Tandom	No	S. Asher
Zhi Jun Wu	No	S. Asher
Guisheng Pan	No	S. Asher
John Holtz	Yes	S. Asher
Nanjun Cho	No	S. Asher
Stewart Getzow	Yes	S. Asher
Xun Meng	No	S. Asher

Undergraduate Students

Gregory Bijak	Peter Magers
James Chronister	A. Prabhaharan
Allen Householder	Ian Bjorhovde
Molly McKernan	J.L. Cherpes
Hang Zhou	S.A. DeForest
James Knicely	S. Lauer
Kevin John	C.D. Rigone
Alan J. Mirarchi	Chris Switala
Jennifer Spear	Jane Valenta
Michelle Rouse	Beth Wise
Christopher Cunningham	J. Huey

Degrees Granted

A. Held	Ph.D.	Chemistry
E. Fan	Ph.D.	Chemistry
A. Nikolopoulos	Ph.D.	Chemical Engineering
D.F. Plusquellic	Ph.D.	Chemistry
T.C. Stoner	Ph.D.	Chemistry
T.P. Pollagi	Ph.D.	Chemistry
M.-J Hua	Ph.D.	Materials Science and Engineering
R. Mutschler	M.S.	Materials Science and Engineering
M. Carper	M.S.	Materials Science and Engineering
R. Lizewski	M.S.	Materials Science and Engineering
T. McNamara	M.S.	Materials Science and Engineering
A. Ali	Ph.D.	Electrical Engineering
H. Rohman	Ph.D.	Electrical Engineering
Y. Li	M.S.	Electrical Engineering

APPENDIX II - PUBLICATIONS

A. Published Papers, In Press

1. X. Xie, T.W. Berger, and G. Barrionuevo, "Isolated NMDA Receptor-Mediated Synaptic Responses Express Both LTP and LTD", J Neurophysiol., 67: 1009-1013 (1992).

2. M.W. Fleck, D.A. Henze, G. Barrionuevo, and A.M. Palmer, "Aspartate and Glutamate Mediate Excitatory Synaptic Transmission in Area CA1 of the Hippocampus", J. Neurosci. 13(9), 3944-3955 (1993).

3. R.B. Langdon, J.W. Johnson, and G. Barrionuevo, "Asynchrony of Mossy Fiber Inputs and Excitatory Postsynaptic Currents in Rat Hippocampus", J. Physiol (London), 472:157-176 (1993).

4. S. Kamat, J. Barrers, E.J. Beckman, and A.J. Russell, "Biocatalytic Synthesis of Acrylates in Organic Solvents and Supercritical Fluids," Biotechnol. Bioeng., 40 158-166 (1992).

5. J.C. Zahorchak R. Kesavamoorthy, R.D. Coalson and S.A. Asher, "Melting of Colloidal Crystals: A Monte Carlo Study", J. Chem. Phys. 96, 6873-6879 (1992).

6. R. Kesavamoorthy, S. Tandon, S. Xu, S. Jagannathan and S.A. Asher, "Self Assembly and Ordering of Electrostatically Stabilized Silica Suspensions", Colloid and Int. Sci. 153, 188-198 (1992).

7. S.A. Asher, R. Kesavamoorthy, S. Jagannathan, P. Rundquist, "New Nonlinear Bragg Diffraction Devices", SPIE Vol 1626, Nonlinear Optics III, 238-241 (1992).

8. R. Kesavamoorthy, M.S. Super and S.A. Asher, "Nanosecond Photothermal Dynamics in Colloidal Dispersions, J. Appl. Phys. 71, 1116-1123 (1992).

9. R.D. Coalson and A. Duncan, "Systematic Ionic Screening Theory of Macroions", J. Chem. Phys. 97, 5653-5661 (1992).

10. A.M. Walsh and R.D. Coalson, "Redfield Theory is Quantitative for Coupled Harmonic Oscillators", Chem. Phys. Lett. 198:293 (1992).

11. A.M. Walsh and R.D. Coalson,"Lattice Field Theory for Spherical Macroions in Solution: Calculation of Equilibrium Pair Correlation Functions", J. Chem. Phys. 100, 1559 (1994).

12. J.C.S. Wu, R. Oukaci, and J.G. Goodwin, Jr., "The Effect of Dealumination on Zeolite-Supported Ru Catalysts", Journ. of. Catalysis, 142, 531-539 (1993).

13. P. Nachtigall and K.D. Jordan, "Theoretical Study of the Low-Lying Triplet and Singlet States at the Triplet Equilibrium Geometry, J. Am. Chem. Soc., 115, 270 (1993).

14. J. Nash, P. Dowd, and K.D. Jordan, "Theoretical Study of the Low-Lying Triplet and Singlet States of Diradicals: Prediction of Ground State Multiplicities in Cyclic Analogs of TME, J.Am. Chem. Soc., 114, 10071 (1993).

15. S.H. Park, M.P. Casey, and J. Falk, "Nonlinear Optical Properties of CdSe Quantum Dots", J. Appl. Phys. 73(12), 8041-8045 (1993).

16. Y. Shi, J. Falk, R. Patel, "Highly Nonlinear Semiconductor-Metal Composites", Bulletin of the American Physical Society, Program of the 1994 March Meeting, Vol. 39, No. 1, March (1994).

17. J. Manna, S.J. Geib, M.D. Hopkins, "π-Conjugated Metallabutadiyne Complexes: Synthesis, Structure, and Bonding", J. Am. Chem. Soc.,114, 9199, (1992).

18. T.P. Pollagi, J. Manna, T.C. Stoner, S.J. Geib, M.D. Hopkins, "Conjugated Complexes and Polymers Derived from Metal - Alkylidyne Building Blocks", in Transition Metal Carbyne Complexes, F.R. Kreissl, Ed.: Kluwer Academic Publishers: Dordrecht, The Netherlands, p. 71 (1993).

19. J. Manna, L.A. Mlinar, R. J. Kuk, R. F. Dallinger, S. J. Geib, M. D. Hopkins, "Methylidyne Complexes: Structures, Spectra, and Bonding" in Transition Metal Carbyne Complexes, F. R. Kreissl, Ed.; Kluwer Academic Publishers: Dordrecht, The Netherlands, p. 75, (1993).

20. T. P. Pollagi, S. J. Geib, M. D. Hopkins, "Molecular and Electronic Structures of Conjugated Metal-Alkylidyne Polymers" Division of Polymeric Materials: Science and Engineering Proceedings, 69, 157 (1993).

21. T. C. Stoner, W. P. Schaefer, R. E. Marsh, M. D. Hopkins, "Synthesis and Characterization of $M_2(CCR)_4(PMe_3)_4$ Dimetallapolyynes", J. Cluster Sci., 5, 107, (1994).

22. P. P. Phulé, R.A. Russell, and M. Carper, " Preparation of PZT Films and Tantalum Zirconate Powders Using Chemical Techniques",

Ceramic Transactions, Vol.32, Dielectric Ceramics (Ed. by K.M. Nair and A.S. Bhalla), p. 333-338, (1993).

23. M.D. Carper and P. P. Phulé, "Preparation of oriented $PbTiO_3$ Thin Films Using a Spin-On Sol-Gel Process", Applied Physics Letters, 63 (2), 153 (1993).

24. T.A. Deis and P.P. Phulé, "Synthesis of Lithium Tantalate Whiskers fromMetal Alkoxide Derived Gels", Mat. Res. Bull., Vol. 28, pp. 167-171 (1993).

25. Issaevitch, T.A., Jasnow, D., and Balazs, A.C., "Copolymer Adsorption onto Regular Surfaces", J. Chem. Phys. 99:8244 (1993).

26. P. Pouly, M.-J. Hua, C.I. Garcia, A.J. DeArdo "Isothermal Transformation Behavior of Near-Gamma TiAl Alloys", Scripta Metallurgica, vol. 29, pp. 1529-1534 (1993).

27. M.-J. Hua, C.I. Garcia, A.J. DeArdo "Chemical Twinning in the $Ti_4C_2S_2$-TiS System", G.W. Bailey and C.L. Rieder, Eds., Proc. 51st Annual Meeting of the Microscopy Society of America, pp. 744-745 (1993).

28. M.-J. Hua, C.I. Garcia and A.J.DeArdo "Multi-phase Precipitates in Interstitial-Free Steels", Scripa Metallurgica, vol. 28, pp. 973-978 (1993).

29. J.M. Aigler, J.L. Brito, P.A. Leach, M. Houalla, A. Proctor, N.J. Cooper, W.K. Hall, D.M. Hercules, "ESCA Study of "Model" Allyl-Based Mo/SiO_2 Catalysts", J. Phys. Chem., ***97***, 5699 (1993).

30. K.Y. Lee, M. Houalla, D.M. Hercules, W.K. Hall,"Catalytic Oxidative Decomposition of Dimethyl Methylphosphonate over Cu-Substituted Hydroxyapatite", J. Catal. ***145***, 223 (1994).

31. J.T. Lindt and A.K. Ghosh, "Blend Morphology Development in Screw Extruders", Special issue (in Japanese) on recent theoretical developments in Polymer Process Engineering, Japan Plastics, 43, 31 (1992).

32. J.T. Lindt and A.K. Ghosh, "Fluid Mechanics of the Formation of Polymer Blends", Polymer Engineering and Science, December (1992).

33. R.V. McVay, P. Williams, G.H. Meier, F.S. Pettit, University of Pittsburgh, and J.L. Smialek, NASA Lewis, "Oxidation of Low Sulfur Single Crystal Nickel Base Superalloys, pp. 807-816, Superalloys

1992, Editors, S.D. Antolovich, R.W. Stusried, R.A. Mackay, D.L. Anton, T. Khan, R.D. Kissinger, D.L. Klarstrom, The Minerals, Metals and Materials Society, Warrendale, PA (1992).

34. D.A. Bertiss, R.R. Cerchiara, E.A. Gulbransen, F.S. Pettit, and G.H. Meier, "Oxidation of $MoSi_2$ and Comparison to Other Silicide Materials", Mater. Sci. + Eng., A155, 165 (1992).

35. J.S. Schultz, " Fiber Optical Methods for bioprocess Monitoring - Promises and Problems. Proceedings 9th International biotechnology Symposium. Harnessing Biotechnology for the 21st Century. Ed M. Ladish and A. Bose. Amer. Chem. Soc. pp 334-336 (1992).

36. J.S. Schultz, "The Use of Recognition Molecules in Biosensors. BioJapan '92, Yokohama. Symposium Proceedings. pp 339-347 (1992).

37. J.S. Schultz, and J.S. Schultz, "Applications of Combinatorial Libraries in Cellular Engineering. Proceedings of the 1st International Conference on Cellular Engineering. pp 73-74 (1992).

38. D.F. Plusquellic and D.W. Pratt, "Exploiting Quantum Interference Effects for the Determination of the Absolute Orientation of an Electronic Transition Moment Vector in an Isolated Molecule", J. Chem. Phys., 97, 8970 (1992).

39. A. Held and D.W. Pratt, "Hydrogen Bonding in Water Complexes. Structures of 2-Pyridone-H_2O and 2-Pyridone-$(H_2O)_2$ in Their S_o and S_1 Electronic States", J. Amer. Chem. Soc., 115, 9708 (1993).

40. S. J. Humphrey, D.W. Pratt, "High Resolution $S_1 \leftarrow S_0$ Fluorescence Excitation Spectra of Hydroquinone. Distinguishing the cis and trans Rotamers by Their Nuclear Spin Statistical Weights", J. Chem. Phys. 99(7), 5078-5086 (1993).

41. A. Held and D.W. Pratt, "Ammonia as a Hydrogen Bond Donor and Acceptor in the Gas Phase. Structures of 2-Pyridone - $(NH_3)_{1,2}$ in Their S_o and S_1 Electronic States", J. Amer. Chem. Soc., 115, 9718-9723, (1993).

42. S.J. Geib, C. Vincent, E. Fan, and A.D. Hamilton, "Selbstorganisation zu einer Helix durch Wasserstoffbrückenbindung" Angew. Chemie, 105, 83 (1993). "A Self-Assembling Hydrogen Bonded Helix" Angew. Chemie. Int. Ed., 32, 119 (1993).

43. E. Fan, S. A. Van Arman, S. Kincaid and Andrew D. Hamilton,

"Molecular Recognition: Hydrogen Bonding Receptors that Function in Highly Competitive Solvents" J. Am. Chem. Soc. 115, 369 (1993).

44. S. J. Geib, E. Fan, F. Garcia-Tellado, C. Vicent, and A. D. Hamilton, "Supramolecular Self-Assembly based on Directed Hydrogen Bonding' Polymer Preprints, 34, 106-107 (1993).

45. A. D. Hamilton, E. Fan, S. A. Van Arman, C. Vicent, F. Garcia Tellado, S. J. Geib, "Molecular Recognition. Design of New Receptors for Complexation and Catalysis" Supramolecular Chem. 1, 247-252 (1993).

46. J. Yang, E. Fan, S, J. Geib, and A. D. Hamilton, "Hydrogen Bonding Control of Molecular Self-Assembly: Formation of a 2+ 2 Complex in Solution and in the Solid State" J. Am. Chem. Soc. 115, 5314-5315 (1993).

47. S. Chatterjee, A.J. Russell, Determination of microscopic rate constants for subtilisin catalyzed transesterification in anhydrous environments, Biotechnol. Bioengin., 40, 1069-1077 (1992).

48. G.A. Ayala, S. Kamat, C. Komives, E.J. Beckman and A.J. Russell, Solubilization and activity of proteins in supercritical fluids. Annals New York Acad. Sci., 672, 283-293 (1992).

49. D.W. Pratt and L.H. Spangler, "Internal Rotation Dynamics from Electronic Spectroscopy in Supersonic Jets and Beams", in Jet Spectroscopy and Molecular Dynamics, ed. J. M. Hollas and D. Phillips, Chapman and Hall, Ltd., (1994).

50. G.H. Meier, F.S. Pettit, and S. Hu, "Oxidation Behavior of Titanium Aluminides" J. de Physique III, 3, 395-402 Dec. (1993).

51. R. Lizewski, G.H. Meier, F.S. Pettit, R. Bormet, S.A. Asher, University of Pittsburgh, J. Shuro and R. Witkowski. Science and Technology Center, Westinghouse Corp., "The Stability of Diamond Films in Oxygen at Temperatures between 400 - 700°C" in Proceedings of the 1992 Coatings for Advanced Heat Engines Workshop, August 3-6, pp. IV-11 -IV-25 (1992).

52. J. Rakowski, D. Monceau, F.S. PEttit and G.H. Meier, University of Pittsburgh, R.A. Perkins, Lockheed Palo Alto Research Lab "The Oxidiation and Embrittlement of α_2 (Ti_3Al) Titanium Aluminides", Microscopy of Oxidation 2 Proceedings of the Second International Conference on the Microscopy of Oxidation, March 29-31 pp. 476-487 (1993).

53. J.T. Lindt and A.K. Ghosh, "Blend Morphology Development in Screw Extruders", Special issue (in Japanese) on recent theoretical developments in Polymer Process Engineering, Japan Plastics, 43, 31 (1992).

54. J.T. Lindt and A.K. Ghosh, "Flow Mechanics of the Formation of Polymer Blends", Polymer Engineering and Science, December 1992.

55. G.H. Meier and F.S. Pettit, "High Temperature Corrosion of Intermetallics, Ceramics, and Carbon-Carbon Composites", to appear in Proc. of the 1992 Tri-Service Conference on Corrosion", U.S. Dept. of Defense (1992).

56. G.H. Meier and F.S. Pettit, "High Temperature Corrosion of Intermetallics, Ceramics, and Carbon-Carbon Composites", to appear in Proc. of the 1992 Tri-Service Conference on Corrosion", U.S. Dept. of Defense (1992).

57. P.P. Phule', "Sol-Gel Synthesis of Ferroelectric Lithium Tantalate Ceramics: FTIR Investigation of the Molecular Modification of Tantalum Ethoxide", J. Materials Research, 8:2, 334-338 (1993).

58. T.A. Deis and P.P.Phule', "Synthesis of Lithium Tantalate Whiskers from Metal Alkoxide Derived Gels", Mat. Res. Bull., Vol 28, 167-171 (1993).

59. H.U. Rahman, D.W. Langer, J. Falk and S.H. Park, "Measurement of Electric Field Dependent Refractive Index Variations in GaAs/AlGaAs Quantum Well Waveguides", Intern. J. Optoelectron., 8, 259-266 (1993).

60. X.M. Fang, Y. Li and D.W. Langer, "Radiative and Nonradiative Transitions in GaAs: Er", J. Appl. Phys., 74, 6993 (1993).

61. R.A. Russell and P.P. Phule', "Chemical Synthesis of Tantalum Zirconate from Alkoxide Precursors", Mat. Sci. and Eng., B21, 88-93 (1993).

62. K. Kim, and K.D. Jordan, "Theoretical Calculation of the OH Rotational Barrier in Phenol", Chem. Phys. Lett., 218, 261-269 (1994).

63. John, K. Wan and J.T.Yates, Jr. "Temperature Measurement for Scanning Tunnel Microscope Samples Using a Detachable Thermocouple", J. Vac. Sci. Technol. B 11(6) 2137-2138, Nov/Dec (1993).

64. A. Kogelbauer, M. Öcal, A. A. Nikolopoulos, J. G. Goodwin, Jr., and G. Marcelin "MTBE Synthesis on Partially Alkali-Exchanged HY Zeolites", Journ. of Catalysis, 147, 1-7 (1994).

65. H.K. Kim, C.C. Li, X.M. Fang, Y. Li, D.W. Langer and J. Solomon, Photoluminescence of Highly Er-Doped Silica Films and Er-Doped GaAs, J. Luminescence 60 and 61, 220 (1994).

66. D.W. Langer, Y. Li, X. Fang, V. Coon "MOCVD Growth and Properties of Erbium Doped GaAs", Mat. Res. Symp. Proc. 301, 15-20 (1993).

67. M.-J. Hua, C.I. Garcia, A.J.DeArdo "Precipitation Studies in Ti and Ti + Nb Stabilized Interstitial-Free Steels", Accepted for publication in Prog Int. Sym. on Low Carbon Steels for the 90's, TMS. Oct. 22.

68. J.C. Hirsch, G. Barrionuevo, and F. Crepel, "Homo-and Heterosynaptic Changes in Efficacy are Expressed in Prefrontal Neurons: An In Vitro Study in the Rat", Synapse, in press.

69. T.A. Blanpied, and T.W. Berger "Characterization In Vivo of the NMDA Receptor-Mediated Component of the Hippocampal Dentate Population Synaptic Response to Perforant Path Input," Hippocampus, in press.

70. T. P. Pollagi, S. J. Geib, M. D. Hopkins, "Synthesis and Structures of Extended-Chain Metal-Alkylidyne Complexes: Conjugated Polymers Composed of Alternating Organic and Transition-Metal Subunits"; J. Am. Chem. Soc., 116, accepted for publication (1994).

71. T.P. Pollagi, S.J. Geib, and M.D. Hopkins, "Molecular Structure of 2-Methyl-4-(4-Pyridyl)-3-butyn-2-ol: A Two-Dimensional Hydrogen-Bonded Network, Acta Crystall. C50, in press.

72. R.D. Coalson, D.K. Pant, A. Ali, and D.W. Langer,"Computing the Eigenmodes of Lossy Field-Induced Optical Waveguides", Journal of Lightwave Technology, accepted for publication (Jan. 1994).

73. M.F. MacMillan, R.P. Devaty, W.J. Choyke, A. Khan, M.E. Lin, H. Morkoc, W.A. Bryden, T.J. Kistenmacher, and S. Nakamura"Cathodoluminescence and FTIR Reflectance of Thin AlN and GaN Films". Accepted for publication in the Proceedings of the International Conference on Silicon Carbide and Related Materials - 1993 (ICSCRM-93), to be published by the Institute of Physics.

74. W.J. Choyke and I. Linkov, "A Short Atlas of Luminescence and Absorption Lines and Bands in SiC, GaN, AlGaN and AlN", accepted

for publication in the Proceedings of the International Conference on Silicon Carbide and Related Materials - 1993 (ICSCRM-93), to be published by the Institute of Physics.

75. P.P. Phule', "Molecularly Modified Alkoxide Precursors for Thin Film Ferroelectrics" Proceedings of the International Symposium on Integrated Ferroelectrics, in press (1994).

76. P. Phulé, " Molecularly Modified Alkoxide Approach for Thin film Ferroelectrics", Integrated Ferroelectrics, 1994 (in press).

77. P. P. Phulé, "Sol-gel Processing of Ceramic Thin Films", in Encyclopedia of Advanced Materials (Eds. S. Mahajan et al.) Elsevier Press (UK) 1994 (in press).

78. A. Kogelbauer, A.A. Nikolopoulos, J.G. Goodwin, Jr., and G. Marcelin, "Gas Phase Synthesis of MTBE on Post-Synthesis Modified Zeolites", accepted for publication in J. Catal.

79. E. Fan, J. Yang, S. J. Geib, C. Vicent, F. Garcia-Tellado, P. Tecilla and A. D. Hamilton, "Supramolecular Self-Assembly based on Directed Hydrogen Bonding' Die Macromoleculare Chemie, In press.

80. W. Li, and A.C. Balazs, "Cluster Formation in Grafted Polymers with Interactive End-Groups", Molecular Simulations, (an invited paper in a special issue devoted to simulations of polymer systems). In press.

81. Z. Yang, D. Williams and A.J. Russell, "Synthesis of protein-containing polymers in organic solvents", in press (1994).

82. Z. Yang, A. Chaudhray and A.J. Russell, Synthesis, activity, and solubility of PEG-modified subtilisin, Biotechnol. Bioengin. in press (1994).

B. <u>Submitted, In Preparation, Presentations</u>

1. D.L. Williams, and A.J. Russell, "Synthesis of Solvent Resistant Biosensor Materials", AICHE Proceedings, submitted.

2. S. A. Asher, J. Holtz, L. Liu, and Z. Wu, "A Self Assembly Motif for Creating Submicron Periodic Materials., J. Am. Chem. Soc., submitted (1994).
3. S.-Y. Chang, L. Liu, and S. A. Asher,"Preparation and Properties of Tailored Morphology, Monodisperse Colloidal Silica-Cadmium Sulfide Nanocomposites", J. Am. Chem. Soc., submitted (1994).

4. S.-Y. Chang, L. Liu, and S. A. Asher, "Creation of Complex Topological Morphologies in Colloidal Silica", J. Am. Chem. Soc., submitted (1994).

5. J.T. Lindt, A.K. Ghosh and B. Flander, "Fluid Mechanics of Polymer Blends II: Break up of Lamellar Structures into Filaments and Globules, submitted to Polym. Eng. Sci.

6. A. A. Nikolopoulos, A. Kogelbauer, J. G. Goodwin, Jr., and G. Marcelin, "Effect of Dealumination on the Catalytic Activity of Acid Zeolites for the Gas Phase Synthesis of MTBE" submitted for publication in Applied Catalysis.

7. A. Kogelbauer, A. A. Nikolopoulos, J. G. Goodwin, Jr., and G. Marcelin,"Impact of Reactant Adsorption on MTBE Synthesis over Zeolites", submitted for publication.

8. A. A. Nikolopoulos, A. Kogelbauer, J.G. Goodwin, Jr., and G. Marcelin, "Synthesis of MTBE on Triflic Acid Post-Synthesis Modified Zeolites", to be submitted for publication.

9. A. A. Nikolopoulos, A. Kogelbauer, J.G. Goodwin, Jr., and G. Marcelin, "Synthesis of MTBE on Ammonium Fluoride Post-Synthesis Modified Zeolites", to be submitted for publication.

10. K.D. Jordan, K. Kim, and M.N. Paddon-Row, "Long-range Interactions in a Series of Rigid Non-conjugated Dienes: 2. Role of Electron Correlation in Determining the Distance Dependence of the π_+,π_- and π_+^*,π_-^* Splittings", J. Phys. Chem., submitted.

11. J. Manna, R. J. Kuk, R. F. Dallinger, M. D. Hopkins, "Nature of the Metal-Carbon Triple Bond. Reevaluation of the M≡C Stretching Frequency and Force Constant" J. Am. Chem. Soc., submitted for publication.

12. M.D. Carper, Yimin Liu and P. P. Phulé, Chemical Processing, Microstructure Evolution and Dielectric Properties of oriented PZT Thin Films", 1994, to be submitted to J. American Ceramic Society.

13. J. N. Valenta, R. P. Dixon, A. D. Hamilton and S. G. Weber,"Enhanced Extraction of Phenobarbital from Serum with a Designed Artificial Receptor", Analytical Chem. Submitted.

14. E. Fan, C. Vicent, S. J. Geib and A. D. Hamilton. "Molecular Recognition in the Solid State: Hydrogen Bonding Control of Molecular Aggregation", Chemistry of Materials, Submitted.

15. X.M. Fang, Y. Li, D.W. Langer and J. Solomon, MOCVD Growth of GaAs: Er $(C_4H_9C_5H_4)_3$, J. Electron Mater. submitted (1993).

16. S. Lee, P. Jernakoff, N.J. Cooper, "Electrophilic Modification of a Cyclopentadienyl Ligand in a Tungstenocene Complex: Oxidative Addition of CCl_4 to $[W(\eta^5\text{-}C_5H_5)_2(CO)]$ to give $[W(\eta^5\text{-}C_5H_5)_2(CO)(\eta^5\text{-}C_5H_5\text{-exo-}CCl_3)(CO)Cl]$" in preparation for J. Am. Chem. Soc.

17. J.P. McNally, S. Lee, N.J. Cooper, "The Addition of Heteroanionic Nucleophiles to an Electrophilic Cyclopentadienyl Ligand in $[W(\eta^5\text{-}C_5H_5(SMe_2)Br]^+$ as a Route to Chiral Tungstenocene Complexes" in preparation for Organometallics.

18. S. Lee, N.J. Cooper, "The Synthesis of Tungstenocene Compounds Constrained to Non-Centrosymmetric Space Groups by the Addition of Enantiomeric Mentholate Substituents to a Cyclopentadienyl Ligand" in preparation for Organometallics.

19. P. Konidaris, N.J. Cooper "The Synthesis and Second Order NLO Properties of Acentric Tungstenocene Compounds with Thiomentholate and NeomenthanethiolateSubstituents on Cyclopentadienyl Ligands" , in preparation for Organometallics.

20. P. Konidaris, N.J. Cooper, "Modification of the Donor/Acceptor Characteristics of Substituted Tungstenocene Compounds through Oxidation of the Thiomentholate and Neomenthanethiolate Substituents on the Cyclopentadienyl Ligands", in preparation for Organometallics.

Some of the Presentations

1. A. A. Nikolopoulos, M. Öcal, A. Kogelbauer, J. G. Goodwin, Jr., and G. Marcelin, "Influence of Catalyst Acidity on MTBE Synthesis Reaction", 13th North American Meeting of the Catalysis Society, Pittsburgh (May 1993).

2. J. G. Goodwin, Jr., "Synthesis of MTBE and Other Ethers", invited paper at the 11th International Symposium on C1 Reactions, Vienna, Austria, (July 1992).

3. A. A. Nikolopoulos, A. Kogelbauer, J. G. Goodwin, Jr., and G. Marcelin, "Adsorption Behavior of Methanol and Isobutene on MTBE Synthesis Catalysts", 31st Annual Spring Symposium of the Pittsburgh-Cleveland Catalysis Society, Cleveland (May 1992).

4. A. A. Nikolopoulos, R. Oukaci, J. G. Goodwin, Jr., and G. Marcelin, "Gas Phase Synthesis of MTBE over Acid Zeolites", 203rd ACS National Meeting, San Francisco, CA, (April 1992).

5. J.S. Schultz, and J.S. Schultz, Sources of Biorecognition Molecules for Biosensors. 20th Annual Meeting Federation of Analytical Chemistry and Spectroscopy Societies. Detroit. Abs. 120 p.71 (1993).

6. J.S. Schultz, The Challenge of Maintaining Biosensor Functionality at Material Interfaces. 40th National Symposium of American Vacuum Society. Orlando. Abs. TC2-TuA1 p. 194 (1993).

7. D.L. Williams, E.J. Beckman, and A.J. Russell, Abstract from AIchE, Annual Meeting (November), Miami. Synthesis of solvent resistant biosensor materials (1992).

8. D. Williams, and A.J. Russell, abstract BIOT 0150 from 205th ACS, Annual Meeting (March), Denver. Synthesis of solvent resistant biomaterials (1993).

9. A.J. Russell, 1994 Advances in Biopolymer Engineering, Palm Coast, FL, Janaury 1993 Proctor and Gamble Corporation, Cincinatti, OH, December (Invited Seminar).*Incorporation of proteins into acrylic* polymers.

10. A.J. Russell, Rohm and Haas, Springhouse, PA July "Incorporation of proteins into acrylic polymers".

11. A.J. Russell, Shearwater Polymers, Huntsville, AL, July. "Incorporation of proteins into acrylic polymers".

12. W. Li., and A.C. Balazs, "Cluster Formation in Grafted Polymers with Interactive End-Groups", Proceedings of the American Chemical Society, Division of Polymer Materials Science and Engineering Division, August 1993 Meeting, Chicago, IL.

13. E.T. Wise and S.G. Weber, "Quantitative Evaluation of a Smart Material: PVA-Borate Gelation and the Gel's Response to Diols", Symposium on New Macromolecular Architecture and Supramolecular Polymers, 205th ACS National Meeting, Denver, CO, April 1993.

14. J.N. Valenta, R.P. Dixon, A.D. Hamilton, and S.G. Weber, "Enhanced Extraction of Phenobarbital Using Synthetic Receptor, Baltimore, April 1993.

15. S.G. Weber, "Sensors Based on Molecular Recognition", FACSS, Detroit, October 1993.

16. J.N. Valenta, S.G. Weber, A.D. Hamilton, and R.P. Dixon, "Further Investigations of the Enhanced Extraction of Phenobarbital from Serum, Pittsburgh Conference, March 1994.

C. Patents

1. S.A. Asher, S. Jagannathan, University of Pittsburgh, Department of Chemistry, "Method of Making Solid Crystalline Narrow Band Radiation Filter", Patent #5,281,370, Date of Patent - January 25, 1994.

   A Patent application was also filed for a "Method of Making an Optically Nonlinear Switched Optical Device and Related Devices" (serial number 07/999,487) and a "Method of Filtering Submicron Particles and Associated Product".

2. A.J. Russell (1992) Disclosure on "Incorporation of Proteins into Acrylic Polymers", filed on December 8, 1993,.